CHEMICAL INDUSTRIES/125

Chemical Reaction Engineering and Reactor Technology

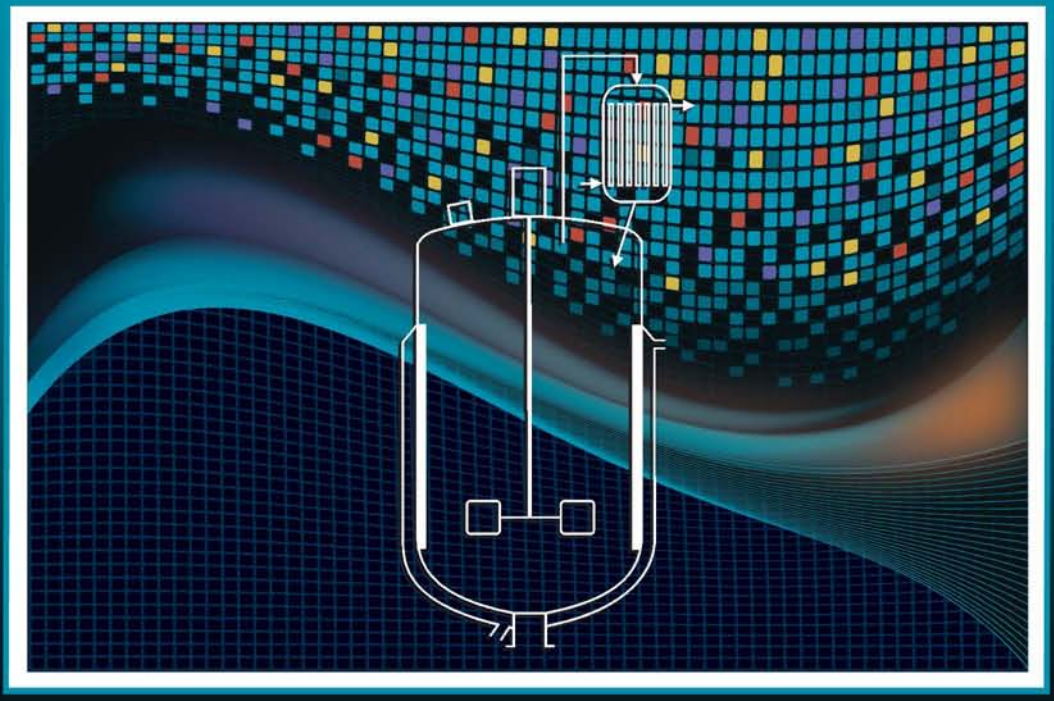

Tapio O. Salmi
Jyri-Pekka Mikkola
Johan P. Wärnå

CRC Press
Taylor & Francis Group

Chemical Reaction Engineering and Reactor Technology

CHEMICAL INDUSTRIES

A Series of Reference Books and Textbooks

Founding Editor

HEINZ HEINEMANN
Berkeley, California

Series Editor

JAMES G. SPEIGHT
CD&W
Laramie, Wyoming

1. *Fluid Catalytic Cracking with Zeolite Catalysts,* Paul B. Venuto and E. Thomas Habib, Jr.
2. *Ethylene: Keystone to the Petrochemical Industry,* Ludwig Kniel, Olaf Winter, and Karl Stork
3. *The Chemistry and Technology of Petroleum,* James G. Speight
4. *The Desulfurization of Heavy Oils and Residua,* James G. Speight
5. *Catalysis of Organic Reactions,* edited by William R. Moser
6. *Acetylene-Based Chemicals from Coal and Other Natural Resources,* Robert J. Tedeschi
7. *Chemically Resistant Masonry,* Walter Lee Sheppard, Jr.
8. *Compressors and Expanders: Selection and Application for the Process Industry,* Heinz P. Bloch, Joseph A. Cameron, Frank M. Danowski, Jr., Ralph James, Jr., Judson S. Swearingen, and Marilyn E. Weightman
9. *Metering Pumps: Selection and Application,* James P. Poynton
10. *Hydrocarbons from Methanol,* Clarence D. Chang
11. *Form Flotation: Theory and Applications,* Ann N. Clarke and David J. Wilson
12. *The Chemistry and Technology of Coal,* James G. Speight
13. *Pneumatic and Hydraulic Conveying of Solids,* O. A. Williams
14. *Catalyst Manufacture: Laboratory and Commercial Preparations,* Alvin B. Stiles
15. *Characterization of Heterogeneous Catalysts,* edited by Francis Delannay
16. *BASIC Programs for Chemical Engineering Design,* James H. Weber
17. *Catalyst Poisoning,* L. Louis Hegedus and Robert W. McCabe
18. *Catalysis of Organic Reactions,* edited by John R. Kosak
19. *Adsorption Technology: A Step-by-Step Approach to Process Evaluation and Application,* edited by Frank L. Slejko
20. *Deactivation and Poisoning of Catalysts,* edited by Jacques Oudar and Henry Wise

21. *Catalysis and Surface Science: Developments in Chemicals from Methanol, Hydrotreating of Hydrocarbons, Catalyst Preparation, Monomers and Polymers, Photocatalysis and Photovoltaics,* edited by Heinz Heinemann and Gabor A. Somorjai
22. *Catalysis of Organic Reactions,* edited by Robert L. Augustine
23. *Modern Control Techniques for the Processing Industries,* T. H. Tsai, J. W. Lane, and C. S. Lin
24. *Temperature-Programmed Reduction for Solid Materials Characterization,* Alan Jones and Brian McNichol
25. *Catalytic Cracking: Catalysts, Chemistry, and Kinetics,* Bohdan W. Wojciechowski and Avelino Corma
26. *Chemical Reaction and Reactor Engineering,* edited by J. J. Carberry and A. Varma
27. *Filtration: Principles and Practices: Second Edition,* edited by Michael J. Matteson and Clyde Orr
28. *Corrosion Mechanisms,* edited by Florian Mansfeld
29. *Catalysis and Surface Properties of Liquid Metals and Alloys,* Yoshisada Ogino
30. *Catalyst Deactivation,* edited by Eugene E. Petersen and Alexis T. Bell
31. *Hydrogen Effects in Catalysis: Fundamentals and Practical Applications,* edited by Zoltán Paál and P. G. Menon
32. *Flow Management for Engineers and Scientists,* Nicholas P. Cheremisinoff and Paul N. Cheremisinoff
33. *Catalysis of Organic Reactions,* edited by Paul N. Rylander, Harold Greenfield, and Robert L. Augustine
34. *Powder and Bulk Solids Handling Processes: Instrumentation and Control,* Koichi Iinoya, Hiroaki Masuda, and Kinnosuke Watanabe
35. *Reverse Osmosis Technology: Applications for High-Purity-Water Production,* edited by Bipin S. Parekh
36. *Shape Selective Catalysis in Industrial Applications,* N. Y. Chen, William E. Garwood, and Frank G. Dwyer
37. *Alpha Olefins Applications Handbook,* edited by George R. Lappin and Joseph L. Sauer
38. *Process Modeling and Control in Chemical Industries,* edited by Kaddour Najim
39. *Clathrate Hydrates of Natural Gases,* E. Dendy Sloan, Jr.
40. *Catalysis of Organic Reactions,* edited by Dale W. Blackburn
41. *Fuel Science and Technology Handbook,* edited by James G. Speight
42. *Octane-Enhancing Zeolitic FCC Catalysts,* Julius Scherzer
43. Oxygen in Catalysis, Adam Bielanski and Jerzy Haber
44. *The Chemistry and Technology of Petroleum: Second Edition, Revised and Expanded,* James G. Speight
45. *Industrial Drying Equipment: Selection and Application,* C. M. van't Land
46. *Novel Production Methods for Ethylene, Light Hydrocarbons, and Aromatics*, edited by Lyle F. Albright, Billy L. Crynes, and Siegfried Nowak
47. *Catalysis of Organic Reactions*, edited by William E. Pascoe
48. *Synthetic Lubricants and High-Performance Functional Fluids*, edited by Ronald L. Shubkin
49. *Acetic Acid and Its Derivatives*, edited by Victor H. Agreda and Joseph R. Zoeller
50. *Properties and Applications of Perovskite-Type Oxides*, edited by L. G. Tejuca and J. L. G. Fierro
51. *Computer-Aided Design of Catalysts*, edited by E. Robert Becker and Carmo J. Pereira

52. *Models for Thermodynamic and Phase Equilibria Calculations*, edited by Stanley I. Sandler
53. *Catalysis of Organic Reactions*, edited by John R. Kosak and Thomas A. Johnson
54. *Composition and Analysis of Heavy Petroleum Fractions*, Klaus H. Altgelt and Mieczyslaw M. Boduszynski
55. *NMR Techniques in Catalysis,* edited by Alexis T. Bell and Alexander Pines
56. *Upgrading Petroleum Residues and Heavy Oils*, Murray R. Gray
57. *Methanol Production and Use*, edited by Wu-Hsun Cheng and Harold H. Kung
58. *Catalytic Hydroprocessing of Petroleum and Distillates*, edited by Michael C. Oballah and Stuart S. Shih
59. *The Chemistry and Technology of Coal: Second Edition, Revised and Expanded,* James G. Speight
60. *Lubricant Base Oil and Wax Processing*, Avilino Sequeira, Jr.
61. *Catalytic Naphtha Reforming: Science and Technology*, edited by George J. Antos, Abdullah M. Aitani, and José M. Parera
62. *Catalysis of Organic Reactions*, edited by Mike G. Scaros and Michael L. Prunier
63. *Catalyst Manufacture,* Alvin B. Stiles and Theodore A. Koch
64. *Handbook of Grignard Reagents,* edited by Gary S. Silverman and Philip E. Rakita
65. *Shape Selective Catalysis in Industrial Applications: Second Edition, Revised and Expanded*, N. Y. Chen, William E. Garwood, and Francis G. Dwyer
66. *Hydrocracking Science and Technology*, Julius Scherzer and A. J. Gruia
67. *Hydrotreating Technology for Pollution Control: Catalysts, Catalysis, and Processes*, edited by Mario L. Occelli and Russell Chianelli
68. *Catalysis of Organic Reactions*, edited by Russell E. Malz, Jr.
69. *Synthesis of Porous Materials: Zeolites, Clays, and Nanostructures,* edited by Mario L. Occelli and Henri Kessler
70. *Methane and Its Derivatives*, Sunggyu Lee
71. *Structured Catalysts and Reactors*, edited by Andrzej Cybulski and Jacob A. Moulijn
72. *Industrial Gases in Petrochemical Processing*, Harold Gunardson
73. *Clathrate Hydrates of Natural Gases: Second Edition, Revised and Expanded*, E. Dendy Sloan, Jr.
74. *Fluid Cracking Catalysts*, edited by Mario L. Occelli and Paul O'Connor
75. *Catalysis of Organic Reactions*, edited by Frank E. Herkes
76. *The Chemistry and Technology of Petroleum: Third Edition, Revised and Expanded*, James G. Speight
77. *Synthetic Lubricants and High-Performance Functional Fluids: Second Edition, Revised and Expanded,* Leslie R. Rudnick and Ronald L. Shubkin
78. *The Desulfurization of Heavy Oils and Residua, Second Edition, Revised and Expanded,* James G. Speight
79. *Reaction Kinetics and Reactor Design: Second Edition, Revised and Expanded,* John B. Butt
80. *Regulatory Chemicals Handbook*, Jennifer M. Spero, Bella Devito, and Louis Theodore
81. *Applied Parameter Estimation for Chemical Engineers*, Peter Englezos and Nicolas Kalogerakis
82. *Catalysis of Organic Reactions,* edited by Michael E. Ford
83. *The Chemical Process Industries Infrastructure: Function and Economics*, James R. Couper, O. Thomas Beasley, and W. Roy Penney
84. *Transport Phenomena Fundamentals*, Joel L. Plawsky

85. *Petroleum Refining Processes*, James G. Speight and Baki Özüm
86. *Health, Safety, and Accident Management in the Chemical Process Industries*, Ann Marie Flynn and Louis Theodore
87. *Plantwide Dynamic Simulators in Chemical Processing and Control*, William L. Luyben
88. *Chemical Reactor Design*, Peter Harriott
89. *Catalysis of Organic Reactions*, edited by Dennis G. Morrell
90. *Lubricant Additives: Chemistry and Applications*, edited by Leslie R. Rudnick
91. *Handbook of Fluidization and Fluid-Particle Systems*, edited by Wen-Ching Yang
92. *Conservation Equations and Modeling of Chemical and Biochemical Processes*, Said S. E. H. Elnashaie and Parag Garhyan
93. *Batch Fermentation: Modeling, Monitoring, and Control*, Ali Çinar, Gülnur Birol, Satish J. Parulekar, and Cenk Ündey
94. *Industrial Solvents Handbook, Second Edition*, Nicholas P. Cheremisinoff
95. *Petroleum and Gas Field Processing*, H. K. Abdel-Aal, Mohamed Aggour, and M. Fahim
96. *Chemical Process Engineering: Design and Economics*, Harry Silla
97. *Process Engineering Economics*, James R. Couper
98. *Re-Engineering the Chemical Processing Plant: Process Intensification*, edited by Andrzej Stankiewicz and Jacob A. Moulijn
99. *Thermodynamic Cycles: Computer-Aided Design and Optimization*, Chih Wu
100. *Catalytic Naphtha Reforming: Second Edition, Revised and Expanded*, edited by George T. Antos and Abdullah M. Aitani
101. *Handbook of MTBE and Other Gasoline Oxygenates*, edited by S. Halim Hamid and Mohammad Ashraf Ali
102. *Industrial Chemical Cresols and Downstream Derivatives*, Asim Kumar Mukhopadhyay
103. *Polymer Processing Instabilities: Control and Understanding*, edited by Savvas Hatzikiriakos and Kalman B. Migler
104. *Catalysis of Organic Reactions*, John Sowa
105. *Gasification Technologies: A Primer for Engineers and Scientists*, edited by John Rezaiyan and Nicholas P. Cheremisinoff
106. *Batch Processes*, edited by Ekaterini Korovessi and Andreas A. Linninger
107. *Introduction to Process Control*, Jose A. Romagnoli and Ahmet Palazoglu
108. *Metal Oxides: Chemistry and Applications*, edited by J. L. G. Fierro
109. *Molecular Modeling in Heavy Hydrocarbon Conversions*, Michael T. Klein, Ralph J. Bertolacini, Linda J. Broadbelt, Ankush Kumar and Gang Hou
110. *Structured Catalysts and Reactors, Second Edition*, edited by Andrzej Cybulski and Jacob A. Moulijn
111. *Synthetics, Mineral Oils, and Bio-Based Lubricants: Chemistry and Technology*, edited by Leslie R. Rudnick
112. *Alcoholic Fuels*, edited by Shelley Minteer
113. *Bubbles, Drops, and Particles in Non-Newtonian Fluids, Second Edition*, R. P. Chhabra
114. *The Chemistry and Technology of Petroleum, Fourth Edition*, James G. Speight
115. *Catalysis of Organic Reactions*, edited by Stephen R. Schmidt
116. *Process Chemistry of Lubricant Base Stocks*, Thomas R. Lynch
117. *Hydroprocessing of Heavy Oils and Residua*, edited by James G. Speight and Jorge Ancheyta
118. *Chemical Process Performance Evaluation*, Ali Cinar, Ahmet Palazoglu, and Ferhan Kayihan

119. *Clathrate Hydrates of Natural Gases, Third Edition*, E. Dendy Sloan and Carolyn Koh
120. *Interfacial Properties of Petroleum Products*, Lilianna Z. Pillon
121. *Process Chemistry of Petroleum Macromolecules*, Irwin A. Wiehe
122. *The Scientist or Engineer as an Expert Witness*, James G. Speight
123. *Catalysis of Organic Reactions,* edited by Michael L. Prunier
124. *Lubricant Additives: Chemistry and Applications, Second Edition,* edited by Leslie R. Rudnick
125. *Chemical Reaction Engineering and Reactor Technology,* Tapio O. Salmi, Jyri-Pekka Mikkola, and Johan P. Wärnå
126. *Asphaltenes: Chemical Transformation during Hydroprocessing of Heavy Oils,* Jorge Ancheyta, Fernando Trejo, and Mohan Singh Rana

Chemical Reaction Engineering and Reactor Technology

Tapio Salmi
Åbo Akademi
Åbo-Turku, Finland

Jyri-Pekka Mikkola
Umeå University,
Umeå, Sweden

Johan Wärnå
Åbo Akademi
Åbo-Turku, Finland

CRC Press
Taylor & Francis Group
Boca Raton London New York

CRC Press is an imprint of the
Taylor & Francis Group, an **informa** business

CRC Press
Taylor & Francis Group
6000 Broken Sound Parkway NW, Suite 300
Boca Raton, FL 33487-2742

Version Date: 20110720

International Standard Book Number-13: 978-1-4398-9485-9 (eBook - PDF)

To my daughter,

Sára Matilda Mikkola
*24.08.1994
†16.06.2007

This is to the memory of my dear daughter, a cross in her favorite color and one piece of art out of her astonishing production, created at the age of nine…

She always saw the bright side of life although since birth she had restrictions in life. For the medical science, it was clear that she was not going to have a life too long, but not for me: a person full of life, intelligence, and sensitivity although not with too much muscle strength. No diagnosis, no prognosis, no cure. I just hope that she is now in some place better…

Your father

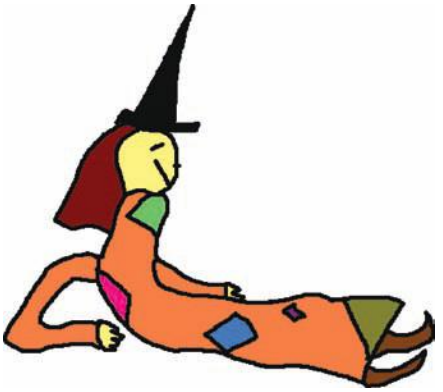

"Witch"

Contents

Preface

The endeavors of this textbook are to define the qualitative aspects that affect the selection of an industrial chemical reactor and coupling the reactor models to the case-specific kinetic expressions for various chemical processes. Special attention is paid to the exact formulations and derivations of mass and energy balances as well as their numerical solutions.

There are several principal sets of problem layouts in chemical reaction engineering: the calculation of reactor performance, the sizing of a reactor, the optimization of a reactor, and the estimation of kinetic parameters from the experimental data. The primary problem is, however, a performance calculation that delivers the concentrations, molar amounts, temperature, and pressure in the reactor. Successful solutions of the remaining problems—sizing, optimization, and parameter estimation—require knowledge of performance calculations. The performance of a chemical reactor can be prognosticated by mass and energy balances, provided that the outlet conditions and the kinetic and thermodynamic parameters are known.

The spectacular emergence of computing technology is characteristic for current chemical reaction engineering. The development of new algorithms for the solution of stiff differential equation systems and initial value problems—both so common in chemical kinetics—and the development of numerical methods for the solutions of boundary value problems of simultaneous chemical reactions and diffusion in heterogeneous systems have enabled reliable simulations of heterogeneous chemical reactions. Numerical methods, together with the powerful computers of today, have transformed the difficulties of yesterday in reactor analysis to the routine calculations of today. The numerical methods are, however, not the main theme of this text, but, nevertheless, a short summary of the most useful methods is introduced in conjunction with each and every type of chemical

reactor. The choice of examples can be attributed, to a large extent, to the authors' research in this area.

Chapters 5 through 8 are mainly concerned with heterogeneous reactors such as two- and three-phase catalytic reactors and gas–liquid reactors for reactive solids. However, we should pay attention to the fact that homogeneous reactors, indeed, form the basis for the analysis and understanding of heterogeneous reactors—therefore, a comprised view of homogeneous reactors is introduced in Chapter 3. The essential stoichiometric, kinetic, and thermodynamic terms needed in the analysis of chemical reactors are discussed in Chapter 2. This book is essentially devoted to reactor technology; thus, the treatment of fundamental kinetics and thermodynamics is kept to a minimum. In Chapter 4, residence time distributions and nonideal flow conditions in industrial reactors are discussed and analyzed. In Appendices 1 and 2, solutions of algebraic equation systems and ordinary differential equation systems are introduced. Appendix 3 contains clarification and the code of the NLEODE (nonlinear equation systems and ordinary differential equation systems) solver. Estimation of gas- and liquid-phase diffusion coefficients is tackled in Appendices 4 and 6, respectively, whereas Appendix 5 discusses the gas film coefficients. Appendix 7 deals with the correlations for gas–liquid systems and Appendix 8 deals with the solubilities of gases in liquids; finally, Appendices 9 and 10 give guidelines for laboratory reactors and the estimation of kinetic parameters.

This book is intended for use by both undergraduates and more advanced students, as well as by industrial engineers. We have tried to follow logical, clear, and rational guidelines that make it feasible for a student to obtain a comprehensive and profound knowledge basis for understanding chemical reactor analysis and design. Furthermore, selected numerical exercises and solutions are helpful in applying the acquired knowledge in practice. Also, engineers working in the field may find the approach of this book suitable as a general reference and as a source of inspiration in the everyday challenges encountered in the profession.

The authors wish to express their gratitude to many of our colleagues in the Laboratory of Industrial Chemistry and Reaction Engineering, Åbo Akademi, and especially to the late Professor Leif Hummelstedt, whose invaluable guidance led many of us into the world of heterogeneous reactors. Professor Lars-Eric Lindfors has contributed numerous interesting discussions dealing with chemical reaction engineering and, especially, heterogeneous catalysis. Professor Erkki Paatero's continuous interest in all the aspects of industrial chemistry has been ever so surprising for all of us. Professor Dmitry Murzin has given valuable comments on the text, particularly to the section concerning catalytic reactors. Many former and present colleagues in our laboratory have contributed to the reactor modeling work: Dr. Jari Romanainen, Dr. Sami Toppinen, Dr. Mats Rönnholm, Dr. Juha Lehtonen, Dr. Esko Tirronen, Dr. Fredrik Sandelin, Dr. Henrik Backman, Dr. Jeannette Aumo, Dr. Johanna Lilja, Dr. Andreas Bernas, and Dr. Matias Kangas.

We are grateful to our family members for their patience during the work.

MATLAB® is a registered trademark of The MathWorks, Inc. For product information, please contact:

The MathWorks, Inc.
3 Apple Hill Drive
Natick, MA 01760-2098 USA
Tel: 508 647 7000
Fax: 508-647-7001
E-mail: info@mathworks.com
Web: www.mathworks.com

Tapio Salmi, Jyri-Pekka Mikkola, and Johan Wärnå

Notations

$\mathbf{a}$	Vector for chemical symbols with the element a_i
a	Variable defined in Equation 8.60, lumped parameters in Table 3.2
A	Mass and heat transfer surface
A	Frequency factor
a, b	Integration constants
a, b, p, r	Concentration exponents in the rate equations, Table 2.1
A'	Frequency factor according to collision theory
A''	Frequency factor according to transition-state theory
a_0	Variable defined in Equation 8.62
a_i	Chemical symbol of component i
a_i	Reacting species i
a_p	Particle surface/reactor volume
A_P	Outer surface of a (catalyst) particle
A_p	Particle surface
a_v	Interfacial area/reactor volume; gas–liquid surface area to reactor volume
b	Temperature exponent according to transition-state theory
C, C', C_1, C_2	Integration constants
C_pm	Molar-based heat capacity
c	Concentration
$\mathbf{c}$	Vector for concentrations
$\mathbf{c}_k$	Vector for the concentrations of key components
c^*	Concentration at the phase boundary, average concentration in Chapter 9
c_0	Total concentration
c_i	Concentration of species i

c_{0i}	Initial concentration of species i
c_A, $c_{R,max}$	Concentration of component A in relation to the concentration maximum of component R
$c_{R,max}$	Concentration maximum of the intermediate product R
c_p	Mass-based heat capacity for a mixture at constant pressure
c_{pmi}	Molar heat capacity of component i at constant pressure
c_{vmi}	Molar heat capacity of component i at constant volume
c_v	Heat capacity of the system at a constant volume
c^s	Surface concentration
$C(t)$	C function, Chapter 4
D	Dispersion coefficient
D_{Ki}	Knudsen diffusion coefficient of component i
D_{ei}	Effective diffusion coefficient of component i
D_i	Diffusion coefficient of component i
D_{mi}	Molecular diffusion coefficient of component i
d_p	Equivalent particle diameter
d_T	Tube diameter
d_b	Bubble diameter
E	Enhancement factor for gas–liquid reactions
E_a	Activation energy
E_i	Factor in van Krevelen–Hoftijzer approximation, Chapter 7
$E(t)$	Population density function, Chapter 4
$F(t)$	Distribution function, Chapter 4
$F*(t)$	Distribution function, complement function of $F(t)$, Chapter 4
ΔF	Gravitation force, Chapter 5
f	Friction factor, Chapter 5
f	General function
f_{kd}	Rate constant for chain initiation
G	Mass flow/reactor tube cross-section
g	Gravitation acceleration
He	Henry's constant, Section 7.2.7
He′	Henry's constant, Section 7.2.7
H_{fi}	Formation enthalpy of component i
h	Heat transfer coefficient for the gas or the liquid film
ΔH_r	Reaction enthalpy
i^T	Vector, $i^T=[1\ 1\ 1\ \ldots\ 1]$
K	Equilibrium constant
K_M	Michaëlis–Menten constant
K_P	Equilibrium constant based on pressure
K_{bc}	Mass transfer coefficient from bubble to cloud phase
$\mathbf{K}_{bc}$	Diagonal matrix for the mass transfer coefficients K_{bc}
K_c	Concentration-based equilibrium constant
K_{ce}	Mass transfer coefficient from cloud to bubble phase
$\mathbf{K}_{ce}$	Diagonal matrix for the mass transfer coefficients K_{ce}

K_i Equilibrium ratio of component i in gas–liquid equilibrium
k Rate constant
k' Empirical rate constant or merged rate constant
k_+ Rate constant of a forward reaction; from left to right
k_- Rate constant of a backward reaction; from right to left
k_{Gi} Mass transfer coefficient of component i in the gas phase
k'_{Gi} Mass transfer coefficient of component i in the gas phase, Section 7.2.7
k_{Li} Mass transfer coefficient of component i in the liquid phase
k_P Rate constant for chain propagation
k_T Rate constant for chain termination
L Reactor length, tube length
l Reactor length coordinate
M Molar mass
M Heat flux, Section 5.2.2.5
M Dimensionless parameter, $M^{1/2}$ = Hatta number, Section 7.2.4.3
$\overline{M}$ Molar mass of a mixture
m Mass
m_{cat} Catalyst mass
$\dot{m}$ Mass flow
m_p Mass of a (catalyst) particle
N Molar flux
$\mathbf{N}$ Flux
N'_i Flux in the absence of mass transfer limitations
n Amount of substance (molar amount)
$\dot{n}$ Flow of amount of substance
n_k Flow of key component k
$\dot{\mathbf{n}}'$ Vector of transformed flows
$\dot{n}'$ Transformed flow, Section 5.2.4
n_T Number of reactor tubes
$\dot{n}$ Vector of flows
$\mathbf{n}'_k$ Vector of flows of key components
n_i Amount of component i
n_k Amount of key component k
n_{0k} Amount of key component k at the beginning or at the inlet
$\dot{n}_i$ Flow of component i
$\dot{n}_k$ Flow of key component k
$\dot{n}_{0i}$ Inflow of component i
$\dot{n}_{0k}$ Inflow of key component k
n_p Number of particles
P Total pressure
P_0 Reference pressure or initial pressure
p Partial pressure
Q Amount of heat transported from or to the system

$\dot{Q}$	Heat flux transported from or to the system
$\Delta\dot{Q}$	Heat flux to or from the system
R	General gas constant, $R = 8.3143$ J/K mol; characteristic dimension of a (catalyst) particle; for spherical objects R = particle radius
R	Reaction rate
$\mathbf{R}$	Vector of reaction rates with the elements R_j
R'	Reaction rates under diffusion influence (not bulk concentrations, see Chapter 5)
R_b	Reaction rate in the bubble phase in a fluidized bed
R_c	Reaction rate in the cloud phase in a fluidized bed
R_e	Reaction rate in the emulsion phase in a fluidized bed
R_j	Rate of reaction j
r	Radial coordinate in a (solid) catalyst particle or in a reactor tube
r	Generation rate
$\mathbf{r}$	Vector of generation rates
r_k	Generation rate of key component k
$\mathbf{r}_k$	Vector of generation rates of key component k
r_i'	Dimensionless generation rate, Equation 5.101
r_1', r_2'	Roots of characteristic equation (second-order linear differential equations)
r_i	Generation rate of component i
S	Number of chemical reactions
S	Heat transfer area of a reactor
ΔS_r	Reaction enthalpy
s	Signal, Chapter 4; form factor, Chapter 5
s_0	Signal of pure fluid, Chapter 4
s_∞	Signal at the system inlet (tracer introduction) (Chapter 4)
s_j	Semiempirical exponent in the Langmuir–Hinshelwood rate equation
T	Temperature
T_ad	Adiabatic temperature
ΔT_ad	Adiabatic temperature change
T_C	Temperature of the surroundings
T_0	Reference temperature
t	Reaction time or residence time
$\bar{t}$	Mean residence time, Chapter 4
t_a	Age of species, Chapter 4
t_c	Clock time, Chapter 4
t_0	Total reaction time, Chapter 8
U	Heat transfer coefficient
ΔU_r	Change in internal energy due to chemical reaction
U_w	Combined heat transfer parameter for the reactor walls and for the fluid film around the reactor wall
V	Volume

V_R Reactor volume
V_b Volume of the bubble phase
V_c Volume of the cloud phase
V_e Volume of the emulsion phase
$\dot{V}_0$ Volumetric flow rate at the reactor inlet
V_p Particle volume
V_S Volume of solid phase
V_{sb} Volume of solid particles in the bubble phase
V_{sc} Volume of solid particles in the cloud phase
V_{se} Volume of solid particles in the emulsion phase
$\dot{V}$ Volumetric flow rate
w Flow rate calculated for the reactor cross-section, superficial velocity
w' Real flow rate, interstitial velocity
w_G Gas velocity in the bubble phase
w_{br} Rise velocity of gas bubbles in a fluidized bed
w_{mf} Velocity at minimum fluidization
w_0 Maximum flow rate in the middle of the tube, Section 4.2.10
x Dimensionless coordinate in a catalyst particle, $x = r/R$
$\mathbf{x}$ Vector for mole fractions
$\mathbf{x}_0$ Vector for mole fractions at the beginning or at the reactor inlet
x_i Mole fraction of component i
x_{0k} Initial mole fraction of key component k
$y, y*$ Dimensionless concentration
y Concentration gradient, Section 8.2.2
$y_{R/A}$ Yield defined as the amount of product formed per total amount of reactant, Section 3.8.1.2
z Length coordinate
Z Compressibility factor
z' Coordinate of the reaction plane for infinitely fast gas and liquid reactions

DIMENSIONLESS GROUPS

a/a_0 Integrated dependencies of the bulk-phase concentrations, Chapter 8
Bi Biot number
Bi_M Biot number of mass transport
Bo Bond number
Da Damköhler number
Ha Hatta number ($Ha = M^{1/2}$)
Fr Froude number
Ga Galilei number

Nu	Nusselt number
Pe	Peclet number
Pe_{mr}	Peclet number of radial mass transfer
Pr	Prandtl number
Re	Reynolds number
Sc	Schmidt number
Sh	Sherwood number
φ	Thiele modulus
$\varphi*$	Thiele modulus for arbitrary kinetics and geometry
φ_s	Generalized Thiele modulus, Equation 5.97

GREEK SYMBOLS

α	Wake volume/bubble volume in Section 5.3.2.1
$\alpha, \beta, \gamma, \delta$	Empirical exponents, Table 2.1
γ	Activity coefficient
γ_{b}	Volume fraction, Section 5.3.2.1
γ_{c}	Volume fraction, Section 5.3.2.1
γ_{e}	Volume fraction, Section 5.3.2.1
δ	Film thickness
ε	Bed porosity
ε	Volume fraction, Section 5.3.2.1
ε_{L}	Liquid holdup
ε_{G}	Gas holdup
$\varepsilon_{\mathrm{mf}}$	Bed porosity at minimum fluidization
ε_{p}	Porosity of catalyst particle
$\phi_{\mathrm{R/A}}$	Momentaneous yield (selectivity), Section 3.8.1
$\phi_{\mathrm{R/A}}$	Integral yield (selectivity), Section 3.8.1
ζ	Dimensionless radial coordinate
η	Conversion; often referred to as X in the literature
η_e	Effectiveness factor
η'_k	Relative of conversion of a key component k
$\boldsymbol{\eta}'_k$	Vector for relative conversion
η_i	Asymptotic effectiveness factor in Section 5.2.2.4
λ	Radial heat conductivity of catalyst bed
λ_{e}	Effective heat conductivity of catalyst particle
λ_{f}	Heat conductivity of fluid film
$\lambda(t)$	Intensity function, Chapter 4
μ	Dynamic viscosity
ν	Stoichiometric matrix with elements ν_{ij}
$\boldsymbol{\nu}$	Stoichiometric matrix
ν	Kinematic viscosity

$\nu_A, \nu_B, \nu_P, \nu_R$	Stoichiometric coefficients of components A, B, P, and R
ν_i	Stoichiometric coefficients of component i
ν_{ij}	Stoichiometric coefficient of component i in reaction j
ν_k	Stoichiometric matrix for the key components
ξ	Reaction extent
$\underline{\xi}$	Vector for reaction extents
ξ'	Specific reaction extent
$\underline{\xi}'$	Vector for specific reaction extents
ξ''	Reaction extent with concentration dimension, Section 3.5
ξ_j	Reaction extent of reaction j
ξ'_j	Specific reaction extent of reaction j, Section 3.5
ρ	Density
ρ_0	Density of feed
ρ_B	Catalyst bulk density; $\rho_B = m_{cat}/V_R$
ρ_{Bb}	Catalyst bulk density in the bubble phase
ρ_{Bc}	Catalyst bulk density in the cloud phase
ρ_{Be}	Catalyst bulk density in the emulsion phase
ρ_P	Density of (catalyst) particle
σ^2	Variance, Chapter 4
τ	Space time, reaction time (BR), residence time (PFR), Section 3.8.5
τ_b	Residence time of a gas bubble
τ_P	Catalyst particle tortuosity
$\tau_{max,PFR}$	Time for the concentration maximum of the intermediate product, case BR or PFR
$\tau_{max,CSTR}$	Time for the concentration maximum of the intermediate product, case CSTR, Chapter 3
ϕ'	Sphericity, Equation 5.257, $\phi' = A_s/A_p$, A_s = the outer surface area of a sphere with the volume equal to the particle, A_p = outer surface area of the particle
$\Phi_{R/A}$	Total yield (selectivity)
φ	Thiele modulus
φ^*	Generalized Thiele modulus for a slab-formed catalyst particle
φ'	Thiele modulus, Equation 8.56
φ''	Thiele modulus, Equation 8.89
φ_s	Generalized Thiele modulus
θ	Surface coverages, Chapter 9
θ	Normalized time, Chapter 4

SUBSCRIPTS AND SUPERSCRIPTS

0	Initial condition or reactor inlet
α, β	General exponents

B, b	Bulk phase
b, c, e	Bubble, cloud, and emulsion phases, Section 5.3.2
C	Reactor surroundings
cat	Catalyst
F	Fluid (gas or liquid)
G	Gas
i	Component index
in	Inlet (feed)
inert	Inert component
j	Reaction index
k	Key component
L	Liquid
MD	Maximum mixed dispersion model
MT	Maximum mixed tanks-in-series model
n	General exponent, for example, in Table 3.3
out	Outlet
p	Particle
R	Reactor
SD	Segregated dispersion model
ST	Segregated tanks in series model
s	Reaction index; in catalytic reactions: surface or phase boundary
sb	Solids in bubble
sc	Solids in cloud
se	Solids in emulsion
T, TS	Tanks in series

ABBREVIATIONS

A, B, C, D, . . . , R, S, T	Component names
AD	Axial dispersion
BR	Batch reactor
CFD	Computational fluid dynamics
CSTR	Continuous stirred tank reactor
E	Enzyme
LFR	Laminar flow reactor
N	Number of reactions
P_n	Component *n*
PFR	Plug flow reactor
R	Reactor
RTD	Residence time distribution
s	Solid
S	Number of reactions, substrate
X	Active complex

UNITS

SI units are used throughout this book. In some exercises, the units used for pressure are 1 atm = 101.3 kPa, 1 bar = 100 kPa, and 1 torr (=1 mm Hg) = 1/760 atm.
For dynamic viscosity 1 cP (centipoise) = 10^{-3} Nsm^{-2} is used.
The occasionally used abbreviation for 1 dm^3 is 1 L (liter).

CHAPTER 1

Introduction

Today, chemical reactors are used for the industrial conversion of raw materials into products. This is naturally facilitated by chemical reactions. Raw material molecules are referred to as reactants. Industrial reactors can be operated batchwise or in a continuous mode. In the batchwise operation mode, the reaction vessel is loaded with reactants, and the chemical reaction is allowed to proceed until the desired conversion of reactants into products has taken place. A more common approach is the continuous operation of a chemical reactor. Reactants are fed continuously into the reaction vessel, and a product flow is continuously taken out of it. If the desired product purity cannot be achieved in the reactor—as is often the case—one or several separation units are installed after the actual reactor. Common separation units include distillation, absorption, extraction, or crystallization equipment. A chemical reactor coupled with a separation unit constitutes the core of a chemical plant, as illustrated in Figure 1.1. The role of the chemical reactor is crucial for the whole process: product quality from the chemical reactor determines the following process steps, such as type, structure, and operation principles of separation units [1].

A brief classification of chemical reactors is presented in Table 1.1. The classification is mainly based on the number of phases present in the reactor. This classification is very natural, as the character of reactive phases to a large extent decides the physical configuration of reactor equipment.

Most industrially relevant chemical processes are carried out in the presence of compounds that enhance the reaction rate. These compounds are referred to as catalysts. Homogeneous or homogeneously catalyzed reactions can be facilitated in a simple tube or tank reactors. For heterogeneous catalytic reactions, usually the reactor has a solid catalyst phase, which is not consumed as the reaction takes place. The catalyst is placed in the reactor to enhance reaction velocity. Heterogeneous catalytic reactions are commonly carried out in packed bed reactors, in which the reacting gas or liquid flows through a stagnant

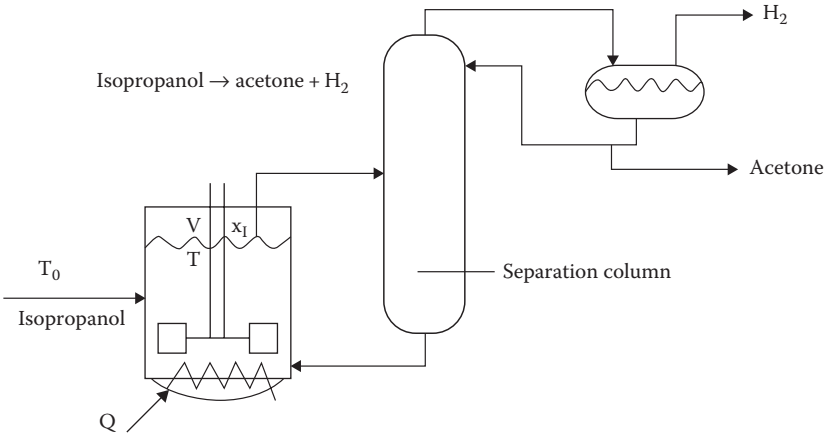

FIGURE 1.1 A chemical reactor and the separation unit.

catalyst layer. If catalyst particles are very small, they can be set in motion and we can talk about a fluidized bed. In case the catalytic reactor contains both a gas phase and a liquid phase, it is referred to as a three-phase reactor. If catalyst particles are immobile, we have a so-called packed bed reactor (trickle bed). If, on the other hand, the catalyst is suspended in a liquid, the reactor is called a slurry reactor.

A special type of catalytic reactor consists of reactive distillation columns, in which the reaction takes place on catalyst particles that are assembled into a column, while the products and reactants are continuously being separated by means of distillation.

Homogeneous and homogeneously catalyzed gas–liquid reactions take place in the liquid phase in which gaseous reactants dissolve and react with other reactants that are primarily present in the liquid phase. Typical constructions to be used as gas–liquid reactors are column and tank reactors. Liquid–liquid reactors principally resemble gas–liquid reactors, but the gas phase is replaced by another liquid phase. The reactions can principally take place in either of, or even both, the liquid phases.

The most complicated systems are represented by reactors in which the solid phase is consumed—or solid particles are generated—while a reaction takes place. For this kind of reaction, similar types of reactors are utilized as for heterogeneous catalytic reactions: packed and fluidized beds.

However, it is not the configuration of the reactor itself but the chemistry involved in the industrial process that plays a central role in the production of new substances. The process chemistry decides, to a large extent, the choice of the reactor. For a review of various industrial processes, see Table 1.2. The classification given here is crude and only indicates the main trends in modern industry. All these processes can be studied by methods that have been developed in chemical reaction engineering.

Projecting a chemical reactor in a factory site is a process with many steps. This procedure—a combination of chemical knowledge and intuition, chemical reaction engineering as well as general engineering knowledge—is not easy to systematize and generalize. One can, however, identify certain characteristic steps [2] as discussed below.

TABLE 1.1 Overview of Industrial Reactors

Reactor-Type Configuration		Characteristics
Homogeneous reactors Tube reactor (plug flow reactor, PFR) Tank reactor (stirred tank reactor, CSTR) Batch reactor Semibatch reactor	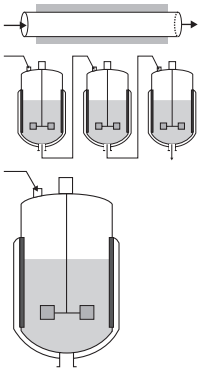	Only one phase (gas or liquid) A homogeneous catalyst can be present
Heterogeneous catalytic two-phase reactors Packed bed Moving bed Fluidized bed	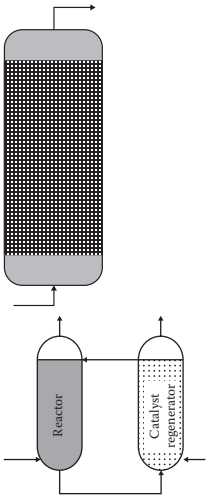	Two phases: one fluid phase (gas or liquid) and a solid catalyst. Reaction takes place on the catalyst surface
Heterogeneous catalytic three-phase reactors	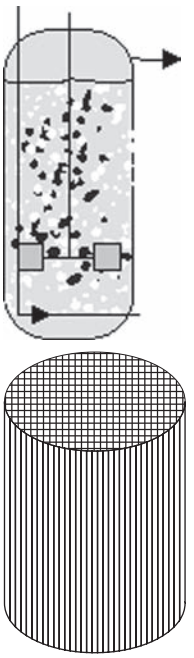	Three phases: gas, liquid, and solid catalyst. Reaction takes place on the catalyst surface

continued

TABLE 1.1 (continued) Overview of Industrial Reactors

Reactor-Type Configuration		Characteristics
Gas–liquid reactors Absorption column Bubble column Tank reactor Reactive distillation column Monolith reactors	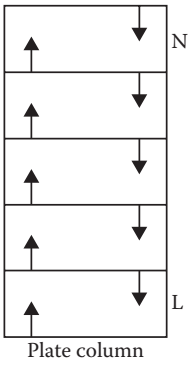 Plate column	A gas phase and a liquid phase Possibly a homogeneous catalyst Reaction takes place in the liquid phase
Liquid–liquid reactors Column reactor Mixer–settler reactor		Two liquid phases. Possibly a homogeneous catalyst Reaction can take place in both phases
Fluid–solid reactors Packed bed Fluidized bed	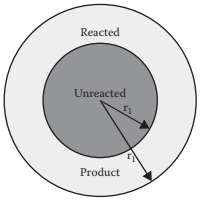	Two or three phases. One fluid phase (gas/liquid). One reactive solid phase Reaction between the solid phase and the gas/liquid phase

1.1 PRELIMINARY STUDIES

1.1.1 REACTION STOICHIOMETRY, THERMODYNAMICS, AND SYNTHESIS ROUTES

These studies show whether the chemical process under consideration is feasible or possible in general. It also provides the answer to questions such as under what conditions (temperature and pressure) the reactor should operate for the projected reaction to be thermodynamically feasible. A literature search and general chemical knowledge give information on the possible synthesis routes and catalysts.

1.2 LABORATORY EXPERIMENTS

If the synthesis route for the product under consideration is unknown, it should be innovated and verified by means of laboratory experiments. For many industrial reactions, the synthesis route is reasonably clear, whereas the reaction velocity, the kinetics, is usually unknown. The role of the reaction velocity is crucial when it comes to the dimensioning of the reactor: The more slowly the reactions proceed, the larger the reactors—or the longer the residence times. By means of laboratory experiments, the kinetics of the reactions involved

TABLE 1.2 Some Industrial Processes and Reactors

Process	Reactor Type
Manufacture of inorganic bulk chemicals (ammonia and methanol synthesis, oxidation of sulfur dioxide in a sulfuric acid plant, manufacture of nitric acid, hydrogen peroxide, and sodium borohydride)	Usually catalytic processes, packed beds, and fluidized beds are used
Oil refinery processes [catalytic cracking, isomerization, hydrogenation (dearomatization), dehydrogenation, reforming, steam reforming, desulfurization, metal removal, hydro-oxygenation, methane activation, etherification, benzene–toluene–xylene (BTX) process]	Catalytic two- and three-phase processes; packed and fluidized beds, trickle beds, bubble columns
Manufacture of synthetic fuels [Fischer–Tropsch reaction, MTG (methanol-to-gasoline) process]	Packed and fluidized beds
Petrochemical processes (manufacture of polyethene, polypropene, polystyrene, polyvinyl chloride, polyethers, maleinic and phthalic anhydride, phenol, acetone, etc.)	Packed beds, tube reactors, tank reactors
Wood-processing processes (wood delignification, bleaching, manufacture of cellulose derivatives such as carboxymethyl cellulose, CMC)	Specially constructed, tailor-made reactors
Organic fine chemicals (manufacture of pharmaceuticals, pesticides, herbicides, cosmetics, reactive intermediates)	Often homogeneous or homogeneously catalyzed reactions but even heterogeneous catalytic reactions exist; batch, tank, and tube reactors, three-phase reactors, bubble columns
Extraction processes (acceleration of metal extraction with chemical reactions)	Columns and mixer–settler
Gas cleaning (absorption of poisonous or harmful gases, e.g., CO, CO_2, and H_2S in liquids with the aid of a reagent)	Absorption columns
Combustion processes (combustion of carbon and other solid fuels)	Packed and fluidized beds
Biochemical processes (enzymatic catalysis, fermentation, biological waste water treatment)	Slurry reactors, packed beds
Processes of the alimentary industry (hydrogenation of xylose to xylitol, margarine production)	Slurry (autoclave) and loop reactors

can be determined. Other unknown quantities such as reaction enthalpies, diffusion coefficients, and other mass and heat transfer parameters are also determined frequently.

1.3 ANALYSIS OF THE EXPERIMENTAL RESULTS

On the basis of kinetic data, a rate equation can be designed and even—if one is lucky—the reaction mechanisms can be determined at the molecular level. The result is thus a

mathematical model of the reaction kinetics. This model has to be verified by means of additional experiments.

1.4 SIMULATION OF REACTOR MODELS

On the basis of the kinetic model developed, a laboratory reactor and the reactors on a larger scale—pilot and factory scale—can be simulated by a computer, and the most promising reactor construction can be selected. The design of new reactors in the industry is today based on experiments and computer simulations. With the kinetic model from the laboratory and a process simulator, the process can be simulated and different possibilities are screened. Even optimization studies can be conducted at this stage.

1.5 INSTALLATION OF A PILOT-PLANT UNIT

In principle, a courageous engineer might base a full-scale process on laboratory experiments and computer simulations. However, for this approach to be successful, all the process parameters should be known with great accuracy. This is not always the case. Therefore, the process is often designed on a half-large scale at first as the so-called pilot-plant unit. This can be used to obtain valuable information on process behavior, and mathematical models can be further refined through additional experiments.

1.6 CONSTRUCTION OF THE FACILITY IN FULL SCALE

Once the previous steps have been successfully completed, the construction of the full-scale process can be initiated. At this stage, one still needs to return to the simulation and optimization calculations [3].

One of the fundamental aspects of the process described above is the mathematical analysis of the behavior of chemical reactors (reactor analysis). Reactor analysis mainly refers to two types of calculations: performance calculations, which indicate the reactor performance, and design calculations, which, for example, determine the required reactor volume for a certain performance requirement such as the desired conversion degree of reactants or the desired production capacity. These problems are tackled in Figure 1.2 [3]. These two tasks are apparently different: as a matter of fact, the problems culminate in the

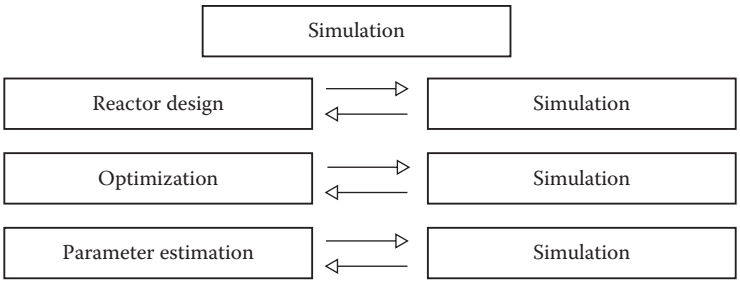

FIGURE 1.2 Typical tasks in reactor analysis.

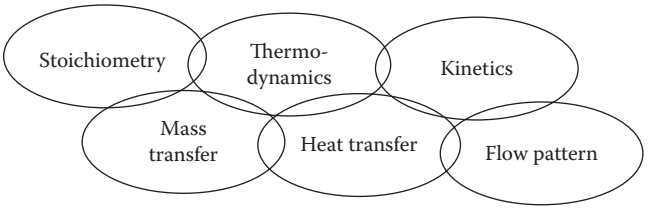

FIGURE 1.3 Factors governing the analysis and design of chemical reactors.

solution of mass and energy balance equations for the reactor in question. The choice of the industrial reactor, as well as the analysis of its performance, is going to be one of the main themes in this text.

Mathematical analysis of chemical reactors is based on mass, energy, and momentum balances. The main features to be considered in reactor analysis include stoichiometry, thermodynamics and kinetics, mass and heat transfer effects, and flow modeling. The different factors governing the analysis and design of chemical reactors are illustrated in Figure 1.3. In subsequent chapters, all these aspects will be covered.

Since the main focus of this text is on chemical reactors, chemical kinetics is briefly discussed (Chapter 2) in order to explain how the kinetic concept is implemented in reactor models. Heat and mass transfer effects along with flow modeling are treated in each chapter devoted to reactors (Chapters 3 through 8).

REFERENCES

1. Trambouze, P., van Landeghem, H., and Wauquier, J.P., *Chemical Reactors—Design/Engineering/Operation*, Editions Technip, Paris, 1988.
2. Villermaux, J., *Génie de la réaction chimique—conception et fonctionnement des réacteurs*, Techniques et Documentation Lavoisier, Paris, 1985.
3. Salmi, T., Modellering och simulering av kemiska reaktioner, *Kemia—Kemi*, 12, 365–374, 1985.

CHAPTER 2

Stoichiometry and Kinetics

In a chemical reactor, one or several simultaneous chemical reactions take place. In an industrial context, some of the reactions tend to be desirable, whereas others are undesirable side reactions yielding by-products.

In case several reactions take place simultaneously in the system, these are called multiple reactions.

An example of a desirable main reaction is methanol synthesis

$$CO + 2H_2 \leftrightarrows CH_3OH,$$

which is carried out industrially on a solid catalyst bed. Along with the main reaction, a side reaction also takes place because the feed into the reactor always contains CO_2:

$$CO_2 + H_2 \leftrightarrows CO + H_2O.$$

These reactions in the methanol synthesis are *parallel* reactions in H_2, since H_2 reacts simultaneously with CO_2 and CO to yield CO and CH_3OH. On the other hand, the reaction scheme can be interpreted to be *consecutive* in CO, as CO is produced by the latter reaction and consumed by the first one.

A classical example of coupled reactions is illustrated by a reaction scheme that is parallel in one reactant and consecutive in another. For instance, in the chlorination of *p*-cresol, mono- and dichloro-*p*-cresols are produced according to the following scheme

$$p\text{-cresol} + Cl_2 \rightarrow \text{monochloro-}p\text{-cresol} + HCl$$

$$\text{monochloro-}p\text{-cresol} + Cl_2 \rightarrow \text{dichloro-}p\text{-cresol} + HCl.$$

This reaction system is consecutive with respect to the intermediate product, monochloro-*p*-cresol, whereas it is parallel with respect to chlorine. These kinds of reaction systems are called consecutive-competitive reactions.

The rates of these different reactions vary case by case: some of the reactions are relatively fast, whereas others might be considerably slow. The reaction stoichiometry relates the generation and consumption velocities of the various components to the velocities of the corresponding chemical reactions. For a qualitative treatment of the stoichiometry of the chemical reactions and kinetics, some fundamental concepts need to be defined.

2.1 STOICHIOMETRIC MATRIX

The stoichiometry for a chemical system, in which only *one* chemical reaction takes place, is described by

$$\sum_{i}^{N} \nu_i a_i = 0, \tag{2.1}$$

where ν_i denotes the stoichiometric coefficient for component i, whose chemical symbol is a_i. This principle can be illustrated by using methanol synthesis as an example,

$$CO + 2H_2 \leftrightarrows CH_3OH,$$

which can be rewritten in the form

$$-CO - 2H_2 + CH_3OH = 0.$$

The vector for the chemical symbols can be arranged to

$$\mathbf{a} = [CO\ H_2\ CH_3OH]^T,$$

in which $\mathbf{a}_1 = CO$, $\mathbf{a}_2 = H_2$, and $\mathbf{a}_3 = CH_3OH$. The stoichiometric coefficients of CO, H_2, and CH_3OH are -1, -2, and $+1$, respectively. We thus obtain the vector $\boldsymbol{\nu}$ for the stoichiometric coefficients

$$\boldsymbol{\nu} = [-1\ -2\ +1]^T.$$

The above reaction equations can also be written in the form

$$[-1\ -2\ +1] \begin{bmatrix} CO \\ H_2 \\ CH_3OH \end{bmatrix} = 0.$$

It is easy to understand that the stoichiometric Equation 2.1 can equally well be written using the vector notation

$$\boldsymbol{\nu}^T \mathbf{a} = \mathbf{0}. \tag{2.2}$$

For a system in which several (S) chemical reactions take place simultaneously, for every reaction, we can write an equation analogous to Equation 2.1; here the stoichiometric coefficient for component i in reaction j is denoted by ν_{ij},

$$\sum_{i}^{N} \nu_{ij} a_i = 0, \quad j = 1, \ldots, S. \tag{2.3}$$

Instead of a vector for the stoichiometric coefficients, we now have a stoichiometric matrix $\boldsymbol{\nu}$ with the elements ν_{ij}.

Let us continue with the methanol synthesis example:

$$CO + 2H_2 \leftrightarrows CH_3OH.$$

Besides the main reaction, a side reaction takes place in this process, which is the above-mentioned conversion reaction

$$CO_2 + H_2 \leftrightarrows CO + H_2O.$$

The vector for the chemical symbols can, for example, be selected in the following manner:

$$\mathbf{a} = [CO\ H_2\ CH_3OH\ CO_2\ H_2O]^{\mathrm{T}}.$$

The stoichiometric coefficients for components CO, H_2, CH_3OH, CO_2, and H_2O for the first reaction will be $-1, -2, +1, 0$, and 0. Accordingly, we obtain the stoichiometric coefficients for the second reaction: $+1, -1, 0, -1$, and $+1$. We can thus write the stoichiometric matrix $\boldsymbol{\nu}$ for the whole system:

$$\boldsymbol{\nu} = \begin{bmatrix} -1 & -2 & +1 & 0 & 0 \\ +1 & -1 & 0 & -1 & +1 \end{bmatrix}^{\mathrm{T}} \begin{bmatrix} -1 & -2 & +1 & 0 & 0 \\ +1 & -1 & 0 & -1 & +1 \end{bmatrix} \begin{bmatrix} CO \\ H_2 \\ CH_3OH \\ CO_2 \\ H_2O \end{bmatrix} = 0.$$

By means of a simple multiplication, one can indeed confirm that Equation 2.3

$$\boldsymbol{\nu}^{\mathrm{T}} \mathbf{a} = 0$$

is also valid for a system with several chemical reactions. For a system consisting of few components and chemical reactions, the stoichiometric matrix can easily be constructed just by glancing at the system; for a system with dozens of components and chemical reactions, it is easiest to utilize computer programs that calculate the stoichiometric matrix on the basis of the entered alphanumerical equations of the type $CO + 2H_2 = CH_3OH$, $CO_2 + H_2 = CO + H_2O$, and so on.

2.2 REACTION KINETICS

If a chemical reaction is taking place in the system, the molar amounts of compounds in the reactor will vary. This is due to the fact that some of the compounds—the reactants—are consumed and some others—the products—are formed. The transformation of reactants to products takes place at a certain rate. The field of science devoted to the rates of chemical reactions is called chemical kinetics [1–5]. A system with only *one* chemical reaction is consequently characterized by a single reaction rate, R. This rate, R, describes the number of moles of substance generated per time unit and reactor volume unit. This is why the classical methanol synthesis example

$$CO + 2H_2 \leftrightarrows CH_3OH$$

has a characteristic reaction velocity, R (mol/s m^3), which defines the number of moles of product generated with a certain reactive mixture composition, pressure, and temperature. The value of R naturally depends on the stoichiometric equation that forms the basis of the mathematical treatment. The stoichiometric equation can, in principle, be selected from a group of an indefinitely large number of choices. For instance, the methanol synthesis example discussed above can also be written as follows:

$$\tfrac{1}{2}CO + H_2 \leftrightarrows \tfrac{1}{2}CH_3OH,$$
$$2CO + 4H_2 \leftrightarrows 2CH_3OH,$$

and so on.

In any case, stoichiometric equations are usually chosen so that the coefficients represent the collection of the smallest possible integers. If this selection simultaneously reflects the course of actions at the molecular level, the reaction defined by the stoichiometric equation is referred to as elementary. In all other cases, the reaction is said to be nonelementary.

The central problem is to answer the question of how the velocities of chemical reactions are related to the generation velocities of individual components. For a system with a single chemical reaction, the generation velocity of component i (r_i) is given by the equation

$$r_i = \nu_i R. \tag{2.4}$$

In other words, the reaction velocity is multiplied by the corresponding components of stoichiometric coefficients and thus we obtain the generation velocity of the components. The generation velocity of a component can be either positive or negative.

For the previously introduced methanol synthesis example, the generation velocity of hydrogen is defined by the equation

$$r_{H_2} = -2R$$

and the generation velocity of methanol by the equation

$$r_{CH_3OH} = +1R.$$

In a system where several chemical reactions take place simultaneously, the generation velocities of components are obtained by summarizing the contribution of every reaction:

$$r_i = \sum_{j-1}^{S} \nu_{ij} R_j. \tag{2.5}$$

This can be neatly expressed with arrays:

$$\mathbf{r} = \boldsymbol{\nu}\mathbf{R} \tag{2.6}$$

Equation 2.6 is practical for use in calculations.

2.2.1 ELEMENTARY REACTIONS

Determination of the exact form of the reaction rate for a chemical reaction is one of the most central tasks in chemical kinetics. Provided that reaction stoichiometry reflects the events at the molecular level, the reaction is elementary and the reaction kinetics is determined directly by stoichiometry. As an example, we will look at an elementary and reversible reaction

$$2\mathrm{A} + \mathrm{B} \rightleftarrows 2\mathrm{C}$$

and assume that it is elementary. Consequently, the reaction rate is given by the expression

$$R = k_+ c_\mathrm{A}^2 c_\mathrm{B} - k_- c_\mathrm{C}^2, \tag{2.7}$$

that is, the absolutes of the stoichiometric coefficients appear directly in the rate expression. This is based on the fact that the reaction is proportional to the number of intermolecular collisions—the above-mentioned reaction requires a collision frequency, and thus the reaction rate is proportional to c_A, c_B, and c_C. The coefficients k_+ and k_- are forward and backward rate constants, respectively.

The rate constants are strongly temperature-dependent. The general temperature dependence of the rate constant is described as

$$k = A' T^b \mathrm{e}^{-E_\mathrm{a}/(RT)}, \tag{2.8}$$

where E_a is the activation energy, A' is the frequency (preexponential) factor, and b is an exponent that can be obtained empirically or from the transition-state theory [1,2]. A requirement for using a theoretical approach is that the reaction mechanism at the molecular level is known or a reasonable hypothesis for the mechanism can be proposed.

In many cases, temperature T^b in Equation 2.8 is much less pronounced than the exponential term, $\exp(-E_\mathrm{a}/(RT))$. Thus, a simpler version of Equation 2.8 can be presented,

where b ≈ 0 is most often used in chemical reaction engineering, that is, the Arrhenius equation

$$k = A\mathrm{e}^{-E_\mathrm{a}/(RT)}. \tag{2.9}$$

For elementary reactions, the following relation is valid for the rate constants k_+ and k_-:

$$K_\mathrm{c} = \frac{k_+}{k_-}, \tag{2.10}$$

where K_c is the concentration-based equilibrium constant for the elementary reaction. At chemical equilibrium, the rate is zero. For our example, this implies that

$$R = k_+ c_\mathrm{A}^2 c_\mathrm{B} - k_- c_\mathrm{C}^2 = 0, \tag{2.11}$$

which can be rewritten as

$$\frac{c_\mathrm{C}^2}{c_\mathrm{A}^2 c_\mathrm{B}} = \frac{k_+}{k_-}. \tag{2.12}$$

On the other hand, the left-hand side is recognizable. It is equivalent to the equilibrium constant K_c:

$$K_\mathrm{c} = \frac{c_\mathrm{C}^2}{c_\mathrm{A}^2 c_\mathrm{B}}. \tag{2.13}$$

It is easy to prove that Equation 2.10 is valid for an arbitrary reaction. Equation 2.7 can thus be expressed with the equilibrium constant:

$$R = k_+ \left(c_\mathrm{A}^2 c_\mathrm{B} - \frac{c_\mathrm{C}^2}{K_\mathrm{c}} \right). \tag{2.14}$$

The equilibrium constant is temperature-dependent according to the van't Hoff law [1–5]. For exothermic reactions, which produce heat, K decreases with temperature. For endothermic reactions, which consume heat, K increases with temperature.

The treatment presented hitherto concerns ideal mixtures, for which the equilibrium can be expressed with concentrations. For nonideal mixtures, concentrations should be replaced by activities (a_i) of the reaction components. The rate of our example would thus be expressed as

$$R = k_+ \left(a_\mathrm{A}^2 a_\mathrm{B} - \frac{a_\mathrm{C}^2}{K_\mathrm{p}} \right), \tag{2.15}$$

where K_p is the thermodynamic equilibrium constant.

The activities are obtained from concentrations (mole fractions) and activity coefficients (γ): $a = \gamma c$. Theories for estimating activity coefficients have been developed and are summarized in Ref. [6]. This is a subtask in reactor modeling, which is not treated further here.

For nonelementary reactions, the rate expression is not at all self-evident. For such reactions, the concentration dependence of reaction velocities can be determined empirically from experimental data. A more sustainable way is to derive the rate expression as a function of concentration $\mathbf{R} = f(\mathbf{c})$ starting from molecular mechanisms. This subject is treated in detail in specialized literatures [1–5], but the methods for nonelementary kinetics are summarized in the next section. Typical rate expressions for common homogeneously and heterogeneously catalyzed reactions are provided in Table 2.1. In reactor modeling, such expressions can be utilized in an operative manner, without penetrating their physical and chemical background. The estimation of numerical values of rate constants is in most cases based on experimental data. The procedure is described in detail in Appendices 9 and 10.

TABLE 2.1 Typical Examples of Reaction Kinetics

Reaction	Kinetic Equation
Elementary kinetics $\lvert\nu_A\rvert A + \lvert\nu_B\rvert B + \cdots \rightleftarrows \lvert\nu_P\rvert P + \lvert\nu_R\rvert R + \cdots$	$R = k\left(c_A^a c_B^b \cdots - c_P^p c_R^r \cdots / K\right)$ $a, b, \ldots = \lvert\nu_A\rvert, \lvert\nu_B\rvert \cdots$ for reactants $p, r, \ldots = \lvert\nu_P\rvert, \lvert\nu_R\rvert \cdots$ for products $k = k_+, K = k_+/k_-$
Potency law $\lvert\nu_A\rvert A + \lvert\nu_B\rvert B + \cdots \lvert\nu_P\rvert P + \lvert\nu_R\rvert R + \cdots .$	$R = k' c_A^\alpha c_B^\beta c_P^\gamma c_R^\delta$ $\alpha, \beta, \gamma, \ldots =$ empirical exponents, often $\alpha \neq \lvert\nu_A\rvert$, $\beta \neq \lvert\nu_B\rvert \cdots$
Langmuir–Hinshelwood kinetics (heterogeneous catalytic reactions) $\lvert\nu_A\rvert A + \lvert\nu_B\rvert B + \cdots \lvert\nu_P\rvert P + \lvert\nu_R\rvert R + \cdots .$	$R = \dfrac{k\left(c_A^a c_B^b \cdots - c_P^p c_R^r \cdots / K\right)}{\left(1 + \sum K_i c_i^{s_i}\right)^\gamma}$ $K_i =$ adsorption parameter for component i $s_i =$ exponent $s_i = 1$ for nondissociative adsorption $s_i = 1/2$ for dissociative adsorption *Note:* Many other types of Langmuir–Hinshelwood expressions exist
Polymerization kinetics	$R = k_P \sqrt{\dfrac{f_{kd}}{k_T}} c_A^a c_B^b$ $k_P =$ rate constant for chain propagation $k_T =$ rate constant for termination $f_{kd} =$ constant for chain initiation *Note:* The rate expression for the above polymerization is valid for chain polymerization processes
Enzyme kinetics $S + E \overset{1}{\rightleftarrows} X \overset{2}{\rightleftarrows} E + P$ S = substrate E = enzyme P = product X = active complex	$R = \dfrac{k_2 k_{-1} (c_S - c_P/K)\, c_0}{k_{-1} K_M (1 + c_S/K_M) + k_2 c_P/K}$ $K = \dfrac{k_1}{k_{-1}} \cdot \dfrac{k_2}{k_{-2}}, \quad K_M = \dfrac{k_2 + k_{-1}}{k_1}$ $c_0 =$ total enzyme concentration $K_M =$ Michaëlis–Menten constant

2.2.2 KINETICS OF NONELEMENTARY REACTIONS: QUASI-STEADY-STATE AND QUASI-EQUILIBRIUM APPROXIMATIONS

Derivation of rate equations for nonelementary reactions is a huge challenge. It can be done, provided that the details of the underlying reaction mechanism, the elementary steps, are known. The elementary steps of a chemical reaction have characteristic rate and equilibrium constants. Typically, some of the steps are rapid, while others are slow, rate-limiting steps. Furthermore, some reaction intermediates can be unstable, having high production and consumption rates. Typical examples of reactions in which intermediates appear are radical reactions, reactions between ions in organic and inorganic media, and catalytic processes (homogeneously and heterogeneously catalyzed reactions and enzyme reactions; catalytic processes and reactors are discussed in detail in Chapters 5 and 6). An overview of reaction intermediates is given in Table 2.2. In most cases, it is impossible to measure quantitatively the concentrations of the intermediates by standard methods of chemical analysis, such as chromatography and spectroscopy.

For rapidly reacting intermediates, the quasi-steady-state hypothesis can be applied to eliminate the concentrations of the intermediates from the rate equations. For rapid reaction steps, the quasi-equilibrium hypothesis is used to eliminate the concentrations of the intermediates.

The principles of quasi-steady-state and quasi-equilibrium hypotheses are illustrated in Figures 2.1 and 2.2. If we consider the reversible reaction sequence $A \rightleftarrows R \rightleftarrows S$ and assume that R is a rapidly reacting intermediate, its concentration remains at a low, practically constant level during the reaction: Figure 2.1 shows the concentrations of A, R, and S in a batch reactor (Chapter 3) as a function of the reaction time. The net generation rate of R is practically zero ($R_R = 0$), except during a short initial period of time. On the other hand, if one of the reaction steps is very rapid compared with the others, for instance,

TABLE 2.2 An Overview of Reactive Intermediates in Chemical Reactions

	Intermediate	Example Reactions
Radical reactions	Radical	$CH_3^{\cdot} + OH^{\cdot} \rightarrow CH_3OH$
Reactions in liquid phase	Ion (carbenium ions, carbon ions, inorganic ionic complexes)	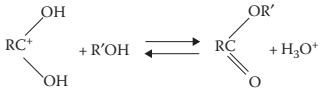
Catalytic reactions		
*Heterogeneous catalysis	Adsorbed surface species	$CO^* + O^* \rightleftharpoons CO_2 + 2^*$
*Homogeneous catalysis	Complex formed from the catalyst and the reactant	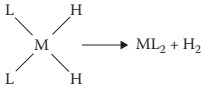
		L = ligand, M = metal
*Enzyme reactions	Complex formed from the enzyme and the substrate (substrate = reactant)	$E + S \rightleftharpoons ES$ $ES \rightarrow P + E$ E = enzyme, S = substrate, P = product

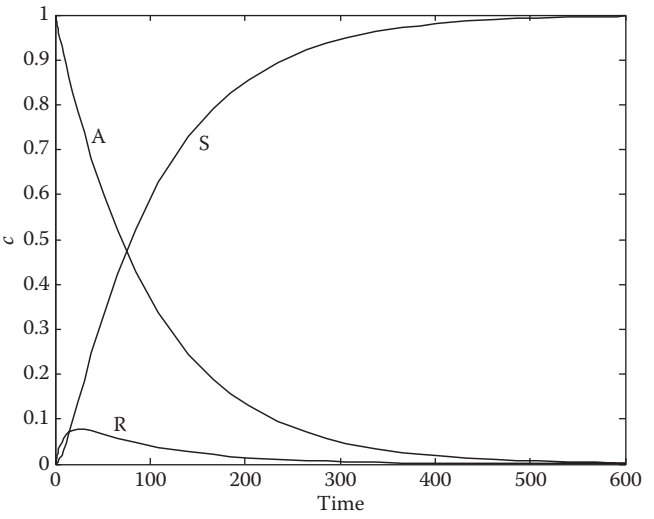

FIGURE 2.1 Quasi-steady-state hypothesis applied to the reaction system $A \rightleftharpoons R \rightleftharpoons S$, where R is a rapidly reacting intermediate in a batch reactor.

$R_1 \gg R_2$, the rates can be denoted by the vectors shown in Figure 2.2. The difference $R_{+1} - R_{-1} = R_{+2} - R_{-2}$, where the indices + and − refer to the forward and backward rates of the elementary steps, respectively. However, since R_{+1} and R_{-1} are large, their ratio approaches one, $R_{+1}/R_{-1} \simeq 1$, which implies that the quasi-equilibrium hypothesis can be applied: $R_{+1}/R_{-1} = k_{+1}c_A/k_{-1}c_R = K_1 c_A/c_R = 1$, that is, $K_1 = c_R/c_A$, which is the well-known equilibrium expression for an elementary step.

A general mathematical approach to the quasi-steady-state can be developed. The generation rates of the detectable (by standard chemical analysis) main components are expressed by the stoichiometry

$$\mathbf{r} = \boldsymbol{\nu}\mathbf{R}(c, c^*), \tag{2.16}$$

whereas the generation rates of the intermediates ($\boldsymbol{c}^*$) are given by

$$r^* = \boldsymbol{\nu}^*\mathbf{R}(c, c^*), \tag{2.17}$$

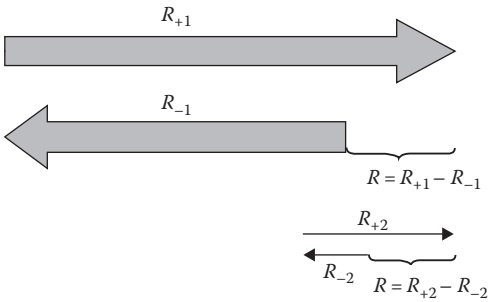

FIGURE 2.2 Quasi-equilibrium hypothesis: a two-step reaction $A \rightleftharpoons R \rightleftharpoons S$, first step is rapid; $R = R_{+1} - R_{-1} = R_{+2} - R_{-2}$, but $R_{+1}/R_{-1} \simeq 1$.

where $\boldsymbol{\nu}^{*\mathrm{T}}$ denotes the stoichiometric matrix of the intermediates. Application of the quasi-steady-state hypothesis implies that

$$r^* = 0. \tag{2.18}$$

Consequently, the concentrations of the intermediates are solved by Equation 2.18 as a function of the concentrations of the main components ($\mathbf{c}$). If the reaction mechanism is linear with respect to the intermediates, an analytical solution is possible. For the linear case, Equation 2.18 is rearranged to

$$\mathbf{A}\mathbf{c}^* = \mathbf{B} \tag{2.19}$$

from which $\mathbf{c}^* = \mathbf{A}^{-1}\mathbf{B}$. Matrix $\mathbf{A}$ and vector $\mathbf{B}$ contain rate and equilibrium constants and concentrations of the detectable main components only. The concentrations of the intermediates are substituted back in to the rate equations of the main components (Equation 2.16).

If the reaction mechanism is nonlinear with respect to the intermediates, the solution of Equation 2.18 becomes more complicated and an iterative procedure is applied in most cases. It should be noticed that an assumption of each rapid intermediate reduces the number of adjustable rate parameters by one. For example, the application of the quasi-steady-state hypothesis in the system $\mathrm{A} \rightleftharpoons \mathrm{R} \rightleftharpoons \mathrm{S}$ implies that

$$r_\mathrm{R} = k_{+1}c_\mathrm{A} - k_{-1}c_\mathrm{R} - k_{+2}c_\mathrm{R} + k_{-2}c_\mathrm{S} = 0 \tag{2.20}$$

and

$$\left(\frac{k_{+1}}{k_{-2}}\right)c_\mathrm{A} - \left[\left(\frac{k_{-1}}{k_{-2}}\right) + \left(\frac{k_{+2}}{k_{-2}}\right)\right]c_\mathrm{R} + c_\mathrm{S} = 0, \tag{2.21}$$

that is, from the set of initial parameters (k_{+1}, k_{-1}, k_{+2}, and k_{-2}), we obtain three parameters ($a_1 = k_{+1}/k_{-2}$, $a_{-1} = k_{-1}/k_{-2}$, and $a_2 = k_{+2}/k_{-2}$).

2.2.2.1 Ionic and Radical Intermediates

The application of quasi-steady-state and quasi-equilibrium hypotheses will be illustrated with the example reaction

$$\mathrm{A} + \mathrm{B} \rightleftharpoons \mathrm{D},$$

which is presumed to have a two-step mechanism

$$\mathrm{A} \rightleftharpoons \mathrm{A}^*, \tag{I}$$

$$\frac{\mathrm{A}^* + \mathrm{B} \rightleftharpoons \mathrm{D}}{\mathrm{A} + \mathrm{B} \rightleftharpoons \mathrm{D}}, \tag{II}$$

where A* is the intermediate (a radical or an ionic species). The rates of the elementary steps are

$$\underline{R} = \begin{bmatrix} R_1 \\ R_2 \end{bmatrix} = \begin{bmatrix} k_{+1}c_{\mathrm{A}} - k_{-1}c_{\mathrm{A}^*} \\ k_{+2}c_{\mathrm{A}^*}c_{\mathrm{B}} - k_{-2}c_{\mathrm{D}} \end{bmatrix}. \tag{2.22}$$

The vectors for chemical symbols are fixed to $\mathbf{a}^{\mathrm{T}} = [\mathrm{A\ B\ D}]$ and $\mathbf{a}^{*\mathrm{T}} = [\mathrm{A}^*]$. The generation rates of the main components are given by

$$\underline{r} = \underline{\nu}\underline{R} = \begin{bmatrix} -1 & 0 \\ 0 & -1 \\ 0 & -1 \end{bmatrix} \begin{bmatrix} R_1 \\ R_2 \end{bmatrix}. \tag{2.23}$$

The generation rate of the intermediate (A*) is

$$\underline{r}^* = \underline{\nu}^*\underline{R} = [1\ -1] \begin{bmatrix} R_1 \\ R_2 \end{bmatrix} = 0. \tag{2.24}$$

After inserting the expressions R_1 and R_2, we obtain

$$k_{+1}c_{\mathrm{A}} - k_{-1}c_{\mathrm{A}^*} - k_{+2}c_{\mathrm{B}}c_{\mathrm{A}^*} + k_{-2}c_{\mathrm{D}} = 0 \tag{2.25}$$

from which c_{A^*} is easily solved:

$$c_{\mathrm{A}^*} = \frac{k_{+1}c_{\mathrm{A}} + k_{-2}c_{\mathrm{D}}}{k_{-1} + k_{+2}c_{\mathrm{B}}}. \tag{2.26}$$

The expression for c_{A^*} is inserted into the expression for R_1 (or R_2), and the final rate equation is obtained:

$$R = R_1 = R_2 = \frac{k_{+1}k_{+2}c_{\mathrm{A}}c_{\mathrm{B}} - k_{-1}k_{-2}c_{\mathrm{D}}}{k_{-1} + k_{+2}c_{\mathrm{B}}}. \tag{2.27}$$

Recalling that $k_{+1}/k_{-1} = K_1$, $k_{+2}/k_{-2} = K_2$, and $K_{\mathrm{c}} = K_1K_2$ (the equilibrium constant of the overall reaction), Equation 2.27 is rewritten as

$$R = \frac{k'[c_{\mathrm{A}}c_{\mathrm{B}} - (c_{\mathrm{D}}/K_{\mathrm{c}})]}{k_{-1} + k_{+2}c_{\mathrm{B}}}, \tag{2.28}$$

where $k' = k_{+1}k_{+2}$.

We thus obtain a rate equation in which the intermediate does not appear anymore and the generation rates of the components are calculated from $r_i = \nu_i R$, where ν_i denotes the stoichiometric coefficients of the main components ($\nu_{\mathrm{A}} = \nu_{\mathrm{B}} = -1$ and $\nu_{\mathrm{D}} = 1$).

From the general solution obtained with the quasi-steady-state hypothesis, the solutions corresponding to the quasi-equilibrium hypothesis can be obtained as special cases. If step I is much more rapid than step II, $k_{-1} \gg k_{+2}c_B$ in Equation 2.27, the reaction rate becomes

$$R = k_{+2}K_1 c_A c_B - k_{-2}c_D, \tag{2.29}$$

which can be rewritten as

$$R = k_{+2}K_1 \left(c_A c_B - \frac{c_D}{K_c} \right). \tag{2.30}$$

On the other hand, if step II is the rapid one, $k_{+2}c_B \gg k_{-1}$, the general rate equation is reduced to

$$R = \left(\frac{k'}{k_{+2}c_B} \right) \left(c_A c_B - \frac{c_D}{K_c} \right), \tag{2.31}$$

which attains the final form

$$R = \left(\frac{k_{+1}}{c_B} \right) \left(c_A c_B - \frac{c_D}{K_c} \right). \tag{2.32}$$

The rate equations valid for one rapid step (Equation 2.30 or 2.32) can be obtained more easily by applying the quasi-equilibrium assumption directly. For instance, if step I is rapid, we can write

$$K_1 = \frac{c_{A^*}}{c_A}, \tag{2.33}$$

that is, $c_{A^*} = K_1 c_A$, which is inserted into Equation 2.22,

$$R_2 = k_{+2}c_{A^*}c_B - k_{-2}c_D \tag{2.34}$$

yielding ($R_2 = R$)

$$R = k_{+2}K_1 c_A c_B - k_{-2}c_D, \tag{2.35}$$

which is equal to Equation 2.29 and leads to Equation 2.30. On the other hand, if step II is rapid, we can write

$$K_2 = \frac{c_D}{c_{A^*}c_B} \tag{2.36}$$

and proceed further, obtaining Equation 2.32.

2.2.2.2 Catalytic Processes: Eley–Rideal Mechanism

For heterogeneous catalytic processes in which solid surface sites (*) play a crucial role, an analogous treatment is applied. Let us consider a linear two-step mechanism:

$$\mathrm{A} + {}^* \rightleftharpoons \mathrm{A}^* + \mathrm{C}, \tag{I}$$

$$\frac{\mathrm{A}^* + \mathrm{B} \rightleftharpoons \mathrm{D} + {}^*}{\mathrm{A} + \mathrm{B} \rightleftharpoons \mathrm{C} + \mathrm{D}}, \tag{II}$$

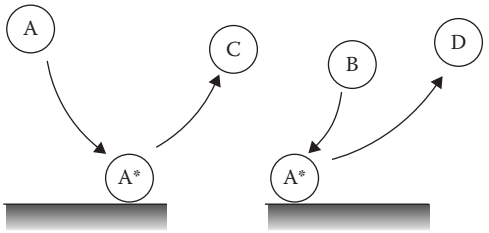

FIGURE 2.3 Schematic illustration of a catalytic process $A + B \rightleftharpoons C + D$ on a solid surface (Eley–Rideal mechanism).

where A, B, C, and D are the experimentally detectable main components, * denotes a vacant surface site, and A is a molecule adsorbed on the surface site. Adsorbed A (denoted by A*) reacts with a B-molecule from the bulk phase (gas or liquid phase) to form D and release the surface site (*). The process is illustrated in Figure 2.3 and is called the Eley–Rideal mechanism. The nature of the surface site depends on the chemical case and the solid catalyst material used. The surface site can be a metal site, an oxide site, and an acidic or a basic site, depending on the catalyst material used. Heterogeneous catalysts are described in more detail in Chapter 5.

The rates of the elementary steps are defined by

$$R = \begin{bmatrix} k_{+1}c_{\mathrm{A}}c_{*} - k_{-1}c_{\mathrm{A}^*}c_{\mathrm{C}} \\ k_{+2}c_{\mathrm{B}}c_{\mathrm{A}^*} - k_{-2}c_{\mathrm{D}}c_{*} \end{bmatrix}. \tag{2.37}$$

After defining the vectors $\mathbf{a}^{\mathrm{T}} = [\mathrm{A\ B\ C}]$ and $\mathbf{a}^{*\mathrm{T}} = [^*\ \mathrm{A}^*]$, the generation rates become

$$r = \nu \mathrm{R} = \begin{bmatrix} -1 & 0 \\ 0 & -1 \\ 0 & -1 \end{bmatrix} \begin{bmatrix} R_1 \\ R_2 \end{bmatrix} = \begin{bmatrix} -R_1 \\ -R_2 \\ -R_2 \end{bmatrix}, \tag{2.38}$$

$$\underline{r}_{*} = \underline{\nu}_{*}\underline{\mathrm{R}} = \begin{bmatrix} -1 & +1 \\ +1 & -1 \end{bmatrix} \begin{bmatrix} R_1 \\ R_2 \end{bmatrix} = \begin{bmatrix} -\mathrm{R}_1 & +\mathrm{R}_2 \\ \mathrm{R}_1 & -\mathrm{R}_2 \end{bmatrix}. \tag{2.39}$$

Equation 2.39 reveals an interesting fact: $\mathbf{r}_{*} = -\mathbf{r}_{\mathrm{A}^*} = 0$, which implies that the two equations contain the same information. To solve the concentrations of the intermediates (* and A*) as a function of the bulk-phase components, the total balance of the active sites is used:

$$\sum c_{*j} = c_0, \tag{2.40}$$

where c_{*j} refers to the surface species and c_0 is the total concentration of the active sites. We now have the equation system

$$\begin{bmatrix} R_1 & -R_2 \\ \sum c_{*j} & -c_0 \end{bmatrix} = \begin{bmatrix} 0 \\ 0 \end{bmatrix}. \tag{2.41}$$

The concentrations are inserted into the equation system, which becomes

$$\begin{bmatrix} k_{+1}c_{\mathrm{A}}c_{*} - k_{-1}c_{C}c_{\mathrm{A}^{*}} - k_{+2}c_{\mathrm{B}}c_{\mathrm{A}^{*}} + k_{-2}c_{\mathrm{D}}c_{*} \\ c_{\mathrm{A}^{*}} + c_{*} - c_{0} \end{bmatrix} = \begin{bmatrix} 0 \\ 0 \end{bmatrix}, \tag{2.42}$$

that is,

$$\begin{bmatrix} (k_{+1}c_{\mathrm{A}} + k_{-2}c_{\mathrm{D}}) & (-k_{-1}c_{\mathrm{C}} - k_{+2}c_{\mathrm{B}}) \\ 1 & 1 \end{bmatrix} \begin{bmatrix} c_{*} \\ c_{\mathrm{A}^{*}} \end{bmatrix} = \begin{bmatrix} 0 \\ c_{0} \end{bmatrix}. \tag{2.43}$$

Equation 2.41 can be written as

$$\begin{bmatrix} (a_{1} + a_{-2}) & (-a_{-1} - a_{2}) \\ 1 & 1 \end{bmatrix} \begin{bmatrix} c_{*} \\ c_{\mathrm{A}^{*}} \end{bmatrix} = \begin{bmatrix} 0 \\ c_{0} \end{bmatrix} \tag{2.44}$$

from which the concentrations of the surface species are solved according to Equation 2.19,

$$\frac{c_{*}}{c_{0}} = \frac{a_{-1} + a_{2}}{a_{1} + a_{-1} + a_{2} + a_{-2}}, \tag{2.45}$$

$$\frac{c_{\mathrm{A}^{*}}}{c_{0}} = \frac{a_{1} + a_{-2}}{a_{1} + a_{-1} + a_{2} + a_{-2}}. \tag{2.46}$$

The quantity $c_{\mathrm{A}^{*}}/c_{0}$ is called the surface coverage of A and is often denoted by θ_{A}.

Substitution of the concentrations of the intermediates into the rate equation yields

$$R = \frac{(a_{1}a_{2} - a_{-1}a_{-2})c_{0}}{a_{1} + a_{-1} + a_{2} + a_{-2}}. \tag{2.47}$$

Back-substitution of the original quantities finally yields

$$R = \frac{(k_{+1}k_{+2}c_{\mathrm{A}}c_{\mathrm{B}} - k_{-1}k_{-2}c_{\mathrm{C}}c_{\mathrm{D}})c_{0}}{k_{+1}c_{\mathrm{A}} + k_{-1}c_{\mathrm{C}} + k_{+2}c_{\mathrm{B}} + k_{-2}c_{\mathrm{D}}}, \tag{2.48}$$

that is,

$$R = \frac{k'c_{0}[c_{\mathrm{A}}c_{\mathrm{B}} - (c_{\mathrm{C}}c_{\mathrm{D}}/K_{\mathrm{c}})]}{k_{+1}c_{\mathrm{A}} + k_{-1}c_{\mathrm{C}} + k_{+2}c_{\mathrm{B}} + k_{-2}c_{\mathrm{D}}}, \tag{2.49}$$

where $k' = k_{+1}k_{+2}$ and $K_{\mathrm{c}} = K_{1}K_{2} = k_{+1}k_{+2}/(k_{-1}k_{-2})$.

If step I is rapid and step II is rate-limiting, $k_{+1}c_{\mathrm{A}} + k_{-1}c_{\mathrm{C}} \gg k_{+2}c_{\mathrm{B}} + k_{-2}c_{\mathrm{D}}$, we obtain

$$R = \frac{k_{+2}K_{1}[c_{\mathrm{A}}c_{\mathrm{B}} - (c_{\mathrm{C}}c_{\mathrm{D}}/K_{\mathrm{c}})]c_{0}}{K_{1}c_{\mathrm{A}} + c_{\mathrm{C}}}. \tag{2.50}$$

If step II is rapid and step I is rate-limiting, $k_{+2}c_{\mathrm{B}} + k_{-2}c_{\mathrm{D}} \gg k_{+1}c_{\mathrm{A}} + k_{-1}c_{\mathrm{C}}$, we obtain

$$R = \frac{k_{+1}K_{2}[c_{\mathrm{A}}c_{\mathrm{B}} - (c_{\mathrm{C}}c_{\mathrm{D}}/K_{\mathrm{c}})]c_{0}}{K_{2}c_{\mathrm{B}} + c_{\mathrm{D}}}. \tag{2.51}$$

Equations 2.50 and 2.51 could, of course, have been obtained directly by applying the quasi-equilibrium hypothesis in reaction steps I and II, respectively.

The quasi-equilibrium assumption is frequently used in the heterogeneous catalysis, since the surface reaction steps are often rate-limiting, while the adsorption steps are rapid. This is not necessarily true for large molecules. Here we consider the application of the quasi-equilibrium hypothesis on two kinds of reaction mechanisms, an Eley–Rideal mechanism and a Langmuir–Hinshelwood mechanism. The rate expressions obtained with this approach are referred to as Langmuir–Hinshelwood–Hougen–Watson (LHHW) equations in the literature, in honor of the pioneering researchers.

A simple Eley–Rideal mechanism, a reaction between adsorbed species and a molecule from the fluid (gas or liquid) phase, can be written as

$$\mathrm{A}+^* \rightleftharpoons \mathrm{A}^*, \tag{I}$$

$$\frac{\mathrm{A}^* + \mathrm{B} \rightleftharpoons \mathrm{C}+^*}{\mathrm{A} + \mathrm{B} \rightleftharpoons \mathrm{C}} \tag{II}$$

which means that A is adsorbed on the catalyst surface and then it reacts with B from the fluid phase.

Application of the quasi-equilibrium hypothesis on the adsorption step yields

$$K_1 = \frac{c_{\mathrm{A}^*}}{c_{\mathrm{A}} c_*} \tag{2.52}$$

from which c_{A^*} is solved: $c_{\mathrm{A}^*} = K_1 c_{\mathrm{A}} c_*$. The total balance of the surface sites, $c_{\mathrm{A}^*} + c_* = c_0$, then yields

$$K_1 c_{\mathrm{A}} c_* + c_* = c_0 \tag{2.53}$$

from which c^* is solved:

$$c^* = \frac{c_0}{1 + K_1 c_{\mathrm{A}}} \tag{2.54}$$

and

$$c_{\mathrm{A}^*} = \frac{K_1 c_0 c_{\mathrm{A}}}{1 + K_1 c_{\mathrm{A}}}. \tag{2.55}$$

Equation 2.55 is called the *Langmuir adsorption isotherm*. The rate equation then becomes

$$R(= R_2) = \frac{k_{+2} c_{\mathrm{B}} K_1 c_{\mathrm{A}} c_0}{1 + K_1 c_{\mathrm{A}}} - \frac{k_{-2} c_{\mathrm{C}} c_0}{1 + K_1 c_{\mathrm{A}}}. \tag{2.56}$$

A rearrangement of Equation 2.56 yields the final form

$$R = \frac{k_{+2} K_1 c_0 [c_{\mathrm{A}} c_{\mathrm{B}} - (c_{\mathrm{C}}/K_{\mathrm{c}})]}{1 + K_1 c_{\mathrm{A}}}. \tag{2.57}$$

In practical applications, the parameters $k_{+2} K_1 c_0$ are often merged to a single parameter $k' = k_{+2} K_1 c_0$.

2.2.2.3 Catalytic Processes: Langmuir–Hinshelwood Mechanism

A classical example of LHHW equations is the bimolecular reaction case, in which the surface reaction between the adsorbed reactants is the rate-limiting step. The adsorption and desorption steps are presumed to be rapid enough to reach quasi-equilibria. For instance, the overall reaction A + B ⇌ C comprises the steps

$A+^* \rightleftharpoons A^*$	Adsorption	(I)
$B+^* \rightleftharpoons B^*$	Adsorption	(II)
$A^* + B^* \rightleftharpoons C^* +^*$	Surface reaction	(III)
$C^* \rightleftharpoons C +^*$	Desorption	(IV)
$A + B \rightleftharpoons C$		

The rate is determined by step III, the surface reaction

$$R = k_+ c_{A^*} c_{B^*} - k_- c_{C^*} c_*. \tag{2.58}$$

The adsorption and desorption quasi-equilibria (steps I, II, and IV) are defined as

$$K_i = \frac{c_{i^*}}{c_i c_*}, \tag{2.59}$$

where i = A, B, and C. Each quasi-equilibrium yields $c_{i*} = K_i c_i c^*$, which is inserted into the site balance

$$\sum_j c_{j^*} + c^* = c_0. \tag{2.60}$$

This yields the concentration of vacant sites

$$c_* = \frac{c_0}{1 + \sum K_j c_j}. \tag{2.61}$$

The rate expression is rewritten using the concentration of vacant sites,

$$R = k_+ K_A K_B c_A c_B c_*^2 - k_- K_C c_C c_*^2. \tag{2.62}$$

After inserting the concentration of vacant sites, Equation 2.58, the final form of the rate equation becomes

$$R = \frac{k_+ K_A K_B c_0^2 \left[c_A c_B - (c_C/K)\right]}{\left(1 + \sum K_j c_j\right)^2}, \tag{2.63}$$

where $\sum K_j c_j = K_A c_A + K_B c_B + K_C c_C$ and $(k_+/k_-) K_A K_B / K_C = K$, the equilibrium constant of the overall reaction. If a nonreactive species, for example, a catalyst poison (P),

adsorbs on the surface blocking active sites, its contribution is included in the sum of the denominator of Equation 2.63: the term is added to the sum $\sum K_j c_j$.

A special feature is the dissociative adsorption of a component, for example, hydrogen and oxygen. For this case, we have the adsorption step

$$B_2 + 2^* \rightleftharpoons 2B^*$$

and the adsorption quasi-equilibrium for B becomes $K_B = c_{B^*}^2/(c_B c_*^2)$, yielding $c_{B^*} = \sqrt{K_B c_B} c^*$. This implies that the term $K_B c_B$ is replaced by $\sqrt{K_B c_B}$ in the denominator of Equation 2.63 for dissociative adsorption.

A more detailed treatment of kinetics of catalytic reactions can be found in the special literature, for example, in Ref. [5]. By definition, a catalyst retains its activity forever. In practice, the situation is different, and the catalyst lifetime can be from years to seconds. Severe catalyst deactivation takes place, for instance, in cracking of hydrocarbons to smaller molecules, in catalytic hydrogenation and dehydrogenation, in general, and in many transformations of organic molecules. Organic molecules have the tendency to form carbonaceous deposits, which block the active sites on the catalyst surface. Components in the reactor feed, such as sulfur-containing species, often act as strong catalyst poisons. Active metal sites on the catalyst surface can agglomerate at high temperatures leading to sintering, which reduces the overall activity of the catalyst. Catalyst deactivation influences the kinetics, leading to an impaired performance of the chemical reactor. The impact of catalyst deactivation on reaction kinetics and reactor modeling is discussed in Chapter 5.

REFERENCES

1. Laidler, K.J., *Chemical Kinetics*, 3rd Edition, Harper & Row, New York, 1987.
2. Smith Sørensen, T., *Reaktionskinetik—systemteori for kemikere*, Polyteknisk Förlag, Köbenhavn, 1984.
3. Hougen, O. and Watson, K., *Chemical Process Principles, Part III, Kinetics and Catalysis*, 7th Edition, Wiley, New York, 1959.
4. Boudart, M., *Kinetics of Chemical Processes*, Prentice-Hall, Englewood Cliffs, NJ, 1968.
5. Murzin, D. and Salmi, T., *Catalytic Kinetics*, Elsevier, Amsterdam, 2005.
6. Reid, R.C., Prausnitz, J.M., and Poling, B.E., *The Properties of Gases and Liquids*, 5th Edition, McGraw-Hill, New York, 1988.

CHAPTER 3

Homogeneous Reactors

3.1 REACTORS FOR HOMOGENEOUS REACTIONS

For a homogeneous reactor, it is characteristic that just *one* phase, usually a *gas* or a *liquid phase*, is present. Chemical reactions thus take place in this phase. In this chapter, we will examine three reactors most commonly used industrially for homogeneous reactions: a batch reactor (BR), a tube reactor, and a tank reactor. Figure 3.1 illustrates a BR. A BR is operated by at first charging the reactor contents with a reaction mixture that is usually heated to the reaction temperature, allowing the reaction to proceed until the desired conversion of the reactants has been reached. After this, the reactor vessel is emptied.

On an industrial scale, BRs are primarily intended for homogeneous liquid-phase reactions and less frequently for gas-phase reactions. On a laboratory scale, however, BRs with a constant volume are often used for the determination of the kinetics of homogeneous gas-phase reactions. BRs are typically used industrially for the production of fine chemicals via organic liquid-phase reactions, such as drug synthesis, and the manufacture of paints, pesticides, and herbicides.

The construction of a BR is simple in principle; standard vessels are easily available in the market. See Table 3.1 for examples of commercially available standard reactors. When choosing a reactor vessel, the following factors should be taken into account: the desired production capacity, operation temperature and pressure, construction material, cleaning of the reactor, mixing of the reactor contents, and heat exchange properties. Organic liquid-phase reactions are often strongly exothermic, and efficient cooling is necessary to prevent a very rapid increase in temperature, which can result in gasification of the reactor contents, consequently leading to critical pressure increase, undesired product distribution, and even explosion of the reactor vessel. Some standard constructions are presented in Figure 3.2 to solve the heat exchange problem. In the simplest case, it is enough to provide the reactor

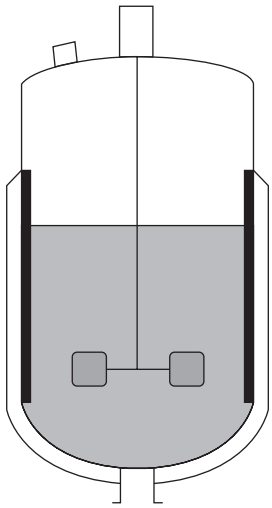

FIGURE 3.1 An industrial BR.

wall with a double shell. The cooling that can be realized by means of this construction is, however, limited. One way to increase the heat exchange area is to mount a cooling (heating) coil in the reactor (Figure 3.2). In an extreme case, the reactor contents are continuously circulated through an outer heat exchanger. In principle, one can reach an infinitely large heat exchange area by utilizing an outer heat exchanger. Analogous outer heat exchangers are used, for instance, in batchwise polymerizations.

A BR has several advantages in the realization of industrial reactions. It is flexible, allowing the same reactor to be used for multiple, chemically different reactions. This is a clear advantage for the manufacture of an assortment of fine chemicals; the production can be adjusted and rearranged according to market demand. Different reactions often require very different reaction times (batch time), since reaction velocities vary considerably. For a BR, this is, however, a minor problem: the reaction time can easily be altered, as required, by allowing a longer or a shorter reaction time until the desired product distribution is obtained.

For certain types of reactions, it is desirable to change the operation conditions during the course of the reaction. For instance, in the case of reversible exothermic reactions, it is favorable to have a higher temperature at the beginning of the reaction to enhance the reaction kinetics, whereas toward the end of the reaction the temperature should be reduced. This procedure (decreasing temperature ramp) is favorable, since the equilibrium composition is more favorable at lower temperatures. The desired conditions in a BR can be established by a computer-controlled temperature trajectory; the optimal temperature–time scheme can be theoretically determined in advance and realized by cooling control.

The scaleup of kinetic data obtained in the laboratory to a BR operating on an industrial scale is fairly simple, as the reaction time in the laboratory corresponds directly to the reaction time on the factory scale, provided that the reactors in general operate under similar conditions. This advantage has diminished in importance, however, since the tremendous increase in the theoretical knowledge of chemical reaction engineering.

TABLE 3.1 Characteristics of Some Commercially Available Standard Reactor Vessels

Capacity (m^3)	8	14	25	32	10	20	25	1	4	10	25	0.7
Diameter (m)	2	2.5	2.8	3.1	2.4	2.8	3	1.2	1.8	2.4	3	0.9
Total weight (kg)	9450	13,900	21,300	24,100	11,000	18,000	21,800	1830	2500	5200	7900	800
Exchange area (m^2)[a]	18.6 DE	26.6 DE	40.0 DE	45.6 DE	19.8 DE	33 DE	38.8 DE	4.45 DE	10.90 DE	11.15 SE	19.5 SE	3.4 DE
Service pressure (bar)	15	15	15	15	6	6	6	6	6	6	6	1.5
Material[b]	AV	AV	AV	AV	AV	AV	AV	Al	Al	Al	Al	V

Source: Data from Trambouze, P., van Langenhem, H., and Wauquier, J.P., *Chemical Reactors—Design/Engineering Operation*, Editions Technip, Paris, 1988.

[a] DE = double jacket, SE = welded external coil.

[b] AV = glass-lined steel, Al = stainless steel, V = glass.

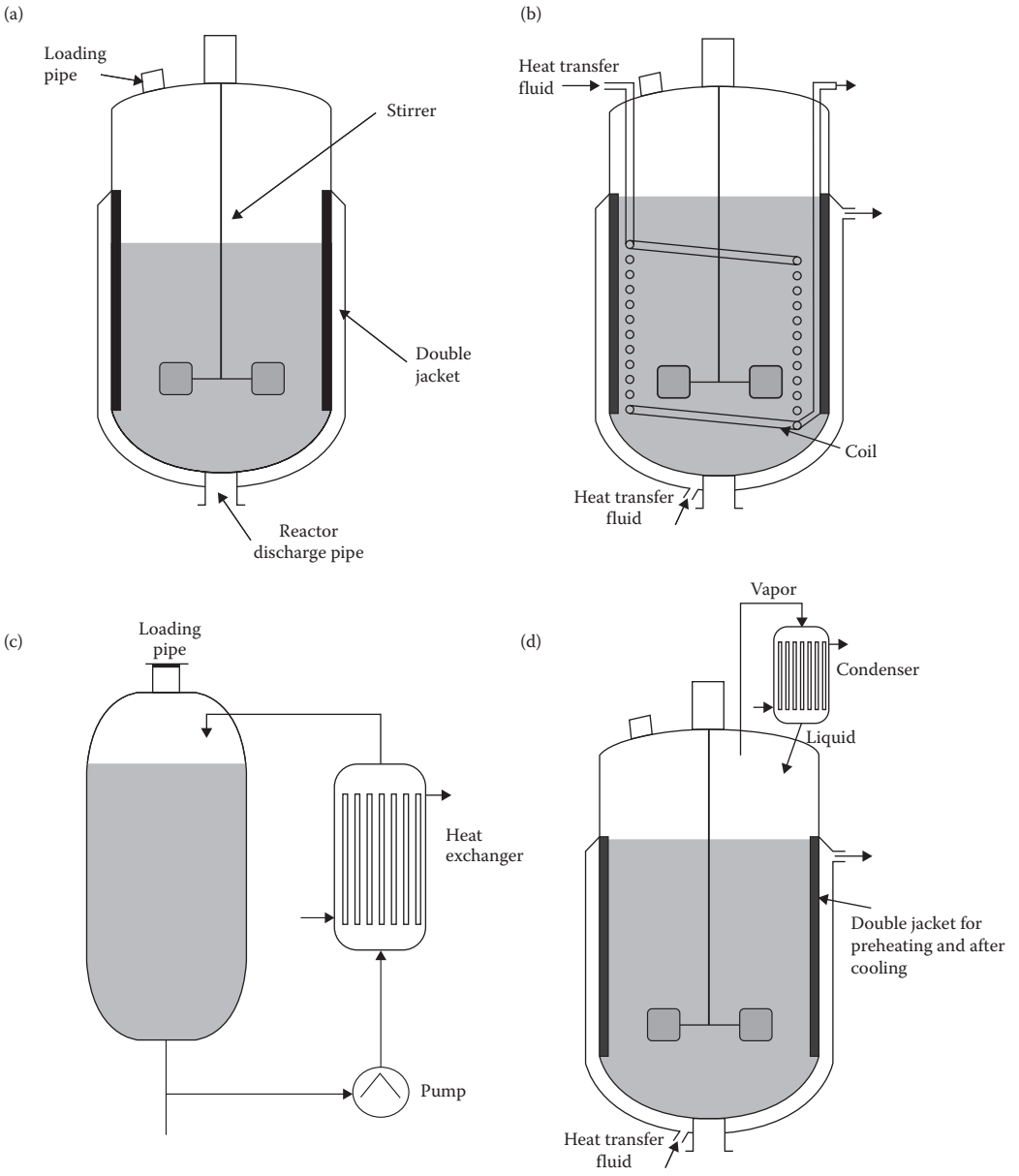

FIGURE 3.2 Various ways of constructing a BR: (a) a BR vessel with a double wall; (b) a BR vessel with a double wall and a cooling coil; (c) a BR vessel with an external heat exchanger; and (d) a BR vessel equipped with condenser cooling.

From the kinetic point of view, a BR is often presented as an attractive alternative. For the majority of various kinds of reaction kinetics—simple reactions with approximately elementary reaction kinetics, consecutive reactions, and mixed reactions—the BR gives a higher yield as well as a higher amount of desired intermediate products than a continuous stirred tank reactor (CSTR), and this is why the BR competes with a tube reactor in efficiency.

In any case, the production capacity of a BR is reduced by the time required for filling and emptying the reactor vessel between the batches.

A BR always operates under nonstationary, transient conditions. This can sometimes cause problems such as in terms of controlling the temperature; for strongly exothermic reactions, there exists a risk of an uncontrolled increase in temperature (*temperature runaway*). The nonstationary mode of operation can also cause problems with product quality.

A BR is sometimes operated in a semicontinuous (semibatch) mode: one or several of the reactants are fed into the reactor during the course of the reaction. This mode of operation is typical in the case of strongly exothermic reactions, thus avoiding excessively high temperatures in the reactor. By the semicontinuous operation mode, the product distribution can also be optimized for certain types of mixed reactions. For instance, in a mixed reaction of the types $A + B \rightarrow R$ and $R + B \rightarrow S$, the yield of the intermediate, R, can be maximized by adding B in a batch containing an excess of A.

A continuously operating stirred tank reactor can be called a backmix reactor. Typically, in a backmix reactor, the reaction mixture is completely mixed and has a composition similar to the production flow at the reactor outlet. Three principally different constructions of the reaction vessel are used industrially: a tank reactor equipped with a propeller mixer is in principle constructed in a manner similar to a corresponding BR (Table 3.1), in which the reactants are pumped in continuously and a product flow is taken out of the reactor continuously (Figure 3.3). Complete mixing can also be realized by a *multistage reactor*, in which a multilevel mixer is mounted. This reactor is introduced in Figure 3.4. A third way to realize complete backmixing is to utilize a circulation pump to loop the production flow. See Figure 3.5 for an illustration of the reactor construction. At sufficiently high levels of backmixing, the reactor behaves like a stirred tank reactor, and no mechanical mixing is required. This is actually a practical way of facilitating complete backmixing in the case of gas-phase reactions.

The biggest advantage of a stirred tank reactor is that it operates in a continuous manner under stationary conditions after the steady state has been attained. The product quality is therefore very even. Good heat exchange can be achieved, as reactants are continuously being fed into the reactor. The reactant in-flow can be either cooled or preheated to a suitable temperature as necessary. For specific reactions, such as reversible exothermic reactions, the optimal reaction temperature can be calculated *a priori*, and the reaction conditions can thereafter be chosen in such a way that the reactor actually operates at this temperature.

The disadvantage of a stirred tank reactor is that it usually operates at low reactant concentrations in comparison with the product mixture concentrations. This, in practice, implies that in case of the most common reaction kinetics, a stirred tank delivers a lower yield and a lower level of intermediates than a tube reactor and a BR with the same residence time.

By coupling several stirred tank reactors in a series, the performance level of a tube reactor can be approached. Usually two or three stirred tanks are used in a series; to use more is often uneconomical, because the capital costs increase considerably.

For a certain type of production kinetics, a stirred tank reactor is in any case the best choice from the kinetic point of view. A backmixed reactor always favors the reaction with the lowest reaction order among parallel reactions of different orders: for instance, in the

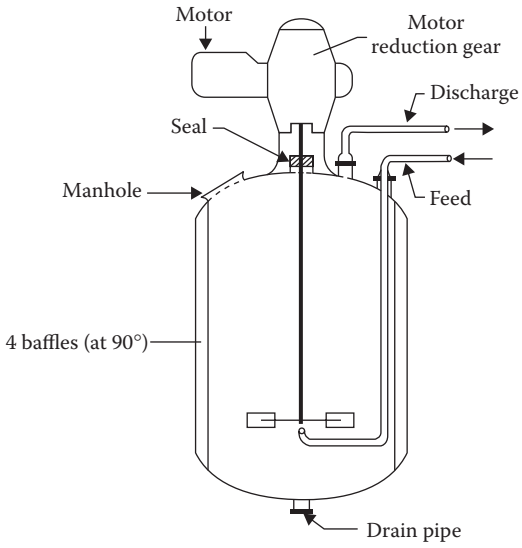

FIGURE 3.3 Tank reactor. (Data from Trambouze, P., van Langenhem, H., and Wauquier, J.P., *Chemical Reactors—Design/Engineering Operation*, Editions Technip, Paris, 1988.)

case of elementary reactions, $2A \rightarrow R$ and $A \rightarrow S$, the latter reaction is favored. This may be of importance when choosing a reactor. In the case of autocatalytic reactions, in which the reaction velocity increases monotonously with the product concentration, a backmixed reactor gives a higher product yield than that of a tube reactor with the same residence time.

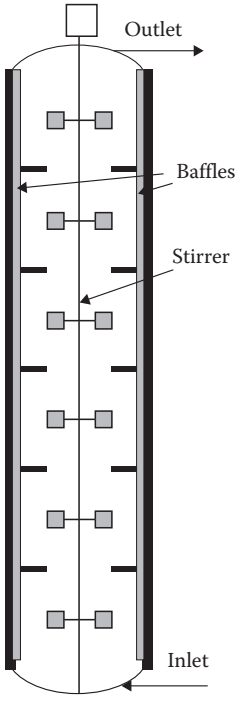

FIGURE 3.4 Multistage reactor.

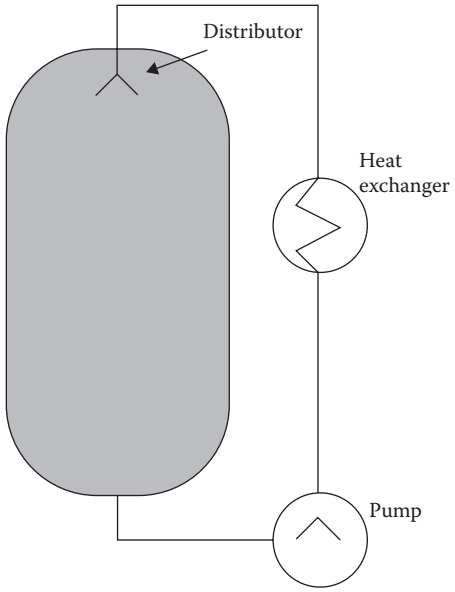

FIGURE 3.5 Loop reactor.

A tube reactor is used industrially for both homogeneous and liquid-phase reactions. If the length of the tube is long compared with the tube diameter and the flow velocity is sufficiently high, axial dispersion and diffusion effects disappear and the fluid can be assumed to flow just like a piston in a cylinder. This is when we can speak of a tube reactor. In principle, two types of constructions are applied as tube reactors for homogeneous reactions in the industry: either a tube reactor with concentric tubes, in which the reaction mixture flows in the inner part and the heat exchange medium in the outer part, or a tube reactor installed in a heated oven. These reactors are illustrated in Figures 3.6 and 3.7. Tube reactors installed inside an oven are primarily used for exothermic cracking and dehydrogenation reactions. Reactors with concentric tubes are used, for example, in the polymerization of ethene and propene. The tubes are bent, thus ensuring tubular flow conditions. A tube reactor is highly suitable for rapid gas-phase reactions.

The biggest advantage of a tube reactor is that it can produce the highest yield and the highest amounts of intermediate products for the most common reaction kinetics. It is superior to the stirred tank reactor and, usually, even better than a BR in this sense. Problems can occur when using a tube reactor, as it is not very stable when dealing with strongly exothermic reactions: a so-called hot spot (overheated section of the reactor) can be formed. The temperature of the hot spot thus dictates the operating conditions: this maximal temperature must not exceed the limit set by the product distribution requirements, construction material limitations, and safety aspects. Usually, these factors can be administered and sufficient cooling can be arranged. Due to the reaction engineering benefits and its simple construction, a tube reactor is popular in industrial applications of homogeneous reactions.

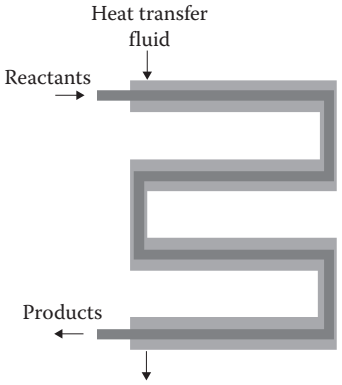

FIGURE 3.6 Tube reactor.

The desired production capacity and the required reaction time (residence time) are two of the most important criteria when selecting a reactor suitable for a homogeneous process. Trambouze et al. [1] have proposed a chart that suggests the applicability limits of different kinds of reactors for various reactions (Figure 3.8). For slow reactions and low production capacities, a BR is typically chosen, whereas for larger production volumes, a continuous reactor is preferred: a cascade of stirred tank reactors or a tube reactor. In the next section, the mass and energy balances for homogeneous reactors will be considered in detail.

3.2 HOMOGENEOUS TUBE REACTOR WITH A PLUG FLOW

In this section, we will discuss a homogeneous tube reactor, in which gas- or liquid-phase reactions are assumed to proceed. Further, diffusion and dispersion in the axial direction

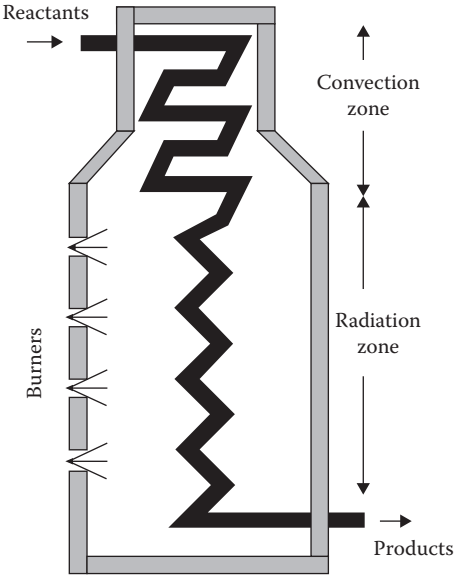

FIGURE 3.7 Tube reactor for high-temperature reactions.

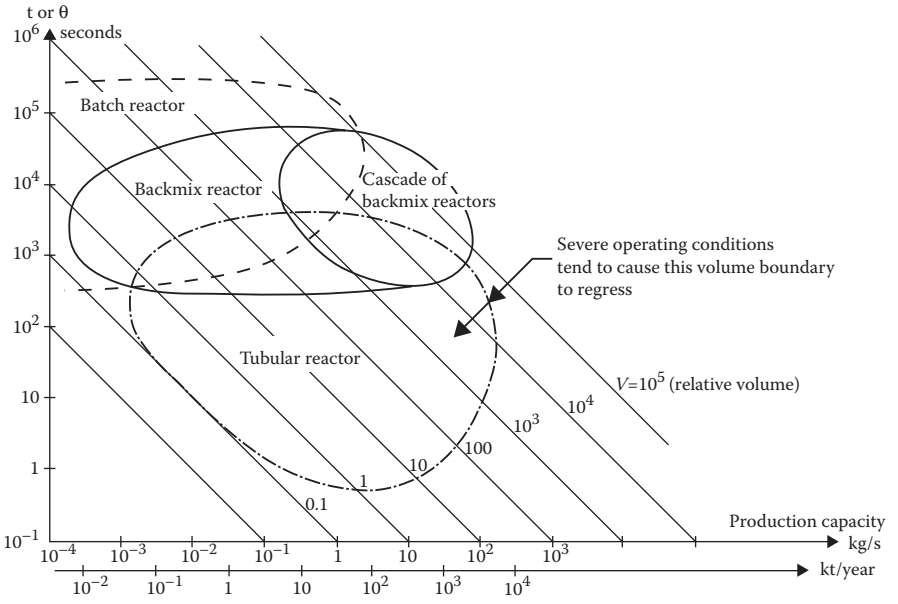

FIGURE 3.8 Applicability limits of different kinds of reactors for various reactions, according to Trambouze et al. (Data from Trambouze, P., van Langenhem, H., and Wauquier, J.P., *Chemical Reactors—Design/Engineering Operation*, Editions Technip, Paris, 1988.)

are assumed to be negligible. Turbulence in the radial direction is presumed to be so efficient that the radial temperature, concentration, and velocity gradients in the fluid flow disappear. In this case, the flow characteristics of the tube coincide with those prevailing in a plug flow and, consequently, all fluid elements have equal residence times in the reactor. The conduction of heat in the axial direction is ignored. The convection of heat in the radial direction is assumed to be so efficient that no radial temperature gradients are generated. A pressure drop can occur in longer reactor tubes, which can be estimated based on equations known from fluid mechanics, such as the Fanning equation [2]. This section, however, focuses on the most fundamental equations relevant to the design of chemical reactors: mass and energy balances under steady-state conditions. Steady-state conditions imply that the reactor is operating under unchanged conditions, regardless of the time dimension. The equations derived thus do not apply at the start-up of the reactor or during transient periods after a change in the operating conditions, such as a temperature change or an alteration in the feed composition. In this section, we will consider only a single tube reactor. In the industry, multiple—even hundreds of—tube reactors coupled in parallel are often operated; it is, however, trivial to expand our scope of study to multiple similar units.

3.2.1 MASS BALANCE

In this section, we will consider the tube reactor volume element. An inflow, $\dot{n}_{i,\text{in}}$ (mol/s), enters this element, and an outflow, $\dot{n}_{i,\text{out}}$, leaves it. The volume element is illustrated in Figure 3.9.

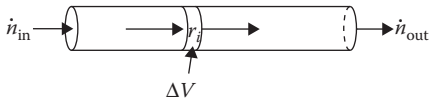

FIGURE 3.9 Volume element ΔV in a homogeneous tube reactor.

For component i, the following general mass balance is established:

$$\left[\text{incoming } i\right] + \left[\text{generated } i\right] = \left[\text{outgoing } i\right] + \left[\text{accumulated } i\right]. \tag{3.1}$$

Under steady-state conditions (no accumulation), Equation 3.1 is reduced to the following form:

$$\left[\text{incoming } i\right] + \left[\text{generated } i\right] = \left[\text{outgoing } i\right], \tag{3.2}$$

since no accumulation takes place under steady-state conditions. Quantitatively, Equation 3.2 can be expressed by the molar flows $\left(\dot{n}_{i,\text{in}}, \dot{n}_{i,\text{out}}\right)$ and the generation velocity (r_i):

$$n_{i,\text{in}} + r_i \Delta V = n_{i,\text{out}}, \tag{3.3}$$

in which the difference, $n_{i,\text{out}} - n_{i,\text{in}}$, can be denoted as follows:

$$\dot{n}_{i,\text{out}} - \dot{n}_{i,\text{in}} = \Delta \dot{n}_i. \tag{3.4}$$

After inserting Equations 3.3 and 3.4 and taking into account that $\Delta V \rightarrow 0$, Equation 3.3 transforms to the following differential equation:

$$\frac{\mathrm{d}\dot{n}_i}{\mathrm{d}V} = r_i, \tag{3.5}$$

where r_i is given by either Equation 2.4 or 2.5, depending on whether one or several chemical reactions proceed simultaneously in the reactor.

In the design of chemical reactors, the space time, τ, is often a central parameter. Space time is defined by

$$\tau = \frac{V_\text{R}}{\dot{V}_0}, \tag{3.6}$$

where V_R denotes the reactor volume and V_0 denotes the volumetric feed flow. One should observe that $\tau = \bar{t}$, where $\bar{t}$ is the residence time in the reactor (the time when a volume element resides inside the reactor). This is only true for a system with a constant volumetric flow. Typical systems with practically constant volumetric flows are isothermic liquid-phase reactions.

Equation 3.6 gives the following expression for the volume element $\mathrm{d}V$:

$$\mathrm{d}V = \dot{V}_0 \, \mathrm{d}\tau, \tag{3.7}$$

which can be combined with the molar balance (Equation 3.5):

$$\frac{\mathrm{d}\dot{n}_i}{\mathrm{d}\tau} = r_i \dot{V}_0. \tag{3.8}$$

Balance Equations 3.5 and 3.8 are very general and thus applicable to both liquid- and gas-phase reactions.

3.2.2 ENERGY BALANCE

We continue to study the volume element, $\mathrm{d}V$, in the reactor tube—this time from the perspective of energy balance. Let us assume that a *single* chemical reaction proceeds in the volume element with velocity R and the reaction enthalpy given by ΔH_r. The mixture is presumed to have a mass-based heat capacity, c_p. The heat flux to—or from—the environment to the reactor vessel is described by $\Delta\dot{Q}$. The energy effects in the volume element are illustrated in Figure 3.10.

At steady state, the energy balance for volume element ΔV can be written as follows:

$$R\,(-\Delta H_\mathrm{r})\,\Delta V = \Delta\dot{Q} + \dot{m} c_\mathrm{p} \Delta T. \tag{3.9}$$

Intuitively, Equation 3.9 can be understood as an exothermic reaction: heat is released due to the chemical reaction proceeding in the system at the rate $R(-\Delta H_\mathrm{r})\Delta V$ $[W]$; this heat, in turn, is partially transported to the environment at the rate $\Delta\dot{Q}$ and is partially consumed by increasing the temperature of the reaction mixture from T to $T + \Delta T$. For an endothermic reaction, an analogous reasoning is applied: $R(-\Delta H_\mathrm{r})\Delta V$ is negative and often causes a temperature suppression (excluding the effect of $\Delta\dot{Q}$: ΔT is thus negative).

The heat flux term, $\Delta\dot{Q}$, can often be described with an expression of the following type:

$$\Delta\dot{Q} = U\,(T - T_\mathrm{C})\,\Delta S. \tag{3.10}$$

In the previous expression (Equations 3.10 and 3.153), ΔS denotes the heat transfer area, U is an overall heat transfer coefficient comprising the reactor wall and the stagnant layers (films) inside and outside the reactor, and T_C denotes the temperature of the environment.

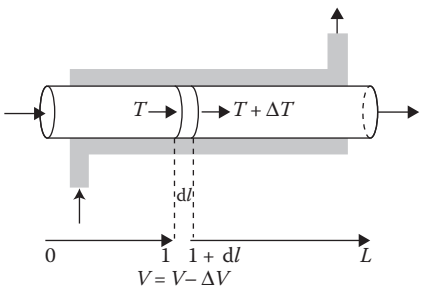

FIGURE 3.10 Energy effects in a volume element ΔV in a homogeneous tube reactor.

After combining Equations 3.9 and 3.10, we obtain

$$\frac{\Delta T}{\Delta V} = \frac{1}{\dot{m}c_p}\left[R\left(-\Delta H_r\right) - \frac{U\Delta S}{\Delta V}\left(T - T_C\right)\right]. \tag{3.11}$$

If the relation between heat transfer surface and reactor volume, $\Delta S/\Delta V$, can be assumed to be constant then $\Delta S/\Delta V = S/V_R$, where S denotes the total heat transfer surface. Thus Equation 3.11 is converted into Equation 3.12:

$$\frac{dT}{dV} = \frac{1}{\dot{m}c_p}\left[R\left(-\Delta H_r\right) - \frac{US}{V_R}\left(T - T_C\right)\right]. \tag{3.12}$$

For several chemical reactions in the system, Equation 3.12 can simply be generalized by taking into account the heat effects from all of the reactions. In the case of S chemical reactions taking place in the system, the total heat effect can be described by $\sum R_j\left(\Delta H_{rj}\right)$. Equation 3.12 can be rewritten in the following form:

$$\frac{dT}{dV} = \frac{1}{\dot{m}c_p}\left[\sum_{j=1}^{s} R_j\left(-\Delta H_{rj}\right) - \frac{US}{V_R}\left(T - T_C\right)\right]. \tag{3.13}$$

Using the definition of space time, τ, and substituting Equation 3.6 into Equations 3.12 and 3.13, Equation 3.14 assumes the following form. The equation describes systems with just *one* ongoing chemical reaction,

$$\frac{dT}{d\tau} = \frac{1}{\rho_0 c_p}\left[R\left(-\Delta H_r\right) - \frac{US}{V_R}\left(T - T_C\right)\right], \tag{3.14}$$

whereas Equation 3.15 is valid for systems with *multiple*, simultaneous ongoing chemical reactions:

$$\frac{dT}{d\tau} = \frac{1}{\rho_0 c_p}\left[\sum_{j=1}^{s} R_j\left(-\Delta H_{rj}\right) - \frac{US}{V_R}\left(T - T_C\right)\right]. \tag{3.15}$$

In Equations 3.14 and 3.15, the density of the incoming mixture, ρ_0, is shown since $\dot{m}/\dot{V}_0 = \rho_0$ according to the definition. The product, $\rho_0 c_p$, is often called the heat capacity of the reaction mixture. Equations 3.13 through 3.15 are valid for both liquid- and gas-phase reactions. The heat capacity, $\rho_0 c_p$, is often relatively constant in liquid-phase systems, whereas this is not the case for gas-phase reactors. For gas-phase reactions, it is often practical to replace the product $\dot{m}c_p$ with $\sum \dot{n}_i C_{pm,i}$, in which the sum includes all—even the nonreactive—components in the system. The volumetric flow, $\dot{V}_0$, included in Equations 3.14 and 3.15 and the space time are taken into account and the product $\rho_0 c_p$ can be replaced by the following term if necessary:

$$\frac{1}{\rho_0 c_p} = \frac{\dot{V}}{\sum \dot{n}_i C_{pm,i}}.$$

The volumetric flow rate should be calculated in an appropriate equation of state for the gas, in the simplest case, by the ideal gas law. This problem is dealt with in greater detail in Section 3.5.

Under isothermal conditions—if the reactor temperature is controlled to remain at a constant level or the heat effects are negligible—no energy balances need to be taken into account when proceeding with the reactor calculations. In this case, the molar balances can be solved analytically for certain special cases in chemical kinetics. These kinds of special cases are studied in detail in Section 3.7.

Generally, the molar balances of a tube reactor comprise a system of coupled differential equations that can be solved numerically using an appropriate algorithm, such as the Runge–Kutta method (Appendix 2). If the values of the kinetic constants vary within a large range in a system, this implies that some of the reactions are slow, whereas some proceed so rapidly that they can be regarded as almost having reached their equilibria. In this case, the differential equations describing the system become stiff and need to be solved using special techniques such as semi-implicit Runge–Kutta methods or backward difference (BD) methods. The numerical algorithms are studied in more detail in Appendix 2. Some results from a simultaneous solution of molar and energy balances are illustrated principally in Figure 3.11 for the case of an exothermic reaction. If the reactor is operated under adiabatic conditions, the temperature will increase until the adiabatic temperature is reached (Section 3.7). If the heat is removed instead, the temperature is bound to decrease after the hot spot in the reactor. At extremely high values of the heat transfer coefficient, no temperature maximum can be observed and the temperature in the reactor decreases monotonously.

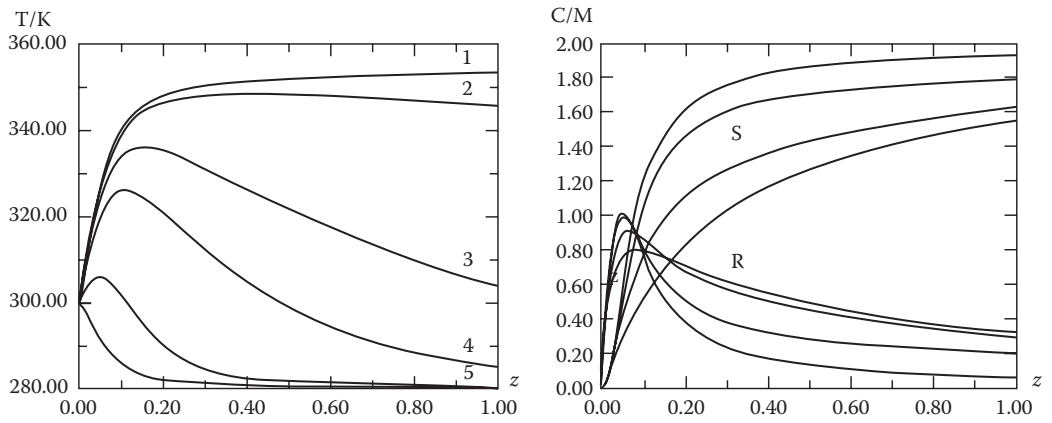

FIGURE 3.11 Temperature (left) and concentration (right) profiles in a homogeneous tube reactor. Curve 1—adiabatic reactor; curve 2—small heat transfer coefficient; curves 3 and 4—intermediate heat transfer coefficient; and curve 5—very high heat transfer coefficient. Saponification of ethyl adipate with NaOH [3]: A + B → R + E, A = diethyl adipate, B = NaOH, E = ethanol R + B → S + E, R = primary hydrolysis product, and S = secondary hydrolysis product (Na salt of adipic acid).

3.3 HOMOGENEOUS TANK REACTOR WITH PERFECT MIXING

In a homogeneous tank reactor with perfect mixing, or a CSTR, the whole reactor contents have the same temperature and chemical composition. No temperature, concentration, or pressure gradients exist in a CSTR. However, the composition and temperature of the in-flow (feed) can hugely differ from the characteristics of the reactor contents, since a chemical reaction proceeds in the reactor. Here we will take into account the molar and energy balances of a CSTR, which is assumed to be operating at steady state. Industrially, CSTRs are often coupled in a series—usually a maximum of three pieces—to form a reactor cascade. Thus, the required yield of the product can be reached. Below we will concentrate on a single building block or a tank reactor.

3.3.1 MASS BALANCE

Since no concentration gradients exist in a CSTR, the whole reactor volume can be considered as an entity when deriving the balance equations. For a schematic illustration of a CSTR, see Figure 3.12.

At steady state, the molar balance for component i in the reactor is qualitatively given by Equation 3.2:

$$[\text{incoming } i] + [\text{generated } i] = [\text{outgoing } i].$$

Quantitatively, this means the following for component i in the entire reactor volume:

$$\dot{n}_{0i} + r_i V_R = \dot{n}_i. \tag{3.16}$$

Analogously with the balance written for the tubular reactor Equation 3.5, Equation 3.16 can be rewritten as

$$\frac{\dot{n}_{0i} - \dot{n}_i}{V_R} = -r_i. \tag{3.17}$$

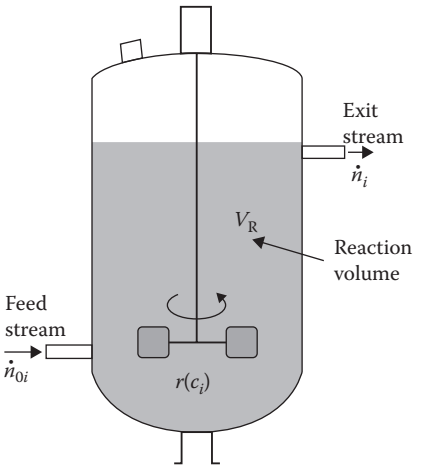

FIGURE 3.12 Continuous stirred tank reactor.

Using the definition of space time, Equation 3.6, into the above balance equation, we will obtain

$$\frac{\dot{n}_{0i} - \dot{n}_i}{\tau} = -\dot{V}_0 r_i. \tag{3.18}$$

Balance Equations 3.16 through 3.18 are valid for both liquid- and gas-phase reactions.

3.3.2 ENERGY BALANCE

A CSTR is illustrated from the point of view of energetics in Figure 3.13. For the sake of simplicity, we will at first assume that just *one* chemical reaction proceeds in the system. In addition, we will presume that the reactor operates at steady state. At steady state, the energy balance can be written as follows:

$$R\,(-\Delta H_r)\,V_R = \dot{Q} + \dot{m}\int_{T_0}^{T} c_p\,\mathrm{d}T. \tag{3.19}$$

A similar conclusion can be drawn when considering the energy balance of the tank reactor as that of a tube reactor (Equation 3.9). For instance, in the case of an exothermic reaction, the term $R(-\Delta H_r)V_R$ represents the heat effect that can be observed due to the occurrence of a chemical reaction. This heat is partially dissipated to the surroundings ($\dot{Q}$) and is partially consumed by the increase in the temperature of the reactor contents from the initial temperature T_0 to the reaction temperature T. If heat is supplied from an outside source into the reactor, the term $\dot{Q}$ assumes a negative value. An a analogous reasoning can be applied in the case of an endothermic reaction. Expression 3.19 is valid in all cases.

The term $\dot{Q}$ is often given as

$$\dot{Q} = US\,(T - T_C)\,, \tag{3.20}$$

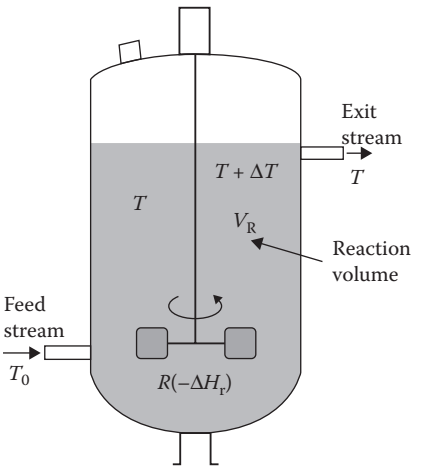

FIGURE 3.13 Energy effects in a homogeneous CSTR.

where S denotes the total heat transfer surface of the reactor and T_C is the temperature of the surroundings. If an internal cooling coil is used along with a cooling jacket, an additional expression is added to Equation 3.20.

Further treatment of Equation 3.19 will only be possible after the integral $\int c_p \, dT$ has been calculated. This can be achieved if a function describing the temperature dependence of the heat capacity is available. For gas-phase reactions, it is often practical to replace the integral in $\dot{m} \int c_p \, dT$ by $\sum \dot{n}_i \int c_{pmi} \, dT$, since the molar-based heat capacity as a function of temperature, $C_{pmi}(T)$, is easily available for many gases (Section 2.3).

For the special case in which the heat capacity can be approximated as temperature-independent, the insertion of $\dot{Q}$ into Equation 3.19 gives the simple equation

$$\frac{T - T_0}{V_R} = \frac{1}{\dot{m} c_p} \left[R \left(-\Delta H_r \right) - \frac{US}{V_R} \left(T - T_C \right) \right]. \tag{3.21}$$

Equation 3.21 is analogous to the energy balance of the tube reactor (Equation 3.12). In the case of several, simultaneous chemical reactions taking place in the system, the energy balance (Equation 3.21) can be easily generalized by taking into account the heat effects from all reactions in the system:

$$\frac{T - T_0}{V_R} = \frac{1}{\dot{m} c_p} \left[\sum_{j=1}^{S} R_j \left(-\Delta H_{rj} \right) - \frac{US}{V_R} \left(T - T_C \right) \right]. \tag{3.22}$$

After inserting the space time τ into Equations 3.21 and 3.22, we obtain

$$\frac{T - T_0}{V_R} = \frac{1}{\rho_0 c_p} \left[R \left(-\Delta H_r \right) - \frac{US}{V_R} \left(T - T_C \right) \right] \tag{3.23}$$

for *single* reactions and

$$\frac{T - T_0}{\tau} = \frac{1}{\rho_0 c_p} \left[\sum_{j=1}^{s} R_j \left(-\Delta H_{rj} \right) - \frac{US}{V_R} \left(T - T_C \right) \right] \tag{3.24}$$

for *multiple* reactions. Equations 3.22 through 3.24 are analogous to the corresponding balances for a tube reactor (Equations 3.13 through 3.15).

Under isothermal conditions, the reaction temperature is known beforehand, and no energy balance is required to calculate the composition of the reaction mixture. The molar balances can thus be solved analytically for certain special cases of chemical kinetics. These special cases are studied further in Section 3.8.

Generally, the molar and energy balances of a CSTR form a coupled algebraic equation system that should be solved numerically to obtain the values of molar flows and the reactor temperature under given conditions. The coupled molar and energy balances are most

efficiently solved numerically by the Newton–Raphson method. For a detailed description of this, refer to Appendix 1.

In exothermic reactions, a special phenomenon can occur that has important consequences concerning the solution of the balance equations and, in particular, the operational features of a CSTR: the balance equations can have multiple real solutions, with multiple sets of values for the molar flows and temperatures, satisfying the equation system. This implies that the reactor can de facto operate under multiple steady-state conditions, depending on how it has been started. This kind of problem is tackled in depth in the literature [2]. Iterative numerical methods such as the Newton–Raphson method are able to find *one* of the solutions, one of the steady states. The one detected by numerical computation depends on the initial guesses of the parameters (estimates) given by the algorithm. Thus, it is of utmost importance to attempt several initial estimates for exothermic reactions to find all the solutions. For a system with a single chemical reaction in progress, all the steady states can be found by a graphical study [3–5]. Another alternative is to solve the transient molar and energy balances numerically. The stable steady states can thus be found after solving the equation system for different initial conditions of the reaction/reactor. This problem is, however, not discussed here in greater detail.

The fact that multiple steady states are indeed a real phenomenon has been illustrated by various experimental studies. An example is given by Figure 3.14 in which the experimentally observed and theoretically calculated steady states [4] are shown for a bimolecular reaction between hydrogen peroxide (H_2O_2) and sodium thiosulfate ($Na_2S_2O_3$). The experiments were performed in an adiabatic CSTR. A similar phenomenon has been predicted even for multiple industrially important reactions such as the polymerization of styrene [5]. When designing a CSTR for exothermic reactions, one should always be alert to the possibility of *steady-state multiplicity.*

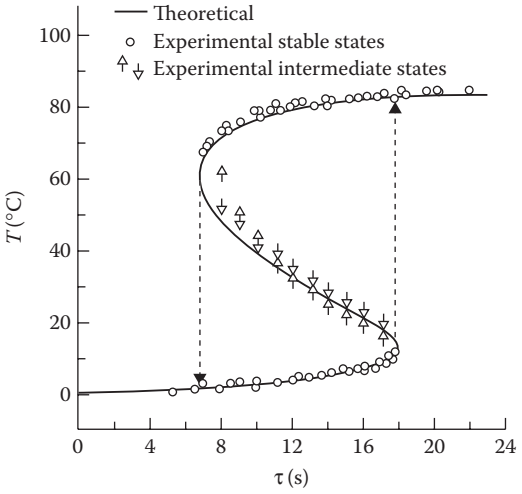

FIGURE 3.14 Multiple steady states in an adiabatic CSTR. A reaction between H_2O_2 and $Na_2S_2O_3$ [4].

3.4 HOMOGENEOUS BR

The characteristic of a homogeneous BR with perfect mixing is that neither a concentration nor a temperature gradient exists in the reaction mass. In this sense, a BR resembles a CSTR. The crucial difference between these two reactors is that neither an inflow nor an outflow of reactants takes place in a BR, either to or from the reactor. This also implies that a BR should never operate at a steady state but, instead, under constantly transient conditions. A steady state is reached—philosophically—after an infinitely long period of reaction time: at that point, all chemical reactions have achieved their equilibria and neither the concentration nor the temperature change in the reactor as a function of time. Usually, however, batchwise reactions are interrupted at an earlier time.

This section provides an introduction to the transient molar and energy balances for a homogeneous BR with ongoing gas- or liquid-phase reactions.

3.4.1 MASS BALANCE

A BR is illustrated in Figure 3.15. The general molar balance (1) that was introduced in connection with the tube reactor is considerably reduced in the case of a BR, as the inflows and outflows of reactants are zero. We thus obtain for component i (Equation 3.1):

$$[\text{incoming } i] + [\text{generated } i] = [\text{outgoing } i] + [\text{accumulated } i].$$

Qualitatively, this implies that the molar balance is acquired in the following simple form:

$$\frac{\mathrm{d}n_i}{\mathrm{d}t} = V_\mathrm{R} r_i, \tag{3.25}$$

where the term $V_\mathrm{R} r_i$ denotes the generated i (mol/s) and the derivative $\mathrm{d}n_i/\mathrm{d}t$ denotes the accumulated i (mol/s). The above balance Equation 3.25 bears a mathematical analogy to

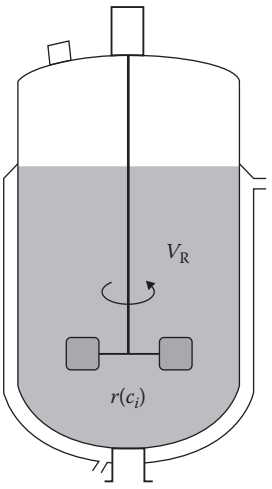

FIGURE 3.15 Batch reactor.

an earlier balance Equation 3.8, which is valid for the PFR. This means that mathematical solutions for the balance equations of a PFR can sometimes be utilized as solutions for those of a BR. Naturally, the reverse is true as well.

3.4.2 ENERGY BALANCE

Energy effects in a BR are illustrated in Figure 3.16. Let us again consider a system in which only a single chemical reaction takes place. For most cases that are relevant in practice, the energy balance of a homogeneous BR can be given with sufficient accuracy by

$$R\,(-\Delta H_{\mathrm{r}})\,V_{\mathrm{R}} = \dot{Q} + mc_{\mathrm{p}}\frac{\mathrm{d}T}{\mathrm{d}t}. \tag{3.26}$$

The background for Equation 3.26 can be illustrated by the following mental exercise: let us assume that an exothermic chemical reaction proceeds in a reactor for an infinitesimally short period of time, $\mathrm{d}t$. Subsequently, an amount of heat $R(-\Delta H_{\mathrm{r}})V_{\mathrm{R}}\,\mathrm{d}t$ (in J) is released. This heat partially escapes from the reactor ($\mathrm{d}\dot{Q} = \dot{Q}\,\mathrm{d}t$) and is partially consumed to increase the temperature of the reaction mixture by the amount $\mathrm{d}T$: $mc_{\mathrm{p}}\mathrm{d}T$. Consequently, balance Equation 3.26 is obtained, which can be proved valid even in the case of an endothermic reaction. The heat flux $\dot{Q}$ can be either positive or negative, depending on the temperature of the reactor (T) and its surroundings (T_{C}). $\dot{Q}$ is typically given as

$$\dot{Q} = US(T - T_{\mathrm{C}}), \tag{3.27}$$

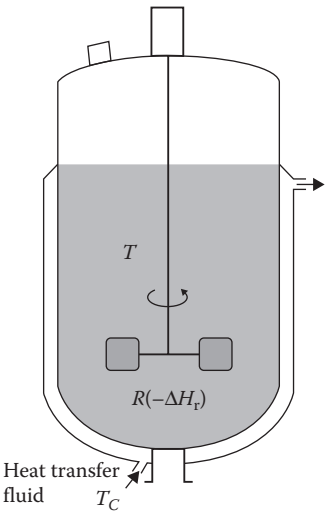

FIGURE 3.16 Energy effects in a homogeneous BR.

where S denotes the heat transfer area of the BR. A combination of Equations 3.26 and 3.27 yields the differential equation

$$\frac{\mathrm{d}T}{\mathrm{d}t} = \frac{1}{mc_\mathrm{p}} \left[R\left(-\Delta H_\mathrm{r}\right) V_\mathrm{R} - US(T - T_\mathrm{C})\right]. \tag{3.28}$$

Using the initial properties of the solution $\rho_0 = m/V_\mathrm{R}$ at time $t = 0$, Equation 3.28 is transformed to the following form:

$$\frac{\mathrm{d}T}{\mathrm{d}t} = \frac{1}{\rho_0 c_\mathrm{p}} \left[R\left(-\Delta H_\mathrm{r}\right) - \frac{US}{V_\mathrm{R}} (T - T_\mathrm{C})\right]. \tag{3.29}$$

Equation 3.29 is mathematically analogous to the energy balance of the PFR, namely Equation 3.14.

For systems with multiple simultaneously ongoing chemical reactions, the energy balance can easily be generalized accordingly as

$$\frac{\mathrm{d}T}{\mathrm{d}t} = \frac{1}{\rho_0 c_\mathrm{p}} \left[\sum_{j=1}^{s} R_j \left(-\Delta H_{\mathrm{r}j}\right) - \frac{US}{V_\mathrm{R}} (T - T_\mathrm{C})\right]. \tag{3.30}$$

Even this equation is mathematically analogous to the corresponding energy balance of the PFR (Equation 3.15).

It is worth mentioning the approximations in the background of the energy balance equations presented in this section. In fact, the term $mc_\mathrm{p}(\mathrm{d}T/\mathrm{d}t)$ represents the storage of internal energy in the system $(\mathrm{d}U/\mathrm{d}t)$. The derivative, $\mathrm{d}U/\mathrm{d}t$, can be written as $\mathrm{d}U/\mathrm{d}t = (\mathrm{d}U/\mathrm{d}T)(\mathrm{d}T/\mathrm{d}t)$. As a definition, we can write that the derivative $\mathrm{d}U/\mathrm{d}T = c_\mathrm{v}m$. Here the heat capacity of the system at a constant volume is c_v. For liquid-phase systems, the difference between c_v and c_p is usually negligible, but for gas-phase systems, the molar heat capacities of a gas are related to each other by the following expression, provided that the ideal gas law is valid:

$$c_{\mathrm{v}mi} = c_{\mathrm{p}mi} - R_\mathrm{G}.$$

Here R_G denotes the general gas constant ($R_\mathrm{G} = 8.3143$ J/mol K). For a gas-phase system, it is more practical to utilize the sum $\sum n_i C_{\mathrm{v}mi}$ instead of the term mc_p in Equations 3.26 and 3.27. Instead, one should replace the term $\rho_0 c_\mathrm{p}$ in Equations 3.29 and 3.30 with the term $V_\mathrm{R}/\sum n_i C_{\mathrm{v}mi}$. Batchwise gas-phase reactions are usually carried out in an autoclave at a constant volume, but allowing the pressure to change during the course of the reaction. However, if the number of molecules remains unchanged during the reaction, the pressure remains constant under isothermal conditions. This indicates that ΔH_r in the previous equations should actually be replaced by ΔU_r, that is, the change in the internal energy of the system. However, the term ΔH_r is usually utilized as a good approximation of

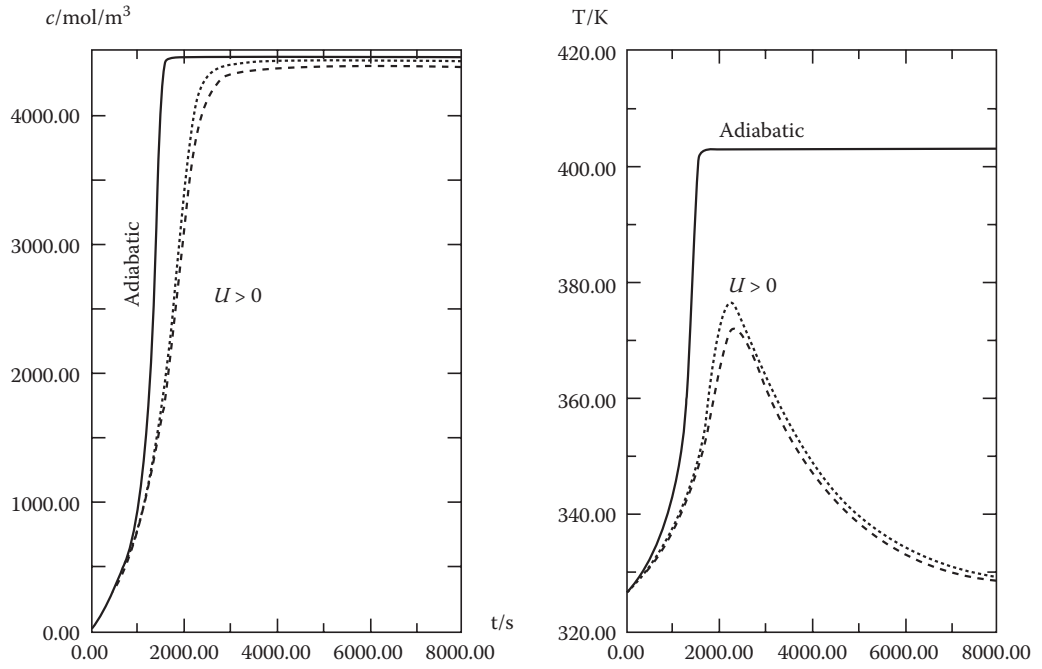

FIGURE 3.17 Concentration and temperature profiles in a homogeneous BR. An exothermic liquid-phase reaction between maleic acid and hexanol to maleic acid ester (left figure) in an adiabatic BR (continuous line) and in a BR with external cooling (dotted line).

ΔU_r. For gas-phase reactions under constant pressure, as well as for liquid-phase reactions, $\Delta U_r \approx \Delta H_r$.

In mathematical terms, the molar and energy balances of a BR form a system of coupled differential equations similar to the corresponding stationary balance equations of a PFR (Section 3.2). Even in this case, special numerical techniques and methods need to be utilized, if the values of the kinetic constants vary within wide boundaries. The numerical methods are explained in greater detail in Appendix 2. Under isothermal conditions, the energy balance can be decoupled and, for some special cases of chemical kinetics, analytical solutions of balance equations can be derived. A few examples will be given in Section 3.8.

The behavior of a BR during an exothermic reaction is illustrated in Figure 3.17. The numerically calculated concentration and temperature profiles in the production of maleic acid monoether are displayed. During adiabatic operation, the temperature will augment until a maximum is attained and, in theory, the temperature then remains at this maximum level until the reaction is completed. If the reactor is externally cooled, the temperature initially increases and begins to decrease after sometime. This *hot spot* phenomenon in the time plane of a BR is analogous to that occurring inside a reactor tube (Figure 3.11).

3.5 MOLAR AMOUNT, MOLE FRACTION, REACTION EXTENT, CONVERSION, AND CONCENTRATION

In the previous section, the balance equations were derived on the basis of a fundamental quantity, either a molar amount or a molar flow. The reaction velocity in the balances is, however, usually expressed by concentrations. We should thus be aware of the way in which these may be related to each other. In the context of reaction engineering, even other quantities appear when describing a reaction system: mole fraction, extent of reaction, and conversion. It is even possible to reduce the number of balance equations required to describe a system using such quantities as the extent of reaction and conversion. In the following section, stoichiometric relations will be derived for liquid- and gas-phase systems.

3.5.1 DEFINITIONS

If the molar amounts in a BR and the molar flows in a continuous reactor are denoted by n_i and $\dot{n}_i$, respectively, the total molar amounts and molar flows for a component i are described by the following set of equations:

$$\dot{n} = \sum_{i=1}^{N} \dot{n}_i, \tag{3.31}$$

$$n = \sum_{i=1}^{N} n_i. \tag{3.32}$$

The sum in Equations 3.31 and 3.32 should contain all—even nonreactive—components of the system. Equation 3.31 is valid for any arbitrary location (coordinate) inside a continuous reactor, whereas Equation 3.32 is valid for any arbitrary reaction time in a BR. At the reactor inlet, at the reaction time $t = 0$, Equations 3.33 and 3.34 for continuous and BRs are obtained:

$$\dot{n}_0 = \sum_{i=1}^{N} \dot{n}_{0i}, \tag{3.33}$$

$$n_0 = \sum_{i=1}^{N} n_{0i}. \tag{3.34}$$

The molar fraction for component i is defined by

$$x_i = \frac{\dot{n}_i}{\dot{n}} \tag{3.35}$$

or

$$x_i = \frac{n_i}{n}, \tag{3.36}$$

where $\dot{n}$ is the total molar flow and n is the total molar amount in a system. Depending on whether the reactor is a continuous or discontinuous (batch) one, either Equation 3.35 or 3.36 should be used. It is worth mentioning that the latter definition of molar fraction, Equation 3.36, is also valid for a continuous reactor. At the reactor inlet, at the initial state (reaction time, $t = 0$), the following is naturally true:

$$x_{0i} = \frac{\dot{n}_i}{\dot{n}_0}, \tag{3.37}$$

$$x_{0i} = \frac{n_i}{n_0}. \tag{3.38}$$

The concentration of component i can be given by several alternative expressions; by definition, the concentration is the relation between molar amount and volume or—in the case of continuous reactors—the relation between molar flow and volumetric flow rate:

$$c_i = \frac{\dot{n}_i}{\dot{V}}, \tag{3.39}$$

$$c_i = \frac{n_i}{V}. \tag{3.40}$$

Equation 3.40 is valid for both continuous and discontinuous reactors, whereas Equation 3.39 is only valid for continuous reactors.

The volumetric flow rate depends on the mass flow and density of the mixture accordingly:

$$\dot{V} = \frac{\dot{m}}{\rho}. \tag{3.41}$$

The total mass flow is the sum of the molar flows in the system, taking into account the molar masses (M_i) of the components:

$$\dot{m} = \sum_{i=1}^{N} \dot{n}_i M_i. \tag{3.42}$$

The volumetric flow rate is thus given by

$$\dot{V} = \sum_{i=1}^{N} \frac{\dot{n}_i M_i}{\rho} = \frac{\dot{n}}{\rho} \sum_{i=1}^{N} x_i M_i, \tag{3.43}$$

where $\sum x_i M_i = \bar{M}$ in which $\bar{M}$ denotes the molar mass of the mixture.

By taking into account the definitions of molar fraction, Equations 3.35 and 3.36, the concentrations in Equations 3.39 and 3.40 can alternatively be

$$c_i = x_i \frac{\dot{n}}{\dot{V}} = x_i c, \tag{3.44}$$

$$c_i = x_i \frac{n}{V} = x_i c, \tag{3.45}$$

where c denotes the total concentration in the system, that is, the sum of the concentrations of all components.

In connection with chemical reactors, one or some of the components are selected as *key compounds* (*limiting compounds*). With the aid of molar amounts, molar flows, or concentrations of these compounds, the corresponding values of the remaining components can be expressed. For a system with S independent chemical reactions, S key components should be chosen for the system to become uniquely defined. If we consider a system with a single chemical reaction, most commonly one of the reactants, such as compound A, is selected as the key component. The conversion of A is thus defined by

$$\eta_A = \frac{\dot{n}_{0A} - \dot{n}_A}{\dot{n}_{0A}} \tag{3.46}$$

for continuous reactors, where $\dot{n}_{0A}$ and $\dot{n}_A$ denote the inlet and outlet flows, respectively. For a BR, the definition of η_A is analogous:

$$\eta_A = \frac{n_{0A} - n_A}{n_{0A}}, \tag{3.47}$$

where n_{0A} denotes the amount of reactant at the beginning and n_A is the amount left after a certain reaction time.

In a system with S independent chemical reactions, one is obliged to select S components as key components. If all these components are reacting species, the conversions of these species are defined by

$$\eta_k = \frac{\dot{n}_{0k} - \dot{n}_k}{\dot{n}_{0k}}. \tag{3.48}$$

This is the case for continuous reactors. For a BR, the analogous definition becomes

$$\eta_k = \frac{n_{0k} - n_k}{n_{0k}}. \tag{3.49}$$

Naturally, Equations 3.48 and 3.49 are only valid if $\dot{n}_{0k} \neq 0$ and $n_{0k} \neq 0$, for all of the key components. This problem can be resolved by introducing a new definition: relative conversion, which is defined by

$$\eta'_k = \frac{\dot{n}_{0k} - \dot{n}_k}{n_0}, \tag{3.50}$$

$$\eta'_k = \frac{n_{0k} - n_k}{\dot{n}_0}, \tag{3.51}$$

where n_0 and $\dot{n}_0$ denote the total molar amount and the corresponding molar flow in the system, respectively. A comparison of Equation 3.50 with 3.48 or of Equation 3.51 with 3.49 indicates that η'_k and η_k are related by the following expression:

$$\eta_k = \frac{\eta'_k}{x_{0k}}. \tag{3.52}$$

The relative conversion can never obtain an undefined value; it is positive for reactants and negative for products.

3.5.2 RELATION BETWEEN MOLAR AMOUNT, EXTENT OF REACTION, CONVERSION, AND MOLAR FRACTION

3.5.2.1 A System with a Single Chemical Reaction

For systems in which only a single chemical reaction takes place, the extent of reaction, ξ, is defined by the following set of equations:

$$\dot{n}_i = \dot{n}_{0i} + \nu_i \xi, \tag{3.53}$$

$$n_i = n_{0i} + \nu_i \xi. \tag{3.54}$$

Equations 3.53 and 3.54 are valid for continuous and discontinuous reactors, respectively. In practice, the most practical quantity is the *specific reaction extent*, ξ', that is obtained by dividing the reaction extent, ξ, by the total molar flow or amount. We thus obtain Equations 3.55 and 3.56 for continuous and discontinuous reactors, respectively,

$$\xi' = \frac{\xi}{\dot{n}_0}, \tag{3.55}$$

$$\xi' = \frac{\xi}{n_0}. \tag{3.56}$$

Dividing Equations 3.53 and 3.54 by $\dot{n}_0$ and n_0, respectively, yields the following equations:

$$\frac{\dot{n}_i}{\dot{n}_0} = x_{0i} + \nu_i \xi', \tag{3.57}$$

$$\frac{n_i}{n_0} = x_{0i} + \nu_i \xi'. \tag{3.58}$$

If all molar flows or amounts are added together, the total relative molar flow or amount is obtained by Equations 3.59 and 3.60:

$$\frac{\dot{n}}{\dot{n}_0} = 1 + \sum_{i=1}^{N} \nu_i \xi', \tag{3.59}$$

$$\frac{n}{n_0} = 1 + \sum_{i=1}^{N} \nu_i \xi'. \tag{3.60}$$

After taking into account the definition of molar fraction, Equations 3.35 and 3.36, the following expression for x_i is obtained for both continuous and discontinuous reactors:

$$x_i = \frac{x_{0i} + \nu_i \xi'}{1 + \sum \nu_i \xi'}. \tag{3.61}$$

Formally, Equation 3.61 is obtained by dividing Equation 3.57 with 3.59 or by dividing Equation 3.58 with 3.60. One should, however, recall that ξ' has a dissimilar definition for continuous (Equation 3.55) and discontinuous (Equation 3.56) reactors. For continuous reactors, x_{0i} denotes the molar fraction of component i at the reactor inlet, whereas in the case of discontinuous reactors, it is the molar fraction at the initial state.

If the conversion of key component A is utilized, the definition of the conversion of A (either Equation 3.46 or 3.47) can be utilized in Equations 3.53 and 3.54:

$$\dot{n}_A = \dot{n}_{0A} + \nu_A \xi, \tag{3.62}$$

$$n_A = n_{0A} + \nu_A \xi. \tag{3.63}$$

By substituting $\dot{n}_A - \dot{n}_{0A} = -\dot{n}_{0A}\eta_A$ and $n_A - n_{0A} = -n_{0A}\eta_A$ into Equations 3.62 and 3.63, respectively, we obtain a relation between ξ and η_A:

$$\xi = \frac{\dot{n}_{0A}\eta_A}{-\nu_A} \tag{3.64}$$

and

$$\xi = \frac{n_{0A}\eta_A}{-\nu_A}. \tag{3.65}$$

By taking into account the specific reaction extent, ξ', these equations attain the following form in both cases:

$$\xi' = \frac{x_{0A}\eta_A}{-\nu_A}. \tag{3.66}$$

By inserting the expression for ξ' from Equation 3.66 into the expression for the molar fraction (Equation 3.61), all the molar fractions (x_i) can be expressed through the conversion of A:

$$x_i = \frac{x_{0i} + (\nu_i x_{0A}\eta_A / -\nu_A)}{1 + \left(\left(\sum \nu_i\right) x_{0A}\eta_A / -\nu_A\right)}. \tag{3.67}$$

3.5.2.2 A System with Multiple Chemical Reactions

If there are multiple ongoing chemical reactions in the system, an independent extent of reaction, ξ_j ($j = 1, \ldots, S$), should be defined for each and every reaction. Equations 3.53 and 3.54 are then consequently replaced by analogous definitions for continuous and discontinuous reactors:

$$\dot{n}_i = \dot{n}_{0i} + \sum_{j=1}^{S} \nu_{ij}\xi_i, \tag{3.68}$$

$$n_i = n_{0i} + \sum_{j=1}^{S} \nu_{ij}\xi_i. \tag{3.69}$$

Thus we have here i reacting components and S chemical reactions in the system. Analogously, the specific extent of reaction can be defined for a system with multiple chemical reactions:

$$\xi_j' = \frac{\xi_j}{\dot{n}_0}. \tag{3.70}$$

Equations 3.68 and 3.69 can thus be rewritten in the following form:

$$\frac{\dot{n}_i}{\dot{n}_0} = x_{0i} + \sum_{j=1}^{S} \nu_{ij}\xi_j', \tag{3.71}$$

$$\frac{n_i}{n_{0i}} = x_{0i} + \sum_{j=1}^{S} \nu_{ij}\xi_j'. \tag{3.72}$$

After adding the molar amounts and flows of all components, Equations 3.71 and 3.72 transform to

$$\frac{\dot{n}_i}{\dot{n}_0} = 1 + \sum_{i=1}^{N}\sum_{j=1}^{S} \nu_{ij}\xi_j', \tag{3.73}$$

$$\frac{n}{n_0} = 1 + \sum_{i=1}^{N}\sum_{j=1}^{S} \nu_{ij}\xi_j' \tag{3.74}$$

The definition of molar fraction gives us, starting from Equations 3.71 and 3.72, as well as from Equations 3.73 and 3.74, an expression for the molar fraction x_i:

$$x_i = \frac{x_{0i} + \sum_{j=1}^{S} \nu_{ij}\xi_j'}{1 + \sum_{i=1}^{N}\sum_{j=1}^{S} \nu_{ij}\xi_j'}. \tag{3.75}$$

Equation 3.75 can be written in a compact form with arrays as

$$x = \frac{x_0 + \nu\xi'}{1 + i^{\mathrm{T}}\nu\xi'}, \tag{3.76}$$

where $x_0 = [x_1 x_2 \ldots x_N]^{\mathrm{T}}$, $\xi' = [\xi_1'\xi_2' \ldots \xi_s']^{\mathrm{T}}$, and $i^{\mathrm{T}} = [1\,1\,\ldots\,1]$. Also, ν is the stoichiometric matrix that contains the stoichiometric coefficients and can be defined as

$$\nu = \begin{bmatrix} \nu_{11} & \nu_{12} & \cdots & \nu_{1S} \\ \nu_{12} & \nu_{22} & \cdots & \nu_{2S} \\ \vdots & & & \vdots \\ \nu_{N1} & \nu_{N2} & \cdots & \nu_{NS} \end{bmatrix}$$

according to Section 2.1.

If the conversions of the key components are utilized in the calculations,

$$\dot{n}_k = \dot{n}_{0k} + \sum_{j=1}^{S} \nu_{kj}\xi_j \tag{3.77}$$

$$n_k = n_{0k} + \sum_{j=1}^{S} \nu_{kj}\xi_j \tag{3.78}$$

and the appropriate substitutions are taken into account, $\dot{n}_k - \dot{n}_{0k} = -\dot{n}_{0k}\eta_k$ and $n_k - n_{0k} = -n_{0k}\eta_k$, the following equations are obtained for continuous and discontinuous reactors, respectively:

$$\dot{n}_{0k}\eta_k = -\sum_{j=1}^{S} \nu_{kj}\xi_j, \tag{3.79}$$

$$n_{0k}\eta_k = -\sum_{j=1}^{S} \nu_{kj}\xi_j. \tag{3.80}$$

After the transformation to the specific extent of reactions, ξ', Equations 3.79 and 3.80 are transformed to a new form:

$$x_{0k}\eta_k = -\sum_{j=1}^{S} \nu_{kj}\xi'_j, \tag{3.81}$$

which is valid for both continuous and discontinuous reactors. After taking into account the definition for the relative conversion, η'_k,

$$\eta'_k = x_{0k}\eta_k. \tag{3.82}$$

Equation 3.82 takes on a new form, using the matrix and vector notations:

$$\eta'_k = -\nu_k\xi', \tag{3.83}$$

where ν_k denotes the submatrix containing stoichiometric coefficients for the key components. If ν_k is a quadratic and nonsingular matrix—this is the case if key components have been selected in the correct way—then ξ' can be solved by Equation 3.83:

$$\xi' = -\nu_k^{-1}\eta'_k. \tag{3.84}$$

This expression for ξ' can now, in turn, be incorporated into the expression for x in Equation 3.76. The result is written as follows:

$$x = \frac{x_0 + \nu(-\nu_k^{-1})\eta'_k}{1 + i^{\mathrm{T}}\nu(-\nu_k^{-1})\eta'_k}. \tag{3.85}$$

The analogy to Equation 3.67, which is valid for single-reaction systems, is elegant. Equation 3.85 allows the possibility of calculating the molar fractions, x_i, for all components, from the relative conversions, η'_{ki}, of the key components.

3.5.3 RELATIONSHIP BETWEEN CONCENTRATION, EXTENT OF REACTION, CONVERSION, AND VOLUMETRIC FLOW RATE IN A CONTINUOUS REACTOR

In reactor calculations, the important quantities in reaction kinetics, or concentrations of the components, are related to the stoichiometric quantities such as the extent of reaction and conversion. For practical reasons, gas- and liquid-phase reactions are discussed separately. For gas-phase reactions, the ideal gas law is assumed to be valid.

3.5.3.1 Gas-Phase Reactions

Relationships 3.44 and 3.45 can be utilized to calculate the concentrations in a mixture constituting an "ideal" gas. The total concentration in the mixture is given according to the ideal gas law:

$$P = cRT, \tag{3.86}$$

where P denotes the total pressure and T is the temperature (in K). The concentration therefore becomes

$$c = \frac{P}{RT}. \tag{3.87}$$

For a system with a single chemical reaction, Equations 3.61 and 3.67 are inserted into the expression of c_i; if the relation (Equation 3.87) is taken into account simultaneously, the result becomes

$$c_i = \frac{x_{0i} + \nu_i \xi'}{1 + \sum_{i=1}^{N} \nu_i \xi'} \frac{P}{RT} \tag{3.88}$$

and

$$c_i = \frac{x_{0i} + \nu_i x_{0\mathrm{A}} \eta_\mathrm{A} / (-\nu_\mathrm{A})}{1 + x_{0\mathrm{A}} \eta_\mathrm{A} \sum_{i=1}^{N} \nu_i / (-\nu_\mathrm{A})} \frac{P}{RT}. \tag{3.89}$$

For a system with multiple chemical reactions, the expression for the total concentration (Equation 3.87) is naturally still valid. By inserting expressions of the molar fractions, Equations 3.76 and 3.85, into the definition of the concentration, Equations 3.44 and 3.45, the following expressions are obtained for the concentrations:

$$c = \frac{x_0 + \nu \xi'}{1 + i^\mathrm{T} \nu \xi'} \frac{P}{RT}, \tag{3.90}$$

$$c = \frac{x_0 + \nu (\nu_k^{-1}) \eta'_k}{1 + i^\mathrm{T} \nu (\nu_k^{-1}) \eta'_k} \frac{P}{RT}. \tag{3.91}$$

The change in the volumetric flow rate is obtained by applying the ideal gas law to the entire reaction mixture, at the reactor inlet and in an arbitrary reactor coordinate (location):

$$\dot{V}_0 = \frac{\dot{n}_0 R T_0}{P_0}, \tag{3.92}$$

$$\dot{V} = \frac{\dot{n} R T}{P}. \tag{3.93}$$

The above-mentioned equations yield

$$\frac{\dot{V}}{\dot{V}_0} = \frac{\dot{n}}{\dot{n}_0} \frac{T}{T_0} \frac{P_0}{P}. \tag{3.94}$$

For $\dot{n}/\dot{n}_0$, different expressions can be inserted, depending on whether one or several chemical reactions are in progress in the reactor. If only *one* reaction is taking place, Equations 3.94 and 3.57 yield

$$\frac{\dot{V}}{\dot{V}_0} = \left(1 + \sum_{i=1}^{N} \nu_i \xi'\right) \frac{T}{T_0} \frac{P_0}{P}, \tag{3.95}$$

and, in case the relationship between ξ' and η_A, Equation 3.66, is incorporated into Equation 3.95, a new expression is obtained:

$$\frac{\dot{V}}{\dot{V}_0} = \left(1 + \frac{x_{0A}\eta_A}{-\nu_A} \sum_{i=1}^{N} \nu_i\right) \frac{T}{T_0} \frac{P_0}{P}. \tag{3.96}$$

In case multiple chemical reactions take place, the corresponding expressions for $\dot{n}/\dot{n}_0$ should be inserted. Combining Equations 3.73 and 3.94 yields

$$\frac{\dot{V}}{\dot{V}_0} = \left(1 + i^{\mathrm{T}} \nu \xi'\right) \frac{T}{T_0} \frac{P_0}{P}, \tag{3.97}$$

where $i^{\mathrm{T}} \nu \xi' = \sum_{i=1}^{N} \sum_{i=1}^{S} \nu_{ij} \xi'_j$.

If ξ' (in Equation 3.84) is replaced by the relative conversions of key components, Equation 3.97 is transformed to

$$\frac{\dot{V}}{\dot{V}_0} = \left(1 + i^{\mathrm{T}} \nu (-\nu_k^{-1}) \eta'_k\right) \frac{T}{T_0} \frac{P_0}{P}. \tag{3.98}$$

Equations 3.95 through 3.98 also yield the change in the density of the reaction mixture since the mass flow $\dot{m}$ is constant:

$$\frac{\dot{V}}{\dot{V}_0} = \frac{\rho_0}{\rho}. \tag{3.99}$$

The interpretation of Equations 3.95 and 3.96, as well as Equations 3.97 and 3.98, is simple: if the number of molecules in the chemical reaction increases, the expression $\sum \nu_i \xi$ attains a positive value (since $\xi' > 0$ and $\sum \nu_i > 0$). Simultaneously, the terms in parentheses, in Equations 3.95 through 3.98, become larger than *unity* (>1) inside the reactor. Under isothermal conditions ($T = T_0$), the volumetric flow rate inside the reactor is thus increased. Under nonisothermal conditions—with strongly exothermic or endothermic reactions—the temperature effect, that is, the term T/T_0, results in a considerable change in the volumetric flow rate.

In case the ideal gas law is not valid, the equation of state is $PV=ZnRT$, where Z is the compressibility factor ($Z \neq 1$). The term RT in the above equation is thus replaced by ZRT. Z is a function of mole fraction, pressure, and temperature (x, P, and T), which implies, for instance, that an iterative procedure should be applied to Equations 3.90 and 3.91. Nonideal gases are discussed in detail in Ref. [8].

3.5.3.2 Liquid-Phase Reactions

The change in the density of a mixture is mostly negligible for liquid-phase reactions and can, therefore, often be excluded from the calculations. The definition of ξ, Equation 3.53, for a system with *one* ongoing chemical reaction yields

$$\dot{n}_i = \dot{n}_{0i} + \nu_i \xi. \tag{3.100}$$

Equation 3.100 is divided by the volumetric flow rate at the reactor inlet, $\dot{V}_0$, and we obtain

$$\frac{\dot{n}_i}{\dot{V}_0} = c_{0i} + \frac{\nu_i \xi}{\dot{V}_0}. \tag{3.101}$$

By assuming that $\dot{n}_i/\dot{V}_0 \simeq \dot{n}_i/\dot{V} = c_i$ and defining a new extent of reaction with the concentration dimension, ξ'',

$$\xi'' = \frac{\xi'}{\dot{V}_0}. \tag{3.102}$$

Equation 3.101 is transformed to a new form:

$$c_i = c_{0i} + \nu_i \xi''. \tag{3.103}$$

For systems with *multiple* chemical reactions, Equation 3.103 can easily be generalized to

$$c_i = c_{0i} + \sum_{j=1}^{S} \nu_{ij} \xi_j'' \tag{3.104}$$

or

$$c = c_0 + \nu \xi''. \tag{3.105}$$

If conversion is used as a variable, Equation 3.101 takes the following form, provided that Equation 3.64 is included:

$$\frac{\dot{n}_i}{\dot{V}_0} = c_{0i} + \frac{\nu_i}{-\nu_A} c_{0A} \eta_A. \tag{3.106}$$

This is approximately true for liquid-phase reactions,

$$c_i = c_{0i} + \frac{\nu_i}{-\nu_A} c_{0A} \eta_A \tag{3.107}$$

in the case of a single chemical reaction.

If the system comprises *multiple* chemical reactions, the quantity ξ'' should be replaced with a vector, ξ'', defined as

$$\xi'' = \frac{\xi}{\dot{V}_0} = \frac{\dot{n}_0 \xi'}{\dot{V}_0} = c_0 \xi', \tag{3.108}$$

where ξ is given by Equation 3.84—if the relative conversions are used:

$$\xi' = -\nu_k^{-1} \eta_k'. \tag{3.109}$$

Equation 3.68 can be rewritten as

$$\dot{n} = \dot{n}_0 + \nu \xi. \tag{3.110}$$

We obtain $\xi = c_0 \dot{V}_0 (-\nu_k^{-1} \eta_k')$, which is inserted into Equation 3.110, and the resulting expression is divided by the volumetric flow $\dot{V}_0$. The result attains the following form:

$$\frac{\dot{n}}{\dot{V}_0} = c_0 + \nu(-\nu_k^{-1}) \eta_k' c_0. \tag{3.111}$$

For liquid-phase reactions, $\dot{n}/\dot{V}_0$ can often be regarded as a good approximation that is equal to the concentrations in the system: $c \approx \dot{n}/\dot{V}_0$.

The product, $\eta_k' c_0$, in Equation 3.111, can naturally be developed further. The definition of relative conversion for the key component k, η_k', indicates that $\eta_k'' c_0$ is given by

$$\eta_k' c_0 = \frac{\dot{n}_{0k} - \dot{n}_k}{\dot{n}_0}, \tag{3.112}$$

Since $\dot{n}_0 = c_0 \dot{V}_0$, Equation 3.112 becomes

$$\eta_k' c_0 = \frac{\dot{n}_{0k} - \dot{n}_k}{\dot{V}_0}. \tag{3.113}$$

If $\dot{V}_0$ can be approximated as $\dot{V}_0 \approx \dot{V}$, Equation 3.113 attains a new form:

$$\eta_k' = \frac{c_{0k} - c_k}{c_0}, \tag{3.114}$$

which implies that we obtain a simplified definition for the relative conversions in the liquid-phase system:

$$\boldsymbol{\eta}'_k = \frac{\mathbf{c}_{0k} - \mathbf{c}_k}{c_0} \tag{3.115}$$

The product, $\eta'_k c_0$, in Equation 3.112 can in fact often be approximated by the difference $c_{0k} - c_k$ in the liquid-phase system.

3.5.4 RELATIONSHIP BETWEEN CONCENTRATION, EXTENT OF REACTION, CONVERSION, AND TOTAL PRESSURE IN A BR

In this section, we will study the relationship between concentrations and stoichiometric quantities. We will look at gas- and liquid-phase reactions separately. For batchwise reactions, the total pressure in the reactor plays an important role: the total pressure may vary during the course of reaction due to changes in the number of molecules in the system and due to temperature variations. The treatment of gas-phase systems in this section is based on the ideal gas law.

3.5.4.1 Gas-Phase Reactions

In a BR, the reaction volume (V_R) is usually constant. By applying the ideal gas law to the entire amount of gas in a BR, at the initiation of the reaction ($t = 0$) and at an arbitrary moment in time, we obtain

$$P_0 V = n_0 RT \tag{3.116}$$

and

$$PV = nRT. \tag{3.117}$$

A combination of Equations 3.116 and 3.117 gives us the pressure relationship

$$\frac{P}{P_0} = \frac{n}{n_0}\frac{T}{T_0}. \tag{3.118}$$

Different kinds of expressions for the molar ratio, n/n_0, can be used in Equation 3.118, depending on whether the extent of reaction or conversion is used as a variable and, whether one or several reactions are in progress in the system. For a system with a single chemical reaction, for instance, the alternative formulae 3.119 and 3.120 are available for the change in pressure:

$$\frac{P}{P_0} = \left(1 + \left(\sum_i \nu_i\right)\xi'\right)\frac{T}{T_0}, \tag{3.119}$$

$$\frac{P}{P_0} = \left(1 + \frac{x_{0\mathrm{A}}\eta_\mathrm{A}}{-\nu_\mathrm{A}}\sum_i \nu_i\right)\frac{T}{T_0}. \tag{3.120}$$

For systems with multiple chemical reactions, the corresponding expressions, Equations 3.121 and 3.122, are obtained:

$$\frac{P}{P_0} = \left(1 + i^{\mathrm{T}} \nu \xi'\right) \frac{T}{T_0}, \tag{3.121}$$

$$\frac{P}{P_0} = \left(1 + i^{\mathrm{T}} \nu \left(-\nu_k^{-1}\right) \eta_k'\right). \tag{3.122}$$

A comparison between the equations describing the change in the volumetric flow rate, in continuous reactors, Equations 3.95 through 3.98, shows that similar correction terms appear in Equations 3.119 through 3.122: the effect of chemical reactions is reflected by the volumetric flow rate of continuous reactors operating at a constant pressure, whereas the same is true for the total pressure in BRs (autoclaves) with constant volumes.

The concentration expressions in Equations 3.88 through 3.91 presented in the context of continuous reactors are also valid for a BR with a constant volume; the corresponding expression for the total pressure (Equations 3.118 through 3.121) should, however, be replaced in Equations 3.88 through 3.91 for a BR. The correction terms for the total pressure and the denominator in the corresponding concentration expression always cancel each other out. The results—the surprisingly elegant and simple dependencies—can be summarized as follows:

For a system with only *one* chemical reaction, the following is valid:

$$c_i = \left(x_{0i} + \nu_i \xi'\right) \frac{P}{RT_0}, \tag{3.123}$$

$$c_i = \left(x_{0i} + \nu_i \frac{x_{0\mathrm{A}} \eta_{\mathrm{A}}}{-\nu_{\mathrm{A}}}\right) \frac{P_0}{RT_0}, \tag{3.124}$$

where $P_0/RT_0 = c_0$ in terms of the total concentration.

For a system with *multiple* chemical reactions, we obtain analogously

$$c = \left(x_0 + \nu \xi'\right) \frac{P}{RT_0}, \tag{3.125}$$

$$c = \left(x_0 + \nu \left(-\nu_k^{-1}\right) \eta_k'\right) \frac{P}{RT_0}. \tag{3.126}$$

3.5.4.2 Liquid-Phase Reactions

In BRs, in connection with liquid-phase reactions, no pressure changes usually take place due to chemical reactions. Expression 3.99 is thus valid for BRs as well,

$$c_i = c_{0i} + \nu_i \xi'' \tag{3.127}$$

in case only a single chemical reaction takes place in the system. The concentration-based extent of reaction, ξ'', is, however, defined by

$$\xi'' = \frac{\xi}{V_0} = \frac{\xi}{V_R}. \tag{3.128}$$

For a system with multiple chemical reactions, Equation 3.127 is generalized to

$$c = c_0 + \nu\xi'', \tag{3.129}$$

where ξ'' is defined analogously to Equation 3.107:

$$\xi'' = \frac{\xi}{V_0} = \frac{\xi}{V_R}. \tag{3.130}$$

If conversion or relative conversion is used as a variable, relationships 3.130 and 3.132 for *one* and *multiple* chemical reactions become, respectively,

$$c_i = c_{0i} + \frac{\nu_i}{-\nu_A} c_{0A}\eta_A \tag{3.131}$$

and

$$c = c_0 + \nu\left(-\nu_k^{-1}\right)\eta'_k c_0. \tag{3.132}$$

Even in Equation 3.132, the relative conversion for the key component k, η'_k, is given by

$$\eta'_k = \frac{c_{0k} - c_k}{c_0}, \tag{3.133}$$

that is, similar to continuous liquid-phase reactors.

3.6 STOICHIOMETRY IN MASS BALANCES

If a reduction in the number of molar balances is desired for the calculations, the stoichiometric relationships developed in the previous section must be utilized. We can thus reduce the number of necessary balance equations from N to S; one should keep in mind that the number of chemical reactions is usually much lower than the number of components in a system. The molar flows, $\dot{n}_i$, can be replaced by expressions containing reaction extent, specific reaction extent, and reaction extent with concentration dimension or conversion (ξ, ξ', ξ'', or η_A) in a system containing a single chemical reaction. For systems with multiple chemical reactions, $\dot{n}$ is replaced by an expression containing ξ, ξ', ξ'', or $\boldsymbol{\eta}'$.

In the following, different kinds of transformations of molar balances are introduced. These transformations are obtained using the extent of reaction, conversion, concentrations of the key components, or their molar flows. The treatment is directly applied to systems

with multiple reactions. The definition for reaction velocities of components, r_i, Equation 3.6 (Chapter 2), can be written using arrays

$$\mathbf{r} = \boldsymbol{\nu}\mathbf{R}, \tag{3.134}$$

where $\mathbf{r}$ and $\mathbf{R}$ contain the elements $\mathbf{r} = [r_1\ r_2\ \ldots\ r_N]^T$ and $\mathbf{R} = [R_1\ R_2\ R_S]^T$. If we only take into account the generation velocities of the key components, a vector, $\mathbf{r}_k$, can be defined based on the corresponding stoichiometric submatrices, $\boldsymbol{\nu}_k$, containing the stoichiometric coefficients of the key components:

$$\mathbf{r}_k = \boldsymbol{\nu}_k\mathbf{R}. \tag{3.135}$$

The molar balances of the three ideal reactor types, *tube reactor*, *BR*, and *CSTR*, Equations 3.8, 3.18, and 3.25, can be written in the following form—provided that only the molar balances of the key components are taken into account:

$$\frac{\mathrm{d}\dot{n}_k}{\mathrm{d}\tau} = \dot{V}_0\nu_k R, \tag{3.136}$$

$$\frac{\mathrm{d}n_k}{\mathrm{d}t} = V_R h\nu_k R, \tag{3.137}$$

$$\frac{\dot{n}_k - \dot{n}_{0k}}{\tau} = \dot{V}_0\nu_k R. \tag{3.138}$$

The relationships between the extent of reaction and molar flows, as well as the molar amounts, of the key components are given by

$$\dot{n}_k = \dot{n}_{0k} + \nu_k\xi \tag{3.139}$$

and

$$n_k = n_{0k} + \nu_k\xi. \tag{3.140}$$

The above-mentioned equations provide us with the derivatives $\mathrm{d}\dot{n}_k/\mathrm{d}\tau$ and $\mathrm{d}\mathbf{n}_k/\mathrm{d}t$ for *tube reactors* and *BRs*, respectively,

$$\frac{\mathrm{d}\dot{n}_k}{\mathrm{d}\tau} = \nu_k\frac{\mathrm{d}\xi}{\mathrm{d}\tau} \tag{3.141}$$

and

$$\frac{\mathrm{d}n_k}{\mathrm{d}t} = \nu_k\frac{\mathrm{d}\xi}{\mathrm{d}t}, \tag{3.142}$$

as well as the difference

$$\dot{n}_k - \dot{n}_{0k} = \nu_k\xi \tag{3.143}$$

in the case of a *CSTR*.

After the replacement of Equations 3.141 through 3.143 by Equations 3.136 through 3.138, as well as the elimination of the stoichiometric matrix, ν_k, the balances can be expressed by reaction extents, ξ:

$$\frac{d\xi}{d\tau} = \dot{V}_0 R, \tag{3.144}$$

$$\frac{\xi}{\tau} = \dot{V}_0 R, \tag{3.145}$$

$$\frac{d\xi}{dt} = V_R R. \tag{3.146}$$

If the *specific extent of the reaction* (ξ'), defined by Equations 3.55 and 3.56, is utilized, the balance Equations 3.144 through 3.146 are transformed to

$$\frac{d\xi'}{d\tau} = \frac{1}{c_0} R, \tag{3.147}$$

$$\frac{\xi'}{\tau} = \frac{1}{c_0} R, \tag{3.148}$$

$$\frac{d\xi'}{dt} = \frac{1}{c_0} R, \tag{3.149}$$

where c_0 denotes the total concentration. Alternatively, the use of the definition of concentration-dependent extent of the reaction, ξ'', for continuous reactors, Equation 3.108:

$$\xi'' = \frac{\xi}{\dot{V}_0}$$

for a BR, Equation 3.130:

$$\xi'' = \frac{\xi}{V_R}$$

transforms the balance Equations 3.144 through 3.146 into Equations 3.150 through 3.152:

$$\frac{d\xi''}{d\tau} = R, \tag{3.150}$$

$$\frac{\xi''}{\tau} = R, \tag{3.151}$$

$$\frac{d\xi''}{dt} = R. \tag{3.152}$$

If the relative conversion, η'_k, is considered as a variable, Equation 3.84 gives us the relationship

$$\xi' = -\nu_k^{-1} \eta'_k.$$

Substituting Equation 3.84 into Equations 3.147 through 3.149 yields a set of equations,

$$\frac{\mathrm{d}\eta_k'}{\mathrm{d}\tau} = -\frac{1}{c_0}\nu_k R, \tag{3.153}$$

$$\frac{\eta_k'}{\tau} = -\frac{1}{c_0}\nu_k R, \tag{3.154}$$

$$\frac{\mathrm{d}\eta_k'}{\mathrm{d}t} = -\frac{1}{c_0}\nu_k R, \tag{3.155}$$

which are valid for the ideal reactor types.

If the volumetric flow rate is constant, which is approximately true in the case of liquid-phase reactions and isothermal gas-phase reactions with $\sum_j \sum_i \nu_{ij} = 0$, in continuous reactors or if no volume changes take place (this is true for most of the BRs regardless of whether the system comprises a gas or a liquid phase), balance Equations 3.136 through 3.138 can be expressed with the concentrations of the key components:

$$\frac{\mathrm{d}c_k}{\mathrm{d}\tau} = \nu_k R, \tag{3.156}$$

$$\frac{c_k - c_{0k}}{\tau} = \nu_k R, \tag{3.157}$$

$$\frac{\mathrm{d}c_k}{\mathrm{d}t} = \nu_k R. \tag{3.158}$$

If the molar flows of the key components are used, Equation 3.139 yields the extents of the reactions, ξ:

$$\xi = \nu_k^{-1}(\dot{n}_k - \dot{n}_{0k}). \tag{3.159}$$

These can be substituted into the definition of ξ, Equation 3.66, to obtain all molar flows:

$$\dot{n} = \dot{n}_0 + \nu\nu_k^{-1}(\dot{n}_k - \dot{n}_{0k}). \tag{3.160}$$

The above-stated equation naturally contains new information about the remaining components, but not about the key components.

For ideal gas-phase reactions, the concentrations of the key components are obtained from

$$c_k = \frac{\dot{n}_k}{\dot{V}}, \tag{3.161}$$

in which the volumetric flow rate, $\dot{V}$, is delivered by inserting Equation 3.162

$$\xi' = \nu_k^{-1}\left(\frac{\dot{n}_k}{\dot{n}_0} - x_{0k}\right) \tag{3.162}$$

into Equation 3.97:

$$\frac{\dot{V}}{\dot{V}_0} = \left[1 + i^{\mathrm{T}} \nu \nu_k^{-1} \left(\frac{\dot{n}_k}{\dot{n}_0} - x_{0k}\right)\right] \frac{T}{T_0} \frac{P_0}{P}. \tag{3.163}$$

The concentrations of the remaining components are thereafter given by

$$c = \frac{\dot{n}}{\dot{V}}, \tag{3.164}$$

in which the molar flow vector, $\dot{\mathbf{n}}$, can be obtained from Equation 3.160 and the volumetric flow, $\dot{V}$, from Equation 3.163.

For liquid-phase reactions, the procedure is analogous, with one exception: the volumetric flow rate. Expression 3.163 is thus not used, but instead it is often replaced by the assumption $\dot{V} \approx \dot{V}_0$. If the extent of a reaction or the specific extent of a reaction is used, the concentrations of all components can be obtained from Equation 3.90 for gas-phase reactions. For liquid-phase reactions, Equation 3.105 is valid if the volumetric flow rate can be assumed to be constant. When using Equations 3.90 and 3.105, one should take into account the following relationship:

$$\underline{\xi} = \underline{\xi}' \cdot \dot{n}_0 = \underline{\xi}'' \dot{V}_0. \tag{3.165}$$

If the relative conversions of the key components are used, the remaining relative conversions are obtained from Equation 3.166:

$$\eta' = \nu \nu_k^{-1} \eta_k'. \tag{3.166}$$

The previous equation was obtained by applying the definition of relative conversion, η', to Equation 3.83.

The concentrations and volumetric flow rates are obtained from Equations 3.91 and 3.98 in the case of ideal gases; in the case of liquid-phase reactions with constant volumetric flow rates, the concentrations are given by Equation 3.111.

If the concentrations of key components are utilized as variables in the calculation of flow reactors with a constant volumetric flow rate, the remaining component concentrations are given by the key component concentrations as follows:

$$c = c_0 + \nu \nu_k^{-1} (c_k - c_{0k}). \tag{3.167}$$

For a BR with a constant volume, the transformation from molar amounts, extents of reactions, and conversions become much simpler than for flow reactors. As the molar amounts of the key components are used as variables, the molar amounts of the remaining components are obtained by noting Equation 3.140:

$$\xi = \eta_k^{-1} (n_k - n_{0k}), \tag{3.168}$$

which is substituted into the definition for the specific reaction extent vector, ξ, Equation 3.69:

$$n = n_0 + \nu\nu_k^{-1}(n_k - n_{0k}). \tag{3.169}$$

The concentrations of the components are thus given by

$$c = \frac{n}{V_R}. \tag{3.170}$$

If the extent of reaction or the specific extent of reaction is used, the concentrations are given by the expression

$$c = c_0 + \nu\underline{\xi}'' \tag{3.171}$$

together with taking into account the relationship

$$\underline{\xi} = \underline{\xi}' n_0 = \underline{\xi}'' V_R. \tag{3.172}$$

If the relative conversion is utilized in the calculations, Equations 3.126 and 3.132 give the concentrations of all components for gas- and liquid-phase reactions, respectively.

The most simple means of performing calculations on BRs with constant volumes is to utilize the concentrations of the key components according to balance Equation 3.157. The concentration-dependent extent of reaction will then give for the key components

$$\underline{\xi}'' = \nu_k^{-1}(c_k - c_{0k}), \tag{3.173}$$

which, after back-substitution in Equation 3.171, gives an expression for the other concentrations in the system:

$$c = c_0 + \nu\nu_k^{-1}(c_k - c_{0k}). \tag{3.174}$$

3.7 EQUILIBRIUM REACTOR: ADIABATIC TEMPERATURE CHANGE

Sometimes, especially when referring to commercial process simulators, the term *equilibrium reactor* is used. A chemical system can be approximated with a so-called equilibrium reactor, in which the reaction rates are so high that one can assume that the chemical reaction resides at the equilibrium at the given temperature. The extreme performance limits of a chemical reactor can be mapped with the aid of the equilibrium approximation, which does not, however, help in the design of a real reactor.

3.7.1 MASS AND ENERGY BALANCES

In the following, a backmixed reactor unit is examined, in which all reactions are in equilibria. The molar balances of the reactor are, thus, given by Equation 3.138:

$$\frac{\dot{n}_k - \dot{n}_k}{\tau} = \dot{V}_0 \nu_k R.$$

After combining Equations 3.143 and 3.138, we obtain

$$\frac{\nu_k \xi}{\tau} = \dot{V}_0 \nu_k R \tag{3.175}$$

from which the extent of the reaction, ξ, is obtained:

$$\xi = \tau \dot{V}_0 R. \tag{3.176}$$

From the viewpoint of each reaction, we can write

$$\xi_j = \tau \dot{V}_0 R_j = R_j V_\mathrm{R}. \tag{3.177}$$

The energy balance for a completely backmixed reactor unit is given by Equation 3.22:

$$\frac{T - T_0}{V_\mathrm{R}} = \frac{1}{\dot{m} c_\mathrm{p}} \left(\sum_{j=1}^{S} R_j \left(-\Delta H_{\mathrm{r}j} \right) - \frac{US}{V_\mathrm{R}} \left(T - T_\mathrm{C} \right) \right).$$

Inserting R_j (from Equation 3.176) into the above equation yields

$$\frac{T - T_0}{V_\mathrm{R}} = \frac{1}{\dot{m} c_\mathrm{p}} \left(\frac{1}{V_\mathrm{R}} \sum_{j=1}^{S} \xi_j \left(-\Delta H_{\mathrm{r}j} \right) - \frac{US}{V_\mathrm{R}} \left(T - T_\mathrm{C} \right) \right), \tag{3.178}$$

which can be simplified ($\tau \dot{V}_0 = V_\mathrm{R}$) to

$$T - T_0 = \frac{1}{\dot{m} c_\mathrm{p}} \left(\sum_{j=1}^{S} \xi_j \left(-\Delta H_{\mathrm{r}j} \right) - US \left(T - T_\mathrm{C} \right) \right). \tag{3.179}$$

If the reaction enthalpies, $\Delta H_{\mathrm{r}j}$, can be approximately constant, the reactor temperature can be solved using the above-stated equation:

$$T = \frac{T_0 + (US/\dot{m} c_\mathrm{p}) T_\mathrm{C} + (1/\dot{m} c_\mathrm{p}) \left(\sum_{j=1}^{S} \left(-\Delta H_{\mathrm{r}j} \right) \xi_j \right)}{1 + (US/\dot{m} c_\mathrm{p})}. \tag{3.180}$$

It should be noted that the exact form of the balance Equation 3.22 *cannot* be directly applied to the equilibrium reactor, since $\mathbf{R} = 0$ in equilibria but $\xi \neq 0$.

Each reaction is assumed to reside at equilibrium, and all of the reaction velocities in principle depend on the concentrations and reaction temperatures of all involved components. This is why at an equilibrium state we can state that

$$R_j(c, T) = 0, \quad j = 1 \ldots S, \tag{3.181}$$

that is, the net rate of each reaction is zero.

The relationship between concentrations and extents of reactions implies that

$$c\dot{V} = c_0\dot{V}_0 + \underline{\nu}\underline{\xi} \tag{3.182}$$

both for liquid- and for gas-phase reactions. Equation 3.182 implies that Equation 3.181 can even be expressed as follows:

$$R(\underline{\xi}, T) = 0. \tag{3.183}$$

The task thus comprises solving S algebraic equations similar to Equation 3.183, if the temperature is *a priori* known. If the temperature is unknown, it can be calculated from the CSTR model according to Equation 3.180. An iterative procedure should be applied, since the reaction rates, **R**, are temperature-dependent.

An important extreme case is the so-called *adiabatic reactor*. In an adiabatic reactor, no heat exchange takes place with the surroundings, that is, $U = 0$. In this case, Equation 3.179 is simplified to the form

$$T_{\mathrm{ad}} = T_0 + \frac{1}{\dot{m}c_{\mathrm{p}}}\left(\sum_{j=1}^{S}\left(-\Delta H_{\mathrm{r}j}\right)\xi_j\right). \tag{3.184}$$

The difference, $T_{\mathrm{ad}} - T_0$, is often denoted here as ΔT_{ad}, the adiabatic temperature difference in the reactor. Equation 3.184 was originally developed for the CSTR model; it is, however, easy to prove mathematically that it gives the adiabatic temperature of a PFR as well. For a BR, a formula analogous to Equation 3.183 can be written as

$$T_{\mathrm{ad}} = T_0 + \frac{1}{mc_{\mathrm{p}}}\left(\sum_{j=1}^{S}\left(-\Delta H_{\mathrm{r}j}\right)\xi_j\right) \tag{3.185}$$

for the adiabatic reaction temperature. Expressions 3.184 and 3.185 provide important information: since $\Delta H_{\mathrm{r}j}$ is usually relatively independent of the temperature, the adiabatic temperature change becomes directly proportional to the extent of reaction, ξ_j. Expressions 3.184 and 3.185 are also valid for nonequilibrium reactions.

3.8 ANALYTICAL SOLUTIONS FOR MASS AND ENERGY BALANCES

In some simple cases of reaction kinetics, it is possible to solve the balance equations of the ideal, homogeneous reactors analytically. There is, however, a precondition: isothermicity; if nonisothermal conditions prevail, analytical solutions become impossible or, at least, extremely difficult to handle, since the energy and molar balances are interconnected through the exponential temperature dependencies of the rate and equilibrium constants (Sections 2.2 and 2.3). Analytical solutions are introduced in-depth in the literature dealing

TABLE 3.2 Analytical Solution for a First-Order Reaction in Various Ideal Reactors

$A \rightarrow P, \quad r_A = \nu_A R = -1kc_A$
$\dot{V} = \text{constant } (=\dot{V}_0)$

Plug flow reactor, PFR

$\frac{d\dot{n}_A}{d\tau} = r_A \dot{V}_0$ (Equation 3.8)
$\dot{n}_A = c_A \dot{V} = c_A \dot{V}_0, \quad \frac{d\dot{n}_A}{d\tau} = \frac{dc_A}{d\tau}\dot{V}_0,$ we obtain
$\frac{dc_A}{d\tau} = r_A \Rightarrow \frac{dc_A}{d\tau}_t = -kc_A$ separation of variables yields
$\int_{c_{0A}}^{c_A} \frac{dc_A}{c_A} = -k \int_0^t d\tau \quad \ln\left(\frac{c_A}{c_{0A}}\right) = -k\tau \quad \frac{c_A}{c_{0A}} = e^{-k\tau}$

Continuous stirred tank reactor, CSTR

$\frac{\dot{n}_A - \dot{n}_{0A}}{\tau} = r_A \dot{V}_0$ (Equation 3.18)
Again, we can introduce $\dot{n}_A = c_A \dot{V}_0$ and $\dot{n}_{0A} = c_{0A}\dot{V}_0$ (see the above, PFR) and obtain
$\frac{c_A - c_{0A}}{\tau} = r_A$, where $r_A = -kc_A$, the solution of the equation becomes
$\frac{c_A}{c_{0A}} = (1 + k\tau)^{-1}$

Batch reactor, BR

$\frac{dn_A}{dt} = r_A V_R$ (Equation 3.25)
here $n_A = c_A V_R$, V_R = constant, and we obtain
$\frac{dc_A}{dt} = -kc_A$, which is analogous to PFR (τ is replaced by t), $\frac{c_A}{c_{0A}} = e^{-kt}$

with chemical kinetics and reaction engineering [2,3,5,7,9,10], as well as in a summarized work [6]. The procedure for obtaining analytical solutions is illustrated in Table 3.2 for first-order reactions.

In Table 3.3, the concentration expressions of the key components are given for some common types of reaction kinetics. The concentration expressions in Table 3.3 are valid for isothermal conditions, for systems in which the volumetric flow rate and the reaction volume are kept constant. In practice, this implies isothermal liquid-phase reactions in a BR, PFR, and CSTR, isothermal gas-phase reactions in a BR with a constant volume, and isothermal gas-phase reactions with a constant molar amount $\left(\sum\sum \nu_{ij} = 0\right)$ in a PFR or CSTR. The equations in Table 3.3 were developed from balance equations introduced in Sections 3.2 through 3.4 as well as from the stoichiometric relationships that were presented in Sections 3.5 and 3.6. The equations are written in such a way that the concentrations of key components are expressed explicitly; for simple reactions, the corresponding design expressions are obtained by solving the space time (τ) or the reaction time (t) in the equations.

For isothermal gas-phase reactions, in CSTRs and PFRs, analytical design equations can sometimes be derived. In this case, we should begin with expressions such as Equations 3.136 and 3.138 or Equations 3.185 and 3.148. Further, we should utilize a correction term for the volumetric flow rates, such as Equation 3.97. Usually, these kinds of expressions become so complicated that a numerical solution of the balance equations is preferable. In Section 3.8, the analytical solutions of some simple systems are considered in detail.

TABLE 3.3 Concentrations in Ideal Reactors at a Constant Temperature, Pressure, and Volumetric Flow Rate

	Reaction Type	Kinetic Equation	PFR and BR
Simple reactions	$\lvert\nu_A\rvert\,A \rightarrow \lvert\nu_P\rvert\,P + \cdots$	$R = kc_A^n$	$c_A = \left(c_{0A}^{1-n} + \lvert\nu_A\rvert\,(n-1)k\tau\right)^{(1/1-n)}, \quad n \neq 1$ $c_A = c_{0A}e^{-\lvert\nu_A\rvert k\tau}, \quad n = 1$
	$\lvert\nu_A\rvert\,A + \lvert\nu_B\rvert\,B \rightarrow \lvert\nu_P\rvert\,P + \cdots$	$R = kc_Ac_B$	$c_A = \dfrac{c_{0A}ae^{ak\tau}}{\lvert\nu_B\rvert\,c_{0A}e^{ak\tau} - \lvert\nu_A\rvert\,c_{0B}}, \quad a \neq 0$ $a = (\lvert\nu_B\rvert\,c_{0A} - \lvert\nu_A\rvert\,c_{0B})$ $c_A = \left(c_{0A}^{-1} + \lvert\nu_B\rvert\,k\tau\right)^{-1}, \quad a = 0$
	$\lvert\nu_A\rvert\,A \Longleftrightarrow \lvert\nu_P\rvert\,P$	$R = k_+(c_A - c_P/K)$	$c_A = \dfrac{\lvert\nu_A\rvert\,c_{0P} + \lvert\nu_P\rvert\,c_{0A}}{aK} + \dfrac{\lvert\nu_A\rvert}{a}\left(c_{0A} - \dfrac{c_{0P}}{K}\right)e^{-ak_+\tau}$ $a = \lvert\nu_A\rvert + \lvert\nu_P\rvert/K$
Coupled parallel reactions	$\lvert\nu_{A1}\rvert\,A \rightarrow \lvert\nu_P\rvert\,P$ $\lvert\nu_{A2}\rvert\,A \rightarrow \lvert\nu_R\rvert\,R$	$R_1 = k_1c_A$ $R_2 = k_2c_A$	$c_A = c_{0A}e^{-a\tau}, \quad a = \lvert\nu_{A1}\rvert k_1 + \lvert\nu_{A2}\rvert k_2$ $c_P = c_{0P} + \dfrac{\lvert\nu_P\rvert k_1c_{0A}}{a}(1 - e^{-a\tau})$ $c_R = c_{0R} + \dfrac{\lvert\nu_R\rvert k_2c_{0A}}{a}(1 - e^{-a\tau})$
Coupled consecutive reactions	$\lvert\nu_A\rvert\,A \rightarrow \lvert\nu_{B1}\rvert\,B$ $\lvert\nu_{B2}\rvert\,B \rightarrow \lvert\nu_C\rvert\,C$	$R_1 = k_1c_A$ $R_2 = k_2c_B$	$c_B = c_{0B}e^{-\lvert\nu_{B2}\rvert k_2\tau} + \dfrac{\lvert\nu_{B1}\rvert\,k_1c_{0A}}{a} \cdot \left(e^{-\lvert\nu_A\rvert k_1\tau} - e^{-\lvert\nu_{B2}\rvert k_2\tau}\right)$ $a = \lvert\nu_{B2}\rvert\,k_2 - \lvert\nu_A\rvert\,k_1, \quad a \neq 0$ $c_B = (\lvert\nu_{B1}\rvert\,k_1c_{0A}\tau + c_{0B})\,e^{-\lvert\nu_A\rvert k_1\tau}, \quad a = 0$ $c_C = c_{0C} + \dfrac{\lvert\nu_{B1}\rvert\,\lvert\nu_C\rvert}{\lvert\nu_{B2}\rvert\,\lvert\nu_A\rvert}(c_{0A} - c_A) + \dfrac{\lvert\nu_C\rvert}{\lvert\nu_{B2}\rvert}(c_{0B} - c_B)$
	Reaction Type	**Kinetic Equation**	**CSTR**
Simple reactions	$\lvert\nu_A\rvert\,A \rightarrow \lvert\nu_P\rvert\,P + \cdots$	$R = kc_A^n$	$c_A = \dfrac{c_{0A}}{1 + \lvert\nu_A\rvert\,k\tau}, \quad n = 1$ $c_A = \dfrac{(1 + 4\,\lvert\nu_A\rvert\,c_{0A}k\tau)^{1/2} - 1}{2\,\lvert\nu_A\rvert\,k\tau}, \quad n = 2$
	$\lvert\nu_A\rvert\,A + \lvert\nu_B\rvert\,B \rightarrow \lvert\nu_P\rvert\,P + \cdots$	$R = kc_Ac_B$	$c_A = \dfrac{\left(()^2 + 4\,\lvert\nu_A\rvert\,c_{0A}k\tau\right)^{1/2} - ()}{2\,\lvert\nu_A\rvert\,k\tau}$ $() = 1 + (\lvert\nu_A\rvert\,c_{0B} - \lvert\nu_B\rvert\,c_{0A})\,k\tau$
	$\lvert\nu_A\rvert\,A \Longleftrightarrow \lvert\nu_P\rvert\,P$	$R = k_+(c_A - c_P/K)$	$c_A = \dfrac{c_{0A} + (k_+\tau/K)\left(\lvert\nu_A\rvert\,c_{0P} + \lvert\nu_P\rvert\,c_{0A}\right)}{1 + ak_+\tau}$ $a = \lvert\nu_{A1}\rvert + \lvert\nu_P\rvert/K$
Coupled parallel reactions	$\lvert\nu_{A1}\rvert\,A \rightarrow \lvert\nu_P\rvert\,P$ $\lvert\nu_{A2}\rvert\,A \rightarrow \lvert\nu_R\rvert\,R$	$R_1 = k_1c_A$ $R_2 = k_2c_A$	$c_A = \dfrac{c_{0A}}{1 + a\tau}$ $c_P = c_{0P} + \dfrac{\lvert\nu_P\rvert\,k_1c_{0A}\tau}{1 + a\tau}$ $c_R = c_{0R} + \dfrac{\lvert\nu_R\rvert\,k_2c_{0A}\tau}{1 + a\tau}$ $a = \lvert\nu_{A1}\rvert\,k_1 + \lvert\nu_{A2}\rvert\,k_2$
Coupled consecutive reactions	$\lvert\nu_A\rvert\,A \rightarrow \lvert\nu_{B1}\rvert\,B$ $\lvert\nu_{B2}\rvert\,B \rightarrow \lvert\nu_C\rvert\,C$	$R_1 = k_1c_A$ $R_2 = k_2c_B$	$c_A = \dfrac{c_{0A}}{1 + \lvert\nu_A\rvert\,k_1\tau}$ $c_B = \dfrac{c_{0B} + (\lvert\nu_A\rvert\,c_{0B} + \lvert\nu_{B1}\rvert\,c_{0A})\,k_1\tau}{(1 + \lvert\nu_A\rvert\,k_1\tau)\,(1 + \lvert\nu_{B2}\rvert\,k_2\tau)}$ c_C, see PFR and BR

Note: τ = space time in a PFR and CSTR and $\tau = t$ = reaction time in a BR.

For simple reactions, the concentrations of the other components are given by the stoichiometric relation $c_i = (\nu_i/\nu_A)\,(c_A - c_{0A}) + c_{0i}$.

3.8.1 MULTIPLE REACTIONS

In the following, we will discuss the analytical solution of some multiple chemical reaction systems in detail. The terms *multiple reactions* or *composite reactions* are usually used in this context. Multiple, simultaneous reactions occur in many industrial processes such as oil refining, polymer production, and, especially, organic synthesis of fine chemicals. It is thus of utmost importance to be able to optimize the reaction conditions, so that the yield of the desired product is maximized and the amounts of by-products are minimized.

We will observe three main categories of composite reactions and, in addition, try and provide an overview of the treatment of complex reaction systems in general. The temperature and density of the reaction mixture are assumed to remain constant, which implies that the volume and volumetric flow rate should remain at a constant level. The three principal categories of composite reactions are *parallel*, *consecutive*, and *consecutive-competitive* reactions. The following reaction schemes illustrate it better:

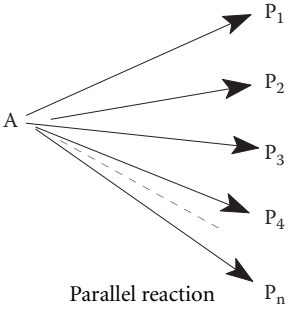

Consecutive reaction	$A \rightarrow R \rightarrow S \rightarrow T \ldots$
Consecutive-competitive reaction	$A + B \rightarrow R + D$ $R + B \rightarrow S + D$ $S + B \rightarrow T + D$ $T + B \ldots$

The extent of a reaction may alter naturally; for instance, parallel reactions of a higher order do exist. In connection with consecutive-competitive reactions, in many cases, secondary reaction products that react further appear (D), such as in the case of chlorination of organic substances, where hydrogen chloride is always generated. Another example is the polyesterification of dicarboxylic acids, upon which water formation takes place. Some industrially relevant multiple reaction systems are shown in Figure 3.18.

3.8.1.1 First-Order Parallel Reactions

Undesirable, parallel side reactions are a common complication in industrial processes. The desire to avoid side reactions can justify the choice of another reactor type or different

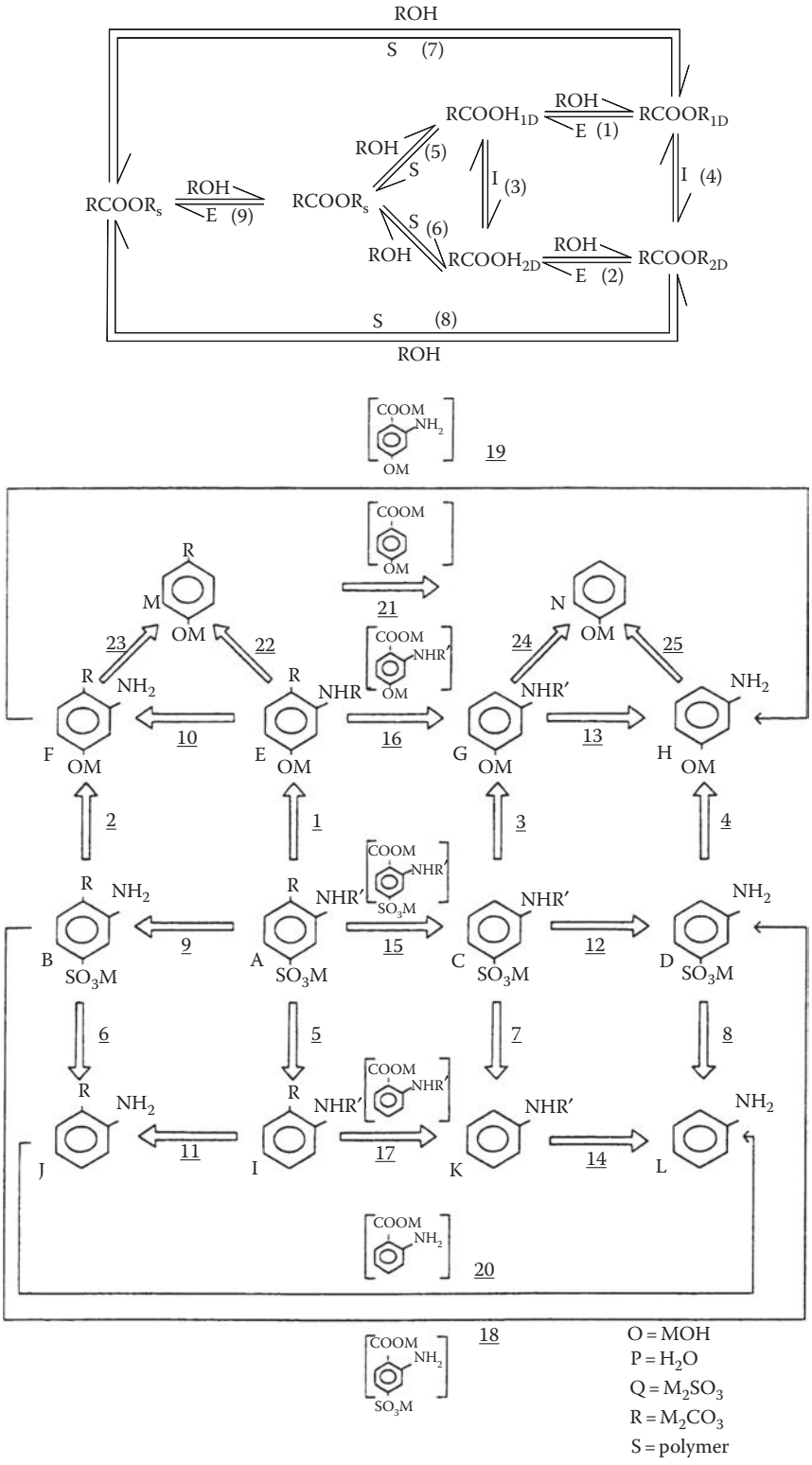

FIGURE 3.18 Sample multiple reaction systems that are industrially relevant: polyesterification of unsaturated carboxylic acids and alkali fusion.

reaction conditions than what might be natural in the absence of side reactions. We will limit our discussion to homogeneous isothermal first-order reaction systems, for which the volume and volumetric flow rate of the reaction mixture remain constant.

The simplest possible parallel reaction scheme for two first-order reactions is written as follows:

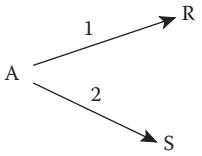

The reaction rates for steps (1) and (2) become

$$r_1 = k_1 c_A, \tag{3.186}$$

$$r_2 = k_2 c_A. \tag{3.187}$$

The generation velocities of the components can be written as

$$r_A = -r_1 - r_2, \tag{3.188}$$

$$r_R = r_1, \tag{3.189}$$

$$r_S = r_2. \tag{3.190}$$

The relationships between the concentrations of the components and the (average) space times can then consequently be derived from the mass balances of the ideal reactors.

3.8.1.1.1 BR and PFR

For a BR and a PFR, the molar balances are

$$\frac{dc_i}{d\tau} = r_i, \quad i = A, R, S, \tag{3.191}$$

in which r_A, r_R, and r_s are given by Equation 3.191. For component A, we obtain

$$\frac{dc_A}{d\tau} = -(k_1 + k_2)\, c_A, \tag{3.192}$$

which is easily integrated:

$$\int_{c_{0A}}^{c_A} \frac{dc_A}{c_A} = -(k_1 + k_2) \int_0^{\tau} d\tau. \tag{3.193}$$

The relationship between the concentration and time becomes

$$\ln\left(\frac{c_A}{c_{0A}}\right) = -(k_1 + k_2)\, \tau, \tag{3.194}$$

that is,

$$\frac{c_A}{c_{0A}} = e^{-(k_1+k_2)\tau}. \tag{3.195}$$

The concentrations, c_R and c_s, can then be calculated from

$$\frac{dc_R}{dt} = k_1 c_A \tag{3.196}$$

and

$$\frac{dc_S}{dt} = k_2 c_A \tag{3.197}$$

by separation and insertion of c_A (from Equation 3.195),

$$\int_{c_{0R}}^{c_R} dc_R = \int_0^\tau k_1 c_{0A} e^{-(k_1+k_2)\tau}\, d\tau, \tag{3.198}$$

$$\int_{c_{0B}}^{c_B} dc_S = \int_0^\tau k_2 c_{0A} e^{-(k_1+k_2)\tau}\, d\tau. \tag{3.199}$$

The final result takes the following form:

$$c_R = c_{0R} + \frac{k_1 c_{0A}}{k_1 + k_2}\left(1 - e^{-(k_1+k_2)\tau}\right), \tag{3.200}$$

$$c_S = c_{0S} + \frac{k_2 c_{0A}}{k_1 + k_2}\left(1 - e^{-(k_1+k_2)\tau}\right). \tag{3.201}$$

This solution is shown in Table 3.2 (previous section). In many cases, the initial concentrations of components R and S are equal to zero. In the case of extremely long residence times, the exponential term in Equations 3.200 and 3.201 disappears; the ratio between R and S approaches the limiting value:

$$\frac{c_R - c_{0R}}{c_S - c_{0S}} \cdots \rightarrow \cdots \frac{k_1}{k_2} \quad \text{in case that } \tau \rightarrow \infty \tag{3.202}$$

In other words, the ratio between the rate constants determines the product distribution.

3.8.1.1.2 Continuous Stirred Tank Reactor

For a CSTR, the mass balance can be written separately for each and every component as

$$\frac{c_i - c_{0i}}{\tau} = r_i, \tag{3.203}$$

where $i = A, R, S$.

The concentration of A can be solved from Equation 3.203 by inserting the rate equation, Equation 3.190:

$$\frac{c_A - c_{0A}}{\tau} = -k_1 c_A - k_2 c_A. \tag{3.204}$$

Thus, an explicit value for c_A is obtained:

$$c_A = \frac{c_{0A}}{1 + (k_1 + k_2)\,\tau}. \tag{3.205}$$

The concentrations of R and S are obtained from Equation 3.203, which, after inserting the expression for c_A, yield

$$c_R = c_{0R} + \frac{c_{0A} k_1 \tau}{1 + (k_1 + k_2)\,\tau}, \tag{3.206}$$

$$c_S = c_{0S} + \frac{c_{0A} k_1 \tau}{1 + (k_1 + k_2)\,\tau}. \tag{3.207}$$

The solution can be found in Table 3.2.

In case the inflow to the reactor is free from R and S, the initial concentrations are zero: $c_{0R} = c_{0S} = 0$. One can observe that even in this case, the product distribution dependence

$$\frac{c_R - c_{0R}}{c_S - c_{0S}} \tag{3.208}$$

approaches the limiting value, k_1/k_2, for very long space times.

For a general system of parallel reactions,

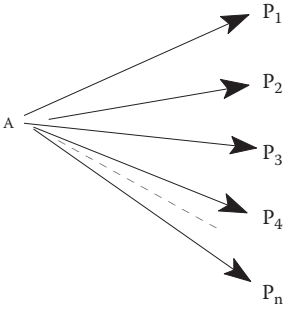

The following expressions are obtained for BRs and PFRs:

$$\frac{c_A}{c_{0A}} = e^{-\sum_{j=1}^{n} k_j \tau}, \tag{3.209}$$

$$\frac{c_i}{c_{0A}} = \frac{c_{0i}}{c_{0A}} + \frac{k_i}{\sum_{j=1}^{n} k_j}\left(1 - e^{-\sum k_j \tau}\right). \tag{3.210}$$

For a CSTR, the solution of mass balances yields

$$\frac{c_A}{c_{0A}} = \frac{1}{\left(1 + \sum_{j=1}^{n} k_j \tau\right)}, \tag{3.211}$$

$$\frac{c_i}{c_{0A}} = \frac{c_i}{c_{0A}} + \frac{k_i \tau}{\left(1 + \sum_{j=1}^{n} k_j \tau\right)}. \tag{3.212}$$

3.8.1.2 Momentaneous and Integral Yield for Parallel Reactions

As a measure of the product distribution, integral (total) and momentaneous yields are often used. Let us assume that component A is consumed by two composite reactions with the following stoichiometry:

$$|\nu_{A1}|\,A \rightarrow |\nu_R|\,R,$$
$$|\nu_{A2}|\,A \rightarrow |\nu_S|\,S.$$

The total yield, $\Phi_{R/A}$, is thus defined as

$$\Phi_{R/A} = \frac{|\nu_{A1}|\,(c_R - c_{0R})}{|\nu_R|\,(c_A - c_{0A})}. \tag{3.213}$$

In other words, it describes the generated amount of R per A, normalized by the stoichiometric coefficients.

The momentaneous yield, $\varphi_{R/A}$, in contrast, describes the normalized ratio between the production rate of R and the consumption rate of A:

$$\varphi_{R/A} = \frac{|\nu_{A1}|\,r_R}{|\nu_R|\,(-r_A)}. \tag{3.214}$$

Analogous expressions can be developed for the product, S, just by replacing r_R and $|\nu_R|$ by r_s and $|\nu_s|$ in Equations 3.213 and 3.214.

With the aid of molar mass balances, one can prove that the total and momentaneous yields obtain similar expressions for a CSTR. The balances for R and A consequently become

$$\frac{c_R - c_{0R}}{\tau} = r_R, \tag{3.215}$$

$$\frac{c_A - c_{0A}}{\tau} = r_A. \tag{3.216}$$

After dividing the previous balances with each other, we obtain

$$\frac{r_R}{-r_A} = \frac{c_R - c_{0R}}{c_A - c_{0A}}. \tag{3.217}$$

This, for instance, can be inserted into the expression for $\Phi_{R/A}$, which thus transforms to a form similar to that of $\varphi_{R/A}$, Equation 3.214.

For BRs and PFRs, the momentaneous and integral yields naturally take different forms, since the reaction rates vary as a function of time or inside the reactor. By setting up the mass balances,

$$\frac{dc_R}{d\tau} = r_R, \tag{3.218}$$

$$\frac{dc_A}{d\tau} = r_A, \tag{3.219}$$

and after combining them, we obtain a differential equation

$$\frac{dc_R}{dc_A} = \frac{r_R}{r_A}, \tag{3.220}$$

which can formally be integrated as follows:

$$\int_{c_{0R}}^{c_R} dc_R = \int_{c_{0A}}^{c_A} \frac{r_R}{r_A}\, dc_A, \tag{3.221}$$

$$c_R - c_{0R} = -\frac{|\nu_R|}{|\nu_A|} \int_{c_{0A}}^{c_A} \varphi_{R/A}\, dc_A. \tag{3.222}$$

Dividing Equation 3.222 by the term $c_{0A} - c_A$, that is, the concentration of unreacted A, yields

$$\frac{c_R - c_{0R}}{c_{0A} - c_A} = \frac{-|\nu_R|}{|\nu_A|\,(c_{0A} - c_A)} \int_{c_{0A}}^{c_A} \varphi_{R/A}\, dc_A. \tag{3.223}$$

After taking into account Equation 3.213, we obtain the total yield and can thus replace the ratio of $\varphi_{R/A}$ and $\varphi_{R/A}$

$$\phi_{R/A} = \frac{\int_{c_A}^{c_{0A}} \varphi_{R/A}\, dc_A}{c_{0A} - c_A} \tag{3.224}$$

This indicates that the integral yield can be obtained as an *integral of the momentaneous yield*. The result is mainly of theoretical interest, since the integral yield is in practice calculated from the definition (Equation 3.213). For the yield of S, analogous expressions are obtained $|\nu_{A1}|$, $|\nu_R|$, c_R, and c_{0R} should just be replaced by $|\nu_{A2}|$, $|\nu_S|$, c_S, and c_{0S} in the above-mentioned equations.

The quantity that we refer to here as *yield* is often denoted as *selectivity* by synthetic chemists. Last but not the least, the reader ought to be reminded of the fact that the term "yield" is used in another context with a different meaning: yield is defined as the amount of product formed per total amount of the reactant—naturally normalized with the stoichiometric coefficients. This "yield" ($y_{R/A}$) would thus assume the following form for the product R:

$$y_{R/A} = \frac{|\nu_{A1}|\,(c_R - c_{0R})}{|\nu_R|\,c_{0A}}. \tag{3.225}$$

3.8.1.3 Reactor Selection and Operating Conditions for Parallel Reactions

In this section, we will discuss the qualitative aspects of selecting the reactor and operating conditions for parallel reactions. We will assume that component A undergoes two irreversible reactions, of which the former gives the desired product, R, and the latter the nondesired product, S:

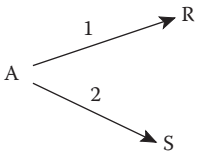

If the generation rates of R and S are given by the empirical expressions:

$$r_R = k_1 c_A^{a_1} \tag{3.226}$$

$$r_S = k_2 c_A^{a_2}, \tag{3.227}$$

one should apparently aim at as large a value as possible for the ratio r_R/r_s. Since this dependence, the so-called *selectivity*, can be written as

$$\frac{r_R}{r_S} = \frac{k_1}{k_2} c_A^{(a_1 - a_2)}, \tag{3.228}$$

we should try and maintain the concentration, c_A, at as high a level as possible, provided that the difference, $a_1 - a_2$, is positive, and at as low a level as possible in case the difference is negative. If $a_1 = a_2$, that is, the reactions are of the same order, the ratio r_R/r_s becomes independent of the concentration level of A. In the latter case, one can eventually force the ratio toward the desired direction by means of a correctly chosen operation temperature, provided that the activation energies of these (parallel) composite reactions have values different from each other. Another possibility would be the addition of an appropriate, selective catalyst. In case parallel, composite reactions are of a different order, the product purity can thus be influenced by the choice of the concentration level in the process. If the concentration of component A, c_A, has to be maintained at a high level, the reactor choice is obvious: a BR or a PFR. At the same time, one should be satisfied with a relatively low conversion, η_A—somewhat worse than in a cascade reactor (Figure 3.19).

In the case of a gas-phase system, the product purity can, in our example, be increased by a higher total pressure or a reduced amount of inert components. If a low value for c_A is desired, then a CSTR is the correct choice for the reactor. The reactor should further be operated so that as high a value for the conversion, η_A, as possible is obtained. In gas-phase reactions, the desired reaction is now promoted by the low total pressure and a high amount of inert components in the system.

Undesirable parallel reactions can thus force us to select a CSTR, although the low production capacity requires a considerably larger reactor volume than in the case of a PFR or a BR.

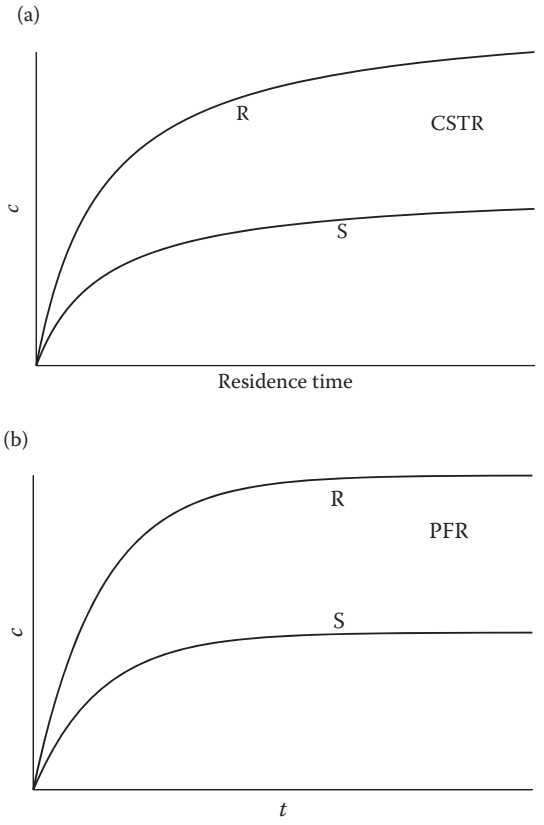

FIGURE 3.19 Concentration evolvements of the components for a composite reaction in a (a) CSTR, and (b) PFR.

For reactions with more complex kinetics, the product quality (purity) may be dependent on the concentration levels of two or more reactive components. For instance, if the generation rates of components R and S are given by the expressions:

$$r_R = k_1 c_A^{a_1} c_B^{b_1}, \tag{3.229}$$

$$r_S = k_2 c_A^{a_2} c_B^{b_2}, \tag{3.230}$$

the selectivity is expressed as

$$\frac{r_R}{r_S} = \frac{k_1}{k_2} c_A^{(a_1 - a_2)} c_B^{(b_1 - b_2)}. \tag{3.231}$$

If component R is the desired product, one should evidently keep both c_A and c_B at as high levels as possible, if both the exponents $(a_1 - a_2)$ and $(b_1 - b_2)$ are positive. If both the exponents are negative, then one should aim at low concentration levels of both reactants. It is often the case that the exponents have different signs—one positive and the other negative. In this case, the desired reaction is favored if the concentration of one of

the reactants is maintained at a relatively high level, whereas the concentration of the other reactant is kept at a relatively low level. This can be achieved in a batchwise operation by a pulsed or a continuous overdose (in relation to the stoichiometry) of one of the reactants. In a continuous operation, different levels of concentrations for different reactants can be realized by adding one of the components as separate side-streams to the separate CSTRs of a cascade reactor, whereas the whole inflow of another component is supplied in the very first reactor in the series.

3.8.1.4 First-Order Consecutive Reactions

In this section, we will discuss the calculation principles for consecutive reactions, that is, situations in which two or more reactions are coupled in a series. An especially interesting question in this connection is how the reactor should be operated in order to obtain the best possible yield of a reactive *intermediate* product. The ideal reactor types are compared in this context. As before, the temperature, density, volume, and volumetric flow rate of the reaction mixture are assumed to remain constant.

Let us consider the case in which a component (A) undergoes two consecutive, irreversible reactions of first order:

$$\mathrm{A} \xrightarrow{k_1} \mathrm{R} \xrightarrow{k_2} \mathrm{S}.$$

Furthermore, an assumption is made that the initial concentrations of R and S are equal to zero.

Since the residence time in a PFR completely coincides with that of a BR, it is evident that the expressions derived for a BR can also be used in connection with a PFR by implementing the residence time, $\tau = V/\dot{V}$. A CSTR, in contrast, requires a separate mathematical analysis. The generation rates for A, R, and S can be written as follows:

$$r_\mathrm{A} = -r_1 = -k_1 c_\mathrm{A}, \tag{3.232}$$

$$r_\mathrm{R} = r_1 - r_2 = k_1 c_\mathrm{A} - k_2 c_\mathrm{R}, \tag{3.233}$$

$$r_\mathrm{S} = r_2 = k_2 c_\mathrm{R}. \tag{3.234}$$

3.8.1.4.1 PFRs and BRs

The molar mass balances for a BR and PFR converge into similar mathematical expressions and can thus be treated simultaneously. The mass balances assume the following form (Equation 3.235):

$$\frac{\mathrm{d}c_i}{\mathrm{d}t} = r_i \tag{3.235}$$

where i = A, R, and S.

After taking into account the rate expressions, these equations can be rewritten as

$$\frac{\mathrm{d}c_\mathrm{A}}{\mathrm{d}\tau} = -k_1 c_\mathrm{A}, \quad \frac{\mathrm{d}c_\mathrm{R}}{\mathrm{d}\tau} = k_1 c_\mathrm{A} - k_2 c_\mathrm{R}, \quad \frac{\mathrm{d}c_\mathrm{S}}{\mathrm{d}\tau} = -k_2 c_\mathrm{R}. \tag{3.236}$$

After integrating Equation 3.236, we obtain

$$c_A = c_{0A} e^{-k_1 t\tau}. \tag{3.237}$$

Inserting this expression for c_A into Equation 3.237 yields

$$\frac{dc_R}{d\tau} = k_1 c_{0A} e^{-k_1\tau} - k_2 c_R, \tag{3.238}$$

which is conveniently written in its more usual form for a linear differential equation of first order:

$$\frac{dc_R}{d\tau} + k_2 c_R = k_1 c_{0A} e^{-k_1\tau}. \tag{3.239}$$

In case c_R equals zero, at $t = 0$, expression 3.239 yields the following form for $c_R(t)$:

$$c_R = \frac{k_1 c_{0A}}{k_2 - k_1}\left(e^{-k_1\tau} - e^{-k_2\tau}\right). \tag{3.240}$$

For the given stoichiometry, $A \rightarrow R \rightarrow S$, the sum of concentrations is obviously constant and equal to c_{0A}, since $c_{0R} = c_{0S} = 0$. We thus obtain

$$c_S = c_{0A} - c_A - c_R, \tag{3.241}$$

which in combination with Equations 3.237 and 3.240 yields the following equation for $c_s(t)$:

$$c_S = c_{0A}\left[1 - \frac{k_1 k_2}{k_2 - k_1}\left(\frac{1}{k_1}e^{-k_1\tau} - \frac{1}{k_2}e^{-k_2\tau}\right)\right]. \tag{3.242}$$

The concentration profiles of A and R are shown in Figure 3.3.

The concentration of the intermediate product, R, goes through a maximum at a certain time, $\tau_{max,PFR}$. This time, $\tau_{max,PFR}$, can be calculated by differentiating Equation 3.240 against time and by solving the equation $dc_R/dt = 0$:

$$\frac{dc_R}{dt} = 0 = \frac{k_1 c_{0A}}{k_2 - k_1}\left(-k_1 e^{-k_1\tau_{max}} + k_2 e^{-k_2\tau_{max}}\right). \tag{3.243}$$

The final result becomes

$$\tau_{max,PFR} = \frac{\ln(k_2/k_1)}{k_2 - k_1}. \tag{3.244}$$

Equation 3.236 indicates that $dc_R/dt = 0$, if $k_1 c_A = k_2 c_R$. Thus, if the maximum value of c_R is denoted as C_{Rmax}, the following is true:

$$\frac{c_{R,max}}{c_A} = \frac{k_1}{k_2}. \tag{3.245}$$

According to Equation 3.237, we know that

$$c_A = c_{0A} e^{-k_1 \tau_{max,CSTR}} \tag{3.246}$$

and the combination of Equations 3.244 through 3.246, finally, leads to an elegant expression:

$$\frac{c_{R,max}}{c_{0A}} = \left(\frac{k_1}{k_2}\right)^{k_2/(k_2-k_1)}. \tag{3.247}$$

In case $k_1 = k_2$, one can show that Equation 3.247 approaches

$$\frac{c_{R,max}}{c_{0A}} = e^{-1} \approx 0.368. \tag{3.248}$$

Thus, the ratio c_{Rmax}/c_{0A} is a universal constant and is independent of the values of rate constants, as given by Equation 3.248.

3.8.1.4.2 Continuous Stirred Tank Reactor

If the consecutive, irreversible reactions of first order (A → R → S) take place in a CSTR, we will assume, as previously, that $c_{0R} = c_{0S} = 0$. The following mass balance is valid:

$$\frac{c_i - c_{0i}}{\tau} = r_i. \tag{3.249}$$

By taking into account the rate expressions, Equations 3.232 through 3.234, one can rewrite these mass balances (the generation rates for A, R, and S) for the case $c_{0R} = c_{0S} = 0$:

$$\frac{c_A - c_{0A}}{\tau} = -k_1 c_A, \tag{3.250}$$

$$\frac{c_R}{\tau} = k_1 c_A - k_2 c_R, \tag{3.251}$$

$$\frac{c_S}{\tau} = k_2 c_R. \tag{3.252}$$

Thus, concentration c_A becomes

$$c_A = \frac{c_{0A}}{1 + k_1 \tau}. \tag{3.253}$$

Inserting Equation 3.251 yields, after a few rearrangements,

$$\frac{c_R}{c_{0A}} = \frac{k_1 \tau}{(1 + k_1 \tau)(1 + k_2 \tau)}. \tag{3.254}$$

After inserting Equation 3.254 into Equation 3.252, we obtain for c_S

$$\frac{c_S}{c_{0A}} = \frac{k_1 k_2 \tau^2}{(1 + k_1 \tau)(1 + k_2 \tau)}. \tag{3.255}$$

TABLE 3.4 Comparison of the Performance of a PFR and BR with a CSTR: The Values of c_{Rmax}/c_{0A} versus k_2/k_1, $k_1\tau_{max,PFR}$, and $k_1\tau_{max,CSTR}$

CSTR		PFRs and BRs		
$k_1\tau_{max,CSTR}$	c_{Rmax}/c_{0A}	k_2/k_1	$k_1\tau_{max,PFR}$	c_{Rmax}/c_{0A}
3.16	0.578	0.10	2.56	0.775
1.41	0.344	0.50	1.39	0.500
1	0.250	1.00	1.00	0.368
0.707	0.172	2	0.693	0.250
0.316	0.0578	10.00	0.256	0.0775

Differentiating Equation 3.254 and solving it for the case in which the equation equals zero yield the residence time, $\tau_{max,CSTR}$, for which c_R reaches a maximum:

$$\tau_{max} = \frac{1}{\sqrt{k_1 k_2}}. \tag{3.256}$$

Inserting the value of $\tau_{max,CSTR}$ into Equation 3.254 finally yields the following expression:

$$\frac{c_{Rmax}}{c_{0A}} = \frac{1}{\left(1 + \sqrt{k_2/k_1}\right)^2}. \tag{3.257}$$

Table 3.4 illustrates how the ratio c_{Rmax}/c_{0A} and the dimensionless groups, $k_1\tau_{max,PFR}$ and $k_1\tau_{max,CSTR}$ (Damköhler number), respectively, depend on the ratio k_2/k_1 in case the initial concentration of species R is zero, $c_{0R} = 0$.

Thus, for a given value of k_1 the value of $\tau_{max(CSTR)}$ is apparently larger than $\tau_{max,PRF}$ for a PFR or a BR, unless $k_2/k_1 = 1$ when $\tau_{max,CSTR} = \tau_{max,PRF}$. The difference in the performance of these reactor classes becomes larger and larger, the further away from unity (1) the value for the ratio k_2/k_1 resides. We can further observe that the ratio c_{Rmax}/c_{0A} in the case of a PFR or a BR always yields values larger than those for a CSTR. In case $k_2/k_1 = 1$, the maximum concentration of the component R obtained in a CSTR is only around 68% of that obtained in the other two reactor classes; when the value $k_2/k_1 = 0.10$ or, alternatively, 10, the percentage is around 75%. We can therefore deduce that the difference in the performance of the different reactor classes is reduced more, further away from unity (1) the value of the ratio k_2/k_1 resides. The mathematical treatment has, consequently, shown that the reactor of choice should be a PFR or a BR, provided that the goal is to obtain a maximum yield of the intermediate product, R, in the system under consideration. Although the analysis is valid for consecutive reactions of first order, the conclusions are also qualitatively valid for all intermediate products for a larger series of irreversible, consecutive reactions.

3.8.1.5 Consecutive-Competitive Reactions

When talking about mixed reactions (series-parallel reactions, consecutive-competitive reactions), we refer to interrelated reactions that contain subprocesses that can be regarded

as both parallel and consecutive, depending on which reaction component is considered. The following reaction is a significant example:

$$A + B \xrightarrow{k_1} R \quad R + B \xrightarrow{k_2} S$$

where A can be considered to undergo consecutive reactions to R and S, whereas B undergoes parallel reactions with A and R. For instance, halogenation and nitrification of aromatic hydrocarbons, as well as reactions between ethene oxide and water or ammonium, belong to these types of reactions. This is often a case of homogeneous reactions of second order.

In our example, the following generation rates of the components are valid in case the reactions can be considered irreversible and elementary:

$$r_A = -k_1 c_A c_B, \tag{3.258}$$

$$r_B = -k_1 c_A c_B - k_2 c_R c_B, \tag{3.259}$$

$$r_R = k_1 c_A c_B - k_2 c_R c_B, \tag{3.260}$$

$$r_S = k_2 c_R c_B. \tag{3.261}$$

A qualitative reasoning soon reveals that the product distribution in this example depends on the relative concentrations of A and B. If component A is introduced extremely slowly in a large excess of B, the intermediate product, R, reacts further with B to yield S. It should thus be possible to carry out the reaction in such a manner that the intermediate product can barely be seen in the analysis. If, on the other hand, B is slowly introduced into an excess of A, R is almost solely formed at the beginning, and the formation of S is initiated only after the concentration of R has reached such a high level that R can compete with A for species B. The concentration of R as a function of supplied B should thus pass through a maximum. Even if we deliver A and B in large quantities from the beginning, c_R should pass through a similar maximum as a function of reacted B.

These mental exercises illustrate the fact that the concentration of B does not influence the product distribution (although it naturally influences the reaction time) in case the concentration of A is high. In both cases, the concentration of R, c_R, has a maximum. On the other hand, if c_A is low and c_B high, in practice, only the final product S is obtained. The underlying reason for the differences in the concentration dependence of the product distribution is that A undergoes consecutive reactions, whereas B undergoes parallel reactions that are both of the same order from the viewpoint of B. An analysis according to these guidelines considerably simplifies the treatment of mixed reactions and, consequently, the reactor selection.

3.8.1.6 Product Distributions in PFRs and BRs

A quantitative treatment of the example discussed above is, as expected, the same for both a PFR and a BR, whereas the case of a CSTR will be tackled separately.

In case both reactions are assumed to proceed irreversibly and to be of second order, the following molar balances can be written for the two first-mentioned types of reactors:

$$\frac{dc_A}{d\tau} = r_A = -k_1 c_A c_B, \tag{3.262}$$

$$\frac{dc_B}{d\tau} = r_B = -k_1 c_A c_B - k_2 c_R c_B, \tag{3.263}$$

$$\frac{dc_R}{d\tau} = r_R = k_1 c_A c_B - k_2 c_R c_B, \tag{3.264}$$

$$\frac{dc_S}{dt} = r_S = k_2 c_R c_B, \tag{3.265}$$

where τ denotes reaction time, for a BR, or residence time ($\tau = V/\dot{V}$; note that here $\dot{V}$ is assumed to be constant), for a PFR. A system of equations of this kind can easily be solved by numerical computations. However, it is difficult to obtain analytical expressions as a function of τ. To study *product distribution*, it is possible to eliminate the time variable by simple means. Equation 3.264 is divided by Equation 3.262 and thus an analytical solution becomes feasible:

$$\frac{dc_R}{dc_A} = -1 + \frac{k_2 c_R}{k_1 c_A}. \tag{3.266}$$

Here c_B disappears, indicating that the ratio dc_R/dc_A does not depend on the concentration level of B. It is of interest to note that for consecutive reactions, A $\rightarrow$ R $\rightarrow$ S, an equation similar to Equation 3.266 is obtained. Therefore, the product distribution should become similar to the consecutive, irreversible reactions of first order. This can be verified by solving Equation 3.266. Consequently, we obtain the following equations for c_R and dc_R/dc_A:

$$c_R = z c_A, \tag{3.267}$$

$$\frac{dc_R}{dc_A} = z + c_A \frac{dz}{dc_A}, \tag{3.268}$$

which, after inserting into Equation 3.266, yields

$$z + c_A \frac{dz}{dc_A} = -1 + \frac{k_2}{k_1} z. \tag{3.269}$$

The separation of variables is now trivial,

$$\int_{z=c_{0R}/c_{0A}}^{z=c_R/c_A} \frac{dz}{((k_2/k_1)-1)\,z - 1} = \int_{c_{0A}}^{c_A} \frac{dc_A}{c_A} \tag{3.270}$$

and we obtain the solution

$$\frac{k_1}{k_2 - k_1} \ln\left[\frac{((k_2/k_1)-1)\,(c_R/c_A) - 1}{((k_2/k_1)-1)\,(c_{0R}/c_{0A}) - 1}\right] = \ln\left(\frac{c_A}{c_{0A}}\right). \tag{3.271}$$

From Equation 3.271, the following expression for c_R as a function of c_A is obtained:

$$\frac{c_R}{c_{0A}} = \frac{k_1}{k_2 - k_1}\left[\left(\frac{c_A}{c_{0A}}\right) - \left(\frac{c_A}{c_{0A}}\right)^{k_2/k_1}\right] + \frac{c_{0R}}{c_{0A}}\left(\frac{c_A}{c_{0A}}\right)^{k_2/k_1}. \tag{3.272}$$

This formula cannot be applied directly as such if k_1 happens to be equal to k_2. For this special case, Equation 3.268 has the following solution:

$$\frac{c_R}{c_{0A}} = \frac{c_A}{c_{0A}}\left[\frac{c_{0R}}{c_{0A}} - \ln\left(\frac{c_A}{c_{0A}}\right)\right]. \tag{3.273}$$

The expressions above, Equations 3.272 and 3.273, thus give the relationship between concentrations c_R and c_A, for BRs and PFRs. The reaction stoichiometry of the reactions implies that

$$c_{0A} - c_A = (c_R - c_{0R}) + (c_S - c_{0S}) \tag{3.274}$$

and, therefore, we obtain the following relationship for c_S:

$$c_S = c_{0A} + c_{0R} + c_{0S} - c_A - c_R. \tag{3.275}$$

Further, the overall stoichiometry yields

$$c_{0B} - c_B = c_R - c_{0R} + 2\,(c_S - c_{0S})\,, \tag{3.276}$$

from which the concentration c_B can be calculated.

Differentiating Equation 3.272 with respect to c_A yields dc_R/dc_A, which should be equal to zero, corresponding to a ratio of c_A/c_{0A} that yields c_{Rmax}. The result is

$$\left(\frac{c_A}{c_{0A}}\right)_{c_{Rmax}} = \left[\frac{k_1^2 c_{0A}}{k_1 k_2 c_{0A} - k_2(k_2 - k_1)c_{0R}}\right]^{k_1/(k_2-k_1)}. \tag{3.277}$$

If c_{0R} is zero, then the equation is simplified to

$$\left(\frac{c_A}{c_{0A}}\right)_{c_{Rmax}} = \left(\frac{k_1}{k_2}\right)^{k_1/(k_2-k_1)}. \tag{3.278}$$

Inserting the ratio c_A/c_{0A}, according to Equation 3.278, into Equation 3.271, yields, for the case c_{0R}=0, the relation

$$\frac{c_{Rmax}}{c_{0A}} = \left(\frac{k_1}{k_2}\right)^{k_2/(k_2-k_1)}, \tag{3.279}$$

which, as expected, is identical to Equation 3.279 for the consecutive reaction, A → R → S.

The derivations presented here support the hypothesis that the concentration level of c_B does not affect that of c_{Rmax}—in the case of mixed reactions where the participating reactions are of the same order in B. For the calculation of $\tau_{max,PFR}$, Equation 3.262 can be integrated numerically, assuming that the concentration of species B, c_B, corresponding to the given concentration of species A, c_A, can *a priori* be calculated from Equation 3.276. Naturally, the same principle can generally be applied for the calculation of the residence time, τ, as a function of c_A in BRs and PFRs.

3.8.1.7 Product Distribution in a CSTR

In case the mixed reactions tackled in the previous section occur in a CSTR, the following molar balances are valid in the steady state:

$$\frac{c_i - c_{0i}}{\tau} = r_i, \tag{3.280}$$

where $i = A, R, S$.

After insertion of the rate expressions for $r_A \ldots r_s$ and the space time, $\tau = V/\dot{V}$, the above balances are transformed to a new form:

$$c_{0A} - c_A = \tau k_1 c_A c_B, \tag{3.281}$$

$$c_{0B} - c_B = \tau(k_1 c_A c_B + k_2 c_R c_B), \tag{3.282}$$

$$c_{0R} - c_R = \tau(k_2 c_R c_B - k_1 c_A c_B), \tag{3.283}$$

$$c_{0S} - c_S = -\tau k_2 c_R c_B. \tag{3.284}$$

Dividing Equation 3.283 by Equation 3.281 yields

$$\frac{c_{0R} - c_R}{c_{0A} - c_A} = -1 + \frac{k_2 c_R}{k_1 c_A}, \tag{3.285}$$

from which the following form is obtained for the concentration c_R:

$$c_R = \frac{c_A\,(c_{0A} - c_A + c_{0R})}{c_A + (k_2/k_1)\,(c_{0A} - c_A)}. \tag{3.286}$$

The stoichiometric equations for the system, as well as all the concentrations, can, therefore, easily be calculated for a given value of the concentration of A. The space time for a CSTR is given by Equation 3.287:

$$\tau = \frac{c_{0A} - c_A}{k_1 c_A c_B} \tag{3.287}$$

For the special case $c_{0R} = 0$, one obtains through derivating Equation 3.286, which is set to be equal to zero, the following expression for the value of c_A that is related to the maximum value of c_R:

$$c_{A,C_{Rmax}} = \frac{c_{0A}}{1 + (k_1/k_2)}. \tag{3.288}$$

Inserting this value of c_A into Equation 3.286 yields the maximum concentration of component R, c_{Rmax}, for the case in which the initial concentration $c_{0R} = 0$:

$$c_{R,max} = \frac{c_{0A}}{\left(1 + \sqrt{(k_2/k_1)}\right)^2}. \tag{3.289}$$

Expression 3.289 is, evidently, the same as that obtained for consecutive reactions $A \rightarrow R \rightarrow S$.

3.8.1.8 Comparison of Ideal Reactors

On the basis of the derivations of the previous section, it is evident that the ratio c_{Rmax}/c_{0A} for that specific mixed reaction depends on the ratio k_2/k_1, according to the principles illustrated in the table presented for consecutive reactions (Table 3.4). Thus, PFRs and BRs produce a higher concentration of the intermediate product than we can achieve in a CSTR. The values given in Table 3.4 for $k_1\tau_{max,CSTR}$ and $k_1\tau_{max,PFR}$ are therefore valid for two consecutive reactions of first order only (Figure 3.20).

Generally, one can state that in mixed reactions, it is possible to classify the reaction species into two categories, one of which contains species undergoing consecutive and the other parallel (composite) reactions. If component A undergoes consecutive reactions, the highest yield of the intermediate product, R, is obtained by avoiding mixing mixtures with different values of conversion, η_A. Therefore, PFRs and BRs give higher yields of the intermediate product than a CSTR, in which the inflow containing unreacted species ($\eta_A = 0$) is mixed with a solution in which η_A has a relatively high value. If component B undergoes parallel reactions that are of the same order from B's point of view, the concentration level of B does not affect product distribution. However, it affects the reaction time that is required (average residence time). In case parallel reactions are of a different order from B's point of view, the concentration of B, c_B, does indeed affect the product distribution.

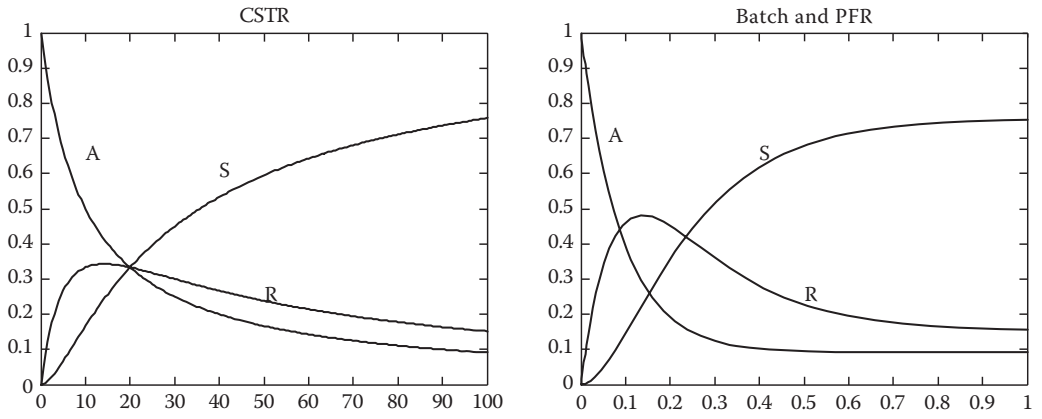

FIGURE 3.20 A consecutive reaction $A \rightarrow R \rightarrow S$. Concentration evolvements in a CSTR (left) and in BR and PFRs, respectively (right).

3.9 NUMERICAL SOLUTION OF MASS BALANCES FOR VARIOUS COUPLED REACTIONS

As discussed above, the possibilities of solving balance equations analytically are very limited, but numerical simulations provide a general approach. Examples of reaction systems are given in Figure 3.21 on numerical simulations of concentration profiles; as a function of residence time (BRs and PFRs) and average residence time (CSTR), they are illustrated in Figure 3.22. The reactors were assumed to be isothermal, and the density of the reaction mixture was constant during the course of the reaction. In the simulation of BRs and PFRs, the BD method was applied. The CSTR model was solved using the Newton–Raphson method, and the space time (τ) was used as a *continuity parameter* in the solution of the balance equations. At the space time, $\tau + \Delta\tau$, the solution of the previous space time, τ, was utilized as the initial estimate. In this way, convergence toward the correct solution was easily guaranteed [10]. For some of the reaction systems presented in Figure 3.21, analytical solutions of the balance equations can be found; this is true, for instance, for the first-order consecutive and parallel reactions (1) and (3) (Table 3.3). In case the reactions are reversible, however, the analytical solutions tend to become cumbersome.

Reaction systems (1) and (3) represent cases in which all reactions are of first order. For reaction systems (2) and (4), it is, however, characteristic that reactions of different orders occur in the consecutive or composite (parallel) reaction scheme. Scheme (5) represents mixed reactions (*consecutive-competitive reactions*) that commonly occur in an industrial context.

Reaction scheme (6) is typical in the oxidation of hydrocarbons (A, R, and S) in the presence of a large amount of oxygen. Therefore, the reactions become pseudo-first-order from the viewpoint of hydrocarbons, and the practically constant oxygen partial pressure can be included in the rate constants. The intermediate product, R, represents a partial oxidation product (such as phthalic anhydride in the oxidation of *o*-xylene or maleic anhydride in the oxidation of benzene), whereas S represents the undesirable byproducts (CO_2, H_2O). The triangle system (7) represents monomolecular reactions such as isomerizations: A, for instance, can be 1-butene, which is subject to an isomerization to *cis*-2-butene and *trans*-2-butene.

Simulation results in Figure 3.22 require a few explanat ions and comments. A plug flow model usually gives a higher concentration maximum of the intermediate product, R, than a CSTR model. On the other hand, the concentration level decreases more slowly with increased residence time in a CSTR. The gap between the conversion of the reactants for CSTR and plug flow models expands rapidly with increasing residence time. Most of the effects illustrated in Figure 3.22 can be predicted qualitatively, although some effects are not a priori as evident. For instance, Figure f shows that a concentration maximum of the product R in a parallel system $A \leftrightarrow R$, $A \leftrightarrow S$ is possible, if the first reaction proceeds rapidly and reversibly, whereas the second reaction proceeds irreversibly. Irreversibility is, however, a necessary condition for a concentration maximum in a parallel scheme. This is illustrated by Figures g and h for the scheme $A \leftrightarrow R$, $A + B \leftrightarrow S$: if one of the reactions proceeds faster than the other one obtains, at first, a large amount of the

(a)

1. $\mathrm{A} \underset{k_2}{\overset{k_1}{\rightleftharpoons}} \mathrm{R} \underset{k_4}{\overset{k_3}{\rightleftharpoons}} \mathrm{S}$

2. $\mathrm{A} + \mathrm{B} \underset{k_2}{\overset{k_1}{\rightleftharpoons}} \mathrm{R} \underset{k_4}{\overset{k_3}{\rightleftharpoons}} \mathrm{S}$

3. $\mathrm{A} \underset{k_4}{\overset{k_3}{\rightleftharpoons}} \mathrm{S}$, $\mathrm{A} \underset{k_2}{\overset{k_1}{\rightleftharpoons}} \mathrm{R}$

4. $\mathrm{A} + \mathrm{B} \underset{k_4}{\overset{k_3}{\rightleftharpoons}} \mathrm{S}$, $\mathrm{A} + \mathrm{B} \underset{k_2}{\overset{k_1}{\rightleftharpoons}} \mathrm{R}$

5. $\mathrm{A} + \mathrm{B} \xrightarrow{k_1} \mathrm{R}$; $\mathrm{R} + \mathrm{B} \xrightarrow{k_3} \mathrm{S}$; $\mathrm{S} + \mathrm{B} \xrightarrow{k_5} \mathrm{T}$

6. $2\mathrm{A} \xrightarrow{k_1} \mathrm{R} \xrightarrow{k_3} \mathrm{S}$, $2\mathrm{A} \xrightarrow{k_5} \mathrm{S}$

7. $\mathrm{A} \underset{k_2}{\overset{k_1}{\rightleftharpoons}} \mathrm{R}$, $\mathrm{A} \underset{k_4}{\overset{k_3}{\rightleftharpoons}} \mathrm{S}$, $\mathrm{R} \underset{k_6}{\overset{k_5}{\rightleftharpoons}} \mathrm{S}$

(b) Example (case 5)

$\mathrm{A} + \mathrm{B} \rightarrow \mathrm{R}$ Step 1

$\mathrm{R} + \mathrm{B} \rightarrow \mathrm{S}$ Step 2

$\mathrm{S} + \mathrm{B} \rightarrow \mathrm{T}$ Step 3

$$N^{\mathrm{T}} = \begin{bmatrix} -1 & -1 & 1 & 0 & 0 \\ 0 & -1 & -1 & 1 & 0 \\ 0 & -1 & 0 & -1 & 1 \end{bmatrix} \begin{matrix} \text{Step 1} \\ \text{Step 2} \\ \text{Step 3} \end{matrix} \qquad R = \begin{bmatrix} k_1 & c_{\mathrm{A}} & c_{\mathrm{B}} \\ k_3 & c_{\mathrm{R}} & c_{\mathrm{B}} \\ k_5 & c_{\mathrm{S}} & c_{\mathrm{B}} \end{bmatrix} = \begin{bmatrix} R_1 \\ R_2 \\ R_3 \end{bmatrix}$$

$$\begin{matrix} A & B & R & S & T \end{matrix}$$

$$NR = \begin{bmatrix} -1 & 0 & 0 \\ -1 & -1 & -1 \\ 1 & -1 & 0 \\ 0 & 1 & -1 \\ 0 & 0 & 1 \end{bmatrix} \begin{bmatrix} R_1 \\ R_2 \\ R_3 \end{bmatrix} = \begin{bmatrix} r_{\mathrm{A}} \\ r_{\mathrm{B}} \\ r_{\mathrm{R}} \\ r_{\mathrm{S}} \\ r_{\mathrm{T}} \end{bmatrix} = r$$

FIGURE 3.21 Selected isothermal model reactions (a); examples of numerical solutions to the model reaction (5) (b).

product from the faster reaction. This reaction product thereafter reacts reversibly back to the original reactant, which, in turn, reacts along the other, slower, reaction pathway to the second product molecule. Therefore, it is feasible to assume that there exists an optimal residence time for the maximum concentration of the product, although we are dealing with a parallel reaction. Those concentration maxima that exceed the equilibrium concentrations obtainable at infinitely long residence times are called *superequilibrium concentrations*.

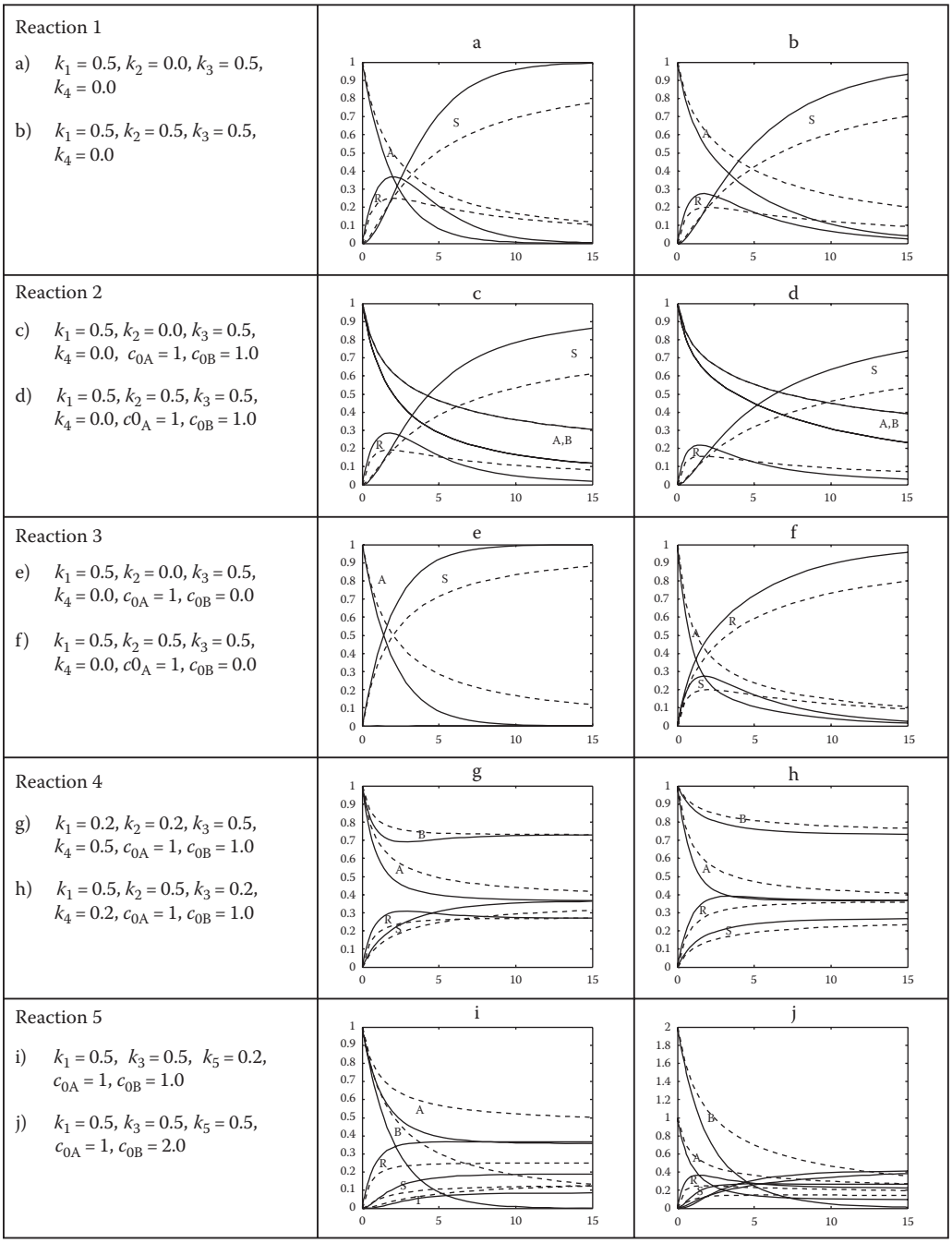

FIGURE 3.22 Simulated concentration profiles for the model reactions in Figure 3.21. — A PFR or a BR; - - - a CSTR.

The simulation results from the combined reaction scheme (5), in Figure 3.21, illustrate clearly the differences between the ideal reactor types, as well as the effect of the concentration of the composite (parallel) reactant, B, on product distribution. If the amount of B is maintained at a low level (Figure 3.21), a great deal of the intermediate product,

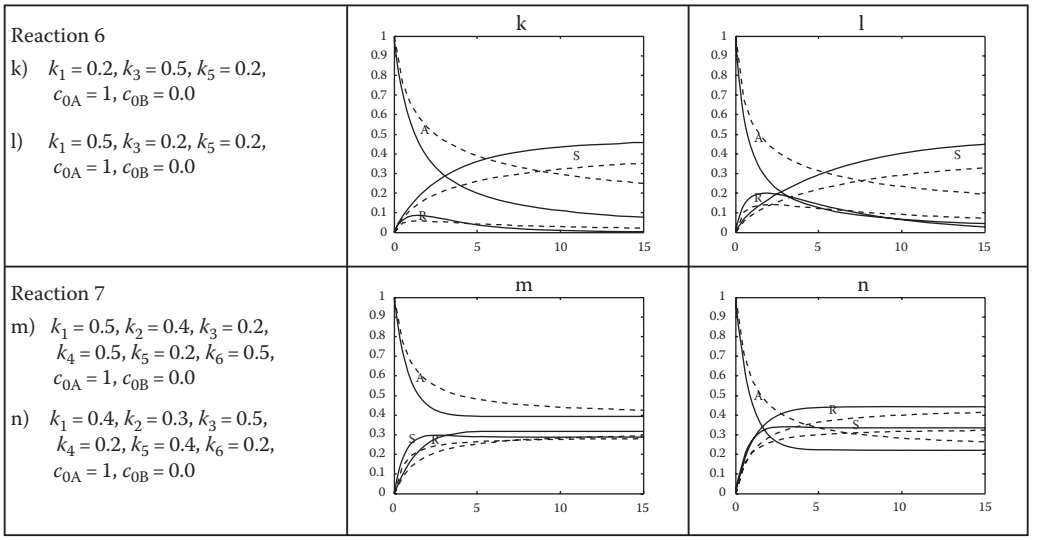

FIGURE 3.22 continued.

R, is obtained. Its relative amount is also quite stable within a wide range of residence times. If the proportion of B is high (Figure 3.21j), the proportion of the final product, S, increases dramatically. Simultaneously, the concentration of R just attains a minimum or a maximum.

REFERENCES

1. Trambouze, P., van Langenhem, H., and Wauquier, J.P., *Chemical Reactors—Design/Engineering Operation*, Editions Technip, Paris, 1988.
2. Froment, G. and Bischoff, K., *Chemical Reactor Analysis and Design*, 2nd Edition, Wiley, New York, 1990.
3. Levenspiel, O., *Chemical Reaction Engineering*, 3rd Edition, Wiley, New York, 1999.
4. Vejtasa, S.A. and Schmitz, R.A., An experimental study of steady state multiplicity and stability in an adiabatic stirred reactor, *AIChE J.*, 16, 410–419, 1970.
5. Nauman, E.B., *Chemical Reactor Design, Optimization and Scaleup*, McGraw-Hill, New York, 2001.
6. Rodigin, N.M. and Rodigina, E.N., *Consecutive Chemical Reactions*, Van Nostrand, New York, 1964.
7. Reid, R.C., Prausnitz, J.M., and Poling, B.E., *The Properties of Gases and Liquids*, 4th Edition, McGraw-Hill, New York, 1988.
8. Salmi, T. and Lindfors, L.-E., A program package for simulation of coupled chemical reactions in flow reactors, *Comput. Ind. Eng.*, 10, 45–68, 1986.
9. Salmi, T., A computer exercise in chemical reaction engineering and applied kinetics, *J. Chem. Edu.*, 64, 876–878, 1987.
10. Fogler, H.S., *Elements of Chemical Reaction Engineering*, Prentice-Hall, Englewood Cliffs, NJ, 1999.

CHAPTER 4

Nonideal Reactors: Residence Time Distributions

4.1 RESIDENCE TIME DISTRIBUTION IN FLOW REACTORS

Several reactors deviate from the ideal flow patterns presented in the previous chapters. This is why it is important to understand the meaning of residence time distribution (RTD) in the system under consideration. In this chapter, a basic characterization of RTDs will be presented. It is relevant, however, to emphasize that in studies of purely physical systems, such as different kinds of mixing chambers, knowledge of the RTD of the system can be considerably beneficial. Before the actual, detailed treatment of the problem, we will briefly define the concepts of residence time and RTDs.

4.1.1 RESIDENCE TIME AS A CONCEPT

Let us assume that we have a reactor system with the volume V_R as in Figure 4.1. A volumetric flow rate $\dot{V}$ passes through this volume. Consequently, at a certain point of time, we will notice one of the incoming elements, which we will follow on its journey through the reactor. In terms of its stay, the element has the age zero seconds (0 s) at the specific moment at which it emerges in the inlet of the reactor. Nevertheless, its age (t_a) increases, consequently, in parallel with the "normal" clock time (t_c). When this element—sooner or later—leaves the reactor, it would have reached a certain age. We refer to this time as the residence time of the element. The residence time of an element—or a *volume element*—is thus defined as the period that passes between the time an element enters the reactor and the time it leaves the reactor (at certain points in time). To simplify the illustrative scheme below, index r has been excluded. Thus, the residence time is denoted as t.

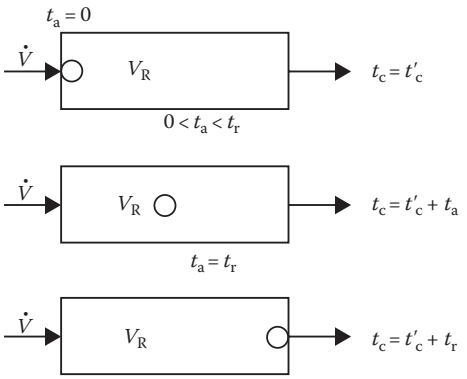

FIGURE 4.1 A reactor system at three different points in time.

The above illustration reflects the same reactor system at three different points in time. At the time it leaves the reactor, the particle under consideration has reached its maximum age that is equal to its residence time, t_r, which we will denote hereafter as t.

If the reactor is a plug flow one, all particles in the same, arbitrarily chosen cross-section will be of the same age. All volume elements would have thus reached the same age once they leave the reactor. This is why they also have the same residence time. As a consequence, in an ideal PFR, there is no distribution of residence times of any kind.

In reactors with some degree of backmixing, however, this cannot be achieved, and there is always a distribution of the residence times of the volume elements. The largest possible distribution of residence times is found in CSTRs, in which the residence times of individual volume elements are spread throughout the time frame, from zero to infinity.

A PFR can serve as the initial starting point for further analysis and for study of the reasons for the deviations from the initial state in which the reactor is assumed to reside. In reactors equipped with a stirrer, it is possible to create an RTD that ranges from one close to a plug flow to almost complete backmixing. Various flow conditions can be realized in one reactor, simply by varying the stirring speed or the stirrer type (Figure 4.2). Sometimes, as efficient mixing as possible is required. Abnormally large deviations from the desired ideal case can occur as a result of a failed design as indicated in Figure 4.2.

In packed beds used for catalytic processes (Chapter 5), the actual packing causes a certain amount of backmixing and, therefore, related deviations in the residence time. We should, however, note that the packing in many cases favors good radial backmixing as well as limited axial backmixing. In fact, in these cases, the reactor will resemble a PFR considerably (Figure 4.3). An RTD can even be created in a packed bed as a result of "short-circuiting" of a part of the flow. This, in turn, can be caused by unsuccessful packing of the solid phase, such as a catalyst.

Differences in the length of the residence time can even be caused by *convective backmixing*. This in turn is caused by temperature gradients. A plausible explanation for this can be given by the following example: If we assume that an exothermic reaction takes place in a tube reactor in the absence of external cooling, it is very likely that a temperature profile illustrated in Figure 4.4a will emerge, in the given cross-section (the flow direction coincides

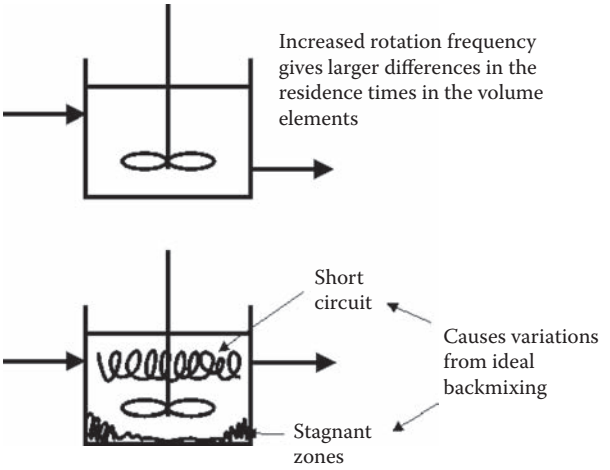

FIGURE 4.2 A reactor equipped with a mixer. Effects of different mixing rates and an illustration of stagnant zones due to inappropriate mixing.

with that of the T coordinate), since the flow velocity close to the reactor wall is lower than that in the center. Therefore, the reaction would have proceeded further close to the reactor walls. At this point, if we apply external cooling, the two separate effects result in the final temperature profile illustrated in Figure 4.4b.

The presence of an RTD in a chemical reactor is—in most cases—considered as an undesirable phenomenon. For this reason, the volume of a CSTR in most reactions has to be larger than that of a PFR to reach the same degree of conversion. On the other hand, one should keep in mind that there are situations in which we wish to create a certain, well-defined RTD. There may be several reasons for this: for example, process control or product quality aspects. Regardless of whether an RTD is desired or not, its experimental determination is often inevitable.

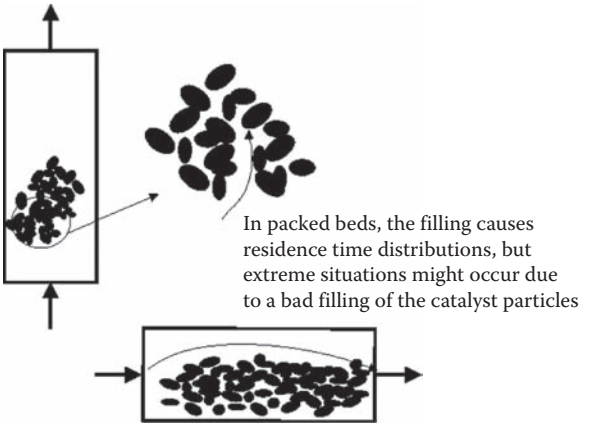

FIGURE 4.3 Effect of packing on RTD.

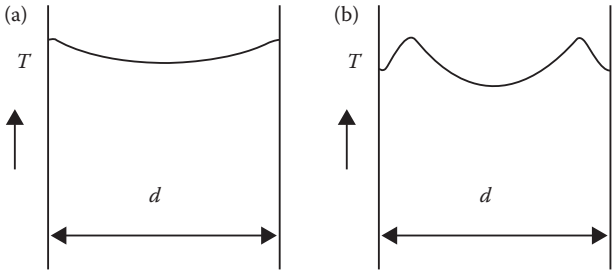

FIGURE 4.4 Plausible temperature profiles in a tube reactor (a) without and (b) with external cooling. Case: convective remixing.

4.1.2 METHODS FOR DETERMINING RTDs

The RTD of a chemical reactor can be determined by using tracer substances and, consequently, by tracing every volume element that passes through the reactor. We attempt to determine the length of the time the volume elements reside in the reactor. In other words, we attempt to determine the RTD of the species.

4.1.2.1 Volume Element

As the name already indicates, the tracer technique is based on the use of a suitable added substance that we can easily detect or trace (Figure 4.5). This is realized by introducing the tracer in the reactor system (usually via the inlet) and monitoring its concentration at a certain location (usually via the outlet). The approach is illustrated in the scheme below.

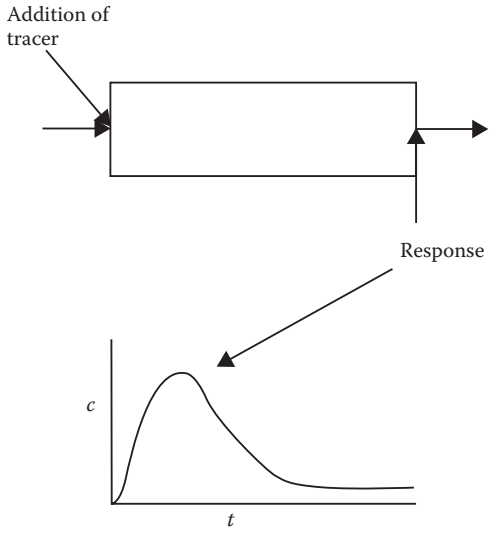

FIGURE 4.5 An example of the implementation of a marker substance (tracer) technique, together with its response curve.

For a tracer to be suitable for dynamic studies, it should satisfy certain criteria. The most important ones are listed below:

- There should be a correspondence between the flowing media and the tracer, that is, the tracer should behave as similarly as possible to the component under consideration.
- The tracer should not be adsorbed by the reactor system.
- The tracer should not undergo a chemical or any other transformation. However, if it does, the transformation process should be known in detail.

In an industrial context, we often use radioactive isotopes as tracers. These do break down, but the breakdown process is well known, defined, and easy to take into account. The isotopes can be introduced into the system in several ways, which makes it significantly easier to attain the correspondence mentioned above. Keeping in mind the radiation risks, we generally choose isotopes with a relatively short half-life. Species other than radioactive ones with other measurable properties can also be utilized as tracers.

4.1.2.2 Tracer Experiments

Experimental methods for determining RTDs can be classified into three major categories, depending on how the tracer is introduced into the system. The use of all of these three methods yields specific variations in the concentration at the outlet. This in turn affects the mathematical treatment of the experimental measurement results. Some of the most common methods are briefly summarized below:

- In the *pulse method*, the tracer is introduced momentarily (as a pulse) and the resulting response shows a maximum as illustrated in Figure 4.6a. If the tracer is introduced over a very short time interval—infinitesimally short—the pulse is called an *impulse*, and the mathematical treatment then becomes quite simple. The tracer can also be introduced by including several consecutive pulses of varying lengths in the system. In this case, we discuss a so-called pulse train.
- A stepwise introduction of the tracer would result in abrupt changes in the measurable properties, maintaining the new level. In other words, a constant level is replaced by another constant level. This method (Figure 4.6b) induces a stepwise response that more or less slowly approaches—from the first constant level—the newly established constant level, a new steady state.
- Sometimes, a *periodically changing* (oscillating) supply of the tracer is applied. The response obtained is illustrated in Figure 4.6c. Although this approach has some theoretical advantages, we should mention that there may be significant experimental difficulties.

4.2 RESIDENCE TIME FUNCTIONS

The functions discussed in this section form the theoretical foundation of RTDs. The fundamental concept of RTD functions was presented by P.V. Danckwerts in a classical paper in the 1950s [1]. The derivation of the residence time functions starts on a microscale,

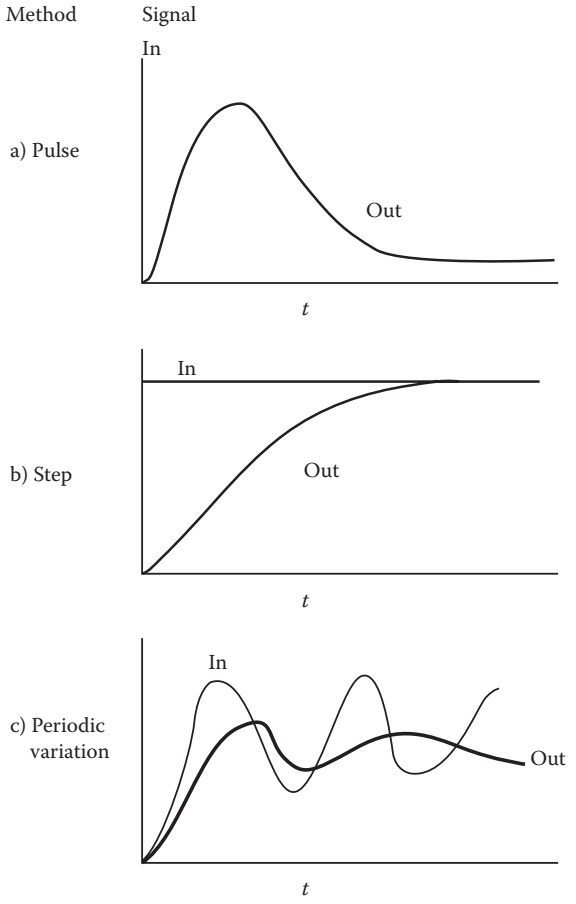

FIGURE 4.6 Illustration of a (a) pulse-wise, (b) stepwise, and (c) oscillating supply of the tracer.

that is, the flowing medium is thought to consist of small volume elements. The population under consideration consists of elements in the reactor outflow. Below, we will study the single species, the elements, and compare them with each other in terms of their respective residence times that represent the variable.

1. *Population*: elements in the outflow.
2. *Object*: a single species, elements.
3. *Variable*: the residence times of the elements.

In the following, the most important residence time functions are described.

4.2.1 POPULATION DENSITY FUNCTION $E(t)$

At an arbitrarily chosen moment of time, t_c, over an infinitesimal time interval, dt_c, if we analyze the outflow, $\dot{V}$, from a reactor (with volume V_R, see below) operating at

a steady state, we find that the volume element, $\dot{V}\,\mathrm{d}t_c$, contains elements with variable residence times.

If we consider the amount of substance to correspond with the number of elements, the number of elements in the volume element at the outlet can be expressed as follows:

$$\dot{V}\,\mathrm{d}t_c \cdot \frac{n}{V} \tag{4.1}$$

or

$$\frac{n}{V}\,\mathrm{d}V, \tag{4.2}$$

where the ratio n/V denotes the number of the substance divided by the volume of the mixture. In this amount of species, most of the volume elements have different residence times. However, some of the elements do have similar—or almost similar—residence times, which can be ascribed to the fact that they reside in the interval $t + \mathrm{d}t$. The total number of the latter species (illustrated in Figure 4.7 by dots inside the volume element) that can be found in the volume element under consideration is given by the following expression:

$$\frac{n'}{V}\,\mathrm{d}V. \tag{4.3}$$

It is practical to give the number of species with residence times between t and $t + \mathrm{d}t$ as a fraction of the total number of elements in the volume element under consideration. This fraction, with the ratio n'/n, is denoted as $E(t)\,\mathrm{d}t$, where $E(t)$ is the so-called density function:

$$\frac{n'}{n} = E(t)\,\mathrm{d}t. \tag{4.4}$$

An integration of $E(t)\,\mathrm{d}t$ from the residence time zero to infinity ($0 \rightarrow \infty$) implies that all the species in the volume element are taken into account, that is, the sum of the amounts n', n'', n''', and so on. If this sum is equal to n, on the basis of Equation 4.4, we obtain

$$\int_0^\infty E(t)\,\mathrm{d}t = 1. \tag{4.5}$$

We can observe that the density function has the unit s^{-1} (Equations 4.4 and 4.5). The principal form of the function for an arbitrary reactor is illustrated in Figure 4.8.

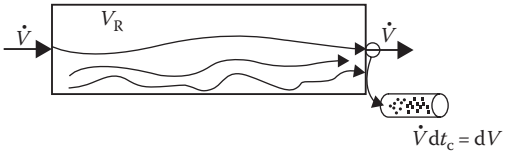

FIGURE 4.7 A reactor with the volume V_R operating in a steady state.

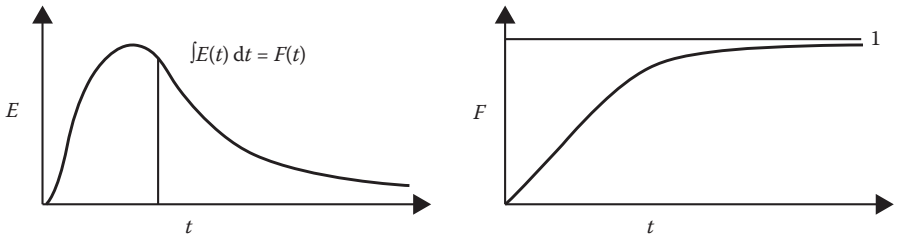

FIGURE 4.8 $E(t)$ and $F(t)$, appearance and principal form.

Thus, on its way out of the reactor, in the volume element, there are species with variable residence times. The species in the volume element that have similar residence times, however, must have been introduced into the reactor at the same time. This is why we can even derive Equations 4.4 and 4.5 on the basis of a volume element *entering* the reactor. In this case, function $E(t)\,\mathrm{d}t$ describes that portion of the elements in the volume element that attains residence times between t and $t + \mathrm{d}t$. If the distribution pattern of the species is known in the volume element leaving the reactor (at the outlet), it is possible to predict the RTD in an incoming volume element. A precondition for this, however, is that the system should have reached its steady state and that the flow conditions should remain constant during the time the volume element passes the system.

4.2.2 DISTRIBUTION FUNCTIONS $F(t)$ AND $F^*(t)$

Starting from the density function, $E(t)$, it is possible to derive two so-called distribution functions: $F(t)$ and $F^*(t)$. The first one, $F(t)$, is the integral function of $E(t)$ and can, therefore, be written as follows:

$$F(t) = \int_0^t E(t)\,\mathrm{d}t \tag{4.6}$$

$F(t)$ is dimensionless and monotonously increasing, and its appearance and the principal form are illustrated in Figure 4.8.

Equations 4.5 and 4.6 readily yield

$$F(t_\infty) = \int_0^\infty E(t)\,\mathrm{d}t = 1. \tag{4.7}$$

The physical explanation of $F(t)$ is as follows: $F(t)$ describes the portion of the incoming volume element that remains inside the reactor for a period of time between 0 and t or that specific portion of the outflowing volume element that has reached a residence time between 0 and t.

The latter distribution function, $F^*(t)$, is a complement function to $F(t)$ and is defined according to the following expression.

$$F^*(t) = 1 - F(t) = 1 - \int_0^t E(t)\,\mathrm{d}t. \tag{4.8}$$

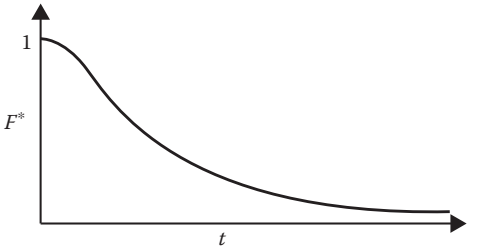

FIGURE 4.9 The appearance of $F^*(t)$.

$F^*(t)$ is monotonously decreasing and has the following principal form:

$F^*(t)$ describes that portion of the volume element flowing in or out that has the residence time $\geq t$ and remains, therefore, inside the reactor for the period of time denoted by t (Figure 4.9).

4.2.3 INTENSITY FUNCTION $\lambda(t)$

An expression for the intensity function $\lambda(t)$ can be formed from the functions $E(t)$ and $F^*(t)$:

1. $F^*s(t)$: that portion of the incoming volume element that has the residence time $\geq t$, that is, that portion that resides inside the reactor at the time t.
2. $E(t)\,\mathrm{d}t$: that portion of the incoming volume element that leaves the reactor within the time interval from t to $t + \mathrm{d}t$.
3. $\lambda(t)\,\mathrm{d}t$: that fraction of $F^*(t)$ that leaves the reactor within the time interval from t to $t + \mathrm{d}t$, that is, the fraction that separates from the fraction inside the reactor at the exact moment in question.

After taking into account the above definitions, we can create the following expression:

$$\lambda(t) = \frac{E(t)}{F^*(t)}. \tag{4.9}$$

4.2.4 MEAN RESIDENCE TIME

The concept of average residence time is defined here in a manner similar to the expected value in mathematical statistics:

$$\bar{t} = \int_0^\infty tE(t)\,\mathrm{d}t. \tag{4.10}$$

Thus, time $\bar{t}$ can be determined by a numerical integration from t versus $E(t)$ data:

$$\bar{t} = \int_0^\infty t\,\mathrm{d}F(t). \tag{4.11}$$

4.2.5 *C* FUNCTION

All the functions treated so far are of a theoretical nature. The association between them and the *C* function is relatively simple. The *C* function is determined on the basis of real experiments with tracers. The information in the *C* function is illustrated by the following derivation. The notations are related to Figure 4.10 below.

On the basis of the applied principles, it is possible to write $c(t)'_c \dot{V}\, dt_c = n\, E(t)\, dt$. Since $t'_c - t_c = t$, the concentration at the outlet can even be related to the residence time, t, so that $c(t'_c) = c(t)$ and $dt_c = dt$. This implies that

$$E(t) = \frac{c(t)\dot{V}}{n}. \tag{4.12}$$

Insertion of the time, t, into the equations implies that the counting of time starts from the time of injection. If n/V_R is denoted as $c(0)$, Equation 4.12 transforms to a new form:

$$E(t) = \frac{c(t)\dot{V}}{c(0)V_R} = \frac{\dot{V}}{V_R} C(t). \tag{4.13}$$

The *C* function is, consequently, defined as the ratio $c(t)/c(0)$ or as a response to the impulse. By combining Equations 4.5 and 4.12, one is able to show that

$$\int_0^\infty C(t)\, dt = \frac{V_R}{\dot{V}}. \tag{4.14}$$

4.2.6 DIMENSIONLESS TIME

The calculations can often be simplified by introducing a new kind of time, dimensionless time. Furthermore, the comparison of residence times obtained from different types of equipment becomes more informative if they are expressed as normalized residence times. In the following, the normalized time will be denoted as θ with the following definition:

$$\theta = \frac{t}{V_R/\dot{V}} \quad \text{or} \quad \frac{V_R}{\dot{V}} = \bar{t}, \quad \theta = \frac{t}{\bar{t}}. \tag{4.15}$$

Based on this definition, Equation 4.15, as well as the functions derived earlier, new relations between the functions can be derived. Some of these are listed in Table 4.1.

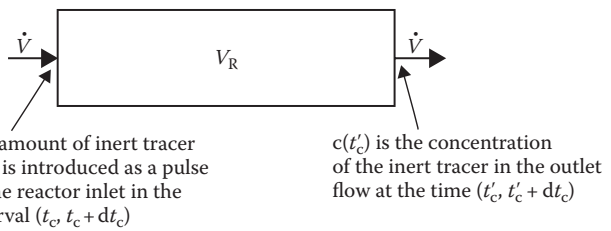

FIGURE 4.10 Determination of the *C* function.

TABLE 4.1 Relationships between Residence Time Functions

$\theta = \dfrac{t}{V_r/\dot{V}} \quad \theta = \dfrac{t}{\bar{t}} \quad \text{if} \quad \bar{t} = \dfrac{V_r}{\dot{V}}$
$E(t)\,dt = E(\theta)\,d\theta \quad \lambda(t)\,dt = \lambda(\theta)\,d\theta$
$F(t) = F(\theta) \quad F^*(t) = F^*(\theta) \quad C(t) = C(\theta)$
$E(t) = \dfrac{dF(t)}{dt} = -\dfrac{dF^*(t)}{dt} = \dfrac{1}{\bar{t}}C(t) = \dfrac{1}{\bar{t}}E(\theta)$
$F(t) = \int_0^t E(t)\,dt = 1 - F^*(t) = F(\theta)$
$\lambda(t) = \dfrac{E(t)}{F^*(t)} = \dfrac{E(t)}{1 - F(t)} = \dfrac{E(t)}{\bar{t}I(t)} = \dfrac{1}{\bar{t}}\lambda(\theta)$
$C(t) = \bar{t}E(t) = \bar{t}\dfrac{dF(t)}{dt} = C(\theta)$
$\int_0^\infty E(t)\,dt = \int_0^\infty E(\theta)\,d\theta = 1$
$\int_0^\infty I(t)\,dt = 1 = \dfrac{1}{\bar{t}}\int_0^\infty F^*(t)\,dt = \int_0^\infty F^*(\theta)\,d\theta$
$\int_0^\infty C(t)\,dt = \int_0^\infty tE(t)\,dt = \bar{t} = \bar{t}\int_0^\infty C(\theta)\,d\theta$

4.2.7 VARIANCE

In the treatment of the theoretically calculated and experimentally obtained residence time functions, the concept of variance is useful, particularly for the comparison of different theories of RTD. Variance is defined as, in mathematical statistics, that is, the quadratic value of standard deviation:

$$\sigma_t^2 = \int_0^\infty (t - \bar{t})^2 E(t)\,dt = \int_0^\infty t^2 E(t)\,dt - \bar{t}^2. \tag{4.16}$$

The variance can also be expressed with the dimensionless time θ. The following expression is obtained:

$$\sigma_\theta^2 = \int_0^\infty (\theta - 1)^2 E(\theta)\,d\theta = \int_0^\infty \theta^2 E(\theta)\,d\theta - \bar{t}^2. \tag{4.17}$$

There exists, naturally, a simple relation between the variances, σ_t^2, and σ_θ^2, which is obtained from Equations 4.15 and 4.16. The result is represented by Equation 4.18:

$$\sigma_t^2 = \bar{t}^2\sigma_\theta^2. \tag{4.18}$$

4.2.8 EXPERIMENTAL DETERMINATION OF RESIDENCE TIME FUNCTIONS

The distribution functions, $E(t)$ and $F(t)$, can easily and efficiently be determined by tracer experiments. In this section, we will discuss the ways in which distribution functions can be obtained from primary experimental data. Let us assume that a continuously operating analytical instrument is available. The instrument should be installed at the outlet of

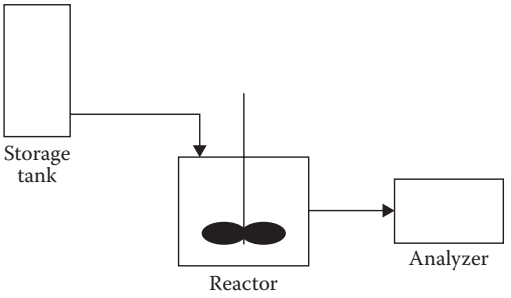

FIGURE 4.11 Measuring the signal from tracer experiments on-line.

the reactor (Figure 4.12). Typically, the concentration of the tracer can be related to the measured signal (s) by means of a linear dependence:

$$s = a + bc(t), \tag{4.19}$$

where a and b are constants depending on the characteristics of the apparatus and the chemical composition of the system. Different analytical methods are summarized in Table 4.2.

Let us now assume that we conduct a *pulse experiment* and register the measured signal, s, as a function of time (Figure 4.13). The pure fluid free from a tracer yields the measured signal

$$s_0 = a \tag{4.20}$$

and the concentration, $c(t)$, is obtained from

$$c(t) = \frac{s(t) - s_0}{b}. \tag{4.21}$$

The total amount of the tracer is obtained through integration of the $c(t)$ curve (Figure 4.6):

$$n = \int_0^\infty c(t)\dot{V}\,\mathrm{d}t. \tag{4.22}$$

TABLE 4.2 Common Analytical Methods for Tracer Experiments

Method	Measuring Principle	Operation
Conductometry	Electrical conductivity	Continuous
Photometry	Light absorbance (visible or UV light)	Continuous
Mass spectroscopy	Different mass numbers of components	Continuous
Paramagnetic analysis	Paramagnetic properties of compounds	Continuous
Radioactivity	Radioactive radiation	Continuous
Gas chromatography	Adsorption of a compound on a carrier material (gas phase)	Discontinuous
Liquid chromatography	Adsorption of a compound on a carrier material (liquid phase)	Discontinuous

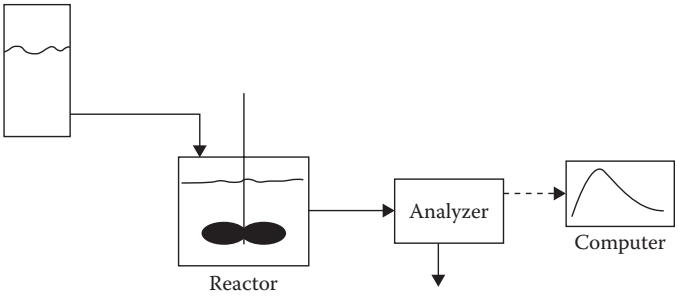

FIGURE 4.12 Apparatus for the experimental determination of an RTD in a continuous reactor.

The density function, $E(t)$, is defined as

$$E(t) = \frac{c(t)\dot{V}}{n}. \tag{4.23}$$

In case that $\dot{V}$ = constant, a combination of Equations 4.22 and 4.23 yields

$$E(t) = \frac{c(t)}{\int_0^\infty c(t)\,\mathrm{d}t} \tag{4.24}$$

and

$$E(t) = \frac{s(t) - s_0}{\int_0^\infty (s(t) - s_0)\,\mathrm{d}t}. \tag{4.25}$$

Equation 4.25 implies that $E(t)$ can be directly determined from the measured primary signal. The procedure is illustrated in Figures 4.12 and 4.13.

A *stepwise experiment* is illustrated in Figure 4.14. The signal has an initial level, s_0, and an asymptotic level, s_∞. Apparently, s_0 corresponds to the conditions in a tracer-free fluid, whereas s_∞ is related to the concentration at the inlet, c_0, similar to that in Equation 4.21.

$$c_0 = \frac{s_\infty - s_0}{b} \tag{4.26}$$

After dividing Equation 4.21 by Equation 4.26, we obtain

$$\frac{c(t)}{c_0} = \frac{s(t) - s_0}{s_\infty - s_0}. \tag{4.27}$$

At the time, $t = 0$, $s(t) = s_0$, and $c(t)/c_0 = 0$. After an infinitely long period of time $s(t) = s_\infty$. Thus $c(t)/c_0 = 1$. Finally, we can conclude that the ratio $c(t)/c_0$ directly yields the distribution function

$$F(t) = \frac{s(t) - s_0}{s_\infty - s_0}. \tag{4.28}$$

The procedure is illustrated in Figure 4.14.

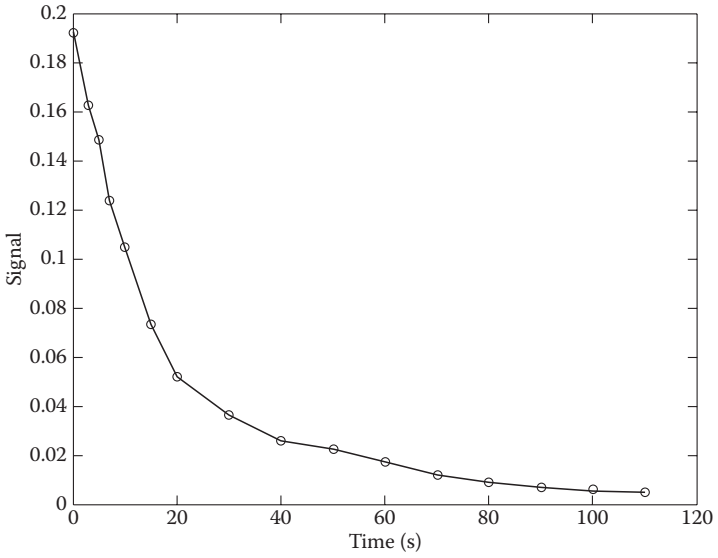

FIGURE 4.13 Determination of $E(t)$ based on the measured signal (impulse experiment).

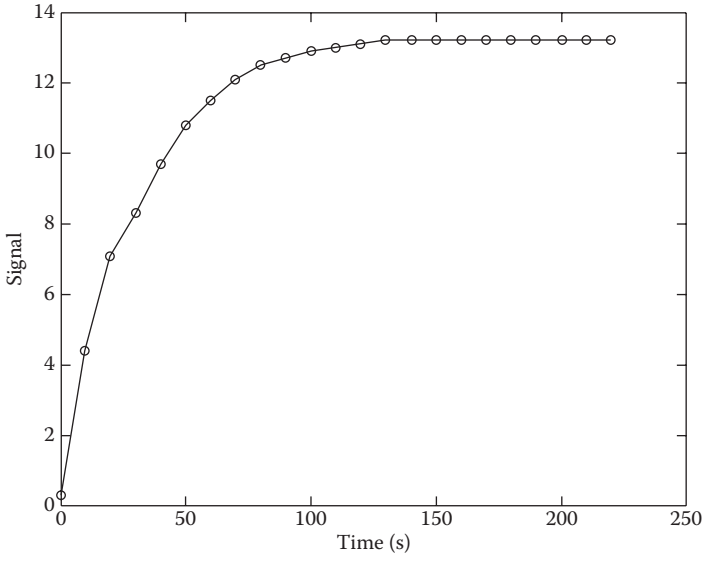

FIGURE 4.14 Determination of $F(t)$ from a stepwise experiment.

4.2.9 RTD FOR A CSTR AND PFR

For a CSTR, the RTD can be determined from a pulse experiment. During such an experiment, a quantity of an inert tracer, n, is injected into the reactor. The resulting concentration becomes

$$c(0) = \frac{n}{V}, \tag{4.29}$$

where V denotes the reactor volume. The reactor is continuously fed with a tracer-free feed, $\dot{V}$. The molar balance for a component can be expressed qualitatively as follows:

$$\text{supplied} + \text{generated} = \text{removed} + \text{accumulated}.$$

In this particular case, the terms on the left-hand side are equal to zero (0), since no tracer is present in the feed and nothing is generated via a chemical reaction. The balance becomes

$$0 = c\dot{V} + \frac{\mathrm{d}n}{\mathrm{d}t}. \tag{4.30}$$

The accumulated amount, $\mathrm{d}n/\mathrm{d}t$, can be expressed with the concentration (c) and the volume (V):

$$n = cV.$$

Provided that the reactor volume remains constant, the $\mathrm{d}n/\mathrm{d}t$ is simplified to $V\,\mathrm{d}c/\mathrm{d}t$. We denote the ratio $V/\dot{V}\,\bar{t}$, as a result of which balance Equation 4.30 becomes

$$\frac{\mathrm{d}c}{\mathrm{d}t} = -\frac{c}{\bar{t}}, \tag{4.31}$$

which is solved by variable separation, followed by integration:

$$\int_{c(0)}^{c} \frac{\mathrm{d}c}{c} = -\int_{0}^{t} \frac{\mathrm{d}t}{\bar{t}}, \tag{4.32}$$

$$\ln\left(\frac{c}{c(0)}\right) = -\frac{t}{\bar{t}}. \tag{4.33}$$

The fraction of the tracer that leaves the reactor within the time interval $t \rightarrow t + \mathrm{d}t$ is given by

$$\frac{c(t)}{c(0)}\frac{\dot{V}\,\mathrm{d}t}{V} = \frac{1}{\bar{t}}\,\mathrm{e}^{-t/\bar{t}}\,\mathrm{d}t = E(t)\,\mathrm{d}t. \tag{4.34}$$

According to the definition of the density function, $E(t)$, this fraction in fact represents the density function. Equation 4.34 yields

$$E(t) = \frac{\mathrm{e}^{-t/\bar{t}}}{\bar{t}} \tag{4.35}$$

for a CSTR with perfect backmixing. The distribution function, $F(t)$, is obtained through integration of the density function, $E(t)$, within the interval $0 \rightarrow t$:

$$F(t) = \int_{0}^{t} E(t)\,\mathrm{d}t = \int_{0}^{t} \frac{\mathrm{e}^{-t/\bar{t}}}{\bar{t}}\,\mathrm{d}t. \tag{4.36}$$

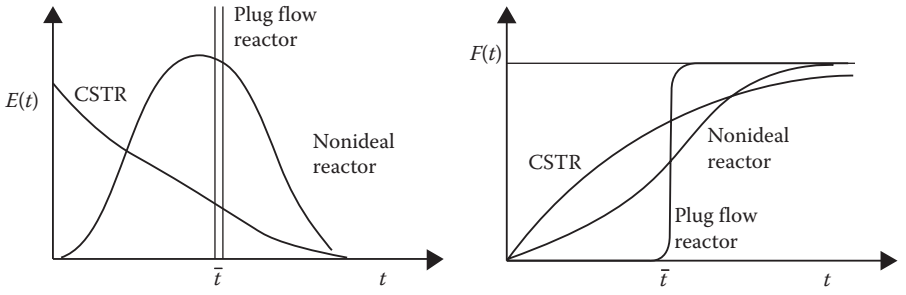

FIGURE 4.15 RTDs in various reactors.

The result assumes the following form:

$$F(t) = 1 - e^{-t/\bar{t}}. \tag{4.37}$$

Alternatively, all these functions can be expressed with the dimensionless coordinate, $\theta = t/\bar{t}$. The relations $E(t)\,dt = E(\theta)\,d\theta$ and $F(t) = F(\theta)$ in Table 4.1 are taken into account, and we obtain

$$E(\theta) = e^{-\theta}, \tag{4.38}$$

$$F(\theta) = 1 - e^{-\theta}. \tag{4.39}$$

The residence time functions for a *tube reactor with plug flow* (a PFR) are trivial. Let us assume that we suddenly inject an amount of inert tracer into the inlet of the reactor. The whole amount of the tracer resides in the reactor tube for a period of time $t = L/w$, in which L and w denote the reactor length and the flow velocity, respectively. We can even see that the time t can be expressed as the reactor volume and the volumetric flow rate ($t = V/\dot{V}$).

A tube reactor, in which turbulent flow characteristics prevail, the radial velocity profile, is flattened so that, as a good approximation, it can be assumed to be flat. Function $E(t)$ becomes extremely narrow and infinitely high at the residence time of the fluid. This function is called a *Dirac* δ *function*. The residence time functions $E(\theta)$ and $F(\theta)$ for the plug flow and backmix models are presented in Figure 4.15. In this figure, the differences between these extreme flow models are dramatically emphasized.

4.2.10 RTD IN TUBE REACTORS WITH A LAMINAR FLOW

In reactor tubes in which the flow velocity is low, the flow profiles deviate from that of the plug flow. The reason is that the *Reynolds* number, $Re = wd/\nu$ (where w denotes the flow velocity in m/s, d is the diameter of the tube, and ν is the kinematic viscosity), yields values that are typical for a laminar flow. The kinematic viscosity, ν, is obtained from the dynamic viscosity, μ, and density, ρ, of the flowing media ($\nu = \mu/\rho$). A typical boundary value for the Reynolds number is 2000: values below this indicate that the flow with a

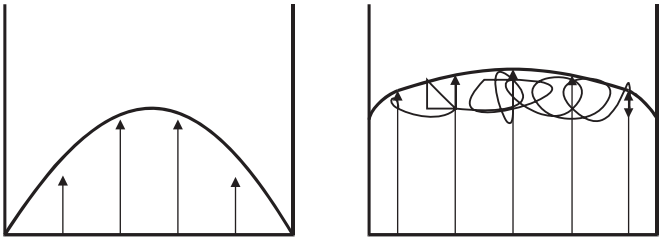

FIGURE 4.16 Laminar and turbulent flows in a tube.

high probability is laminar. A laminar flow emerges in a tube reactor (Figure 4.16) in which the residence time is long. A long residence time, in turn, is required if the chemical reaction is slow. Furthermore, in monolith reactors, a laminar flow profile is often desired. Figure 4.17 illustrates the typical metallic and ceramic monolith structures. Monoliths are often used in the cleaning of flue gases from internal combustion engines. In this case, the flow characteristics are usually laminar. A laminar flow is illustrated in Figure 4.18. The flow characteristic, that is, the flow velocity in a circular tube, is parabolic and follows the law of *Hagen–Poiseuille*,

$$w(r) = w_0 \left(1 - \left(\frac{r}{R}\right)^2\right), \tag{4.40}$$

where w_0 denotes the flow velocity in the middle of the tube, r is the axial coordinate position, and R is the radius of the tube ($R = d/2$ for circular, cylindrical tubes). In the vicinity of the tube walls, the flow velocity approaches zero, according to Equation 4.40. The residence time for a fluid element at the coordinate position r becomes

$$t(r) = \frac{L}{w(r)}. \tag{4.41}$$

A reactor tube in which laminar flow conditions prevail can therefore be considered as a system of parallel, coupled PFRs, in which the residence time varies between $t_{\min} = L/w_0$ ($r = 0$) and an infinitely long period of time. L represents the length of the tube and $w(r)$ is given by Equation 4.40. The total volumetric flow rate, $\dot{V}$, through the tube is obtained by integrating the flow velocity over the whole reactor cross-section. The element is $\mathrm{d}A = 2\pi r\,\mathrm{d}r$ (Figure 4.18), and we thus obtain the following expression for the total

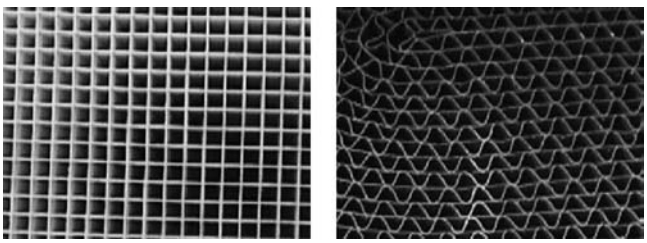

FIGURE 4.17 Ceramic (left) and metallic (right) monolith structures.

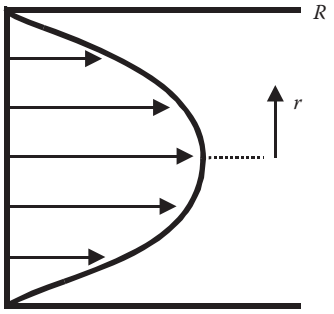

FIGURE 4.18 Laminar flow in circular tubes.

volumetric flow rate:

$$\dot{V} = \int_0^R w 2\pi r \, \mathrm{d}r. \tag{4.42}$$

Substituting w, according to Equation 4.40, yields

$$\dot{V} = 2\pi w_0 \int_0^R \left(1 - \left(\frac{r}{R}\right)^2\right) r \, \mathrm{d}r. \tag{4.43}$$

Further

$$\dot{V} = 2\pi R^2 w_0 \int_0^1 (1 - y^2)\, y = 2\pi R^2 w_0 \left[\frac{1}{2}y^2 - \frac{1}{4}y^4\right]_0^1. \tag{4.44}$$

The total volume flow, $\dot{V}$, can even be defined as the multiplication of the average velocity by the cross-section A:

$$\dot{V} = \pi R^2 \overline{w}. \tag{4.45}$$

A comparison of Equation 4.44 with Equation 4.45 yields a simple expression for the average velocity,

$$\overline{w} = \frac{w_0}{2}. \tag{4.46}$$

The average velocity is one half of the value of the maximum velocity (w_0) in the middle of the tube.

The average residence time can therefore apparently be defined with the help of the average velocity:

$$\bar{t} = \frac{V}{\dot{V}} = \frac{L}{\overline{w}} = \frac{2L}{w_0}. \tag{4.47}$$

The RTD for a tube can be derived by focusing on the fraction of the volumetric flow rate that has a residence time between $t_{\min}$ ($= L/w_0$) and an arbitrary value of t. This part of the volumetric flow rate is apparently

$$\int \mathrm{d}\dot{V} = \int_0^R w \, 2\pi r \, \mathrm{d}r. \tag{4.48}$$

After a transfer into the dimensionless coordinate system ($y = r/R$), according to Equation 4.44, we can write

$$\int \mathrm{d}\dot{V} = 2\pi R^2 w_0 \int_0^{r/R} (1 - y^2) y \, \mathrm{d}y. \tag{4.49}$$

After insertion of the boundaries, we obtain

$$\int \mathrm{d}\dot{V} = 2\pi R^2 w_0 \left(\frac{1}{2} \left(\frac{r}{R} \right)^2 - \frac{1}{4} \left(\frac{r}{R} \right)^4 \right) = \pi R^2 w_0 \left(\frac{r}{R} \right)^2 \left(1 - \frac{1}{2} \left(\frac{r}{R} \right)^2 \right). \tag{4.50}$$

The radial coordinates are related to time by Equations 4.40 and 4.41, yielding

$$\left(\frac{r}{R} \right)^2 = 1 - \frac{L}{w_0 t}. \tag{4.51}$$

Substituting Equation 4.51 into Equation 4.50, followed by some rearrangements, we obtain

$$\int \mathrm{d}\dot{V} = \frac{\pi R^2 w_0}{2} \left(1 - \left(\frac{L}{w_0 t} \right)^2 \right). \tag{4.52}$$

The distribution function, $F(t)$, is given by the fraction of the volumetric flow rate that has a residence time between $t_{\min} = L/w_0$ and t:

$$F(t) = \frac{\int_{t_{\min}}^{t} \mathrm{d}\dot{V}}{\dot{V}}. \tag{4.53}$$

Expressions 4.52 and 4.45 can be inserted into Equation 4.53, yielding

$$F(t) = 1 - \left(\frac{L}{w_0 t} \right)^2. \tag{4.54}$$

Alternatively, this can be written as follows:

$$F(t) = 1 - \left(\frac{t_{\min}}{t} \right)^2, \quad t \geq t_{\min} \tag{4.55}$$

or

$$F(t) = 1 - \left(\frac{\bar{t}}{2t} \right)^2, \quad t \geq \bar{t}/2. \tag{4.56}$$

The density function, $E(t)$, can be obtained easily by differentiation of $F(t)$:

$$E(t) = \frac{2t_{\min}^2}{t^3}, \quad t \geq t_{\min}, \tag{4.57}$$

$$E(t) = \frac{\bar{t}^2}{2t^3}, \quad t \geq \bar{t}/2. \tag{4.58}$$

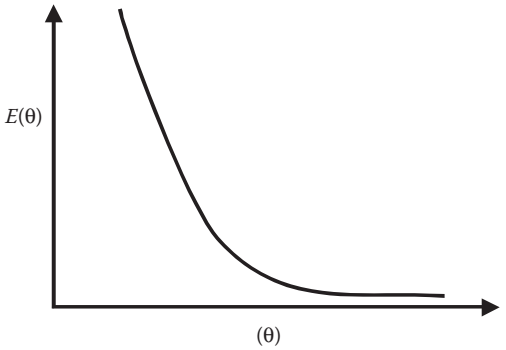

FIGURE 4.19 $E(\theta)$ for laminar flow.

The residence time functions, $E(t)$ and $F(t)$, can be expressed by the dimensionless time coordinate, $\theta = t/\bar{t}$, and thus the following relationships are valid: $F(\theta) = F(t)$ and $E(t)\,dt = E(\theta)\,d\theta$ (Table 4.1). In this way, we obtain

$$F(\theta) = 1 - \frac{1}{4\theta^2}, \quad \theta \geq \frac{1}{2} \tag{4.59}$$

and

$$E(\theta) = \frac{1}{2\theta^3}, \quad \theta \geq \frac{1}{2}. \tag{4.60}$$

The functions $E(\theta)$ and $F(\theta)$ are illustrated in Figures 4.19 and 4.20, which show that the first volume element reaches the reactor outlet at $\theta = 0.5$. Thereafter, the F curve increases rapidly but still, nevertheless, approaches the limit value, $F = 1$, very slowly. This is understandable, as the flow velocity has very low values in the vicinity of the tube wall ($r \approx R$).

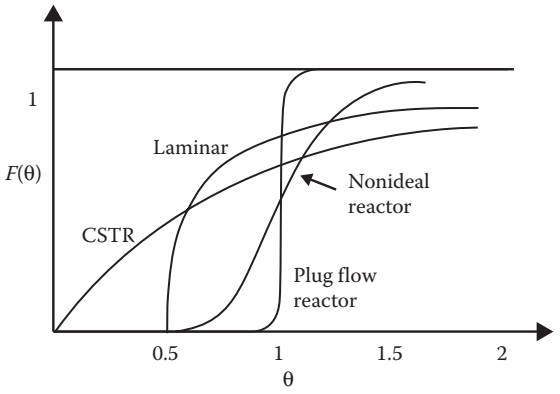

FIGURE 4.20 $F(\theta)$ for different flow models.

4.3 SEGREGATION AND MAXIMUM MIXEDNESS

As demonstrated in the previous section, the residence time functions provide a quantitative measure of the duration of time various species reside inside such a flow reactor. However, we still do not know what happens to the individual elements/species. This is by no means without inconsequential, but instead quite decisive for the conversion level that can be reached in a chemical reactor. An example can be provided by an often-applied model comprising a PFR and a CSTR in series, in one of the two ways in which they can be coupled (Figure 4.21). These two ways of coupling yield the same density function, $E(t)$, but different conversions are obtained for various reactions. Figure 4.20 shows, in other words, that every single flow model yields a special RTD, whereas the opposite is not true. This, in a strict sense, indicates that a direct utilization of the residence time functions for the calculation of the conversion in a chemical reactor is possible only for reactions with linear rate equations. However, there are exceptions to this general rule when dealing with the so-called *macrofluids*. In those cases, we will indeed be able to calculate the conversion degrees according to a segregation model.

4.3.1 SEGREGATION MODEL

A reactor following the segregation model can be considered to act in such a manner that the reactor itself consists of small droplets containing the reactants. Every droplet acts as a small BR, and thus the residence time functions for the entire system are also valid for the droplets (Figure 4.22). Using the segregation model, it is possible to calculate the degree of conversion for a chemical reaction, if the density function of the droplets and the reaction kinetics within the droplets are known. This is why the segregation model yields the same result for the two couplings in Figure 4.21, regardless of the nature of the kinetics of the chemical reactions.

The highest conversion value of the segregation model can be determined since it yields an extreme value of the degree of reactant conversion, that is, the highest or the lowest, depending on the reaction kinetics. We can show that the conversion obtained with the

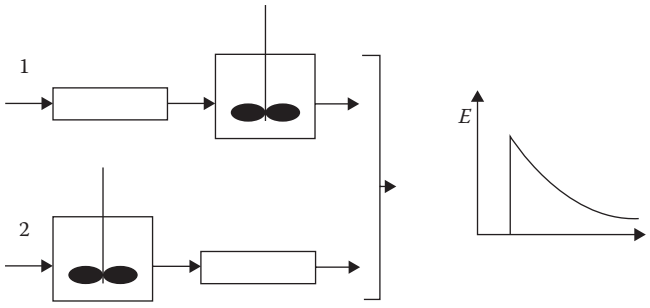

FIGURE 4.21 Coupling (1) yields a better conversion in case of, for example, a reaction with the following rate equation: $-r_A = k_A c_A^m$, if $m > 1$. Both modes of coupling will yield the same result if the rate equation is $-r_A = k_A c_A$. Coupling (2) yields a better conversion, if in the previous rate equation $-r_A = k_A c_A^m, m < 1$.

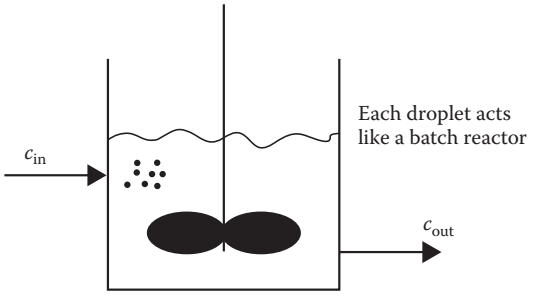

FIGURE 4.22 The principle of the segregation model.

segregation model represents a maximum, as the reaction from the kinetics viewpoint has an order higher than one (1). The minimum is obtained for reaction orders less than one (1).

It is necessary to know the density function, $E(t)$, if the segregation model is applied. $E(t)$ can be determined either experimentally or theoretically. Since it is possible to derive the residence time functions for many flow models, the segregation model is very flexible. According to the segregation model, the average concentration at the reactor outlet is obtained from the relation

$$\bar{c}_i = \int_0^\infty c_{i,\text{batch}}(t)E(t)\,\mathrm{d}t, \tag{4.61}$$

where the concentration $c_{i,\text{batch}}$ is obtained from the BR model, and $E(t)$ is either determined experimentally or a theoretically derived $E(t)$ function is used (e.g., backmixed model, tanks-in-series model, and dispersion model).

4.3.2 MAXIMUM MIXEDNESS MODEL

Even for the maximum mixedness model, the calculation of an extreme concentration value is possible. This extreme value, in comparison with the previous one for the segregation model, represents the opposite end of the scale. The maximum mixedness model is relevant to microfluids and yields, even in this case, results that do not differ considerably from those that can be obtained by means of direct utilization of separate flow models. The model is, however, of importance in cases in which experimentally determined residence time functions are available for a reactor system. The maximum mixedness model is more difficult to visualize than the segregation model. However, its underlying philosophy can be described as follows:

- The elements that leave the reactor, at different times, have been completely segregated during their entire period of stay in the reactor.
- All elements that leave the reactor simultaneously in a volume element have been completely backmixed with each other at the first possible opportunity.

It is worth mentioning that the first claim is also valid for the segregation model, whereas the second claim suggests that a volume element residing inside the reactor can attract new species. Additionally, this happens immediately at the time of entry into the system. Zwietering [2] described the maximum mixedness model mathematically. The derivation was based on the time that reveals the *life expectation* of a species in a reactor, which will be denoted here as t_λ. Since the variable in question yields the time (t_λ) that an element with the age t_a is going to remain in the reactor, the sum of these times must be equal to the residence time of the species, t:

$$t = t_a + t_\lambda. \tag{4.62}$$

Zwietering [2] concluded that the maximum mixedness model can be expressed as follows in terms of the generation rate:

$$\frac{dc_i}{dt_\lambda} = -r_i(c_i) + \lambda(t_\lambda)(c_i - c_{0i}). \tag{4.63}$$

In Equation 4.63, the expression $\lambda(t_\lambda)$ denotes the intensity function of t_λ. Equation 4.63 can be solved by taking into account that $dc_i/dt_\lambda = 0$ at $t_\lambda = \infty$. The c_i-value at $t_\lambda = 0$ has to be determined. It should be noted that $t_\lambda = 0$ at the time the species leaves the reactor. Since a detailed description of Zwietering's philosophy would take too long, here it will suffice to state that he proved that $\lambda(t_\lambda)$, in Equation 4.63, can be replaced by $\lambda(t)$. If, further, the ratio c_i/c_{0i} is denoted by y, and $t_\lambda/\bar{t}$ as θ_λ, the left-hand side in Equation 4.63, dc_i/dt_λ, becomes equal to $c_{0i}\, dy/\bar{t}\, d\theta_\lambda$. Since we are still able to show that the result of the calculation will be the same, although θ_λ would be replaced by θ ($= t/\bar{t}$), we will finally obtain t, an expression of practical use

$$\frac{dy}{d\theta} = -\frac{\bar{t}}{c_{0i}} r_i(y) + \lambda(\theta)(y - 1) \tag{4.64}$$

with the following boundary condition:

$$\frac{dy_i}{d\theta} = 0 \quad \text{at} \quad \theta = \infty. \tag{4.65}$$

Equations 4.64 and 4.65 yield the final value of y_i at $\theta = 0$, as the solution is obtained backwards, by starting with large values of θ (in addition to the λ values valid at these points) and ending up with $\theta = 0$. Similar to the segregation model, a precondition for the maximum mixedness model is that the residence time functions—or more precisely the intensity function—are available, either from theory or from experiments.

4.4 TANKS-IN-SERIES MODEL

The tanks-in-series model can sometimes be used to describe the flow characteristics of real reactors. In its simplest form, this model consists of a number of equally large tanks coupled

in series so that the flow between them moves in only one direction (irreversible flow). The model approaches the plug flow model with an increasing number of tanks in series, whereas it approaches the CSTR model with a decreasing number of tanks, respectively. Consequently, this implies that by varying the number of tanks, it is possible to cover the residence time functions within the widest boundaries possible.

4.4.1 RESIDENCE TIME FUNCTIONS FOR THE TANKS-IN-SERIES MODEL

In the setup displayed in Figure 4.23, a series of tanks consisting of j CSTRs of an equal size are shown. The derivations to follow are based on notations given in the scheme. The volumetric flow rate, V, is assumed to be constant.

The density function can be derived on the basis of a mass balance that, for an inert component i, yields

$$\dot{V}c_{i-1} = \dot{V}c_i + V_i\frac{\mathrm{d}c_i}{\mathrm{d}t} \tag{4.66}$$

where $V_i/\dot{V} = t_i$.

If we assume that an *inert* tracer is supplied as a pulse to the first reactor, the expression $c_{i>1}(0) = 0$ is valid. The Laplace transformation thus yields

$$sc_i(s) - c_i(0) + \frac{1}{t_i}c_i(s) - \frac{1}{t_i}c_{i-1}(s) = 0 \tag{4.67}$$

or generally for a reactor i:

$$c_i(s) = \frac{c_{i-1}(s)}{\bar{t}_i[s + (1/\bar{t}_i)]}. \tag{4.68}$$

If we begin with the last reactor in the series, Equation 4.68 yields a general expression

$$c_j(s) = \frac{c_1(s)}{\bar{t}_i^{j-1}[s + (1/\bar{t}_i)]^{j-1}}. \tag{4.69}$$

An expression for the concentrations $c_1(s)$ in Equation 4.69 was derived previously:

$$c_1(t) = \frac{n}{V_i}\,\mathrm{e}^{-t/\bar{t}_i}. \tag{4.70}$$

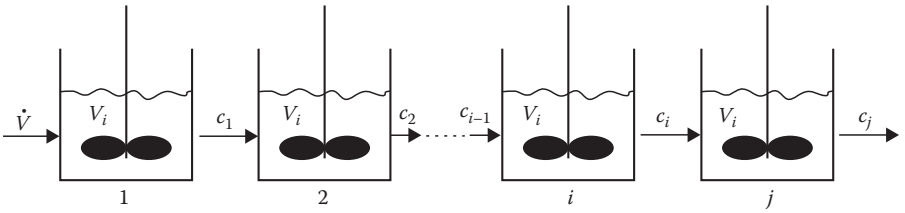

FIGURE 4.23 Tanks in series.

The Laplace transformation of Equation 4.70 yields

$$c_1(s) = \frac{n}{V_i} \frac{n}{[s + (1/\bar{t}_i)]} \tag{4.71}$$

and Equations 4.69 and 4.71, finally, yield

$$c_j(s) = \frac{c(0)\bar{t}}{\bar{t}_i^j [s + (1/\bar{t}_i)]^j}. \tag{4.72}$$

The reader should, however, be reminded of the fact that the average residence time, $\bar{t}$, incorporated into Equation 4.72, accounts for the whole system and is defined by

$$\bar{t} = j\frac{V_i}{\dot{V}} = \frac{V_r}{\dot{V}} = j\bar{t}_i. \tag{4.73}$$

The concentration $c(0)$ in Equation 4.72 denotes the ratio n/V_R, where n is the amount of the tracer inserted at that moment and V_R denotes the entire reactor volume. The variable $c_j(s)$ is back-transformed into the variable t, and we obtain

$$\frac{c_j(t)}{c(0)} = C(t) = \frac{j^j}{(j-1)!} \left(\frac{t}{\bar{t}}\right)^{j-1} e^{-jt/\bar{t}}. \tag{4.74}$$

This expressed with the normalized time and using the relation $C(t) = \bar{t}\, E(t) = E(\theta)$ finally yields

$$E(\Theta) = \frac{j^j}{(j-1)!} \Theta^{j-1} e^{-j\Theta}. \tag{4.75}$$

It can additionally be shown that the distribution function $F^*(\theta)$ becomes

$$F^*(\Theta) = e^{-j\Theta} \sum_{i=0}^{j-1} \frac{(j\Theta)^i}{i!}. \tag{4.76}$$

By division of Equations 4.75 and 4.76, the intensity function becomes

$$\lambda(\Theta) = \frac{j^j \Theta^{j-1}}{(j-1)! \sum_{i=0}^{j-1} [(j\Theta)^i / i!]}. \tag{4.77}$$

The principal forms of functions $E(\theta)$, $F^*(\theta)$, and $\lambda(\theta)$ for a tank series are illustrated in Figures 4.24 through 4.26.

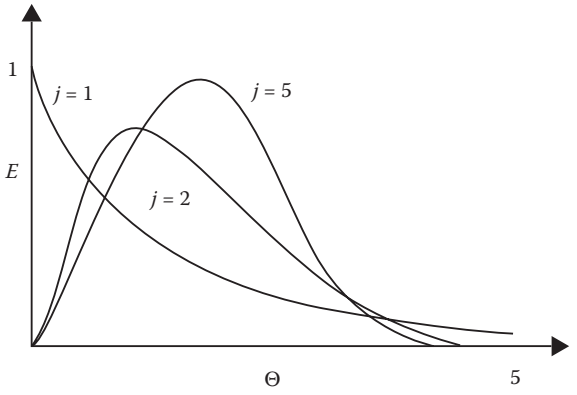

FIGURE 4.24 Density functions for a tanks-in-series model.

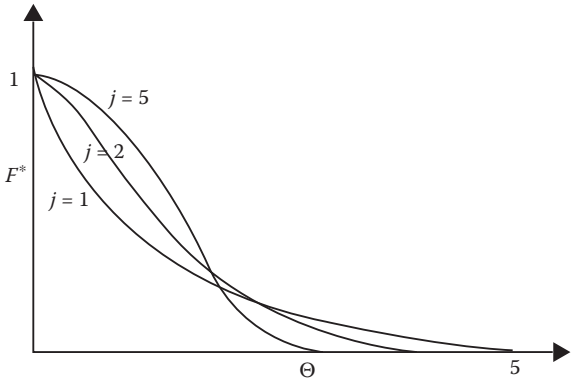

FIGURE 4.25 Distribution functions for a tank series.

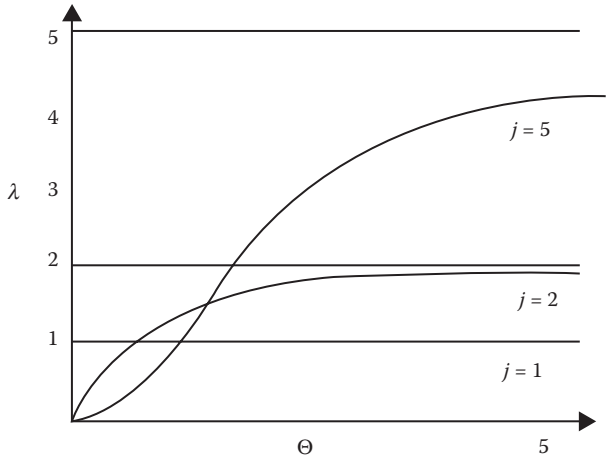

FIGURE 4.26 Intensity functions for a tank series.

Of these functions, especially the intensity function, $\lambda(\theta)$, has the interesting feature that with increasing values of θ, it asymptotically approaches the number of tanks coupled in series. This can even be proved mathematically:

$$\lim_{\Theta\to\infty}\lambda(\Theta) = \lim_{\Theta\to\infty}\left(\frac{j^j\Theta^{j-1}}{(j-1)! + \left[1 + j\Theta/1! + (j\Theta)^2/2! + \cdots + j^{j-1}\Theta^{j-1}/(j-1)!\right]}\right)$$

$$= \frac{j^j}{j^{j-1}} = j. \tag{4.78}$$

Since it is true that the variance, σ_θ^2, is equal to $1/j$, the relation

$$j = \frac{1}{\sigma_\Theta^2} = \lim_{\Theta\to\infty}\lambda(\Theta) \tag{4.79}$$

is valid. Equation 4.78 shows that it is possible to determine an equivalent number (j) of tanks coupled in series, on the basis of the relation between the number of reactors coupled in series, the variance, and the limiting value for the intensity function. This can be done by determining the variance, since the tanks-in-series model is adequate for a reactor system. This, in turn, can be done by starting with, for example, experimentally determined density functions. On the basis of Equation 4.79, it is clear that the number of tanks coupled in a sequence can be obtained from the limiting value of the intensity function. The model was derived for an integer number of tanks, but it can be generalized to encompass a noninteger number of tanks by recalling that $(j-1)!$ in Equations 4.75 and 4.76 is the gamma function $(j-1)! = \Gamma(j)$.

4.4.2 TANKS IN SERIES AS A CHEMICAL REACTOR

It is possible to derive explicit expressions for concentrations in a tanks-in-series system, provided that the reactions are of the first order (Table 3.3). Thus, for concentrations of reactant A (A $\rightarrow$ P), starting with the outlet concentration in the reactor j and ending with the inlet concentration in the first reactor, we obtain

$$\frac{c_{Aj}}{c_{0A}} = \frac{1}{(1 + k\bar{t}/j)^j}. \tag{4.80}$$

In Equation 4.80, $\bar{t}$ is the entire reactor system, in agreement with the definition in Equation 4.73. It should be emphasized that the concentrations c_{Aj} and c_{0A} denote a reactant that undergoes a chemical reaction—in contrast to the previous section where the concentrations, as a rule, accounted for inert tracers. In the case of nonlinear kinetics, no analytical solutions can be obtained. Numerical solution techniques are therefore required. For some reaction types, there are even ready-made diagrams that give the order of magnitude for the conversion; see Figure 4.27 for examples of such diagrams. In addition to the tanks-in-series reactor that was under consideration so far, we shall now discuss two additional, closely related models: the maximum mixedness tanks-in-series and the segregated tanks-in-series models.

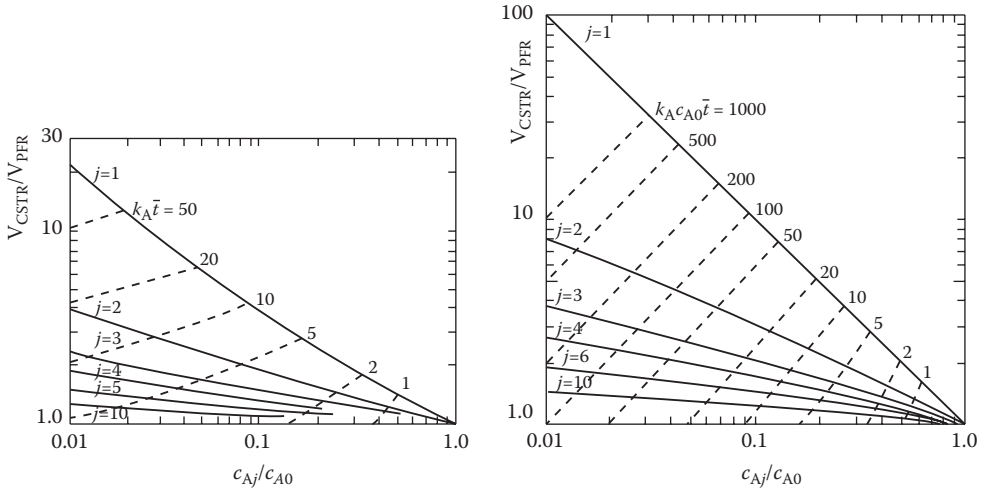

FIGURE 4.27 Comparison of tanks-in-series volumes with PFR volumes; first-order reaction, $-r_A = k_A c_A$ (left), and second-order reaction $-r_A = k_A c_A^2$ (right).

4.4.3 MAXIMUM-MIXED TANKS-IN-SERIES MODEL

Some common guidelines are presented here on how the derived residence time functions can be utilized for calculating the conversion for a maximum mixedness tanks-in-series model. It is necessary, in this context, to state that if each tank in a series is completely backmixed, the model provides the same result as the tanks-in-series model. In this case, no special treatment is required. If, on the contrary, the tanks in series as an entity are considered to be completely backmixed, one has to turn to an earlier equation, Equation 4.64, together with the boundary condition, Equation 4.65. Instead of the original expression for the intensity function, a new one that is valid for the tanks-in-series model, Equation 4.77, is utilized.

4.4.4 SEGREGATED TANKS IN SERIES

Two different cases should be mentioned for the segregated tanks-in-series model: firstly, every reactor in the series can be segregated, and secondly, the tanks in series as an entity can be segregated. These two initial assumptions lead to different results.

Let us first consider the case in which the tank series as an entity is segregated. Thus, for a reactant A, we obtain

$$c_{A,out} = \int_0^\infty c_{A,batch}(t)\, E(t)\, dt. \tag{4.81}$$

After combining Equations 4.81 and 4.75, a new expression is obtained:

$$c_{A,out} = \frac{j^j}{(j-1)!} \int_0^\infty c_{A,batch}(\Theta)\Theta^{j-1}\, e^{-j\Theta}\, d\Theta. \tag{4.82}$$

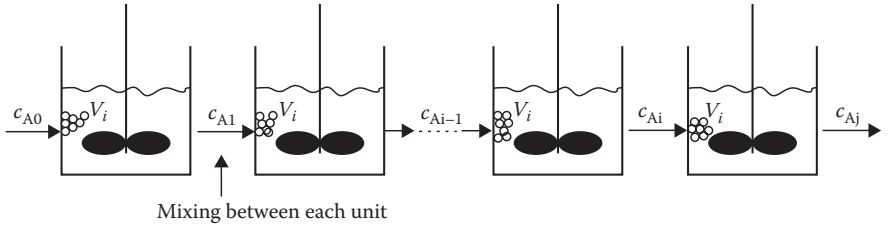

FIGURE 4.28 An individually segregated tank series (complete backmixing between each unit).

In the second case, let us assume that each individual CSTR is segregated. As a result, the following derivation is valid, provided that the volume elements are broken up and mixed with each other between each step in the series:

$$c_{A,1} = \int_0^\infty c_{A,\text{batch}}(t)\frac{1}{\bar{t}_1}\,\mathrm{e}^{-t/\bar{t}_1}\,\mathrm{d}t, \quad c_{A,\text{in}} = c_{A,0}, \tag{4.83}$$

$$c_{A,i} = \int_0^\infty c_{A,\text{batch}}(t)\frac{1}{\bar{t}_i}\,\mathrm{e}^{-t/\bar{t}_1}\,\mathrm{d}t, \quad c_{A,\text{in}} = c_{A,i-1}. \tag{4.84}$$

For definitions of the symbols in the equations, see Figure 4.28.

4.4.5 COMPARISON OF TANKS-IN-SERIES MODELS

For irreversible, second-order reaction kinetics with an arbitrary stoichiometry, the generation rates of the reactants are as follows:

$$r_A = \nu_A k c_A c_B,$$

$$r_B = \nu_B k c_A c_B.$$

The above expressions are inserted into the appropriate balance equations, for example, for tanks-in-series, segregated tanks-in-series, and maximum-mixed tanks-in-series models. The models are solved numerically [3], and the results are illustrated in the diagrams presented in Figure 4.29, which displays the differences between the above models for second-order reactions. The figure shows that the differences between the models are the most prominent in moderate Damköhler numbers (Figure 4.29). For very rapid and very slow reactions, it does not matter in practice which tanks-in-series model is used. For the extreme cases, it is natural to use the simplest one, that is, the ordinary tanks-in-series model.

4.4.6 EXISTENCE OF MICRO- AND MACROFLUIDS

The existence of segregation in a real reactor system can be investigated by means of three time constants, t_r, the relaxation time of a chemical process, t_D, the time of micromixing, and $\bar{t}$, the mean residence time. The relaxation time (t_r) is a characteristic parameter for reaction kinetics and it is the time required to reduce the relative concentration c_i/c_{0i} from 1 to the value e^{-1}. For instance, for a first-order reaction ($r_i = -kc_i$) in a BR, the

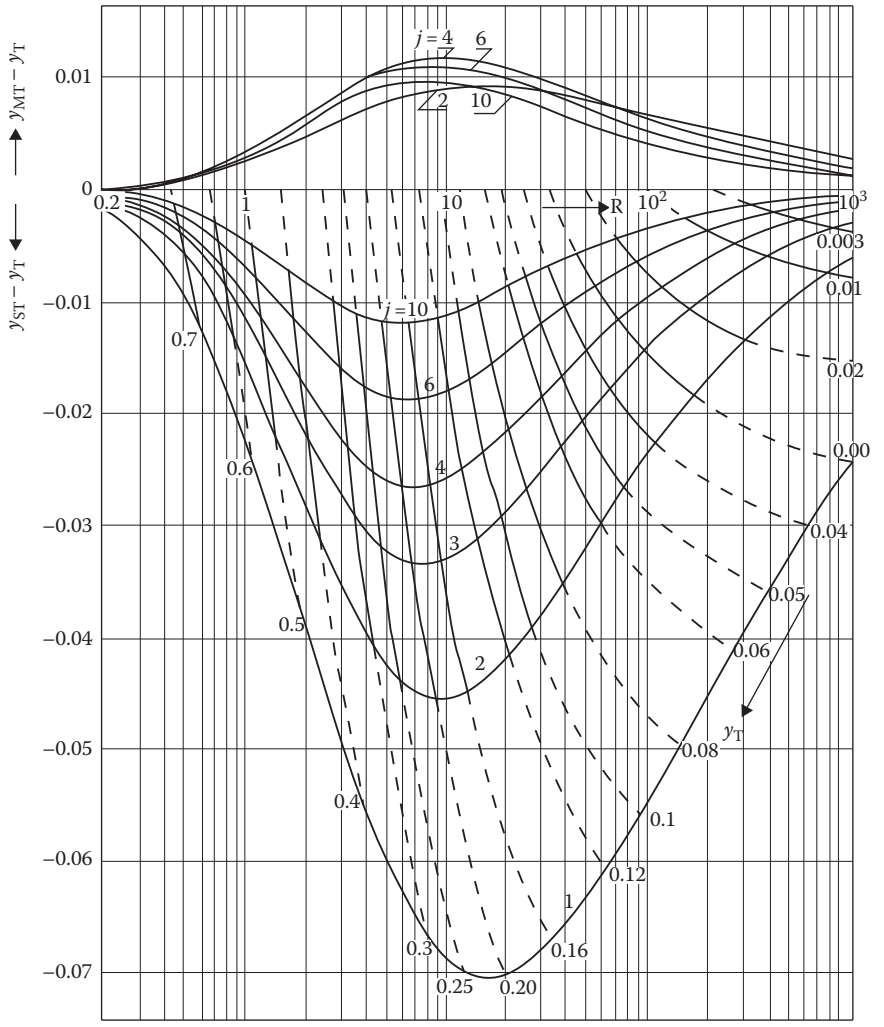

FIGURE 4.29 y_T (tanks in series), y_{MT} (maximum-mixed tanks in series), and y_{ST} (segregated tanks in series) at $M = 1.00$, $M = \nu_A c_{0B}/(\nu_B c_{0A})$, $R = k_A \bar{t} c_{0A} \nu_B / \nu_A$, $R =$ Damköhler number.

relative concentration of a reactant is given by $c_i/c_{0i} = e^{-kt}$. This yields the relaxation time $e^{-kt_r} = e^{-1}$, that is, $t_r = k^{-1}$. In an analogous manner, the relaxation time can be obtained for other kinetics.

The micromixing time (t_D), that is, the time required for complete backmixing on a molecular level, can be estimated from turbulence theories. Molecular diffusion plays a decisive role in mixing if the molecular aggregates are of the same size as microturbulent eddies, whose sizes are given by the turbulence theory of Kolmogoroff:

$$l = \left(\frac{\nu}{\varepsilon}\right)^{1/4}, \tag{4.85}$$

where ν is the kinematic viscosity of the fluid ($\nu = \mu/\rho$) and ε is the energy dispatched per mass unit (in J/kg), for instance, via stirring. The time required for micromixing is then

obtained from

$$t_D = \frac{l^2}{D_{mi}}, \tag{4.86}$$

where D_{mi} is the molecular diffusion coefficient. Correlation expressions for estimating the molecular diffusion coefficients for gases and liquids are provided in Appendices 4 and 6, respectively.

Segregation plays a central role in the process if the relaxation time (t_r) is of the same order of magnitude as the micromixing time (t_D), particularly if the residence time ($\bar{t}$) is short. Segregation is an important phenomenon for rapid reactions. For example, the energy dissipated to the system is $\varepsilon = 1.0\,\text{W/kg}$ and the kinematic viscosity has the value $10^{-6}\,\text{m}^2/\text{s}$ (i.e., $\mu = 1.0\,\text{cP}$ and $\rho = 1.0\,\text{kg/dm}^3$); the length of microturbulent eddies is $32\,\mu\text{m}$. A typical value for the molecular diffusion coefficient in the liquid phase is $D_m = 10^{-9}\,\text{m}^2/\text{s}$. The time of micromixing becomes $t_D = 1\,\text{s}$ in this case. For large molecules, such as polymers, the diffusion coefficient can have much smaller values, and the time for micromixing increases. The viscosity of the fluid strongly influences the micromixing time. As shown in Appendix 6, the molecular diffusion coefficient in liquids is proportional to μ^{-1}. The micromixing time (t_D) is thus proportional to 1^2, that is, to $\nu^{3/2}$ and $\mu^{3/2}$. Consequently, the micromixing time is proportional to $\mu^{5/2} = \mu^{2.5}$. An evaluation of the viscosity of the reaction medium is thus crucial to ascertain the segregation effect.

4.5 AXIAL DISPERSION MODEL

The concept of "dispersion" is used to describe the degree of backmixing in continuous flow systems. Dispersion models have been developed to correct experimentally recorded deviations from the ideal plug flow model. As described in previous sections, the residence time functions $E(t)$ and $F(t)$ can be used to establish whether a real reactor can be described by the ideal flow models (CSTR, PFR, or laminar flow) or not. In cases where none of the models fits the residence time distribution (RTD), the tanks-in-series model can be used, as discussed in Section 4.4. However, the use of a tanks-in-series model might be somewhat artificial for cases in which tanks do not exists in reality but only form a mathematical abstraction. The concept of a dispersion model thus becomes actual.

Mathematically, dispersion can be treated in the same manner as molecular diffusion, but the physical background is different: dispersion is caused not only by molecular diffusion but also by turbulence effects. In flow systems, turbulent eddies are formed and they contribute to backmixing. Therefore, the operative concept of dispersion, the dispersion coefficient, consists principally of two contributions, that is, the one caused by molecular diffusion and the second one originating from turbulent eddies. Below we shall derive the RTD functions for the most simple dispersion model, namely, the axial dispersion model.

4.5.1 RTDs FOR THE AXIAL DISPERSION MODEL

We will study a cylindrical element residing in a tube (Figure 4.30). The RTD functions can be obtained by assuming a step change of an inert, nonreactive tracer, which is introduced

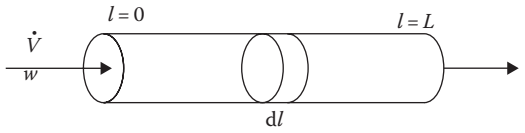

FIGURE 4.30 Cylindrical volume element.

into the reactor tube. The general balance equation of the inert tracer can be expressed as follows:

$$[\text{tracer inflow}] = [\text{outflow of tracer}] + [\text{accumulated tracer}].$$

The inflow and outflow consist of two contributions: the molar flow itself (expressed as $\dot{n}_i$, in mol/s) and the contribution of axial dispersion. The description of axial dispersion is a widely debated topic in chemical engineering. A standard expression for dispersion is expressed by a mathematical analogy of Fick's law,

$$N_i' = -D\frac{\mathrm{d}c_i}{\mathrm{d}l}, \tag{4.87}$$

where the coefficient D denotes the overall dispersion coefficient. It should be noted that D is different from the molecular diffusion coefficient and is usually treated as an independent component in the simplest versions of dispersion models. Quantitatively, the balance equation for the inert tracer in a volume element can be expressed as

$$\dot{n}_{i,\text{in}} + \left(-D\frac{\mathrm{d}c_i}{\mathrm{d}l}A\right)_{\text{in}} = \dot{n}_{i,\text{out}} + \left(-D\frac{\mathrm{d}c_i}{\mathrm{d}l}A\right)_{\text{out}} + \frac{\mathrm{d}n_i}{\mathrm{d}t}, \tag{4.88}$$

where A stands for the reactor cross-section. The difference, $\dot{n}_{i,\text{out}} - \dot{n}_{i,\text{in}}$, is denoted by $\Delta\dot{n}_i$ and the difference $(D(\mathrm{d}c/\mathrm{d}l)\mathrm{A})_{\text{out}} - (D(\mathrm{d}c/\mathrm{d}l)\mathrm{A})_{\text{in}} = \Delta(D(\mathrm{d}c/\mathrm{d}l)\mathrm{A})$:

$$\Delta\left(D\frac{\mathrm{d}c_i}{\mathrm{d}l}A\right) = \Delta\dot{n}_i + \frac{\mathrm{d}n_i}{\mathrm{d}t}. \tag{4.89}$$

The molar amounts (n_i) and flows ($\dot{n}_i$) are expressed as concentrations as follows:

$$\Delta\,\dot{n}_i = \Delta(c_i\dot{V}) = (\Delta\, c_i w)A, \tag{4.90}$$

$$n_i = c_i\Delta V.$$

The constant, cross-section of the tube, is

$$A = \pi R^2. \tag{4.91}$$

The difference equation becomes

$$\frac{\mathrm{d}c}{\mathrm{d}t}\Delta V = \Delta\left(D\frac{\mathrm{d}c_i}{\mathrm{d}l}A\right) - \Delta(c_i w)A. \tag{4.92}$$

Dividing by ΔV and recalling that $A/\Delta V = l/\Delta L$ yield

$$\frac{dc_i}{dt} = \frac{\Delta(D\, dc_i/dl)}{\Delta l} - \frac{\Delta(c_i w)}{\Delta l}. \tag{4.93}$$

By allowing the volume element to shrink, we obtain the differential equation

$$\frac{dc_i}{dt} = \frac{d(D\, dc_i/dl)}{dl} - \frac{d(c_i w)}{dl}. \tag{4.94}$$

Equation 4.94 describes the general behavior of an inert tracer for gas- and liquid-phase processes. Typically, the dispersion coefficient is presumed to be constant, which simplifies the differential equation to

$$\frac{dc_i}{dt} = D\frac{d^2 c_i}{dl^2} - \frac{d(c_i w)}{dl}. \tag{4.95}$$

For cases in which the flow rate (w) is constant, a further development is possible: $d(c_i w)/dl = w\, dc_i/dl$. The commonly used form of the axial dispersion model is

$$\frac{dc_i}{dt} = D\frac{d^2 c_i}{dl^2} - w\frac{dc_i}{dl}. \tag{4.96}$$

The model can be transformed to a dimensionless form by introducing the dimensionless concentration, $y_i = c_i/c_0$, where c_0 denotes the concentration of the tracer at the inlet, $z = l/L$, where L is the reactor length, and $\Theta = t/\bar{t}$, that is, the dimensionless time. The balance Equation 4.95 is thus rewritten as

$$\frac{\partial^2 y_i}{Pe\, \partial z^2} - \frac{\partial y_i}{\partial z} - \frac{\partial y_i}{\partial \theta} = 0 \tag{4.97}$$

or

$$\frac{\partial^2 (c/c_0)}{Pe\, \partial z^2} - \frac{\partial (c/c_0)}{\partial z} - \frac{\partial (c/c_0)}{\partial \theta} = 0, \tag{4.98}$$

where the dimensionless quantity, the Peclet number, is described as $Pe = wL/D$.

As revealed by the definition of the Peclet number, it is de facto a measure of the degree of dispersion. For a plug flow, $D = 0$ and $Pe = \infty$; on the other hand, complete backmixing implies that $D = \infty$ and $Pe = 0$.

Solutions to Equations 4.97 and 4.98 are dependent on the boundary conditions chosen, and these boundary conditions, in turn, are governed by the assumptions made concerning the reactor arrangement. In the case of chemical reactors, a so-called closed system is usually selected. By this we mean that no dispersion takes place either at the reactor inlet or outlet. Moreover, the dispersion inside the reactor is considered equal in each volume element of the system. For the closed system, the following initial and boundary conditions can be set:

$$\theta = 0, \quad z < 0, \quad c/c_0 = 1; \qquad 0 < z < 1, \quad c/c_0 = 0 \tag{4.99}$$

$$\theta > 0, \quad z = 0, \quad 1 = c/c_0 - \frac{\partial (c/c_0)}{Pe \partial z}, \quad z = 1, \quad \frac{\partial (c/c_0)}{\partial z} = 0 \tag{4.100}$$

If Equations 4.97 and 4.98 are solved by applying the boundary conditions, Equations 4.99 and 4.100 above, the distribution function, $F(\Theta)$, for the dispersion model becomes

$$F(\theta) = 1 - 4pe^{p} \sum_{i=1}^{\infty} \frac{(-1)^{i+1}\,\alpha_i^2}{(\alpha_i^2 + \mathbf{p}^2)(\alpha_i^2 + \mathbf{p}^2 + \mathbf{2p})}\, e^{-(\theta(\alpha_i^2+\mathbf{p}^2)/\mathbf{2p})}. \tag{4.101}$$

After differentiating Equation 4.101, the following equation for the density function, $E(\Theta)$, is obtained:

$$E(\theta) = 2e^{p} \sum_{i=1}^{\infty} \frac{(-1)^{i+1}\,\alpha_i^2}{(\alpha_i^2 + \mathbf{p}^2 + \mathbf{2p})}\, e^{-(\theta(\alpha_i^2+\mathbf{p}^2)/\mathbf{2p})}. \tag{4.102}$$

In Equations $F(\Theta)$ and $E(\Theta)$ above, the parameter $p = Pe/2$, whereas the parameter α denotes the roots of the transcendent equations below:

$$\frac{\alpha_i}{2} \tan \frac{\alpha_i}{2} = \frac{p}{2}, \quad i = 1, 3, 5, \ldots, \tag{4.103}$$

$$\frac{\alpha_i}{2} \cot\left(\frac{\alpha_i}{2}\right) = -\frac{p}{2}, \quad i = 2, 4, 6, \ldots. \tag{4.104}$$

Since the intensity function denotes the ratio between the density and the distribution functions, we obtain the following expression using the equations for $F(\Theta)$ and $E(\Theta)$:

$$\lambda(\theta) = \frac{1}{2p} \frac{\sum_{i=1}^{\infty}(-1)^{i+1}\,\alpha_i^2/\left(\alpha_i^2 + \mathbf{p}^2 + \mathbf{2p}\right)\, e^{-(\theta(\alpha_i^2+\mathbf{p}^2)/\mathbf{2p})}}{\sum_{i=1}^{\infty}(-1)^{i+1}\,\alpha_i^2/\left(\alpha_i^2 + \mathbf{p}^2\right)\left(\alpha_i^2 + \mathbf{p}^2 + \mathbf{2p}\right)\, e^{-(\theta(\alpha_i^2+\mathbf{p}^2)/2\mathbf{p})}}. \tag{4.105}$$

It is possible to prove that the intensity function, according to Equation 4.105, obtains constant values at relatively low values of the parameter Θ, provided that the value of the Peclet number is below a limit value (around 12). Additionally, we can easily show that the constant value obtained can be calculated using the following equation:

$$\lambda(\theta)_{\text{const}} = \frac{\alpha_1^2 + p^2}{2p}. \tag{4.106}$$

Functions $E(t)$, $F(t)$, and $\lambda(t)$ are displayed in Figure 4.31. As indicated by the figures, the intensity function (λ) really approaches a limit. This enables a straightforward determination of the Peclet number from experimental data, according to Figure 4.31. Furthermore, $\lambda(\theta)_{\text{const}}$, as a function of the Peclet number, is almost linear, as illustrated in Figure 4.32.

The normalized mean residence time and variances are given here, since they are important from the calculation point of view:

$$\bar{\theta} = 1, \tag{4.107}$$

$$\sigma_{\theta}^2 = \frac{2}{Pe^2}\left(Pe - 1 + e^{-Pe}\right). \tag{4.108}$$

As the value of the Peclet number increases, the behavior of the axial dispersion model in fact approaches that of a plug flow model. As a result of this, it is possible to simplify

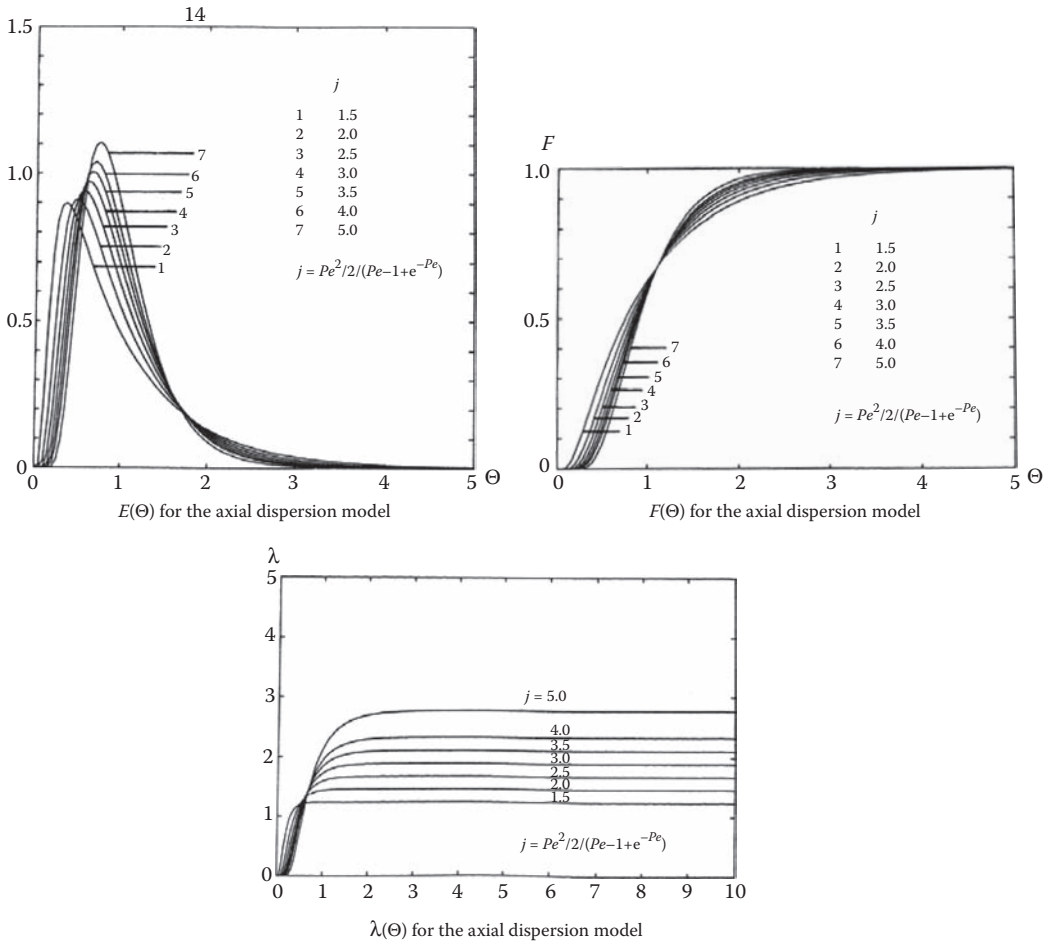

FIGURE 4.31 RTD functions for $E(\theta)$, $F(\theta)$, and $\lambda(\theta)$ for the axial dispersion model $\left(\sigma_\theta^2 = 1/j = \text{Equation 4.108}\right)$.

the boundary condition, Equation 4.97, with large values of the Peclet number (in practice greater than 50), to the following form:

$$\begin{aligned} z &= 0 \quad \theta > 0 \\ z &< 0 \quad \theta = 0 \quad c/c_0 = 1 \end{aligned} \tag{4.109}$$

In sum, we can say that if Equation 4.97 is solved with the boundary conditions, Equations 4.99, 4.100, and 4.106, an equation is obtained that is approximately valid at $Pe > 50$:

$$F(\theta) = \frac{1}{2}\left[1 - \text{erf}\left(\frac{1-\theta}{\sqrt{\theta}}\sqrt{\frac{Pe}{4}}\right)\right], \tag{4.110}$$

$$E(\theta) = \frac{e^{-Pe(1-\theta)^2/4}}{\sqrt{4\pi/Pe}}. \tag{4.111}$$

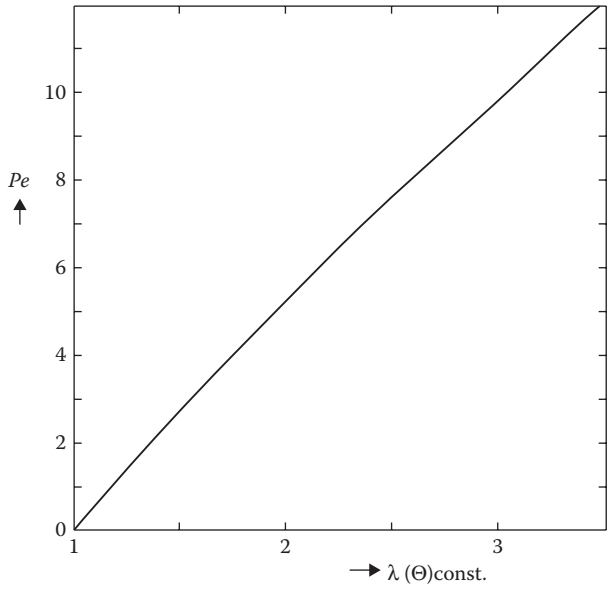

FIGURE 4.32 Relation between *Pe* and $\lambda(\Theta)_{\text{const.}}$ for the axial dispersion model.

As can be easily understood, this approaches the variance σ^2_Θ, along with increasing values of the Peclet number, so that the following expression can also be used at large values of the Peclet number ($Pe > 50$).

$$\sigma^2_\theta \approx \frac{2}{Pe} \quad \text{at } Pe > 50. \tag{4.112}$$

Because of their fundamentally different basic assumptions, the axial dispersion and tanks-in-series models can be compared on the basis of several criteria such as conversion or parameters j and Pe. From the comparison, it is evident that the conditions selected are such that both models obtain similar values of variances ($\sigma^2_\theta = 1/j$ for the tanks-in-series model).

4.5.2 AXIAL DISPERSION MODEL AS A CHEMICAL REACTOR

The final goal of the axial dispersion model is its utilization in the modeling of chemical reactors. Below we will consider steady-state models only, which imply that the mass balance of a reacting component i can be written as

$$[\text{inflow of } i] + [\text{generation of } i] = [\text{outflow of } i].$$

Quantitatively, this is expressed for the reactor volume element as

$$\dot{n}_{i,\text{in}} + \left(-D\frac{\mathrm{d}c_i}{\mathrm{d}l}A\right)_{\text{in}} + r_i \Delta V = \dot{n}_{i,\text{out}} + \left(-D\frac{\mathrm{d}c_i}{\mathrm{d}l}A\right)_{\text{out}}. \tag{4.113}$$

The following notations are introduced:

$$\dot{n}_{i,\text{out}} - \dot{n}_{i,\text{in}} = \Delta\dot{n}, \tag{4.114}$$

$$\left(D\frac{\mathrm{d}c_i}{\mathrm{d}l}A\right)_{\text{out}} - \left(D\frac{\mathrm{d}c_i}{\mathrm{d}l}A\right)_{\text{in}} = \Delta\left(D\frac{\mathrm{d}c_i}{\mathrm{d}l}A\right), \tag{4.115}$$

yielding

$$\Delta\left(D\frac{\mathrm{d}c_i}{\mathrm{d}l}A\right) - \Delta\dot{n}_{i,\text{in}} + r_i\Delta V = 0. \tag{4.116}$$

The molar flow difference, $\Delta\dot{n}_i$, is given by $\Delta(c_i w)A$. After a straightforward algebraic treatment, ($\Delta V = \mathrm{A}\Delta l$), we obtain

$$\frac{\Delta(D\,\mathrm{d}c_i/\mathrm{d}l)}{\Delta l} - \frac{\Delta(c_i w)}{\Delta l} + r_i = 0. \tag{4.117}$$

By allowing $\Delta l \to 0$, a differential equation is obtained:

$$\frac{\mathrm{d}(D\,\mathrm{d}c_i/\mathrm{d}l)}{\mathrm{d}l} - \frac{\mathrm{d}(c_i w)}{\mathrm{d}l} + r_i = 0. \tag{4.118}$$

Equation 4.118 is the most general one and can be applied to arbitrary kinetics. Usually, the dispersion coefficient is regarded as a constant that leads to

$$D\frac{\mathrm{d}^2c_i}{\mathrm{d}l^2} - \frac{\mathrm{d}(c_i w)}{\mathrm{d}l} + r_i = 0. \tag{4.119}$$

Equation 4.119 is valid for both gas- and liquid-phase reactions. For liquid-phase reactions, the density and flow rate (w) remain virtually constant and, consequently, Equation 4.119 can be simplified to

$$D\frac{\mathrm{d}^2c_i}{\mathrm{d}l^2} - w\frac{\mathrm{d}c}{\mathrm{d}l} + r_i = 0. \tag{4.120}$$

By introducing the dimensionless quantities, $z = l/L$, $y = c_i/c_{0i}$, the balance equation becomes

$$Pe^{-1}\frac{\mathrm{d}^2y}{\mathrm{d}z^2} - \frac{\mathrm{d}y}{\mathrm{d}z} + \frac{\bar{t}}{c_{0i}}r_i = 0. \tag{4.121}$$

The classical boundary conditions are

$$z = 0 \quad y - \frac{1}{Pe}\frac{\mathrm{d}y}{\mathrm{d}z} = 1, \tag{4.122}$$

$$z = 1 \quad \frac{\mathrm{d}y}{\mathrm{d}z} = 0. \tag{4.123}$$

Equation 4.121 is analytically solvable for linear (zero- and first-order) kinetics only. The solution of first-order kinetics, that is, $r_i = \nu_i k c_i$, after accounting for the boundary conditions above, Equations 4.122 and 4.123, becomes

$$y(z) = \frac{2\left[(1+\beta)\,\mathrm{e}^{-Pe(1-\beta)(1-z)/2} - (1-\beta)\,\mathrm{e}^{-Pe(1+\beta)(1-z)/2}\right]}{(1+\beta)(1+\beta)\,\mathrm{e}^{-Pe(1-\beta)/2} - (1-\beta)(1-\beta)\,\mathrm{e}^{-Pe(1+\beta)/2}}, \tag{4.124}$$

where

$$\beta = \sqrt{1 + 4k_A\bar{t}/Pe}. \tag{4.125}$$

The calculations can be performed to illustrate the above equation with the help of a kind of graph presented in Figure 4.33.

For nonlinear reaction kinetics, a numerical solution of the balance Equation 4.121 is carried out. For example, for second-order kinetics, $R = kc_Ac_B$, with an arbitrary stoichiometry, the generation rate expressions, $r_A = -\nu_A k c_A c_B$ and $r_B = -\nu_B k c_A c_B$, are inserted into the mass balance expression, which is solved numerically using, for example, a polynomial approximation (orthogonal collocation method). The performances of the "normal" dispersion model and its segregated or maximum-mixed variants are compared in Figure 4.34. The symbols are explained in the figure. The comparison reveals that the differences between the segregated, maximum-mixed, and normal axial dispersion models are notable at moderate Damköhler numbers (R = Damköhler number).

The axial dispersion model can further be compared with the tanks-in-series model using the concept of equal variances. A typical concentration pattern obtained for a complex

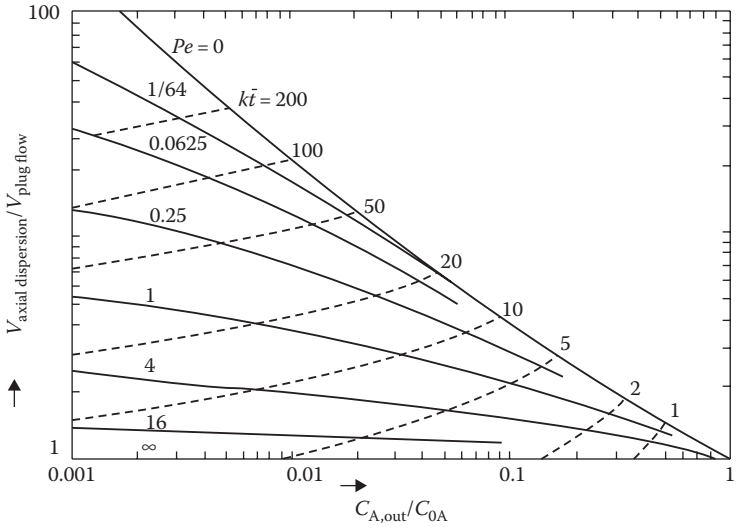

FIGURE 4.33 Reactor size predicted by an axial dispersion model compared with the size predicted by a plug flow model. First-order reaction, $-r_A = k_A c_A$.

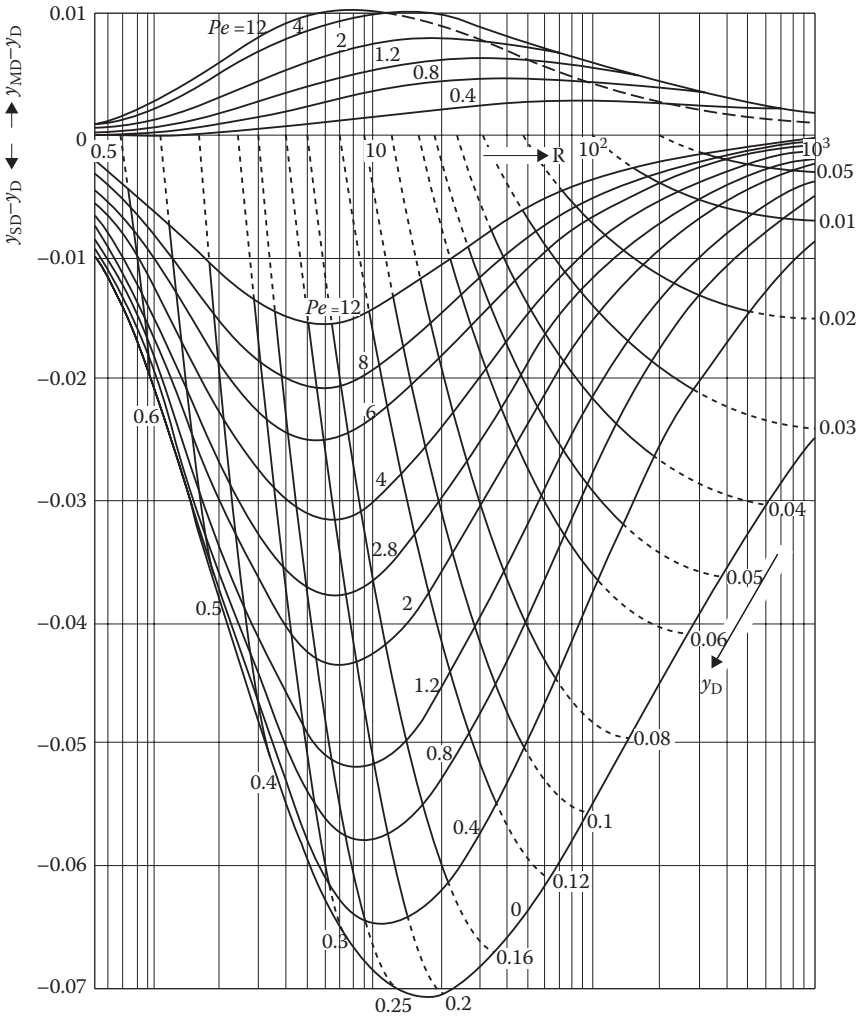

FIGURE 4.34 y_T (axial dispersion model), y_{MD} (maximum-mixed axial dispersion model), and y_{SD} (segregated axial dispersion model) at $M = 1.00$. $\mathrm{M} = \nu_A c_{0B}/(\nu_B c_{0A})$, $R = K_A \bar{t} c_{0A} \nu_B / \nu_A$.

reaction system

$$\mathrm{A} + \mathrm{B} \rightarrow \mathrm{R} + \mathrm{E}$$

$$\mathrm{R} + \mathrm{B} \rightarrow \mathrm{S} + \mathrm{E}$$

is shown in Figure 4.35. The concentration profiles were obtained by orthogonal collocation [4]. The product concentrations as a function of the mean residence time are shown in the figures. As shown in the figure, the concentrations predicted by the tanks-in-series and axial dispersion models are very similar, provided that equal variances are used in the calculations.

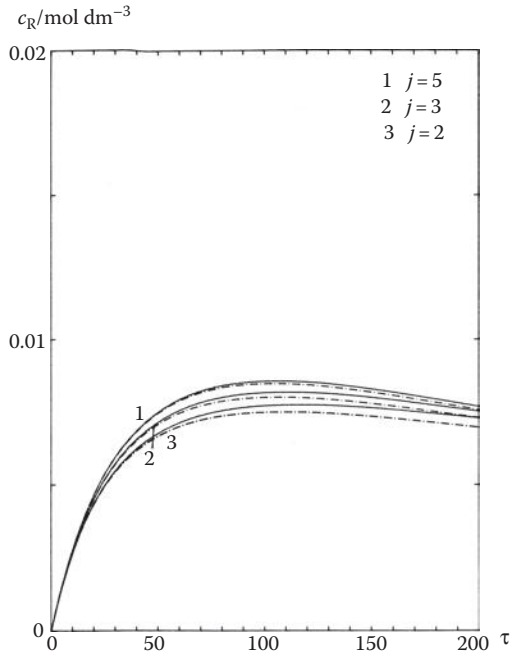

Axial dispersion (___) and tanks-in-series (_._._) models

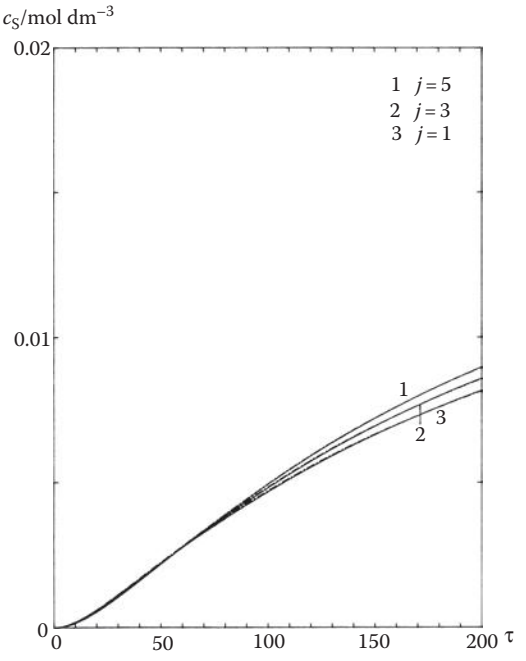

Axial dispersion (___) and tanks-in-series (_._._) models

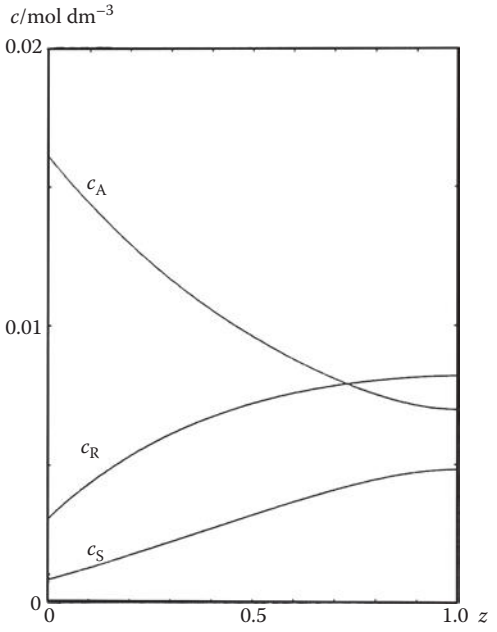

Concentration profiles in an axial dispersion reactor

FIGURE 4.35 Comparison of axial dispersion and tanks-in-series models for a consecutive-competitive reaction system (A + B → R + E, R + B → S + E).

4.5.3 ESTIMATION OF THE AXIAL DISPERSION COEFFICIENT

The axial dispersion coefficient can be determined experimentally, for instance, by finding the numerical value of the Peclet number, in impulse or step-response experiments. This is, however, possible, provided that experimental equipment (reactor) is available to carry out the experiments. This is not always the case. If no reactor experiments can be performed, the best approach is to estimate the value of the axial dispersion coefficient from the available correlations.

In tube reactors with laminar flow profiles, the axial dispersion coefficient (D) is related to the molecular diffusion coefficient (D_m), the average flow velocity, and the tube diameter (d):

$$D = D_m + \frac{w^2 d^2}{192\ D_m} \quad 1 < Re < 2000. \tag{4.126}$$

The above equation is valid for the values of *Reynolds number* below 2000 only. By incorporating the *Peclet number* (Pe) for a tube, $Pe_R = w\,d/D$, the same relation can be expressed using two dimensionless quantities, namely, the *Reynolds number* (Re) and *Schmidt number* (Sc) [5]:

$$\frac{1}{Pe_R} = \frac{1}{Re\ Sc} + \frac{Re\ Sc}{192}. \tag{4.127}$$

The above equation is valid for the intervals $1 < Re < 2000$ and $0.23 < Sc < 1000$, where $Re = wd/\nu$ and $Sc = \nu/D_m$. Here ν denotes the kinematic viscosity, $\nu = \mu/\rho$, where μ and ρ, in turn, denote the dynamic viscosity and the density, respectively. This relationship is illustrated in Figure 4.36. As shown in the figure, the value of Pe_R reaches a maximum ($0.5\sqrt{192}$) at $Re\ Sc = \sqrt{192}$. In the case of completely developed turbulent flow conditions, we refer to semiempirical correlations. It has been found that in these cases, the value of Pe_R is proportional to $Re^{1/8}$. A semiempirical correlation that is also able to describe the transition area between laminar and turbulent flow regimes can be written in the following form:

$$\frac{1}{Pe_R} = \frac{a}{Re^{\alpha}} + \frac{b}{Re^{\beta}} \quad Re > 2000, \tag{4.128}$$

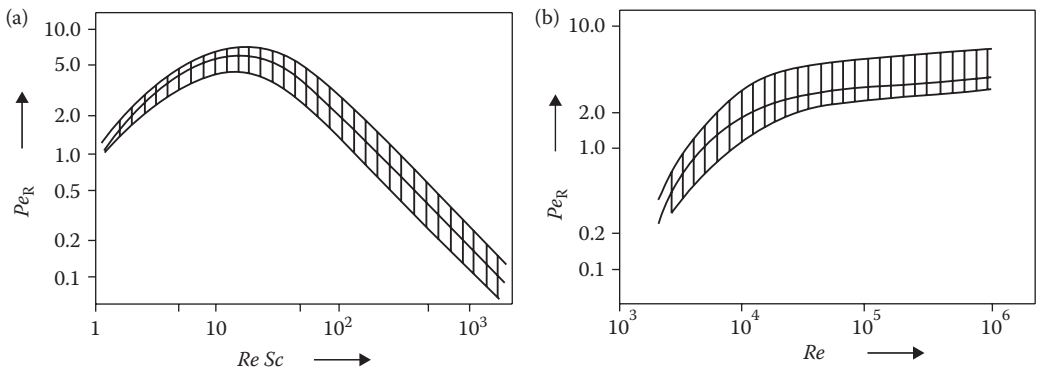

FIGURE 4.36 *Pe* for laminar (a) and turbulent (b) flows.

where $a = 3 \times 10^7$, $b = 1.35, \alpha = 2.1$, and $\beta = 1/8$. The relationship is illustrated in Figure 4.36. It is evident that the value of Pe_R at first rapidly increases as a function of the Reynolds number while the turbulence is developing. However, a limiting value of less than 20 is reached as the value of Reynolds number continues to increase. In case the Peclet number is based on the reactor diameter, the Peclet number based on the tube length is related accordingly:

$$Pe = Pe_R \frac{L}{d}. \tag{4.129}$$

The advantage of using the kind of correlations presented above is that the Peclet number can be estimated from the flow velocity and from easily measured physical material parameters (μ, ρ, D_m) only.

4.6 TUBE REACTOR WITH A LAMINAR FLOW

A tube containing a laminar flow can be considered as coaxial PFRs coupled in series, where the residence time varies according to the parabolic velocity profile ($t = L/w$, $w = w_0[1 - [r/R^2]]$) from the value of L/w_0, at the reactor axis, to the value of ∞ (infinity), at the reactor wall ($r = R$). Thanks to these differences in the residence times of radial volume elements, radial concentration profiles emerge. For instance, for a first-order reaction, the reactant concentration is higher at the location $r = 0$ than at a different location, $r > 0$. The reason for this is that a reactant molecule does not have enough time to undergo a complete chemical reaction at the reactor axis, thanks to the shorter time it resides in the reactor. At the reactor walls, on the contrary, we expect a practically complete conversion of the reactant to the product to have taken place. These radial concentration differences, concentration gradients, are countereffected by molecular diffusion, which is, in this context, denoted as radial diffusion. This phenomenon illustrates the constant tendency of "mother nature" to even up any gradients, to increase the total entropy. How the influence of radial diffusion on the reactor performance should be accounted for depends on the value of the diffusion coefficient, the reactor diameter, and the average residence time of the fluid in the reactor. In this section, a laminar reactor with both a negligible and a large radial diffusion are treated briefly.

4.6.1 LAMINAR REACTOR WITHOUT RADIAL DIFFUSION

Let us first assume that the radial diffusion is negligible. In this case, the laminar reactor operates just like a series of coaxial PFRs in parallel, where the average residence time varies between $t = L/w_0$ (in the middle axis) and $t = \infty$ (at the reactor wall). A mass balance for a component A, residing in an infinitesimal volume element with the volume $\Delta V = 2\pi r \Delta r \Delta l$, can be written, provided that steady-state conditions prevail (Figure 4.37):

$$(c_A w 2\pi r \Delta r)_{in} + r_A 2\pi r \Delta r \Delta l = (c_A w 2\pi r \Delta r)_{out}. \tag{4.130}$$

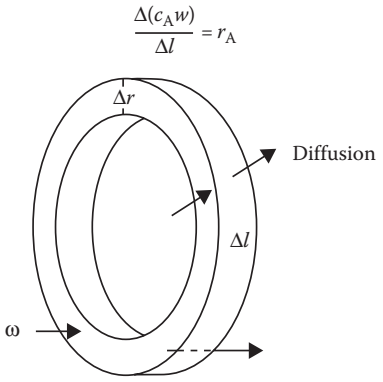

FIGURE 4.37 Volume element in a laminar reactor.

The above equation can be rewritten in the following form:

$$\frac{\Delta(c_A w)}{\Delta l} = r_A. \tag{4.131}$$

Since the volume element diminishes, the left-hand side of the derivative of $c_A w$ is

$$\frac{\mathrm{d}(c_A w)}{\mathrm{d}l} = r_A. \tag{4.132}$$

The above equation is valid for both gas- and liquid-phase reactions. In the case of gas-phase reactions, the flow velocity varies even in the length coordinate of the reactor, since the total molar amount changes as the reaction proceeds, causing pressure changes in the reactor tube. In the case of liquid-phase reactions, the velocity can often be considered as approximately constant, simplifying Equation 4.132 to

$$w\frac{\mathrm{d}c_A}{\mathrm{d}l} = r_A. \tag{4.133}$$

After insertion of Equation 4.130 for the flow velocity, we obtain

$$w_0\left(1 + (r/R)^2\right)\frac{\mathrm{d}c_A}{\mathrm{d}l} = r_A. \tag{4.134}$$

On the other hand, let us take into account that $\mathrm{d}l/w = \mathrm{d}t$, that is, equal to the residence time element. The balance Equation 4.133 can therefore be written in a new form,

$$\frac{\mathrm{d}c_A}{\mathrm{d}t} = r_A, \tag{4.135}$$

where $t = l/(w_0(1 - (r/R)^2))$, $0 \le r \le R$ and $0 \le l \le L$. The differential Equation 4.135 can be solved as a function of t, and the radial and longitudinal concentration distributions are obtained. However, the total molar flow and the average concentration ($c_{A,\mathrm{average}}$) at the

reactor outlet are of maximum interest to us. The total molar flow ($\dot{n}_A$) at the reactor outlet is obtained by means of integration of the whole reactor cross-section:

$$\dot{n}_A = \int_0^R c_A(r, L) w(r)\, 2\pi r\, dr = \bar{c}_A \dot{V}. \tag{4.136}$$

Recalling an earlier derivation for volume flow, $V = \pi R^2 w_0/2$, inserting it into Equation 4.136, and performing a few rearrangements, we obtain

$$\bar{c}_A = (4/R^2) \int_0^R c_A(r, L)(1 - (r/R)^2) r\, dr, \tag{4.137}$$

where $c_A(r, L)$ represents the solution of Equation 4.137 at $t = L/(w_0(1 - (r/R)^2))$, that is, at the reactor outlet. After incorporating a dimensionless coordinate, $x = r/R$, Equation 4.137 can be rewritten in an elegant form:

$$\bar{c}_A = 4 \int_0^1 c_A(x, L)(1 - x^2) x\, dx. \tag{4.138}$$

Let us now illustrate the use of the above equation by means of a first-order, irreversible, elementary reaction, A → P. The generation velocity of A is given by the expression $r_A = -kc_A$. The solution is obtained from $dc_A/dt = -kc_A$, $c_A/c_{0A} = e^{-kt}$, that is, $c_A/c_{0A} = \exp(-kL/(w_0(1 - x^2)))$. The average value for the concentration at the reactor outlet thus becomes [6]

$$\bar{c}_A = 4c_{0A} \int_0^1 e^{-kL/w_0(1-x^2)}(1 - x^2) x\, dx. \tag{4.139}$$

After using the notation $\bar{t} = 1$, $\bar{w} = 2L/w_0$, we arrive at

$$\frac{\bar{c}_A}{c_{0A}} = 4 \int_0^1 e^{-k\bar{t}/2(1-x^2)}(1 - x^2) x\, dx. \tag{4.140}$$

The result obtained, as above, can be compared with that obtained for a PFR,

$$\frac{c_A}{c_{0A}} = e^{-k\bar{t}}, \tag{4.141}$$

and for a completely backmixed reactor,

$$\frac{c_A}{c_{0A}} = \frac{1}{1 + k\bar{t}}. \tag{4.142}$$

The above expression, Equation 4.140, should be integrated numerically.

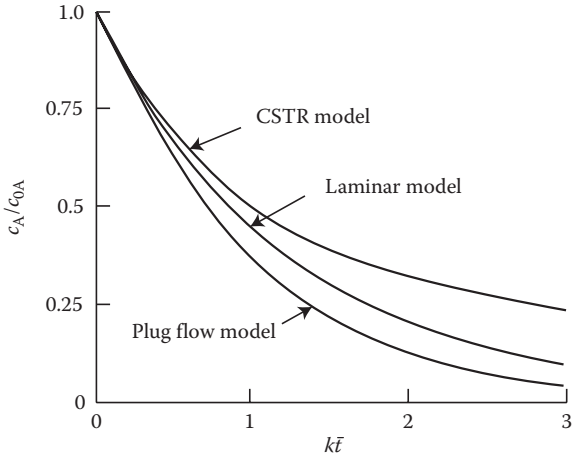

FIGURE 4.38 Comparison of PFR, CSTR, and laminar flow models for a first-order reaction.

A comparison shown in Figure 4.38 reveals that the laminar flow predicts a value for the reactant concentration that resides between those predicted for a PFR and a completely backmixed reactor. Corresponding comparisons can be performed for reactions with arbitrary reaction kinetics; Equation 4.140 needs to be solved, either analytically or numerically, as a function of t and, consequently, the average value is calculated using the numerical integration of Equation 4.138.

4.6.2 LAMINAR REACTOR WITH A RADIAL DIFFUSION: AXIAL DISPERSION MODEL

In cases in which radial diffusion plays a significant role in the reactor performance, its influence needs to be accounted for via the diffusion term. The simplest formulation of the diffusion term is given by Fick's law, which, for component A, is written as

$$N_A = -D_{mA}\frac{dc_A}{dr}, \tag{4.143}$$

where N_A denotes the flow of component A [for instance, in mol/(m^2 s)], D_{mA} is the molecular diffusion coefficient, and dc_A/dr is the radial concentration gradient of A. The diffusion takes place toward the surface element, $2\pi r\Delta l$ (Figure 5.10), whereby the flow (expressed in mol/time unit), for the volume element, becomes $N_A 2\pi r\Delta l$. The mass balance for component A, in the volume element, is thus obtained:

$$(c_A w\, 2\pi r\, \Delta r)_{in} + \left(-D_{mA}\frac{dc_A}{dr}2\pi r\, \Delta l\right)_{in} + r_A c_A w\, 2\pi r\, \Delta r \Delta l$$
$$= (c_A w\, 2\pi r \Delta r)_{out} + \left(-D_{mA}\frac{dc_A}{dr}2\pi r\, \Delta l\right)_{out}. \tag{4.144}$$

The difference between the diffusion terms, $(\cdot)_{\text{out}} - (\cdot)_{\text{in}}$, is denoted by $\Delta(\cdot)$ and the Equation 4.144 is transformed to

$$\Delta\left(D_{\text{mA}}\frac{\mathrm{d}c_{\text{A}}}{\mathrm{d}r}r\right)\Delta l + r_{\text{A}}r\Delta r\Delta l = \Delta(c_{\text{A}}w)r\Delta r, \tag{4.145}$$

which after division with $r\Delta r\Delta l$ yields

$$\frac{\Delta(D_{\text{mA}}\,(\mathrm{d}c_{\text{A}}/\mathrm{d}r)\,r)}{r\Delta r} + r_{\text{A}} = \frac{\Delta(c_{\text{A}}w)}{\Delta l}. \tag{4.146}$$

Let us allow the volume element shrink ($\Delta r \to 0, \Delta l \to 0$) to obtain the following differential equation:

$$\frac{\mathrm{d}(c_{\text{A}}w)}{\mathrm{d}l} = \frac{\mathrm{d}\,(D_{\text{mA}}\,(\mathrm{d}c_{\text{A}}/\mathrm{d}r)\,r)}{r\,\mathrm{d}r} + r_{\text{A}}. \tag{4.147}$$

The result, Equation 4.147, is a general expression for a laminar reactor tube under radial diffusion. A comparison with expression 4.132 illustrates the significance of the diffusion term as a whole. In most cases, the flow velocity (w) for liquid-phase reactions can be considered constant in the length coordinate, provided that D_{mA} is only weakly concentration-dependent. Consequently, in this case, Equation 4.147 is simplified to

$$w\frac{\mathrm{d}c_{\text{A}}}{\mathrm{d}l} = D_{\text{mA}}\left(\frac{\mathrm{d}^2c_{\text{A}}}{\mathrm{d}r^2} + \frac{1}{r}\frac{\mathrm{d}c_{\text{A}}}{\mathrm{d}r}\right) + r_{\text{A}}, \tag{4.148}$$

where $w = w_0(1 - (\mathrm{r}/R)^2)$. The dimensionless coordinates, $z = 1/L$ and $x = r/R$, are introduced. As a result, the balance is transformed to the elegant and simple form of

$$\frac{\mathrm{d}c_{\text{A}}}{\mathrm{d}z} = \frac{D_{\text{mA}}L}{w\mathrm{R}^2}\left(\frac{\mathrm{d}^2c_{\text{A}}}{\mathrm{d}x^2} + \frac{1}{x}\frac{\mathrm{d}c_{\text{A}}}{\mathrm{d}x}\right) + \frac{L}{w}r_{\text{A}}. \tag{4.149}$$

After insertion of the expression for $w(w = w_0(1 - (r/R)^2))$, we obtain

$$(1 - x^2)\frac{\mathrm{d}c_{\text{A}}}{\mathrm{d}z} = \frac{D_{\text{mA}}L}{w_0R^2}\left(\frac{\mathrm{d}^2c_{\text{A}}}{\mathrm{d}x^2} + \frac{1}{x}\frac{\mathrm{d}c_{\text{A}}}{\mathrm{d}x}\right) + \frac{L}{w_0}r_{\text{A}}. \tag{4.150}$$

The quantity D_{mA}/w_0R^2 is dimensionless and therefore represents a measure of the importance of radial diffusion. The average residence time, $\bar{t}$, is defined by $\bar{t} = L/\bar{w} = 2L/w_0$. The dimensionless term is thus $D_{\text{mA}}\bar{t}/R^2$. Let us present a recommended criterion for negligible radial diffusion:

$$D_{\text{mA}}\bar{t}/R^2 < 3 \cdot 10^{-3}. \tag{4.151}$$

Utilization of this criterion is simple, since the incorporated measures, $D_{\text{mA}}, \bar{t}$, and R, are known parameters for a reactor system.

The model Equation 4.149 is a parabolic, partial differential equation that can be solved numerically with appropriate initial and boundary conditions:

$$c_A = c_{0A} \quad \text{at } z = 0,\ 0 \le x \le 1, \tag{4.152}$$

$$\frac{dc_A}{dx} = 0 \quad \text{at } x = 0,\ x = 1. \tag{4.153}$$

The boundary condition $x = 0$, Equation 4.153, emerges for the sake of symmetry, and the boundary condition $x = 1$ indicates that the walls of the reactor are nonpenetrable for component A. Naturally, the radial diffusion flow, N_A, should be zero at the reactor wall.

The models presented for laminar flow with radial diffusion can be replaced with the somewhat simpler axial dispersion model by introducing individual dispersion coefficients of the type D_A.

REFERENCES

1. Danckwerts, P.V., Continuous flow systems. Distribution of residence times, *Chem. Eng. Sci.*, 2, 1–13, 1953.
2. Zwietering, T., The degree of mixing in continuous flow systems, *Chem. Eng. Sci.*, 11, 1–15, 1959.
3. Lindfors, L.-E., A study of the combined effects of kinetic parameters and flow models on conversions for second order reactions, *Can. J. Chem. Eng.*, 53, 647–652, 1975.
4. Salmi, T. and Lindfors, L.-E., A program package for simulation of coupled chemical reactions in flow reactors, *Comput. Ind. Eng.*, 10, 45–68, 1986.
5. Baerns, M., Hofmann, H., and Renken, A., *Chemische Reaktionstechnik*, Georg Theme, Verlag, Stuttgart, 1992.
6. Nauman, E.B., *Chemical Reactor Design*, Wiley, New York, 1987.

CHAPTER 5

Catalytic Two-Phase Reactors

A catalyst is a chemical compound that has the ability to enhance the rate of a chemical reaction without being consumed by the reaction. The catalytic effect was discovered by the famous British physician, Michael Faraday, who observed that the presence of a metal powder enhanced oxidation reactions. The catalytic effect was first described by the Swedish chemist, Jöns Jacob Berzelius, in 1836. The Baltic chemist and the Nobel Prize winner, Wilhelm Ostwald, described homogeneous, heterogeneous, and enzymatic catalysis separately—a definition that is valid even today. Homogeneous catalysts, such as organic and inorganic acids and bases, as well as metal complexes, are dissolved in reaction media. They enhance the reaction rate, but their effect is limited to the reaction kinetics. Heterogeneous catalysts, on the other hand, form a separate (solid) phase in a chemical process. Mass and heat transfer effects thus often become prominent when using heterogeneous catalysts. Heterogeneous catalysts are typically metals and metal oxides, but many other materials have been found to possess a catalytic effect (e.g., zeolites and other alumina silicates). Heterogeneous catalysts are the dominant ones in the chemical industry, mainly because they are easier to recover and recycle. Enzymes are highly specific catalysts of biochemical systems. They are, for instance, used in the manufacture of alimentary products and pharmaceuticals. Although enzymes are homogeneous catalysts, they can be immobilized by several methods on solid materials, and a heterogeneous catalyst is thus obtained.

The word "catalysis" has a Greek origin, meaning "dissolve." This is exactly what a catalyst does: it helps facilitate close contact between reacting molecules and thus lowers the activation energy. Typical examples can be listed from any branch of industry. Solid iron-based catalysts are able to adsorb hydrogen and nitrogen molecules on their surface, hydrogen and nitrogen molecules are dissociated to atoms on the surface, and, consequently, ammonia molecules are gradually formed. In the cleaning of automotive exhaust gases, for instance, carbon monoxide and oxygen are adsorbed on the solid noble metal surface, and they react on the surface, forming carbon dioxide. In the production of margarine, fatty

acid molecules are hardened by adding hydrogen molecules to the double bonds of acid molecules. This takes place in the liquid phase, on the surface of a finely dispersed catalyst powder. About 90% of the chemical industry is based on the use of catalysts, the vast majority being heterogeneous ones. Without catalysts our society cannot function.

The key issue is the development of catalytic materials, which, in most cases, consist of an active metal or a metal oxide deposited on a carrier material. To attain adequate contact surface for the molecules, the carrier material has a high surface area, typically between 50 and 1000 m^2/g. It is clear that such high surface areas can only be achieved with highly porous materials. The surface areas of some typical carrier materials are listed in the table below:

Aluminum oxide (Al_2O_3)	$\leq 200\ m^2/g$
Silica (SiO_2)	$\leq 200\ m^2/g$
Zeolite materials	$\geq 500\ m^2/g$
Active carbon materials	up to $2000\ m^2/g$

It is possible to deposit catalytically active metals on these carrier materials. The sizes of the metal particles are typically very small, usually a few nanometers. With modern techniques, it is possible to observe not only catalyst particles but also the metal particles on their surfaces (e.g., transmission electron microscopy, TEM). The below-mentioned figures show the support material and the catalytic metal particles. The metal particles on the surface have an average diameter of 5–10 nm.

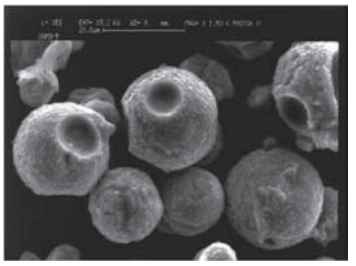

A scanning electron microscopy image of a typical zeolite catalyst.

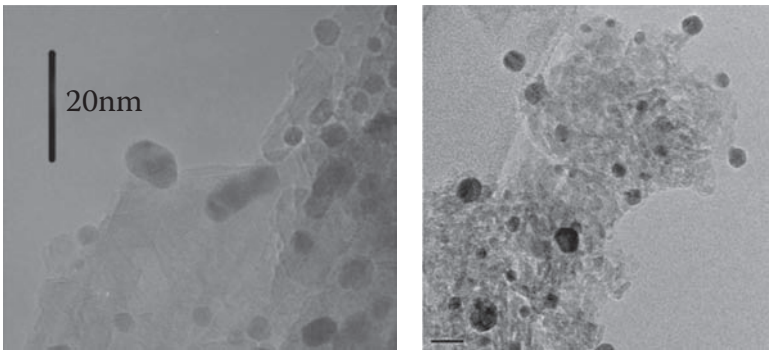

Metal particles on a catalyst support ($Pt/A1_2O_3$). TEM image.

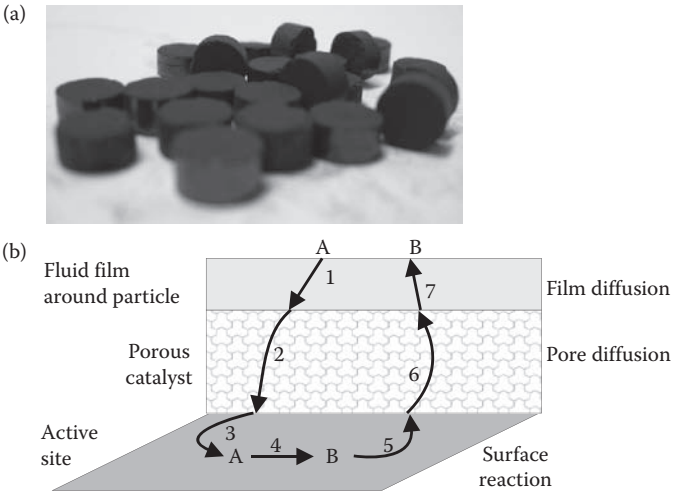

FIGURE 5.1 (a) Typical catalyst particles and (b) steps of a heterogeneously catalyzed process. (1) Film diffusion of A, (2) pore diffusion of A, (3) adsorption of A on active site, (4) surface reaction, (5) desorption of B, (6) pore diffusion of B, and (7) film diffusion of B.

The catalyst particle sizes and shapes (Figure 5.1) vary considerably depending on the reactor applications. In fixed beds, the particle size varies roughly between 1 mm and 1 cm, whereas for liquid-phase processes with suspended catalyst particles (slurry), finely dispersed particles ($<100\,\mu m$) are used. Heterogeneous catalysis in catalytic reactors implies an interplay of chemical kinetics, thermodynamics, mass and heat transfer, and fluid dynamics. Laboratory experiments can often be carried out under conditions in which mass and heat transfer effects are suppressed. This is not typically the case with industrial catalysis. Thus, a large part of the discussion here is devoted to reaction–diffusion interaction in catalytic reactors.

5.1 REACTORS FOR HETEROGENEOUS CATALYTIC GAS- AND LIQUID-PHASE REACTIONS

What is characteristic for heterogeneous catalytic reactors is the presence of a solid catalyst that accelerates the velocity of a chemical reaction without being consumed in the process. The reacting species, the reactants, can be in a gas and/or liquid form. The reactant molecules diffuse onto the outer surface of the solid catalyst and, if catalyst particles are porous, into the catalyst pore system. Inside the pores, the reactant molecules are adsorbed on catalytically active sites and, consequently, react with each other. The product molecules thus formed desorb from the surface and diffuse out through the pores into the bulk of the reaction mixture [2,9]. This process is illustrated in Figure 5.1 [1].

Rate expressions for heterogeneously catalyzed processes are derived on the basis of the steps illustrated in Figure 5.1. Typical rate expressions are listed in Table 5.1. Details of the derivation of the rate expressions are provided in Chapter 2.

TABLE 5.1 Processes Where Catalytic Packed Beds Are Applied

Chemical Bulk Industry	Oil Refining	Petrochemical Industry
Steam reforming	Reforming	Manufacturing
Carbon monoxide conversion	Isomerization	Ethene oxide
Carbon monoxide methanization	Polymerization	Ethene dichloride
Methanol synthesis	Dehydrogenation	Vinyl acetate
Oxo-synthesis	Desulfurization	Butadiene
	Hydrocracking	Maleic acid anhydride
		Phthalic acid anhydride
		Cyclohexane
		Styrene
		Hydrodealkylations

A typical rate expression for catalytic processes on ideal solid surfaces (i.e., surfaces for which each catalytic site is equal) is

$$R = \frac{k\left(c_A^a c_B^b - c_P^p c_R^r / K\right)}{\left(1 + \sum K_i c^{s_i}\right)^\gamma} \tag{5.1}$$

where A, B, . . . denote the reactants and P, R, . . . denote the products (Table 2.1). The values of the exponents depend on the detailed reaction mechanism. Parameter k is a merged rate parameter comprising the surface reaction as well as the sorption effects. Parameter K_i describes the adsorption strengths of various species.

In practically oriented catalysis, particularly in catalysis applied to industrially relevant reactions, the decline of catalyst activity is a profound phenomenon. The reasons for catalyst deactivation are several: merging of metal spots to larger ones through sintering, deposition of a reactive species (reactant or product) on the catalyst surface (fouling), or deposition of any species in the reactor feed on the surface (poisoning). Detailed mechanistic models can be derived for these cases, treating the deactivation process as a fluid–solid reaction. This approach is complicated and requires a molecular-level understanding of the process. In many cases, simpler semiempirical models are used. They are based on the principle of separable kinetics, according to which the real, time-dependent rate (R') is obtained from

$$R' = aR, \tag{5.2}$$

where a is a catalyst activity factor. Suitable equations for activity factors are given below:

$$a = a^* + \left(a_0 - a^*\right) \mathrm{e}^{-k't}, \quad n = 1, \tag{5.3}$$

$$a = a^* + \left[\left(a_0 - a^*\right)^{1-n} + k'\,(n-1)\,t\right]^{1/(1-n)}, \quad n \neq 1, \tag{5.4}$$

where a_0 is the initial activity (often $a_0 = 1$) and a^* is the asymptotic activity (for irreversible deactivation $a^* = 0$); n is the order of the deactivation process; and k' is the (semi)empirical

deactivation constant. The advantage of this approach is that standard steady-state kinetic and reactor models can be used. Parameters a_0, a^*, n, and k' are typically determined experimentally.

Even multiple phases such as gas or liquid phases may be simultaneously present in a catalytic reactor. In such a case, the gas molecules are, at first, dissolved in the liquid bulk, after which they diffuse to the surface of the catalyst. This is where the actual reaction takes place. The industrial system is called a three-phase reactor. Three-phase reactors are discussed in Chapter 6; here, we will concentrate on catalytic two-phase reactors, in which a fluid—gas or liquid—reacts on the surface of a solid catalyst. The most commonly encountered types of catalytic two-phase reactors that are used industrially are a packed (fixed) bed reactor, a fluidized bed reactor, and a moving bed reactor.

A packed (fixed) bed is the most commonly applied reactor in the chemical industry, often called "the working horse of the chemical industry" [2]. The operating principle of a packed bed is illustrated in Figure 5.2. Catalyst particles are placed in a tube, through which the fluid is passed. Generally, catalyst particles are in the form of pellets (the diameter varying from a few millimeters to several centimeters) and stagnant. Excessively small particle sizes are avoided since they start moving as the flow velocity increases. Additionally, very small particles cause a high pressure drop in the reactor. On the other hand, when using large catalyst particles, the diffusion distance to the active sites inside the catalyst increases.

A few examples of catalytic two-phase processes are given in Table 5.1. As can be seen in the table, the processes introduced are, first and foremost, reactions in the inorganic bulk chemical industry such as the manufacture of ammonia, sulfuric acid, nitric acid, and reactions in the petrochemical industry such as the manufacture of monomers, synthetic fuels, hydrogenations, dehydrogenations, dearomatizing reactions, and so on.

An extraordinary type of packed bed is utilized in the oxidation of ammonia to nitrogen oxide, in connection with the nitric acid production: the oxidation reaction takes place at a high temperature (890°C) on a metal net, on which the active catalyst (Pt metal) is dispersed. This reactor type, which can be treated mathematically as a packed bed reactor, is called a gauze reactor. An illustration of a gauze reactor is given in Figure 5.3 [3].

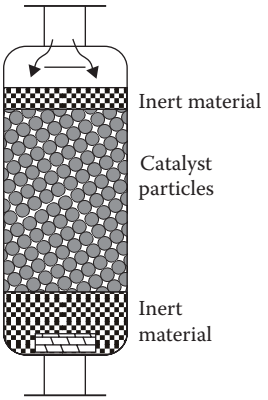

FIGURE 5.2 Typical packed bed reactor.

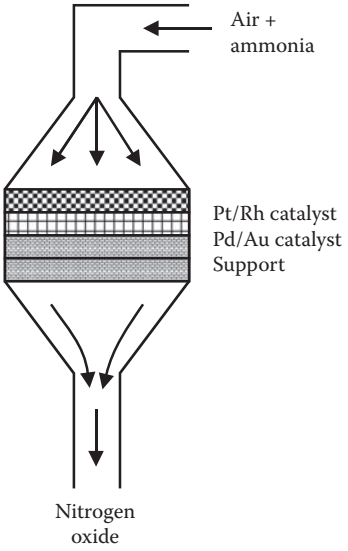

FIGURE 5.3 Gauze reactor.

An automotive catalyst, that is, a catalytic converter for internal combustion engines, can be regarded as a packed bed reactor, in which the active metals (the most important ones being Pt, Pd, and Rh) reside on a carrier substance, which in turn is attached to a ceramic or a metallic monolith structure. A catalytic converter for internal combustion engines is illustrated in Figure 5.4 [1]. Similar monolith structures can also be utilized in conventional industrial processes such as catalytic hydrogenations [4].

For industrial processes on a large scale, two different constructions of packed beds are very common: *multibed* and *multitubular* reactors. These reactors are illustrated in Figures 5.5 and 5.6.

What is characteristic for a multibed reactor is that several, often adiabatic catalyst beds are coupled in series. Heat exchangers are placed in between the beds: heat should be supplied in the case of an endothermic reaction (so that the reaction is not extinguished in the following step), and heat should be removed in the case of an exothermic reaction (to

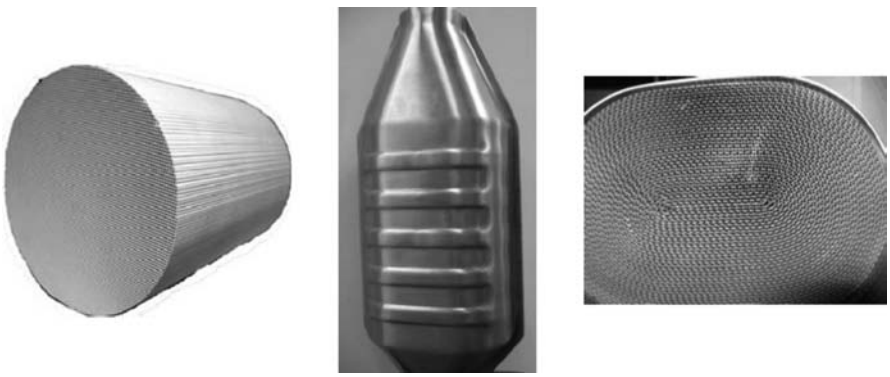

FIGURE 5.4 Ceramic and metallic monolith catalysts.

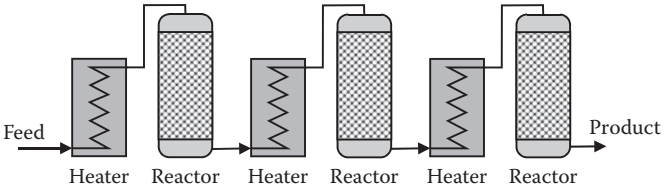

FIGURE 5.5 Multibed reactor system.

avoid catalyst deactivation due to sintering or to prevent a temperature runaway). Even in case the reaction is a reversible and exothermic one, heat needs to be removed. The reason for this is that the equilibrium composition becomes unfavorable at high temperatures. Multibed reactors typically have a low length-to-diameter ratio. The principal layout of a multibed reactor is simple and affordable—in comparison to other types of catalytic reactors. Typical examples of using a multibed reactor are oxidation of sulfuric dioxide (SO_2) in the production of sulfuric acid, ammonia synthesis, and catalytic reforming processes.

This kind of multibed reactor system is utilized in reforming processes (Figure 5.7). Catalytic reforming is an endothermic process; the Pt catalyst is placed in packed beds coupled in series, and between the beds, heating elements are present at an elevated temperature, since the temperature falls in the reaction zone due to the occurrence of endothermic reactions.

A multibed reactor system that is used in the oxidation of SO_2 to SO_3, on a V_2O_5 catalyst, is illustrated in Figure 5.8. The reactors operate at atmospheric pressure, and the heat of the reaction is removed by external heat exchangers, which are also used to preheat the feed into the reactor. In modern sulfuric acid factories, at least four catalyst beds in series

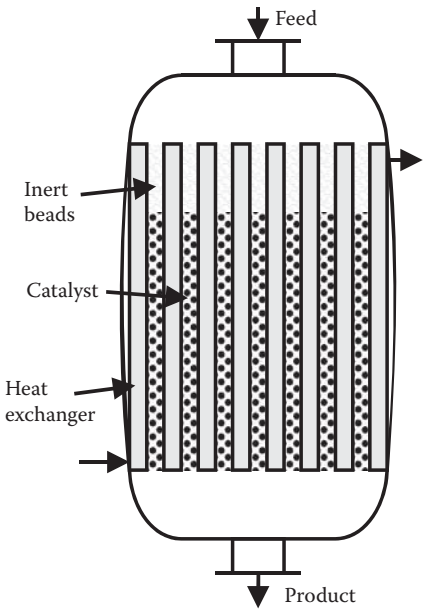

FIGURE 5.6 Multitubular reactor.

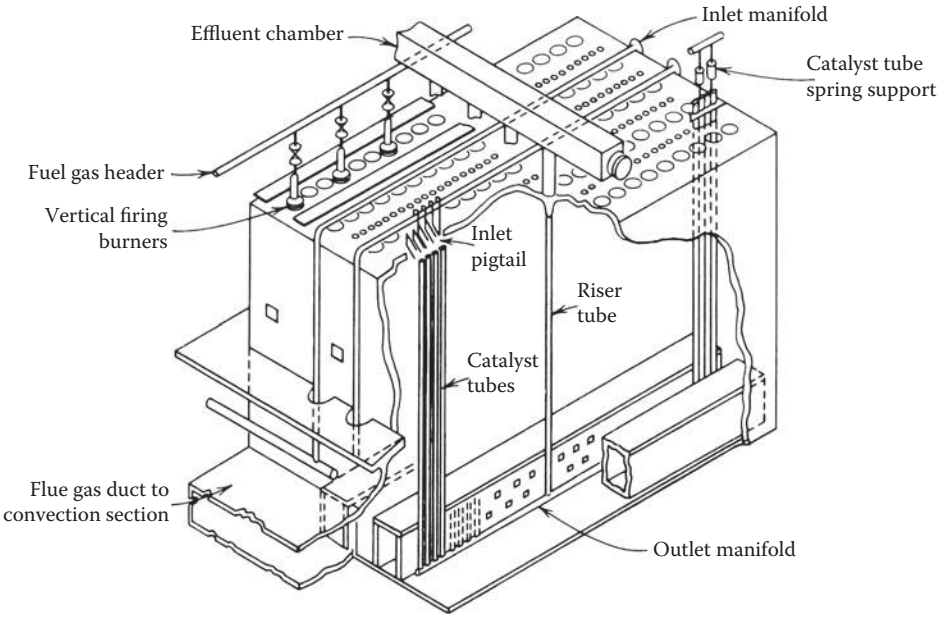

FIGURE 5.7 Packed bed for steam reforming. (Data from Froment, G. and Bischoff, K., *Chemical Reactor Analysis and Design*, 2nd Edition,Wiley, New York, 1990.)

(contact steps) are used, primarily to minimize the environmental impact caused by flue gases containing sulfur.

In the synthesis of ammonia (NH_3), a multibed reactor is used. The reaction takes place on an iron catalyst, and ammonia is synthesized from hydrogen and nitrogen. Extraordinary

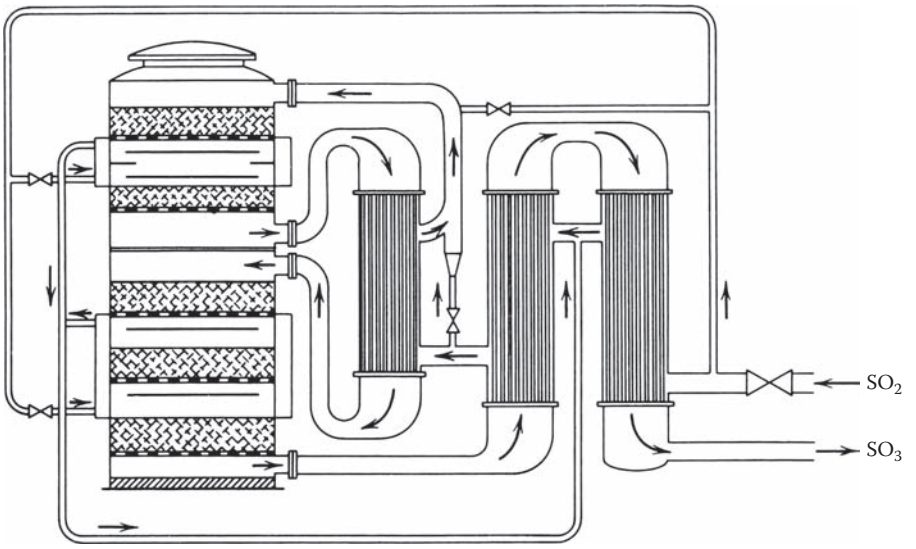

FIGURE 5.8 Multibed reactor for oxidation of SO_2 to SO_3. (Data from Froment, G. and Bischoff, K., *Chemical Reactor Analysis and Design*, 2nd Edition,Wiley, New York, 1990.)

demands on the reactor construction arise from the fact that the reactor operates at a high pressure (300 atm) in order to reach a favorable equilibrium point. To maintain the pressure, the construction needs to be as compact as possible. This is why external heat exchangers are out of question. Sample design layouts of various ammonium synthesis reactors are introduced in Figures 5.9 through 5.11. The exchange of heat is ensured by internal heat exchangers, in which the cold feed is heated by the product gas flow (Figure 5.9). In the most recent constructions, such as Haldor Topsøe's radial ammonia converter (Figure 5.11), even the reactants are heated by product gases via an internal heat exchanger. The inflows are further fed radially through several short beds to minimize the pressure drop and obtain as good as possible a contact with the catalyst. In methanol synthesis, similar packed beds are used as in the synthesis of ammonia, since this reversible as well as exothermal reaction requires a high pressure.

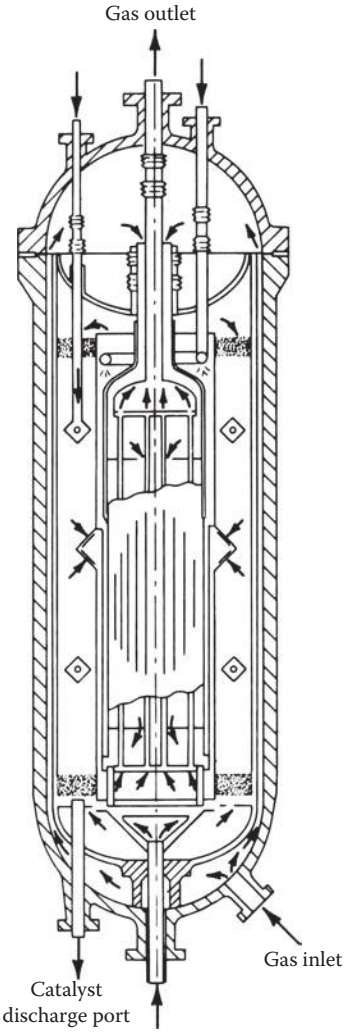

FIGURE 5.9 ICI reactor. (Data from Froment, G. and Bischoff, K., *Chemical Reactor Analysis and Design*, 2nd Edition,Wiley, New York, 1990.)

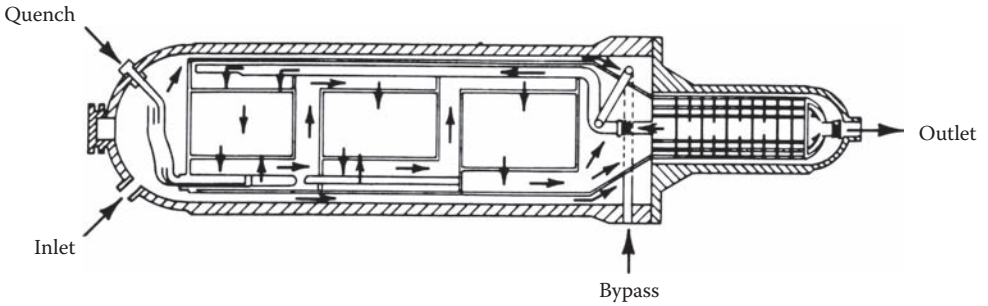

FIGURE 5.10 Horizontal multibed Kellogg reactor. (Data from Froment, G. and Bischoff, K., *Chemical Reactor Analysis and Design*, 2nd Edition,Wiley, New York, 1990.)

In very strongly exothermic reactions such as the oxidation of aromatic hydrocarbons, a multibed construction becomes uneconomical: too many beds would be required to keep up with the heat generated and to maintain the increase in temperature in the beds within reasonable limits. In this case, a *multitubular* bed offers an attractive alternative: up to thousands of small tubes (diameter in the range of a few centimeters) are coupled parallel to

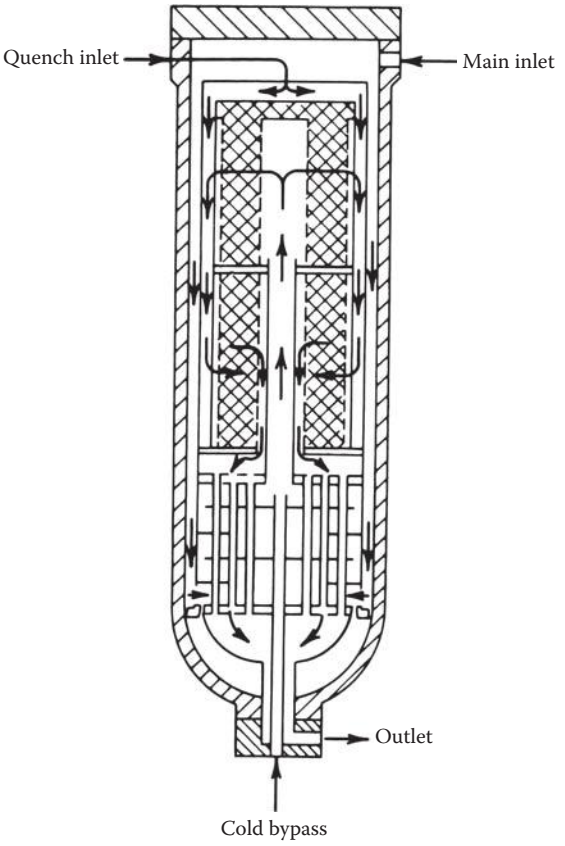

FIGURE 5.11 Radial Haldor–Topsøe converter. (Data from Froment, G. and Bischoff, K., *Chemical Reactor Analysis and Design*, 2nd Edition,Wiley, New York, 1990.)

each other and placed in a heat exchanger. A heat carrier liquid, such as a salt–melt mixture, circulates in the heat exchanger and releases its heat content into a secondary heat exchanger that produces steam. An example of a multitubular reactor that is used in the selective oxidation of *o*-xylene to phthalic acid anhydride on a V_2O_5 catalyst is shown in Figure 5.12.

There are a number of reasons why packed bed reactors are so dominant in the realization of heterogeneous catalytic processes. The flow conditions in packed beds are very close to that of a plug flow, which implies that a packed bed construction gives the highest conversion for the most common reaction kinetics. In the case of consecutive and consecutive-competitive reactions, a packed bed also favors the formation of intermediate products. Further, the principal construction of a packed bed reactor is simple, since no moving parts are required. The reactor is well known, and there are several commercial manufacturers. Optimizing the operation of the bed is also a straightforward task. As an example, one can mention the optimization of reactor cascades (multibed) so that the total reactor volume becomes the smallest possible, or optimization of the catalyst distribution in the bed so that no hot spots emerge. The fact that mathematical modeling of a packed bed is well known today is also a clear advantage: we are able to theoretically calculate the performance of a future reactor with relative reliability, provided that the kinetic and transport parameters are determined *a priori* accurately enough. This results in considerable savings in the design of a new process.

A packed bed reactor has, nevertheless, some characteristic disadvantages. A pressure drop in the bed can cause problems, if too long beds or too small catalyst particles are utilized. These problems can, however, be resolved. A more serious disadvantage is the

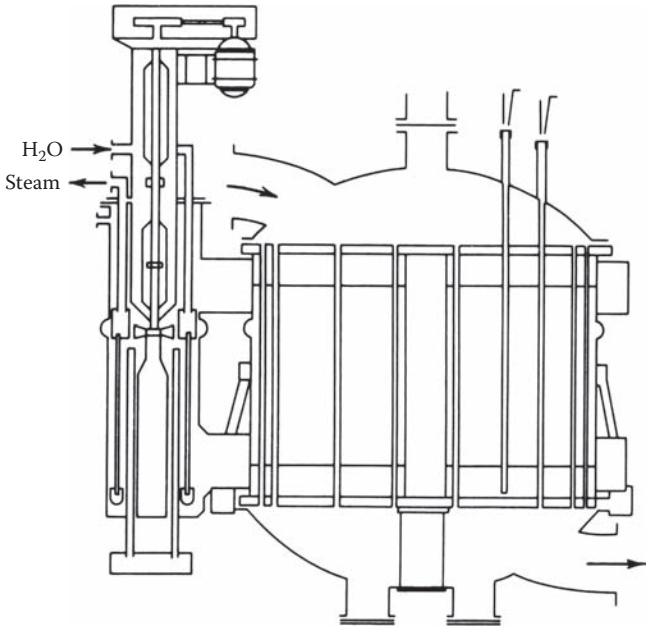

FIGURE 5.12 Multitubular reactor for the oxidation of *o*-xylene to phthalic acid anhydride. (Data from Froment, G. and Bischoff, K., *Chemical Reactor Analysis and Design*, 2nd Edition,Wiley, New York, 1990.)

emergence of *hot spots* in exothermic reactions. If an exothermic reaction proceeds in a tube filled with a catalyst and it is cooled externally, the temperature is initially bound to increase rapidly toward a maximum (hot spot). Due to cooling and lower reactant concentrations, the reaction velocity is bound to decrease after the last hot spot, and the overall temperature will consequently follow suit. This phenomenon is illustrated well in Figure 5.13, which shows catalytic hydrogenation of toluene on a Ni catalyst [6]. The temperature in the narrow hot spot itself dictates the reaction construction to a large extent: the maximum temperature should remain below the maximally allowed temperature, which is set by the heat tolerance of the catalyst material and the reactor, the desired product distribution (i.e., selectivity), and safety aspects. The hot spot effect can sometimes have serious consequences. This can be illustrated well by a sample reaction: oxidation of aromatic hydrocarbons. In Figure 5.14, the temperature evolution in a packed bed reactor is shown for the oxidation of *o*-xylene, at various temperatures [7]. If the feed and coolant temperatures exceed a certain limiting value, a temperature decrease no longer takes place after a hot spot, but instead the temperature starts to increase exponentially (*temperature runaway*). In this case, the desired intermediate product (phthalic acid anhydride) reacts further to yield valueless final products (CO_2 and H_2O). At the same time, the catalyst is destroyed! In fact, this phenomenon is sometimes called an "explosion." The hot spot phenomenon can, to a certain degree, be controlled by an uneven catalyst distribution in the reactor: at the beginning of the reactor, the catalyst concentration can be diluted using an inert solid material mixed with the actual catalyst. Subsequently, further away from the inlet, the catalyst amount is increased, as the reaction rate tends to decline due to the consumption of reactants.

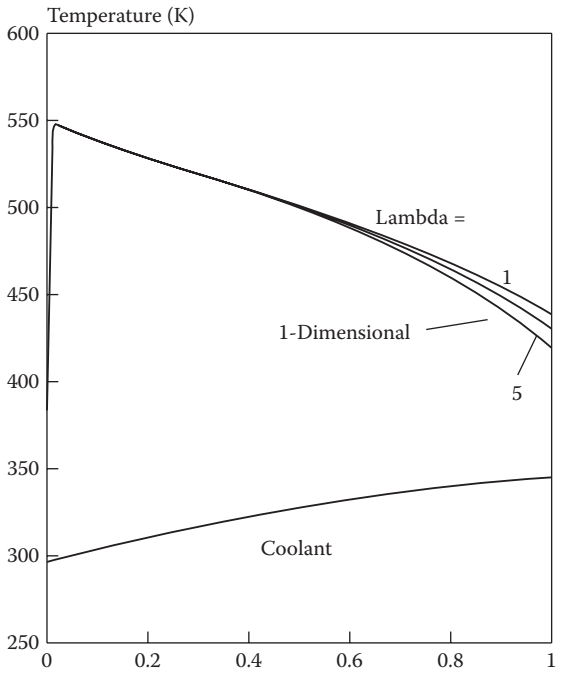

FIGURE 5.13 A hot spot at catalytic hydrogenation of toluene in a packed bed.

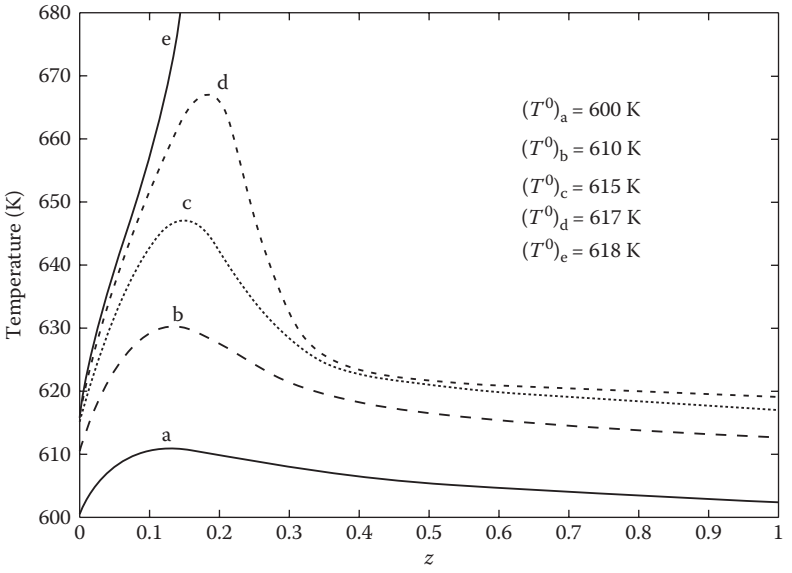

FIGURE 5.14 Dependence of the hot spot on the feed temperature. Catalytic oxidation of *o*-xylene.

For some catalytic processes, the use of packed beds leads to problems. This has led to the development and innovation of new reactors. In catalytic cracking of hydrocarbons—one of the core processes in an oil refinery—*coke deposits* are accumulated on the surface of the zeolite catalyst. This leads to deactivation and requires a replacement or a regeneration of the catalyst. Catalyst regeneration is cumbersome in a packed bed: the bed must be taken off-line in production, emptied, and refilled with a fresh catalyst. The first solution to this dilemma was the *moving bed* construction. The catalyst moved downward in the reactor, and the reactant gas mixture flowed upward. The removed catalyst was transported to a regeneration unit, and the regenerated catalyst was fed into the top of the reactor. A moving bed reactor construction is shown in Figure 5.15 [5].

Further advancement of the moving bed reactor was realized by reducing the particle sizes and increasing the flow velocities, so that a fraction of the particles is transported out of the reactor into the regeneration unit. It turned out that this kind of a bed closely resembles a huge quantity of boiling liquid in its visual characteristics. The gases were collected into bubbles with very few catalyst particles, whereas the main bulk of the reactor contents comprised a so-called emulsion phase, which was much richer in catalyst particles. The particles float freely in the reactor. This innovation was called a *fluidized bed*. A sketch of the principal layout of a fluidized bed is shown in Figure 5.16 [8].

Fluidized beds experienced an industrial breakthrough during the late 1940s, in connection with catalytic cracking. Subsequently, several modifications of this reactor have been developed. A few of these are shown in Figure 5.17. There are two parts, however, that are characteristic to any construction: the reactor unit and the regeneration unit. Examples of commercial applications in fluidized beds are presented in Table 5.2 [3]. This shows that the fluidized bed technology is absolutely dominant in catalytic cracking, whereas it struggles

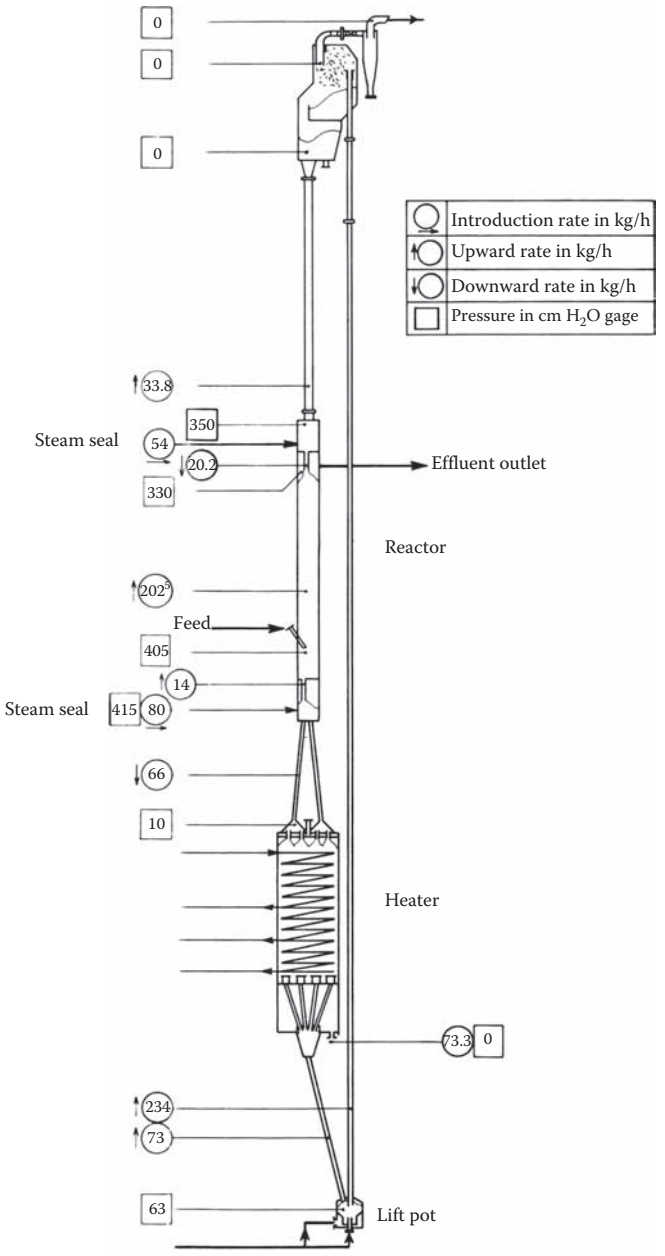

FIGURE 5.15 Moving bed reactor construction. (Data from Trambouze, P., van Landeghem, H., and Wauquier, J.P., *Chemical Reactors—Design/Engineering/Operation*, Edition Technip, Paris, 1988.)

to compete with the fixed bed technology in several other processes (reforming, production of phthalic acid anhydride, dehydrogenation of isobutane, etc.).

There are, however, situations in which we should carefully consider the fluidized bed as an option. If large amounts of catalyst materials need to be transported, for example, due to deactivation and regeneration, a fluidized bed is the most advantageous—and often the only possible construction alternative. If the reactions are so rapid that short residence times are

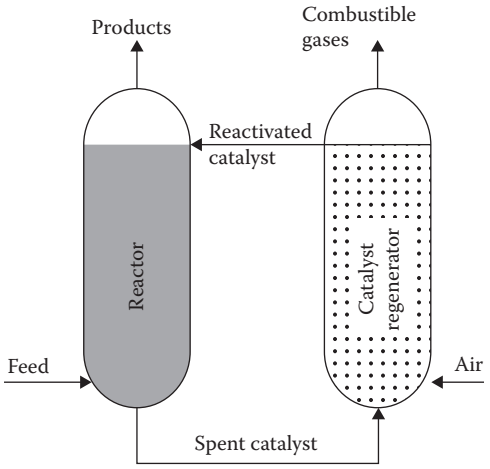

FIGURE 5.16 Fluidized bed reactor with incorporated catalyst regeneration. (Data from Chen, N.C., *Process Reactor Design*, Allyn and Bacon, Boston, 1983.)

sufficient to reach the desired degree of conversion, a fluidized bed can be used: thanks to high gas velocities, the residence time becomes short in fluidized beds. A fluidized bed is a significant candidate if a precise control of the reactor temperature is needed in the process for selectivity reasons: a fluidized bed is isothermal, the whole bed has an equal temperature, and with correct selection of the process conditions, the optimum temperature can be achieved.

A fluidized bed has, however, significant disadvantages that have slowed down its utilization in the chemical industry. The reactor construction itself is complicated and expensive compared with a packed bed. The flow conditions in the reactor vary between a plug flow and complete backmixing. Under bad operating conditions, a fraction of the gas in the bubble phase can even pass through the reactor without coming into contact with the catalyst. These lead to a lower conversion of the reactants and can sometimes result in undesired product distribution. The flow conditions can, however, be modified so that plug flow is approached in a *riser* reactor illustrated in Figure 5.18 [9].

Solid particles in a fluidized bed have a very vigorous movement. Particle attrition, breakdown, or agglomeration can occur in different parts of the reactor. The reactor walls are eroded by the catalyst particles: the conditions inside the reactor are similar to sand-blowing. This is why the running costs of a fluidized bed can become high. The most serious problems with fluidized beds are, however, the environmental aspects. Catalyst particles are very small (<1 mm) at the beginning, and they are further reduced in size by erosion and attrition during the operation. Removing very fine particles from the product gas is expensive. On the other hand, certain catalyst metals (such as Cr) are considered poisons (heavy metals) that cannot be released into the biosphere. This aspect is perhaps going to be the most decisive factor when considering the use of a fluidized bed in new processes. On the other hand, in various environmental applications as well as in the combustion of solid fuels (such as biofuels, black liquor, etc.), the fluidized bed technology has proven its excellence well. One of its advantages in combustion processes is the possibility of feeding substances such as limestone directly into the fluidized bed furnace, together with the fuel to absorb harmful substances such as sulfur dioxide.

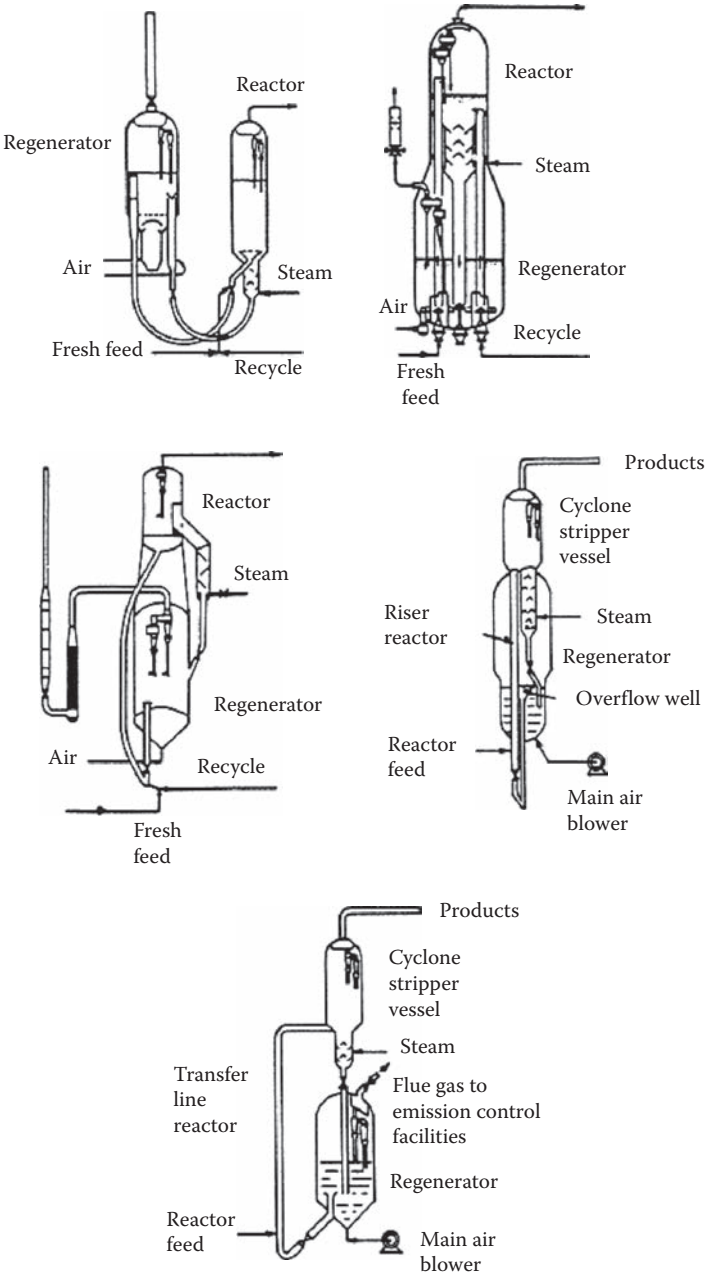

FIGURE 5.17 Various constructions of fluidized beds. (Data from Rase, H.F., *Chemical Reactor Design for Process Plants*, Wiley, New York, 1977.)

5.2 PACKED BED

Mathematical models for a catalytic packed bed reactor can be classified into two main categories: pseudohomogeneous and heterogeneous models. For a pseudohomogeneous model, it is characteristic that the fluid phase (gas or liquid) and the solid catalyst are considered as a continuous phase in which chemical reactions take place at a certain velocity. The entire

TABLE 5.2 Commercially Applied Processes Utilizing Fluidized Beds

Process	Catalyst Deactivation	Reaction Rate and Operating Conditions	Catalyst or Solid Circulation Rate	Heat Transfer	Assessment
Catalytic cracking	Rapid coking necessitating frequent regeneration	Fast, <1 s contact time. Longer times are not catastrophic, 450–525°C, 1–2 atm	Large	Important, high thermal efficiency possible by providing reaction heat from exothermic heat of regeneration	Unqualified success
Catalytic reforming	Early catalyst coked slowly and required regenerating	Relatively slow, ~500°C, 14–15 atm	Low, poor control because of low ΔP compared with operating pressure	Poor thermal efficiencies because of low circulation rate	Fixed bed process is favored, new catalysts do not require frequent regeneration
Acrylonitrile	Negligible if process control of temperature and excess oxygen is effective. Catalyst easily destroyed at runaway temperatures	Rapid, 2–3 s contact time, 450–470°C, 1–5 atm (18)	None	Control of temperature in narrow range essential for high reaction rate	Highly successful, new fixed bed process with similar catalyst coated on a relatively nonporous crystalline core reported to be controllable and effective
Phthalic anhydride	Modest, 1 kg/1000 kg of feed added while unit in operation to maintain activity	Slow, low-activity catalyst chosen deliberately to prevent side reactions caused by backmixing. Contact time: 10–20 s, 750–950°C, 1–3 atm	Small addition rate	Control of temperature increase within a few degrees essential for preventing explosions and assuring good selectivity	Successful, lower capital cost than multitubular fixed bed, but fixed bed is returning in favor because of feedstock flexibility
Maleic anhydride	Similar to phthalic anhydride	Similar to phthalic anhydride	Similar to phthalic anhydride	Similar to phthalic anhydride	Similar to phthalic anhydride
Oxyhydro-chlorination	Modest, catalyst is lost by attrition	Rapid contact time, probably 2 s, 200–350°C, up to 10 atm	Small amount added to make up for attrition	Control of temperature within narrow limits essential to avoid undesired by-products	Appears to be a major new use for fluidized beds. New fixed bed catalysts on highly conductive supports could overcome fixed bed disadvantages

Source: Data from Rase, H.F., *Chemical Reactor Design for Process Plants*, Wiley, New York, 1977.

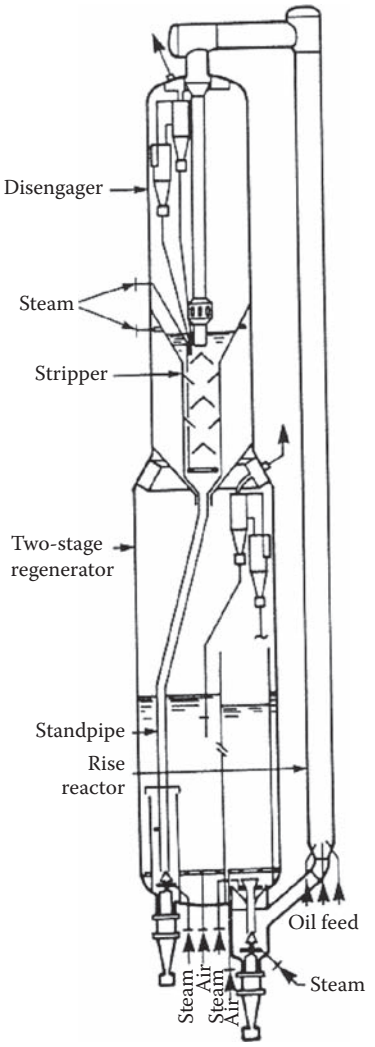

FIGURE 5.18 Riser reactor. (Data from Yates, J.G., *Fundamentals of Fluidized-bed Chemical Processes*, Butterworths, London, 1983.)

reactor can thus be described by mass balance equations that consider only the fluid phase, often called the bulk phase of the reactor. The concentrations and temperature inside the catalyst pores are assumed to remain at the same level as those of the bulk phase in a pseudohomogeneous model. This is valid for catalyst particles, for which the diffusion resistance is negligible and the heat conductivity of the particle is so good that no temperature gradient exists inside the particles. The latter condition is often satisfied for catalyst particles, whereas concentration gradients frequently exist due to pore diffusion. Even in these cases, the pseudohomogeneous model is usable to some extent: the effect of pore diffusion can be taken into account using a correction term, the catalyst *effectiveness factor*.

For a completely realistic interpretation of diffusion effects within catalyst particles, a heterogeneous reactor model is required. In a heterogeneous model, separate balance

equations are introduced for the fluid that exists inside the catalyst pores and for the fluid in the bulk phase surrounding the catalyst particles.

Especially in the case of strongly exothermic reactions, radial temperature gradients appear in the reactor tube. The existence of these gradients implies that the chemical reaction proceeds at different velocities in various radial positions and, consequently, radial concentration gradients emerge. Because of these concentration gradients, dispersion of the material is initiated in the direction of the radial coordinate. Dispersion of heat and material can be described with radial dispersion coefficients, and the mathematical formulation of dispersion effects resembles that of Fick's law (Chapter 4) for molecular diffusion.

If the radial effects are negligible, a packed bed can be described using the plug flow model in a fluid phase. Industrial packed beds are long compared with their reactor diameter, and the dispersion effects in the axial direction can therefore generally be ignored. If the plug flow model can be applied to the fluid phase, the model is called *one-dimensional*. If radial effects are taken into account, the model can be considered *two-dimensional*. We can thus utilize pseudohomogeneous as well as one- and two-dimensional models to describe catalytic beds. The model categories are summarized in Table 5.3. In the next section, the treatment is mainly limited to the mathematically simplest model: the pseudohomogeneous model.

We will first assume that the reactor can be described using a plug flow model and that the reaction rate can be expressed through concentrations in the main bulk of the fluid. Axial dispersion and diffusion effects in the fluid phase are assumed to be negligible. Even the flow of heat (conductivity) in a solid catalyst material is ignored. The pressure drop can—in contrast with the homogeneous tube reactors—often become important, and the pressure drop should therefore always be checked *a priori* when designing packed beds. The reactor is presumed to operate at steady state. In practice, multiple packed beds are sometimes coupled together, parallel to each other (*multitubular reactor*). Here, we will limit our observations and balance equations to a single bed that comprises the basic unit in both commercial applications of bed reactors (*multitubular* and *multibed reactors*).

TABLE 5.3 Models for Catalytic Packed Bed Reactors

Model	Characteristic Features
Pseudohomogeneous Model	Diffusion limitations inside the catalyst neglected
One-dimensional	Plug flow or axial dispersion; neither radial concentration nor temperature gradients in the reactor
Two-dimensional	Plug flow or axial dispersion; radial concentration and temperature gradients in the reactor
Heterogeneous Model	Diffusion resistance in the catalyst notable
One-dimensional	Plug flow or axial dispersion; neither radial concentration nor temperature gradients in the reactor; concentration and temperature gradients inside the catalyst particles
Two-dimensional	Plug flow or axial dispersion; radial concentration and temperature gradients in the reactor; concentration and temperature gradients inside the catalyst particles

5.2.1 MASS BALANCES FOR THE ONE-DIMENSIONAL MODEL

The reaction rate expressions for heterogeneous catalytic reactions are based on the catalyst mass or the surface area. This implies that the generation rate of component i is given by

$$r_i = (\,)\text{mol/s/kg of catalyst} \tag{5.5}$$

and the reaction rate is given accordingly:

$$R_j = (\,)\text{mol/s/kg of catalyst.} \tag{5.6}$$

To relate these reaction velocities to the reactor volume, a new concept, the catalyst bulk density, ρ_B, is introduced. The catalyst bulk density gives the catalyst mass per reactor volume:

$$\rho_B = (\,)\,\text{kg of catalyst/m}^3\text{ of reactor volume.} \tag{5.7}$$

The generation rates of component i, on the basis of the reactor volume, are therefore given by

$$r_i\rho_B = (\,)\,\text{mol s}^{-1}\text{m}^3\text{ of reactor volume.} \tag{5.8}$$

In the derivation of the molar mass balances, the volume element ΔV is considered (Figure 5.19). The general balance equation

$$[\text{incoming } i] + [\text{generated } i] = [\text{outgoing } i] + [\text{accumulated } i] \tag{5.9}$$

is also valid here. For steady-state models, the accumulation term is ignored. The mass balance for the volume element ΔV becomes for component i:

$$\dot{n}_{i,\text{in}} + r_i\rho_B\Delta V = \dot{n}_{i,\text{out}}, \tag{5.10}$$

where the difference, $\dot{n}_{i,\text{out}} - \dot{n}_{i,\text{in}}$, is given by

$$\Delta\dot{n} = \dot{n}_{i,\text{out}} - \dot{n}_{i,\text{in}}. \tag{5.11}$$

After inserting the definition, Equation 5.11 into Equation 5.10, and allowing $\Delta V \to 0$, the balance Equation 5.10 is transformed to

$$\frac{\mathrm{d}\dot{n}_i}{\mathrm{d}V} = r_i\rho_B. \tag{5.12}$$

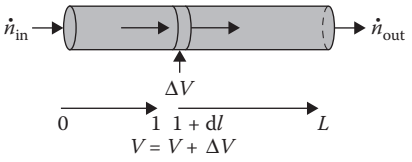

FIGURE 5.19 The volume element, ΔV, in a packed bed.

For a system with *one* single chemical reaction, Equation 5.12 assumes a new form:

$$\frac{\mathrm{d}\dot{n}_i}{\mathrm{d}V} = \rho_\mathrm{B} \nu_i R. \tag{5.13}$$

In case *multiple* chemical reactions are taking place, the following form is attained:

$$\frac{\mathrm{d}\dot{n}_i}{\mathrm{d}V} = \rho_\mathrm{B} \sum_j \nu_{i,j} R. \tag{5.14}$$

This can even be conveniently written as arrays:

$$\frac{\mathrm{d}\dot{\mathbf{n}}}{\mathrm{d}V} = \rho_\mathrm{B} \boldsymbol{\nu} \mathbf{R}. \tag{5.15}$$

If the space time $\tau = V_\mathrm{R}/\dot{V}_0$ is selected as the independent variable, Equations 5.12 and 5.15 assume a new form:

$$\frac{\mathrm{d}\dot{\mathbf{n}}}{\mathrm{d}\tau} = \dot{V}_0 \rho_\mathrm{B} \mathbf{r} \tag{5.16}$$

The earlier definition for the extent of reaction (homogeneous reactors, Chapter 3) is valid for the following pseudohomogeneous model:

$$\dot{\mathbf{n}} = \dot{\mathbf{n}}_0 + \nu \xi. \tag{5.17}$$

Application of this relationship, Equation 5.17, into balance Equation 5.16, yields

$$\frac{\mathrm{d}\xi}{\mathrm{d}\tau} = \dot{V}_0 \rho_\mathrm{B} \mathbf{R}. \tag{5.18}$$

If molar flows of the key components, $\dot{n}_k$, are used, the balance equation transforms to

$$\frac{\mathrm{d}\dot{\mathbf{n}}_k}{\mathrm{d}\tau} = \dot{V}_0 \rho_\mathrm{B} \nu_k \mathbf{R}. \tag{5.19}$$

If relative conversions, η_k, are used as variables, the following balance equation is obtained:

$$\frac{\mathrm{d}\eta'_k}{\mathrm{d}\tau} = -\frac{\rho_\mathrm{B}}{c_0} \nu_k \mathbf{R}, \tag{5.20}$$

where c_0 denotes the total concentration of the fluid at the reactor inlet.

The analogy between the different forms of balance Equations 5.18 through 5.20 and the corresponding balance equations for a homogeneous tube reactor is apparent; the only difference is the term ρ_B that is included in the catalytic reactor model, since the reaction velocity has a definition different from that of homogeneous reactors.

The relationships that were derived in an earlier chapter between concentrations and the volume flow, as well as the stoichiometric measures ($\dot{n}_k, \xi, \eta'_k$) for homogeneous flow reactors (Chapter 3), are also valid for the pseudohomogeneous model for a packed bed discussed here.

When using catalysts, however, we encounter phenomena that complicate reactor calculations. Molecular diffusion through the fluid film around the particle and the diffusion of molecules into the catalyst pores influence the reaction rate. Because of diffusion, the concentrations of reactant molecules inside the catalyst are lower than their concentrations in the bulk fluid. This means that the reaction velocities, R, in the balance equations also need to be calculated based on local concentrations. For practical reasons, it would, however, be highly desirable to use the bulk concentrations. If the velocity calculated using the concentrations of the bulk phase is denoted as $R(c^{\mathrm{b}})$, the real, true reaction velocity under diffusion influence, R', can be expressed using a correction term, η_{ej}, according to the following:

$$R'_j = \eta_{ej} R_j(c^{\mathrm{b}}). \tag{5.21}$$

The term η_{ej} is called the effectiveness factor. Expression 5.14 should be inserted into the balance equations instead of R. If diffusion does not affect the reaction rates, all effectiveness factors, η_{ej}, become equal to unity (=1). In the following, the logical and theoretical appearance of the effectiveness factor is discussed by studying the (molar) mass and energy balances of porous catalyst particles in detail.

5.2.2 EFFECTIVENESS FACTOR

5.2.2.1 Chemical Reaction and Diffusion inside a Catalyst Particle

In a porous catalyst particle, the reacting molecules must first diffuse through the fluid film surrounding the particle surface. They subsequently diffuse into the pores of the catalyst, where chemical reactions take place on active sites. The product molecules thus formed need, of course, to follow an opposite diffusion path. The phase boundary area is shown in Figure 5.20.

The diffusion resistance in the fluid film around the particle, as well as inside the particle, is the reason why the concentrations of the reactant molecules inside the particle are lower than those in the main bulk of the fluid. The result, in the case of most common reaction kinetics, is that even the reaction rates inside the pores assume lower values than what would be expected for the concentration levels of the main bulk.

Let us study a component i that diffuses into a catalyst particle—or out of the particle (Figure 5.20). The species i has the flux N_i(mol/m^2/s) in an arbitrary position in the particle. The flux N_i can often be described (with a sufficient accuracy) using the concentration gradients of the components ($\mathrm{d}c_i/\mathrm{d}r$) and their effective diffusion coefficient (D_{ei}):

$$N_i = -D_{ei}\frac{\mathrm{d}c_i}{\mathrm{d}r}. \tag{5.22}$$

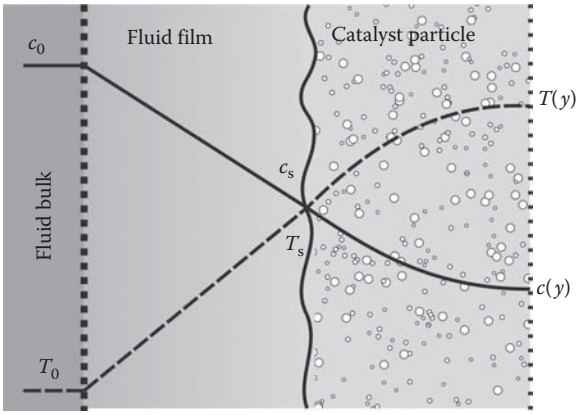

FIGURE 5.20 Phase boundary in a porous catalyst particle.

Equation 5.22 is often called *Fick's law* (Chapter 4). More advanced diffusion models are presented in the literature [10].

A volume element, ΔV, in a spherical catalyst particle is shown in Figure 5.20. The following general balance equations can be established for a volume element and component i at steady state:

[incoming i, by means of diffusion] + [generated i] = [outgoing i, by means of diffusion].

Quantitatively, this implies

$$(N_i A)_{\text{in}} + r_i \Delta m = (N_i A)_{\text{out}}\,, \tag{5.23}$$

where A denotes the diffusion area and Δm is the mass of the catalyst inside the volume element. Various catalyst geometries can be considered, but let us start with a special particle: the diffusion area for a spherical element is

$$A = 4\pi r^2. \tag{5.24}$$

The catalyst mass inside the volume element can be expressed by the density of the catalyst particle (ρ_{P}) and the element volume:

$$\Delta m = \rho_{\text{p}} \Delta V = \rho_{\text{p}} 4\pi r^2 \Delta r. \tag{5.25}$$

After inserting Equations 5.22, 5.24, and 5.25 into balance Equation 5.23, we obtain

$$\left(-D_{\text{e}i}\frac{\text{d}c_i}{\text{d}r}4\pi r^2\right)_{\text{in}} + r_i \rho_{\text{P}} 4\pi r^2 \Delta r = \left(-D_{\text{e}i}\frac{\text{d}c_i}{\text{d}r}4\pi r^2\right)_{\text{out}}. \tag{5.26}$$

The difference, $(D_{ei}\ \mathrm{d}c_i/\mathrm{d}r\ r^2)_{\mathrm{out}} - (D_{ei}\ \mathrm{d}c_i/\mathrm{d}r\ r^2)_{\mathrm{in}}$, is denoted as $\Delta(D_{ei}\,\mathrm{d}c_i/\mathrm{d}r\ r^2)$, and Equation 5.26 transforms to a new form:

$$\Delta\left(-D_{ei}\frac{\mathrm{d}c_i}{\mathrm{d}r}r^2\right) + r_i\rho_{\mathrm{p}}r^2\Delta r = 0. \tag{5.27}$$

Dividing Equation 5.27 by Δr and allowing $\Delta r \to 0$, a differential equation is obtained:

$$\frac{1}{r^2}\frac{\mathrm{d}\left(D_{ei}(\mathrm{d}c_i/\mathrm{d}r)r^2\right)}{\mathrm{d}r} + r_i\rho_{\mathrm{p}} = 0. \tag{5.28}$$

The above derivation was conducted for a *spherical particle*. It is easy to show that this treatment can be extended to an arbitrary geometry, as the form (shape) factor s is applied. Equation 5.28 can then be written in a general form:

$$\frac{1}{r^s}\frac{\mathrm{d}(D_{ei}(\mathrm{d}c_i/\mathrm{d}r)r^s)}{\mathrm{d}r} + r_i\rho_{\mathrm{p}} = 0. \tag{5.29}$$

The form factor, s, obtains the following values: $s = 2$ for a sphere, $s = 1$ for an infinitely long cylinder, and $s = 0$ for a catalyst in the disk form. The ideal catalyst geometries are shown in Figure 5.21.

A real catalyst geometry—such as a short cylinder—can be described by Equation 5.22 by choosing a suitable noninteger value for the form factor. The form factor (s) for an arbitrary geometry can be estimated using the relationship

$$\frac{A_{\mathrm{p}}}{V_{\mathrm{p}}} = \frac{s+1}{R}, \tag{5.30}$$

where A_{p} denotes the outer surface area and V_{p} denotes the volume of the particle. R stands for the characteristic dimension of the particle. The selection of the characteristic dimension is illustrated in Figure 5.21.

The balance Equation 5.29 is usually solved with the following boundary conditions, which are valid for the center point ($r = 0$) and the outer surface of the particle ($r = R$):

$$\frac{\mathrm{d}c_i}{\mathrm{d}r} = 0, \quad r = 0, \tag{5.31}$$

$$c_i = c_i^{\mathrm{s}}, \quad r = R. \tag{5.32}$$

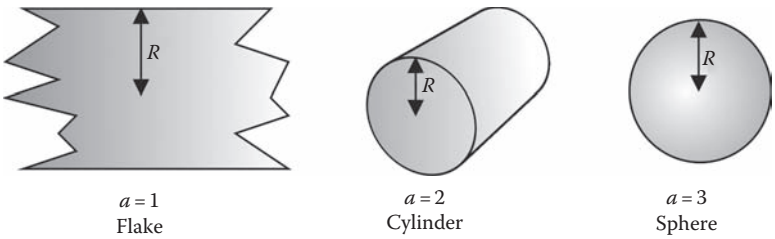

FIGURE 5.21 The ideal catalyst geometries, $a = s + 1$.

Here, c_i^s denotes the concentration at the outer surface of the particle. The first boundary condition, at $r = 0$, follows from the symmetry.

A balance equation similar to Equation 5.29 can, in principle, be set up for the fluid film around the catalyst particle. However, since no reactions take place in the fluid film, r_i is zero (0) for the film. The fluid film balance Equation 5.21 is therefore reduced to

$$\frac{1}{r^s}\frac{\mathrm{d}(D_i(\mathrm{d}c_i/\mathrm{d}r)r^s)}{\mathrm{d}r} = 0. \tag{5.33}$$

In Equation 5.33, the diffusion coefficient is naturally not the same as for the porous particle, but instead the *molecular* diffusion coefficient D_i for the component should be used. Equation 5.33 has the following boundary conditions:

$$c_i = c_i^s, \quad r = R, \tag{5.34}$$

$$c_i = c_i^b, \quad r = R + \delta, \tag{5.35}$$

where the symbol c_i^b denotes the concentration in the fluid bulk and δ denotes the thickness of the fluid film. The fluid film is extremely thin compared with the catalyst particle ($\delta = R$), which means that the change in the term r^s is very small in the film. If the diffusion coefficient D_i, is, in addition, assumed to be concentration-independent, Equation 5.33 is reduced to

$$D_i\frac{\mathrm{d}^2c_i}{\mathrm{d}r^2} = 0, \tag{5.36}$$

which in turn implies that

$$\frac{\mathrm{d}c_i}{\mathrm{d}r} = a, \tag{5.37}$$

where a is an integration constant. Integrating Equation 5.37 yields

$$c_i = ar + b, \tag{5.38}$$

that is, the concentration profile in the fluid film is linear. Inserting the boundary conditions

$$c_i = c_i^s, \quad r = R \tag{5.39}$$

$$c_i = c_i^b, \quad r = R + \delta \tag{5.40}$$

into Equations 5.38 through 5.40 allows us to determine the constants a and b:

$$a = \frac{c_i^b - c_i^s}{\delta}, \tag{5.41}$$

$$b = \frac{c_i^s\,(R + \delta) - Rc_i^b}{\delta}. \tag{5.42}$$

The concentration profiles in the film are, consequently, given by

$$c_i(r) = \frac{\left(c_i^{\mathrm{b}} - c_i^{\mathrm{s}}\right) r}{\delta} + \frac{c_i^{\mathrm{s}}\,(R+\delta) - R c_i^{\mathrm{b}}}{\delta} = \frac{\left(c_i^{\mathrm{b}} - c_i^{\mathrm{s}}\right)(r-R)}{\delta} + c_i^{\mathrm{s}} \tag{5.43}$$

and the concentration gradient becomes

$$\frac{\mathrm{d}c_i}{\mathrm{d}r} = \frac{c_i^{\mathrm{b}} - c_i^{\mathrm{s}}}{\delta}. \tag{5.44}$$

The diffusion flux inside the fluid film is constant and equal to the flux on the outer surface of the particle:

$$N_{i,(r=R)} = -D_{ei}\left(\frac{\mathrm{d}c_i}{\mathrm{d}r}\right)_{r=R}. \tag{5.45}$$

Equation 5.44 yields

$$N_{i,(r=R)} = -\frac{D_i}{\delta}\left(c_i^{\mathrm{b}} - c_i^{\mathrm{s}}\right). \tag{5.46}$$

The ratio D_i/δ is often denoted as $k_{\mathrm{G}i}$, $k_{\mathrm{G}i}$ being the gas film coefficient according to the film theory. Thus, we obtain

$$N_{i,(r=R)} = -k_{\mathrm{G},i}\left(c_i^{\mathrm{b}} - c_i^{\mathrm{s}}\right). \tag{5.47}$$

In the case of liquid-phase processes, $k_{\mathrm{G}i}$ is replaced by the liquid film coefficient $k_{\mathrm{L}i}$. The mass flow of component i, at the surface of the particle, is then given by

$$N_{i,(r=R)}A_{\mathrm{p}} = -D_{\mathrm{e}i}\left(\frac{\mathrm{d}c_i}{\mathrm{d}r}\right)A_{\mathrm{p}} = -k_{\mathrm{G}i}\left(c_i^{\mathrm{b}} - c_i^{\mathrm{s}}\right)A_{\mathrm{p}}. \tag{5.48}$$

The two latter equalities in Equation 5.48 imply that the fluxes calculated in the fluid film and at the outer surface of the particle should be equal. If the reaction proceeds everywhere in the particle with the same velocity, r_i (c^{b}), the molar flow at the surface of the particle would be

$$N'_{i,(r=R)}A_{\mathrm{p}} = r_i(c^{\mathrm{b}})\,\rho_{\mathrm{p}}V_{\mathrm{p}}. \tag{5.49}$$

This, however, would mean that the diffusion resistance has no influence on the reaction rate.

Let us now define the effectiveness factor for component i from a theoretical viewpoint:

$$\eta_i = \frac{N_{i,(r=R)}A_{\mathrm{p}}}{r_i\left(c^{\mathrm{b}}\right)\rho_{\mathrm{p}}V_{\mathrm{p}}}. \tag{5.50}$$

The general definition of the effectiveness factor states that the factor describes the ratio between the real molar flux (N_i) and the molar flux (N'_i) that would be obtained if the reaction proceeded in the absence of diffusion resistance.

The effectiveness factor, η_i, can also be expressed in another way. Differential Equation 5.29 can be formally integrated as follows:

$$\int_0^y \mathrm{d}\left(D_{ei}\frac{\mathrm{d}c_i}{\mathrm{d}r}r^s\right) = -\rho_\mathrm{p}\int_0^R r_i r^s\,\mathrm{d}r, \tag{5.51}$$

where the upper integration limit, y, is given by

$$y = D_{ei}\left(\frac{\mathrm{d}c_i}{\mathrm{d}r}\right)_{r=R} R^s. \tag{5.52}$$

The lower integration limit is zero because of symmetry ($\mathrm{d}c_i/\mathrm{d}r = 0$, at $r = 0$). The integration of Equation 5.51 thus yields

$$N_{i,(r=R)} = -D_{ei}\left(\frac{\mathrm{d}c_i}{\mathrm{d}r}\right)_{r=R} = \frac{\rho_\mathrm{p}}{R^s}\int_0^R r_i r^s\,\mathrm{d}r. \tag{5.53}$$

Inserting expression 5.53 into the definition of the effectiveness factor, Equation 5.50, yields

$$\eta_i = \frac{\int_0^R r_i r^s\,\mathrm{d}r}{r_i\left(c^\mathrm{b}\right)R^s}\,\frac{A_\mathrm{p}}{V_\mathrm{p}}. \tag{5.54}$$

As the definition of the form factor, Equation 5.30, is also taken into account, we obtain

$$\eta_i = \frac{(s+1)\int_0^R r_i r^s\,\mathrm{d}r}{r_i\left(c^\mathrm{b}\right)R^{s+1}}. \tag{5.55}$$

Equations 5.54 and 5.55 show that the effectiveness factor represents the ratio between a weighted average rate and the rate that would be obtained if the conditions were similar to those in the bulk phase. If no concentration gradients emerge in the particle, r_i in Equation 5.55 can be replaced with a constant, $r_i\,(c^\mathrm{b})$, and the integration of Equation 5.55 yields the effectiveness factor, $\eta_i = 1$.

For arbitrary reaction kinetics, the balance equation for a catalyst particle, Equation 5.29, must be solved numerically with the boundary conditions, Equations 5.31 and 5.32. The effectiveness factors can subsequently be obtained from Equation 5.50 or 5.55. For some limited cases of chemical kinetics, it is, however, possible to solve the balance Equation 5.29 analytically and thus obtain an explicit expression for the effectiveness factor. We shall take a look at a few of these special cases.

5.2.2.1.1 First-Order Reaction

If the diffusion coefficient D_{ei} is assumed to remain constant inside the catalyst particle, Equation 5.29 is transformed as follows:

$$\frac{\mathrm{d}^2c_i}{\mathrm{d}r^2} + \frac{s}{r}\frac{\mathrm{d}c_i}{\mathrm{d}r} = -\frac{\rho_\mathrm{p}r_i}{D_{ei}}. \tag{5.56}$$

As this reaction is of the first order with respect to the reactant i, the reaction rate, R, is given by

$$R = kc_i \tag{5.57}$$

and the generation velocity becomes

$$r_i = \nu_i R = \nu_i k c_i. \tag{5.58}$$

The substitution $y = c_i r$ is subsequently inserted into Equation 5.56. This implies that

$$\frac{\mathrm{d}c_i}{\mathrm{d}r} = \frac{\mathrm{d}y}{\mathrm{d}r}\frac{1}{r} - \frac{y}{r^2} \tag{5.59}$$

and

$$\frac{\mathrm{d}^2 c_i}{\mathrm{d}r^2} = \frac{\mathrm{d}^2 y}{\mathrm{d}r^2}\frac{1}{r} - \frac{2}{r^2}\frac{\mathrm{d}y}{\mathrm{d}r} + \frac{2}{r^3}y. \tag{5.60}$$

Inserting the derivatives, Equations 5.58 and 5.59, into balance Equation 5.56, yields

$$\frac{1}{r}\frac{\mathrm{d}^2 y}{\mathrm{d}r^2} + \frac{(s-2)}{r^2}\frac{\mathrm{d}y}{\mathrm{d}r} - \frac{(s-2)}{r^3}y = \frac{\rho_\mathrm{p}\nu_i k}{D_{ei}}\frac{y}{r}, \tag{5.61}$$

which is simplified to

$$r^2\frac{\mathrm{d}^2 y}{\mathrm{d}r^2} + (s-2)r\frac{\mathrm{d}y}{\mathrm{d}r} + \left((2-s) + \frac{\rho_\mathrm{p}\nu_i k}{D_{ei}}r^2\right)y = 0. \tag{5.62}$$

Equation 5.62 is a transformed Bessel's differential equation, which has a solution for arbitrary values of the form factor, s, that can be expressed with the Bessel functions.

5.2.2.2 Spherical Particle

For a spherical geometry, however, the analytical solution becomes particularly simple: $s = 2$, and Equation 5.62 is reduced to

$$\frac{\mathrm{d}^2 y}{\mathrm{d}r^2} + \frac{\rho_\mathrm{p}\nu_i k}{D_{ei}}y = 0. \tag{5.63}$$

The second-order differential Equation 5.63 can be written as

$$r'^2 + \frac{\nu_i \rho_\mathrm{p} k}{D_{ei}} = 0 \tag{5.64}$$

with the roots

$$r'_{1,2} = \pm\sqrt{\frac{-\nu_i \rho_\mathrm{p} k}{D_{ei}}}. \tag{5.65}$$

The analytical solution to Equation 5.63 can now be written accordingly:

$$y = C_1 e^{r_1' r} + C_2 e^{r_2' r}, \tag{5.66}$$

$$y = C_1 e^{\sqrt{(-\nu_i \rho_p k/D_{ei})} r} + C_2 e^{-\sqrt{(-\nu_i \rho_p k/D_{ei})} r}. \tag{5.67}$$

Let us introduce a dimensionless parameter, φ, defined as

$$\phi^2 = \frac{-\nu_i \rho_p k}{D_{ei}} R^2, \tag{5.68}$$

as well as a dimensionless coordinate, $x = r/R$. The parameter φ is called the *Thiele modulus*, and it is very frequently encountered in the catalytic literature. Equation 5.67 can now be simply rewritten as

$$y = C_1 e^{\phi x} + C_2 e^{-\phi x}. \tag{5.69}$$

The boundary conditions, Equations 5.31 and 5.32, yield $y = 0$, at $x = 0$, and $y = y^s$, at $x = 1$ ($r = R$). Inserting these conditions into Equation 5.69 allows us to determine the constants C_1 and C_2, which assume the following values:

$$C_1 = \frac{y^s}{e^{\phi} - e^{-\phi}}, \tag{5.70}$$

$$C_2 = \frac{y^s}{e^{-\phi} - e^{\phi}}. \tag{5.71}$$

Inserting Equations 5.70 and 5.71 into Equation 5.69 yields

$$y = y^s \frac{e^{\phi x} - e^{-\phi x}}{e^{\phi} - e^{-\phi}}, \tag{5.72}$$

which can be conveniently expressed by the hyperbolic functions

$$y = y^s \frac{\sinh(\phi x)}{\sinh(\phi)}. \tag{5.73}$$

The concentration profiles can, consequently, be obtained from Equation 5.74, since $y^s = c^s R$, and, $y = c_i r$,

$$c_i = c^s \frac{\sinh(\phi x)}{x \sinh(\phi)}. \tag{5.74}$$

The concentration profiles are illustrated in Figure 5.22. The profiles are plotted with the Thiele modulus (φ) as parameters. The higher the value the Thiele module attains, the more profound the diffusion resistance inside the particle.

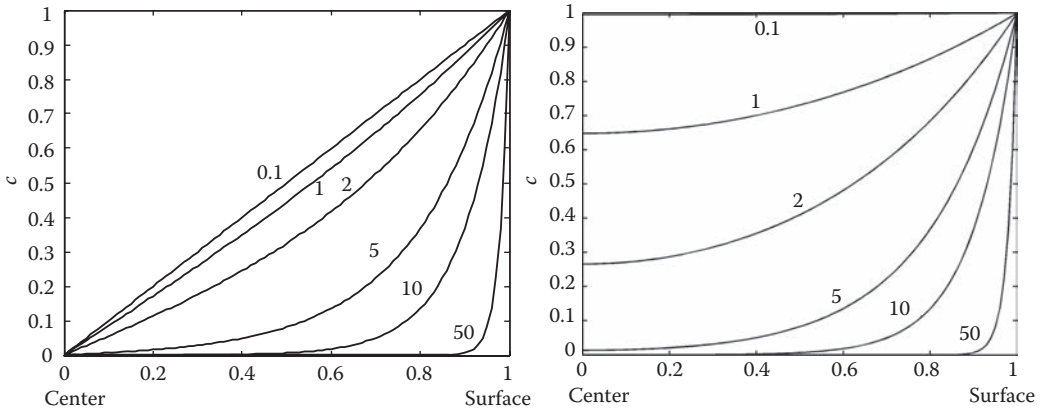

FIGURE 5.22 Concentration profiles of a reactant in porous catalysts: sphere (left) and slab (right), for different values of the Thiele module.

For calculation of the flux, N_i, at the outer surface of the catalyst, Equation 5.74 needs to be differentiated, taking into account the x coordinate

$$\frac{\mathrm{d}c_i}{\mathrm{d}x} = \frac{\mathrm{d}c_i}{\mathrm{d}r}R = \frac{c_i^{\mathrm{s}}}{\sinh(\phi)}\left(\frac{\phi\cosh(\phi x)}{x} - \frac{\sinh(\phi x)}{x^2}\right), \tag{5.75}$$

which, on the surface of the particle ($x = 1$), becomes

$$\frac{\mathrm{d}c_i}{\mathrm{d}x_{x=1}} = \frac{c_{\mathrm{s}}}{\sinh(\phi)}\left(\phi\,\cosh(\phi) - \sinh(\phi)\right). \tag{5.76}$$

On the surface of the spherical particle, the flux is

$$N_i = -D_{\mathrm{e}i}\left(\frac{\mathrm{d}c_i}{\mathrm{d}r}\right)_{r=R} = -\frac{D_{\mathrm{e}i}c_i^{\mathrm{s}}}{R\,\sinh(\phi)}(\phi\cosh(\phi) - \sinh(\phi)) = -\frac{D_{\mathrm{e}i}c_i^{\mathrm{s}}}{R}\left(\frac{\phi}{\tanh(\phi) - 1}\right). \tag{5.77}$$

This flux is equal to the expression of flux through the fluid film, according to Equation 5.48:

$$N_i = -k_{\mathrm{G}i}\left(c_i^{\mathrm{b}} - c_i^{\mathrm{s}}\right) = -\frac{D_{\mathrm{e}i}c_i^{\mathrm{s}}}{R}\left(\frac{\phi}{\tanh(\phi)} - 1\right). \tag{5.78}$$

The unknown surface concentration, c_i^{s}, is now solved by Equation 5.78:

$$c_i^{\mathrm{s}} = \frac{c_i^{\mathrm{b}}}{1 + (D_{\mathrm{e}i}/Rk_{\mathrm{G}i})\phi\,((1/\tanh(\phi)) - (1/\phi))}. \tag{5.79}$$

The spontaneously appearing dimensionless quantity, Rk_{Gi}/D_{ei}, is denoted as the *Biot* number for mass transport:

$$Bi_M = \frac{Rk_{Gi}}{D_{ei}}. \tag{5.80}$$

The *Biot* number gives the ratio between the diffusion resistances in a fluid film and in a catalyst particle. Usually $Bi_M \gg 1$ is true for porous catalyst particles (Appendix 5). Equation 5.79 can now be rewritten as

$$c_i^s = \frac{c_i^b}{1 + (\phi/Bi_M)\,((1/\tanh(\phi)) - (1/\phi))}. \tag{5.81}$$

Inserting the surface concentration c_i^s into the same expression 5.78 yields

$$N_i = -\frac{D_{ei}c_i^b\phi\,((1/\tanh(\phi)) - (1/\phi))}{R\,(1 + (\phi/Bi_M)\,((1/\tanh(\phi)) - (1/\phi)))}. \tag{5.82}$$

The final goal, the effectiveness factor η_i, is now obtained from Expression 5.55. After inserting the ratio A_p/V_p for the spherical geometry, and N_i for first-order kinetics, into Equation 5.55, we obtain

$$\eta_i = \frac{3N_i}{R\nu_i k c_i^b \rho_p}, \tag{5.83}$$

$$\eta_i = \frac{3D_{ei}}{-\nu_i R^2 k \rho_p} \frac{\phi((1/\tanh(\phi)) - (1/\phi))}{1 + (\phi/Bi_M)((1/\tanh(\phi)) - (1/\phi))}. \tag{5.84}$$

The final result can be rewritten in the following form:

$$\eta_i = \frac{3}{\phi}\left(\frac{(1/\tanh(\phi)) - (1/\phi)}{1 + (\phi/Bi_M)((1/\tanh(\phi)) - (1/\phi))}\right). \tag{5.85}$$

Equation 5.85 yields the effectiveness factor for first-order reactions in a spherical catalyst particle. Certain limiting cases are of interest: if diffusion resistance in the fluid film can be ignored—as often is the case, since Bi_M is large—η_i becomes

$$\eta_i = \frac{3}{\phi}\left(\frac{1}{\tanh(\phi)} - \frac{1}{\phi}\right). \tag{5.86}$$

If the Thiele modulus (φ) has a high value—in other words, if the reaction is strongly diffusion resistant—the asymptotic value for the effectiveness factor is obtained:

$$\eta_i = \frac{3}{\phi} \tag{5.87}$$

since $\lim(\varphi \to \infty) \tanh \varphi = 1$.

5.2.2.3 Slab

Another simple geometry of interest is a flake-formed catalyst particle, a slab ($s = 0$). Particularly in three-phase systems, in which often only the outer surface of the catalyst is effectively used, the slab approximation ($s = 0$) is a good representation of the catalyst particle. Differential Equation 5.56 is transformed—for a slab-formed catalyst particle and first-order kinetics—to the equation

$$\frac{\mathrm{d}^2 c_i}{\mathrm{d}r^2} + \frac{\rho_\mathrm{p} \nu_i k c_i}{D_{\mathrm{e}i}} = 0. \tag{5.88}$$

Equation 5.88 is directly analogous to the transformed equation for a spherical catalyst particle, Equation 5.63. We can thus write the solution of Equation 5.88 in line with Equation 5.69 as

$$c_i = C_1 \mathrm{e}^{\phi x} + C_2 \mathrm{e}^{-\phi x}, \tag{5.89}$$

where the Thiele modulus is $\phi^2 = (-\nu_i,\ \rho_\mathrm{p} k)/(D_{\mathrm{e}i})R^2$ and x denotes the dimensionless coordinate, $x = r/R$.

The boundary conditions, Equations 5.31 and 5.32, are valid for the concentration profile, Equation 5.89. Inserting these boundary conditions into Equation 5.89 enables us to determine the constants C_1 and C_2, which become

$$C_1 = C_2 = \frac{c_i^\mathrm{s}}{\mathrm{e}^{\phi} + \mathrm{e}^{-\phi}}. \tag{5.90}$$

The concentration profile then assumes the following form:

$$c_i = c_i^\mathrm{s} \frac{\cosh(\phi x)}{\cosh(\phi)}. \tag{5.91}$$

The concentration profile is illustrated in Figure 5.22.

The concentration gradient becomes

$$\frac{\mathrm{d}c_i}{\mathrm{d}x} = \frac{\mathrm{d}c_i}{\mathrm{d}r} R = \frac{c_i^\mathrm{s} \phi \sinh(\phi x)}{\cosh(\phi)}. \tag{5.92}$$

At the outer surface of the particle ($x = 1$), the concentration gradient is

$$\frac{\mathrm{d}c_i}{\mathrm{d}x_{(x=1)}} = c_i^\mathrm{s} \phi \tanh(\phi). \tag{5.93}$$

The flux on the surface of the particle is thus given by

$$N_i = -D_{\mathrm{e}i} \left(\frac{\mathrm{d}c_i}{\mathrm{d}r} \right)_{r=R} = -\frac{D_{\mathrm{e}i} c_i^\mathrm{s} \phi}{R} \tanh(\phi)\,. \tag{5.94}$$

By setting the fluxes through the fluid film and on the particle surface equal, we obtain

$$N_i = k_{Gi}\left(c_i^b - c_i^s\right) = -\frac{D_{ei}c_i^s\phi\ \tanh(\phi)}{R}. \tag{5.95}$$

The surface concentration, c_i^s, can now be solved by Equation 5.95. The result becomes

$$c_i^s = \frac{c_i^b}{1 + (\phi\ \tanh(\phi)/Bi_M)}, \tag{5.96}$$

where *Biot's* number is defined according to Equation 5.80. For the flux through the outer surface of the particle, we obtain

$$N_i = -\frac{D_{ei}c_i^b}{R}\frac{\phi\ \tanh(\phi)}{1 + (\phi\ \tanh(\phi)/Bi_M)}. \tag{5.97}$$

The definition of the effectiveness factor, Equation 5.50, for a flake-formed geometry ($A_p/V_p = 1/R$) yields

$$\eta_i = \frac{N_i}{Rv_i k c_i^b \rho}. \tag{5.98}$$

The final result, the effectiveness factor, for a first-order reaction and a catalyst flake is

$$\eta_i = \frac{\tanh(\phi)}{\phi}\left[1 + \frac{\phi\ \tanh(\phi)}{Bi_M}\right]^{-1}. \tag{5.99}$$

In case the diffusion resistance in the fluid film is negligible, $Bi_M \to \infty$, Equation 5.99 is reduced to

$$\eta_i = \frac{\tanh(\phi)}{\phi}. \tag{5.100}$$

If the Thiele modulus has a high value, an asymptotic value is again obtained for the effectiveness factor, η_i,

$$\eta_i = \frac{1}{\phi} \tag{5.101}$$

since $\lim(\varphi \to \infty)\tanh(\varphi) = 1$.

A comparison of the expressions before, Equations 5.85 through 5.87 and Equations 5.99 through 5.101, for spherical and flake-formed geometries, shows that the particle geometry is of less importance for the effectiveness factor. Let us recall the definition of the Thiele modulus, as in Equation 5.68:

$$\phi^2 = \frac{-v_i\rho_p k}{D_{ei}}R^2. \tag{5.102}$$

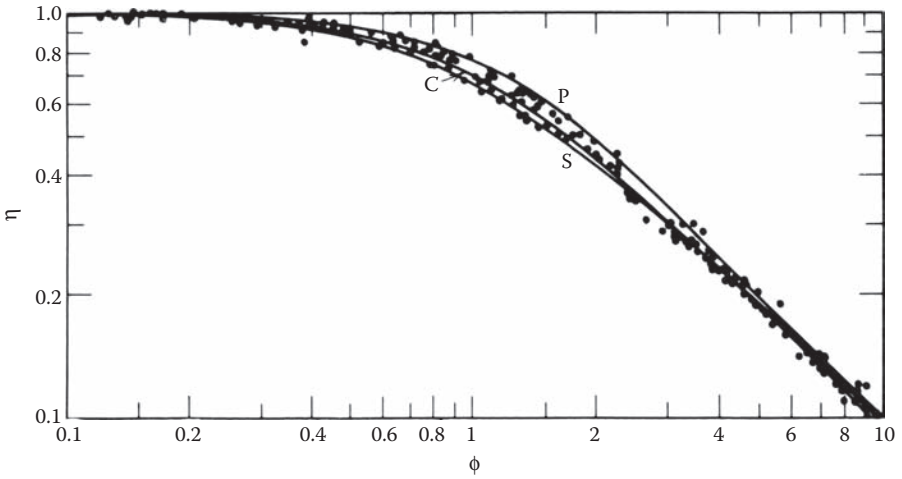

FIGURE 5.23 Isothermal effectiveness factors, for slab-formed (P), cylindrical (C), and spherical (S) catalysts, for a first-order reaction. (Data from Froment, G. and Bischoff, K., *Chemical Reactor Analysis and Design*, 2nd Edition,Wiley, New York, 1990.)

The asymptotic results, Equations 5.87 and 5.101, indicate that an asymptotic value for η_i, for an arbitrary geometry, might be

$$\eta_i = \frac{s+1}{\phi}. \tag{5.103}$$

Let us now define the generalized Thiele modulus, φ_s, for a first-order reaction as follows:

$$\phi_s^2 = \frac{-\nu_i \rho_p k}{D_{ei}} \frac{R^2}{(s+1)^2} = \frac{-\nu_i \rho_p k}{D_{ei}} \left(\frac{V_p}{A_p}\right)^2. \tag{5.104}$$

This implies that the asymptotic value of the effectiveness factor for an arbitrary geometry can be written as

$$\eta_i = \frac{1}{\phi_s}, \tag{5.105}$$

where $\phi_s = \phi/(s+1)$.

We will now investigate how good the approximation given in Equation 5.105 is of the results of exact calculations, for different geometries and a first-order reaction; these are compared in Figure 5.23. The figure shows that the approximation is good, as long as the Thiele modulus has a value above unity ($\varphi_s > 1$).

5.2.2.4 Asymptotic Effectiveness Factors for Arbitrary Kinetics

Even for arbitrarily reaction kinetics, useful semianalytical expressions can be derived for the effectiveness factor. Here, we will restrict ourselves to the flake-formed geometry ($s = 0$).

Consequently, the balance Equation 5.29 is reduced to

$$\frac{\mathrm{d}^2 c_i}{\mathrm{d}r^2} + \frac{\rho_\mathrm{p} r_i}{D_{\mathrm{e}i}} = 0. \tag{5.106}$$

The dimensionless coordinate, $x = r/R$, and the dimensionless concentration, $y = c_i/c_i^\mathrm{b}$, are introduced. Equation 5.106 is thus transformed to

$$\frac{\mathrm{d}^2 y}{\mathrm{d}x^2} + \frac{\rho_\mathrm{p} R^2}{c_i^\mathrm{s} D_{\mathrm{e}i}} r_i = 0. \tag{5.107}$$

Let us define the relationship r_i' as follows:

$$r_i' = \frac{r_i}{r_i\left(c^\mathrm{b}\right)}, \tag{5.108}$$

where $r_i(c^\mathrm{s})$ denotes the reaction velocity calculated with the surface concentrations, c^s. Now, a generalized Thiele modulus can be defined, according to Equation 5.109,

$$\phi^2 = \frac{-\rho_\mathrm{p} r_i\left(c^\mathrm{b}\right)}{D_{\mathrm{e}i} c_i^\mathrm{b}} R^2, \tag{5.109}$$

and Equation 5.107 can be comfortably rewritten as

$$\frac{\mathrm{d}}{\mathrm{d}x}\left(\frac{\mathrm{d}y}{\mathrm{d}x}\right) - \phi^2 r_i' = 0. \tag{5.110}$$

Multiplying Equation 5.110 by dy, followed by integration, leads to

$$\int_0^{\mathrm{d}y/\mathrm{d}x} \frac{\mathrm{d}}{\mathrm{d}x}.\mathrm{d}\left(\frac{\mathrm{d}y}{\mathrm{d}x}\right) = \phi^2 \int_{y^*}^{y^\mathrm{s}} r'\,\mathrm{d}y. \tag{5.111}$$

The result becomes

$$\left(\frac{\mathrm{d}y}{\mathrm{d}x}\right)^2 = 2\phi^2 \int_{y^*}^{y^\mathrm{s}} r'\,\mathrm{d}y \tag{5.112}$$

where $y*$ denotes the dimensionless concentration in the middle of the particle

$$y^* = \frac{c_{i,(r=0)}}{c_i^\mathrm{b}} \tag{5.113}$$

and $\mathrm{d}y/\mathrm{d}x$ denotes the dimensionless concentration gradient on the outer surface of the particle. The concentration gradient consequently becomes

$$\frac{\mathrm{d}y}{\mathrm{d}x} = \phi \left(2 \int_{y^*}^{y^s} r' \, \mathrm{d}y \right)^{1/2} . \tag{5.114}$$

The flux of component i on the particle surface is

$$N_i = -D_{ei} \frac{\mathrm{d}c_i}{\mathrm{d}r} = -D_{ei} \frac{c_i^b}{R} \frac{\mathrm{d}y}{\mathrm{d}x} \tag{5.115}$$

and the ratio, A_p/V_p, for a flake-formed particle ($s = 0$), is $1/R$. After taking into account Equations 5.114 and 5.115, together with the definition of the effectiveness factor, Equation 5.50, we obtain the following expression for the effectiveness factor:

$$\eta_i = \frac{D_{ei} c_i^b}{-r_i \left(c^b \right) \rho_p R^2} \left(2 \int_{y^*}^{y^s} r' \, \mathrm{d}y \right)^{0.5} . \tag{5.116}$$

By taking into account the definition of the Thiele modulus, Equation 5.109, a new form of the equation describing the effectiveness factor is obtained:

$$\eta_i = \frac{1}{\phi} \left(2 \int_{y^*}^{y^s} r' \, \mathrm{d}y \right)^{0.5} . \tag{5.117}$$

The surface concentration, y^s, is affected by the diffusion resistance in the fluid film around the catalyst particle.

After setting the fluxes at the outer surface of the catalyst equal ($x = 1$),

$$N_i = -k_{Gi} \left(c_i^b - c_i^s \right) = -\frac{D_{ei}}{R} \frac{\mathrm{d}c_i}{\mathrm{d}x}, \tag{5.118}$$

the following relation is obtained:

$$\frac{D_{ei}}{R} \frac{\mathrm{d}c_i}{\mathrm{d}x} = k_{Gi} \left(1 - y^s \right) . \tag{5.119}$$

This equation gives the dimensionless surface concentration, y^s:

$$y^s = 1 - \frac{1}{Bi_M} \frac{\mathrm{d}y}{\mathrm{d}x} \quad \text{at } x = 1. \tag{5.120}$$

The *Thiele* modulus, according to the definition, Equation 5.109, becomes

$$\phi^2 = -\frac{\rho_p r_{i,(y=1)}}{D_{ei} c_i^b} R^2. \tag{5.121}$$

The effectiveness factor, Equation 5.117, approaches a limiting value as the Thiele modulus assumes increasing values. For large values of the Thiele modulus, the concentration in the center of the particle approaches zero (0). In other words, lim $(\varphi \to \infty)$ $y^* = 0$. Consequently, the effectiveness factor becomes

$$\eta_i = \frac{1}{\phi} \left(2 \int_0^{y^s} r' \, dy \right)^{0.5}, \tag{5.122}$$

where y^s is determined by the relationship

$$y^s = 1 - \frac{\phi}{Bi_M} \left(2 \int_0^{y^s} r' \, dy \right)^{0.5}. \tag{5.123}$$

Calculating the right-hand side of Equation 5.123 gives an algebraic equation from the viewpoint of the dimensionless surface concentration, y^s. From this expression, it (y^s) can be solved iteratively. Subsequently, the effectiveness factor can be obtained from Equation 5.122. If the diffusion resistance in the fluid film is negligible ($Bi_M \to \infty$), $y^s = 1$ (the dimensionless surface concentration) and, consequently, Equation 5.122 is transformed to

$$\eta_i = \frac{1}{\phi} \left(2 \int_0^{1} r' \, dy \right)^{0.5}, \tag{5.124}$$

where φ is given by Equation 5.121.

Defining a Thiele modulus for arbitrary kinetics, φ^*, according to

$$\phi^* = \frac{\phi}{\left(2 \int_0^1 r' \, dy \right)^{0.5}}, \tag{5.125}$$

the asymptotic effectiveness factor, η_i, can be expressed as

$$\eta_i = \frac{1}{\phi^*}. \tag{5.126}$$

This expression, in fact, is the same equation as the asymptotic effectiveness factor obtained for first-order kinetics in Equation 5.105 ($\varphi = \varphi_s$ since $s = 0$ in the present case).

With the technique described above, the asymptotic values for effectiveness factors can be determined easily for flake-formed catalyst particles, since the integral $\int r'\,\mathrm{d}y$ is usually rather simple to evaluate. The results for some kinetic equations are summarized in Table 5.4 [11]. The asymptotic effectiveness factor is a good approximation, provided that the reaction order with respect to the reactant is positive, while a serious error can occur, if the reaction order is negative: in this case, the reaction is accelerated with a decreasing reactant concentration. Certain Langmuir–Hinshelwood rate equations are also similarly "dangerous" kinetic expressions, in which the numerator is of a lower order than the denominator. For such reaction kinetics, the effectiveness factor can, in extreme cases, exceed the value 1. This can be intuitively understood: the reaction rate increases because the reactant concentration inside the particle becomes lower than that in the bulk phase. Such cases are discussed in greater detail in specialized literature [12]. A few examples are illustrated in Figure 5.24a and b.

TABLE 5.4 Some Asymptotic Effectiveness Factors According to Ref. [11]

Kinetic Model	Thiele Modulus	
Reversible first-order reaction $A \rightleftarrows B$		
Equal diffusivity of reactant and product	$\phi^* = \sqrt{\frac{k\rho_p}{D_{eff}}\frac{1+K}{K}} \cdot R$	Froment and Bischoff [2]
Diffusivity of reactant and product not equal	$\phi^* = \sqrt{\rho_p\left(\frac{k_{+1}}{D_{e,A}} + \frac{k_{-1}}{D_{e,B}}\right)} \cdot R$	Aris [12]
Irreversible power law $r = kc_A^n$	$\phi^* = \sqrt{\frac{k\rho_p}{D_{e,A}} c_A^{s\,n-1}\left(\frac{n+1}{2}\right)} \cdot R$	Aris [12]
First-order Langmuir–Hinshelwood, $A \rightarrow R$ $r = \frac{kc_A}{1 + K_A c_A + K_R c_R}$	$\phi^* = \sqrt{\rho_p \frac{r_A^s((K_A/D_{e,A}) - (K_R/D_{e,B}))}{2(1+K)(1-K\,\ln((1+K)/K))}} \cdot R$ $r_A^s = \frac{kc_A^s}{1 + K_A c_A^s + K_R c_R^s}$ $K = K_A c_A + K_R c_R$	Aris [12]
Second-order Langmuir–Hinshelwood, $A + B \rightarrow R$ $r = \frac{kc_A c_B}{1 + K_A c_A + K_B c_B + K_R c_R}$	$\phi^* = \sqrt{\frac{\rho_p r_A^s\left((K_A/D_{e,A}) + (K_B/D_{e,B}) - (K_R/D_{e,R})\right)}{M}} \cdot R$ $M = (1+K)\sqrt{\frac{2}{1+\varepsilon_0}(\varepsilon_0 - 2K)\ln\left(\frac{1+K}{K}\right) + \frac{1+2x-\varepsilon}{1+K}}$ $K = K_A c_A^s + K_B c_B^s + K_R c_R^s,$ $\varepsilon_0 = \frac{D_{e,B} c_B^s}{D_{e,A} c_A^s} - 1, \quad \varepsilon_0 \geq 0$	

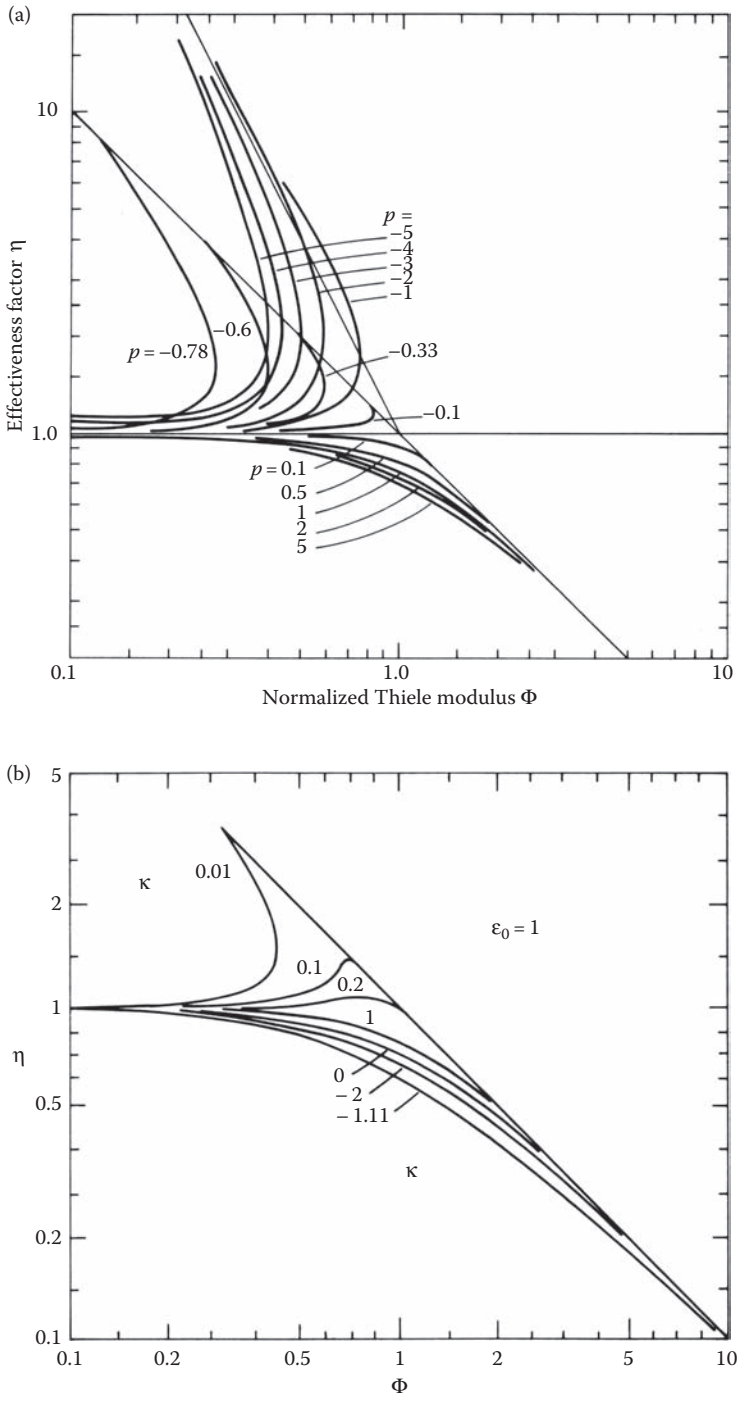

FIGURE 5.24 Isothermal effectiveness factors for a *p*th ($p = 1 \ldots$)-order reaction (a) and for a Langmuir–Hinshelwood kinetics (b). (Data from Aris, R., *The Mathematical Theory of Diffusion an Reaction in Permeable Catalysts*, Vol. I, Clarendon Press, Oxford, 1975.)

Figure 5.24a shows an interesting effect: for reaction kinetics of the order p, with respect to the reactant, even multiple solutions can be obtained for the catalyst particle balance equation, if the reaction order is negative. This phenomenon is called *multiple steady states*. The same effect appears in Langmuir–Hinshelwood kinetics, which is illustrated in Figure 5.24b.

For arbitrary kinetics, a numerical solution of the balance Equation 5.28 taking into account the boundary conditions, Equations 5.31 and 5.32, is necessary. From the concentration profiles thus obtained, we are able to obtain the effectiveness factor by integrating expression 5.55. This is completely feasible using the tools of the modern computing technology, as shown in Refs. [6,10]. Analytical and semianalytical expressions for the effectiveness factor η_i, are, however, always favored if they are available, since the numerical solution of the boundary value problem, Equation 5.29, is not a trivial task.

5.2.2.5 Nonisothermal Conditions

Heat effects caused by chemical reactions inside the catalyst particle are accounted for by setting up an energy balance for the particle. Let us consider the same spherical volume element as in the case of mass balances. Qualitatively, the energy balance in the steady state can be obtained by the following reasoning:

$$\begin{aligned}&\left[\text{the energy flux transported in by means of heat conduction}\right]\\&\quad+\left[\text{the amount of heat generated by the chemical reaction}\right]\\&\quad=\left[\text{the flux of energy transported out by means of heat conduction}\right].\end{aligned}\tag{5.127}$$

Heat conduction is described by the law of Fourier, and several simultaneous chemical reactions are assumed to proceed in the particle. Quantitatively, expression 5.127 implies that

$$\left(-\lambda_e\frac{dT}{dr}4\pi r^2\right)_{in}+\sum_j R_j\left(-\Delta H_{rj}\right)\rho_p 4\pi r^2\Delta r=\left(-\lambda_e\frac{dT}{dr}4\pi r^2\right)_{out},\tag{5.128}$$

where λ_e denotes the effective heat conductivity of the particle.

The difference, $(\lambda_e(dT/dr)4\pi r^2)_{out}-(\lambda(dT/dr)4\pi r^2)_{in}$, is denoted as $\Delta(\lambda_e(dT/dr)\times 4\pi r^2)$. Equation 5.128 then becomes

$$\Delta\left(\lambda_e\frac{dT}{dr}r^2\right)+\sum R_j\left(-\Delta H_{rj}\right)\rho_p r^2\Delta r=0.\tag{5.129}$$

After dividing Equation 5.129 by $r^2\Delta r$ and allowing $\Delta r\to 0$, Equation 5.129 is transformed to the following differential equation:

$$\frac{1}{r^2}\frac{d\left(\lambda_e(dT/dr)r^2\right)}{dr}+\sum R_j\left(-\Delta H_{rj}\right)\rho_p=0.\tag{5.130}$$

This expression is valid for a *spherical geometry* only. It is trivial to show that for an arbitrary geometry, the energy balance can be written using the form factor (s):

$$\frac{1}{r^s}\frac{d(\lambda_e(dT/dr)r^s)}{dr}+\sum R_j\left(-\Delta H_{rj}\right)\rho_p=0.\tag{5.131}$$

The energy balance Equation 5.131 has the following boundary conditions:

$$\frac{\mathrm{d}T}{\mathrm{d}r} = 0, \quad r = 0, \tag{5.132}$$

$$T = T^{\mathrm{s}}, \quad r = R. \tag{5.133}$$

The first boundary condition, Equation 5.132, follows for symmetry reasons.

In practice, the effective heat conductivity of the catalyst, λ_{e}, is often so high that the temperature gradients inside the particle are minor. On the contrary, a temperature gradient often emerges in the fluid film around the catalyst particle, since thermal conduction of the fluid is limited. The energy balance of the fluid film is reduced to

$$\frac{1}{r^s}\frac{\mathrm{d}(\lambda_{\mathrm{f}}(\mathrm{d}T/\mathrm{d}r)r^s)}{\mathrm{d}r} = 0, \tag{5.134}$$

since no reaction takes place in the film itself. The heat conductivity λ_{f}, in Equation 5.134, denotes the conductivity of the fluid. Because the fluid film is extremely thin compared with the catalyst particle, and the heat conductivity of the fluid can be assumed as approximately constant, Equation 5.134 can be simplified to

$$\frac{\mathrm{d}^2T}{\mathrm{d}r^2} = 0 \tag{5.135}$$

having the boundary conditions

$$\begin{aligned} T &= T^{\mathrm{s}}, \quad r = R, \\ T &= T^{\mathrm{b}}, \quad r = R + \delta, \end{aligned} \tag{5.136}$$

where δ denotes the thickness of the fluid film. The equation system, Equations 5.135 and 5.136, is analogous to that of mass balances for the film, Equations 5.34 through 5.36. We can directly apply the solution of Equation 5.36 and write for the temperature profile in the film

$$T(r) = \frac{\left(T^{\mathrm{b}} - T^{\mathrm{s}}\right)(r - R)}{\delta} + T^{\mathrm{s}} \tag{5.137}$$

The temperature gradient in the film becomes

$$\frac{\mathrm{d}T}{\mathrm{d}r} = \frac{T^{\mathrm{b}} - T^{\mathrm{s}}}{\delta}. \tag{5.138}$$

The heat flux through the film, M, becomes

$$M_{r=R} = -\lambda_{\mathrm{e}}\left(\frac{\mathrm{d}T}{\mathrm{d}r}\right)_{r=R}, \tag{5.139}$$

$$M_{r=R} = -\frac{\lambda_{\mathrm{f}}}{\delta}\left(T^{\mathrm{b}} - T^{\mathrm{s}}\right). \tag{5.140}$$

The quantity λ_f/δ is called the heat transfer coefficient of the film, h. We thus obtain

$$M_{r=R} = -h\left(T^b - T^s\right). \tag{5.141}$$

The energy balance for the catalyst particle, Equation 5.131, can be integrated as follows:

$$\int_0^y \mathrm{d}\left(\lambda_e \frac{\mathrm{d}T}{\mathrm{d}r} r^2\right) = -\rho_p \int \sum R_j \left(-\Delta H_{rj}\right) r^s \,\mathrm{d}r, \tag{5.142}$$

where y denotes the upper integration limit, $y = \lambda_e R^s \left(\mathrm{d}T/\mathrm{d}r\right)_{r=R}$. We thus obtain for heat flux at the surface of the particle:

$$M_{r=R} = -\lambda_e \left(\frac{\mathrm{d}T}{\mathrm{d}r}\right)_{r=R} = \frac{\rho_p}{R^s} \int_0^R \sum R_j \left(-\Delta H_{rj}\right) r^s \,\mathrm{d}r. \tag{5.143}$$

The heat fluxes, Equations 5.141 and 5.143, are set equal and a new relationship is obtained:

$$-h\left(T^b - T^s\right) = \frac{\rho_p}{R^s} \int_0^R \sum R_j \left(-\Delta H_{rj}\right) r^s \,\mathrm{d}r. \tag{5.144}$$

Equation 5.144 gives an expression for the temperature of the surface, T^s:

$$T^s = T^b + \frac{\rho_p}{hR^s} \int_0^R \sum R_j \left(-\Delta H_{rj}\right) r^s \,\mathrm{d}r. \tag{5.145}$$

If the dimensionless variable x, $r = xR$, is applied, Equation 5.145 is transformed to

$$T^s = T^b + \frac{\rho_p R}{h} \int_0^1 R_j \left(-\Delta H_{rj}\right) x^s \,\mathrm{d}x. \tag{5.146}$$

Equation 5.146 is global and general: it is valid for those cases in which the temperature varies inside the particle, $T(r) \neq T^s$, as well as for cases in which the whole particle has the same temperature, $T(r) = T^s$. In the latter case, Equation 5.146 can be applied through an iterative calculation of the surface temperature: the mass balance equation for the particle is solved for an assumed (guessed) temperature, the concentration profiles are obtained, and, finally, the integration of Equation 5.146 can be conducted. Equation 5.146 thus gives a better estimate of the surface temperature, and the mass balance equation of the particle can be solved *da capo*, and so on.

If considerable temperature gradients emerge inside the particle, the original energy balance needs to be solved together with the molar balance equation for the particle, Equation 5.29. The effective heat conductivity of the particle λ_e is, however, constant in practice. Therefore, Equation 5.131 can be simplified to

$$\lambda_e\left(\frac{d^2T}{dr^2}+\frac{s}{r}\frac{dT}{dr}\right)+\sum R_j\left(-\Delta H_{rj}\right)\rho_p=0. \tag{5.147}$$

The boundary conditions, Equations 5.132 and 5.133, are still valid. However, whether a temperature gradient does indeed exist in the fluid film or not, the boundary condition is applied accordingly. The boundary condition

$$\frac{dT}{dr}=0, \quad r=0 \tag{5.148}$$

is always valid, whereas the boundary condition

$$T=T^b, \quad r=R \tag{5.149}$$

is valid in case no temperature gradients emerge in the fluid film. The boundary condition

$$\frac{dT}{dr}=\frac{h}{\lambda_e}\left(T^b-T\right), \quad r=R \tag{5.150}$$

is valid if a temperature gradient exists in the fluid film.

The solution of this coupled system of molar mass balances (Equation 5.29) and the energy balance (Equation 5.147) always needs to be conducted numerically: analytical solutions cannot be applied, since the energy and mass balances are coupled through concentrations in the reaction rate expressions and through the exponential temperature dependencies of the rate constants. The numerical solution procedure is discussed in Ref. [10].

For exothermic processes, the reactions cause an increase in temperature inside the particle. This usually leads to increased values of the rate constants. This increase in the rate constants can sometimes overcompensate for the lower concentrations (compared with those in the main fluid bulk) caused by the diffusion limitations in the particle. As a result, the reaction rate becomes higher than the one obtained with the concentrations in the bulk phase and temperature. Consequently, the effectiveness factor exceeds 1! Another interesting phenomenon can emerge under nonisothermal conditions, for strongly exothermic reactions: there will be multiple solutions to the coupled system of energy (Equation 5.131) and mass balances (Equation 5.29)—even for the simplest first-order reaction. This is called *steady-state multiplicity* and is illustrated in Figure 5.25 [13], where nonisothermal effectiveness factors are presented for a first-order reaction. We should, however, note that the phenomenon in practice is rather rarely encountered—as can be understood from a comparison of real parameter values in Figure 5.25. The parameter values for some industrially relevant systems are given in Table 5.5 [2,14].

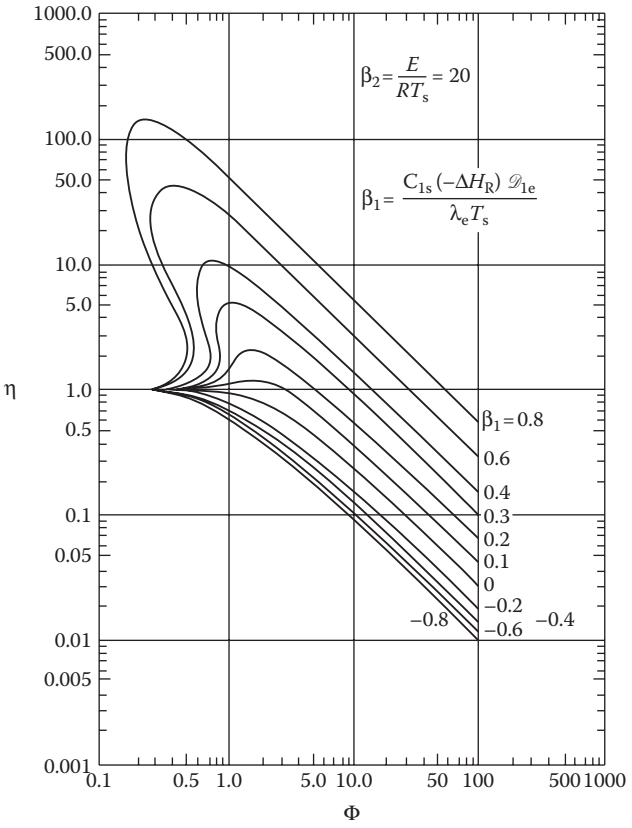

FIGURE 5.25 Nonisothermal effectiveness factors for a first-order reaction in a spherical catalyst particle. (Data from Weisz, P.B. and Hicks, J.S., *Chem. Eng. Sci.*, 17, 265–275, 1962.)

TABLE 5.5 Parameters for Nonisothermal Effectiveness Factors

Reaction	β	γ	γβ	Lw'	φ_s
NH_3 synthesis	0	29.4	0.0018	0.00026	1.2
Synthesis of higher alcohols from CO and H_2	0	28.4	0.024	0.0002	—
Oxidation of CH_3OH to CH_2O	0.011	16	0.175	0.0015	1.1
Synthesis of vinyl chloride from acetylene and HCl	0.25	6.5	1.65	0.1	0.27
Hydrogenation of ethylene	0.066	23–27	2.7	0.11	0.2–2.8
Oxidation of H_2	0.1	6.75–7.52	0.21–2.3	0.036	0.8–2.0
Oxidation of ethylene to ethylene oxide	0.13	13.4	1.76	0.065	0.08
Dissociation of N_2O	0.64	22	1.0–2.0	—	1–5
Hydrogenation of benzene	0.12	14–16	1.7–2.0	0.006	0.05–1.9
Oxidation of SO_2	0.012	14.8	0.175	0.0415	0.9

Note: Case: exothermic reactions [2,14]. For parameters β, γ, γβ, Lw', and φ_s, see Figure 5.25.

5.2.3 ENERGY BALANCES FOR THE ONE-DIMENSIONAL MODEL

In a derivation of the energy balance equation for a packed bed, the same volume element is under consideration as in Section 5.2.1. The energy effects in the volume element are

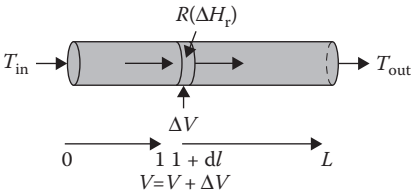

FIGURE 5.26 Energy effects in a packed bed.

illustrated in Figure 5.26. In line with the homogeneous PFR, the energy balance for a volume element, ΔV, can be written in the following manner—provided that only *one* chemical reaction proceeds in the system:

$$\rho_B R\,(-\Delta H_r)\,\Delta V = \Delta\dot{Q} + \dot{m}c_p\Delta T. \tag{5.151}$$

The term $\rho_B R(-\Delta H_r)\Delta V$ describes the energy that is released in an exothermic reaction in catalyst particles. Alternatively, it describes the energy effect that is consumed in an endothermic reaction. $\Delta\dot{Q}$ denotes the heat transfer to or from the surroundings, and the term $\dot{m}c_p\Delta T$ describes the change in the temperature of the flowing media (fluid).

The term for heat transfer from the reactor to the surroundings, $\Delta\dot{Q}$, is typically given by the following expression:

$$\Delta\dot{Q} = U\Delta S\,(T - T_C)\,, \tag{5.152}$$

where ΔS denotes the heat transfer area of the reactor volume element. Inserting Equations 5.10 and 5.152 into Equation 5.151 and dividing the result by the volume element, ΔV, yield

$$\frac{\Delta T}{\Delta V} = \frac{1}{\dot{m}c_p}\left(\rho_B R\,(-\Delta H_r) - U\frac{\Delta S}{\Delta V}\,(T - T_C)\right). \tag{5.153}$$

If the ratio between the heat transfer area, ΔS, and the volume element, ΔV, is assumed to remain constant throughout the reactor, the term $\Delta S/\Delta V = S/V_R$, and we obtain, as $\Delta V \to 0$:

$$\frac{dT}{dV} = \frac{1}{\dot{m}c_p}\left(\rho_B R\,(-\Delta H_r) - U\frac{S}{V_R}(T - T_C)\right). \tag{5.154}$$

In the case of systems with multiple chemical reactions, Equation 5.154 can be easily generalized; the energy balance is then written as follows:

$$\frac{dT}{dV} = \frac{1}{\dot{m}c_p}\left(\rho_B \sum_{j=1}^{s} R_j\left(-\Delta H_{rj}\right) - U\frac{S}{V_R}(T - T_C)\right). \tag{5.155}$$

The energy balances Equations 5.154 and 5.155 are valid for both liquid- and gas-phase reactions. If the definition of the space time, $\tau = V_R/V_0$, is inserted into the energy balance

Equations 5.154 and 5.155, we obtain

$$\frac{\mathrm{d}T}{\mathrm{d}\tau} = \frac{1}{\rho_0 c_\mathrm{p}}\left(\rho_\mathrm{B} R\,(-\Delta H_\mathrm{r}) - U\frac{S}{V_\mathrm{R}}(T - T_\mathrm{C})\right) \tag{5.156}$$

and

$$\frac{\mathrm{d}T}{\mathrm{d}\tau} = \frac{1}{\rho_0 c_\mathrm{p}}\left(\rho_\mathrm{B}\sum_{j=1}^{s} R_j\left(-\Delta H_{\mathrm{r}j}\right) - U\frac{S}{V_\mathrm{R}}(T - T_\mathrm{C})\right). \tag{5.157}$$

A comparison of the energy balance Equations 5.156 and 5.157 with the corresponding balance equations for a homogeneous tube reactor shows a self-evident analogy. There is only one difference: dissimilar definitions for the reaction velocities.

Balance Equations 5.154 through 5.157 are strictly considered as valid for the pseudohomogeneous model, in other words, cases in which neither concentration nor temperature gradients appear in the catalyst particle. In case diffusion inside the catalyst particles—or in the fluid film surrounding the particle—is notable, the term $\rho_\mathrm{B}\Sigma R_j(-\Delta H_{\mathrm{r}j})$ in the energy balance is affected. Furthermore, the heat transfer capacity of the catalyst and the heat conductivity of the fluid film affect this term. Let us consider the effects of temperature gradients on the energy balance equations of the bed, Equation 5.157. Equation 5.143 gives the heat flux, M, on the outer surface of the catalyst:

$$M = -\lambda_\mathrm{e}\left(\frac{\mathrm{d}T}{\mathrm{d}r}\right)_{r=R} = \frac{\rho_\mathrm{p}}{R^\mathrm{s}}\int\sum R_j\,(-\Delta H_\mathrm{r})\,r^\mathrm{s}\,\mathrm{d}r. \tag{5.158}$$

The total heat effect per reactor volume unit is thus given by $M\Delta A/\Delta V$, where ΔA is the heat transfer area in the volume element. Let us assume that we have n_p pieces of spherical particles in the volume element, ΔV. We then obtain

$$\frac{M\Delta A}{\Delta V} = -\lambda_\mathrm{e}\frac{\mathrm{d}T}{\mathrm{d}r}\cdot\frac{n_\mathrm{p}4\pi R^2}{\Delta V}. \tag{5.159}$$

After inserting expression 5.143 into $-\lambda_\mathrm{e}(\mathrm{d}T/\mathrm{d}r)$ and transforming to the dimensionless coordinate, $r = xR$, into the integral (Equation 5.144), we obtain a new expression:

$$\frac{M\Delta A}{\Delta V} = \frac{n_\mathrm{p}4\pi R^3}{(s+1)\,\Delta V}\int_0^1 (s+1)\sum R_j\,(-\Delta H_r)\,x^s\,\mathrm{d}x. \tag{5.160}$$

For a spherical particle $s + 1 = 3$, for the coefficient in front of the integral in Equation 5.160, we obtain the relation

$$\frac{n_\mathrm{p}4/3\pi R^3\rho_\mathrm{p}}{\Delta V} = \frac{m_\mathrm{cat}}{\Delta V} = \rho_\mathrm{B}, \tag{5.161}$$

that is, the catalyst bulk density spontaneously appears in the relationship. The ratio, $\Delta A/\Delta V$, the heat transfer area per reactor volume, is often denoted as a_v. Therefore, as a final result, we obtain

$$Ma_v = \rho_B \int_0^1 (s+1) \sum R_j \left(-\Delta H_{rj}\right) x^s \, dx. \tag{5.162}$$

Equation 5.162 was derived for a spherical particle geometry. However, it is easy to prove that it is indeed valid for arbitrary geometries. The terms $R(-\Delta H_r)$ and $\Sigma R_j(-\Delta H_{rj})$ in energy balance Equations 5.154 through 5.157 should be replaced by the following *averaged* expression, as any concentration or temperature gradients emerge in the catalyst particle:

$$[R\,(-\Delta H_r)]_{average} = \int_0^1 (s+1) R\,(-\Delta H_r)\, x^s \, dx. \tag{5.163}$$

Expression 5.163 is valid for systems with a single chemical reaction, but it is conveniently generalized for systems with multiple chemical reactions:

$$\left(\sum_j R_j \left(-\Delta H_{rj}\right)\right)_{average} = \int_0^1 (s+1) \sum R_j \left(-\Delta H_{rj}\right) x^s \, dx. \tag{5.164}$$

It is easy to understand that expressions 5.163 and 5.164 are reduced to the simple reaction terms in Equations 5.154 through 5.157, provided that terms $R_j(-\Delta H_{rj})$ remain constant. The integrals in Equations 5.163 and 5.164 need to be solved numerically.

For a nonisothermal catalytic packed bed, the energy balance Equation 5.158 is coupled to the mass balances and the system therefore consists of $N + 1$ (number of components + 1) of ordinary differential equations (ODEs), which are solved applying the same numerical methods that were used in the solution of the homogeneous plug flow model (Chapter 2). If the key components are utilized in the calculations, the system can be reduced to $S + 1$ (number of reactions + 1) differential equations—provided that the number of reactions (S) is smaller than the number of components (N).

Examples of a simultaneous numerical solution of molar and energy balance equations for the gas bulk and catalyst particles are introduced in Figure 5.27, in which the concentration and temperature profiles in a methanol synthesis reactor are analyzed. The methanol synthesis reaction, $CO + 2H_2 \leftrightarrow CH_3OH$, is a strongly exothermic and diffusion-limited reaction. This implies that concentration gradients emerge in the catalyst particles, whereas the heat conductivity of the particles is so good that the catalyst particles are practically isothermal.

In the methanol synthesis reactor, the equilibrium composition is attained (Figure 5.27b) and the temperature in the reactor increases to the adiabatic temperature (Figure 5.27c).

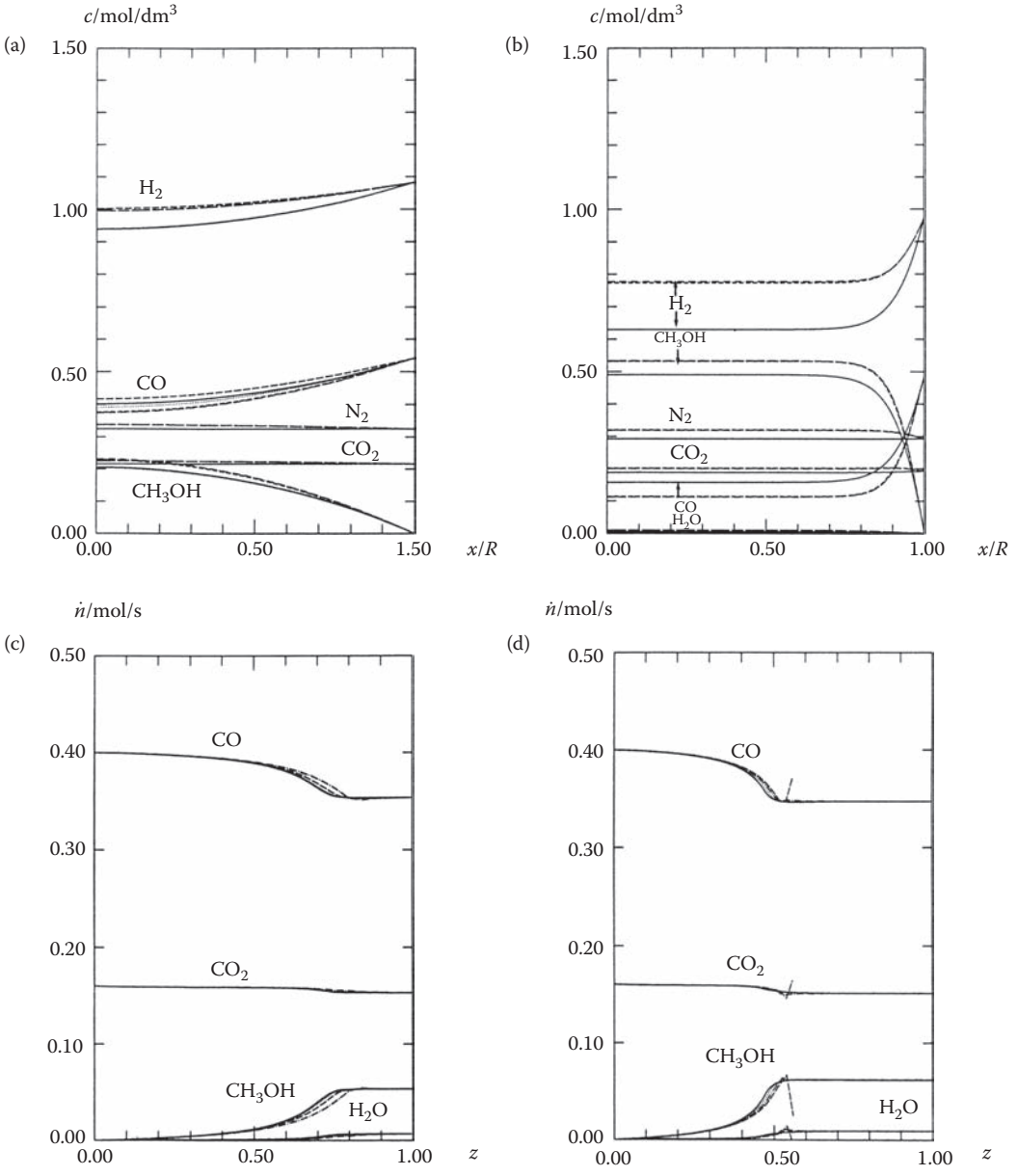

FIGURE 5.27 Concentration profiles in a catalyst particle (a,b) (methanol synthesis, Section 5.2.1) and molar amounts (c,d). An adiabatic packed bed was simulated with different numerical strategies; continuous lines represent the most accurate solution.

Small amounts of water are formed in the process via the side reaction, the reverse water–gas shift reaction, $CO_2 + H_2 \leftrightarrow CO + H_2O$, since the inflow to the synthesis reactor contains some CO_2. Simulation of the concentration and temperature profiles involves relatively tedious calculations for the actual case. The reason for this is that diffusion phenomena in the catalyst particles affect the system: in all solutions of the bulk phase molar and energy

balances, with the BD *method* (Appendix 2), the molar and energy balances for the catalyst particle are solved with polynomial approximations, utilizing the orthogonal collocation method. This strategy is discussed in greater detail in Ref. [10].

The model for packed beds presented above can, in principle, be used for both *multitubular* and *multibed* reactors, since the basic unit in both these reactors is a single reactor tube. We should, however, note certain lamination of the model: in case of very short reactors, the axial dispersion of the material may eventually be important. This is why the plug flow model might not give exactly the correct answer. For strongly exothermic or endothermic reactions, a radial temperature gradient emerges and, consequently, the energy balances, Equations 5.154 through 5.157, are no longer exact. The radial concentration and temperature gradients are treated in greater detail in Section 5.2.4.

For a reactor unit in a *multibed* reactor cascade, the required reactor volume V_R is obtained immediately after determination of the space time, τ:

$$V_R = \tau \dot{V}_0. \tag{5.165}$$

A *multitubular* reactor system consists of identical tubes in parallel (Figure 5.6). The tube length and diameter are usually decided on the basis of practical aspects, such as pressure drop, which restricts the tube length typically to 5–6 m. At the same time, efficient enough heat transfer sets requirements on the tube diameter that should be within the range of a few centimeters. The number of reactor tubes, n_T, can be calculated after the determination of the reactor volume, V_R, from

$$V_R = n_T \frac{\pi d_T^2}{4} L, \tag{5.166}$$

where d_T denotes the tube diameter and L denotes the tube length.

5.2.4 MASS AND ENERGY BALANCES FOR THE TWO-DIMENSIONAL MODEL

If the heat effect that is caused by the chemical reactions is considerable and if the heat conductivity of the catalyst material is low, radial temperature gradients emerge in a reactor tube. This implies, accordingly, that the rate of the chemical reaction varies in the radial direction, and, as a result, concentration gradients emerge in a reactor tube. This phenomenon is illustrated in Figure 5.28. Radial heat conduction can be described with the radial dispersion coefficient as will be shown below.

Let us consider a cylindrical reactor volume element shown in Figure 5.29. The volume element, ΔV, is given by

$$\Delta V = 2\pi r \cdot \Delta r \Delta l, \tag{5.167}$$

as in Figure 5.29. The surface toward which the species are transported in radial dispersion is given by

$$\Delta A = \varepsilon 2\pi r \Delta l, \tag{5.168}$$

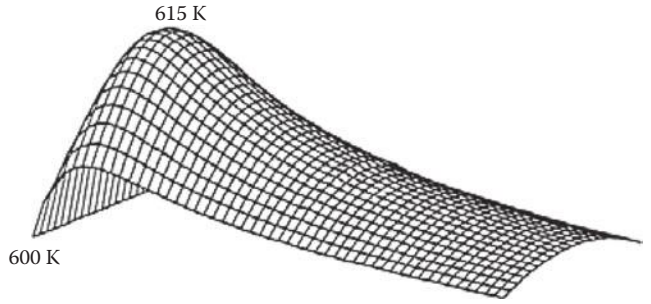

FIGURE 5.28 Radial and axial temperature profiles in a packed bed upon oxidation of *o*-xylene to phthalic anhydride.

where r denotes the radial coordinate and ΔL denotes the length coordinate of the reactor tube. The symbol ε denotes the bed porosity of the catalyst bed.

Qualitatively, the mass balance of component i in a volume element ΔV is given by the following reasoning:

$$\begin{aligned}&[\text{incoming } i \text{ via plug flow}] + [\text{incoming } i \text{ via radial dispersion}] + [\text{generated } i]\\ &\quad = [\text{outgoing } i \text{ via plug flow}] + [\text{outgoing } i \text{ via radial dispersion}]\\ &\qquad + [\text{accumulated } i].\end{aligned} \tag{5.169}$$

The accumulation of component i is discharged, since a steady state is assumed to prevail. Quantitatively, balance (Equation 5.169) is given by

$$\dot{n}_{i,\text{in}} + \left(-D\frac{\mathrm{d}c_i}{\mathrm{d}r}\Delta A\right)_{\text{in}} + r_i\rho_{\text{B}}\Delta V = \dot{n}_{i,\text{out}} + \left(-D\frac{\mathrm{d}c_i}{\mathrm{d}r}\Delta A\right)_{\text{out}}, \tag{5.170}$$

where the term $-D(\mathrm{d}c_i/\mathrm{d}r)\Delta A$ describes radial dispersion; D is the radial dispersion coefficient that presumably has the same value for all components. The molar flow via plug flow, $\dot{n}_i$, in the volume element can be expressed using the concentration, c_i, and the flow velocity, w, as follows:

$$\dot{n}_i = c_i\dot{V} = c_iAw = c_i2\pi r\Delta rw. \tag{5.171}$$

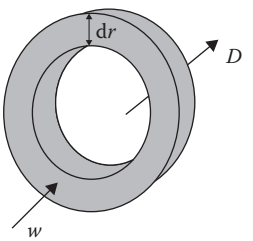

FIGURE 5.29 A cylindrical volume element in a packed bed.

The flow velocity (w) is based on the entire cross-section of the reactor (superficial velocity). The real average flow velocity (w'), interstitial velocity, is higher, since the fluid *de facto* passes through the empty spaces between the particles. The velocities, w and w', are related by the bed porosity:

$$w = \varepsilon w'. \tag{5.172}$$

Relation 5.171 indicates that the difference, $\Delta\dot{n}_i = \dot{n}_{i,\text{out}} - \dot{n}_{i,\text{in}}$, can be expressed as

$$\Delta\dot{n}_i = \dot{n}_{i,\text{out}} - \dot{n}_{i,\text{in}} = 2\pi r \Delta r \Delta(c_i w). \tag{5.173}$$

The difference between the dispersion terms is described according to the following relation

$$\Delta\left(D\frac{\mathrm{d}c_i}{\mathrm{d}r}\Delta A\right) = \left(D\frac{\mathrm{d}c_i}{\mathrm{d}r}\Delta A\right)_{\text{out}} - \left(D\frac{\mathrm{d}c_i}{\mathrm{d}r}\Delta A\right)_{\text{in}} = \Delta\left(D\frac{\mathrm{d}c_i}{\mathrm{d}r}\varepsilon 2\pi r \Delta l\right). \tag{5.174}$$

If the relationships, Equations 5.173 and 5.174, as well as the definition of a volume element, Equation 5.167, are inserted into the mass balance Equation 5.170, we obtain

$$\Delta(c_i w)\cdot 2\pi r \Delta r = \Delta\left(\varepsilon D\frac{\mathrm{d}c_i}{\mathrm{d}r}2\pi r \Delta l\right) + r_i \rho_\text{B}\cdot 2\pi r \Delta r \Delta l. \tag{5.175}$$

Dividing Equation 5.175 by the volume element, $2\pi\Delta r\Delta l$, yields

$$\frac{\Delta(c_i w)}{\Delta l} = \frac{\Delta(\varepsilon D(\mathrm{d}c_i/\mathrm{d}r)r)}{r\Delta r} + r_i\rho_\text{B}. \tag{5.176}$$

By allowing the volume element to shrink, that is, $\Delta l \to 0$ and $\Delta r \to 0$, we achieve a very general form of the molar balance equation for a two-dimensional model:

$$\frac{\mathrm{d}(c_i w)}{\mathrm{d}l} = \frac{1}{r}\frac{d(\varepsilon D(\mathrm{d}c_i/\mathrm{d}r)r)}{\mathrm{d}r} + r_i\rho_\text{B}. \tag{5.177}$$

It is now possible to implement some approximations: the bed porosity, ε, and the dispersion coefficient, D, are assumed to be practically independent of the position. They can therefore be considered as constants in the development of the derivatives in Equation 5.177. We thus obtain the balance equation in the following form:

$$\frac{\mathrm{d}(c_i w)}{\mathrm{d}l} = \varepsilon D\left(\frac{\mathrm{d}^2 c_i}{\mathrm{d}r^2} + \frac{1}{r}\frac{\mathrm{d}c_i}{\mathrm{d}r}\right) + r_i\rho_\text{B}. \tag{5.178}$$

A dimensionless axial coordinate, z, and a dimensionless radial coordinate, ζ, are embraced as follows:

$$l = zL, \tag{5.179}$$

$$r = \zeta R, \tag{5.180}$$

where L and R denote the reactor length and the reactor radius, respectively. When the definitions, Equations 5.179 and 5.180, are inserted into the balance Equation 5.178, we obtain

$$\frac{\mathrm{d}(c_i w)}{\mathrm{d}z} = \frac{\varepsilon D L}{R^2}\left(\frac{\mathrm{d}^2 c_i}{d\zeta^2} + \frac{1}{\zeta}\frac{\mathrm{d}c_i}{d\zeta}\right) + L\rho_B r_i. \tag{5.181}$$

After dividing Equation 5.181 by the velocity w_0 at the reactor inlet, Equation 5.181 transforms to

$$\frac{1}{w_0}\frac{\mathrm{d}(c_i w)}{\mathrm{d}z} = \left(\frac{\varepsilon^2 D}{w_0 d_p}\right)\left(\frac{d_p L}{\varepsilon R^2}\right)\left(\frac{\mathrm{d}^2 c_i}{\mathrm{d}\zeta^2} + \frac{1}{\zeta}\frac{\mathrm{d}\dot{n}}{\mathrm{d}z}\right) + \frac{L}{w_0}\rho_B r_i. \tag{5.182}$$

The ratio L/w_0 is the space time τ:

$$\tau = \frac{L}{w_0}, \tag{5.183}$$

and the term $w_0(d_p/\varepsilon^2 D)$ (d_p denotes the diameter of the catalyst particle) is the Peclet number for radial mass transfer:

$$Pe_{mr} = \frac{w_0 d_p}{\varepsilon^2 D} = \frac{w_0' d_p}{\varepsilon D}. \tag{5.184}$$

The balance Equation 5.182 can consequently be written in the following form:

$$\frac{1}{w_0}\frac{\mathrm{d}(c_i w)}{\mathrm{d}z} = \frac{a}{Pe_{mr}}\left(\frac{\mathrm{d}^2 c_i}{\mathrm{d}\zeta^2} + \frac{1}{\zeta}\frac{\mathrm{d}c_i}{\mathrm{d}\zeta}\right) + \tau\rho_B r_i, \tag{5.185}$$

where $a = d_p L/(\varepsilon R^2)$. Equation 5.185 has the following initial condition at the reactor inlet:

$$c_i = c_{0i} \quad \text{at } z = 0, \tag{5.186}$$

as well as the following boundary conditions at the reactor axis ($\zeta = 0$) and at the outer wall:

$$\frac{\mathrm{d}c_i}{\mathrm{d}\zeta} = 0 \quad \text{at } \zeta = 0, \tag{5.187}$$

$$\frac{\mathrm{d}c_i}{\mathrm{d}\zeta} = 0 \quad \text{at } \zeta = 1. \tag{5.188}$$

The first boundary condition follows for symmetry reasons, whereas the latter implies that the species cannot diffuse through the reactor wall.

When considering the numerical solution of the balance Equation 5.185, further rearrangements are needed. That is, further approximations become actual. The best

approximation is to replace the concentration derivatives in the radial dispersion terms with the following expressions:

$$\frac{\mathrm{d}c_i}{\mathrm{d}\zeta} = \frac{1}{w}\frac{\mathrm{d}(c_i w)}{\mathrm{d}z}, \tag{5.189}$$

$$\frac{\mathrm{d}^2 c_i}{\mathrm{d}\zeta^2} = \frac{1}{w}\frac{\mathrm{d}(c_i w)}{\mathrm{d}z^2}. \tag{5.190}$$

Further, if $c_i w$ is multiplied by the cross-sectional area of the reactor tube πR^2, a quantity with the same dimension as the molar flow is obtained ($\dot{n}$, in mol/s):

$$n_i' = c_i w \pi R^2. \tag{5.191}$$

Equation 5.185 can be rewritten as

$$\frac{\mathrm{d}n_i'}{\mathrm{d}z} = \frac{a w_0}{Pe_{\mathrm{mr}} w}\left(\frac{\mathrm{d}^2 \dot{n}_i'}{\mathrm{d}\zeta^2} + \frac{1}{\zeta}\frac{\mathrm{d}\dot{n}_i'}{\mathrm{d}\zeta}\right) + \rho_{\mathrm{B}} V_{\mathrm{R}} r_i, \tag{5.192}$$

which is analogous to the plug flow model: if the radial dispersion coefficient is small, the variable $Pe_{\mathrm{mr}} = \infty$ and the first term in the right-hand side of Equation 5.192 becomes negligible, and the plug flow model is obtained. The ratio $a w_0 / Pe_{\mathrm{mr}} w$ can be simplified to

$$\frac{a w_0}{Pe_{\mathrm{mr}} w} = \left(\frac{L}{R}\right)\left(\frac{\varepsilon D}{wR}\right) = \frac{L/R}{Pe'}, \tag{5.193}$$

where Pe' denotes another radial Peclet number: $Pe' = (wR)/(\varepsilon D)$. Using arrays, the balance Equation 5.192 becomes

$$\frac{\mathrm{d}\dot{n}'}{\mathrm{d}z} = \frac{L/R}{Pe'}\left(\frac{\mathrm{d}^2 \dot{n}'}{\mathrm{d}\zeta^2} + \frac{1}{\zeta}\frac{\mathrm{d}\dot{n}'}{\mathrm{d}\zeta}\right) + \rho_{\mathrm{B}} \nu R \cdot V_{\mathrm{R}}. \tag{5.194}$$

The quantity $(L/R)/Pe'$ can be used as a criterion for whether to include radial dispersion in the model or not.

The definition of the extent of reaction can be inserted analogously into Equation 5.17:

$$\dot{n}' = \dot{n}_0' + \nu\xi, \tag{5.195}$$

where $\dot{n}_0'$ is obtained from the concentrations at the inlet:

$$\dot{n}_0' = c_0 w_0 \pi R^2. \tag{5.196}$$

If the concept of key components is applied to Equation 5.194, the system is reduced to

$$\frac{\mathrm{d}\dot{n}_k'}{\mathrm{d}z} = \frac{L/R}{Pe'}\left(\frac{\mathrm{d}^2 \dot{n}_k'}{\mathrm{d}\zeta^2} + \frac{1}{\zeta}\frac{\mathrm{d}\dot{n}_k'}{\mathrm{d}\zeta}\right) + \rho_{\mathrm{B}} V_{\mathrm{R}} \nu_k R. \tag{5.197}$$

Multiplying Equation 5.197 by ν_k^{-1} and utilizing the relations below, Equations 5.198 and 5.199,

$$\frac{\mathrm{d}\dot{n}_k'}{\mathrm{d}z} = \nu_k \frac{\mathrm{d}\xi}{\mathrm{d}z}, \tag{5.198}$$

$$\frac{\mathrm{d}\dot{n}_k'}{\mathrm{d}\zeta} = \nu_k \frac{\mathrm{d}\xi}{\mathrm{d}\zeta}, \frac{\mathrm{d}^2\dot{n}_k'}{\mathrm{d}\zeta^2} = \nu_k \frac{\mathrm{d}^2\xi}{\mathrm{d}\zeta^2}, \tag{5.199}$$

give the molar balance expressed with the aid of the *extents of reactions*:

$$\frac{\mathrm{d}\xi}{\mathrm{d}\zeta} = \frac{L/R}{Pe'}\left(\frac{\mathrm{d}^2\xi}{\mathrm{d}\zeta^2} + \frac{1}{\zeta}\frac{\mathrm{d}\xi}{\mathrm{d}\zeta}\right) + \rho_\mathrm{B} V_\mathrm{R} R. \tag{5.200}$$

The balance Equation 5.200 has the following boundary conditions:

$$\frac{\mathrm{d}\xi}{\mathrm{d}\zeta} = 0 \quad \text{at } \zeta = 0, \tag{5.201}$$

$$\frac{\mathrm{d}\xi}{\mathrm{d}\zeta} = 0 \quad \text{at } \zeta = 1. \tag{5.202}$$

When calculating the reactor performance, the total molar flow at the reactor outlet is of interest. If the molar flow of the component i at the reactor outlet is denoted as $\dot{n}_i$, we can obtain it by integrating the flow over the reactor cross-section:

$$\dot{n}_i = \int_0^R c_i w 2\pi r \,\mathrm{d}r = 2\int_0^1 n_i' \zeta \,\mathrm{d}\zeta. \tag{5.203}$$

When calculating the conversions or the molar flows that are needed in the process steps following the reactor, the relationship in Equation 5.203 should be used. Equation 5.203 also provides a comparison with the one-dimensional model.

The energy balance for the volume element, ΔV, can be derived in the same manner as the mass balance. In the steady state, the energy balance is given by

$$\left(-\lambda \frac{\mathrm{d}T}{\mathrm{d}r}\Delta A'\right)_\mathrm{in} + \rho_\mathrm{B}\sum_j R_j\left(-\Delta H_{\mathrm{r}j}\right)\Delta V = \left(-\lambda \frac{\mathrm{d}T}{\mathrm{d}r}\Delta A'\right)_\mathrm{out} + \Delta\dot{m} c_\mathrm{p} \Delta T. \tag{5.204}$$

The term $-\lambda(\mathrm{d}T/\mathrm{d}r)\Delta A'$ describes the heat effect caused by radial heat conduction in the bed; the term $\rho_\mathrm{B}\Sigma R_j(-\Delta H_{\mathrm{r}j})\Delta V$ is the heat effect caused by the chemical reactions and $\Delta\dot{m}\Delta T$ describes the change in temperature of the flowing fluid. The mass flow, $\Delta\dot{m}$, in the volume element is given by

$$\Delta\dot{m} = \rho_0 w_0' \varepsilon 2\pi r \Delta r = \rho_0 w_0 2\pi r \Delta r. \tag{5.205}$$

By taking into account Equation 5.205, as well as the definitions of the volume element, ΔV, Equation 5.167, and the surface element, $\Delta A'$ ($\Delta A' = 2\pi\Delta l$), Equation 5.204 is transformed to

$$\Delta\left(\lambda\frac{\mathrm{d}T}{\mathrm{d}r}2\pi r\Delta l\right) + \rho_B\sum_j R_j\left(-\Delta H_{rj}\right)2\pi r\Delta r\Delta l = \rho_0 w_0 2\pi r\Delta r c_p\Delta T. \tag{5.206}$$

Dividing Equation 5.206 by the volume element, $2\pi r\Delta r\Delta l$, yields

$$c_p\rho_0 w_0\frac{\Delta T}{\Delta l} = \frac{1}{r}\frac{\Delta(\lambda(\mathrm{d}T/\mathrm{d}r)r)}{\Delta r} + \rho_B\sum_j R_j(-\Delta H_{rj}). \tag{5.207}$$

If we allow $\Delta l \to 0$ and $\Delta r \to 0$, the energy balance is obtained as a differential equation:

$$\frac{\mathrm{d}T}{\mathrm{d}l} = \frac{1}{c_p\rho_0 w}\left(\frac{1}{r}\frac{\mathrm{d}(\lambda(\mathrm{d}T/\mathrm{d}r)r)}{\mathrm{d}r} + \rho_B\sum_j R_j(-\Delta H_{rj})\right). \tag{5.208}$$

Here, we can safely assume that the effective radial heat conductivity of the bed, λ, remains approximately constant in the radial direction. Therefore, Equation 5.208 is simplified to

$$\frac{\mathrm{d}T}{\mathrm{d}l} = \frac{1}{c_p\rho_0 w}\left(\lambda\left(\frac{\mathrm{d}^2T}{\mathrm{d}r^2} + \frac{1}{r}\frac{\mathrm{d}T}{\mathrm{d}r}\right) + \rho_B\sum_j R_j(-\Delta H_{rj})\right). \tag{5.209}$$

The energy balance Equation 5.209 bears a mathematical resemblance to the mass balance Equation 5.178. Let us now introduce the *dimensionless coordinates*, z and ζ, according to expressions 5.179 and 5.180. Consequently, the energy balance Equation 5.209 is transformed to

$$\frac{\mathrm{d}T}{\mathrm{d}z} = \frac{1}{c_p\rho_0}\left(\lambda\left(\frac{\mathrm{d}^2T}{\mathrm{d}\zeta^2} + \frac{1}{\zeta}\frac{\mathrm{d}T}{\mathrm{d}\zeta}\right) + \rho_B\sum_j R_j(-\Delta H_{rj})\right). \tag{5.210}$$

This form of the energy balance Equation 5.210 has the following initial boundary conditions at the reactor inlet:

$$T = T_0 \quad \text{at } z = 0, \tag{5.211}$$

$$\frac{\mathrm{d}T}{\mathrm{d}\zeta} = 0 \quad \text{at } \zeta = 0, \tag{5.212}$$

$$-\frac{\lambda}{(\mathrm{d}_T/2)}\left(\frac{\mathrm{d}T}{\mathrm{d}\zeta}\right)_{\zeta=1} = U_w(T - T_C) \quad \text{at } \zeta = 1. \tag{5.213}$$

The first boundary condition, Equations 5.211 and 5.212, follows for symmetry reasons, whereas the second one, Equation 5.213, denotes that the heat flux at the reactor wall should be equal to the heat flux through the reactor wall, $U_w(T - T_C)$, where U_w is a heat transfer coefficient that includes the fluid film at the inner surface of the wall, the reactor wall itself, and the fluid film at the outer surface of the reactor. The value of the heat flux, U_w, can be estimated from standard correlations for heat transfer in tubes.

The pseudohomogeneous two-dimensional model is truly homogeneous if the reaction rates, R_j, remain constant inside the catalyst particles, in other words, when diffusion in the porous catalyst particles does not affect the reaction rate. In case diffusion effects are notable, the terms r_i and $\Sigma R_j(-\Delta H_{rj})$ should be replaced with the terms $\eta_i r_i$ and $\Sigma\left[R_i(-\Delta H_\eta)\right]_{average}$, as was described in Equations 5.55 and 5.164.

Mathematically, the two-dimensional model (balance Equations 5.194 and 5.209) forms a system of parabolic partial differential equations. The best way to numerically solve this system is to convert the partial differential equation

$$\frac{dy}{dz} = f\left(y, \frac{d^2y}{d\zeta^2}, \frac{dy}{d\zeta}\right) \tag{5.214}$$

to an ODE with respect to the length coordinate, z. This can be done by describing the derivatives, $dy/d\zeta$ and $d^2y/d\zeta^2$, by the central differences (the *finite difference method*), or by describing the radial concentration and temperature profiles with approximate functions, such as special polynomial functions (*orthogonal collocation*) [15]. Orthogonal collocation is a more precise method, whereas the finite difference method is easier to implement in computers. The method is described in greater detail in Refs. [15] and [16]. In both cases, the retrieved initial value problem is solved with the help of standard computer codes, Runge–Kutta, Adams–Moulton, or BD methods (Appendix 2).

An important question is raised: when should we use the two-dimensional model and when is the one-dimensional model accurate enough? This issue unfortunately cannot be solved with certainty *a priori*. If the reaction is strongly exothermic, the radial temperature gradient is an important factor. The effect can, for instance, be illustrated through an industrial example: hydrogenation of toluene on a Ni catalyst; the simulated temperature profiles are shown in Figure 5.30 [6]. The two-dimensional model predicts a higher *hot spot* temperature than the one-dimensional model. A similar phenomenon has been shown to exist in the catalytic oxidation of *o*-xylene to phthalic anhydride [2,7] (Figure 5.28). The two-dimensional model can give a conservative—and conservatory—criterion for the highest temperature in the reactor. The problem in the utilization of the two-dimensional model is most often related to the estimation of the radial heat conductivity, λ, for the bed. The radial dispersion coefficient can, on the contrary, be estimated relatively reliably based on the experimental fact that the Peclet number for mass transfer often has the value $Pe_{mr} = 10–12$ in packed beds [2]. The parameters for the one- and two-dimensional models will be discussed in greater detail in Section 5.4.

When comparing the one- and two-dimensional models, the radial heat conductivity, λ, and the heat transfer coefficient, U_w, should thus be related to the heat transfer coefficient,

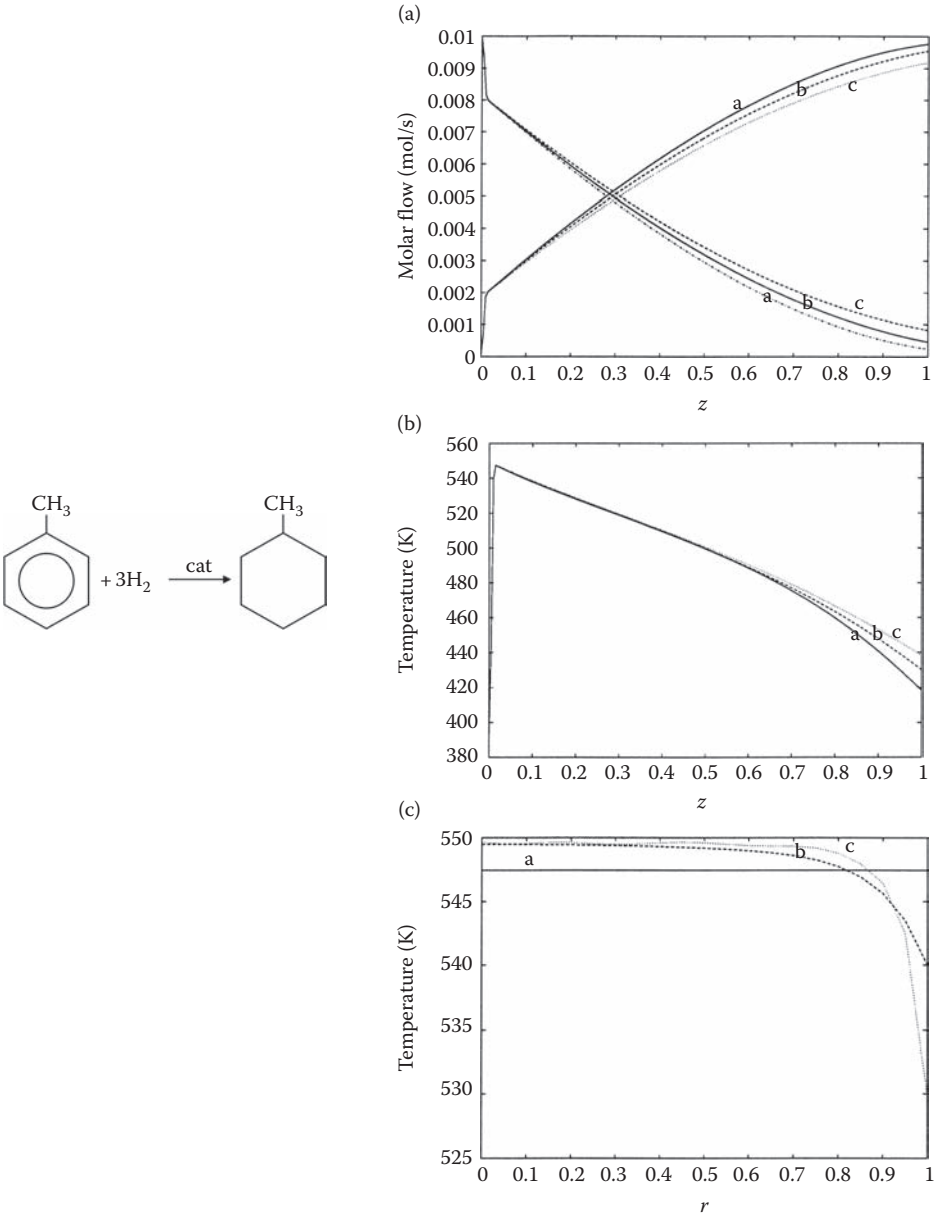

FIGURE 5.30 Molar flows (a), temperatures (b), and radial temperature profiles (c) in a packed bed in catalytic hydrogenation of toluene to methylcyclohexane.

U, of the one-dimensional model. Various theories are presented in the literature, and a frequently used dependence is [3]

$$\frac{1}{U} = \frac{1}{U_w} + \frac{d_T}{8\lambda}. \tag{5.215}$$

If the parameters of the two-dimensional model are known, the parameter U of the one-dimensional model can be obtained easily from Equation 5.215.

5.2.5 PRESSURE DROP IN PACKED BEDS

In packed beds filled with catalyst particles, a pressure drop occurs, since the particles restrict the flow. This phenomenon is important both for industrial and for laboratory scale beds. Although beds in the laboratory are typically short, the pressure drop is of importance even here because the catalyst particles used on the laboratory scale are small. The pressure drop can be estimated from the following equation:

$$\frac{\mathrm{d}P}{\mathrm{d}l} = -f\frac{\rho w^2}{\phi' d_\mathrm{p}}, \tag{5.216}$$

where f is a friction factor, w is the superficial velocity of the fluid, d_p is the diameter of the catalyst particle, and ϕ' denotes the sphericity of the particle. Many correlations are suggested for the estimation of the friction factor, f. Ergun [2,17] has proposed the following expression for the friction factor:

$$f = \frac{(1-\varepsilon)^2}{\varepsilon^3}.\frac{a}{(\phi' d_\mathrm{p} G/\mu)} + \frac{(1-\varepsilon)b}{\varepsilon^3}, \tag{5.217}$$

where $a = 150$, $b = 1.75$, and G is the mass flow per cross-section surface of the tube, that is,

$$G = \frac{\dot{m}}{\pi d_T^2/4} \tag{5.218}$$

and μ is the dynamic viscosity of the fluid. The pressure drop Equation 5.216 is coupled to the molar and energy balances, since the density and velocity of the fluid in particular depend on the temperature and the mixture composition. A rough estimate of the level of the pressure drop can, however, be obtained by integrating Equation 5.216, taking into account estimated values for density, gas velocity, and viscosity. Thus, it is most practical to apply Equation 5.216 in the following form in the case of gas-phase reactions:

$$\frac{\mathrm{d}P}{\mathrm{d}l} = -\frac{fG^2RT}{\phi' d_\mathrm{p} P\overline{M}}. \tag{5.219}$$

In Equation 5.219, $\overline{M}$ is the molar mass of the mixture. If a maximum temperature, T_max, is assumed, a conservative criterion for the pressure drop is obtained in the gas phase—provided that the value $\overline{M}$ is approximately constant:

$$P^2 \geq P_0^2 - \frac{2fG^2RT_\mathrm{max}L}{\phi' d_\mathrm{p}\overline{M}}. \tag{5.220}$$

In Equation 5.220, P and P_0 denote the total pressure at the reactor outlet and inlet, respectively. For an exact calculation, the pressure drop expression, Equation 5.216, needs to be solved simultaneously with the mass and energy balances of one- and two-dimensional models.

5.3 FLUIDIZED BED

The concept of fluidization can be visualized as follows: let us consider small, solid particles located in a vertical, packed bed. The gas flow through the bed comes from below. At low gas velocities, the particles remain immobile, but they begin to float at higher gas velocities. In fact, the drag force that is caused by the flow of gas compensates for gravity. The bed expands, and the particles remain suspended in the gas phase. This phenomenon takes place at a specific gas velocity, the *minimum fluidization velocity*, w_{mf}. If the velocity is further increased, gas bubbles are formed in the bed; this bubble phase is rich in gas but poor in particles. The rest of the bed consists of an emulsion phase, where the majority of the solid particles remain. A fluidized bed is illustrated in Figure 5.31. A fluidized bed resembles a boiling liquid to a large extent in terms of its characteristics. If the gas velocity is increased further, the bubble diameter increases until it is equal to the bed diameter. In this case, the flow is called a slug flow, and the flow is characterized by a limiting velocity, slug velocity, w_s, above which large bubbles are formed [18].

Fluidization is simple to observe visually. However, it can also be registered exactly by measuring the pressure drop over the bed as a function of the gas velocity. This is illustrated in Figure 5.32. In a packed bed, the pressure drop increases monotonously with increasing gas velocity—exactly the pressure drop predicted by the correlation equation. At a minimum fluidization velocity, the increase in the pressure drop stagnates, and at even higher flow values, the pressure drop simply remains at this constant level (Figure 5.32). The minimum fluidization velocity and bed porosity in minimum fluidization are thus very central criteria in the design of fluidized beds.

In a closer study of the hydrodynamics of the fluidized bed, we discover that the gas bubbles have a certain special structure illustrated in Figure 5.33. A *cloud phase* is found around the bubble. At the lower end of the bubble, a particle-rich area is present: a *wake phase*. The catalytic reactions proceed everywhere across the bed, on the surfaces, and in the pores of the solid particles—in the emulsion, bubble, cloud, and wake phases. The reaction velocities in the emulsion and the wake phases are higher than that in the bubble phase. This

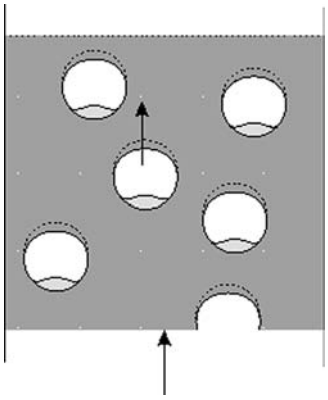

FIGURE 5.31 Flow characteristics of a fluidized bed. (Data from Levenspiel, O., *Chemical Reaction Engineering*, 3rd Edition, Wiley, New York, 1999.)

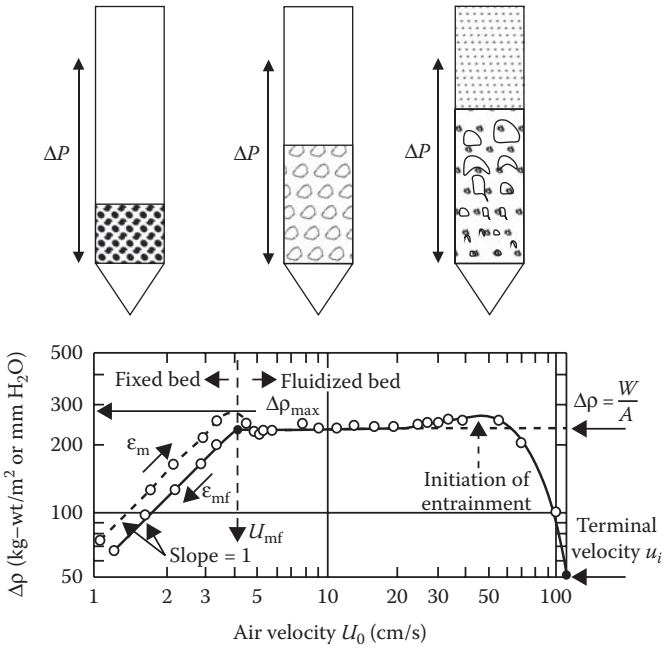

FIGURE 5.32 Pressure drop in a catalytic bed and transformation to a fluidized bed. (Data from Trambouze, P., van Landeghem, H., and Wauquier, J.P., *Chemical Reactors—Design/Engineering/Operation*, Edition Technip, Paris, 1988.)

leads to a mass transfer between the phases: generally, the reactants are transported from the bubbles to the emulsion and the reaction products from the emulsion to the bubbles. Because of the bubble formation, a significant bypass of gases can take place. In these cases, a significantly lower conversion for the reactants is achieved than a CSTR model would predict. Generally, the PFR model gives the extreme boundary values for the performance of a fluidized bed (the highest possible performance level), whereas the CSTR model does *not* provide the other extreme boundary value for the reactor performance (the lowest possible performance level).

A realistic hydrodynamic model for a fluidized bed should therefore contain separate balance studies for each of the phases. The catalyst particles in a fluidized bed are very small, and this is why the inner and outer transport processes in the catalyst particles are

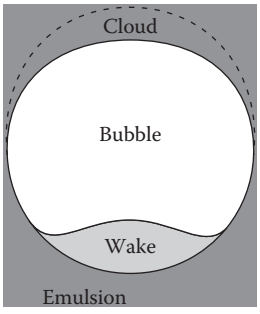

FIGURE 5.33 A bubble in a fluidized bed.

often neglected. Backmixing of phases also implies that the temperature in a fluidized bed is virtually constant over the entire bed. This is why our treatment concentrates on mass balance equations.

5.3.1 MASS BALANCES ACCORDING TO IDEAL MODELS

In this section, we will investigate three kinds of mass balances for a fluidized bed: the plug flow, the CSTR, and the hydrodynamical Kunii–Levenspiel models [18]. The ideal models can be utilized only for rather crude, approximate calculations only; the design of a fluidized bed should comprise a hydrodynamical model coupled with experiments on a pilot scale.

If the one-dimensional plug flow model is applied to a fluidized bed, all equations derived in Section 5.2.1 are applicable. The balance Equations 5.16 through 5.20 are therefore used to describe a fluidized bed. Although the balance equations are nonrealistic from the physical point of view, they can, however, provide an interesting comparison by delivering the extreme performance of the fluidized bed in question. For the sake of a comparison, even the CSTR model for a fluidized bed is described below. The mass balance for component i encompasses, in the case of a backmix model, the entire reactor volume and is given, at the steady state, by the following equation:

$$\dot{n}_{0i} + \rho_B r_i V_R = \dot{n}_i, \tag{5.221}$$

where $\dot{n}_{0i}$ and $\dot{n}_i$ denote the incoming and the outgoing molar flows, respectively. Further, $r_i \rho_B V_R$ denotes the generation rate of component i. Equation 5.221 can be rewritten as

$$\frac{\dot{n}_i - \dot{n}_{0i}}{V_R} = \rho_B r_i. \tag{5.222}$$

For a system with a single chemical reaction, the balance Equation 5.221 can be expressed using the reaction rate, R:

$$\frac{\dot{n}_i - \dot{n}_{0i}}{V_R} = \nu_i R \rho_B. \tag{5.223}$$

In case of multiple chemical reactions, Equation 5.222 is transformed to

$$\frac{\dot{n}_i - \dot{n}_{0i}}{V_R} = \rho_B \sum_j \nu_{ij} R_j, \tag{5.224}$$

which is conveniently expressed with arrays

$$\frac{\dot{\mathbf{n}} - \dot{\mathbf{n}}_0}{V_R} = \rho_B \nu \mathbf{R}. \tag{5.225}$$

As the space time ($\tau = V_R/V_0$) is inserted, Equations 5.224 and 5.225 assume new forms:

$$\frac{\dot{n}_i - \dot{n}_{0i}}{\tau} = \dot{V}_0 \rho_B r_i, \tag{5.226}$$

$$\frac{\dot{n}_i - \dot{n}_{0i}}{\tau} = \dot{V}_0 \rho_B r_i. \tag{5.227}$$

According to the guidelines set in Equations 5.18 through 5.20, the alternative forms of the balance equations, expressed with the extents of reactions, the molar flows of the key components, and the relative conversions, are obtained:

$$\frac{\zeta}{\tau} = \dot{V}\rho_B \mathbf{R}, \tag{5.228}$$

$$\frac{\dot{\mathbf{n}}_k - \dot{\mathbf{n}}_{0k}}{\tau} = \dot{V}_0 \rho_B \nu_k \mathbf{R}, \tag{5.229}$$

$$\frac{\eta'_k}{\tau} = -\frac{\rho_B}{c_0}\nu_k \mathbf{R}. \tag{5.230}$$

The tanks-in-series model (Chapter 4) is sometimes used to describe a fluidized bed. In this case, Equations 5.227 through 5.230 are applied separately for each tank in the system. If the reactor is described using n pieces of equally large units coupled together in a series, the space velocity is $\tau_j = \tau/n$, for each unit; τ_j is thus used in Equations 5.226 through 5.230 instead of τ. Additionally, $\dot{n}_{0i}$ and $\dot{n}_i$ are replaced by $\dot{n}_{j-1,i}$ and $\dot{n}_{j,i}$, respectively.

5.3.2 KUNII–LEVENSPIEL MODEL FOR FLUIDIZED BEDS

The most advanced and realistic description of fluidized beds is the Kunii–Levenspiel model [18]. According to this model, the bubble phase is assumed to move in the reactor following the characteristics of a plug flow, while the gas flow in the emulsion phase is assumed to be negligible. The cloud and wake phases are presumed to possess similar chemical contents. The transport of the reacting gas from the bubble phase to the cloud and wake phases and vice versa prevails. The volume element, ΔV, therefore consists of three parts, as in Figure 5.34:

$$\Delta V = \Delta V_b + \Delta V_c + \Delta V_e. \tag{5.231}$$

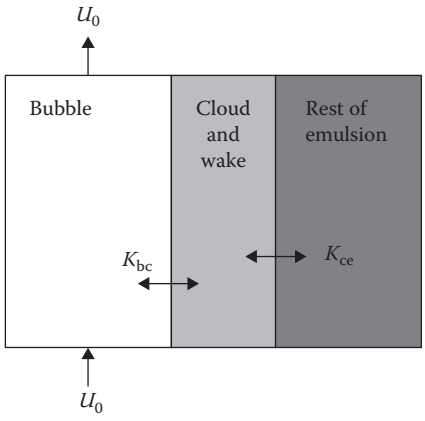

FIGURE 5.34 Schematic structure of a fluidized bed according to the Kunii–Levenspiel model. (Data from Levenspiel, O., *Chemical Reaction Engineering*, 3rd Edition, Wiley, New York, 1999.)

In Equation 5.231, the indexes b, c, and e refer to the bubble, cloud, and emulsion phases, respectively. The mass balance for component i is valid in the bubble phase

$$\dot{n}_{\mathrm{b}i,\mathrm{in}} + r_{\mathrm{b}i}\rho_{\mathrm{Bb}}\Delta V_{\mathrm{b}} = \dot{n}_{\mathrm{b}i,\mathrm{out}} + K_{\mathrm{bc}i}(c_{\mathrm{b}i} - c_{\mathrm{c}i})\Delta V_{\mathrm{b}}, \tag{5.232}$$

where the last term describes the transfer from the bubble phase to the cloud and wake phases and vice versa. Allowing $\Delta V_{\mathrm{b}} \to 0$ and denoting the difference by the expression $\dot{n}_{\mathrm{b}i,\mathrm{out}} - \dot{n}_{\mathrm{b}i,\mathrm{in}} = \Delta\dot{n}_{\mathrm{b}i}$, Equation 5.232 assumes a new form:

$$\frac{\mathrm{d}\dot{n}_{\mathrm{b}i}}{\mathrm{d}V_{\mathrm{b}}} = r_{\mathrm{b}i}\rho_{\mathrm{Bb}} - K_{\mathrm{bc}i}(c_{\mathrm{b}i} - c_{\mathrm{c}i}). \tag{5.233}$$

The following balance equation is valid for the cloud and wake phases:

$$K_{\mathrm{bc}i}\,(c_{\mathrm{b}i} - c_{\mathrm{c}i})\,V_{\mathrm{b}} + r_{\mathrm{c}i}\rho_{\mathrm{Bc}}\Delta V_{\mathrm{c}} = K_{\mathrm{ce}i}\,(c_{\mathrm{c}i} - c_{\mathrm{e}i})\,\Delta V_{\mathrm{b}} \tag{5.234}$$

and Equation 5.234 is transformed to

$$K_{\mathrm{bc}i}\,(c_{\mathrm{b}i} - c_{\mathrm{c}i}) + r_{\mathrm{c}i}\rho_{\mathrm{Bc}}\frac{V_{\mathrm{c}}}{V_{\mathrm{b}}} = K_{\mathrm{ce}i}\,(c_{\mathrm{c}i} - c_{\mathrm{e}i})\,, \tag{5.235}$$

provided that $\Delta V_{\mathrm{b}} \to 0$ and $\Delta V_{\mathrm{c}} \to 0$. Furthermore, $\Delta V_{\mathrm{c}}/\Delta V_{\mathrm{b}} = V_{\mathrm{c}}/V_{\mathrm{b}}$.

To the emulsion phase, the following balance equation is applied:

$$K_{\mathrm{ce}i}\,(c_{\mathrm{c}i} - c_{\mathrm{e}i})\,\Delta V_{\mathrm{b}} + r_{\mathrm{e}i}\rho_{\mathrm{Be}}\Delta V_{\mathrm{e}} = 0. \tag{5.236}$$

Furthermore, if $\Delta V_{\mathrm{b}} \to 0$ and $\Delta V_{\mathrm{e}} \to 0$, as well as if $\Delta V_{\mathrm{b}}/\Delta V_{\mathrm{e}} = V_{\mathrm{b}}/V_{\mathrm{e}}$, Equation 5.236 is simplified to

$$K_{\mathrm{ce}i}\,(c_{\mathrm{e}i} - c_{\mathrm{e}i}) + r_{\mathrm{e}i}\rho_{\mathrm{Be}}\frac{V_{\mathrm{e}}}{V_{\mathrm{b}}} = 0. \tag{5.237}$$

After elimination of the terms $K_{\mathrm{ce}i}\,(c_{\mathrm{c}i} - c_{\mathrm{e}i})$ in Equation 5.235 with the help of Equation 5.237 and, consequently, after insertion of the expression for $K_{\mathrm{bc}i}\,(c_{\mathrm{b}i} - c_{\mathrm{c}i})$ thus obtained in Equation 5.233, we obtain

$$\frac{\mathrm{d}\dot{n}_{\mathrm{b}i}}{\mathrm{d}V_{\mathrm{b}}} = r_{\mathrm{b}i}\rho_{\mathrm{Bb}} + r_{\mathrm{c}i}\rho_{\mathrm{Bc}}\frac{V_{\mathrm{c}}}{V_{\mathrm{b}}} + r_{\mathrm{e}i}\rho_{\mathrm{Be}}\frac{V_{\mathrm{e}}}{V_{\mathrm{b}}}. \tag{5.238}$$

Equation 5.238 illustrates the contributions of reactions proceeding in the bubble, cloud, and emulsion phases, respectively. If the reactions in the cloud and wake phases—or in the bubble phase—are negligible, the corresponding terms disappear from the balance Equation 5.238.

Provided that the volumetric flow rate can be assumed to be (approximately) constant in the bubble phase, the derivative $(\mathrm{d}\dot{n}_{\mathrm{b}i}/\mathrm{d}V_{\mathrm{b}})$ can be written in the following form:

$$\frac{\mathrm{d}\dot{n}_{\mathrm{b}i}}{\mathrm{d}V_{\mathrm{b}}} = \frac{\mathrm{d}c_{\mathrm{b}i}}{\mathrm{d}\tau_{\mathrm{b}}}, \tag{5.239}$$

where $\tau_{\mathrm{b}} = V_{\mathrm{b}}/V_{\mathrm{b}}$. Consequently, Equation 5.238 is transformed to

$$\frac{\mathrm{d}c_{\mathrm{b}i}}{\mathrm{d}\tau_{\mathrm{b}}} = r_{\mathrm{b}i}\rho_{\mathrm{Bb}} + r_{ci}\rho_{\mathrm{Bc}}\frac{V_{\mathrm{c}}}{V_{\mathrm{b}}} + r_{ei}\rho_{\mathrm{Be}}\frac{V_{\mathrm{e}}}{V_{\mathrm{b}}}, \tag{5.240}$$

which, together with Equations 5.235 and 5.237, yields the mathematical model for a fluidized bed. Equations 5.235, 5.237, and 5.240 are valid for systems with multiple chemical reactions. If the volumetric flow rate changes due to chemical reactions, Equation 5.239 is not valid, but an updated formula for $\dot{V}$ should be used, based on the equation of state:

$$P\dot{V} = Z\dot{n}_G RT, \quad \dot{n}_G = \sum \dot{n}_{\mathrm{G}i}. \tag{5.241}$$

The number of variables in the system can be reduced by selecting the extents of reactions for each phase. Let us first consider a system with a single chemical reaction. The extent of the reaction, for the bubble phase, is chosen accordingly:

$$\xi_{\mathrm{b}} = \frac{c_{\mathrm{b}i} - c_{\mathrm{b}0i}}{\nu_i}. \tag{5.242}$$

For the cloud, wake, and emulsion phases, the modified extents of reactions are defined as follows:

$$\xi_{\mathrm{c}} = \frac{K_{\mathrm{bc}i}(c_{\mathrm{b}i} - c_{ci})}{\nu_i} \tag{5.243}$$

and

$$\xi_{\mathrm{e}} = \frac{K_{\mathrm{ce}i}(c_{ci} - c_{ei})}{\nu_i}. \tag{5.244}$$

Equation 5.243 is valid for both cloud and wake phases, whereas Equation 5.244 is restricted to the emulsion phase. Inserting the extent of reaction, ξ_{b}, into Equation 5.240 and taking into account that $r_{\mathrm{b}i} = \nu_i R_{\mathrm{b}}$, $r_{ei} = \nu_i R_{\mathrm{e}}$, and $r_{ci} = \nu_i R_{\mathrm{c}}$, we obtain

$$\frac{\mathrm{d}\xi_{\mathrm{b}}}{\mathrm{d}\tau_{\mathrm{b}}} = R_{\mathrm{b}}\rho_{\mathrm{Bb}} + R_c\rho_{\mathrm{Bc}}\frac{V_{\mathrm{c}}}{V_{\mathrm{b}}} + R_{\mathrm{e}}\rho_{\mathrm{Be}}\frac{V_{\mathrm{c}}}{V_{\mathrm{b}}}. \tag{5.245}$$

Inserting ξ_{c} and ξ_{e}, according to Equations 5.243 and 5.244 into Equations 5.235 and 5.237, respectively, yields

$$\xi_{\mathrm{c}} - \xi_{\mathrm{e}} + R_{\mathrm{c}}\rho_{\mathrm{Bc}}\frac{V_{\mathrm{c}}}{V_{\mathrm{b}}} = 0, \tag{5.246}$$

$$\xi_{\mathrm{e}} + R_{\mathrm{e}}\rho_{\mathrm{Be}}\frac{V_{\mathrm{e}}}{V_{\mathrm{c}}} = 0. \tag{5.247}$$

Equations 5.245 through 5.247 thus form a reduced system of three balance equations. For a system with multiple chemical reactions, the procedure can be generalized using the definitions for the extents of reactions, $\xi_b = [\xi_{1b}\ \xi_{2b} \ldots \xi_{Sb}]^T$, $\xi_c = [\xi_{1c}\ \xi_{2c} \ldots \xi_{Sc}]^T$, and $\xi_e = [\xi_{1e}\ \xi_{2e} \ldots \xi_{Se}]^T$, according to the following:

$$c_b - c_{0b} = \nu\xi_b, \tag{5.248}$$

$$K_{bc}\,(c_b - c_c) = \nu\xi_c, \tag{5.249}$$

$$K_{ce}\,(c_c - c_e) = \nu\xi_e, \tag{5.250}$$

where $\mathbf{K}_{bc}$ and $\mathbf{K}_{ce}$ are diagonal matrices with the elements K_{bci} and K_{cei}, respectively.

Equations 5.235, 5.237, and 5.240 can, consequently, be rewritten with arrays as

$$\frac{dc_b}{d\tau_b} = \nu\left(\rho_{Bb}R_b + \rho_{Bc}R_c\frac{V_c}{V_b} + \rho_{Be}R_e\frac{V_e}{V_b}\right), \tag{5.251}$$

$$K_{bc}(c_b - c_c) - K_{ce}(c_c - c_e) + \nu R_c\rho_{Bc}\frac{V_c}{V_b} = 0, \tag{5.252}$$

$$K_{ce}(c_c - c_e) + \nu R_e\rho_{Be}\frac{V_e}{V_b} = 0. \tag{5.253}$$

After insertions we obtain the very compressed form introduced below:

$$\frac{d\xi_b}{d\tau_b} = \rho_{Bb}R_b + \rho_{Bc}\frac{V_c}{V_b}R_c + \rho_{Be}\frac{V_e}{V_b}R_e \tag{5.254}$$

$$\xi_c - \xi_e + \rho_{Bc}\frac{V_c}{V_b}R_c = 0, \tag{5.255}$$

$$\xi_e + \rho_{Be}\frac{V_e}{V_b}R_e = 0. \tag{5.256}$$

As a summary, we can conclude that the Kunii–Levenspiel model for a fluidized bed consists of $3 \cdot N$ (N = number of components) molar balances (Equations 5.251 through 5.253) if all the components are utilized, or, $3 \cdot S$ (S = number of reactions) balances, if the key components are used as in Equations 5.251 through 5.253. The $3 \cdot S$ balances comprise the model in case the extents of reactions are used in Equations 5.254 through 5.256. In the latter two cases, the concentrations of the components are related through Equations 5.248 through 5.250.

Solving the model of a fluidized bed implies that a simultaneous solution of N ODEs, Equation 5.251, and $2 \cdot N$ algebraic Equations 5.252 and 5.253 is required. Alternatively, S ODEs and $2 \cdot S$ algebraic equations have to be solved simultaneously for the reduced system, Equations 5.254 through 5.256. For systems of first-order reactions, analytical solutions are achievable [18].

5.3.2.1 Kunii–Levenspiel Parameters

For the mass transfer coefficients, K_{bi} and K_{cej}, as well as for the volume fractions, V_c/V_b and V_e/V_b, empirical correlations exist. The average residence time for the bubbles is defined as

$$\tau_b = \frac{L}{w_b}, \tag{5.257}$$

where w_b is the average velocity of the bubbles.

For the estimation of the average bubble velocity, w_b, the minimum fluidization velocity w_{mf} is required. If the bed resides in a condition of minimum fluidization, the particles float freely. The gravitation force is thus compensated for by the pressure drop in the bed. Let us consider a bed cross-section (A), where there are n pieces of particles. The gravitation force, ΔF, is then given by

$$\Delta F = nV_p\rho_p g - nV_p\rho_G g = -\Delta PA, \tag{5.258}$$

where V_p is the particle volume, ρ_P and ρ_G denote the particle and gas densities, respectively, ΔP is the pressure difference, and A is the reactor cross-sectional area. The combined particle volume, nV_P, is given by

$$nV_p = \Delta V_S = \Delta V_R - \Delta V_G = (1 - \varepsilon_{mf})\,\Delta V_R, \tag{5.259}$$

where ΔV_S and ΔV_G are the volume fractions of the particle and the gas, respectively, in a reactor volume element ΔV_R, and ε_{mf} is the bed porosity at minimum fluidization. The volume fraction $\Delta V_R = A\Delta l$ and therefore Equation 5.258 can be written as

$$\frac{dP}{dl} = -(1 - \varepsilon_{mf})(\rho_p - \rho_G)g. \tag{5.260}$$

This pressure drop can be regarded as equal to the pressure drop in Equation 5.216. Let us consider the following expression:

$$\frac{dP}{dl} = -f\frac{\rho_G w_{mf}^2}{\phi' d_p}, \tag{5.261}$$

where φ' is the sphericity of the particle. We should remember that the friction factor f is dependent on the flow velocity w_{mf} (at minimum fluidization) through the mass flow divided by the cross-sectional area (G); according to Equation 5.217, the friction factor f is obtained from

$$f = \frac{(1 - \varepsilon_{mf})}{\varepsilon_{mf}^3}\cdot\frac{a}{(\phi' d_p G/\mu)} + \frac{(1 - \varepsilon_{mf})b}{\varepsilon_{mf}^3}, \tag{5.262}$$

where μ denotes the dynamic viscosity and G is defined by

$$G = -\frac{\dot{m}}{A} = \rho_G w_{mf}. \tag{5.263}$$

Moreover, $a = 150$ and $b = 1.75$. Inserting Equations 5.262 and 5.263 into Equation 5.261, followed by a setting of Equation 5.260 equal to Equation 5.261, gives the following expression for the calculation of the minimum fluidization velocity (w_{mf}):

$$f = \frac{(1-\varepsilon_{mf})^2}{\varepsilon_{mf}^3} \cdot \frac{a\mu}{\left(\phi' d_p\right)^2} w_{mf} + \frac{(1-\varepsilon_{mf})}{\varepsilon_{mf}^3} \frac{b\rho_G}{\left(\phi' d_p\right)^2} w_{mf}^2 = (1-\varepsilon_{mf})\left(\rho_p - \rho_G\right) g, \quad (5.264)$$

where φ' is the sphericity of the particle (see notation). The velocity, w_{mf}, can be calculated from this second-order equation, provided that the bed porosity ε_{mf} at the minimum fluidization point is known. Wen and Yu [19] propose that the following empirical relation can be used for several kinds of particles:

$$\frac{1-\varepsilon_{mf}}{\phi'^2 \varepsilon_{mf}^3} \approx 11. \quad (5.265)$$

For spherical particles ($\varphi' = 1$), Equation 5.265 yields $\varepsilon_{mf} = 0.383$. The average velocity of the bubble velocity, w_b, can now be obtained from the equation [9]

$$w_b = (w - w_{mf}) + 0.711\sqrt{g d_b}, \quad (5.266)$$

where w_0 denotes the superficial velocity, g is the earth gravity acceleration (9.81 m^2/s), and d_b is the bubble diameter. The right-hand side of Equation 5.266 gives the rising velocity of a single bubble in the bed. The difference, $w_0 - w_{mf}$, gives the velocity of the phase between the bubbles. Equation 5.266 requires that the bubble size, d_b, is known.

The volume fractions V_c/V_b (cloud and wake/bubble) and V_e/V_b (emulsion/bubble) are of considerable importance in the design of fluidized beds. They can be obtained from the fractions in the bubbles in the cloud and wake phases as well as in the emulsion phase. Levenspiel [18] has derived the following expressions for the volume fractions:

$$\varepsilon_b = \frac{V_b}{V_R} = \frac{w_0 - w_{mf}}{w_b}, \quad (5.267)$$

$$\varepsilon_c = \frac{V_c}{V_R} = \frac{3(V_b/V_R)(w_{mf}/\varepsilon_{mf})}{w_{br} - (w_{mf}/\varepsilon_{mf})}, \quad (5.268)$$

where w_{br} is the rising velocity of the bubble given by (d_b = bubble diameter)

$$w_{br} = 0.711\sqrt{g d_b}. \quad (5.269)$$

The emulsion fraction is now obtained from

$$\varepsilon_e = \frac{V_e}{V_R} = 1 - \frac{V_b}{V_R} - \frac{V_c}{V_R}. \quad (5.270)$$

The above expressions are used together with the balance equations to predict the volume fractions. The bulk densities ρ_{Bb}, ρ_{Bc}, and ρ_{Be} are often expressed as volume fractions of the solid material in the corresponding phases:

$$\rho_{Bb} = \frac{V_{sb}}{V_b}\rho_p \text{ (bubble)}, \tag{5.271}$$

$$\rho_{Bc} = \frac{V_{sc}}{V_c}\rho_p \text{ (cloud)}, \tag{5.272}$$

$$\rho_{Be} = \frac{V_{se}}{V_e}\rho_p \text{ (emulsion)}, \tag{5.273}$$

where V_{sb}, V_{sc}, and V_{se} denote the volumes of the solid material in the corresponding phases (the indexes are: sb, solids-in-bubble; sc, solids-in-cloud; and se, solids-in-emulsion) and ρ_p is the density of the particles. It has been determined experimentally that

$$\gamma_b = \frac{V_{sb}}{V_b} \approx 0.001 \sim 0.01. \tag{5.274}$$

Levenspiel [18] defines the following volume fractions:

$$\gamma_c = \frac{V_{sc}}{V_b} \text{ (cloud)}, \tag{5.275}$$

$$\gamma_e = \frac{V_{se}}{V_b} \text{ (emulsion)}, \tag{5.276}$$

and gives the following correlation for the fractions γ_c and γ_e:

$$\gamma_c = (1 - \varepsilon_{mf})\left(\frac{3(w_{mf}/\varepsilon_{mf})}{w_{br} - (w_{mf}/\varepsilon_{mf})} + a\right), \tag{5.277}$$

where α = wake volume/bubble volume. The volume fractions are related as follows:

$$\gamma_e = \frac{(1 - \varepsilon_{mf})(1 - \varepsilon_b)}{\varepsilon_b} - (\gamma_c - \gamma_b). \tag{5.278}$$

The fraction wake volume/bubble volume has been experimentally determined in fluidized beds to have values in the following range:

$$\alpha = 0.25 - 1.0. \tag{5.279}$$

Using the correlation equations presented above, all the required quantities ρ_{Bb}, ρ_{Bc}, and ρ_{Be} (bulk densities in the bubble, cloud, and emulsion phases, respectively), as well as the volume fractions for the respective phases (ε_b, ε_c, and ε_e) in the balance equations, can be predicted from the basic quantities, bed porosity at minimum fluidization (ε_{mf}),

minimum fluidization velocity (w_{mf}), superficial flow velocity (w_0), particle density (ρ_p), and gas density (ρ_G).

The following correlations have been found to be valid for the transfer coefficients K_{bc} and K_{ce} [9,18]:

$$K_{bci} = 4.5\left(\frac{w_{mf}}{d_b}\right) + 5.85\left(\frac{D_i^{1/2} g^{1/4}}{d_b^{5/4}}\right) \tag{5.280}$$

and

$$K_{cei} = 6.78\sqrt{\frac{\varepsilon_{mf} D_i w_b}{d_b^3}}, \tag{5.281}$$

where D_i is the molecular diffusion coefficient of the gas-phase component and d_b is the bubble diameter.

It is sometimes interesting to compare the performance of a fluidized bed and a packed bed. The characteristic residence time for the bubbles τ_b defined in Equation 5.239 can be related to the length of a packed bed (L_{packed}) by the following expression [18]:

$$\tau_b = \frac{L}{w_b} = \left(\frac{1-\varepsilon_{packed}}{1-\varepsilon_{mf}}\right)\frac{L_{packed}}{w_{br}}. \tag{5.282}$$

Other models for fluidized beds and industrial processes are discussed in Ref. [9].

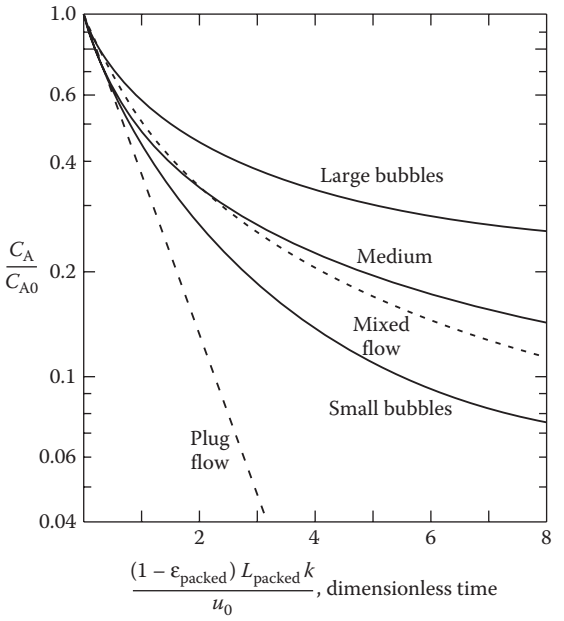

FIGURE 5.35 Comparison of different fluidized bed models for a first-order reaction A→P according to Ref. [18].

5.3.2.1.1 First-Order Reactions in a Fluidized Bed

A comparison between different fluidized bed models for a first-order reaction A→P is presented in Figure 5.35. The figure shows that the plug flow model gives the highest possible conversion of reactant A, whereas the CSTR model does not predict the lowest conversion of A. The conversion obtained by the Kunii–Levenspiel model is highly dependent on the bubble size in the fluidized bed. If the bubbles are small, plug flow conditions are approached, whereas large bubbles give conversion values that are clearly lower than the conversion predicted by the CSTR model. This has also been verified experimentally.

In a general case of nonlinear kinetics, the fluidized bed model is solved numerically with an algorithm suitable for differential algebraic systems. The calculation procedure for fluidized beds with the Kunii–Levenspiel model involves numerous steps, as evidenced by the treatment. As a summary, the path from the minimum fluidization quantities (ε_{mf}, w_{mf}) to the reactor model is presented in Table 5.6. The superficial velocity (w_0) and the physical parameters are assumed to be constant.

5.4 PARAMETERS FOR PACKED BED AND FLUIDIZED BED REACTORS

Several parameters are included in the packed and fluidized bed models. The values of the parameters have to be determined experimentally or estimated theoretically to enable the use of balance equations in the design of real reactors.

TABLE 5.6 Calculation Procedure for Simulation of a Fluidized Bed Model

Quantity	Equation Number
ε_{mf}	5.265
w_{mf}	5.264
w_{br}	5.269
w_b	5.266
ε_b	5.267
ε_c	5.268
ε_e	5.270
γ_b	5.274
γ_c	5.277, α from Equation 5.279
γ_e	5.278
ρ_{Bb}	5.271
ρ_{Bc}	$V_{sc}/V_c = \gamma_c\varepsilon_b/\varepsilon_c$, then Equation 5.272
ρ_{Be}	$V_{se}/V_e = \gamma_e\varepsilon_b/\varepsilon_e$, then Equation 5.273
V_c/V_b	$= \varepsilon_c/\varepsilon_b$
V_e/V_b	$= \varepsilon_e/\varepsilon_b$
K_{bci}	5.280, D_i from Appendix 4
K_{cei}	5.281
Reactor model	5.233, 5.235, 5.237

The effective diffusion coefficient (D_{ei}), which is valid for porous catalyst particles, can be related to the molecular diffusion coefficient D_i with a simple relation:

$$D_{ei} = \left(\frac{\varepsilon_p}{\tau_p}\right) D_i, \tag{5.283}$$

where ε_p and τ_p denote the porosity and the tortuosity of the catalyst particle. Tortuosity describes the difference of the catalyst pores from the ideal linear, cylindrical form. Particle porosity ε_p is always smaller than one, whereas tortuosity τ_p is larger than one. This implies that the effective diffusion coefficient D_{ei} typically is clearly smaller than the molecular diffusion coefficient, D_i. Diffusion in catalyst pores usually takes place according to two parallel mechanisms: molecular diffusion originating from intermolecular collisions and by Knudsen diffusion caused by molecular collisions with the pore walls. The combinatorial diffusion coefficient D_i can be approximately written as

$$\frac{1}{D_i} = \frac{1}{D_{mi}} + \frac{1}{D_{Ki}}, \tag{5.284}$$

where D_{mi} and D_{ki} denote the molecular and the Knudsen diffusion coefficients, respectively. In large pores, molecular diffusion dominates, whereas Knudsen diffusion prevails in small pores, for example, in many zeolite catalysts. The estimation of diffusion coefficients is described in detail in Appendix 4.

The molecular diffusion coefficient, D_{mi}, can be calculated from the binary diffusion coefficients (D_{ij}) obtained from the Fuller–Schettler–Giddings equation [20] for gas-phase systems. The individual diffusion coefficients, D_{mi}, can be estimated from the binary diffusion coefficients using Wilke's approximation [20]. For the Knudsen diffusion

TABLE 5.7 Parameters for Packed Beds

Effective Thermal Conductivities	
1. Effective radial thermal conductivity	1–12 W/mK
2. $\frac{\text{Effective axial thermal conductivity}}{\text{Thermal conductivity of fluid}}$	1–300
3. $\frac{\text{Effective radial thermal conductivity}}{\text{Thermal conductivity of fluid}}$	1–12
4. Static contribution	0.16–0.37 W/mK
Heat Transfer Coefficients	
1. Heat transfer coefficient for the one-dimensional model	15–85 W/m^2K
2. Wall coefficient for the two-dimensional model	100–300 W/m^2K
3. Static contribution (one-dimensional model)	5–25 W/m^2K
4. Static contribution to wall coefficient (two-dimensional model)	15–100 W/m^2K
Dispersion Coefficients	
1. Radial Peclet number	6–20
2. Axial Peclet number	0.1–5

coefficient, an explicit expression is given in Ref. [21]. The gas film coefficients, k_{Gi}, can be obtained from empirical correlations [22]; these correlations require knowledge of molecular diffusion coefficients. For a description of the calculation of gas film coefficients, see Appendix 5.

Estimation of the corresponding parameters for liquid-phase systems is more uncertain. Equation 5.284 is valid for liquid-filled catalyst pores. The molecular liquid-phase diffusion coefficients can be estimated from, that is, the Wilke–Chang equation [20]. Different estimation methods are discussed further in the book *The Properties of Gases and Liquids* [20]. For the liquid phase, the film coefficient, k_L, is always used. Different empirical correlations for the liquid film coefficient are presented and compared, for example, in Ref. [23]. Methods for estimating liquid-phase diffusion coefficients and liquid film coefficients are described in Appendices 6 and 7.

The balances for packed beds contain several other parameters. In the review of Kulkarni and Doraiswamy [22], several expressions are presented for the estimation of the heat transfer parameters (λ, U, . . .); some parameter values are summarized in Table 5.7.

REFERENCES

1. Fogler, H.S., *Elements of Chemical Reaction Engineering*, Prentice-Hall, Englewood Cliffs, NJ, 1999.
2. Froment, G. and Bischoff, K., *Chemical Reactor Analysis and Design*, 2nd Edition, Wiley, New York, 1990.
3. Rase, H.F., *Chemical Reactor Design for Process Plants*, Wiley, New York, 1977.
4. Irandoust, S. and Andersson, B., Monolithic catalysts for nonautomobile applications, *Cat. Rev. Sci. Eng.*, 30, 341–392, 1988.
5. Trambouze, P., van Landeghem, H., and Wauquier, J.P., *Chemical Reactors—Design/Engineering/Operation*, Edition Technip, Paris, 1988.
6. Salmi, T., Wärnå, J., Lundén, P., and Romanainen, J., Development of generalized models for heterogeneous chemical reactors, *Comp. Chem. Eng.*, 16, 421–430, 1992.
7. Lundén, P., Stationära simuleringsmodeller för katalytiska gasfasreaktioner i packade bäddreaktorer, Master's thesis, Åbo Akademi, 1991.
8. Chen, N.C., *Process Reactor Design*, Allyn and Bacon, Boston, 1983.
9. Yates, J.G., *Fundamentals of Fluidized-bed Chemical Processes*, Butterworths, London, 1983.
10. Salmi, T. and Wärnå, J., Modelling of catalytic packed-bed reactors—comparison of different diffusion models, *Comp. Chem. Eng.*, 15, 715–727, 1991.
11. Silveston, P.L., Reaction with porous catalysts—effectiveness factors, in A. Gianetto and P.L. Silveston (Eds), *Multiphase Chemical Reactors*, Hemisphere Publishing Corporation, Washington, DC, 1986.
12. Aris, R., *The Mathematical Theory of Diffusion an Reaction in Permeable Catalysts*, Vol. I, Clarendon Press, Oxford, 1975.
13. Weisz, P.B. and Hicks, J.S., The behavior of porous catalyst particles in view of internal mass and heat diffusion effects, *Chem. Eng. Sci.*, 17, 265–275, 1962.
14. Hlavacek, V., Kubicek, M., and Marek, M., Analysis of nonstationary heat and mass transfer in a porous catalyst particle, *J. Catal.*, 15, 17–30, 1969.
15. Villadsen, J. and Michelsen, M.L., *Solution of Differential Equation Models by Polynomial Approximation*, Prentice-Hall, Englewood Cliffs, NJ, 1978.

16. Salmi, T., Saxén H., Toivonen, H., Aittamaa, J., and Nousiainen, H., *A Program Package for Solving Coupled Systems of Nonlinear Partial and Ordinary Differential Equations by Orthogonal Collocation*, Laboratory of Industrial Chemistry, Åbo Akademi, 1989.
17. Ergun, S., Fluid flow through packed columns, *Chem. Eng. Progr.,* 48, 89–94, 1952.
18. Levenspiel, O., *Chemical Reaction Engineering*, 3rd Edition, Wiley, New York, 1999.
19. Wen, C.Y. and Yu, Y.H., A generalized method for predicting the minimum fluidization velocity, *AIChE J*., 12, 610–612, 1966.
20. Reid, R.C., Prausnitz, J.M., and Poling, B.E., *The Properties of Gases and Liquids*, 4th Edition, McGraw-Hill, New York, 1988.
21. Satterfield, C.N., *Mass Transfer in Heterogeneous Catalysis*, M.I.T. Press, Cambridge, 1970.
22. Kulkarni, B.D. and Doraiswamy, L.K., Estimation of effective transport properties in packed bed reactors, *Catal. Rev. Sci. Eng.*, 22, 1980.
23. Myllykangas, J., *Aineensiirtokertoimen, neste—ja kaasuosuuden sekä aineensiirtopintaalan korrelaatiot eräissä heterogeenisissä reaktoreissa*, Åbo Akademi, Åbo, Finland, 1989.

CHAPTER 6

Catalytic Three-Phase Reactors

6.1 REACTORS USED FOR CATALYTIC THREE-PHASE REACTIONS

In catalytic three-phase reactors, a gas phase, a liquid phase, and a solid catalyst phase coexist. Some of the reactants and/or products are in the gas phase under the prevailing conditions (temperature and pressure). The gas components diffuse through the gas–liquid interface, dissolve in the liquid, diffuse through the liquid film to the liquid bulk phase, and diffuse through the liquid film around the catalyst particle to the catalyst surface, where the chemical reaction takes place (Figure 6.1). If catalyst particles are porous, a chemical reaction and diffusion take place simultaneously in the catalyst pores. The product molecules are transported in the opposite direction.

The size of the catalyst particle is of considerable importance for catalytic three-phase reactors. Catalyst particles can be very small and are suspended in the liquid phase. Catalyst particles of a size similar to those used in two-phase packed bed reactors can also be used in three-phase reactors. The main designs of catalytic three-phase reactors are shown in Figure 6.2. Small catalyst particles are mainly used in bubble columns (Figure 6.2a), stirred tank reactors (Figure 6.2b), and fluidized beds (Figure 6.2d). A common name for this kind of reactor is a slurry reactor. Packed bed reactors are generally filled with large catalyst particles (Figure 6.2c).

Catalytic three-phase processes are of enormous industrial importance. Catalytic three-phase processes exist in the oil and petrochemical industry, in the manufacture of synthetic fuels, as intermediate steps in the processing of organic compounds, in the production of

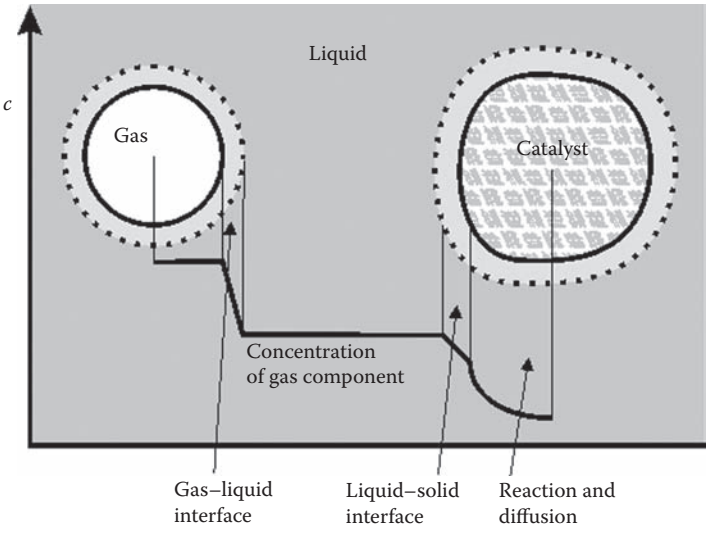

FIGURE 6.1 Various phases in a three-phase reactor.

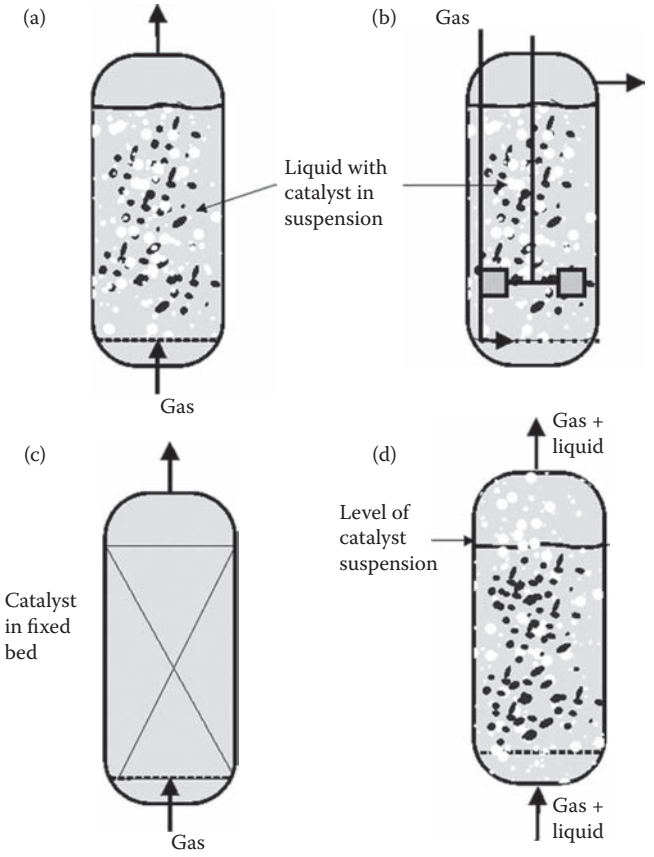

FIGURE 6.2 Typical three-phase reactors: (a) a bubble column, (b) a tank reactor, (c) a packed bed reactor, and (d) a fluidized bed reactor.

TABLE 6.1 Examples of Catalytic Three-Phase Processes

Process	Reactor Type
Hydrogenation (hardening) of fatty acids	Slurry reactor (bubble column and stirred tank reactor)
Desulfurization	Trickle bed, fluidized bed
Hydrocracking	Trickle bed
Fischer–Tropsch synthesis	Bubble column
Hydrogenation of aromatic compounds (dearomatization), that is, hydrogenation of benzene, toluene, and polyaromatics	Trickle bed, slurry reactor
Hydrogenation of anthraquinone in the production of H_2O_2	Bubble column, catalytic monolith, or other structure reactor
Methanol synthesis	Slurry reactor
Hydrogenation of sugars to sugar alcohols (D-glucose to sorbitol, D-xylose to xylitol, D-maltose to maltitol, D-lactose to lactitol, fructose to mannitol and sorbitol)	Slurry reactor, trickle bed reactor, loop reactor, catalytic monolith, or other structured reactor

fine chemicals, in food processing, and in biochemical processes. An overview of industrial three-phase processes is given in Table 6.1.

Catalytic three-phase reactions are used in oil refining, in hydrodesulfurization and hydrometallation processes, for the removal of oxygen and nitrogen from oil fractions (hydrodeoxygenation and hydrodenitrogenation), and in the hydrogenation of aromatic compounds (dearomatization). The production of synthetic fuels (Fisher–Tropsch synthesis) is a three-phase system. In the production of inorganic chemicals, the hydrogen peroxide process (H_2O_2) is a three-phase process in which catalytic hydrogenation of anthraquinone to anthraquinole is an important intermediate step. In food processing, three-phase reactors exist, that is, in the hydrogenation of fatty acids in margarine production and in the hydrogenation of sugars to corresponding sugar alcohols (e.g., xylose to xylitol). For some catalytic two-phase processes, competing three-phase processes have been developed. Oxidation of SO_2 to SO_3 over an active carbon catalyst and methanol synthesis can be carried out in three-phase slurry reactors.

Bubble column reactors are shown in Figures 6.3 and 6.4. Bubble columns are often operated in a semibatch mode (Figure 6.3), with the gas phase as the continuous phase and the liquid with the suspended catalyst particles in batch. This is a typical way of producing chemicals in smaller amounts. Good mixing of the gas–solid–liquid mixture is important in bubble columns. Mixing can be enhanced by the use of a gas lift or a circulation pump with an ejector (Figure 6.4). The backmixing of the suspension of liquid and catalyst particles is more intensive than that of the gas phase. Because of backmixing, bubble columns are mostly rather isothermal.

The flow profile in a bubble column is determined by the gas flow velocity and the cross-sectional area of the column, as in Figures 6.5 and 6.6. At low gas velocities, all gas bubbles are assumed to have the same size. In this regime, we have a *homogeneous bubble flow*. If the gas velocity is increased in a narrow column, a *slug flow* is developed. In a slug flow, the bubbles fill the entire cross-section of the reactor. Small bubbles exist in the liquid between the slugs, but the main part of the gas is in the form of large bubbles. In wider bubble column vessels, a bubble size distribution is developed; this is called *a heterogeneous flow*.

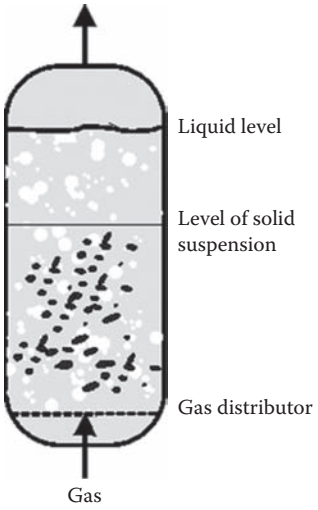

FIGURE 6.3 A semibatch bubble column.

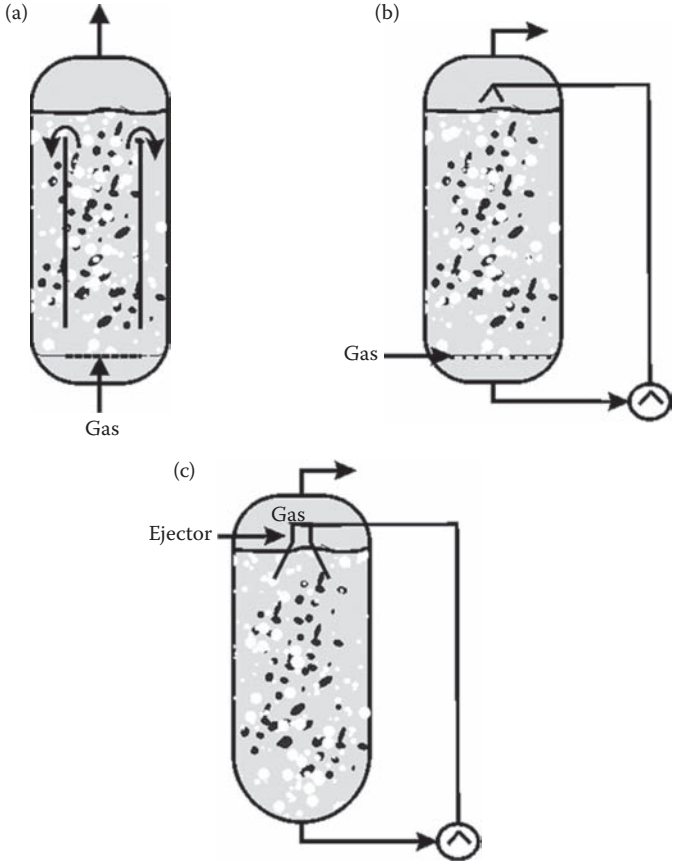

FIGURE 6.4 Different ways to circulate the suspension in a bubble column: (a) gas lift, (b) circulation with a pump, and (c) circulation with a pump and an ejector.

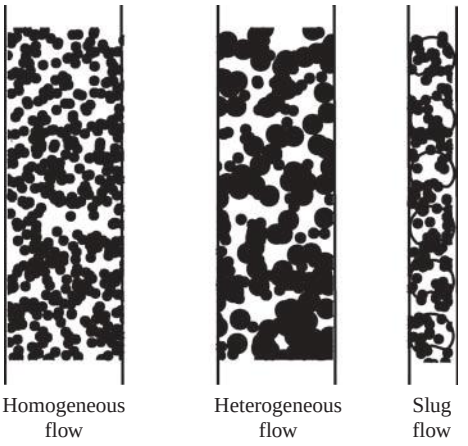

FIGURE 6.5 Flow patterns appearing in a bubble column.

The flow properties in a bubble column are of considerable importance for the performance of three-phase reactors. The flow properties determine the gas volume fraction and the size of the interfacial area in the column. The flow profiles have a crucial impact on the reactor performance.

Another alternative for three-phase catalytic reactors with suspended catalyst particles is to use mechanically agitated tank reactors (Figure 6.7). In a tank reactor, the flow profile can approach complete backmixing.

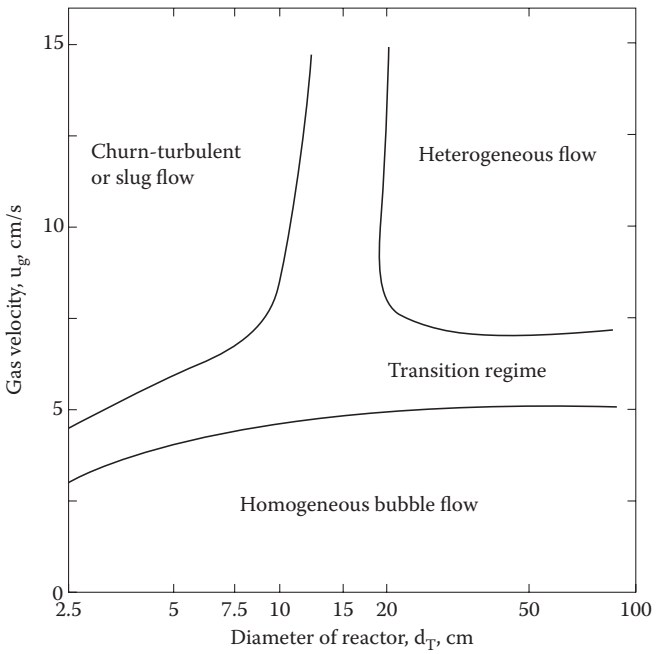

FIGURE 6.6 Flow map for a bubble column. (Data from Ramachandran, P.A. and Chaudhari, R.V., *Three-Phase Catalytic Reactors*, Gordon and Breach Science Publishers, New York, 1983.)

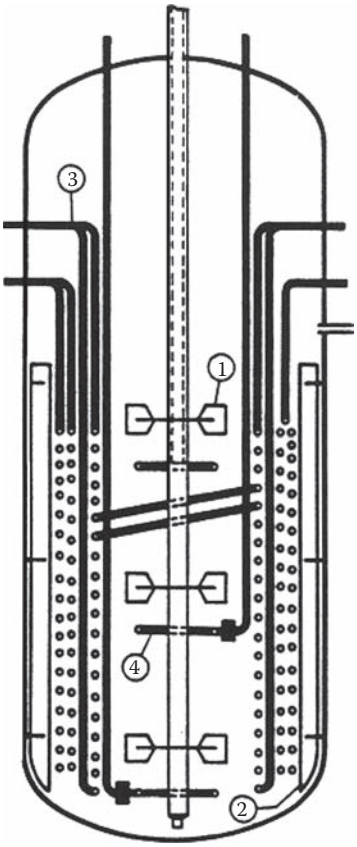

1 Turbine impeller
2 Baffle
3 Cooling and heating coils
4 Perforated ring for hydrogen supply

FIGURE 6.7 A three-phase reactor. (Data from Ramachandran, P.A. and Chaudhari, R.V., *Three-Phase Catalytic Reactors*, Gordon and Breach Science Publishers, New York, 1983.)

Different packed bed reactor designs are illustrated in Figure 6.8. The flow properties are of utmost importance for packed beds used in three-phase reactions. The most common operation policy is to allow the liquid to flow downward in the reactor. The gas phase can flow upwards or downwards, in a concurrent or a countercurrent flow. This reactor is called a *trickle bed* reactor. The name is indicative of flow conditions in the reactor, as the liquid flows downward in a laminar flow wetting the catalyst particles efficiently (*trickling flow*). It is also possible to allow both the gas and the liquid to flow upward in the reactor (Figure 6.8). In this case, no trickling flow can develop, and the reactor is called a *packed bed* or a *fixed bed* reactor.

The flow conditions in a trickle bed reactor are illustrated in Figure 6.9. At low gas and liquid flows, a *trickle flow* dominates; if the flow rates are higher, a *pulsed flow* develops in the reactor. At low gas and high liquid flows, the liquid phase is continuous and gas bubbles flow through the liquid phase. At high gas velocities, the gas phase is continuous and the liquid droplets are dispersed in the gas flow (*spray flow*). Trickle bed reactors are usually

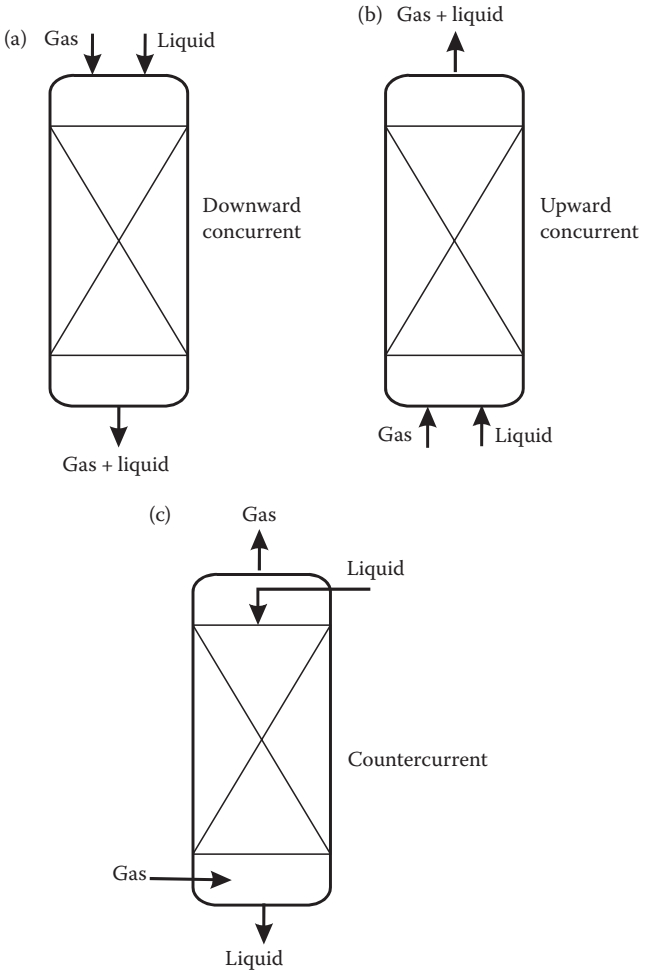

FIGURE 6.8 Different types of packed (fixed) beds; (a) and (c) are called trickle beds; (b) is upflow fixed bed.

operated under *trickle* or *pulse* flow conditions. Both the gas and liquid phases approach plug flow conditions in a *trickle bed* reactor.

For a packed bed, where both the gas and liquid phases flow upward, see Figure 6.10. Different flow patterns also develop in these reactors, depending on the gas and the liquid flow rates. A flow map is displayed in Figure 6.11. At low gas and high liquid flow rates, a bubble flow prevails, the bubbles flowing through the continuous liquid phase. At higher gas and low liquid velocities, the liquid is dispersed in the gas and the flow type is called a *spray flow*. At higher gas and low liquid flow rates, a *slug flow* develops in the reactor, and the bubble size distribution becomes very uneven. In this kind of packed bed reactor, the gas phase is close to a plug flow, but the liquid phase is partially backmixed.

A three-phase fluidized bed is shown in Figure 6.12. In a fluidized bed, the finely crushed catalyst particles are fluidized because of the movement of the liquid. Three-phase fluidized beds usually operate in a concurrent mode with gas and liquid flowing upward. However,

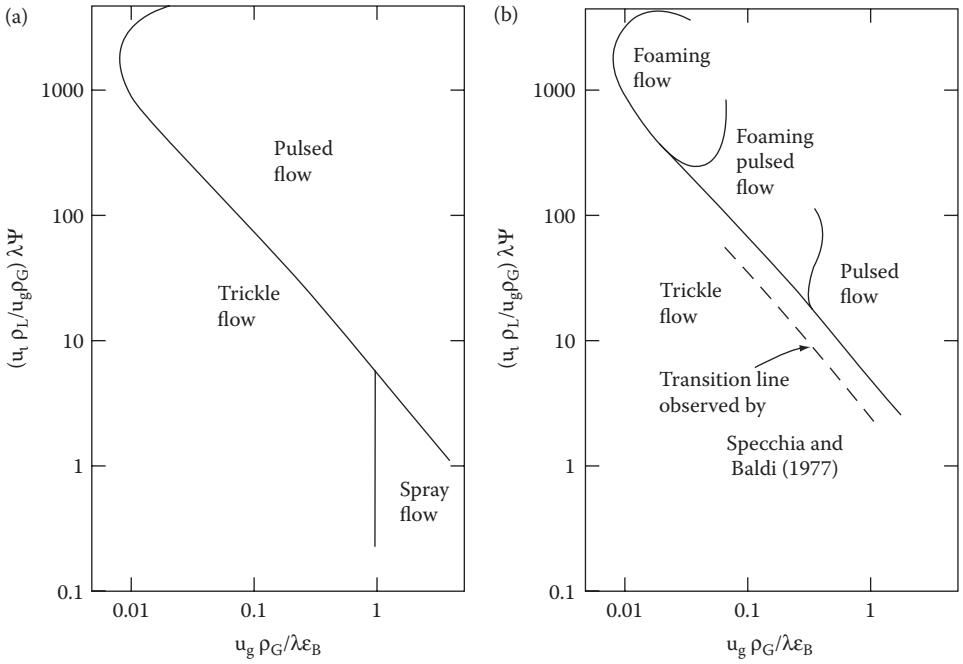

FIGURE 6.9 Flow maps for trickle bed reactors. (Data from Ramachandran, P.A. and Chaudhari, R.V., *Three-Phase Catalytic Reactors*, Gordon and Breach Science Publishers, New York, 1983.)

fluidized beds working in a countercurrent mode also exist. Because of gravity, the particles rise only to a certain level in the reactor (Figure 6.12). The liquid and gas phases are transported out of the reactor and can be separated by decanting.

Three different flow patterns can be observed in a fluidized bed reactor (Figure 6.13). For a *bubble flow*, the solid particles are evenly distributed in the reactor. This flow pattern resembles fluidized beds where only a liquid phase and a solid catalyst phase exist. At high gas velocities, a flow pattern called *aggregative fluidization* develops. In aggregative fluidization, the solid particles are unevenly distributed, and the conditions resemble those of a fluidized bed with a gas phase and a solid catalyst phase. Between these extreme flow areas, there exists a *slug flow* domain, which has the characteristics typical of both extreme cases. An uneven distribution of gas bubbles is characteristic for a *slug flow*.

The flow pattern in a three-phase fluidized bed is usually much closer to complete backmixing than to a plug flow. Because of the higher liquid flow velocities, larger particles can be used than in bubble columns.

Recently, a novel technology for three-phase processes has been developed: the monolith catalyst, sometimes also called the "frozen slurry reactor." Similar to catalytic gas-phase processes (Section 4.1), the active catalyst material and the catalyst carrier are fixed to the monolith structure. The gas and liquid flow through the monolith channels. The flow pattern in the vertical channels is illustrated in Figure 6.14. At low gas velocities, a *bubble flow* dominates, and the bubble size distribution is even. At higher gas flow rates, larger

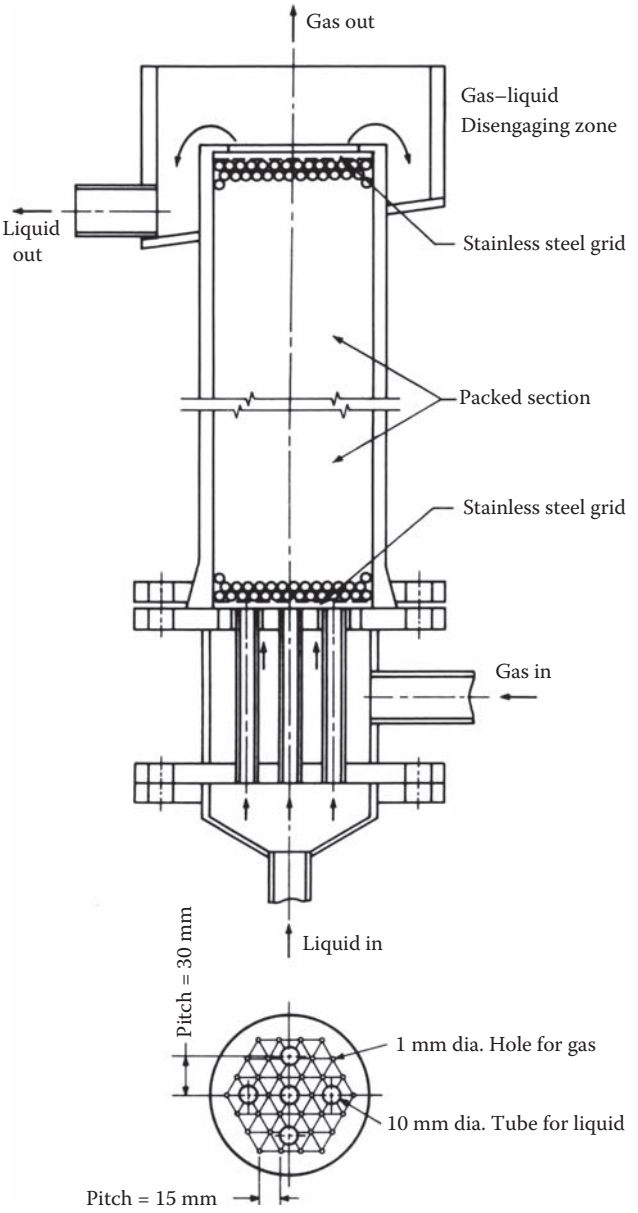

FIGURE 6.10 A packed bed with an upflowing liquid phase. (Data from Ramachandran, P.A. and Chaudhari, R.V., *Three-Phase Catalytic Reactors*, Gordon and Breach Science Publishers, New York, 1983.)

bubbles fill the cross-section of the channels. This flow type is called a *slug flow*. At higher gas flow rates, the smaller bubbles in a *slug flow* merge, and the resulting flow is called a *Taylor flow* or a *churn flow*. At even higher gas flow rates, the gas phase becomes continuous, and a gas–liquid dispersion develops. The flow is called an *annular flow*, and it is very inefficient and undesirable in three-phase systems. A monolith catalyst must always work

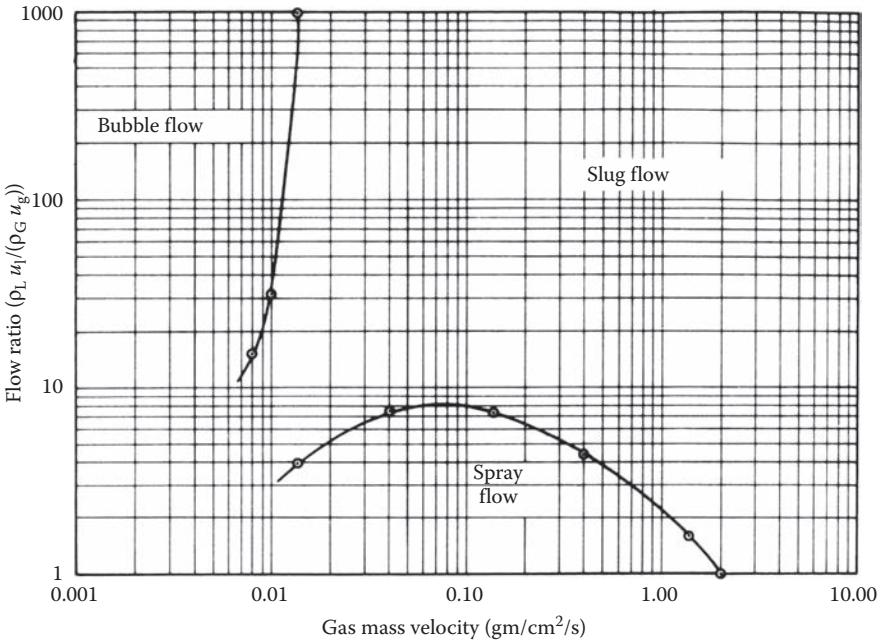

FIGURE 6.11 Flow map for a packed bed with a liquid upflow. (Data from Ramachandran, P.A. and Chaudhari, R.V., *Three-Phase Catalytic Reactors*, Gordon and Breach Science Publishers, New York, 1983.)

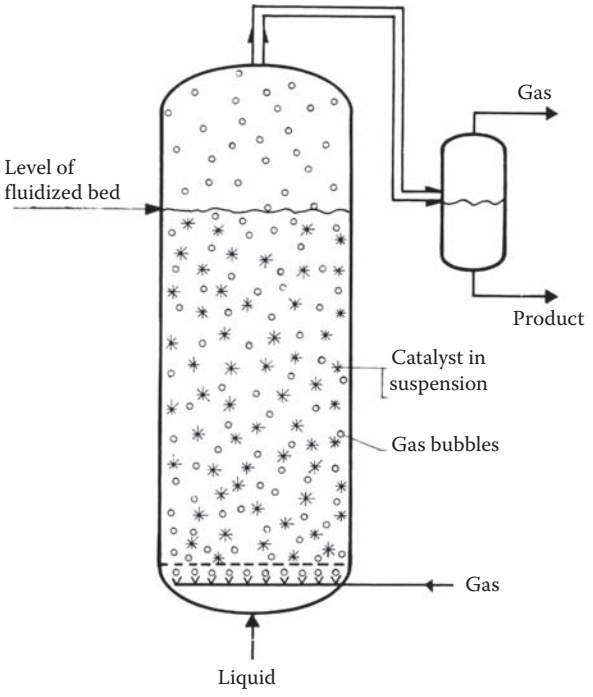

FIGURE 6.12 A three-phase fluidized bed reactor. (Data from Trambouze, P., van Landeghem, H., and Wauquier, J.-P., *Chemical Reactors—Design/Engineering/Operation*, Editions Technip, Paris, 1988.)

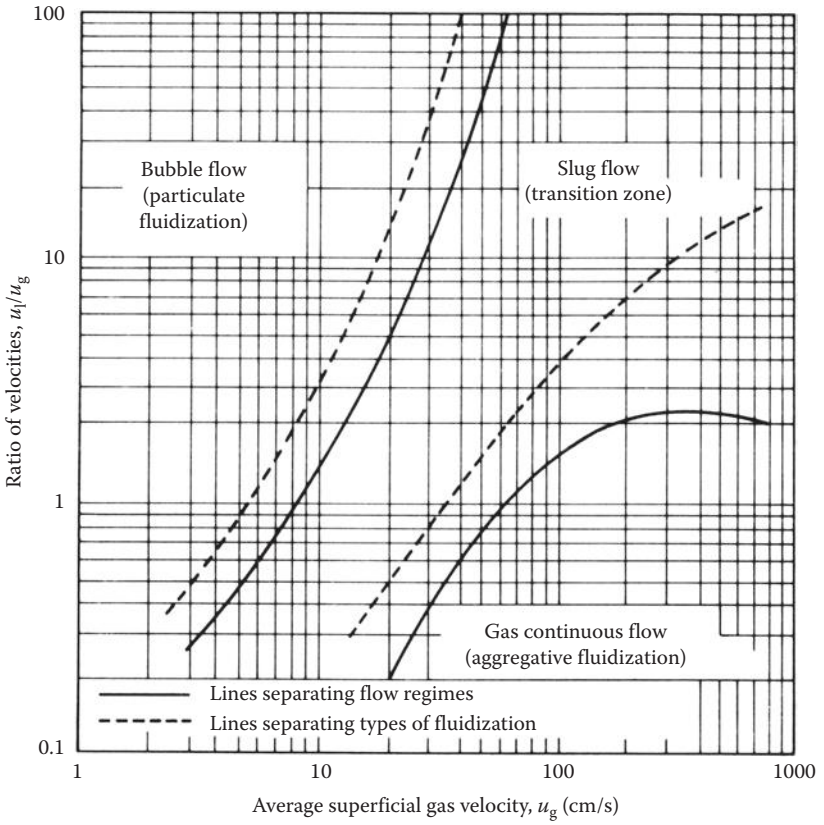

FIGURE 6.13 Flow map for a fluidized bed. (Data from Ramachandran, P.A. and Chaudhari, R.V., *Three-Phase Catalytic Reactors*, Gordon and Breach Science Publishers, New York, 1983.)

under *bubble flow* or *slug flow* conditions; a *slug flow* gives the best mass transfer rates. Monolith catalysts are used in, for example, hydrogenation and dehydrogenation reactions.

As discussed earlier, there are several options for the selection of heterogeneously catalyzed gas–liquid reactors. Trambouze et al. [2] compared various three-phase reactors

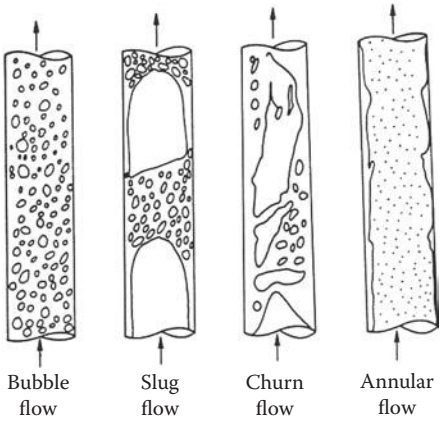

FIGURE 6.14 Flow patterns in a monolith catalyst.

TABLE 6.2 Comparison of Catalytic Three-Phase Reactors

Appreciation Criteria	Catalyst in Suspension	Three-Phase Fluidized Bed	Fixed Bed
		Characteristics with the Catalyst	
Activity	Highly variable, but possible in many cases to avoid the diffusion limitations found in a fixed bed	Highly variable: intra- and extragranular mass transfers may significantly reduce the activity, especially in a fixed bed Backmixing unfavorable	Plug flow favorable
Selectivity	Selectivity generally unaffected by transfers	As for activity, transfers may decrease selectivity Backmixing often unfavorable	Plug flow often favorable
Stability	Catalyst replacement between each batch operation helps to overcome problems of rapid poisoning in certain cases	Possibility of continuous catalyst renewal: the catalyst must nevertheless have good attrition resistance	This feature is essential for fixed bed operation: a plug flow may sometimes be favorable due to the establishment of a poison adsorption front
Cost	Consumption usually depends on the impurities contained in the feed and acting as poisons		Necessarily low catalyst consumption
		Technologies Characteristics	
Heat exchange	Fairly easy to achieve heat exchange	Possibility of heat exchange in the reactor itself	Generally adiabatic operation
Design difficulties	Catalyst separation sometimes difficult: possible problems in pumps and exchangers due to the risks of deposit or erosion		Very simple technology for a downward concurrent adiabatic bed
Scaling-up	No difficulty: generally limited to batch systems and relatively small sizes	System still poorly known, should be scaled up in steps	Large reactors can be built if liquid distribution is carefully arranged

Source: Data from Trambouze, P., van Landeghem, H., and Wauquier, J.-P., *Chemical Reactors—Design/Engineering/Operation*, Editions Technip, Paris, 1988.

(Table 6.2). The advantage of a slurry reactor with small and finely dispersed catalyst particles is that the diffusion resistance inside the catalyst particles seldom limits the reaction, whereas the diffusion resistance can be a limiting factor in packed bed reactors. The temperature in the slurry reactor is rather constant, and no hot spot phenomena occur. In slurry reactors, it is also possible to regenerate the catalyst (fluidized bed). However, the separation of small catalyst particles from the suspension may introduce problems. The high degree of backmixing is usually less efficient for the reaction kinetics, which results in a lower conversion of the reactants than under plug flow conditions. For autocatalytic reactions, we have the opposite effect, since some degree of backmixing can enhance the reaction rate.

The main advantage with packed beds is the flow pattern. Conditions approaching a plug flow are advantageous for most reaction kinetics. Diffusion resistance in catalyst particles may sometimes reduce the reaction rates, but for strongly exothermic reactions, effectiveness factors higher than unity (1) can be obtained. Hot spots appear in highly exothermic

reactions, and these can have negative effects on the chemical stability and physical sustainability of the catalyst. If the catalyst in a packed bed is poisoned, it must be replaced, which is a cumbersome procedure. A packed bed is sometimes favorable, because the catalyst poison is accumulated in the first part of the bed and deactivation can be predicted in advance. In the hydrogenation of sulfur-containing aromatic compounds over nickel catalysts in a packed bed, the sulfur is adsorbed as a multimolecular layer on the catalyst at the inlet of the reactor. However, this layer works as a catalyst poison trap.

6.2 MASS BALANCES FOR THREE-PHASE REACTORS

Let us consider the mass balance of two kinds of three-phase reactors: bubble columns and tube reactors with a plug flow for the gas and the liquid phases, and stirred tank reactors with complete backmixing. Modeling concepts can be implemented in most existing reactors: backmixing is typical for slurry reactors, bubble columns, and stirred tank reactors, whereas plug flow models describe the conditions in a trickle bed reactor. The interface between the gas and the liquid is supposed to be surrounded by gas and liquid films. Around the catalyst particles, there also exists a liquid film. In gas and liquid films, physical diffusion, but no chemical reactions, is assumed to take place. A volume element is illustrated in Figure 6.15.

6.2.1 MASS TRANSFER AND CHEMICAL REACTION

The mass transfer of component i from the gas bulk to the liquid bulk is described by the flux, N_{Li}^{b}, according to Equation 7.69 (Chapter 7):

$$N_{Li}^{b} = \frac{c_{Gi}^{b} - K_i c_{Li}^{b}}{(K_i/k_{Li}) + (1/k_{Gi})}. \tag{6.1}$$

In physical absorption, the fluxes through the gas and liquid films are equal:

$$N_{Li}^{b} = N_{Li}^{s} = N_{Gi}^{s} = N_{Gi}^{b}. \tag{6.2}$$

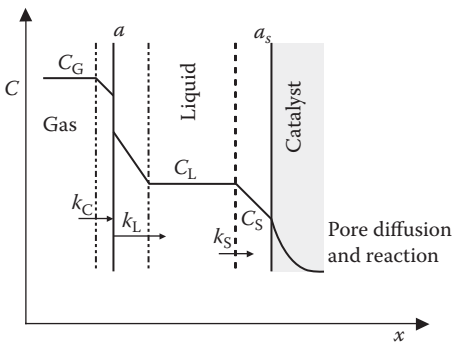

FIGURE 6.15 Schematic description of the concentration profiles in a three-phase reactor.

The flux from the liquid bulk to the liquid film around the catalyst particle at steady state is equal to the generation rate of the component on the catalyst surface. The steady-state mass balance for a catalyst particle thus becomes

$$N_{\mathrm{L}i}^{\mathrm{s}} A_{\mathrm{p}} + r_i m_{\mathrm{p}} = 0, \tag{6.3}$$

where A_{p} and m_{p} are the particle surface and mass, respectively. If the particle density (ρ_{p}) and volume (V_{p}) are introduced, we obtain

$$N_{\mathrm{LS}i} = -\rho_{\mathrm{p}} \frac{V_{\mathrm{p}}}{A_{\mathrm{p}}} r_i. \tag{6.4}$$

The flux, $N_{\mathrm{L}i}^{\mathrm{s}}$, through the liquid film surrounding the catalyst particle is described by the difference in the concentrations and the liquid-film coefficient $k_{\mathrm{L}i}^{\mathrm{s}}$

$$N_{\mathrm{LS}i} = k_{\mathrm{LS}i}(c_{\mathrm{L}i}^{\mathrm{b}} - c_{\mathrm{L}i}^{\mathrm{s}}), \tag{6.5}$$

where $c_{\mathrm{L}i}^{\mathrm{s}}$ is the concentration on the catalyst surface. The reaction rate r_i is a function of the concentration in the catalyst particle, $c_{\mathrm{L}}^{\mathrm{s}}$. After setting Equation 6.4 equal to Equation 6.5, we obtain

$$k_{\mathrm{LS}i}\left(c_{\mathrm{L}i}^{\mathrm{b}} - c_{\mathrm{L}i}^{\mathrm{s}}\right) = -\rho_{\mathrm{p}} \frac{V_{\mathrm{p}}}{A_{\mathrm{p}}} r_i\left(c_{\mathrm{L}}^{\mathrm{s}}\right). \tag{6.6}$$

For three-phase reactors, the catalyst bulk density (ρ_{B}) is usually based on the liquid volume in the reactor:

$$\rho_{\mathrm{B}} = \frac{m_{\mathrm{cat}}}{V_{\mathrm{L}}} = \frac{m_{\mathrm{cat}}}{\varepsilon_{\mathrm{L}} V_{\mathrm{R}}}. \tag{6.7}$$

The ratio, particle area-to-reactor volume, a_{p}, is defined as

$$a_{\mathrm{p}} = \frac{A_{\mathrm{liquid-solid}}}{V_{\mathrm{R}}} = \frac{A_{\mathrm{p}}'}{V_{\mathrm{R}}} \tag{6.8}$$

For n catalyst particles in the reactor volume element, Equation 6.3 becomes

$$k_{\mathrm{LS}i}\left(c_{\mathrm{L}i}^{\mathrm{b}} - c_{\mathrm{L}i}^{\mathrm{s}}\right) n A_{\mathrm{p}} = -\rho_{\mathrm{p}} V_{\mathrm{p}} n r_i\left(c_{\mathrm{L}i}\right), \tag{6.9}$$

where $nA_{\mathrm{p}} = A_{\mathrm{p}}'$ and $n\rho_{\mathrm{p}} V_{\mathrm{p}} = m_{\mathrm{cat}}$. By introducing these into Equation 6.9 and dividing by the reactor volume, we obtain

$$k_{\mathrm{L}i}^{\mathrm{s}}\left(c_{\mathrm{L}i}^{\mathrm{b}} - c_{\mathrm{L}i}^{\mathrm{s}}\right) \frac{A_{\mathrm{p}}'}{V_{\mathrm{R}}} = -\frac{m_{\mathrm{cat}}}{V_{\mathrm{R}}} r_i. \tag{6.10}$$

When Equations 6.7 and 6.8 are introduced into Equation 6.10, the result becomes

$$k_{\mathrm{LS}i}\left(c_{\mathrm{L}i}^{\mathrm{b}}-c_{\mathrm{L}i}^{\mathrm{s}}\right)a_{\mathrm{p}}=-\varepsilon_{\mathrm{L}}\rho_{\mathrm{B}}r_i. \tag{6.11}$$

This implies that the flux, $N_{\mathrm{L}i}^{\mathrm{s}}$, is related to the component generation rate accordingly:

$$N_{\mathrm{LS}i}=-\frac{\varepsilon_{\mathrm{L}}\rho_{\mathrm{B}}}{a_{\mathrm{p}}}r_i. \tag{6.12}$$

The generation rate, r_i, in Equation 6.12 is, of course, defined by Equation 2.4 or 2.6, depending on whether a single reaction or several simultaneous reactions proceed. The most common case is several reactions (Equation 2.6)

$$\mathbf{r}=\boldsymbol{\nu}\mathbf{R}. \tag{6.13}$$

If Equation 6.13 is inserted into Equation 6.12 and the equation is rewritten in the vector form, we obtain

$$\mathbf{N}_{\mathrm{LS}}=-\frac{\varepsilon_{\mathrm{L}}\rho_{\mathrm{B}}}{a_{\mathrm{p}}}\boldsymbol{\nu}\mathbf{R}=\mathbf{k}_{\mathrm{LS}}\left(\mathbf{c}_{\mathrm{L}}^{\mathrm{b}}-\mathbf{c}_{\mathrm{L}}^{\mathrm{s}}\right), \tag{6.14}$$

where the reaction rate is principally a function of all of the concentrations, $\mathbf{R}=\mathbf{f}(\mathbf{c}_{\mathrm{L}}^{\mathrm{s}})$. The concentrations at the catalyst surface, $\mathbf{c}_{\mathrm{L}}^{\mathrm{s}}$, are usually obtained iteratively from Equation 6.14. It is possible to express the reaction rates, $\mathbf{R}$, as a function of concentrations on the outer surface of the reactor. For first- and second-order kinetics, Equation 6.14 can be solved analytically (Table 6.4).

If internal diffusion resistance in the catalyst pores affects the reaction rates, the observed reaction rate, $\mathbf{R}$, is usually lower than the reaction rate obtained with the surface concentrations, $\mathbf{R}'$. The ratio between these rates is called the *effectiveness factor*:

$$\eta_{\mathrm{e}j}=\frac{R_j}{R_j'(c_{\mathrm{Ls}})}. \tag{6.15}$$

If pore diffusion affects the reaction rate and R_j in Equation 6.14 is replaced by $\eta_{ej}R_j'$, the effectiveness factor, η_{ej}, can be obtained the same way as in the case of catalytic two-phase reactions (Section 5.2.2). Equations developed for two-phase reactions in Section 5.2.2 are also valid for three-phase cases, provided that the catalyst particles are completely wetted by the liquid. In this case, we only have one phase: a liquid present inside the catalyst pores. Using the formulae introduced in Section 5.22, the diffusion and mass transfer coefficients of the gas phase are, of course, replaced by those of the liquid phase.

6.2.2 THREE-PHASE REACTORS WITH A PLUG FLOW

Here, we will discuss the mass balances for a PFR with three phases. A volume element in a gas–liquid column reactor is shown in Figure 6.16. The liquid flow direction is set in the

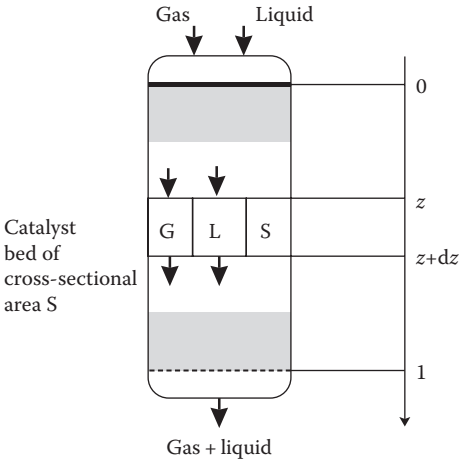

FIGURE 6.16 A volume element in a gas–liquid column reactor.

positive (+) direction. For the volume element, ΔV_L, in the liquid phase, the mass balance for component i can be written in the following form:

$$\dot{n}_{Li,in} + N_{Li}^{b}\Delta A = n_{Li,out} + N_{Lis}\Delta A_p. \tag{6.16}$$

After inserting $\Delta\dot{n}_{Li} = \dot{n}_{Li,out} - \dot{n}_{Li,in}$ and $\Delta A = a_v \Delta A V_R$ (a_v = gas–liquid surface area-to-reactor volume) and recalling the definition of a_p (particle area-to-reactor volume) as in Equation 6.8, Equation 6.16 is transformed to

$$\Delta\dot{n}_{Li} = N_{Li}^{b} a_v \Delta V_R - N_{LSi} a_p \Delta V_R. \tag{6.17}$$

Dividing Equation 6.17 by ΔV_R and allowing $\Delta V_R \to 0$, the mass balance attains the form

$$\frac{d\dot{n}_{Li}}{dV_R} = N_{Li}^{b} a_v - N_{LSi} a_p, \tag{6.18}$$

where N_{Li}^{b} and N_{LSi} are defined by Equations 6.1 and 6.12, respectively.

For a volume element ΔV_G in the gas phase, analogous to Equation 6.16, we obtain the mass balance

$$n_{Gi,in} = n_{Gi,out} + N_{Gi}^{b}\Delta A. \tag{6.19}$$

If the gas and the liquid have the same flow direction, $\Delta\dot{n}_{Gi} = \dot{n}_{Gi,out} - \dot{n}_{Gi,in}$ (concurrent flow), in the case of countercurrent flows, we can write $\Delta\dot{n}_{Gi} = \dot{n}_{Gi,in} - \dot{n}_{Gi,out}$. For the flux, N_{Gi}^{b}, Equation 6.2 is valid and, at the same time, for the area element A, we can write $\Delta A = a_v V_R$. Now the mass balance can be rewritten accordingly as

$$\Delta\dot{n}_{Gi} = \mp N_{Li}^{b} a_v \Delta V_R, \tag{6.20}$$

where the negative and positive signs, (−) and (+), denote the concurrent and the countercurrent cases, respectively. If $\Delta V_R \to 0$, the mass balance equation becomes

$$\frac{d\dot{n}_{Gi}}{dV_R} = \mp N_{Li}^b a_v. \tag{6.21}$$

The initial condition for the liquid phase is

$$\dot{n}_{Li} = \dot{n}_{0Li} \quad \text{at } V_R = 0. \tag{6.22}$$

Equations 6.18 and 6.21 have the initial conditions for both the concurrent and the countercurrent cases, but the initial condition for the gas phase is

$$\dot{n}_{Gi} = \dot{n}_{0Gi} \quad \text{at } V_R = 0 \tag{6.23}$$

in the concurrent case. The boundary condition for the countercurrent flow is

$$\dot{n}_{Gi} = \dot{n}_{0Gi} \quad \text{at } V_R = V_R. \tag{6.24}$$

Mass balance Equations 6.18 and 6.21 can be expressed with the arrays as

$$\frac{d\dot{\mathbf{n}}_L}{dV_R} = N_L^b a_v - N_{LS} a_p, \tag{6.25}$$

$$\frac{d\dot{\mathbf{n}}_G}{V_R} = \mp N_L^b a_v, \tag{6.26}$$

where − and + denotes the concurrent and the countercurrent flow, respectively.

If the space time

$$\tau_L = \frac{V_R}{\dot{V}_{0L}} \tag{6.27}$$

for the liquid phase is inserted into Equations 6.25 and 6.26, alternative forms of the mass balance equations are obtained:

$$\frac{d\dot{\mathbf{n}}_L}{d\tau_L} = \left(N_L^b a_v - N_{LS} a_v\right) \dot{\mathbf{V}}_{0L}, \tag{6.28}$$

$$\frac{d\dot{\mathbf{n}}_G}{d\tau_L} = \mp N_L^b a_v \dot{\mathbf{V}}_{0L}. \tag{6.29}$$

Equations 6.1 and 6.14 give the fluxes, N_L^b and N_{LS}, required in the differential equations, Equations 6.28 and 6.29.

The plug flow model described above works well in the case of a *trickle bed reactor*, where plug flow conditions often prevail. It is also quite good for packed beds, where concurrent

gas and liquid flows take place upward. For bubble columns, the plug flow model is well suited for the gas phase, while the degree of backmixing is quite high in the liquid phase. For the bubble column, a term describing the axial dispersion in the liquid phase has to be included in the mass balance Equation 6.28 [3]. A possible simplification of the bubble column is to consider the liquid phase as completely backmixed.

6.2.3 THREE-PHASE REACTOR WITH COMPLETE BACKMIXING

For a three-phase reactor with complete backmixing, balances for the entire liquid and gas volumes can be set up. For the liquid phase, the mass balance is written as

$$\dot{n}_{0\mathrm{L}i} + N_{\mathrm{L}i}^{\mathrm{b}} A = \dot{n}_{\mathrm{L}i} + N_{\mathrm{L}i}^{\mathrm{s}} A_{\mathrm{p}}. \tag{6.30}$$

After inserting the definitions for A (gas–liquid mass transfer area) and a_{p} (particle area-to-reactor volume), the mass balance is transformed to

$$\frac{\dot{n}_{\mathrm{L}i} - \dot{n}_{0\mathrm{L}i}}{V_{\mathrm{R}}} = N_{\mathrm{L}i}^{\mathrm{b}} a_{\mathrm{v}} - N_{\mathrm{LS}i} a_{\mathrm{p}}. \tag{6.31}$$

The mass balance for the gas phase is expressed similar to Equation 6.30:

$$\dot{n}_{0\mathrm{G}i} = \dot{n}_{\mathrm{G}i} + N_{\mathrm{G}i}^{\mathrm{b}} A. \tag{6.32}$$

After inserting Equation 6.2 and the definition of a_{v} (gas–liquid surface area-to-reactor volume), we obtain

$$\frac{\dot{n}_{\mathrm{G}i} - \dot{n}_{0\mathrm{G}i}}{V_{\mathrm{R}}} = -N_{\mathrm{L}i}^{\mathrm{b}} a_{\mathrm{v}}. \tag{6.33}$$

Equations 6.31 and 6.32 can be rewritten in the vector form as

$$\frac{\dot{\mathbf{n}}_{\mathrm{L}} - \dot{\mathbf{n}}_{0\mathrm{L}}}{V_{\mathrm{R}}} = \mathbf{N}_{\mathrm{L}}^{\mathrm{b}} a_{\mathrm{v}} - \mathbf{N}_{\mathrm{LS}} a_{\mathrm{p}}, \tag{6.34}$$

$$\frac{\dot{\mathbf{n}}_{\mathrm{G}} - \dot{\mathbf{n}}_{0\mathrm{G}}}{V_{\mathrm{R}}} = -\mathbf{N}_{\mathrm{L}}^{\mathrm{b}} a_{\mathrm{v}}. \tag{6.35}$$

If the liquid space time, τ_L, is inserted into Equations 6.34 and 6.35, we obtain

$$\frac{\dot{\mathbf{n}}_{\mathrm{L}} - \dot{\mathbf{n}}_{0\mathrm{L}}}{\tau_{\mathrm{L}}} = \left(\mathbf{N}_{\mathrm{L}}^{\mathrm{b}} a_{\mathrm{v}} - \mathbf{N}_{\mathrm{LS}} a_{\mathrm{p}}\right) V_{0\mathrm{L}}, \tag{6.36}$$

$$\frac{\dot{\mathbf{n}}_{\mathrm{G}} - \dot{\mathbf{n}}_{0\mathrm{G}}}{\tau_{\mathrm{L}}} = -\mathbf{N}_{\mathrm{L}}^{\mathrm{b}} a_{\mathrm{v}} V_{0\mathrm{L}}. \tag{6.37}$$

Equations 6.34 and 6.35 and Equations 6.36 and 6.37 form an algebraic equation system with respect to $\dot{\mathbf{n}}_{\mathrm{G}}$ and $\dot{\mathbf{n}}_{\mathrm{L}}$. The flux at the gas–liquid interface, $\mathbf{N}_{\mathrm{L}}^{\mathrm{b}}$, is defined by Equation 6.1, whereas the flux at the catalyst surface, $\mathbf{N}_{\mathrm{LS}}$, is defined by Equation 6.14.

6.2.4 SEMIBATCH AND BRs

Let us consider a semibatch reactor with a continuously flowing gas phase. The liquid phase is assumed to remain in batch. If the gas flow rate is zero, then the reactor is converted into a BR.

For semibatch and BRs, the mass balance for the liquid phase of the component is given by

$$N_{Li}^{b} A = N_{LSi} A_p + \frac{dn_{Li}}{dt}, \tag{6.38}$$

where the last term, dn_{Li}/dt, describes the accumulation of component i in the reactor. If the definitions of a_v and a_p are inserted, the mass balance becomes

$$\frac{dn_{Li}}{dt} = \left(N_{Li}^{b} a_v - N_{LSi} a_p\right) V_R \tag{6.39}$$

For the gas phase, the mass balance for component i is

$$\dot{n}_{0Gi} = \dot{n}_{Gi} + N_{Gis} A + \frac{dn_{Li}}{dt}. \tag{6.40}$$

Taking into account the definition of a_v as well as Equation 6.2, the differential equation is obtained:

$$\frac{dn_{Gi}}{dt} = -\dot{n}_{Gi} - N_{Li}^{b} a_v + \dot{n}_{0Gi}. \tag{6.41}$$

The balance equations, Equations 6.39 and 6.41, have the following initial conditions:

$$\dot{n}_{Li} = \dot{n}_{0Li} \quad \text{at } t = 0, \tag{6.42}$$

$$\dot{n}_{Gi} = \dot{n}_{0Gi} \quad \text{at } t = 0. \tag{6.43}$$

The mass balances can be rewritten in the vector form as

$$\frac{d\dot{\mathbf{n}}_L}{dt} = \left(\mathbf{N}_L^{b} a_v - \mathbf{N}_{LS} a_p\right) V_R, \tag{6.44}$$

$$\frac{d\dot{\mathbf{n}}_G}{dt} = -\mathbf{N}_L^{b} V_R + \dot{\mathbf{n}}_{0G} - \dot{\mathbf{n}}_G. \tag{6.45}$$

For a semibatch reactor, the gas feed rates are $\dot{\mathbf{n}}_{0G} > 0$ and $\dot{\mathbf{n}}_G > 0$. For a BR, they are both equal to zero ($\mathbf{n}_{0G} = 0$ and $\mathbf{n}_G = 0$). In the differential equations described above, the fluxes, $\mathbf{N}_L^{b}$ and $\mathbf{N}_{LS}$, are defined by Equations 6.1 and 6.14, respectively. The BR model is mathematically analogous to the concurrent plug flow model.

6.2.5 PARAMETERS IN MASS BALANCE EQUATIONS

The values for parameters in the mass balances have to be determined either theoretically or experimentally. These parameters are equilibrium ratio (K_i), mass transfer coefficients (k_{Li} and k_{Gi}), diffusion coefficients in the gas and liquid phases (D_{Li} and D_{Gi}), volume ratios (a_v and a_p), and liquid holdup (ε_L). The equilibrium ratio, K_i, can be estimated using thermodynamic theories [4]; for gases with a low solubility, the equilibrium ratio, K_i, can sometimes be replaced by Henry's constant [5]. In Refs. [6,7], some methods for estimating k_{Li} and k_{Gi} are discussed. The correlation equations for k_{Li} and k_{Gi} contain the diffusion coefficients, D_{Li} and D_{Gi}, in the gas and liquid phases, respectively. The mass transfer coefficients, k_{Li} and k_{Gi}, are formally related to the diffusion coefficients by the film theory:

$$k_{Li} = \frac{D_{Li}}{\delta_L}, \tag{6.46}$$

$$k_{Gi} = \frac{D_{Gi}}{\delta_G}, \tag{6.47}$$

where δ_L and δ_G are the liquid and gas film thicknesses.

In practice, the mass transfer coefficients are obtained from semiempirical correlations that predict a somewhat lower dependence of the mass transfer coefficient on the diffusion coefficient, for example, $k_{Li} \propto D_{Li}^{0.5\ldots0.6}$. The gas-phase diffusion coefficients can be estimated using the Fuller–Schettler-Giddings equation [4], and the liquid-phase diffusion coefficients can be obtained from, for example, the Wilke–Chang equation [4,5]. The estimation methods are discussed in detail in the book *The Properties of Gases and Liquids* [4] and in Appendices 4 and 6. Characteristic values for the volume and area fractions, a_v and a_p, are given in Table 6.3 [2].

TABLE 6.3 Parameters for Three-Phase Reactors

	Catalyst in Suspension		Fixed Bed			
Characteristics	Bubble Column	Mechanically Stirred Tank	Downward Concurrent	Upward Concurrent	Countercurrent	Three-Phase Fluidized Bed
ε_p^a	0.01	0.01	0.6–0.7	0.6–0.7	0.5[b]	0.1–0.5
ε_L^a	0.8–0.9	0.8–0.9	0.05–0.25	0.2–0.3	0.05–0.1	0.2–0.8
ε_G^a	0.1–0.2	0.1–0.2	0.2–0.35	0.05–0.1	0.2–0.4	0.05–0.02
d_p (mm)	$\leq$0.1	$\leq$0.1	1–5	1–5	>5	0.1–5
a_s (m^{-1})	500	500	1000–2000	1000–2000	500	500–1000
a_{GL} (m^{-1})	100–400	100–1500	100–1000	100–1000	100–500	100–1000
η (isothermal)	1	1	<1	<1	<1	$\leq$1

Source: Data from Trambouze, P., van Landeghem, H., and Wauquier, J.-P., *Chemical Reactors—Design/Engineering/Operation*, Editions Technip, Paris, 1988.

[a] The values given here only correspond to part of the reactor occupied by the catalyst and not the entire reactor.

[b] Value corresponding to special shapes of particles.

6.3 ENERGY BALANCES FOR THREE-PHASE REACTORS

6.3.1 THREE-PHASE PFR

Here, we will consider reactors operating in a concurrent mode. Provided that the gas, the liquid, and the solid catalysts have the same temperature, the energy balance for a volume element, ΔV_R, that includes the catalyst mass, Δm_{cat}, can be written as

$$R(-\Delta H_r)\Delta m_{cat} = c_{pL}\dot{m}_L\Delta T + c_{pG}\dot{m}_G\Delta T + \Delta\dot{Q}. \tag{6.48}$$

The term $R(-\Delta H_r)\Delta m_{cat}$ defines the amount of heat released or consumed in an exothermic or endothermic reaction, respectively. This energy effect induces changes in the temperatures of the gas and liquid flows. The change in temperature is described by the terms $c_{pL}\dot{m}_L\Delta T$ and $c_{pL}\dot{m}_G\Delta T$. The heat transfer from or to the surroundings is given by $\Delta\dot{Q}$.

Equation 6.48 is valid for a system with a *single* reaction. The definition for the catalyst bulk density ρ_B, Equation 6.7, implies that

$$\Delta m_{cat} = \rho_B\varepsilon_L\Delta V_R. \tag{6.49}$$

Heat transfer from or to the surroundings is typically described by

$$\Delta\dot{Q} = U\Delta S(T - T_C), \tag{6.50}$$

where U is the overall heat transfer coefficient and ΔS is the heat transfer area in the volume element. Inserting Equations 6.49 and 6.50 into Equation 6.48 yields

$$R(-\Delta H_r)\rho_B\varepsilon_L\Delta V_R = (c_{pL}\dot{m}_L + c_{pG}\dot{m}_G)\Delta T + U\Delta S(T - T_C). \tag{6.51}$$

If the ratio heat transfer area-to-volume of the reactor is constant ($\Delta S/\Delta V_R = S/V_R$) and $\Delta V_R \to 0$ in Equation 6.51, the energy balance is transformed to

$$\frac{dT}{dV_R} = \frac{R(-\Delta H_r)\rho_B\varepsilon_L - U(S/V_R)(T - T_C)}{c_{pL}\dot{m}_L + c_{pG}\dot{m}_G}. \tag{6.52}$$

After inserting the liquid space time τ_L, Equation 6.27, into Equation 6.52, the energy balance becomes

$$\frac{dT}{d\tau_L} = \frac{R(-\Delta H_r)\rho_B\varepsilon_L - U(S/V_R)(T - T_C)}{c_{pL}\rho_L + c_{pG}\rho_{0G}(\dot{V}_{0G}/\dot{V}_{0L})}. \tag{6.53}$$

For systems with several *chemical reactions proceeding simultaneously*, the energy balance can be written in a general form, where the heat effects from all reactions are included:

$$\frac{dT}{dV_R} = \frac{\sum_{j=1}^{s} R_j(-\Delta H_{rj})\rho_B\varepsilon_L - U(S/V_R)(T - T_C)}{c_{pL}\dot{m}_L + c_{pG}\dot{m}_G}. \tag{6.54}$$

If the liquid space time is used, Equation 6.54 is transformed to

$$\frac{\mathrm{d}T}{\mathrm{d}\tau_\mathrm{L}} = \frac{\sum_{j=1}^{s} R_j(-\Delta H_{\mathrm{r}j})\rho_\mathrm{B}\varepsilon_\mathrm{L} - U(S/V_\mathrm{R})(T - T_\mathrm{C})}{c_{\mathrm{pL}}\rho_\mathrm{L} + c_{\mathrm{pG}}\rho_{0\mathrm{G}}(V_{0\mathrm{G}}/\dot{V}_{0\mathrm{L}})}. \tag{6.55}$$

The initial conditions for the energy balances, Equations 6.52 and 6.53 and Equations 6.54 and 6.55, are

$$T = T_0 \quad \text{at } V_\mathrm{R} = 0 \text{ and } \tau_\mathrm{L} = 0. \tag{6.56}$$

The energy balance equations, that is, Equations 6.52, 6.54 through 6.56, are coupled to the mass balance equations through the reaction rates.

6.3.2 TANK REACTOR WITH COMPLETE BACKMIXING

In the modeling of a tank reactor, it is assumed that the gas, liquid, and solid phases exist at the same temperature. The energy balance can then be set up for the entire reactor volume, because the temperature and concentration gradients are absent. For a system with *one* reaction, the balance becomes

$$R(-\Delta H_\mathrm{r})m_\mathrm{out} = \dot{m}_\mathrm{L}\int_{T_0}^{T} c_{\mathrm{pL}}\,\mathrm{d}T + \dot{m}_\mathrm{G}\int_{T_0}^{T} c_{\mathrm{pG}}\,\mathrm{d}T + \dot{Q}. \tag{6.57}$$

The physical interpretation of Equation 6.57 is the same as for the energy balance of a PFR (Equation 6.48).

Equation 6.7 gives an expression for the catalyst mass, and the heat transfer to/from the surroundings is expressed by

$$\dot{Q} = US(T - T_\mathrm{C}). \tag{6.58}$$

Inserting Equations 6.7 and 6.58 into the energy balance, Equation 6.57, yields

$$R(-\Delta H_\mathrm{r})\rho_\mathrm{B}\varepsilon_\mathrm{L}V_\mathrm{R} = \dot{m}_L\int_{T_0}^{T} c_{\mathrm{pL}}\,\mathrm{d}T + \dot{m}_\mathrm{G}\int_{T_0}^{T} c_{\mathrm{pG}}\,\mathrm{d}T + US(T - T_\mathrm{C}). \tag{6.59}$$

If the heat capacities, c_{pL} and c_{pG}, are approximated as temperature-independent, Equation 6.59 can be simplified to

$$R(-\Delta H_\mathrm{r})\rho_\mathrm{B}\varepsilon_\mathrm{L}V_\mathrm{R} = (\dot{m}_\mathrm{L}c_{\mathrm{pL}} + \dot{m}_\mathrm{G}c_{\mathrm{pG}})(T - T_0) + US(T - T_\mathrm{C}). \tag{6.60}$$

Now, Equation 6.60 can be rewritten in a form analogous to the PFR model as

$$\frac{T - T_0}{V_\mathrm{R}} = \frac{R(-\Delta H_\mathrm{r})\rho_\mathrm{B}\varepsilon_\mathrm{L} - U(S/V_\mathrm{R})(T - T_\mathrm{C})}{\dot{m}_\mathrm{L}c_{\mathrm{pL}} + \dot{m}_\mathrm{G}c_{\mathrm{pG}}}. \tag{6.61}$$

If the liquid-phase space time, τ_L, is inserted, the balance becomes

$$\frac{T - T_0}{\tau_L} = \frac{R(-\Delta H_r)\rho_B\varepsilon_L - U(S/V_R)(T - T_C)}{\dot{m}_L c_{pL}\rho_{0L} + \dot{m}_G c_{pG}\rho_{0G}(\dot{V}_{0G}/\dot{V}_{0L})}. \tag{6.62}$$

The energy balances can be generalized to a form that is valid for cases with several chemical reactions:

$$\frac{T - T_0}{V_R} = \frac{\sum R_j(-\Delta H_{rj})\rho_B\varepsilon_L - U(S/V_R)(T - T_C)}{\dot{m}_L c_{pL} + \dot{m}_G c_{pG}} \tag{6.63}$$

and

$$\frac{T - T_0}{\tau_L} = \frac{\sum R_j(-\Delta H_{rj})\rho_B\varepsilon_L - U(S/V_R)(T - T_C)}{\dot{m}_L c_{pL}\rho_{0L} + \dot{m}_G c_{pG}\rho_{0G}(\dot{V}_{0G}/\dot{V}_{0L})}. \tag{6.64}$$

6.3.3 BATCH REACTOR

For a BR where just one reaction takes place, an approximate transient energy balance can be written in the form as

$$R(-\Delta H_r)m_{out} = m_L c_{pL}\frac{dT}{dt} + m_G c_{pG}\frac{dT}{dt} + \dot{Q}. \tag{6.65}$$

In Equation 6.65, it is assumed that the molar heat capacities at constant pressure and temperature have approximately the same values ($c_{pL} \approx c_{vL}$, $c_{pG} \approx c_{vG}$). The catalyst mass m_{cat} and the energy flux can be expressed by Equations 6.7 and 6.58, respectively. By inserting these definitions, the energy balance for a BR becomes

$$\frac{dT}{dt} = \frac{R(-\Delta H_r)\rho_B\varepsilon_L V_R - US(T - T_C)}{m_L c_{pL} + m_G c_{pG}}. \tag{6.66}$$

Division by the reactor volume (V_R) yields

$$\frac{dT}{dt} = \frac{R(-\Delta H_r)\rho_B\varepsilon_L - U(S/V_R)(T - T_C)}{(m_L/V_R)c_{pL} + (m_G/V_R)c_{pG}}. \tag{6.67}$$

The ratios, m_L/V_R and m_G/V_R, can be written as

$$\frac{m_L}{V_R} = \frac{\rho_{0L}V_{0L}}{V_R} = \rho_{0L}\varepsilon_{0L} \tag{6.68}$$

and

$$\frac{m_G}{V_R} = \frac{\rho_{0L}V_{0G}}{V_R} = \rho_{0G}\varepsilon_{0G}, \tag{6.69}$$

where ε_{0L} and ε_{0G} denote the gas and the liquid holdups in the reactor at $t = 0$. The relations, Equations 6.68 and 6.69, are inserted and the energy balance is transformed to

$$\frac{dT}{dt} = \frac{R(-\Delta H_r)\rho_B\varepsilon_L - U(S/V_R)(T - T_C)}{c_{pL}\rho_{0L}\varepsilon_{0L} + c_{pG}\rho_{0G}\varepsilon_{0G}}. \tag{6.70}$$

For several simultaneous chemical reactions, the energy balance is generalized to

$$\frac{dT}{dt} = \frac{\sum R_j(-\Delta H_{rj})\rho_B\varepsilon_L - U(S/V_R)(T - T_C)}{c_{pL}\rho_{0L}\varepsilon_{0L} + c_{pG}\rho_{0G}\varepsilon_{0G}}. \tag{6.71}$$

The initial conditions for the energy balance equations, Equations 6.70 and 6.71, are

$$T = T_0 \quad \text{at } t = 0. \tag{6.72}$$

The energy balance, Equation 6.70 or 6.71, is coupled to the mass balance of the BR, for example, Equations 6.39 and 6.41 or Equations 6.44 and 6.45, via the reaction rates. The mathematical similarity of the batch and plug flow models is apparent. The same numerical methods that are used to solve the plug flow model can thus be used to solve the BR model.

6.3.4 ANALYTICAL AND NUMERICAL SOLUTIONS OF BALANCE EQUATIONS FOR THREE-PHASE REACTORS

An analytical solution of the mass balance equations for three-phase reactors is possible in the case of isothermal reactors and reactions of first-order only. Analytical solutions [1,8] are rather cumbersome even in these cases. Some analytical solutions for effectiveness factors are listed in Table 6.4. This is why a numerical solution is preferred. Case studies will briefly be described below.

The balance equations for column reactors that operate in a concurrent mode as well as for semibatch reactors are mathematically described by ordinary differential equations. Basically, it is an initial value problem, which can be solved by, for example, Runge–Kutta, Adams–Moulton, or BD methods (Appendix 2). Countercurrent column reactor models result in boundary value problems, and they can be solved, for example, by orthogonal collocation [3]. The backmixed model consists of an algebraic equation system that is solved by the Newton–Raphson method (Appendix 1).

6.3.4.1 Sulfur Dioxide Oxidation

Sulfur dioxide can be oxidized catalytically in an aqueous environment. The sample case introduces a catalytic oxidation process of SO_2 in the liquid phase over an active carbon

TABLE 6.4 Calculation of Surface Concentrations

$N_{\mathrm{L}i}^{\mathrm{s}} = -\dfrac{\varepsilon_{\mathrm{L}}\rho_{\mathrm{B}}}{a_{\mathrm{p}}} r_i = k_{\mathrm{L}i}^{\mathrm{s}}\left(c_{\mathrm{L}i}^{\mathrm{b}} - c_{\mathrm{L}i}^{\mathrm{s}}\right)$ [A]

where $r_i = v_i R$

First-order reaction: $R = kc_{\mathrm{L}i}^{\mathrm{s}}$, which is inserted in [A]

$\dfrac{\varepsilon_{\mathrm{L}}\rho_{\mathrm{B}}}{a_{\mathrm{p}}}(-v_i)\,kc_{\mathrm{L}i}^{\mathrm{s}} = k_{\mathrm{L}i}^{\mathrm{s}}\left(c_{\mathrm{L}i}^{b} - c_{\mathrm{L}i}^{\mathrm{s}}\right)$

$c_{\mathrm{L}i}^{\mathrm{s}}$ becomes $c_{\mathrm{L}i}^{\mathrm{s}} = \dfrac{c_{\mathrm{L}i}^{\mathrm{b}}}{1 + \left(\varepsilon_{\mathrm{L}}\rho_{\mathrm{B}}(-v_i)\,k/k_{\mathrm{L}i}^{\mathrm{s}}a_{\mathrm{p}}\right)} = \dfrac{c_{\mathrm{L}i}^{\mathrm{b}}}{\alpha + 1}$

Effectiveness factor for outer mass transfer resistance, $\eta_{ei} = \dfrac{v_i kc_{\mathrm{L}i}^{\mathrm{s}}}{v_i kc_{\mathrm{L}i}^{\mathrm{b}}}$, $\quad \eta_{ei} = \dfrac{1}{1+\alpha}$

Second-order reaction: $R = kc_{\mathrm{L}i}^{\mathrm{s}^2}$

Similarly, we obtain

$\dfrac{\varepsilon_{\mathrm{L}}\rho_{\mathrm{B}}(-v_i)\,kc_{\mathrm{L}i}^{\mathrm{s}^2}}{a_{\mathrm{p}}} = k_{\mathrm{L}i}^{\mathrm{s}}\left(c_{\mathrm{L}i}^{\mathrm{b}} - c_{\mathrm{L}i}^{\mathrm{s}}\right)$ from which $c_{\mathrm{L}i}^{\mathrm{s}}$ is solved:

$c_{\mathrm{L}i}^{\mathrm{s}} = \left(\dfrac{\sqrt{1+4\alpha}-1}{2\alpha}\right)c_{\mathrm{L}i}^{\mathrm{b}}, \quad \alpha = \dfrac{\varepsilon_{\mathrm{L}}\rho_{\mathrm{B}}(-v_i)\,kc_{\mathrm{L}i}^{\mathrm{b}}}{a_{\mathrm{p}}k_{\mathrm{L}i}^{\mathrm{s}}}$,

which can be transformed to $c_{\mathrm{L}i}^{\mathrm{s}} = \dfrac{2}{\sqrt{1+4\alpha}+1}\cdot c_{\mathrm{L}i}^{\mathrm{b}}$

For rapid mass transfer $k_{\mathrm{L}i}^{\mathrm{s}} \to \infty, \alpha \to 0, \sqrt{1+4\alpha} \to 1$, and $c_{\mathrm{L}i}^{\mathrm{s}} \to c_{\mathrm{L}i}^{\mathrm{b}}$

Effectiveness factor is $\eta_{ei} = \left(\dfrac{c_{\mathrm{L}i}^{\mathrm{s}}}{c_{\mathrm{L}i}^{\mathrm{b}}}\right)^2$, $\eta_{ei} = \dfrac{4}{\left(1+\sqrt{1+4\alpha}\right)^2}$

Higher-order reactions: iterative solution of [A] is recommended.

catalyst in a packed bed (*trickle bed*). The reaction consists of the following steps [3]:

$$\mathrm{SO_2(g)} \rightarrow \mathrm{SO_2(l)},$$

$$\mathrm{O_2(g)} \rightarrow \mathrm{O_2(l)},$$

$$\mathrm{SO_2(g)} + \tfrac{1}{2}\mathrm{O_2(l)} + \mathrm{H_2O} \rightarrow \mathrm{H_2SO_4(l)}.$$

The concentration profiles (Figure 6.17) demonstrate the consumption of SO_2 and O_2 in the liquid phase, followed by the production of H_2SO_4. The calculations were performed using orthogonal collocation.

6.3.4.2 Hydrogenation of Aromatics

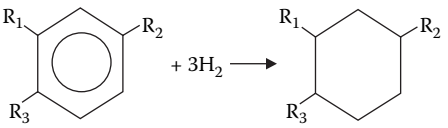

The second example concerns catalytic hydrogenation of aromatic compounds such as benzene, toluene, xylenes, isopropyl benzene, and mesitylene, over a supported nickel catalyst [9,10]. The process is relevant for the production of aromatic-free fuels and solvents. The aromatic ring is hydrogenated in an exothermal reaction in which $R1$, $R2$, and $R3$

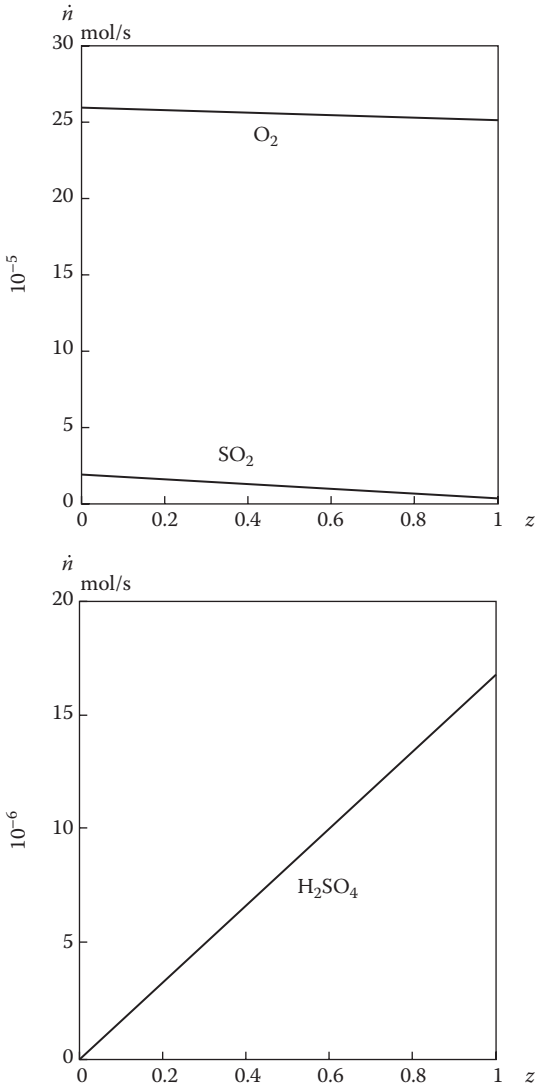

FIGURE 6.17 Concentration profiles in a trickle bed reactor.

denote hydrogen atoms or alkyl chains. The reactions are industrially carried out in fixed beds, but the kinetics can be conveniently measured in laboratory-scale autoclaves. Typical results from the kinetic experiments are displayed in Figure 6.18 and the rate follows the expression

$$R_{\text{tot}} = R + R' = \frac{k_1 K_{\text{A}} K_{\text{H}} c_{\text{A}} c_{\text{H}}}{\left(3K_{\text{A}} c_{\text{A}} + \sqrt{K_{\text{H}} c_{\text{H}} + 1}\right)^3},$$

where k and K denote the rate and the adsorption parameters and R and R' denote the formation rates of *cis*- and *trans*-isomers, respectively [10]. The rate model was coupled to the models of catalyst particles (Chapter 5) and the BR. The textural and transport

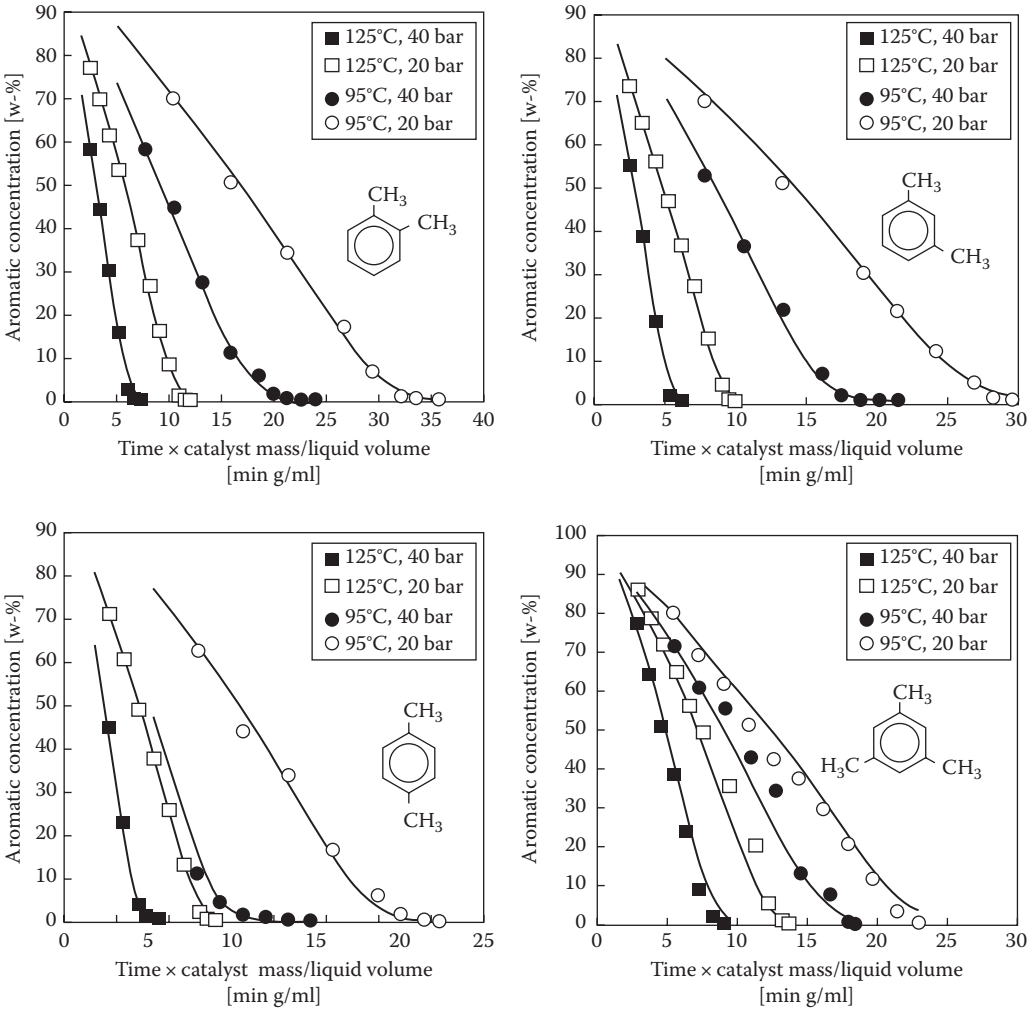

FIGURE 6.18 Kinetic results from the hydrogenation of aromatics.

parameters were calculated *a priori*, and the complete reaction–diffusion model was used in the estimation of kinetic parameters by nonlinear regression. For the results of parameter fitting, see Figure 6.18, in which the continuous curves represent the model predictions.

The dynamic reaction–diffusion model provides valuable information about the diffusional resistance inside the particles as well as the dynamics of the particle and bulk phases. Figure 6.19 shows that the process is heavily influenced by the diffusional limitation of hydrogen at the beginning, whereas the diffusional limitation of the aromatic compound is negligible. The situation, however, changes during the course of the reaction: some diffusional limitation of hydrogen always remains, but the diffusional limitation of the aromatic compound also increases its importance, since the concentration is low at the end of the reaction (Figure 6.19).

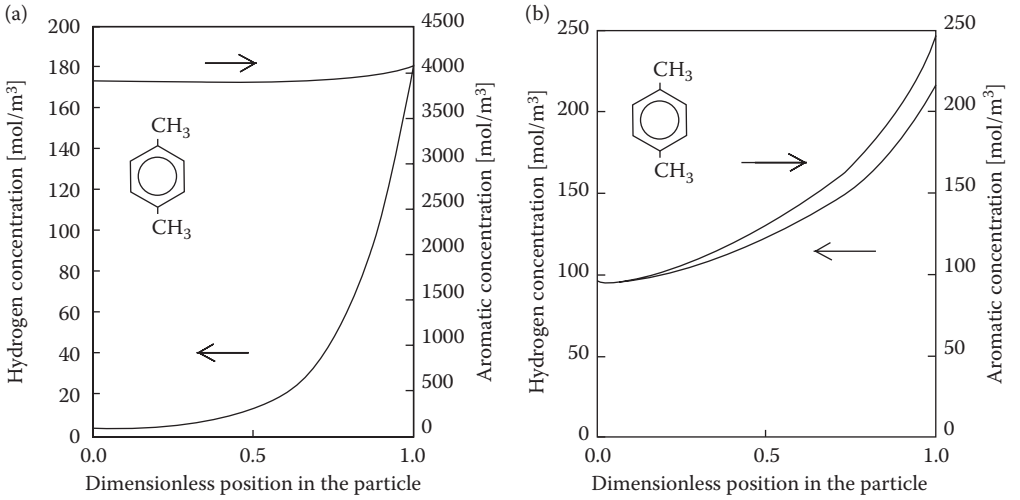

FIGURE 6.19 Diffusional resistances inside the catalyst particle in the hydrogenation of aromatics: (a) at the beginning and (b) at the end of the reaction.

The concentration profiles inside the pellet were simulated for different reaction times. The results are shown in Figure 6.20. The figure shows that the dynamics of catalyst particles is very rapid compared with that of bulk phases: a pseudo-steady-state is established inside the particle within about 10 A, which implies that it is justified to approximate the catalyst particle with a pseudo-steady-state model.

6.3.4.3 Carbonyl Group Hydrogenation

A typical example of the carbonyl group hydrogenation in three-phase systems is the catalytic hydrogenation of sugars to corresponding sugar alcohols. Let us consider, for example, the hydrogenation of D-xylose to xylitol over Raney nickel [11]. Xylitol is an alternative

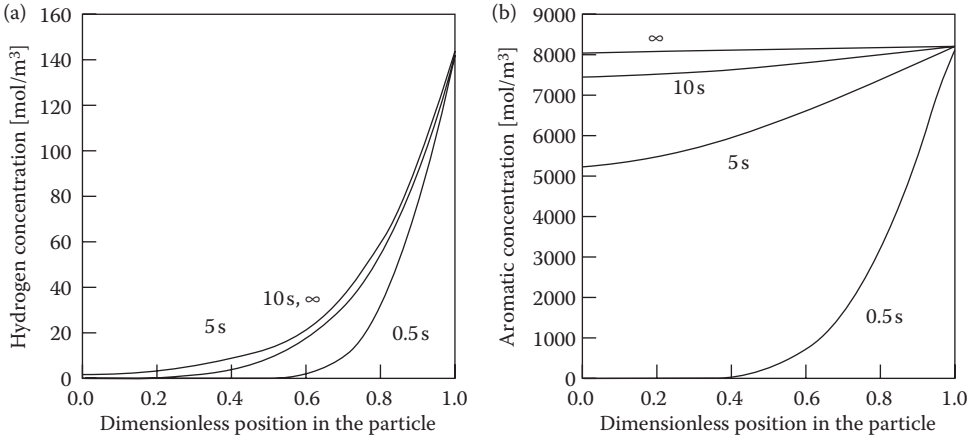

FIGURE 6.20 Dynamics of reaction and diffusion in the hydrogenation of aromatics.

sweetening agent in alimentary products such as chewing gum and chocolate. Its health-promoting properties (such as anticaries, anti-osteoporosis effects) have also started to attract more attention, justifying the use of the term functional food. Besides the main reaction, side reactions proceed in the system, producing D-xylulose, D-arabinitol, D-xylonic acid, and even furfural as undesired byproducts. The reaction scheme is displayed below.

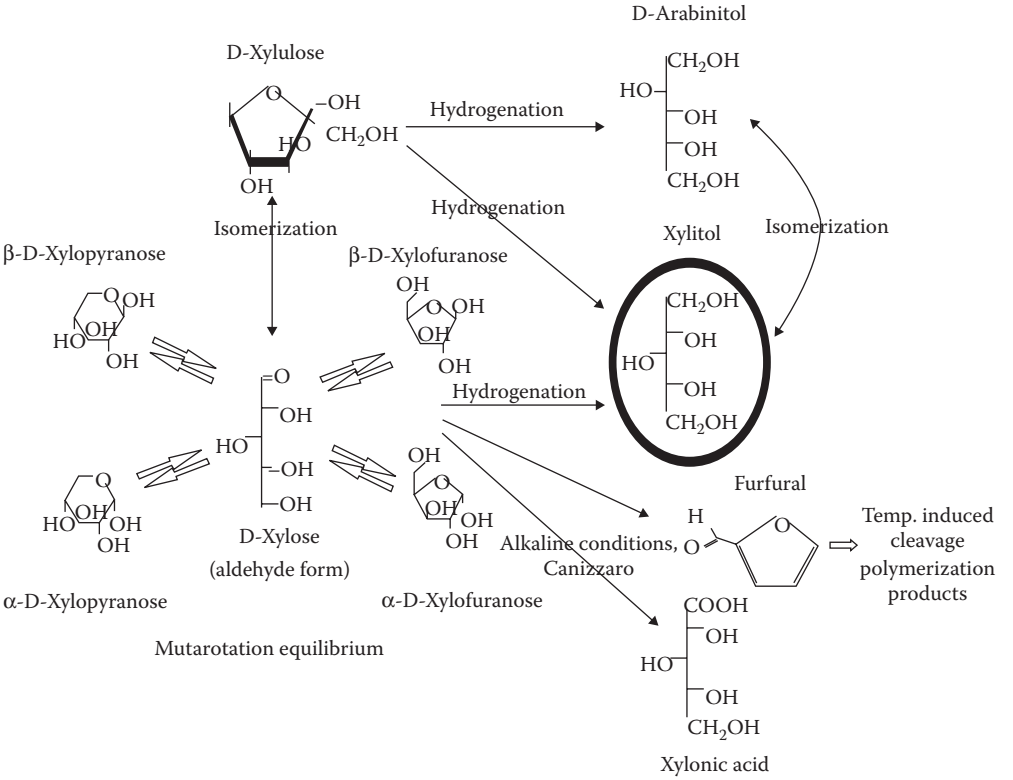

In a simplified form, the reaction scheme can be displayed as follows (xylonic acid and furfural are not formed under standard production conditions, and mutarotation equilibria are rapid).

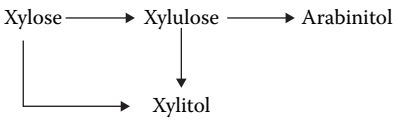

The reaction is carried out in batchwise operating autoclaves on an industrial scale. Typical kinetic results are shown in Figure 6.21. The experiments were carried out with finely dispersed Raney Ni catalyst particles, and a numerical simulation of the concentration profiles inside the particles revealed that the diffusional resistance in the particle was negligible, since the effectiveness factor always exceeded 0.9 [11]. On the other hand, the external mass transfer resistance on the liquid side of the gas–liquid interface can become

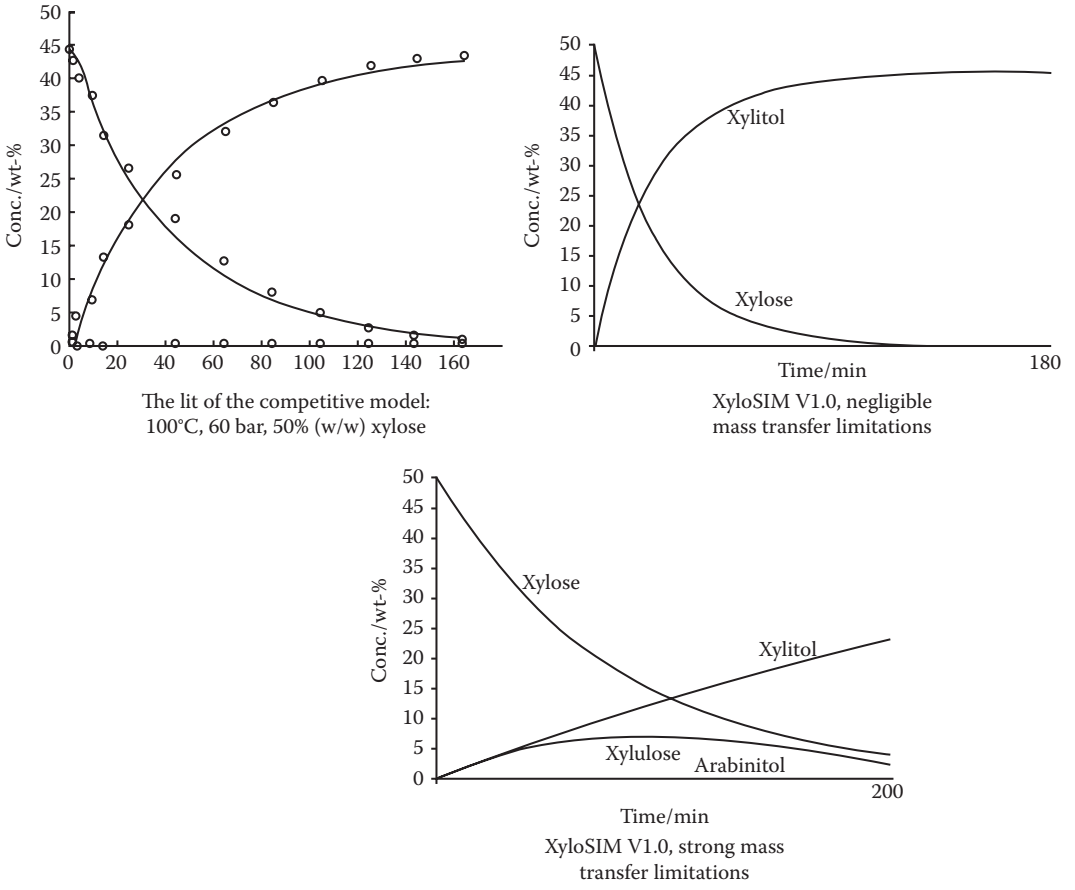

FIGURE 6.21 Xylose hydrogenation to xylitol and by-products. Kinetic data and kinetic modeling (left), simulations in the kinetic regime (center), and in the presence of external mass transfer limitations (right).

important on an industrial scale, if the agitation of the reactor is not efficient enough. The formation of D-xylulose is an isomerization reaction, which is favored if the access of hydrogen is limited. Figure 6.21 illustrates the effect of an external mass transfer limitation on the product distribution: the value of the external mass transfer coefficient of hydrogen (k_{LH}) has to be high in order to suppress the formation of D-xylulose. Under ideal mixing conditions (Figure 6.21), the formation of D-xylulose is minimized and the production of xylitol is maximized.

REFERENCES

1. Ramachandran, P.A. and Chaudhari, R.V., *Three-Phase Catalytic Reactors*, Gordon and Breach Science Publishers, New York, 1983.
2. Trambouze, P., van Landeghem, H., and Wauquier, J.-P., *Chemical Reactors—Design/Engineering/Operation*, Editions Technip, Paris, 1988.

3. Salmi, T., Wärnå, J., Lundén, P., and Romanainen, J., Development of generalized models for heterogeneous chemical reactors, *Comp. Chem. Eng*., 16, 421–430, 1992.
4. Reid, R.C., Prausnitz, J.M., and Poling, B.E., *The Properties of Gases and Liquids*, 4th Edition, McGraw-Hill, New York, 1988.
5. Deckwer, W.-D., *Reaktionstechnik in Blasensäulen*, Otto Salle Verlag, Frankfurt a.M. und Verlag Sauerlander, Aarau, 1985.
6. Myllykangas, J., *Aineensiirtokertoimen, neste—ja kaasuosuuden sekä aineensiirtopintaalan korrelaatiot eräissä heterogeenisissä reaktoreissa*, Åbo Akademi, Turku/Åbo, Finland, 1989.
7. Lee, J.H. and Foster, N.R., Measurement of gas–liquid mass transfer in multiphase reactors, *Appl. Catal*., 63, 1–36, 1990.
8. Goto, S. and Smith, J.M., Performance of slurry and trickle bed reactors: Application to sulphur dioxide removal, *AIChE J*., 24, 286, 294, 1978.
9. Toppinen, S., Rantakylä, T.-K., Salmi, T., and Aittamaa, J., Kinetics of the liquid-phase hydrogenation of benzene and some monosubstituted alkylbenzenes over a nickel catalyst, *Ind. Eng. Chem. Res*., 35, 1824–1833, 1996.
10. Toppinen, S., Rantakylä, T.-K., Salmi, T., and Aittamaa, J., Kinetics of the liquid-phase hydrogenation of di- and trisubstituted alkylbenzenes over a nickel catalyst, *Ind. Eng. Chem. Res.*, 35, 4424–4433, 1996.
11. Mikkola, J.-P, Salmi, T., and Sjöholm, R., Modelling of kinetics and mass transfer in the hydrogenation of xylose over Raney nickel catalyst, *J. Chem. Technol. Biotechnol*., 74, 655–662, 1999.

CHAPTER 7

Gas–Liquid Reactors

7.1 REACTORS FOR NONCATALYTIC AND HOMOGENEOUSLY CATALYZED REACTIONS

The presence of two phases, namely gas and liquid, is characteristic to noncatalytic or homogeneously catalyzed reaction systems. Components in the gas phase diffuse to the gas–liquid interface, dissolve in the liquid phase, and react with components in the bulk liquid phase. The liquid phase may also contain a homogeneous catalyst. Some of the product molecules desorb from the liquid phase to the gas phase, and some product molecules remain in the liquid. The processes taking place in a gas–liquid reactor are displayed in Figure 7.1 [1]. The figure is based on the simplest way of describing the gas–liquid contact, namely the film model. If the catalyst is heterogeneous, the process is dramatically altered, as the reactions take place on the surface of the heterogeneous catalyst and the reactor is obviously a three-phase one (Chapter 6).

Gas–liquid reactions are used in several industrial processes. In the synthesis of chemical compounds, gas–liquid reactions are used in, for example, the oxidation of hydrocarbons. For a synthesis reaction, it is typical that one organic compound is transformed into another organic compound in the presence of a homogeneous catalyst. Typical reactions are, for example, chlorination of aromatic compounds in the production of chlorinated hydrocarbons, chlorination of carboxylic acids (mainly acetic acid), and oxidation of toluene and xylene in the production of benzoic acid and phthalic acid. In the production of hydrogen peroxide (H_2O_2), an oxidation process can also be used, namely oxidation of anthraquinole to anthraquinone.

An important area where gas–liquid reactors are used is the cleaning of industrial gases. A low-concentration gas component is absorbed with the aid of a chemical reaction in the liquid phase. Such an absorption can be purely physical in nature, but when aided by a

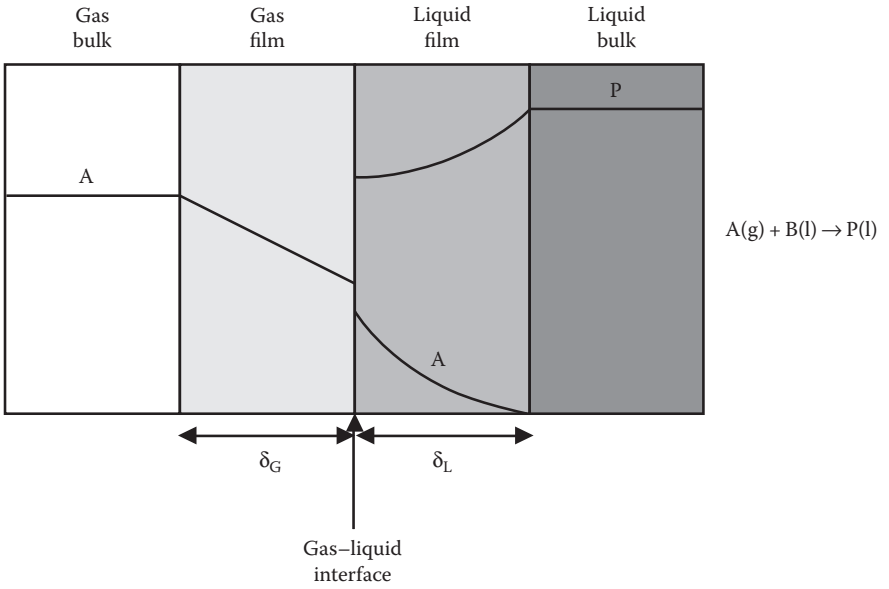

FIGURE 7.1 Phases in a gas–liquid reactor according to the film model.

chemical reaction, the absorption rate may be enhanced. In this case, the absorption unit can be much smaller than in the case of a purely physical absorption. Industrial absorption processes include, for example, the absorption of carbon dioxide (CO_2) in carbonate and hydroxide solutions. Absorption of carbon dioxide in K_2CO_3 is used in the production of syngas for ammonia synthesis. In the desulfurization processes of the petroleum industry, large amounts of H_2S are formed. The H_2S thus produced is absorbed in an amine solution. Gas–liquid reactions are common in biochemical processes. Typical examples include aerobic fermentation and ozonization of wastewater. Aromatic compounds in wastewater can be decomposed by ozonization to carbon dioxide.

For a review of noncatalytic or homogeneously catalyzed gas–liquid reactions, see Table 7.1 [2–4].

Several constructions are available for gas–liquid reactors because of the large number of different application areas. Some of the main reactor types are illustrated in Figure 7.2 [5]. Spray columns, wetted wall columns, packed columns, and plate columns are mainly used for absorption processes. The gas concentrations are low in the case of absorption processes, and to enhance the absorption process, a large interfacial contact area between the gas and the liquid is important. This area is obtained in the previously mentioned reactor types. These column reactors usually operate in a countercurrent mode. The countercurrent operation is the optimal operating mode, because at the gas outlet where the gaseous component concentration is the lowest, the gas comes into contact with a fresh absorption solution. The low concentration of the gaseous component can then partly be compensated by the high concentration of the liquid component.

Two reactor types dominate in the synthesis of chemicals in the case of gas–liquid reactions: the tank reactor and the bubble column. Both types can be operated in a continuous

TABLE 7.1 Industrial Gas–Liquid Reactions

Absorption of NO_2 in H_2O in the production of HNO_3
Absorption of CO_2 in NaOH or KOH
Absorption of CO_2 in carbonate solutions
Absorption of CO_2 in amine solutions
Absorption of CO_2 in ammonia solutions
Absorption of H_2S in amine solutions
Absorption of COS in NaOH or KOH
Oxidation of anthraquinole to anthraquinone in the H_2O_2 process
Oxidation of ethene to acetaldehyde
Oxidation of cumene to cumenehydroxide in the phenol and acetone processes
Oxidation of toluene to benzoic acid
Oxidation of xylene to phthalic acid
Oxidation of wastewater
Chlorination of aromatic hydrocarbons
Chlorination of acetic acid to monochloroacetic acid
Sulfonation of aromatic hydrocarbons
Nitrification of toluene to nitrotoluene

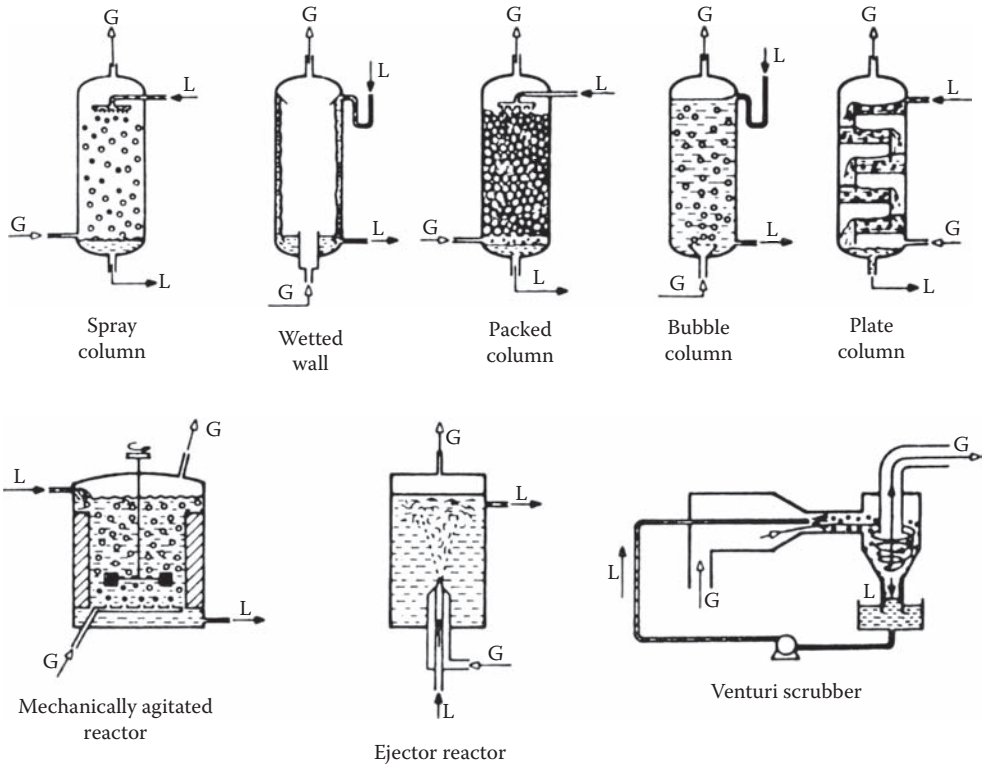

FIGURE 7.2 Typical gas–liquid reactors used industrially. (Data from Charpentier, J.-C., *Advances in Chemical Engineering*, Vol. 11, Academic Press, New York, 1981.)

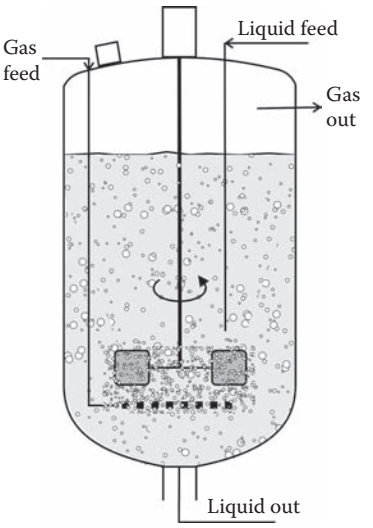

FIGURE 7.3 Gas–liquid tank reactor.

or a semibatch mode. In a semibatch operation, the liquid phase is treated as a batch, and the gas phase flows continuously through the liquid.

A typical tank reactor for gas–liquid reactions is shown in Figure 7.3. For this kind of reactors, it is very important to have good gas dispersion in liquid. The gas is fed through a sparger located under the impeller. The advantage of a tank reactor is its good mixing capabilities that also make it useful in the treatment of highly viscous fluids. The heat transfer capabilities are useful in the case of highly exothermic reactions: the reactor contents can be regulated by feeding in cold reactants to a certain extent. In a semibatch operation, a similar problem of temperature control and product quality can occur as in the case of homogeneous liquid-phase systems. The biggest disadvantage of tank reactors operating in a continuous mode is the low reactant concentrations at which the reactors operate. Another disadvantage is the complex mechanical structure that results in increased investment and operating costs.

A frequently used gas–liquid reactor is the bubble column. Different bubble column constructions are introduced in Figures 7.4 through 7.8. The gas is usually fed from the bottom through a sparger, and the liquid flows either concurrently or countercurrently. A countercurrent operation is more efficient than a concurrent one, but for certain types of parallel reactions, for example, parallel chlorination reactions yielding mono- and dichlorinated products, concurrent operation can provide better selectivity. Bubble columns are often operated in a semibatch mode: the gas bubbles through the liquid. This mode of operation is attractive in the production of fine chemicals produced in small quantities—especially in the case of slow reactions. Different kinds of bubble columns are shown in Figures 7.4 through 7.8. A larger interfacial area can be obtained with a gas injector (Figure 7.6). The coalescence of bubbles reduces the interfacial area at higher levels in the column. In Figures 7.7 and 7.8, two systems for reaction liquid recirculation in the bubble column are displayed. It is often necessary to facilitate recirculation of the liquid phase for improved

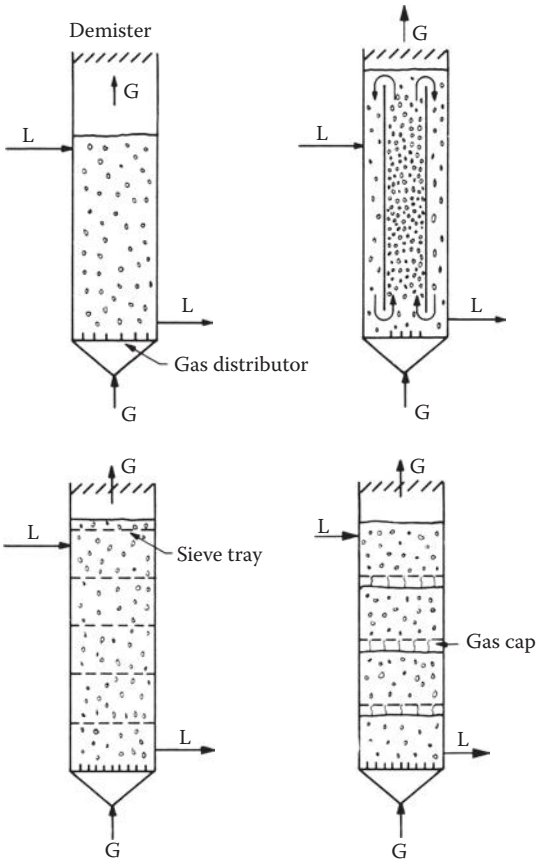

FIGURE 7.4 Various types of bubble columns for gas–liquid reactions. (Data from Trambouze, P., van Landeghem, H., and Wauquier, J.P., *Chemical Reactors—Design/Engineering*, Editions Technip, Paris, 1988.)

temperature control. The flow patterns can vary considerably in a bubble column: generally, as a rule of thumb, the liquid phase is more backmixed than the gas phase. The plug flow model is suitable for the gas phase, whereas the liquid phase can be modeled with the backmixed, dispersion, or plug flow models.

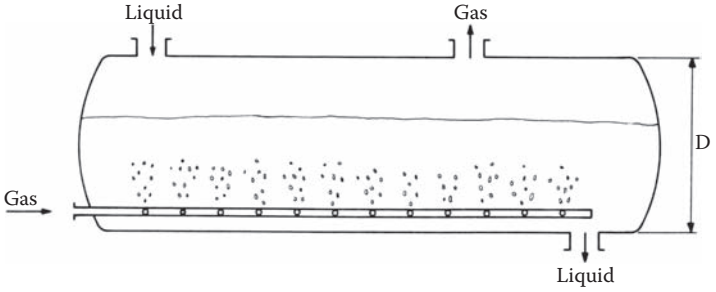

FIGURE 7.5 Horizontal bubble column. (Data from Trambouze, P., van Landeghem, H., and Wauquier, J.P., *Chemical Reactors—Design/Engineering*, Editions Technip, Paris, 1988.)

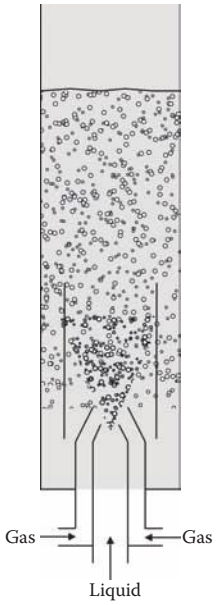

FIGURE 7.6 A bubble column with a gas ejector.

Packed columns are traditionally the most frequently used absorption reactors in the chemical industry. The columns are usually operated in a countercurrent mode; the gas flows upwards and the liquid flows downwards over the packing material. The packing material provides a large enough gas–liquid interfacial contact transfer area in the column.

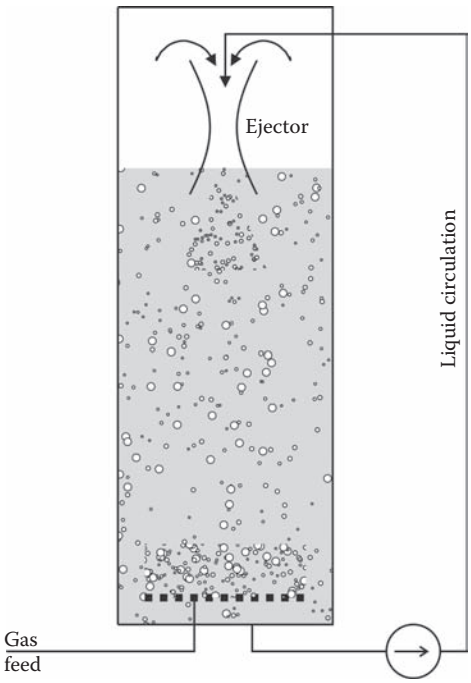

FIGURE 7.7 A bubble column with a recirculation loop for the liquid phase, loop reactor.

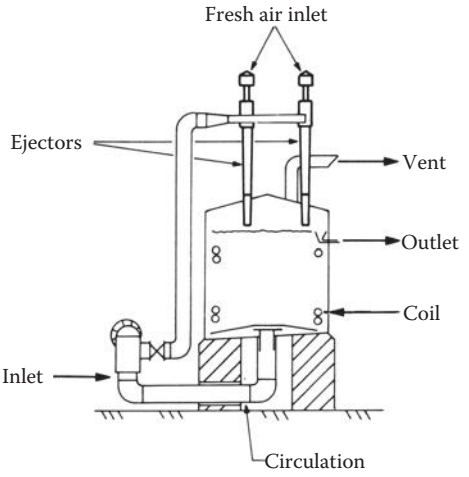

FIGURE 7.8 A bubble column with recirculation of the liquid. (Data from Trambouze, P., van Landeghem, H., and Wauquier, J.P., *Chemical Reactors—Design/Engineering*, Editions Technip, Paris, 1988.)

Some common packing materials are shown in Figure 7.9. The packings are most often manufactured from ceramics, plastics, or metals (Figure 7.10). The gas principally is well distributed in the reactor tanks to the packing material, but channeling can easily occur in the liquid phase. By placing distribution plates in the column, channeling can largely be avoided. Certain types of distribution plates are introduced in Figure 7.11. If a packed column works well, the flow conditions in the gas and liquid phases are close to the plug flow conditions.

A plate column is shown in Figure 7.12. Plate columns are used for the same purposes as packed columns, namely for absorption of gases. The gas and the liquid flow countercurrently, and the plate column is very similar to a distillation column. Contrary to distillation columns, the energy effects in plate columns are of minor importance, since the gas flow rates and the reaction rates are low. Several types of plate columns have been developed; the most typical construction is the bubble-cap tray (Figure 7.13).

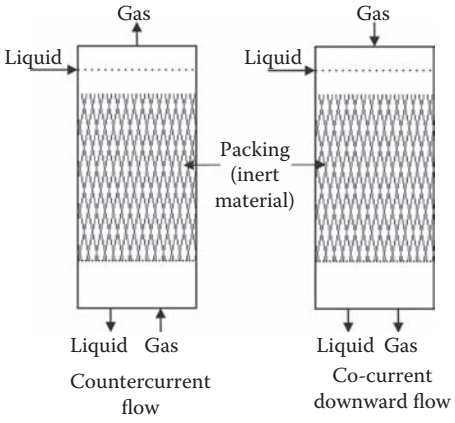

FIGURE 7.9 Packed column for gas–liquid reactions.

FIGURE 7.10 Different kinds of column packings. (Data from Trambouze, P., van Landeghem, H., and Wauquier, J.P., *Chemical Reactors—Design/Engineering*, Editions Technip, Paris, 1988.)

Plate or packed columns are often competing construction alternatives in the design of absorption processes. Trambouze et al. [2] give the following advice for the comparison of plate and packed columns.

1. The pressure drop is usually lower in a packed column than in a plate column.
2. For column diameters <1 m, a packed column is cheaper, and for larger diameters, a plate column is cheaper.
3. The flow conditions are easier to control in a plate column.
4. Plate columns are suitable for reactions that occur partially in the liquid bulk.
5. Short-circuiting of the gas flows may be a problem in packed columns.

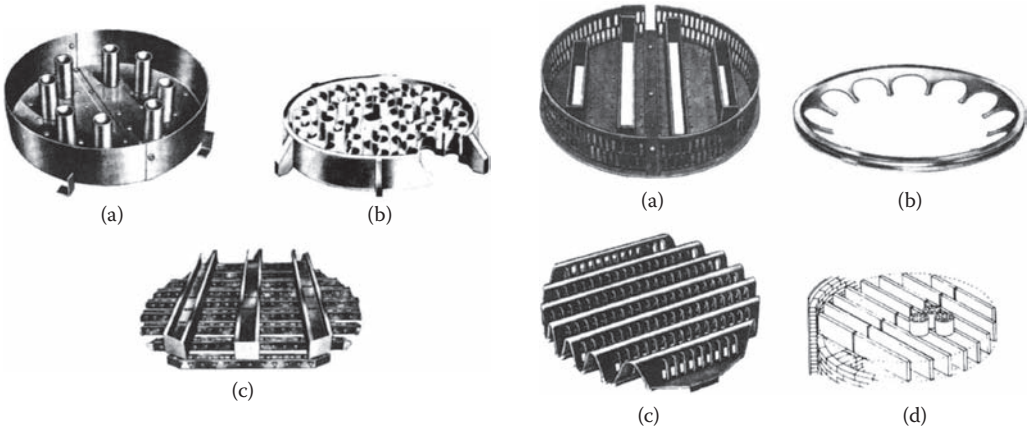

FIGURE 7.11 Distribution plates for packed columns. (Data from Trambouze, P., van Landeghem, H., and Wauquier, J.P., *Chemical Reactors—Design/Engineering*, Editions Technip, Paris, 1988.)

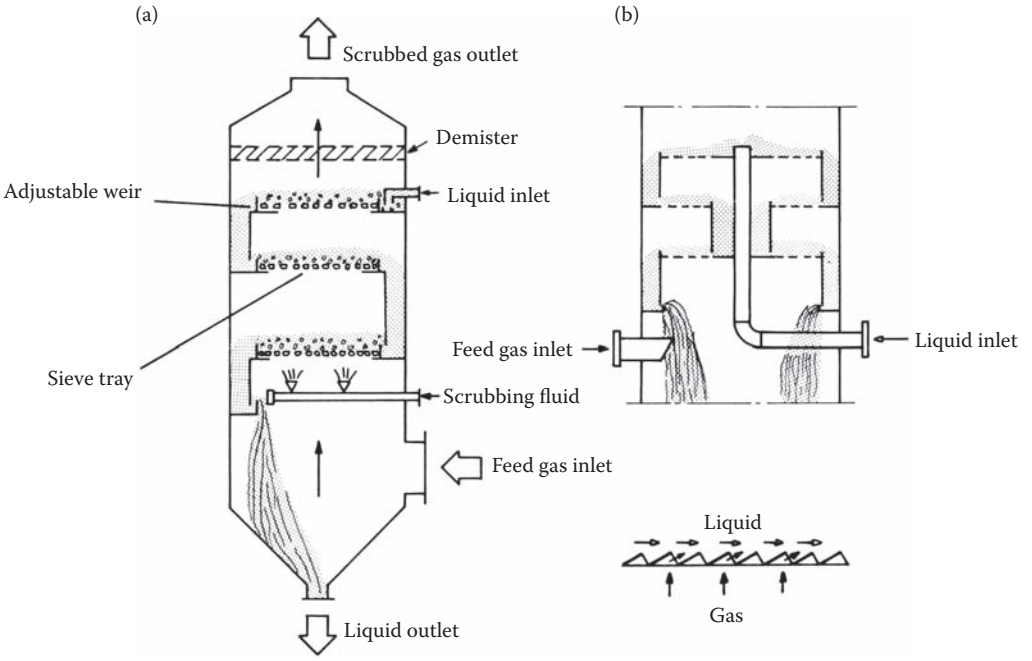

FIGURE 7.12 Plate column. (Data from Trambouze, P., van Landeghem, H., and Wauquier, J.P., *Chemical Reactors—Design/Engineering*, Editions Technip, Paris, 1988.)

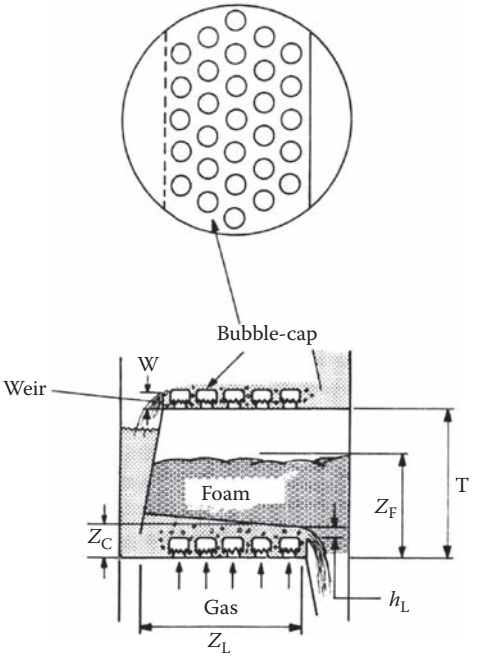

FIGURE 7.13 Bubble-cap bottom. (Data from Trambouze, P., van Landeghem, H., and Wauquier, J.P., *Chemical Reactors—Design/Engineering*, Editions Technip, Paris, 1988.)

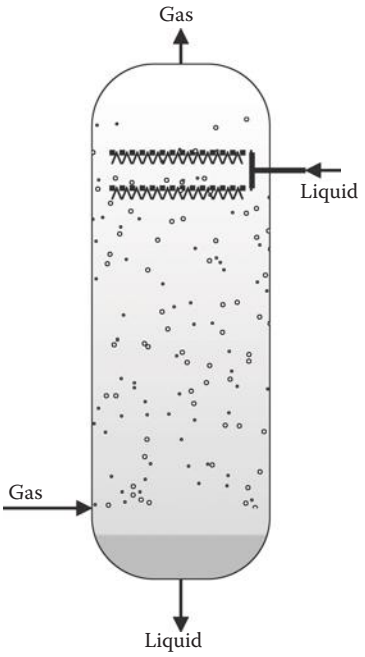

FIGURE 7.14 Spray column.

Gas scrubbers are a special type of gas–liquid reactors. Two main constructions exist: the spray tower and the Venturi scrubber. These reactor types are shown in Figures 7.14 and 7.15. The gas phase is dispersed into the liquid phase with a Venturi tube. The gas flows through the Venturi tube at a high velocity (Figure 7.15). In a spray tower, the liquid is distributed with a distributor and sprayed downwards in the form of small droplets. The gas flows countercurrently upwards. Due to high gas velocities, these kinds of reactors are only useful for very fast reactions.

A variety of different types of gas–liquid reactors exist. The choice of the reactor type is sometimes obvious and sometimes very difficult. A summary of the selection criteria is listed in Table 7.2. For slow reactions, a bubble column is preferred; for fast reactions, a column, a scrubber, or a spray tower should be used. For absorption processes in which a high conversion of the gaseous reactant is the main goal, the self-evident reactor type is a packed bed or a plate column.

7.2 MASS BALANCES FOR IDEAL GAS–LIQUID REACTORS

Mathematical models for different kinds of gas–liquid reactors are based on the mass balances of components in the gas and liquid phases. The flow pattern in a tank reactor is usually close to complete backmixing. In the case of packed and plate columns, it is often a good approximation to assume the existence of a plug flow. In bubble columns, the gas phase flows in a plug flow, whereas the axial dispersion model is the most realistic one for the liquid phase. For a bubble column, the ideal flow patterns set the limit for the reactor capacity for typical reaction kinetics.

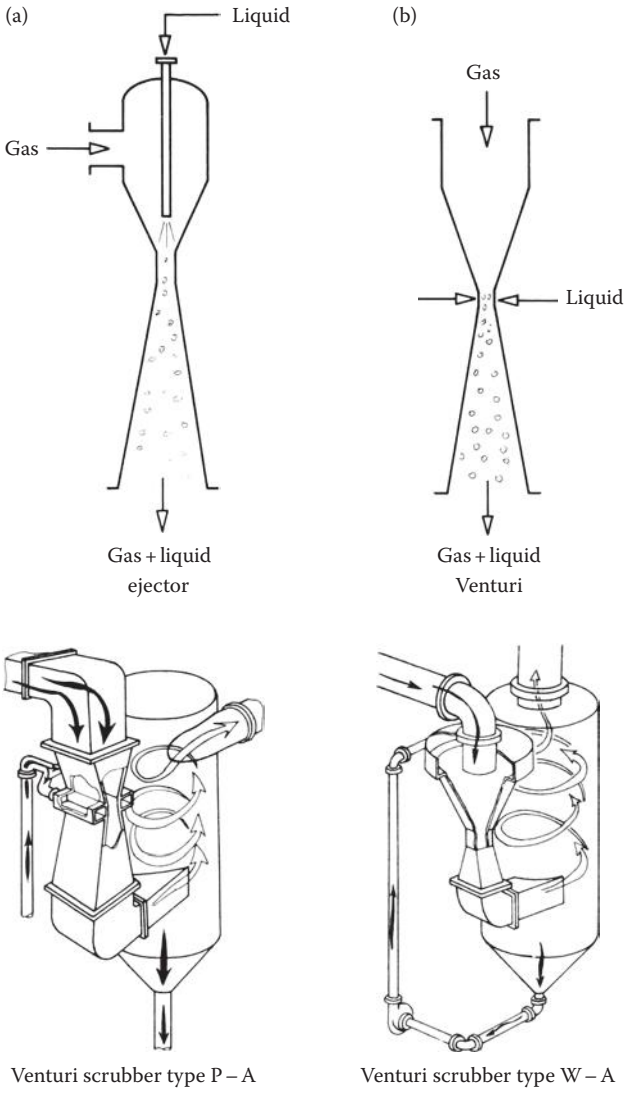

FIGURE 7.15 Venturi scrubbers. (Data from Trambouze, P., van Landeghem, H., and Wauquier, J.P., *Chemical Reactors—Design/Engineering*, Editions Technip, Paris, 1988.)

Below we will look at three ideal gas–liquid reactor types: a column reactor with a plug flow in the gas and liquid phases, a tank reactor with complete backmixing, and a BR. The main volume elements in gas–liquid reactors are displayed in Figure 7.16. The bulk gas and liquid phases are delimited by thin films where chemical reactions and molecular diffusion occur. However, the reactions do take place in the bulk phase of the liquid as well.

The flux of component i from the gas bulk to the gas film is denoted as N_{Gi}^{b}, whereas the flux from the liquid film to the liquid bulk is denoted as N_{Li}^{b}. Qualitatively, the fluxes are given with respect to the interfacial contact area (A) according to a very simple relation:

$$N_i A = (\,)\,\frac{\text{mol}}{\text{m}^2\text{s}}\,(\,)\text{m}^2.$$

TABLE 7.2 Selection Criteria for Gas–Liquid Reactors

	Bubble Column	Partitioned Bubble Column	Horizontal Bubble Column	Bubble Column with Gas Recycle	Mechanically Stirred Tank	Valve Tray Column	Sieve Tray Column	Counter Current Packed Column	Cross-Current or Concurrent	Venturi Scrubber	Spray Tower
Fast reaction	−	−	−	−	0	0	0	+	+	+	+
Slow reaction	+	+	+	+	0	0	0	−	−	−	−
High capacity	+	+	+	0	−	+	+	+	+	+	+
High reactant conversion in the gas phase	−	0	0	0	−	+	+	+	+	0	0
High reactant conversion in the liquid phase	−	0	0	−	0	+	+	+	+	−	−
Low pressure drop for gas	−	−	−	−	−	−	0	+	+	+	+
Fines removal	0	0	0	0	0	−	0	−	−	+	+

Source: Data from Trambouze, P., van Landeghem, H., and Wauquier, J.P., *Chemical Reactors–Design/Engineering*, Editions Technip, Paris, 1988.
Note: +, suitable; −, unsuitable; and 0 acceptable.

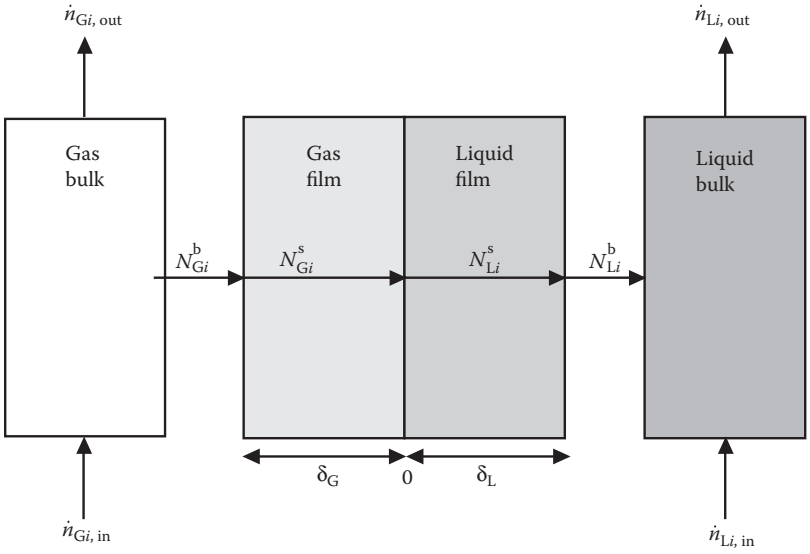

FIGURE 7.16 A volume element in a gas–liquid reactor.

The flows N^{b}_{Li} and N^{b}_{Gi} can have both positive and negative values, depending on the direction of the respective flow. The positive direction is marked in Figure 7.16. The volumes of the gas and liquid films are assumed to be negligible with respect to the bulk-phase volumes. The formulation of the fluxes is treated in detail in Section 7.2.4.

7.2.1 PLUG FLOW COLUMN REACTOR

A column reactor is assumed to operate under steady-state conditions. A positive flow is chosen as the liquid-phase flow direction. For a volume element ΔV_L in the liquid phase, the mass balance can be written as

$$\dot{n}_{Li,in} + N^{b}_{Li}\Delta A + r_i \Delta V_L = \dot{n}_{Li,out}. \tag{7.1}$$

By considering the relation $\dot{n}_{Li,out} - \dot{n}_{Li,in} = \Delta \dot{n}_{Li}$ and by defining the volume fraction (*holdup*) of the liquid

$$\varepsilon_L = \frac{\Delta V_L}{\Delta V_R} \tag{7.2}$$

(liquid volume element-to-reactor volume element) as well as the ratio of interfacial contact area-to-reactor volume, we obtain

$$a_v = \frac{\Delta A}{\Delta V_R}. \tag{7.3}$$

Equation 7.1 can now be written as

$$\Delta \dot{n}_{Li} = N^{b}_{Li} a_v \Delta V_R + r_i \varepsilon_L \Delta V_R. \tag{7.4}$$

After division by the reactor volume element, ΔV_R, and allowing $\Delta V_R \to 0$, we obtain

$$\frac{d\dot{n}_{Li}}{dV_R} = N^{b}_{Li} a_v + \varepsilon_L r_i. \tag{7.5}$$

For a gas-phase volume element, ΔV_G, analogous to Equation 7.1, we obtain

$$\dot{n}_{Gi,in} = N^b_{Gi}\Delta A + \dot{n}_{Gi,out}. \tag{7.6}$$

If the gas and the liquid flow in the same direction, $\Delta\dot{n}_{Gi} = \dot{n}_{Gi,out} - \dot{n}_{Gi,in}$, and the flow directions are opposite, $\Delta\dot{n}_{Gi} = \dot{n}_{Gi,in} - \dot{n}_{Gi,out}$, we can rewrite Equation 7.6 for both concurrent $(-)$ and countercurrent $(+)$ flows, taking into account the definition of a_v, Equation 7.3:

$$\Delta\dot{n}_{Gi} = \pm N^b_{Gi} a_v \Delta V_R. \tag{7.7}$$

Balance Equation 7.7 is transformed to a differential equation

$$\frac{d\dot{n}_{Gi}}{dV_R} = \pm N_{Gi} a_v. \tag{7.8}$$

Equations 7.5 and 7.8 have the initial conditions

$$\dot{n}_{Li} = \dot{n}_{0Li} \quad \text{at } V_R = 0 \tag{7.9}$$

for both concurrent and countercurrent flows. The initial condition is

$$\dot{n}_{Gi} = \dot{n}_{0Gi} \quad \text{at } V_R = 0 \tag{7.10}$$

for a concurrent flow, and the boundary condition is

$$\dot{n}_{Gi} = \dot{n}_{0Gi} \quad \text{at } V_R = V_R \tag{7.11}$$

for a countercurrent flow.

The balance Equations 7.5 and 7.6 can now be written with arrays:

$$\frac{d\dot{\mathbf{n}}_L}{dV_R} = \mathbf{N}^b_L a_v + \varepsilon_L \nu \mathbf{R}, \tag{7.12}$$

$$\frac{d\dot{\mathbf{n}}_G}{dV_R} = \pm \mathbf{N}^b_G a_v. \tag{7.13}$$

If the liquid space time

$$\tau_L = \frac{V_R}{\dot{V}_{0L}} \tag{7.14}$$

is used as an independent variable, Equations 7.12 and 7.13 are transformed to

$$\frac{d\dot{\mathbf{n}}_L}{d\tau_R} = \left(\mathbf{N}^b_L a_v + \varepsilon_L \nu \mathbf{R}\right) \dot{V}_{0L} \tag{7.15}$$

and

$$\frac{d\dot{\mathbf{n}}_G}{dV_R} = \pm \mathbf{N}^b_G a_v \dot{V}_{0L}. \tag{7.16}$$

7.2.2 TANK REACTOR WITH COMPLETE BACKMIXING

The mass balance for a completely backmixed reactor can be rewritten as

$$\dot{n}_{0\mathrm{L}i} + N_{\mathrm{L}i}^{\mathrm{b}} A + r_i V_{\mathrm{L}} = \dot{n}_{\mathrm{L}i}, \tag{7.17}$$

$$\varepsilon_{\mathrm{L}} = \frac{V_{\mathrm{L}}}{V_{\mathrm{R}}}. \tag{7.18}$$

Analogous to Equations 7.1 and 7.2, the liquid holdup and the ratio of interfacial contact area-to-reactor volume is defined as

$$a_{\mathrm{v}} = \frac{A}{V_{\mathrm{R}}}. \tag{7.19}$$

Substituting these ratios into Equation 7.17, we obtain

$$\frac{\dot{n}_{\mathrm{L}i} - \dot{n}_{0\mathrm{L}i}}{V_{\mathrm{R}}} = N_{\mathrm{L}i}^{\mathrm{b}} a_{\mathrm{v}} + \varepsilon_{\mathrm{L}} r_i. \tag{7.20}$$

For the gas phase, analogous to Equation 7.17, we obtain

$$\dot{n}_{0\mathrm{G}i} = N_{\mathrm{G}i}^{\mathrm{b}} A + \dot{n}_{\mathrm{G}i}. \tag{7.21}$$

Insertion of the ratio into Equation 7.19 yields

$$\frac{\dot{n}_{\mathrm{G}i} - \dot{n}_{0\mathrm{G}i}}{V_{\mathrm{R}}} = -N_{\mathrm{G}i}^{\mathrm{b}} a_{\mathrm{v}}. \tag{7.22}$$

Mass balance Equation 7.20 and Equations 7.22 and 7.25 can now be written in the vector form as

$$\frac{\dot{\mathbf{n}}_{\mathrm{L}i} - \dot{\mathbf{n}}_{0\mathrm{L}i}}{V_{\mathrm{R}}} = N_{\mathrm{L}i}^{\mathrm{b}} a_{\mathrm{v}} + \varepsilon_{\mathrm{L}} \mathbf{r}_i \tag{7.23}$$

and

$$\frac{\dot{\mathbf{n}}_{\mathrm{G}i} - \dot{\mathbf{n}}_{0\mathrm{G}i}}{V_{\mathrm{R}}} = -\mathbf{N}_{\mathrm{G}i}^{\mathrm{b}} a_{\mathrm{v}}, \tag{7.24}$$

as well as a function of the liquid space time:

$$\frac{\dot{n}_{\mathrm{L}} - \dot{n}_{0\mathrm{L}}}{\tau_{\mathrm{L}}} = \left(N_{\mathrm{L}}^{\mathrm{b}} a_{\mathrm{v}} + \varepsilon_{\mathrm{L}} \nu \mathrm{R} \right) \dot{V}_{0\mathrm{L}} \tag{7.25}$$

and

$$\frac{\dot{n}_{\mathrm{G}} - \dot{n}_{0\mathrm{G}}}{\tau_{\mathrm{L}}} = -N_{\mathrm{G}}^{\mathrm{b}} a_{\mathrm{v}} \dot{V}_{0\mathrm{L}}. \tag{7.26}$$

7.2.3 BATCH REACTOR

For a BR, the liquid-phase transient mass balance is

$$N_{Li}^{b}A + r_i V_L = \frac{dn_{Li}}{dt}, \tag{7.27}$$

where dn_{Li}/dt accounts for the accumulation of component i in the liquid phase. For a_v and ε_L, the same definitions as for the tank reactor, Equations 7.18 and 7.19, are valid. Inserting Equations 7.18 and 7.19 into the mass balance Equation 7.27 yields

$$\frac{dn_{Li}}{dt} = \left(N_{Li}^{b}a_v + \varepsilon_L r_i\right) V_R. \tag{7.28}$$

For the gas phase, the following mass balance is valid:

$$0 = N_{Gi}^{b}A + \frac{dn_{Gi}}{dt}. \tag{7.29}$$

Insertion of the definition for a_v (interfacial contact area per reactor volume) yields

$$\frac{dn_{Gi}}{dt} = -N_{Gi}^{b}a_v V_R. \tag{7.30}$$

Equations 7.28 and 7.29 have the initial conditions

$$n_{Li} = n_{Li}(0) \quad \text{at } t = 0 \tag{7.31}$$

and

$$n_{Gi} = n_{Gi}(0) \quad \text{at } t = 0. \tag{7.32}$$

These can now be rewritten in the vector form as

$$\frac{d\mathbf{n}_L}{dt} = \left(\mathbf{N}_L^{b}a_v + \varepsilon_L \nu R\right) V_R, \tag{7.33}$$

$$\frac{d\mathbf{n}_G}{dt} = -\mathbf{N}_G^{b}a_v V_R. \tag{7.34}$$

The analogy with the column reactor mass balances is obvious.

7.2.4 FLUXES IN GAS AND LIQUID FILMS

Different theories and methods [6] are available for the calculation of molar fluxes, N_{Gi}^{b} and N_{LA}^{b}, which are needed in the bulk-phase mass balances of ideal gas–liquid reactors, Equations 7.15 and 7.16, Equations 7.22, 7.25, and 7.26, and Equations 7.33 and 7.34. According to the two-film theory, molecular diffusion and a chemical reaction occur simultaneously

in the liquid film, and only molecular diffusion occurs in the gas film. The liquid and gas film thicknesses are denoted as δ_L and δ_G, respectively. *Fick's law* describes the fluxes in gas and liquid films. The transport processes are shown in Figure 7.17.

If Fick's law is valid for both the gas and the liquid films, fluxes N_{Gi}^{b} and N_{LA}^{b} are defined as

$$N_{Gi}^{b} = D_{Gi}\left(\frac{dc_{Gi}}{dz}\right)_{z=\delta_G} \tag{7.35}$$

and

$$N_{Li}^{b} = -D_{Li}\left(\frac{dc_{Li}}{dz}\right)_{z=\delta_L}, \tag{7.36}$$

where D_{Gi} and D_{Li} are the diffusion coefficients in the gas and liquid phases, respectively. Different signs in Equations 7.35 and 7.36 are due to the different coordinate system definitions for the gas and liquid films in Figure 7.16.

Balance Equation 7.37 is valid for component i in the gas film,

$$\left(D_{Gi}\frac{dc_{Gi}}{dz}\right)_{in} A = \left(D_{Gi}\frac{dc_{Gi}}{dz}\right)_{out} A, \tag{7.37}$$

where $(\,)_{in} - (\,)_{out} = \Delta\left[D_{Gi}\left(dc_{Gi}/dz\right)\right]$.

Dividing Equation 7.37 by Δz (distance element in z coordinate) yields

$$\frac{\Delta[D_{Gi}\ (dc_{Gi}/dz)]}{\Delta z} = 0. \tag{7.38}$$

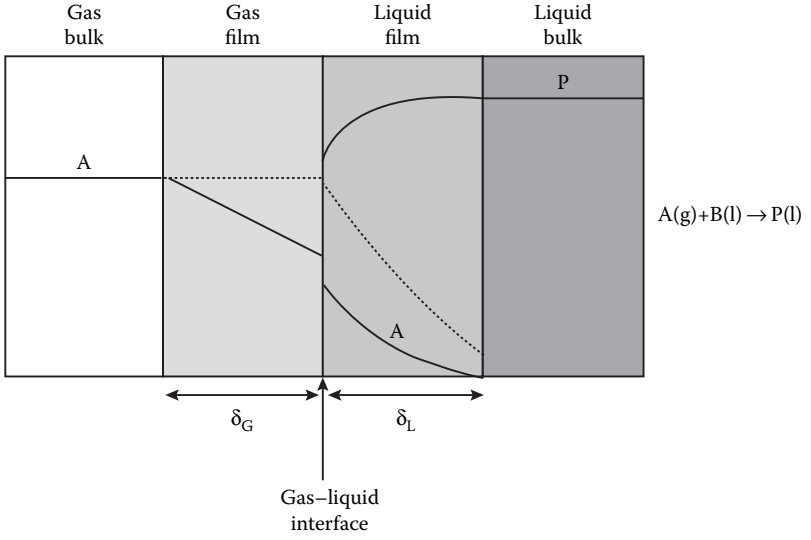

FIGURE 7.17 Diffusion and reaction in gas and liquid films (.... slow diffusion rate, — more rapid diffusion rate).

Assuming that the diffusion coefficient is approximately constant and allowing that $\Delta z \to 0$, we obtain the balance equation

$$D_{Gi}\frac{d^2 c_{Gi}}{dz^2} = 0. \tag{7.39}$$

This balance equation has an analytical solution. Integrating the equation once yields

$$\frac{dc_{Gi}}{dz} = C_1. \tag{7.40}$$

Integrating it once more yields

$$c_{Gi} = C_1 z + C_2. \tag{7.41}$$

The following boundary conditions are valid for Equation 7.39:

$$c_{Gi} = c_{Gi}^{s} \quad \text{at } z = 0, \tag{7.42}$$

$$c_{Gi} = c_{Gi}^{b} \quad \text{at } z = \delta_G. \tag{7.43}$$

The integration constants C_1 and C_2 can be determined by inserting the boundary conditions into Equation 7.41

$$C_1 = \frac{c_{Gi}^{b} - c_{Gi}^{s}}{\delta_G}, \tag{7.44}$$

$$C_2 = c_{Gi}^{s}. \tag{7.45}$$

The expression for the concentration profile, c_{Gi}, can now be written as

$$c_{Gi}(z) = \left(c_{Gi}^{b} - c_{Gi}^{s}\right)\left(\frac{z}{\delta_G}\right) + c_{Gi}^{s}. \tag{7.46}$$

The flux, N_{Gi}^{b}, is obtained according to the definition in Equation 7.35

$$N_{Gi}^{b} = \frac{D_{Gi}}{\delta_G}\left(c_{Gi}^{b} - c_{Gi}^{s}\right). \tag{7.47}$$

The ratio $D_{Gi}/\Delta z$ is often referred to as the gas film coefficient, k_{Gi},

$$k_{Gi} = \frac{D_{Gi}}{\delta_G}. \tag{7.48}$$

The flux N_{Gi}^{b} can be expressed in the form

$$N_{Gi}^{b} = k_{Gi}\left(c_{Gi}^{b} - c_{Gi}^{s}\right). \tag{7.49}$$

The flux in the gas film is, according to Equation 7.49, dependent on the gas film coefficient and the concentration difference between the gas bulk and the gas film interface.

For the liquid film, the mass balance can be written as

$$-\left(D_{\mathrm{L}i}\frac{\mathrm{d}c_{\mathrm{L}i}}{\mathrm{d}z}\right)_{\mathrm{in}}A + r_i\Delta z = -\left(D_{\mathrm{L}i}\frac{\mathrm{d}c_{\mathrm{L}i}}{\mathrm{d}z}\right)_{\mathrm{out}}A, \tag{7.50}$$

where $A\Delta z$ is the volume element in the liquid film and r_i is the generation rate of component i. The difference, $(\,)_{\mathrm{in}} - (\,)_{\mathrm{out}}$, can be written as $\Delta(D_{\mathrm{L}i}(\mathrm{d}c_{\mathrm{L}i}/\mathrm{d}z))$. Dividing Equation 7.50 by the volume element $A\Delta z$ yields

$$\frac{\Delta\left[D_{\mathrm{L}i}\left(\mathrm{d}c_{\mathrm{L}i}/\mathrm{d}z\right)\right]}{\Delta z} + r_i = 0. \tag{7.51}$$

If the diffusion coefficient $D_{\mathrm{L}i}$ is assumed to be independent of the concentration and allowing $\Delta z \to 0$, Equation 7.51 is transformed to

$$D_{\mathrm{L}i}\frac{\mathrm{d}^2c_{\mathrm{L}i}}{\mathrm{d}z^2} + r_i = 0. \tag{7.52}$$

Equation 7.52 describes *simultaneous diffusion and chemical reaction in the liquid film*. The concentration profile of component i, $c_{\mathrm{L}i}(z)$, can in principle be solved by Equation 7.52 and the flux, $N_{\mathrm{L}i}^{\mathrm{b}}$, is obtained from the derivative $\mathrm{d}c_{\mathrm{L}i}/\mathrm{d}z$ in Equation 7.36. Equation 7.52 has the boundary conditions

$$N_{\mathrm{G}i}^{\mathrm{b}} = N_{\mathrm{G}i}^{\mathrm{s}} \quad \text{at } z = 0, \tag{7.53}$$

$$c_{\mathrm{L}i} = c_{\mathrm{L}i}^{\mathrm{b}} \quad \text{at } z = \delta_{\mathrm{L}}. \tag{7.54}$$

The boundary condition, Equation 7.53, means that the component fluxes defined according to the gas and liquid film properties, Equations 7.35 and 7.36, must be equal to each other. At the interface, a chemical equilibrium is assumed to exist mainly; the concentrations in the gas and liquid phases are then related to each other according to

$$K_i = \frac{c_{\mathrm{G}i}^{\mathrm{s}}}{c_{\mathrm{L}i}^{\mathrm{s}}}, \tag{7.55}$$

where K_i is the equilibrium state. For gases with a low solubility, K_i is often called *Henry's constant*. An analytical solution of the differential Equation 7.52 with the boundary conditions, Equation 7.53 and 7.54, is only possible in isothermal cases, in certain special cases. These cases are characterized by the interdependence of reaction and diffusion velocities and by the reaction kinetics.

The following special cases can be distinguished based on their reaction kinetics: physical absorption, very slow reactions, slow reactions, finite speed reactions, fast reactions, and

TABLE 7.3 Classification of Gas–Liquid Processes

Physical absorption	No chemical reaction in the liquid film and in the liquid bulk. Linear concentrations in the films
Very slow reaction	The same reaction velocity in the liquid film and in the liquid bulk. No concentration gradients in the liquid film
Slow reaction	No reaction in the liquid film, chemical reaction in the liquid bulk. Linear concentration gradients in the films
Finite speed reaction (moderate reaction)	Chemical reaction in the liquid film and in the liquid bulk. Nonlinear concentration profiles in the liquid film
Fast reaction	Chemical reaction in the liquid film. No chemical reaction in the liquid bulk. Nonlinear concentration profiles in the liquid film. The gas-phase component concentration is zero in the liquid phase
Instantaneous reaction	Chemical reaction in the reaction zone in the liquid film. The diffusion rates of the components determine reaction velocity

instantaneous reactions. A more detailed description of different reaction types is summarized in Table 7.3. The concentration profiles of components A(2) and B(1) for a bimolecular reaction and for different cases are illustrated in Figure 7.18. In the following pages, analytical expressions will be derived for the fluxes for different reaction types and reaction kinetics. Component A is assumed to be in the gas phase, and it is absorbed continuously by the liquid phase.

7.2.4.1 Very Slow Reactions

If a chemical reaction is very slow, no concentration gradients exist in the liquid film. Two cases can be distinguished depending on whether diffusion resistance in the gas film influences the absorption speed or not.

If diffusion resistance does not affect the reaction velocity, the flux for component A is

$$N_{GA}^{b} = N_{LA}^{b}, \tag{7.56}$$

and the gas–liquid equilibrium at the gas–liquid interface is

$$K_A = \frac{c_{GA}^{b}}{c_{LA}^{b}}. \tag{7.57}$$

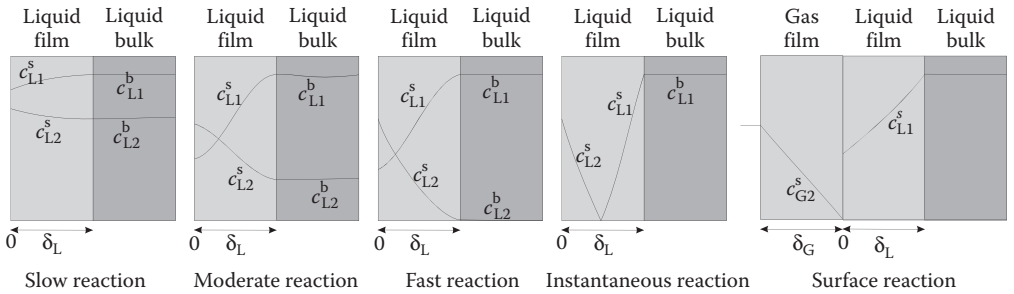

FIGURE 7.18 Influence of reaction kinetics on the concentration gradients in the liquid film for a bimolecular reaction. (Data from Trambouze, P., van Landeghem, H., and Wauquier, J.P., *Chemical Reactors—Design/Engineering*, Editions Technip, Paris, 1988.)

Equation 7.56 states that no reactions occur in the gas and liquid films, whereas Equation 7.57 states that the bulk-phase concentrations can be used to calculate the equilibrium at the gas–liquid interface.

If diffusion resistance is of importance in the gas film, the following equations are valid for the fluxes and equilibrium constant, respectively,

$$N_{GA}^{b} = N_{LA}^{b}, \tag{7.58}$$

$$K_A = \frac{c_{GA}^{s}}{c_{LA}^{b}}. \tag{7.59}$$

The diffusion flux for component A in the gas film is obtained from Equation 7.49 as

$$N_{GA}^{b} = k_{GA}\left(c_{GA}^{b} - c_{GA}^{s}\right). \tag{7.60}$$

Inserting the equilibrium definition, Equation 7.59, into Equation 7.60 yields the following expression for N_{LA}^{b} and N_{GA}^{b}:

$$N_{GA}^{b} = N_{LA}^{b} = k_{GA}\left(c_{GA}^{b} - K_A c_{LA}^{b}\right). \tag{7.61}$$

7.2.4.2 Slow Reactions

Slow reactions are characterized by the fact that diffusion resistances in the gas and liquid films suppress the absorption velocities. No chemical reactions are assumed to occur in the liquid film. For the diffusion flux and gas–liquid equilibrium, the following equations are valid for component A:

$$N_{GA}^{b} = N_{LA}^{b}, \tag{7.62}$$

$$K_A = \frac{c_{GA}^{s}}{c_{LA}^{s}}. \tag{7.63}$$

Equations 7.63 and 7.23 state that concentrations at the gas–liquid interface are different from those in the bulk phase. The flux through the gas film is given by

$$N_{GA}^{b} = k_{GA}\left(c_{GA}^{b} - c_{GA}^{s}\right). \tag{7.64}$$

Because no reactions are assumed to occur in the liquid film ($r_i = 0$), the transport equation, Equation 7.52, for the liquid film can be solved analytically, just like the transport equation for the gas film. The solution is analogous to the gas film reaction solution, Equation 7.46, and the flux through the liquid film is obtained as

$$N_{LA}^{b} = k_{LA}\left(c_{LA}^{s} - c_{LA}^{b}\right), \tag{7.65}$$

where the liquid film coefficient, k_{LA}, is defined in a manner analogous to the gas film coefficient, k_{GA},

$$k_{LA} = \frac{D_{LA}}{\delta_L}. \tag{7.66}$$

Here D_{LA} and δ_L are the liquid-phase diffusion coefficient and the liquid film thickness, respectively.

Equations 7.64 and 7.65 can be set equal to each other, according to Equations 7.63 and 7.23, and the expression for c^s_{GA} is inserted:

$$k_{GA}\left(c^b_{GA} - K_A c^s_{LA}\right) = k_{LA}\left(c^s_{LA} - c^b_{LA}\right). \tag{7.67}$$

The unknown interface concentration, c^s_{LA}, can be solved by Equation 7.67. The result is as follows:

$$c^s_{LA} = \frac{c^b_{GA} + (k_{KA}/k_{GA})\ c^b_{LA}}{K_A + (k_{LA}/k_{GA})}. \tag{7.68}$$

Substitution of the surface concentration, c^s_{LA}, Equation 7.68, into the expression for N^b_{LA}, Equation 7.65, yields

$$N^s_{LA} = \frac{c^b_{GA} - K_A c^b_{LA}}{(K_A/k_{LA}) + (1/k_{GA})}. \tag{7.69}$$

Equation 7.69 shows that the film transport resistances can be added to each other, and an overall transport coefficient can be defined as

$$\frac{1}{k'_A} = \frac{K_A}{k_{LA}} + \frac{1}{k_{GA}}. \tag{7.70}$$

If the diffusion resistance in the gas film is negligible in comparison to that in the liquid film—which is frequently the case for slow reactions—the term $1/k_{GA}$ disappears ($k_{GA} \to 0$) in Equations 7.69 and 7.70.

7.2.4.3 Reactions with a Finite Velocity

For reactions in this regime, no general expressions can be derived for the diffusion flux, N_A, through the gas and liquid films. Chemical reactions proceed in the liquid film and the following conditions are valid for diffusion fluxes through the gas and liquid films:

$$N^b_{GA} \neq N^b_{LA}, \tag{7.71}$$

$$N^b_{GA} = N^s_{GA} = N^s_{LA}. \tag{7.72}$$

The first condition, Equation 7.71, states that the diffusion flux for component A in the liquid phase changes because of the reaction taking place in the liquid film. For the gas–liquid equilibrium at the interface, the following ratio is valid:

$$K_A = \frac{c^s_{GA}}{c^s_{LA}}. \tag{7.73}$$

The transport equation for component A must be solved separately for each type of reaction kinetics. An analytical solution for Equation 7.52 is possible in some special cases. The liquid film must, however, be considered as isothermal, this being a quite reasonable assumption.

Let us now consider an analytical solution for the mass balance equation of the liquid film

$$D_{\mathrm{LA}}\frac{\mathrm{d}^2 c_{\mathrm{LA}}}{\mathrm{d}z^2} + r_{\mathrm{A}} = 0 \tag{7.74}$$

for zero-, first-, pseudo-first-, and second-order reactions.

7.2.4.3.1 Zero-Order Reactions

For zero-order kinetics, the reaction rate r_{A} is

$$r_{\mathrm{A}} = \nu_{\mathrm{A}} R = \nu_{\mathrm{A}} k. \tag{7.75}$$

Substituting r_{A} into Equation 7.74 yields

$$\frac{\mathrm{d}^2 c_{\mathrm{LA}}}{\mathrm{d}z^2} = -\frac{\nu k}{D_{\mathrm{LA}}}. \tag{7.76}$$

By integrating Equation 7.76 twice, the concentration profiles for component A in the liquid film are obtained:

$$c_{\mathrm{LA}}(z) = -\frac{\nu k}{2D_{\mathrm{LA}}} z^2 + C_1 z + C_2. \tag{7.77}$$

Applying the boundary conditions

$$c_{\mathrm{LA}}(\delta_{\mathrm{L}}) = c_{\mathrm{LA}}^{\mathrm{b}} \tag{7.78}$$

and

$$c_{\mathrm{LA}}(0) = c_{\mathrm{LA}}^{\mathrm{s}} \tag{7.79}$$

makes it possible to determine the integration constants C_1 and C_2 in Equation 7.77:

$$C_1 = \frac{c_{\mathrm{LA}}^{\mathrm{b}} - c_{\mathrm{LA}}^{\mathrm{s}}}{\delta_{\mathrm{L}}} + \frac{\nu_k k}{2D_{\mathrm{LA}}}\delta_{\mathrm{L}}, \tag{7.80}$$

$$C_2 = c_{\mathrm{LA}}^{\mathrm{s}}. \tag{7.81}$$

Substituting Equations 7.80 and 7.81 into Equation 7.77 yields the concentration profile $c_{\mathrm{LA}}(z)$:

$$c_{\mathrm{LA}}(z) = -\frac{\nu_{\mathrm{A}} k \delta_{\mathrm{L}}^2}{2D_{\mathrm{LA}}}\left(\frac{z}{\delta_{\mathrm{L}}}\right)^2 + \left(c_{\mathrm{LA}}^{\mathrm{b}} - c_{\mathrm{LA}}^{\mathrm{s}} + \frac{\nu_{\mathrm{A}} k \delta_{\mathrm{L}}^2}{2D_{\mathrm{LA}}}\right)\left(\frac{z}{\delta_{\mathrm{L}}}\right) + c_{\mathrm{LA}}^{\mathrm{s}}. \tag{7.82}$$

To obtain the flux, N_{LA}^{s}, we calculate the derivative

$$\frac{dc_{LA}}{dz} = -\frac{\nu_A k \delta_L}{D_{LA}} \left(\frac{z}{\delta_L}\right) + \left(\frac{c_{LA}^{b} - c_{LA}^{s}}{\delta_L}\right) + \frac{\nu_A k \delta_L}{2D_{LA}}. \tag{7.83}$$

According to the definition, the flux N_{LA}^{s} is obtained as

$$N_{LA}^{s} = -D_{LA}\left(\frac{dc_{LA}}{dz}\right)_{z=0} = -\frac{D_{LA}(c_{LA}^{b} - c_{LA}^{s})}{\delta_L} - \frac{\nu_A k \delta_L}{2D_{LA}}, \tag{7.84}$$

and the term $-\nu_A k \delta_L/2$ can be written as

$$-\frac{\nu_A k \delta_L}{2} = -\frac{\nu_A k D_{LA}}{2k_{LA}}. \tag{7.85}$$

By defining the dimensionless quantity, M, as

$$M = -\frac{\nu_A k D_{LA}}{2k_{LA}^2 c_{LA}^{b}}, \tag{7.86}$$

the expression for flux, N_{LA}^{s}, can be written as

$$N_{LA}^{s} = k_{LA}\left(c_{LA}^{s} - c_{LA}^{b}\right) + k_{LA} c_{LA}^{b} M. \tag{7.87}$$

The flux is also affected by *diffusion through the gas film*. For the gas film diffusion, we have

$$N_{GA}^{s} = N_{GA}^{b} = k_{GA}\left(c_{GA}^{b} - c_{GA}^{s}\right). \tag{7.88}$$

By setting Equations 7.87 and 7.88 equal to each other and using the equilibrium definition, Equation 7.73, the unknown interface concentration c_{LA}^{s} can be determined:

$$c_{LA}^{s} = \frac{k_{LA} c_{LA}^{b}(1 - M) + k_{GA} c_{GA}^{b}}{k_{LA} + k_{GA} K_A}. \tag{7.89}$$

Substituting this c_{LA}^{s} into Equation 7.87 yields the final form of the flux, N_{LA}^{s},

$$N_{LA}^{s} = \frac{c_{GA}^{s} + K_A c_{LA}^{b}(M - 1)}{(K_A/k_{LA}) + (1/k_{GA})}, \tag{7.90}$$

where M is defined by Equation 7.86. If the gas film resistance is negligible, the term k_{GA} disappears in Equation 7.90.

7.2.4.3.2 Enhancement Factor

For gas–liquid reactions, an *enhancement factor* is often defined. The enhancement factor is the ratio between the chemical absorption rate and the physical absorption rate. Equation 7.69 is valid for component A, when only physical absorption occurs in the liquid film. The enhancement factor E_A is in this case defined as

$$E_A = \frac{N_{LA}^s}{\left(c_{GA}^b - K_A c_{LA}^b\right) / \left[(K_A/k_{LA}) + (1/k_{GA})\right]}. \tag{7.91}$$

Applying the relation in Equation 7.90 to a zero-order reaction gives, according to Equation 7.91, the enhancement factor

$$E_A = 1 + \frac{MK_A c_{LA}^b}{c_{GA}^b - K_A c_{LA}^b}. \tag{7.92}$$

The enhancement factor, E_A, always assumes values larger than 1, that is, $E_A \geq 1$.

7.2.4.3.3 First-Order Reactions

For first-order kinetics, the reaction rate for component A is written as

$$r_A = \nu_A R = \nu_A k c_{LA}. \tag{7.93}$$

Applying this definition of r_A to the mass balance Equation 7.74 yields

$$\frac{d^2 c_{LA}}{dz^2} = -\frac{\nu_L k c_{LA}}{D_{LA}}. \tag{7.94}$$

This second-order differential equation

$$\frac{d^2 c_{LA}}{dz^2} + \frac{\nu_A k}{D_{LA}} c_{LA} = 0, \tag{7.95}$$

with constant coefficients, yields the characteristic equation

$$r^2 + \frac{\nu_A k}{D_{LA}} = 0 \tag{7.96}$$

with the roots

$$r_{1,2} = \pm \left[-\frac{\nu_A k}{D_{LA}} \right]^{1/2} = \pm\sqrt{\ }. \tag{7.97}$$

The solution, the concentration profiles of A, can be written as

$$c_{LA}(z) = C_1 e^{r,z} + C_2 e^{r,z}. \tag{7.98}$$

By applying the boundary conditions

$$c_{\mathrm{LA}}(\delta_{\mathrm{L}}) = c_{\mathrm{LA}}^{\mathrm{b}}, \tag{7.99}$$

$$c_{\mathrm{LA}}(0) = c_{\mathrm{LA}}^{\mathrm{s}}, \tag{7.100}$$

the integration constants C_1 and C_2 can be determined. The result is

$$C_1 = \frac{c_{\mathrm{LA}}^{\mathrm{b}} - c_{\mathrm{LA}}^{\mathrm{s}} \mathrm{e}^{-\sqrt{\delta_{\mathrm{L}}}}}{\mathrm{e}^{\sqrt{\delta_{\mathrm{L}}}} - \mathrm{e}^{-\sqrt{\delta_{\mathrm{L}}}}}, \tag{7.101}$$

$$C_2 = \frac{c_{\mathrm{LA}}^{\mathrm{s}} \mathrm{e}^{\sqrt{\delta_{\mathrm{L}}}} - c_{\mathrm{LA}}^{\mathrm{b}}}{\mathrm{e}^{\sqrt{\delta_{\mathrm{L}}}} - \mathrm{e}^{-\sqrt{\delta_{\mathrm{L}}}}}. \tag{7.102}$$

Substituting the integration constants C_1 and C_2 into Equation 7.98 yields the concentration profile in the liquid film:

$$c_{\mathrm{LA}}(z) = \frac{1}{\mathrm{e}^{\sqrt{\delta_{\mathrm{L}}}} - \mathrm{e}^{-\sqrt{\delta_{\mathrm{L}}}}} \left(c_{\mathrm{LA}}^{\mathrm{b}} \left(\mathrm{e}^{\sqrt{z/\delta_{\mathrm{L}}}} - \mathrm{e}^{-\sqrt{z/\delta_{\mathrm{L}}}} \right) + c_{\mathrm{LA}}^{\mathrm{s}} \left[\mathrm{e}^{\sqrt{(\delta_{\mathrm{L}} - z)}} - \mathrm{e}^{-\sqrt{(\delta_{\mathrm{L}} - z)}} \right] \right). \tag{7.103}$$

By defining a dimensionless group, M, as

$$M = -\frac{\nu_{\mathrm{A}} k D_{\mathrm{LA}}}{k_{\mathrm{LA}}^2}, \tag{7.104}$$

we obtain ($k_{\mathrm{LA}} = D_{\mathrm{LA}}/\delta_{\mathrm{L}}$),

$$\left(-\frac{\nu_{\mathrm{A}} k}{D_{\mathrm{LA}}} \right)^{1/2} \delta_{\mathrm{L}} = M^{1/2}. \tag{7.105}$$

This can be inserted into Equation 7.103:

$$\begin{aligned} c_{\mathrm{LA}}(z) = \frac{1}{\mathrm{e}^{M^{1/2}} - \mathrm{e}^{-M^{1/2}}} \Big(& c_{\mathrm{LA}}^{\mathrm{b}} \left(\mathrm{e}^{M^{1/2} z/\delta_{\mathrm{L}}} - \mathrm{e}^{-M^{1/2} z/\delta_{\mathrm{L}}} \right) \\ & + c_{\mathrm{LA}}^{\mathrm{s}} \left[\mathrm{e}^{M^{1/2}(1 - z/\delta_{\mathrm{L}})} - \mathrm{e}^{-M^{1/2}(1 - z/\delta_{\mathrm{L}})} \right] \Big). \end{aligned} \tag{7.106}$$

Equation 7.106 can even be written with hyperbolic functions

$$c_{\mathrm{LA}}(z) = \frac{c_{\mathrm{LA}}^{\mathrm{b}} \sinh\left(M^{1/2}(z/\delta_{\mathrm{L}})\right) + c_{\mathrm{LA}}^{\mathrm{s}} \sinh\left(M^{1/2}(1 - z/\delta_{\mathrm{L}})\right)}{\sinh M^{1/2}}. \tag{7.107}$$

To calculate the flux $N_{\mathrm{LA}}^{\mathrm{s}}$, the derivative of $c_{\mathrm{LA}}(z)$ is required:

$$\begin{aligned} \frac{\mathrm{d}c_{\mathrm{LA}}}{\mathrm{d}z} = \frac{1}{\sinh M^{1/2}} \Bigg(& c_{\mathrm{LA}}^{\mathrm{b}} \cosh\left[M^{1/2}(z/\delta_{\mathrm{L}})\right] \frac{M^{1/2}}{\delta_{\mathrm{L}}} \\ & + c_{\mathrm{LA}}^{\mathrm{s}} \cosh\left[M^{1/2}(1 - z/\delta_{\mathrm{L}})\right] \left(-\frac{M^{1/2}}{\delta_{\mathrm{L}}} \right) \Bigg). \end{aligned} \tag{7.108}$$

N^{s}_{LA} is now obtained according to Equation 7.36:

$$N^{s}_{LA} = -D_{LA}\left(\frac{dc_{LA}}{dz}\right)_{z=0} = \frac{k_{LA}M^{1/2}}{\tanh M^{1/2}}\left(c^{s}_{LA} - \frac{c^{b}_{LA}}{\cosh M^{1/2}}\right). \tag{7.109}$$

If diffusion through the gas film affects the flux, the expression

$$N^{s}_{LA} = N^{b}_{GA} = k_{GA}\left(c^{b}_{GA} - c^{s}_{GA}\right) \tag{7.110}$$

is combined with Equation 7.109 in order to eliminate the unknown surface concentration, c^{s}_{LA}.The result is

$$c^{s}_{LA} = \frac{k_{GA}c^{b}_{GA} + \left(k_{LA}M^{1/2}/\tanh M^{1/2}\right)\left(c^{b}_{LA}/\cosh M^{1/2}\right)}{k_{GA}K_{A} + \left(k_{LA}M^{1/2}/\tanh M^{1/2}\right)}. \tag{7.111}$$

Insertion of the concentration, Equation 7.111, into Equation 7.109 yields the final expression for the flux N^{s}_{LA} for first-order reactions

$$N^{s}_{LA} = \frac{c^{b}_{GA} - \left(K_{A}/\cosh M^{1/2}\right)c^{b}_{LA}}{\left(\tanh M^{1/2}/M^{1/2}\right)(K_{A}/k_{LA}) + (1/k_{GA})}, \tag{7.112}$$

where M is given by Equation 7.104. $M^{1/2}$ is often denoted as the Hatta number, *Ha*.

The enhancement factor E_A is obtained by dividing Equation 7.112 with the expression for physical absorption, Equation 7.112.

$$E_{A} = \left[\frac{(K_{A}/k_{LA}) + (1/k_{GA})}{(K_{A}/k_{LA})\left(\tanh M^{1/2}/M^{1/2}\right) + (1/k_{GA})}\right]\left[\frac{c^{b}_{GA} - \left(K_{A}/\cosh M^{1/2}\right)c^{b}_{LA}}{c^{b}_{GA} - K_{A}c^{b}_{LA}}\right] \tag{7.113}$$

7.2.4.3.4 Second-Order Reactions

For second-order reactions, no analytic expressions for the diffusion equation can be derived. In some cases, it is, however, possible to derive semianalytical, approximate solutions. Here, we will consider a bimolecular reaction

$$|\nu_{A}|\,A(g) + |\nu_{B}|\,B(l) \rightarrow \text{Products} \tag{7.114}$$

with the reaction kinetics

$$R = kc_{LA}c_{LB}. \tag{7.115}$$

Some second-order reactions can be considered to be pseudo-first-order ones, particularly in case one of the reactants (B) is present in large excess.

7.2.4.3.5 Pseudo-First-Order Reactions

For a pseudo-first-order reaction, the liquid-phase bulk concentration of component B is so high that the consumption rate of B in the liquid film is negligible, that is, $c_{LB} \approx$ constant in the liquid film. The reaction rate for component A is then

$$r_A = \nu_A k c_{LA} c_{LB}^b = \nu_A k' c_{LA}, \tag{7.116}$$

where $k' = k c_{LB}^b$. The reaction is of a pseudo-first-order, and the expressions derived for first-order kinetics, for N_{LA}^s and E_A, are valid even in this case. For the molar flux of component A,

$$N_{LA}^s = \frac{c_{GA}^b - \left(K_A/\cosh M^{1/2}\right) c_{LA}^b}{\left(\tanh M^{1/2} K_A / M^{1/2} k_{LA}\right) + (1/k_{GA})}, \tag{7.117}$$

where the Hatta number $Ha = M^{1/2}$ is defined as

$$M = -\frac{\nu_A k c_{LB}^b D_{LA}}{k_{LA}^2}. \tag{7.118}$$

The enhancement factor E_A is

$$E_A = \left[\frac{(K_A/k_{LA}) + (1/k_{GA})}{(K_A/k_{LA})\left(\tanh M^{1/2}/M^{1/2}\right) + (1/k_{GA})}\right]\left[\frac{c_{GA}^b - \left(K_A/\cosh M^{1/2}\right) c_{LA}^b}{c_{GA}^b - K_A c_{LA}^b}\right]. \tag{7.119}$$

7.2.4.3.6 Real Second-Order Reactions

Approximate solutions have been developed for the reaction kinetics

$$r_A = \nu_A R = \nu_A c_{LA} c_{LB} \tag{7.120}$$

for fast reactions where component A is consumed completely in the liquid film, that is, $c_{LA}^b = 0$. The classical expression for the enhancement factor E_A by van Krevelen and Hoftijzer [7] is

$$E_A = \frac{\sqrt{M\ [(E_i - E_A)/(E_i - 1)]}}{\tanh\sqrt{M\ [(E_i - E_A)/(E_i - 1)]}}, \tag{7.121}$$

where the Hatta number $Ha = M^{1/2}$ is defined as

$$M = -\frac{\nu_A k c_{LB}^b D_{LA}}{k_{LA}^2} \tag{7.122}$$

and E_i is defined as

$$E_i = 1 + \frac{\nu_A D_{LB} c_{LB}^b}{\nu D_{LA} c_{LA}^s}. \tag{7.123}$$

The flux at the phase interface is obtained from the relation

$$N_{LA}^{s} = k_{LA} c_{LA}^{s} E_A. \tag{7.124}$$

Note that the physical absorption rate in this case is given by $k_{LA} c_{LA}^{s}$ since c_{LA}^{b} is assumed to be zero. The enhancement factor, according to the van Krevelen–Hoftijzer expression, is shown in Figure 7.19. The figure shows that the enhancement factor approaches a limit, $E_A = E_i$, as the Hatta number, $M^{1/2}$, increases.

If diffusion in the gas film is limited by the absorption rate, then Equation 7.124 is set equal to the relation

$$N_{GA}^{s} = N_{GA}^{b} = k_{GA} \left(c_{GA}^{b} - c_{GA}^{s} \right). \tag{7.125}$$

The concentration c_{LA}^{s} at the gas–liquid interface is now obtained as

$$c_{LA}^{s} = \frac{c_{GA}^{b}}{K_A + E_A k_{LA} / k_{GA}}. \tag{7.126}$$

The expression for c_{LA}^{s} is now inserted into Equation 7.123, and E_i can be written as

$$E_i = 1 + \frac{\nu_A D_{LB} c_{LB}^{b} \left(K_A + E_A k_{LA} / k_{GA} \right)}{\nu_B D_{LA} c_{GA}^{b}} \tag{7.127}$$

and the flux, N_{LA}^{s}, as

$$N_{LA}^{s} = \frac{c_{GA}^{b}}{\left(K_A / E_A k_{LA} \right) + \left(1 / k_{GA} \right)}. \tag{7.128}$$

The molar flux N_{LA}^{s} is obtained from Equation 7.128, whereas the enhancement factor E_A is iteratively calculated from Equations 7.121 and 7.127. If the gas film resistance is negligible, $1/k_{GA}$ is set to zero in Equations 7.127 and 7.128. In this case ($k_{GA} \to \infty$), E_A is iterated directly from Equation 7.121.

To avoid an iterative procedure for E_A, several approximate explicit equations have been developed. They are summarized in Table 7.4.

7.2.4.3.7 Fast Reactions

Fast reactions are a special class of reactions with a finite rate. The basic assumptions, Equations 7.71 through 7.73, are thereby also valid for fast reactions. In these cases, the gas-phase component A is completely consumed in the liquid film, and the liquid-phase concentration of the gaseous component is zero:

$$c_{LA}^{b} = 0. \tag{7.129}$$

The expressions derived in the previous chapters for the enhancement factor E_A and the flux N_A can be used directly for fast reactions by setting the concentration $c_{LA}^{b} = 0$. The equations for N_A and E_A are hereby summarized for zero-, first-, and second-order reactions.

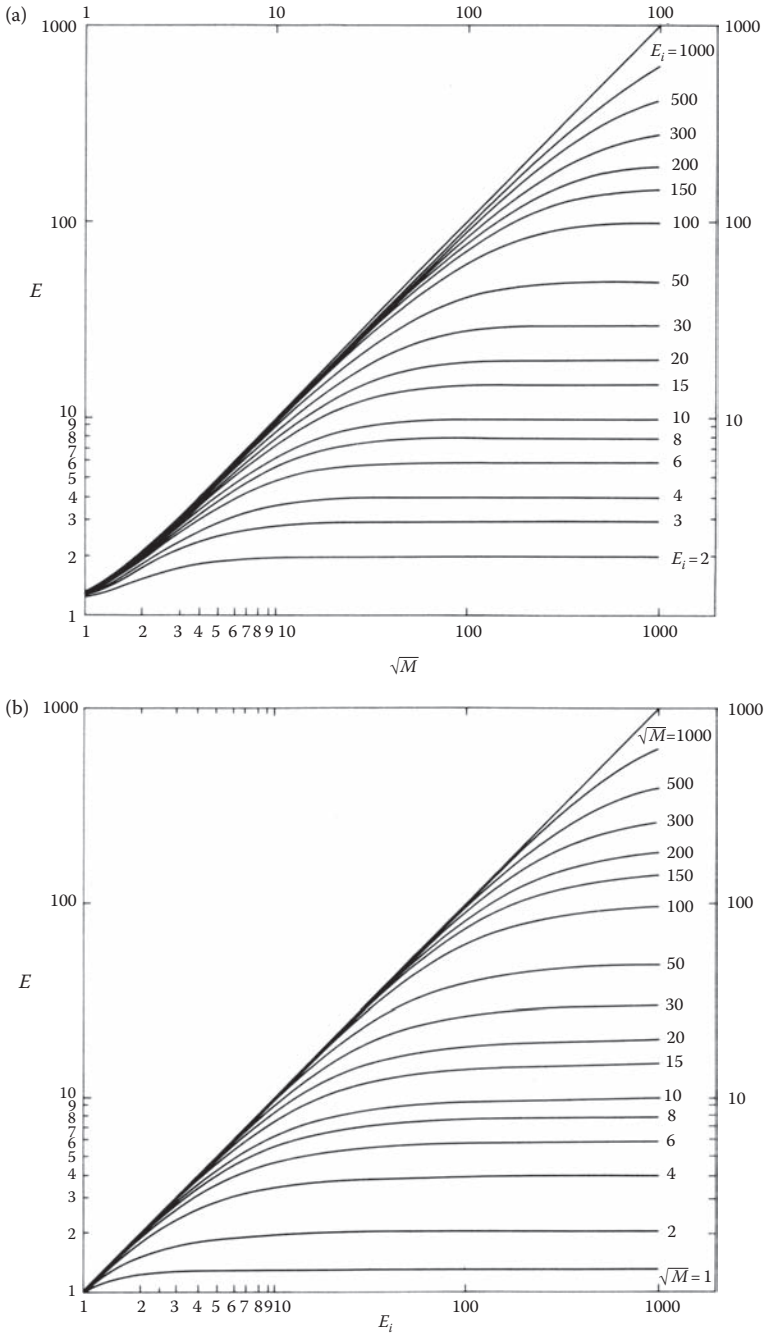

Enhancement factors for second-order reaction; for quiescent liquid or agitated liquid (film or Higbie models). Based on equation

$$E = \sqrt{\left(M \frac{E_i - E}{E_i - E}\right)} \Big/ \tanh \sqrt{\left(M \frac{E_i - E}{E_i - 1}\right)}$$

and corresponding equation for M'

FIGURE 7.19 Enhancement factor according to van Krevelen and Hoftijzer for rapid second-order reactions. (Data from Danckwerts, P.V., *Gas–Liquid Reactions*, McGraw-Hill, New York, 1970; van Krevelen, D.W. and Hoftijzer, P.J., *Rec. Trav. Chim. Pays-Bas*, 67, 563–599, 1948.)

TABLE 7.4 Explicit Expressions for the Enhancement Factor E_A for Second-Order Reactions

Authors	Formula $Ha = M^{1/2}$	m	n	Domain of Validity
Porter (1966)	$E = 1 + (E_i - 1)\left(1 - e^{-(Ha-1)/(E_i-1)}\right)$	1	1	$Ha > 2$
Baldi and Sicardi (1975)	$E = 1 + (E_i - 1)\left(1 - e^{-\left(\sqrt{1+Ha^2}-1\right)/(E_i-1)}\right)$	1	1	$Ha \geq 1$
De Santiago Farina (1970)	$E = -\dfrac{Ha^2}{2(E_i-1)} + \sqrt{\dfrac{Ha^4}{4(E_i-1)^2} + \dfrac{Ha^2}{E_i-1} + Ha^2}$	1	1	$Ha > 3$
De Coursey (1974)	$E = -\dfrac{Ha^2}{2(E_i-1)} + \sqrt{\dfrac{Ha^4}{4(E_i-1)^2} + \dfrac{E_i Ha^2}{E_i-1} + 1}$	1	1	$Ha \geq 1$
Yeramian et al. (1970)	$E = \dfrac{E_1^2}{2(E_i-1)}\left(\sqrt{1 + \dfrac{4(E_i-1)E_i}{E_1^2}} - 1\right)$, where $E_i = \dfrac{Ha}{\tanh(Ha)}$	1	1	$Ha > 1$
Wellek et al. (1978)	$E = 1 + \left(1 + \left(\dfrac{E_i-1}{E_1-1}\right)^{1/1.35}\right)^{1/1.35}$, where $E_1 = \dfrac{Ha}{\tanh(Ha)}$	1	1	$Ha > 1$
Kishnevskii et al. (1971)	$E = 1 + \dfrac{Ha}{\alpha}\left(1 - e^{-0.65Ha\sqrt{\alpha}}\right)$ and $\alpha = \dfrac{Ha}{E_i-1} + e^{[(0.68/Ha)-(0.45Ha/(E_i-1))]}$	1	1	$Ha > 1$
Karlsson and Bjerle (1980)	$E = \dfrac{\left(Ha^{-x} + E_i^{-x}\right)^{-1/x}}{\tanh\left(Ha^{-x} + E_i^{-x}\right)^{-1/x}}$ and $x = \dfrac{1}{2} + \dfrac{1}{m}$	$0.5 \leq m \leq 4$		$E_i \geq 2$

Source: Data from Charpentier, J.-C., *Multiphase Chemical Reactors*, A. Gianetto and P.L. Silveston (Eds), Hemisphere Publishing Corporation, Washington, DC, 1986.

7.2.4.3.8 Zero-Order Reaction

Equation 7.92 is valid, and the term $K_A c_{LA}^b M$ can be written as

$$K_A c_{LA}^b M = K_A c_{LA}^b \left(\frac{-\nu_A k D_{LA}}{2k_{LA}^2 c_{LA}^b}\right) = -\frac{\nu_A k D_{LA} K_A}{2k_{LA}^2}. \tag{7.130}$$

By defining another dimensionless parameter, M', as

$$M' = -\frac{\nu_A k D_{LA} K_A}{2k_{LA}^2 c_{GA}} \tag{7.131}$$

the flux N_{LA}^{s} can now be rewritten as follows, considering that $c_{LA}^{b} = 0$ according to Equation 7.90:

$$N_{LA}^{s} = \frac{c_{GA}^{b}(1 + M')}{(K_A/k_{LA}) + (1/k_{GA})}. \tag{7.132}$$

The enhancement factor, E_A, is obtained from Equation 7.92 with $c_{LA}^{b} = 0$, as

$$E_A = 1 + M'. \tag{7.133}$$

7.2.4.3.9 First-Order Reactions

Equation 7.112 is valid for the molar flux N_{LA}^{s} for first-order reactions. For fast first-order reactions, c_{LA}^{b} is zero and M is large ($M^{1/2}$ is the Hatta number). For large M values, we have

$$\frac{\tanh\sqrt{M}}{\sqrt{M}} \approx \frac{1}{\sqrt{M}} \tag{7.134}$$

because $\lim_{M\to\infty} \tan\sqrt{M} = 1$. Equation 7.112 for fast reactions is therefore

$$E_A = \frac{(K_A/k_{LA}) + (1/k_{GA})}{\left(K_A/k_{LA}\sqrt{M}\right) + (1/k_{GA})}. \tag{7.135}$$

7.2.4.3.10 Second-Order Reactions

For reaction kinetics defined in Equation 7.115, for a pseudo-first-order reaction, the same expressions are obtained for the flux and the enhancement factor, N_{LA}^{s} and E_A, as for fast first-order reactions, from Equations 7.117 and 7.119. Equations 7.130 and 7.131 can, therefore, be used for fast pseudo-first-order reactions, but the parameter M is defined as

$$M = -\frac{\nu_A k c_{LB}^{b} D_{LA}}{k_{LA}^{2}}. \tag{7.136}$$

For "real" second-order reactions, like the reaction kinetics in Equation 7.119, the expressions in Equations 7.121, 7.122, 7.127, and 7.128 are valid for the calculation of the flux and enhancement factor, N_{LA}^{s} and E_A. The van Krevelen–Hoftijzer approximation assumes that the liquid bulk concentration of component A equals zero, $c_{LA}^{b} = 0$.

7.2.4.3.11 Infinitely Fast Reactions

For infinitely fast reactions (instantaneous reactions), it is assumed that the components react completely in the liquid film. The reacting components cannot coexist in the liquid film, since the numerical value of the rate constant is very high. The components diffuse from the phase interface and the liquid bulk to the reaction plane in the liquid film where the reaction occurs. Let us now consider a bimolecular reaction

$$|\nu_A|\,(g) + |\nu_B|\,B(l) \rightarrow \text{Products} \tag{7.137}$$

with the reaction kinetics defined in Equation 7.116, in case of a very high value of the rate constant. The reaction zone coordinate is denoted as "z," and the concentration profiles for components A and B are illustrated in Figure 7.20.

For component A, in the interval $[0, z']$, the equation for diffusion

$$D_{\mathrm{LA}} \frac{\mathrm{d}^2 c_{\mathrm{LA}}}{\mathrm{d}z^2} = 0 \tag{7.138}$$

is analogous to the gas film equation. The molar flux $N^{\mathrm{s}}_{\mathrm{LA}}$ is obtained in a similar way as in Equation 7.65:

$$N^{\mathrm{s}}_{\mathrm{LA}} = \frac{D_{\mathrm{LA}}}{z'} \left(c^{\mathrm{s}}_{\mathrm{LA}} - c_{\mathrm{LA}}(z') \right). \tag{7.139}$$

When the reaction plane is considered, the concentration of component A is zero, $c_{\mathrm{LA}}(z') = 0$, and the flux can be written as

$$N^{\mathrm{s}}_{\mathrm{LA}} = \frac{D_{\mathrm{LA}} c^{\mathrm{s}}_{\mathrm{LA}}}{z'}. \tag{7.140}$$

For component B, in the interval $[z', \delta_{\mathrm{L}}]$, the equation for diffusion is

$$D_{\mathrm{LB}} \frac{\mathrm{d}^2 c_{\mathrm{LB}}}{\mathrm{d}z^2} = 0. \tag{7.141}$$

The molar flux of component B is

$$N^{\mathrm{b}}_{\mathrm{LB}} = -\frac{D_{\mathrm{LB}}}{\delta_{\mathrm{L}} - z'} \left(c^{\mathrm{b}}_{\mathrm{LB}} - c_{\mathrm{LB}}(z') \right). \tag{7.142}$$

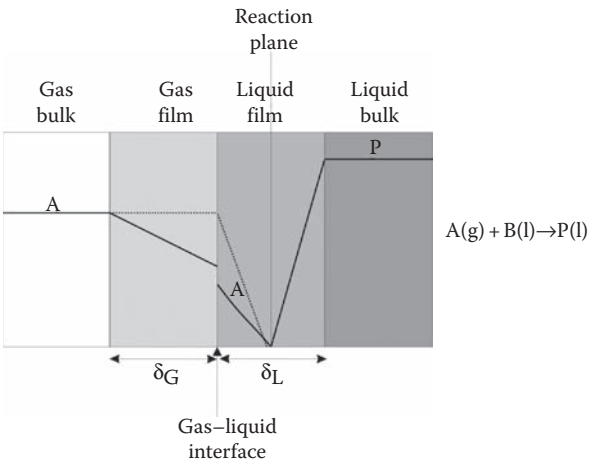

FIGURE 7.20 Concentration profiles in the gas and liquid films for an infinitely fast bimolecular reaction: (−) gas film resistance important and (....) gas film resistance negligible.

If we consider that $c_{LB}(z') = 0$, the flux can be written in a more simple way:

$$N_{LB}^{s} = -\frac{D_{LB}c_{LB}^{b}}{\delta_L - z'}. \tag{7.143}$$

The fluxes N_{LA}^{s} and N_{LB}^{s} are related to each other according to the reaction stoichiometry:

$$\frac{N_{LA}^{s}}{\nu_A} = -\frac{N_{LB}^{s}}{\nu_B}. \tag{7.144}$$

Insertion of Equations 7.140 and 7.143 into Equation 7.144 makes it possible to determine the reaction plane coordinate z':

$$z' = \frac{(\nu_B \delta_L / D_{LB} c_{LB})}{\left(\nu_A / D_{LA} c_{LA}^{s}\right) + \left(\nu_B / D_{LB} c_{LB}^{b}\right)}. \tag{7.145}$$

This expression can now be inserted into Equation 7.140, and a new expression for N_{LA}^{s} is obtained:

$$N_{LA}^{s} = D_{LA} c_{LA}^{s} \left(\frac{\left(\nu_A / D_{LA} c_{LA}^{s}\right) + \left(\nu_B / D_{LB} c_{LB}^{b}\right)}{\left(\nu_B \delta_L / D_{LB} c_{LB}^{b}\right)} \right). \tag{7.146}$$

After insertion of the liquid film coefficient $k_{LA} = D_{LA}/\delta_L$, the flux (N_{LA}^{s}) becomes

$$N_{LA}^{s} = k_{LA} c_{LA}^{s} \left(1 + \frac{\nu_A D_{LB} c_{LB}^{b}}{\nu_B D_{LA} c_{LA}^{s}} \right). \tag{7.147}$$

Note that the expression in the parenthesis, in Equation 7.147, is exactly the same as E_i in the van Krevelen–Hoftijzer approximation, Equations 7.121 and 7.123.

If the diffusion resistance is significant, the equation for the diffusion rate in the gas film

$$N_{GA}^{b} = N_{GA}^{s} = k_{GA} \left(c_{GA}^{b} - c_{GA}^{s} \right) \tag{7.148}$$

and the gas–liquid equilibrium at the interface

$$K_A = \frac{c_{GA}^{s}}{c_{LA}^{s}} \tag{7.149}$$

must be accounted for. After setting Equations 7.147 and 7.148 equal to each other and inserting Equation 7.149 for c_{GA}^{s}, the surface concentration c_{LA}^{s} can be determined explicitly:

$$c_{LA}^{s} = \frac{c_{GA}^{b} - (\nu_A k_{LB} / \nu_B k_{GA})\, c_{LB}^{b}}{K_A + (k_{LA}/k_{GA})}. \tag{7.150}$$

Here, the liquid film coefficient is defined as

$$k_{LB} = \frac{D_{LB}}{\delta_L} = \frac{D_{LB}}{D_{LA}} k_{LA}. \tag{7.151}$$

The expression for c^s_{LA}, Equation 7.150, is inserted into the expression for N^s_{LA}, Equation 7.147, and the final form of the molar flux, N^s_{LA}, is obtained:

$$N^s_{LA} = \frac{c^b_{GA} + (\nu_A D_{LB}/\nu_B D_{LA})\, K_A c^b_{LB}}{(K_A/k_{LA}) + (1/k_{GA})}. \tag{7.152}$$

If the diffusion resistance in the gas film is negligible, $1/k_{GA}$ can be set equal to zero. The enhancement factor, E_A, is obtained by dividing Equation 7.152 by the equation for physical absorption, Equation 7.91:

$$E_A = \frac{c^b_{GA} + (\nu_A D_{LB}/\nu_B D_{LA})\, K_A c^b_{LB}}{c^b_{GA} - K_A c^b_{LA}}. \tag{7.153}$$

For an infinitely fast reaction $c^b_{LA} = 0$, Equation 7.153 is reduced to

$$E_A = 1 + \frac{\nu_A D_{LB} c^b_{LB}}{\nu_B D_{LA} c^b_{GA}} K_A. \tag{7.154}$$

Equations 7.152 and 7.154 for the diffusion flux and the enhancement factor of component A show that the absorption rate of A is only determined by the concentration levels of A and B and their diffusion coefficients. For infinitely fast reactions, component A's absorption rate can be enhanced, if the concentration of component B is high in the liquid bulk. When the concentration of B increases, the reaction plane moves toward the phase interface as shown in Equation 7.145.

The equations derived here are valid for bimolecular, infinitely fast reactions. If several infinitely fast reactions occur simultaneously, a separate derivation of N_A must be performed for each and every reaction. In the case of several simultaneous, infinitely fast reactions, several reaction planes can coexist in the liquid film.

7.2.5 FLUXES IN REACTOR MASS BALANCES

The expressions that we obtained for the molar flux of very slow, slow, normal, fast, and infinitely fast reactions are inserted into the mass balances of the ideal reactor models. The molar flux at the gas–liquid interface was derived for ideal reactor models: for plug flow column reactors (Equations 7.15 and 7.16), for stirred tank reactors (Equations 7.22, 7.25, and 7.26), and for BRs (Equations 7.33 and 7.34):

$$N^b_{Gi} = N^s_{Gi} = N^s_{Li}. \tag{7.155}$$

The expression for molar flux, N_{LA}^{s}, was derived for different kinds of reactions. The flux from the liquid film to the liquid bulk N_{LA}^{b} (required for the mass balances) is equal to the flux from the liquid film to the solid surface, N_{LA}^{s}, for very slow reactions (no reaction in the liquid film). For other types of reactions, the flux N_{LA}^{b} is obtained from the concentration profile of the liquid bulk $c_{LA}(z)$ by calculating the derivative dc_{LA}/dz and inserting it into Equation 7.36.

In its most general form, the problem can be solved with $N + 2$ (N = number of reactions) differential equations (column reactor and BRs) or algebraic equations (CSTR). If the column reactor operates in a countercurrent mode, the mass balances pose a boundary value problem. For concurrent column reactors and BRs, the mass balances are solved as initial value problems.

The same numerical methods as those used to solve the homogeneous reactor models (PFR, BR, and stirred tank reactor) as well as the heterogeneous catalytic packed bed reactor models are used for gas–liquid reactor problems. For the solution of a countercurrent column reactor, an iterative procedure must be applied in case the initial value solvers are used (Adams–Moulton, BD, explicit, or semi-implicit Runge–Kutta). A better alternative is to solve the problem as a true boundary value problem and to take advantage of a suitable method such as orthogonal collocation. If it is impossible to obtain an analytical solution for the liquid film diffusion Equation 7.52, it can be solved numerically as a boundary value problem. This increases the numerical complexity considerably. For coupled reactions, it is known that no analytical solutions exist for Equation 7.52 and, therefore, the bulk-phase mass balances and Equation 7.52 must be solved numerically.

For systems with only one reaction, the number of necessary balance equations can be reduced by setting up a total balance both at the reactor inlet (i.e., liquid feed inlet) and at an arbitrary location in the reactor. This is illustrated for the concurrent case, for components A and B reacting according to

$$|\nu_A|A + |\nu_B|B \rightarrow \text{Products}. \tag{7.156}$$

The extent of the reaction is defined as

$$\xi = \frac{\dot{n}_{LA} + \dot{n}_{GA} - (\dot{n}_{0LA} + \dot{n}_{0GA})}{\nu_A} = \frac{\dot{n}_{LB} + \dot{n}_{GB} - (\dot{n}_{0LB} + \dot{n}_{0GB})}{\nu_B}. \tag{7.157}$$

The previous expression can be used instead of the four balance equations for A(l), A(g), B(l), and B(g). In many cases, component B's volatility is so low that the molar flow $\dot{n}_{0GB} \approx 0$. In this case, the system can be solved using the balance equations for A(l) and A(g), taking into account the stoichiometric relation.

For fast and infinitely fast reactions, the concentration of component A in the bulk phase is zero ($c_{LA} = 0$) and, consequently, the molar flow is also zero ($\dot{n}_{LA} = 0$). In this case, only the balance equation for A(g) and the stoichiometric relation in Equation 7.156 are needed.

The relation between component fluxes can be obtained from systems with only one chemical reaction by integrating the differential Equation 7.52:

$$\int_0^{\delta_L} D_{Li} \frac{d^2 c_{Li}}{dz^2}\, dz = -\int_0^{\delta_L} r_i\, dz = -\nu_i \int_0^{\delta_L} R\, dz. \tag{7.158}$$

By assuming that the diffusion coefficient D_{Li} is constant, the left-hand side yields

$$D_{Li} \frac{dc_{Li}}{dz}(z = \delta_L) - D_{Li} \frac{dc_{Li}}{dz}(z = 0) = -N_{Ni}^{b} + N_{Li}^{s}, \tag{7.159}$$

and a combination with Equation 7.158 yields for all components:

$$\frac{N_{Li}^{b} - N_{Li}^{s}}{\nu_i} = \int_0^{\delta_L} R\, dz. \tag{7.160}$$

For components A and B, Equation 7.160 yields a stoichiometric relation in the liquid film:

$$\frac{N_{LA}^{b} - N_{LA}^{s}}{\nu_A} = \frac{N_{LB}^{b} - N_{LB}^{s}}{\nu_B}. \tag{7.161}$$

If the reaction is a pseudo-first-order one with respect to A, it is necessary to apply Equation 7.156 for the calculation of c_{LB} and Equation 7.161 for the calculation of N_{LB}. The reason for this is that the concentration of B in the liquid bulk and liquid film changes in the reactor, although the concentration gradient in the liquid film is approximately zero.

The liquid volume flow in a continuous gas–liquid reactor can usually be assumed to be constant:

$$\dot{V}_L \approx \dot{V}_{0L}, \tag{7.162}$$

but the gas flow rate can fluctuate because of temperature variations, stoichiometry, differences in the reactant/product solubilities (K_i), and mass transfer properties (k_{Li}).

If the mass balances for all gas-phase components are included, the volumetric flow rate is obtained from the molar flow rate with the aid of the ideal gas law:

$$\dot{V}_G = \frac{\dot{n}_G RT}{P} \quad \text{where } \dot{n}_G = \sum \dot{n}_{Gi}. \tag{7.163}$$

For the simulation of gas–liquid reactors used in the synthesis of chemicals, a complete set of gas- and liquid-phase mass balances is usually needed. The reason is that the concentrations of chemical components are high in both gas and liquid phases, and chemical reactions proceed both in the liquid film and in the liquid bulk phase.

Chemical absorption is used in gas cleaning processes (e.g., gas stripping). The concentration of the absorbing gas is usually low, and the total pressure and volumetric flow of the gas can usually be assumed to be constant. A large mass transfer area is required

and, therefore, absorption processes are usually performed in packed columns. The low gas concentrations and high purification demand make it necessary to perform the process in a countercurrent mode. In the following, the dimensioning of absorption columns for fast and infinitely fast reactions is considered.

7.2.6 DESIGN OF ABSORPTION COLUMNS

Absorption columns are a special type of gas–liquid reactors for gas cleaning, for which a simplified model treatment is possible. For an absorption column, the mass balances can be considered in a simplified way. Let us consider an absorption column where an infinitely fast reaction occurs as

$$|\nu_A|\mathrm{A(g)} + |\nu_B|B(\mathrm{l}) \rightarrow \text{Products}. \tag{7.164}$$

A volume element in an absorption column is shown in Figure 7.21. For component A, according to Equation 7.13, the mass balance in the gas phase is

$$\frac{\mathrm{d}\dot{n}_{GA}}{\mathrm{d}\tau_L} + N_{GA}^{b} a_v \dot{V}_{0L}, \tag{7.165}$$

where the positive (+) sign shows that the column operates in a concurrent mode. The gas phase is assumed to consist only of component A and inert components. The total molar mass balance is obtained as

$$\dot{n}_G = \dot{n}_{G,\mathrm{inert}} + \dot{n}_{GA}, \tag{7.166}$$

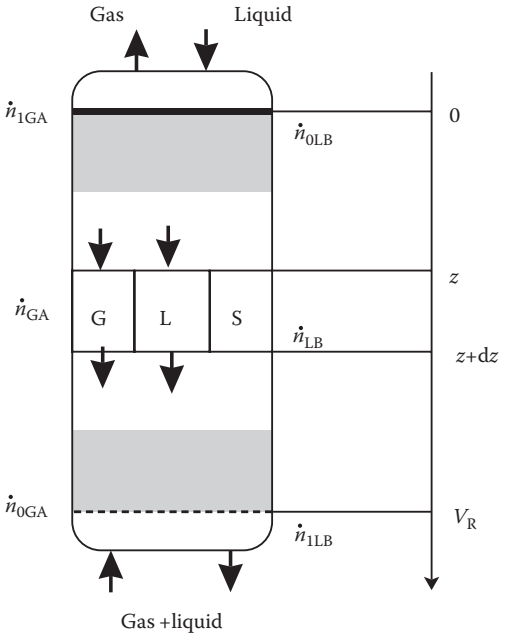

FIGURE 7.21 A volume element in a column reactor.

where $\dot{n}_G$ and $\dot{n}_{GA}$ are obtained from the molar fraction x_A.

$$\dot{n}_{GA} = x_A \dot{n}_G, \tag{7.167}$$

$$\dot{n}_{G,inert} = (1 - x_A)\dot{n}_G. \tag{7.168}$$

The total gas molar flow is expressed as

$$\dot{n}_G = \frac{\dot{n}_{G,inert}}{1 - x_A}. \tag{7.169}$$

At the bottom of the column, where the gas is fed into the column, the feed rate is

$$\dot{n}_{0G} = \frac{\dot{n}_{G,inert}}{1 - x_{0A}}. \tag{7.170}$$

Dividing Equation 7.169 by Equation 7.170 yields

$$\frac{\dot{n}_G}{\dot{n}_{0G}} = \frac{1 - x_{0A}}{1 - x_A} \tag{7.171}$$

and inserting Equation 7.171 into Equation 7.167 yields

$$\dot{n}_{GA} = \frac{x_A\,(1 - x_{0A})\dot{n}_{0G}}{1 - x_A}. \tag{7.172}$$

The derivative of Equation 7.169, as a function of the molar fraction, x_A, yields

$$\frac{d\dot{n}_{GA}}{dx_A} = \frac{(1 - x_{0A})\dot{n}_{0G}}{(1 - x_A)^2}. \tag{7.173}$$

By replacing the term $\dot{V}_{0L}\,d\tau_L$ with dV_R, in Equation 7.13, the volume of the absorption column can be determined from

$$\int_0^{V_R} dV_R = \frac{(1 - x_{0A})\dot{n}_{0G}}{a_v} \int_{x_A}^{x_{0A}} \frac{dx_A}{N_{GA}^b\,(1 - x_A)^2}. \tag{7.174}$$

After integrating and setting the fluxes (from the liquid film to the liquid bulk and from the liquid film to the solid surface) equal, $N_{GA}^b = N_{LA}^s$, the volume is obtained:

$$V_R = \frac{(1 - x_{0A})\dot{n}_{0G}}{a_v} \int_{x_A}^{x_{0A}} \frac{dx_A}{N_{LA}^s\,(1 - x_A)^2}. \tag{7.175}$$

Different expressions for the flux N_{LA}^s can be inserted into Equation 7.174, depending on whether the absorption is physical or chemical in nature. Chemical absorption kinetics is

often expressed with the partial pressure of component A. The relation between the molar fraction x_A and partial pressure p_A is as follows:

$$p_A = x_A P, \tag{7.176}$$

where P denotes the total pressure.

Insertion of Equation 7.176 into the dimensioning Equation 7.174 yields

$$V_R = \frac{(1 - x_{0A})\dot{n}_{0G}\, P}{a_v} \int_{P_A}^{p_{0A}} \frac{dp_A}{N_{LA}^s (P - p_A)^2}. \tag{7.177}$$

For low gas concentrations $(P - p_A)^2 \approx P^2$.

The expressions for the flux, N_{LA}^s, contain the concentration in the gas bulk, c_{GA}^b. If the calculations are performed with a partial pressure value, the relation

$$c_{GA}^b = \frac{p_A}{RT} \tag{7.178}$$

is inserted into the expression for N_{LA}^s. If the molar fraction x_A is used, the gas bulk-phase concentration c_{GA}^b is replaced with

$$c_{GA}^b = x_A \frac{P}{RT} \tag{7.179}$$

in the expressions for the flux N_{LA}^s.

For fast and infinitely fast reactions, the gas bulk-phase concentration is zero ($c_{LA}^b = 0$) in the expressions for the flux N_{LA}^s. c_{LA}^b is therefore eliminated in Equation 7.174.

In the case of equations for bimolecular reactions, the concentration of component B in the bulk phase, c_{LB}^b, is included in the expression for the flux N_{LA}^s. The concentration c_{LB}^b can be eliminated with a molar balance around the column as shown in Figure 7.21.

$$\frac{\dot{n}_{LA} - \dot{n}_{0GB}}{\nu_A} = \frac{\dot{n}_{1,LA} - \dot{n}_{LB}}{\nu_B}. \tag{7.180}$$

This equation assumes that $c_{LA}^b = 0$ and $c_{LB}^b = 0$ in the column. The molar flow $\dot{n}_B$ is given by

$$\dot{n}_{LB} = \dot{n}_{1,LB} + \frac{\nu_B}{\nu_A} \left(\dot{n}_{0,GA} - \dot{n}_{GA}\right). \tag{7.181}$$

The molar flow $\dot{n}_{1,LB}$ can be determined from the mass balance of the column. In an absorption process, the molar inflow of component B, $\dot{n}_{0,LB}$, is known and the outflow of A, $\dot{n}_{1,GA}$, is fixed. Since a certain gas content is assumed at the top of the column, the outflow $\dot{n}_{1,LB}$ is obtained accordingly:

$$\dot{n}_{1,LB} = \dot{n}_{0,LB} - \frac{\nu_B}{\nu_A} \left(\dot{n}_{0,GA} - \dot{n}_{1,GA}\right). \tag{7.182}$$

The liquid-phase density and volume flow are usually quite constant, and the concentration of B can be calculated:

$$\dot{n}_{\mathrm{LB}} = c^{\mathrm{b}}_{\mathrm{LB}} \dot{V}_{\mathrm{L}} \approx c^{\mathrm{b}}_{\mathrm{LB}} \dot{V}_{0\mathrm{L}}. \tag{7.183}$$

After inserting the relation, Equation 7.185, into Equations 7.181 and 7.182 as well as taking into account Equation 7.171 and the ideal gas law, we obtain the following expressions for the concentrations $c^{\mathrm{b}}_{1,\mathrm{LB}}$ and $c^{\mathrm{b}}_{\mathrm{LB}}$:

$$c^{\mathrm{b}}_{1,\mathrm{LB}} = c^{\mathrm{b}}_{0,\mathrm{LB}} - \frac{\nu_{\mathrm{B}}}{\nu_{\mathrm{A}}} \left(\frac{x_{0\mathrm{A}} - x_{1\mathrm{A}}}{1 - x_{1\mathrm{A}}} \right) \frac{\dot{V}_{0\mathrm{G}}}{\dot{V}_{0\mathrm{L}}} \frac{P}{RT}, \tag{7.184}$$

$$c^{\mathrm{b}}_{\mathrm{LB}} = c^{\mathrm{b}}_{1,\mathrm{LB}} + \frac{\nu_{\mathrm{B}}}{\nu_{\mathrm{A}}} \left(\frac{x_{0\mathrm{A}} - x_{\mathrm{A}}}{1 - x_{\mathrm{A}}} \right) \frac{\dot{V}_{0\mathrm{G}}}{\dot{V}_{0\mathrm{L}}} \frac{P}{RT}. \tag{7.185}$$

Insertion of Equations 7.179 and 7.185 instead of the concentrations $c^{\mathrm{b}}_{\mathrm{GA}}$ and $c^{\mathrm{b}}_{\mathrm{LB}}$ into the expressions for the flux $N^{\mathrm{s}}_{\mathrm{LA}}$ means that the flux $N^{\mathrm{s}}_{\mathrm{LA}}$ is written only as a function of the molar fraction x_{A}. In this case, the integral, Equation 7.175, can be solved analytically or numerically in order to determine the column volume.

7.2.7 GAS AND LIQUID FILM COEFFICIENTS, DIFFUSION COEFFICIENTS, AND GAS–LIQUID EQUILIBRIA

Especially in absorption processes, the gas film coefficient k_{GA} is defined with reference to component A's partial pressure. The molar flux of A through the gas film is

$$N^{\mathrm{b}}_{\mathrm{GA}} = N^{\mathrm{s}}_{\mathrm{GA}} = k_{\mathrm{GA}} \left(c^{\mathrm{b}}_{\mathrm{GA}} - c^{\mathrm{s}}_{\mathrm{GA}} \right), \tag{7.186}$$

but the formula can also be written using partial pressures:

$$N^{\mathrm{b}}_{\mathrm{GA}} = N^{\mathrm{s}}_{\mathrm{GA}} = k'_{\mathrm{GA}} \left(p_{\mathrm{A}} - p^{\mathrm{s}}_{\mathrm{A}} \right). \tag{7.187}$$

By implementing the ideal gas law

$$p_{\mathrm{A}} = c^{\mathrm{b}}_{\mathrm{GA}} RT, \quad p^{\mathrm{s}}_{\mathrm{A}} = c^{\mathrm{s}}_{\mathrm{GA}} RT, \tag{7.188}$$

the flux can then be written as

$$N^{\mathrm{b}}_{\mathrm{GA}} = k'_{\mathrm{GA}} \left(c^{\mathrm{b}}_{\mathrm{GA}} - c^{\mathrm{s}}_{\mathrm{GA}} \right) RT. \tag{7.189}$$

By setting Equation 7.186 equal to Equation 7.189, we obtain the relation between the concentration-based coefficient k_{GA} and the pressure-based coefficient k'_{GA}:

$$k_{\mathrm{GA}} = k'_{\mathrm{GA}} RT. \tag{7.190}$$

The gas–liquid equilibrium for component A is defined by the ratio

$$K_A = \frac{c^s_{GA}}{c^s_{LA}}. \tag{7.191}$$

For gases with low solubility, the equilibrium is often expressed with *Henry's constant.*

$$He_A = \frac{p^s_A}{c^s_{LA}}. \tag{7.192}$$

Insertion of the partial pressure p^s_A yields

$$He_A = \frac{c^s_{GA}}{c^s_{LA}} RT. \tag{7.193}$$

The relation between Henry's constant, He_A, and the gas–liquid equilibrium constant, K_A, is

$$K_A = \frac{He_A}{RT}. \tag{7.194}$$

Note that Henry's constant is sometimes defined with the partial pressure in the gas phase and the molar fraction in the liquid phase:

$$He'_A = \frac{p^s_A}{x^s_{LA}}. \tag{7.195}$$

The molar fraction in the liquid phase is defined accordingly:

$$x^s_{LA} = \frac{c^s_{LA}}{c_L}, \tag{7.196}$$

where the concentration c_L is the total liquid-phase concentration. Insertion of Equation 7.196 into Equation 7.195 yields the relation

$$He'_{LA} = \frac{p^s_A}{c^s_{LA}} c_L = He_A c_L. \tag{7.197}$$

For gas–liquid equilibria, it is very important to investigate how the gas–liquid equilibrium constant is defined. The constant for gas–liquid equilibrium (K_A) can be estimated from thermodynamic theories [9]. Henry's constant often yields an acceptable accuracy. Estimation methods for Henry's constant are discussed in reference [4]. There are several correlation equations for the liquid film coefficients (k_{GA} and k_{LA}), phase area-to-reactor volume, and gas holdup. These correlations are discussed in reference [10] and in Appendix 7. Usually, correlations for the mass transfer parameter $k_L a_v$ are more reliable

TABLE 7.5 Parameters for Different Kinds of Gas–Liquid Reactors

Reactor	$k_G \times 10^2$ (m/s)	$k_L \times 10^4$ (m/s)	a_v ($= A_{GL}/V_L$) (L/m)	$k_L a_v \times 10^2$ (L/s)	ε_L (%)
Stirred tank	∞	0.3–4	100–2000	0.3–80	20–95
Bubble column	1–5	1–4	50–600	0.5–24	60–98
Packed column countercurrent	0.07–5	0.4–2	10–350	0.04–7	2–25
Packed column concurrent	0.2–7.5	0.4–6	10–1700	0.04–102	2–95
Plate Column					
1. Sieve	1–15	1–20	100–200	1–40	10–95
2. Bubble-cup	1–5	1–5	100–400	1–20	10–95
Tube					
1. Horizontal	1–10	1–10	50–700	0.5–70	5–95
2. Vertical	1–20	2–5	100–2000	2–100	5–95

than those for the mass transfer coefficient k_L only, because $k_L a_v$ is determined in absorption experiments. Typical values for these entities in different types of gas–liquid reactors are listed in Table 7.5.

The diffusion coefficients in gas and liquid phases play an important role in the correlation equations, because the film thickness, film coefficient, and diffusion coefficient are related to each other. Gas-phase diffusion coefficients can be estimated using the Fuller–Schettler–Giddings equation [9] and the Wilke approximation [9] (Appendix 4). Liquid-phase diffusion coefficients are more difficult to estimate. A frequently used correlation equation for the liquid-phase diffusion coefficient is the Wilke–Chang equation [4,9], which is reliable for poorly soluble gases, in clean liquids and liquid mixtures (Appendix 6). There are also several other methods presented in the literature. The estimation methods are discussed in detail in the book *The Properties of Gases and Liquids* [9].

7.3 ENERGY BALANCES FOR GAS–LIQUID REACTORS

If the reaction enthalpies ($|\Delta H_r|$) obtain large values, the energy balance for the gas–liquid reactor must be taken into account. This is, in principle, a difficult task, since energy balances must be set up for the gas phase, liquid phase, and gas–liquid films. Here, we will only consider simplified cases in which the temperatures of the gas and the liquid are the same. In these cases, the reactor can be described with only one energy balance.

7.3.1 PLUG FLOW COLUMN REACTOR

We will look at a column reactor operating in a concurrent mode. The energy balance for a volume element ΔV_R, resembling the liquid-phase volume element ΔV_L and the surface element ΔA at the gas–liquid interface, can be written for a system with one chemical reaction accordingly:

$$\int_0^{\delta_L} R(-\Delta H_r)\,\mathrm{d}z\Delta A + R(-\Delta H_r)\Delta V_L = \Delta\dot{Q} + \dot{m}_L\, c_{pL}\Delta T + \dot{m}_G c_{pG}\Delta T. \qquad (7.198)$$

The first term describes the heat effects caused by chemical reactions in the liquid film. By applying the relation

$$\Delta\dot{Q} = U\Delta S(T - T_C) \tag{7.199}$$

and the definitions for the liquid holdup and interfacial contact area-to-reactor volume, ε_L and a_v, the energy balance can be written as

$$\int_0^{\delta_L} R(-\Delta H_r)\,\mathrm{d}z\, a_v \Delta V_R + R(\Delta H_r)\varepsilon_L \Delta V_R = U\Delta S(T - T_C) + (\dot{m}_L c_{pL} + \dot{m}_G c_{pG})\Delta T. \tag{7.200}$$

Considering that the ratio of heat transfer area to reactor volume is constant,

$$\frac{\Delta S}{\Delta V_R} = \frac{S}{V_R}, \tag{7.201}$$

and allowing the volume element to approach zero, $\Delta V \to 0$, Equation 7.200 is transformed to a differential equation

$$\frac{\mathrm{d}T}{\mathrm{d}V_R} = \frac{\int_0^{\delta} R(-\Delta H_r)\,\mathrm{d}z\, a_v + R(-\Delta H_r)\varepsilon_L - U(S/V_R)(T - T_C)}{c_{pL}\dot{m}_L + c_{pG}\dot{m}_G}. \tag{7.202}$$

If the liquid space time is included in the energy balance, Equation 7.202 is transformed to

$$\frac{\mathrm{d}T}{\mathrm{d}\tau_L} = \frac{\int_0^{\delta_L} R(-\Delta H_r)\,\mathrm{d}z\, a_v + R(-\Delta H_r)\varepsilon_L - U(S/V_R)(T - T_C)}{c_{pL}\rho_{0L} + c_{pG}\rho_{0G}(\dot{V}_{0G}/\dot{V}_{0L})}. \tag{7.203}$$

Liquids have much higher heat capacities than gases, and the term $c_{pL}\dot{m}_L \gg c_{pG}\dot{m}_G$ in the energy balance, because the heat flux supplied into the system by the liquid flow, is much greater than that supplied by the gas flow. For fast or slow reactions, one of the terms, $R(\Delta H_r)\varepsilon_L$, or the integral $\int_0 R(-\Delta H_r)\,\mathrm{d}z\, a_v$, can be excluded from the energy balance.

In systems with several reactions, the reaction term is replaced with sums of the reaction rates and energies from all reactions:

$$\frac{\mathrm{d}T}{\mathrm{d}V_R} = \frac{\int_0^{\delta_L} \sum_{j=1}^{s} R_j(-\Delta H_{rj})\,\mathrm{d}z\, a_v + \sum_{j=1}^{s} R_j(-\Delta H_{rj})\varepsilon_L - U(S/V_R)(T - T_C)}{c_{pL}\dot{m}_L + c_{pG}\dot{m}_G}. \tag{7.204}$$

and

$$\frac{\mathrm{d}T}{\mathrm{d}\tau_R} = \frac{\int_0^{\delta_L} \sum R_j(-\Delta H_{rj})\,\mathrm{d}z\, a_v + \sum R_j(-\Delta H_{rj})\varepsilon_L - U(S/V_R)(T - T_C)}{c_{pL}\rho_{0L} + c_{pG}\rho_{0G}(\dot{V}_{0G}/\dot{V}_{0L})}. \tag{7.205}$$

The above equations have the initial condition

$$T = T_0 \quad \text{at } V_R = 0 \quad \text{and} \quad \tau_L = 0 \tag{7.206}$$

that must be considered.

7.3.2 TANK REACTOR WITH COMPLETE BACKMIXING

For a completely backmixed tank reactor, an energy balance can be written in a manner similar to Equation 7.198. The energy balance now describes the whole reactor volume. For systems with only one equation, the energy balance obtains the form

$$\int_0^{\delta_L} R(-\Delta H_r)\,\mathrm{d}z\,A + R(-\Delta H_r)V_L = \dot{Q} + \dot{m}_L \int_{T_0}^{T} c_{pL}\,\mathrm{d}T + \dot{m}_G \int_{T_0}^{T} c_{pG}\,\mathrm{d}T. \quad (7.207)$$

If the definitions for liquid holdup ε_L and the ratio of interfacial contact area-to-reactor volume a_v as in Equations 7.18 and 7.19, together with the definition for the heat flux, $\dot{Q}$,

$$\dot{Q} = US(T - T_C) \quad (7.208)$$

are taken into account, balance Equation 7.207 can be written as follows:

$$\dot{m}_L \int_{T_0}^{T} c_{pL}\,\mathrm{d}T + \dot{m}_G \int_{T_0}^{T} c_{pG}\,\mathrm{d}T = \int_0^{\delta_L} R(-\Delta H_r)\,\mathrm{d}z a_v V_R + R(-\Delta H_r)\varepsilon_L V_R - US(T - T_C). \quad (7.209)$$

If the heat capacities can be considered independent of the temperature, the energy balance can be described by

$$\frac{T - T_0}{V_R} = \frac{\int_0^{\delta_L} R(-\Delta H_r)\,\mathrm{d}z\,a_v + R(-\Delta H_r)\varepsilon_L - U(S/V_R)(T - T_C)}{c_{pL}\dot{m}_L + c_{pG}\dot{m}_G}. \quad (7.210)$$

If the liquid residence time and densities are inserted, the energy balance is transformed to

$$\frac{T - T_0}{\tau_L} = \frac{\int_0^{\delta_L} R(-\Delta H_r)\,\mathrm{d}z\,a_v + R(-\Delta H_r)\varepsilon_L - U\,(S/V_R)\,(T - T_C)}{c_{pL}\rho_{0L} + c_{pG}\rho_{0G}}. \quad (7.211)$$

Generalizing this reasoning for an arbitrary number of reactions is easy. For systems with several reactions, the energy balances are

$$\frac{T - T_0}{V_R} = \frac{\int_0^{\delta_L} \sum_{j=1}^{s} R_j(-\Delta H_{rj})\,\mathrm{d}z\,a_v + \sum_{j=1}^{s} R_j(-\Delta H_{rj})\varepsilon_L - U\,(S/V_R)\,(T - T_C)}{c_{pL}\dot{m}_L + c_{pG}\dot{m}_G} \quad (7.212)$$

and, alternatively,

$$\frac{T - T_0}{\tau_L} = \frac{\int_0^{\delta_L} \sum_{j=1}^{s} R_j(-\Delta H_{rj})\,\mathrm{d}z\,a_v + \sum_{j=1}^{s} R_j(-\Delta H_{rj})\varepsilon_L - U\,(S/V_R)\,(T - T_C)}{c_{pL}\rho_{0L} + c_{pG}\rho_{0G}(\dot{V}_{0G}/\dot{V}_{0L})}. \quad (7.213)$$

7.3.3 BATCH REACTOR

For a BR, an approximate energy balance for a single chemical reaction can be written as

$$\int_0^{\delta_L} R(-\Delta H_r)\,dz\,A + R(-\Delta H_r)V_L = \dot{Q} + (m_L c_{pL} + m_G c_{pG})\frac{dT}{dt}. \tag{7.214}$$

If the definitions for liquid holdup, ε_L, interfacial contact area-to-reactor volume, a_v, and heat flux, $\dot{Q}$, Equations 7.18, 7.19, and 7.208, are inserted, the energy balance can be expressed in the form

$$\frac{dT}{dt} = \frac{\int_0^{\delta_L} R(-\Delta H_r)\,dz\,a_v V_R + R(-\Delta H_r)\varepsilon_L V_R - US(T - T_C)}{m_L c_{pL} + m_G c_{pG}}. \tag{7.215}$$

By considering that the mass of liquid per reactor volume is

$$\frac{m_L}{V_R} = \frac{\rho_{0L} V_{0L}}{V_R} \approx \rho_{0L}\varepsilon_{0L} \approx \rho_{0L}\varepsilon_L \tag{7.216}$$

and the mass of gas per reactor volume is

$$\frac{m_G}{V_R} = \frac{\rho_{0G} V_{0G}}{V_R} \approx \rho_{0G}\varepsilon_{0G} \approx \rho_{0G}\varepsilon_G, \tag{7.217}$$

Equation 7.215 assumes a new form:

$$\frac{dT}{dt} = \frac{\int_0^{\delta_L} R(-\Delta H_r)\,dz\,a_v + R(-\Delta H_r)\varepsilon_L - U(S/V_R)(T - T_C)}{c_{pL}\rho_{0L}\varepsilon_{0L} + c_{pG}\rho_{0G}\varepsilon_{0G}}. \tag{7.218}$$

For systems with several reactions, the energy balance can be written as

$$\frac{dT}{dt} = \frac{\int_0^{\delta_L} \sum_{j=1}^{s} R_j(-\Delta H_{rj})\,dz\,a_v + \sum_{j=1}^{s} R_j(-\Delta H_{rj})\varepsilon_L - U(S/V_R)(T - T_C)}{c_{pL}\rho_{0L}\varepsilon_{0L} + c_{pG}\rho_{0G}\varepsilon_{0G}}. \tag{7.219}$$

The initial conditions for the BR energy balance are given accordingly

$$T = T_0 \quad \text{at } t = 0. \tag{7.220}$$

If the pressure varies in a BR (nonisobaric operations), the expressions for heat capacities, c_{pL} and c_{pG}, should be replaced with the heat capacities for a constant volume, c_{vL} and c_{vG}.

7.3.4 COUPLING OF MASS AND ENERGY BALANCES

The energy balances for gas–liquid reactors presented above are coupled to the corresponding mass balances using the reaction rates (R_j). Analytical solutions of coupled energy and mass balances are impossible, because the reaction rate and equilibrium constants have exponential temperature dependencies. Including the energy balances means that the number of differential equations (batch and column reactor) or algebraic equations (CSTR) is increased by one (1). The same numerical methods as those described in Section 7.2.5 can be used. Examples of numerical solutions of reactor models are described in the following section.

7.3.5 NUMERICAL SOLUTION OF GAS–LIQUID REACTOR BALANCES

For nonisothermal cases, higher-order reactions (>1), and for systems with coupled reactions, the mass and energy balances for gas–liquid reactors are solved numerically. An example can be seen in Figure 7.22, in which *p*-cresol is chlorinated to mono- and dichloro-*p*-cresol following the reaction scheme below [11–13].

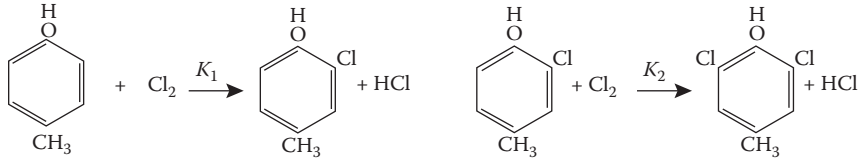

Figure 7.22 illustrates the numerical solution of concentrations in the liquid phase of a tank reactor. The simulation also gives the concentration profiles in the liquid film, as shown in Figure 7.22b. The algebraic equation system describing the gas- and liquid-phase mass balances is solved by the Newton–Raphson method, whereas the differential equation system that describes the liquid film mass balances is solved using orthogonal collocation. To guarantee a reliable solution of the mass balances, the mass balance equations have been solved as a function of the reactor volume. The solution of the mass balances for the reactor volume, V_R, has been used as an initial estimate for the solution for the reactor volume, $V_R + \Delta V_R$. The simulations show an interesting phenomenon: at a certain reactor volume, the concentration of the intermediate product, monochloro-*p*-cresol, passes a maximum. When the reactor volume—or the residence time—is increased, more and more of the final product, dichloro-*p*-cresol, is formed (Figure 7.22a). This shows that mixed reactions in gas–liquid systems behave in a manner similar to mixed reactions in homogeneous reactions (Section 3.8) [11,12].

Comparative simulations for a dynamic bubble column reactor are presented in Figure 7.23. The time-dependent mass balances (axial dispersion model) and the partial differential equations (PDEs) were discretized with respect to the reactor length coordinate. Finite differences were used for the discretization of the reactor length coordinate, while global collocation was used for film equations. The original system of PDEs was

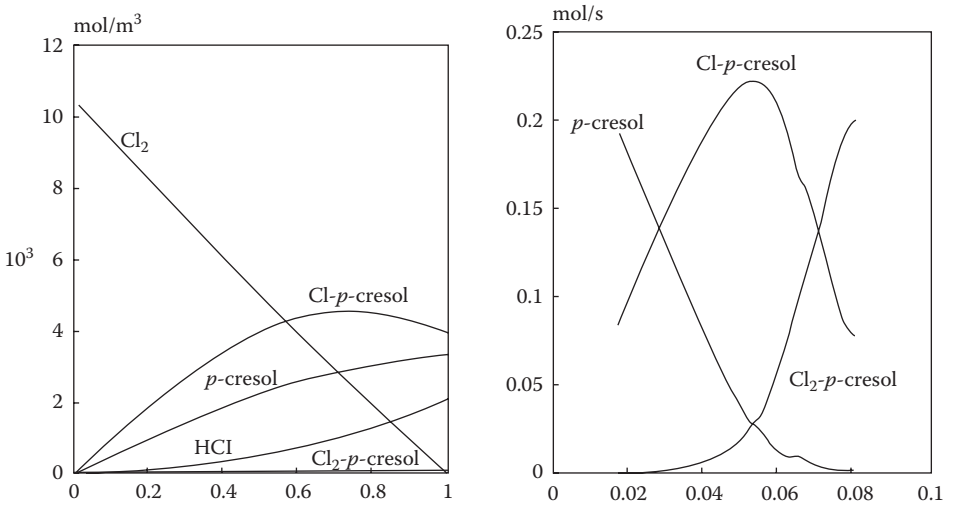

FIGURE 7.22 (a) Simulated concentration profiles in a gas–liquid tank reactor; chlorination of *p*-cresol to monochloro- and dichloro-*p*-cresol. The concentration is given as a function of the reactor volume. (b) Concentrations in the liquid film at the reactor volume $V_R = 0.04\ m^3$.

thus converted into a system of ODEs (an initial value problem), which was integrated forward by the BD method (Appendix 2). For the simulation results, see Figure 7.23, which shows how the concentration profiles of monochloro- and dichloro-*p*-cresol develop.

A requirement for modeling gas–liquid reactors is that the gas and liquid diffusion coefficients and mass transfer coefficients are known. For an estimation of the diffusion coefficients in the gas and liquid phases, see Appendices 4 and 6, respectively. Estimation of mass transfer coefficients is considered in Appendices 5 and 7, and methods for calculating the gas solubilities are discussed in Appendix 8.

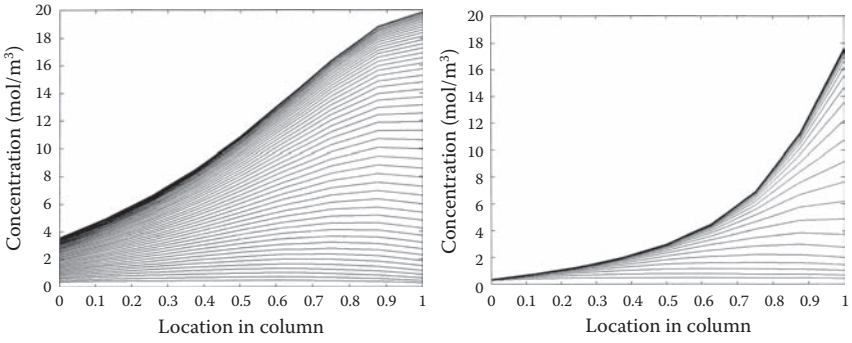

FIGURE 7.23 Simulation of concentration profiles in a bubble column, monochloro-*p*-cresol (left) and dichloro-*p*-cresol (right).

REFERENCES

1. Shah, Y.T., *Gas Liquid Solid Reactor Design*, McGraw-Hill, New York, 1979.
2. Trambouze, P., van Landeghem, H., and Wauquier, J.P., *Chemical Reactors—Design/Engineering*, Editions Technip, Paris, 1988.
3. Doraiswamy, L.K. and Sharma, M.M., *Heterogeneous Reactions: Analysis, Examples and Reactor Design*, Vol. 2, Wiley, New York, 1984.
4. Deckwer, W.D., *Reaktionstechnik in Blasensäulen*, Otto Salle Verlag, Frankfurt a.M. and Verlag Sauerländer, Aarau, 1985.
5. Charpentier, J.-C., Mass-transfer rates in gas–liquid absorbers and reactors, in *Advances in Chemical Engineering*, Vol. 11, Academic Press, New York, 1981.
6. Danckwerts, P.V., *Gas–Liquid Reactions*, McGraw-Hill, New York, 1970.
7. van Krevelen, D.W. and Hoftijzer, P.J., Kinetics of gas–liquid reactions, *Rec. Trav. Chim. Pays-Bas*, 67, 563–599, 1948.
8. Charpentier, J.-C., Mass transfer coupled with chemical reaction, Chapter 2, in A. Gianetto and P.L. Silveston (Eds), *Multiphase Chemical Reactors*, Hemisphere Publishing Corporation, Washington, DC, 1986.
9. Reid, R.C., Prausnitz, J.M., and Poling, P.J., *The Properties of Gases and Liquids*, 4th Edition, McGraw-Hill, New York, 1988.
10. Myllykangas, J., *Aineensiirtokertoimen, neste—ja kaasuosuuden sekä aineensiirtopintaalan korrelaatiot eräissä heterogeenisissä reaktoreissa*, Institutionen for teknisk kemi, Åbo Akademi, Turku/Åbo, Finland, 1989.
11. Romanainen, J.J. and Salmi, T., Numerical strategies in solving gas–liquid reactor models—1. Stagnant films and a steady state CSTR, *Comput. Chem. Eng.*, 15, 767–781, 1991.
12. Salmi, T., Wärnå, J., Lundén, P., and Romanainen, J., Development of generalized models for heterogeneous chemical reactors, *Comput. Chem. Eng.*, 16, 421–430, 1992.
13. Darde, T., Midoux, N., and Charpentier, J.-C., Reactions gaz-liquide complexes: Contribution à la recherche d'un outil de modélisation et de prédiction de la sélectivité, *Entropie*, 109, 92–109, 1983.

CHAPTER 8

Reactors for Reactive Solids

8.1 REACTORS FOR PROCESSES WITH REACTIVE SOLIDS

Chemical processes in which the solid phase changes during the reaction are of considerable industrial importance. Three types of reactions take place in these kinds of processes: reactions between a gas and a solid component; reactions between a liquid and a solid component; and reactions between a gas, a liquid, and a solid component. The majority of the processes with a solid phase are two-phase reactions, but three-phase processes also exist. For three-phase systems, the liquid phase is often used as a solvent, and a suspension is facilitated for the reactive gas and solid phases.

In reactions between a solid and a fluid phase, it is important to note the amount of solid-phase changes during the reaction. If all reaction products are gases, the solid phase shrinks during the reaction. The reacting solid particle decreases in size, even when the differences in densities between the solid reactant and the solid product are large: tensions in the product layer around the solid particle are developed, and the product layer is continuously peeled away from the surface of the reactant.

A few processes with reactive solids are listed in Table 8.1. Oxidation of zinc ore, that is, zinc sulfide, is a process in which the size of the reactive solid particle remains approximately the same: zinc sulfide is oxidated to zinc oxide. Similar reactions occur, for example, in the oxidation process of pyrite to hematite. Reduction processes of metallic oxides with hydrogen in the production of pure metals are also processes in which the size of the solid phase remains unchanged. Another example of a reduction process is the reduction of magnetite to metallic iron.

In organo-chemical processes, there are also reactions involving a solid phase: the cellulose derivative, carboxymethyl cellulose (CMC), is formed from Na-cellulose suspended in a liquid phase and monochloroacetic acid is dissolved in the liquid phase, usually

TABLE 8.1 Processes Involving a Solid Reactive Phase

Oxidation of sulfur-containing ores to oxides

$2ZnS(s) + 3O_2(g) \rightarrow 2ZnO(s) + 2SO_2(g)$

$4Fe_3S_2(s) + 11O_2(g) \rightarrow 8SO_2(g) + 2Fe_2O_3(s)$

Reduction of metal oxides to metals

$Fe_3O_4(s) + H_2 \rightarrow 3Fe + 4H_2O$

Nitration of calcium carbide to cyanamide

$CaC_2(s) + N_2 \rightarrow CaCN_2 + C$ (amorphous)

Combustion of carbon

$C(s) + O_2(g) \rightarrow CO_2(g)$

$2C(s) + O_2(g) \rightarrow 2CO(g)$

$C(s) + CO_2 \rightarrow 2CO(g)$

Water–gas reaction

$C(s) + H_2O(g) \rightarrow CO(g) + H_2(g)$

$C(s) + 2H_2O(g) \rightarrow CO_2 + 2H_2(g)$

Limestone combustion

$CaCO_3(s) \rightarrow CaO(s) + CO_2$

Hydration

$CaO(s) + H_2O(l) \rightarrow Ca(OH_2)$

Production of CS_2

$C(s) + 2S(g) \rightarrow CS_2(g)$

Production of sodium cyanide

$NaNH_2(l) + C(s) \rightarrow NaCN(l) + H_2(g)$

Production of sodium thiosulfate

$NaSO_3(aq) + S(g) \rightarrow Na_2S_2O_3(aq)$

Production of sodium hydride

$2Na(l, \text{dispersed in oil}) + H_2(g) \rightarrow 2NaH(s)$

Production of sodium borohydride

$4NaH(s) + B(OCH_3)_3(l) \rightarrow NaBH_4(s) + 3NaOCH_3(s)$

Production of CMC

$$\underset{\text{(Na-cellulose)}}{\text{cell-O}^-\text{-Na}^+(s)} + CH_2ClCOO^-Na^- \rightarrow \underset{\text{(CMC)}}{\text{cell-O-}CH_2COO^-Na(s)} + NaCl(l)$$

cell = anhydroglucose unit in cellulose

in 2-propanol. The reducing agent, Na-borohydride, is industrially produced from solid sodium hydride and trimethyl borate dissolved in mineral oil. In the above-mentioned processes, the solid phase remains relatively constant in size during the reaction.

The combustion of coal in different forms (wood, peat, and coal) represents an example of a process in which the solid phase disappears almost completely during the reaction. The main products are gases such as CO and CO_2. The production of CS_2, sodium cyanide, and sodium thiosulfate is another process in which the size of the solid phase changes remarkably (Table 8.1).

Several kinds of reactors are used in carrying out reactions involving a solid phase. The most important kinds of fluid–solid reactors are illustrated in Figure 8.1 [1]. Coal

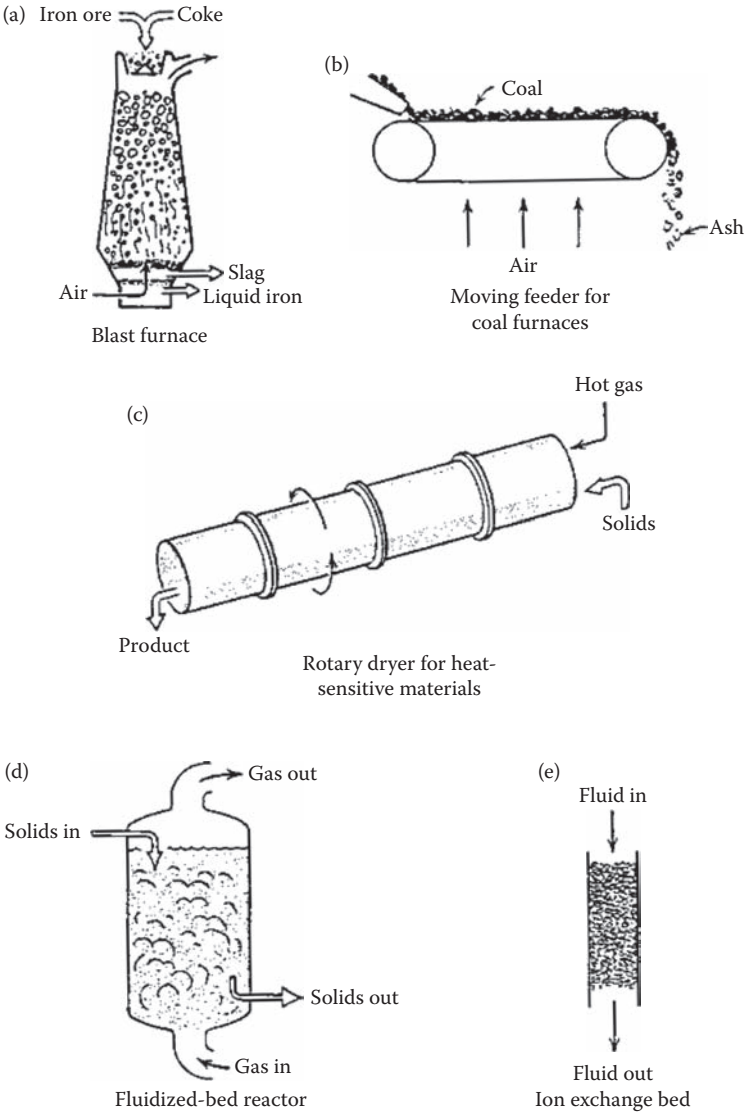

FIGURE 8.1 Typical reactor types for gas–solid and liquid–solid reactions: (a) a blast furnace, (b) a moving bed for coal combustion, (c) a rotary dryer for heat-sensitive materials, (d) a fluidized bed, and (e) an ion exchanger. (Data from Levenspiel, O., *Chemical Reaction Engineering*, 3rd Edition,Wiley, New York, 1999.)

combustion can be facilitated in semicontinuous packed beds where the gas flows through a fixed bed of solid particles. Another similar liquid-phase process is an ion-exchange process in which the liquid phase flows through a packed bed of ion-exchange resin granules (Figure 8.1e).

Combustion processes can very well be carried out in fluidized beds (Figure 8.1d), whose hydrodynamics considerably resemble those of catalytic fluidized beds (Section 4.3). It is sometimes favorable to carry out the gas–solid reaction so that the solid product is

continuously removed from the bed; this type of reactor is called a moving bed reactor (Figure 8.1b). A blast furnace is also a moving bed reactor (Figure 8.1a). It is used for the reduction of iron ore to metallic iron. Tank reactors, BRs, and semibatch reactors are often used for carrying out liquid–solid reactions. For instance, the production of CMC is carried out industrially in a BR, whereas sodium borohydride is produced in continuous tanks-in-series reactors.

In mathematical modeling of reactors with a reactive solid phase, the description of changes in the solid phase is of considerable importance. Several models have been proposed for the reactive solid phase. The solid particle can be assumed to be porous, and the chemical reaction and diffusion are assumed to occur simultaneously in the pores of the particles, similar to porous catalyst particles (Section 4.2.2). This model is called the *porous particle model*. If the particle is nonporous, the chemical reaction only takes place on the outer surface of the particle. If the products are gases/liquids, or if the solid product is continuously peeled away from the surface, the particle shrinks continuously as the reaction proceeds. This model is called the *shrinking particle model*. A reactive nonporous particle often forms a porous product layer or an ash layer around the particle. At the same time, the core of the particle remains unreacted. This is called the *product layer model* or the *ash layer model*. The shrinking particle model and the product layer model are illustrated in Figures 8.2 and 8.3 [1]. More advanced models have also been developed [2], for example, the *grain model*. In the grain model, the solid particle consists of smaller nonporous solid particles. These microparticles form macroparticles. The mass transfer processes occur by diffusion, and the reactions take place on the surfaces of the nonporous microparticles. A particle according to the grain model is shown in Figure 8.4 [4].

The question is, which model should be chosen for a particular case? Experiments have demonstrated that solid particles react with gases, forming a thin reaction zone on the surface of the particle rather than causing a simultaneous reaction in the whole particle. This implies that the shrinking particle model and the ash layer model can often be used for porous particles. The grain model is probably the most realistic one for solid particles, although the mathematical treatment becomes complicated because of the large number of parameters required than in the case of simpler models. From here on, we will concentrate on the shrinking particle and ash layer models, as these are also the basic building blocks of the grain model.

The strongest emphasis is on gas–solid reactions, but the theories presented can also be directly applied to liquid–solid cases. The physical properties and mass transfer parameters for the gas phase, such as the diffusion coefficient (D_{GA}) and the mass transfer coefficient (k_{LA}), must be replaced by equivalent parameters in the liquid phase (D_{LA}, k_{LA}).

8.2 MODELS FOR REACTIVE SOLID PARTICLES

8.2.1 DEFINITIONS

Here, we will mainly consider reactions between a gas-phase component A and a solid-phase component B. The stoichiometry of the reaction is

$$|\nu_A|\,A(g) + |\nu_B|\,B(s) \rightarrow \text{products}.$$

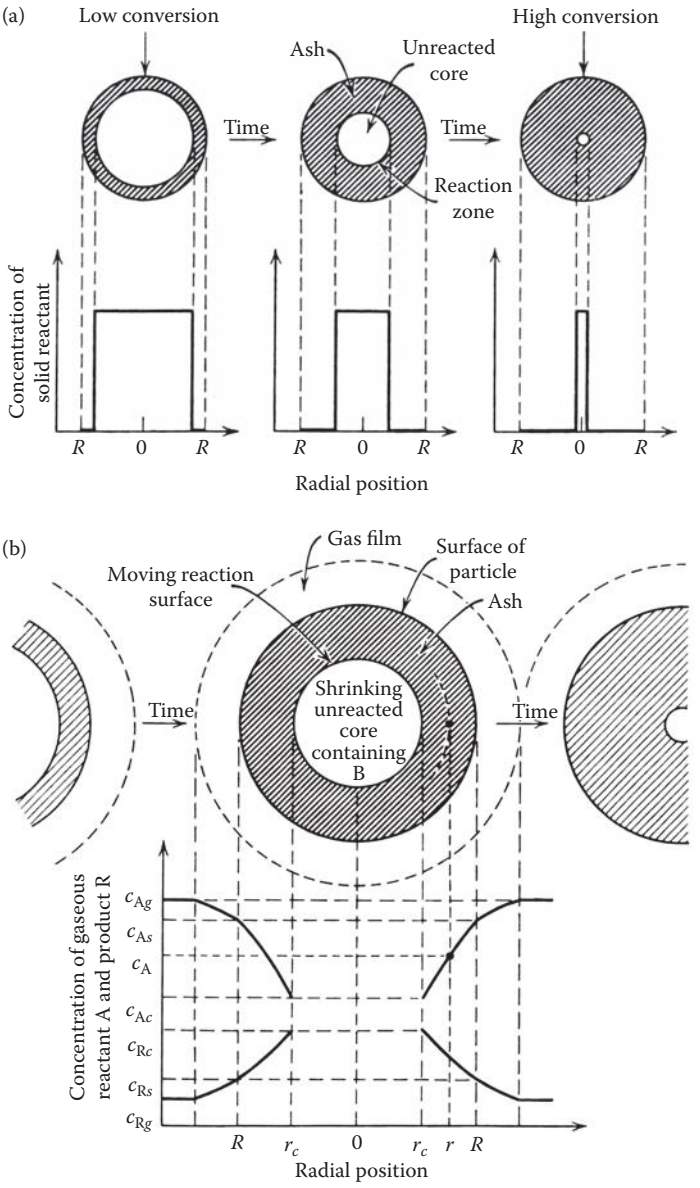

FIGURE 8.2 (a) A reactive particle with a product layer. (b) Reactant and product concentrations for the reaction A(g) + B(s) → R(g) + S(s) in a solid particle with a product layer. (Data from Levenspiel, O., *Chemical Reaction Engineering*, 3rd Edition,Wiley, New York, 1999.)

The products can be either gaseous or solid components (or both). The kinetics of the reaction is defined according to the available particle surface area:

$$RA = (\,)\,\frac{\text{mol}}{\text{m}^2\text{s}}\,(\,)\,\text{m}^2,$$

where R denotes the reaction rate and A denotes the particle area.

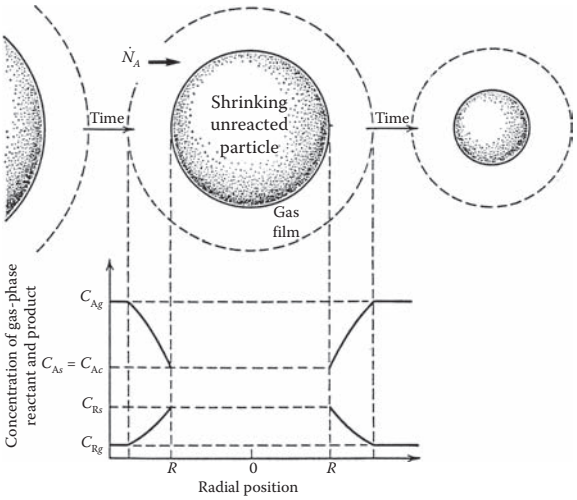

FIGURE 8.3 Reactant and product concentrations for the reaction A(g) + B(s) → R(g) in a shrinking particle. (Data from Levenspiel, O., *Chemical Reaction Engineering*, 3rd Edition,Wiley, New York, 1999.)

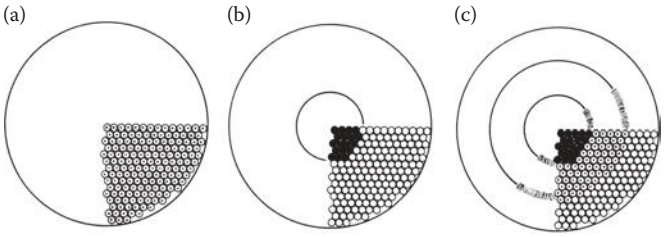

FIGURE 8.4 Particle structures according to the grain model. (Data from Ranz, W.E. and Marshall, W.R., *Chem. Eng. Prog.* , 48, 141–173, 1952.)

The solid reactant B is assumed to be nonporous, and the spherical particle has the radius R at the beginning of the reaction and the radius r after a certain reaction time. The conversion of B, η_B, is related to the particle radius with fundamental relations. The concentration of B in the particle x_B is expressed in molar fractions. The particle has density ρ_p, and the molar mass of B is M_B. The conversion of B is defined as

$$\eta_B = \frac{\eta_{0B} - n_B}{n_{0B}}, \tag{8.1}$$

where n_{0B} is the initial amount of B in the particle and n_B is the amount of B at the reaction time t. The amounts of component B at the beginning and at time t, n_{0B} and n_B, can be

related to molar mass M_B according to

$$\eta_{0B} = \frac{m_{0B}}{M_B}, \quad n_B = \frac{m_B}{M_B}, \tag{8.2}$$

which implies that Equation 8.3 can be written in the form

$$\eta_B = \frac{m_{0B} - m_B}{m_{0B}}. \tag{8.3}$$

The masses m_{0B} and m_B can now be related to the particle volumes:

$$V_{0p} = \frac{4}{3}\pi R^3, \quad V_p = \frac{4}{3}\pi r^3, \tag{8.4}$$

which means that Equation 8.1 can be expressed as

$$\eta_B = 1 - \frac{V_p}{V_{0p}}. \tag{8.5}$$

This gives the relation between the conversion and the particle radius:

$$\eta_B = 1 - \left(\frac{r}{R}\right)^3 \tag{8.6}$$

or

$$\frac{r}{R} = (1 - \eta_B)^{1/3}. \tag{8.7}$$

The mass balance for a solid component B in any kind of reactor with stationary particles is

$$[\text{generated B}] = [\text{accumulated B}]. \tag{8.8}$$

For one particle, according to Equations 8.27 and 8.8, we obtain

$$\frac{dn_B}{dt} = r_B A. \tag{8.9}$$

The stoichiometry $|\nu_A|A + |\nu_B|B \rightarrow$ products gives the generation rates of components A and B; accordingly,

$$r_A = \nu_A R, \tag{8.10}$$

$$r_B = \nu_B R, \tag{8.11}$$

where R is the reaction rate.

The outer surface area A for spherical particles is

$$A = 4\pi r^2. \tag{8.12}$$

The amount of substance B, n_B, in the particles can be related to the particle radius r. The amount of substance is

$$n_B = x_B n, \tag{8.13}$$

where n denotes the total amount of substance in the particle and x_B is component B's molar fraction. The total amount of substance is

$$n = \frac{m}{M}, \tag{8.14}$$

where m is the mass of the particle and M is the molar mass of the solid material. The mass, m, is obtained from

$$m = \rho_p V_p = \rho_p \frac{4}{3}\pi r^3 \tag{8.15}$$

for a spherical particle. The derivative, dn_B/dt, is

$$\frac{dn_B}{dt} = \frac{d}{dt}\left(\frac{x_B \rho_p (4/3)\pi r^3}{M}\right) \tag{8.16}$$

and it can be rewritten as

$$\frac{dn_B}{dt} = \frac{x_B \rho_p}{M} 4\pi r^2 \frac{dr}{dt}. \tag{8.17}$$

The relation in Equation 8.17; the definition of the outer surface area, Equation 8.12; and the stoichiometric relation, Equation 8.11, are inserted into the balance Equation 8.9. The time derivative is now obtained as

$$\frac{dr}{dt} = \frac{M}{x_B \rho_p} \nu_B R\left(c^s\right), \tag{8.18}$$

where $R(c^s)$ denotes the fact that the reaction rate is dependent on the concentration at the phase interface.

Equation 8.18 relates the particle radius to the surface reaction rate in a general way. The surface concentration, c^s, is highly dependent on the conditions on the reactive surface. Let us now consider two extreme cases: a particle with a porous product layer (ash layer model) and the shrinking particle model.

8.2.2 PRODUCT LAYER MODEL

A particle with a porous product layer is divided into three zones: the gas film around the product layer, the porous product layer, and the unreacted solid material. The structure of the particle is shown in Figure 8.2. The gas-phase component A diffuses through the gas film and product layer to the interface, where chemical reactions occur. The gas-phase product, P, has the opposite transport route. The molar flux of A is denoted as N_A, and the positive transport direction is given in Figure 8.2.

For the gas film, the molar flux of component A is

$$N_A = k_{GA}\left(c_A^b - c_A^*\right), \tag{8.19}$$

where c_A^b and c_A^* denote the concentrations in the bulk phase and on the particle surface, respectively. In the porous product layer, the components are transported due to diffusion effects. At steady state, the mass balance for component A in an infinitesimally thin layer, the product layer, can be written as

$$(N_A A)_{in} = (N_A A)_{out}, \tag{8.20}$$

where A is the size of the interface. For a spherical particle, the interface area A is defined by Equation 8.12.

The diffusion flux N_A is expressed using Fick's law:

$$N_A = +D_{eA}\frac{dc_A}{dr}, \tag{8.21}$$

where D_{eA} is the effective diffusion coefficient in a porous layer (Appendix 4); the positive (+) sign in Equation 8.21 depends on the choice of the positive direction of the molar flux (Figure 8.2). If the relations in Equations 8.12 and 8.21 are inserted into Equation 8.20, we obtain

$$\left(D_{eA}\frac{dc_A}{dr}4\pi r^2\right)_{in} = \left(D_{eA}\frac{dc_A}{dr}4\pi r^2\right)_{out}. \tag{8.22}$$

The difference $(\cdot)_{in} - (\cdot)_{out}$ above is denoted as $\Delta(\cdot)$, and the equation is divided by the radius increment Δr:

$$\frac{\Delta(D_{eA}(dc_A/dr)r4\pi r^2)}{r^2\Delta r} = 0. \tag{8.23}$$

By allowing the increment to approach zero ($\Delta r \to 0$), we obtain the differential equation

$$\frac{d\left(D_{eA}(dc_A/dr)r^2\right)}{r^2 dr} = 0, \tag{8.24}$$

which is the basic form of the mass balance of component A in a porous, spherical layer. The diffusion coefficient D_{eA} can usually be taken as constant and independent of the radius r. With these assumptions, and by derivation, we obtain the equation

$$D_{eA}\left(\frac{d^2c_A}{dr^2} + \frac{2}{r}\frac{dc_A}{dr}\right) = 0, \tag{8.25}$$

which implies that

$$\frac{d^2c_A}{dr^2} + \frac{2}{r}\frac{dc_A}{dr} = 0. \tag{8.26}$$

If we use the notation $dc_A/dr = y$, the differential equation is transformed to

$$\frac{dy}{dr} = -\frac{2}{r}y, \tag{8.27}$$

and a differential equation with separable variables can be written as follows:

$$\int \frac{dy}{y} = -2\int \frac{dr}{r}. \tag{8.28}$$

Finally, the solution is obtained:

$$\ln y = -2\ln r + \ln C, \tag{8.29}$$

where C is the integration constant. The solution of Equation 8.29 yields $y = dc_A/dr$:

$$y = \frac{C}{r^2}. \tag{8.30}$$

Taking into account that $y = dc_A/dr$ and integrating Equation 8.30 *once more*, the concentration profile of A is obtained accordingly:

$$c_A = -\frac{C}{r} + C', \tag{8.31}$$

where C is a new integration constant. At the surface of the particle ($r = R$), the concentration of component A, c_A^*, is

$$c_A^* = -\frac{C}{R} + C'. \tag{8.32}$$

According to Equation 8.30, the concentration gradient is obtained from

$$\frac{dc_A^*}{dr} = \frac{C}{R^2}. \tag{8.33}$$

At the particle surface, the flux N_A is defined by Equation 8.21:

$$N_A = D_{eA}\frac{dc_A^*}{dr} = D_{eA}\frac{C}{R^2}. \tag{8.34}$$

This flux is equal to the flux through the gas film according to Equation 8.19:

$$N_A = k_{GA}\left(c_A^b - c_A^*\right) = D_{eA}\frac{C}{R^2}. \tag{8.35}$$

Inserting the concentration onto the particle surface c_A^*, Equation 8.32, yields

$$k_{GA}\left(c_A^b + \frac{C}{R} - C'\right) = D_{eA}\frac{C}{R^2}. \tag{8.36}$$

On the other hand, Equation 8.31 is valid at the interfaces between the porous layer and the unreacted particle:

$$c_{\mathrm{A}}^{\mathrm{s}} = -\frac{C}{r} + C', \tag{8.37}$$

where $c_{\mathrm{A}}^{\mathrm{s}}$ is the concentration at the interface. Based on Equations 8.36 and 8.37, the integration constants C and C' can be determined. An elegant solution is obtained:

$$C = \frac{c_{\mathrm{A}}^{\mathrm{b}} - c_{\mathrm{A}}^{\mathrm{s}}}{(1/r) - (1/R)\,(1 - (D_{\mathrm{eA}}/Rk_{\mathrm{GA}}))} \tag{8.38}$$

and

$$C' = c_{\mathrm{A}}^{\mathrm{b}} + \frac{1}{R}\left(1 - \frac{D_{\mathrm{eA}}}{Rk_{\mathrm{GA}}}\right) C. \tag{8.39}$$

The dimensionless ratio, $Rk_{\mathrm{GA}}/D_{\mathrm{eA}}$, is called the *Biot number* for mass transfer (Equation 4.72):

$$Bi_{\mathrm{M}} = \frac{Rk_{\mathrm{GA}}}{D_{\mathrm{eA}}}. \tag{8.40}$$

The Biot number defines the relation between the gas film and porous layer diffusion resistances. Usually, $Bi_{\mathrm{M}} \gg 1$. The concentration gradient at the interface is now given by

$$\frac{\mathrm{d}c_{\mathrm{A}}}{\mathrm{d}r} = \frac{C}{r^2}. \tag{8.41}$$

Inserting the constant C into Equation 8.42 yields the concentration gradient as follows:

$$\frac{\mathrm{d}c_{\mathrm{A}}}{\mathrm{d}r} = \frac{c_{\mathrm{A}}^{\mathrm{b}} - c_{\mathrm{A}}^{\mathrm{s}}}{r\,[1 - (r/R)\,(1 - (1/Bi_{\mathrm{M}}))]}. \tag{8.42}$$

The flux, N_{A}, at the interface, according to Equation 8.21, is obtained as

$$N_{\mathrm{A}}(r) = +D_{\mathrm{eA}}\frac{\mathrm{d}c_{\mathrm{A}}}{\mathrm{d}r} = \frac{D_{\mathrm{eA}}\left(c_{\mathrm{A}}^{\mathrm{b}} - c_{\mathrm{A}}^{\mathrm{s}}\right)}{r\,[1 - (r/R)\,(1 - (1/Bi_{\mathrm{M}}))]}. \tag{8.43}$$

At the outer surface of the particle ($r = R$), the flux is obtained in a similar way:

$$N_{\mathrm{A}}(R) = +D_{\mathrm{eA}}\left(\frac{\mathrm{d}c_{\mathrm{A}}}{\mathrm{d}r}\right)_{r=R} = k_{\mathrm{GA}}\left(c_{\mathrm{A}}^{\mathrm{b}} - c_{\mathrm{A}}^{\mathrm{s}}\right). \tag{8.44}$$

At steady state, for the interface, the following mass balance for component A is valid:

$$[\text{incoming A due to diffusion}] + [\text{generated A}] = 0. \tag{8.45}$$

This can be expressed in the form

$$N_A A + r_A A = 0, \tag{8.46}$$

where the interfacial area is $A = 4\pi r^2$ for a spherical particle.

By considering the reaction stoichiometry, Equation 8.11, the mass balance is transformed to

$$N_A + \nu_A R = 0, \tag{8.47}$$

where R is the reaction rate according to Equation 8.11. The reaction rates are calculated with the interfacial concentration c^s. Taking into account the equation for flux, Equation 8.43, we obtain the final result:

$$\frac{D_{eA}\left(c_A^b - c_A^s\right)}{r\left[1 - (r/R)\left(1 - (1/Bi_M)\right)\right]} = -\nu_A R\left(\mathbf{c}^s\right). \tag{8.48}$$

A similar expression can be derived for each component in the gas phase. For component i in the gas phase, the mass balance is

$$N_i + \nu_i R = 0 \tag{8.49}$$

and the molar flux at the interface is, consequently,

$$N_i = D_{ei}\frac{dc_i}{dr} = \frac{D_{ei}\left(c_i^b - c_i^s\right)}{r\left[1 - (r/R)\left(1 - (1/Bi_{iM})\right)\right]} = -\nu_i R\left(\mathbf{c}^s\right). \tag{8.50}$$

A general expression can now be written as

$$\frac{D_{ei}\left(c_i^b - c_i^s\right)}{r\left[1 - (r/R)\left(1 - (1/Bi_{iM})\right)\right]} = -\nu_i R\left(\mathbf{c}^s\right). \tag{8.51}$$

For different kinds of reaction kinetics, the unknown surface concentrations c must be solved as a function of concentrations in the bulk phase c^b in the equation system (Equation 8.51). For component B in the solid phase, the time dependence is defined by Equation 8.18.

It is often interesting to couple balance Equation 8.18 to the balance equation of component A, Equation 8.48, which gives an expression for the reaction rate, $R(\mathbf{c}^s)$. The solution of $R(\mathbf{c}^s)$ from Equation 8.48 and substituting the expression for $R(\mathbf{c}^s)$,

$$R\left(\mathbf{c}^s\right) = \frac{D_{eA}\left(c_A^b - c_A^s\right)}{-\nu_A r\left[1 - (r/R)\left(1 - (1/Bi_{AM})\right)\right]}, \tag{8.52}$$

into Equation 8.18 yield

$$\frac{\mathrm{d}r}{\mathrm{d}t} = \frac{\nu_B M D_{eA} \left(c_A^b - c_A^s\right)}{x_B \rho_p \left(-\nu_A\right) r \left[1 - (r/R)\left(1 - (1/Bi_{AM})\right)\right]}. \tag{8.53}$$

With this expression, it is possible to calculate the time dependence of a particle radius for different reactions. The surface concentration c_A^s is thus dependent on the position of the interface, the coordinate of r, as defined in Equation 8.52. In general, c^s must be solved iteratively by Equation 8.52, for each position in the radial direction. In the case of a special kind of reaction kinetics, that is, a first-order reaction, an analytical solution of Equation 8.52 is possible. These special cases are considered below.

8.2.2.1 First-Order Reactions

For a first-order reaction, the reaction kinetics is defined as

$$R = k c_A^s, \tag{8.54}$$

where k is the first-order rate constant. Inserting Equation 8.54 into Equation 8.51, the solution of the surface concentration c_A^s yields

$$c_A^s = \frac{c_A^b}{1 - (-\nu_A k r / D_{eA})[1 - (r/R)(1 - Bi_{AM})]}. \tag{8.55}$$

Let us define the dimensionless quantity, ϕ', as

$$\phi' = \frac{-\nu_A k R}{D_{eA}}, \tag{8.56}$$

which is analogous to the *Thiele modulus* (ϕ) (defined in Chapter 5, Section 5.1). Equation 8.55 can now be rewritten as follows:

$$c_A^s = \frac{c_A^b}{1 + \phi'(r/R)\left[1 - (r/R)\left(1 - (1/Bi_{AM})\right)\right]}. \tag{8.57}$$

The expression (Equation 8.56) for c_A^s is substituted into the kinetic Equation 8.54 and into the balance Equation 8.53. The time dependence of the particle radius is now obtained as

$$\frac{\mathrm{d}r}{\mathrm{d}t} = \frac{M \nu_B k c_A^b}{x_B \rho_p} \frac{1}{\left\{1 + \phi'(r/R)\left[1 - (r/R)\left(1 - (1/Bi_{AM})\right)\right]\right\}}. \tag{8.58}$$

If the rate constant k is independent of time, that is, the temperature in the system is constant, a differential equation can be integrated as

$$\int_R^r \left\{1 + \phi' \frac{r}{R}\left[1 - \frac{r}{R}\left(1 - \frac{1}{Bi_{AM}}\right)\right]\right\} \mathrm{d}r = \frac{M \nu_B k}{x_B \rho_p} \int_0^t c_A^b \, \mathrm{d}t. \tag{8.59}$$

The right-hand side of the integral is denoted by

$$a = \frac{-M\nu_B k}{x_B \rho_p} \int_0^t c_A^b \, dt. \tag{8.60}$$

Integrating the left-hand side of Equations 8.59 and 8.60 and inserting the integration limits yield

$$r - R + \frac{\phi'}{2R}\left(r^2 - R^2\right) - \frac{\phi'}{3R^2}\left(r^3 - R^3\right)\left(1 - \frac{1}{Bi_{AM}}\right) = -a. \tag{8.61}$$

Since all of the solid material has reacted at time t_0 (the total reaction time, $r = 0$), we have

$$a_0 = \frac{M\nu_B k}{x_B \rho_p} \int_0^t c_A^b \, dt. \tag{8.62}$$

This is inserted into Equation 8.62, together with the limit $r = 0$, and the result is

$$-R - \frac{\phi' R}{2} - \frac{\phi' R}{3}\left(1 - \frac{1}{Bi_{AM}}\right) = -a_0. \tag{8.63}$$

Equations 8.62 and 8.63 can be rewritten as

$$R\left(1 - \frac{r}{R}\right) + \frac{\phi' R}{2}\left[1 - \left(\frac{r}{R}\right)^2\right] - \frac{\phi' R}{3}\left[1 - \left(\frac{r}{R}\right)^3\right]\left(1 - \frac{1}{Bi_{AM}}\right) = a \tag{8.64}$$

and

$$R + \frac{\phi' R}{2} - \frac{\phi' R}{3}\left(1 - \frac{1}{Bi_{AM}}\right) = a_0. \tag{8.65}$$

As the next step, the division a/a_0 yields

$$\frac{a}{a_0} = \frac{6\left(1 - (r/R)\right) + 3\phi'\left(1 - (r/R)^2\right) - 2\phi'\left(1 - (r/R)^3\right)\left(1 - (1/Bi_{AM})\right)}{6 + \phi'\left(1 + (2/Bi_{AM})\right)}. \tag{8.66}$$

This ratio, a/a_0, is the relationship between the integrated time dependencies of the bulk-phase concentrations c_A^b:

$$\frac{a}{a_0} = \frac{\int_0^t c_A^b dt}{\int_0^{t_0} c_A^b dt}. \tag{8.67}$$

Some limiting cases of Equation 8.66 are of considerable interest. Let us consider four of these cases:

a. The chemical reaction is rate-determining.
b. Diffusion through the product layer and the gas film is rate-determining.

c. Diffusion through the product layer is rate-determining.
d. Diffusion through the gas film is rate-determining.

If the chemical reaction alone determines the rate, the *Thiele modulus*, φ', assumes very low values ($\varphi' \approx 0$) and Equation 8.66 is simplified to

$$\frac{a}{a_0} = 1 - \frac{r}{R}. \tag{8.68}$$

If diffusion through both the product layer and the gas film is the rate-determining step, the *Thiele modulus* (φ') becomes very large (k is large compared to D_{eA}/R). In this case, the boundary value for the ratio a/a_0 is

$$\frac{a}{a_0} = \frac{3\left(1 - (r/R)^2\right) - 2\left(1 - (r/R)^3\right)\left(1 - (1/Bi_{AM})\right)}{1 + (2/Bi_{AM})}. \tag{8.69}$$

When diffusion through the product layer is much slower than the diffusion through the gas film—which is quite probable—the Biot number for the mass transfer of component A approaches infinity, that is, $Bi_{AM} = \infty$, and Equation 8.69 can be simplified to

$$\frac{a}{a_0} = 1 - 3\left(\frac{r}{R}\right)^2 + 2\left(\frac{r}{R}\right)^3. \tag{8.70}$$

In the relatively rare cases in which diffusion through the gas film could be the rate-determining step, the Biot number for the mass transfer of component A is zero, that is, $Bi_{AM} = 0$, and Equation 8.69 can be written as

$$\frac{a}{a_0} = 1 - \left(\frac{r}{R}\right)^3, \tag{8.71}$$

denoting the relationship between the integrated time dependencies of the bulk-phase concentrations c_A^b, that is, the ratio between the current and the initial concentration profiles throughout the "ash layer." In other words, it relates the reduction of the particle radius from the initial value R to the new value r, and the concentration profiles in a certain time domain (Table 8.2).

TABLE 8.2 Summary: The Equation of Choice in Case of Diffusion as the Rate-Determining Step

Rate-Determining Step	a/a_0
Diffusion through the fluid film and the product layer	Equation 8.69
Diffusion through the product layer	Equation 8.70
Diffusion through the fluid film	Equation 8.71

8.2.2.2 General Reaction Kinetics: Diffusion Resistance as the Rate-Determining Step

Deriving an explicit expression for a/a_0 in a general case of reaction kinetics is very difficult and often impossible. The reason for this is that the surface concentrations must be solved in Equation 8.51. When the rate-determining step is diffusion-resistant both in the product layer and in the gas film, a generally applicable derivation is possible.

If the diffusion steps are slow compared with the chemical reaction, reactant A is instantaneously consumed after it has diffused to the interface. At the same time, the surface concentration c_A^s is very small in comparison to the bulk-phase concentration c_A^b. The difference $c_A^b - c_A^s$ in Equation 8.53 can be approximated with sufficient accuracy accordingly, $c_A^b - c_A^s \approx c_A^b$, and Equation 8.53 can be directly integrated.

It is easy to show that the result obtained actually is Equation 8.69, which was obtained for first-order reactions. In cases in which diffusion resistances in the gas film and/or in the product layer are rate-determining, we can use the general expressions for a/a_0 as given in Table 8.2 (the relationship between the integrated time dependencies of the bulk-phase concentrations c_A^b).

8.2.3 SHRINKING PARTICLE MODEL

In the case of a shrinking particle, we will consider two areas (or sections): the interface and the gas film around the particle. The solid- or gas-phase products are immediately transported away from the particle surface, and they have no direct influence on the reaction rate. The structure of such a particle is shown in Figure 8.3. Component A diffuses through the gas film to the particle surface and reacts with the solid phase of product P. The flux of A through the gas film is denoted as N_A. The positive (+) direction for N_A is shown in Figure 8.3.

For the gas film around the particle, the flux N_A is expressed as

$$N_A = k_{GA}\left(c_{GA}^b - c_A^s\right), \tag{8.72}$$

where c_{GA}^b and c_A^s denote component A's concentrations in the gas bulk phase and on the particle surface, respectively.

The following mass balance at steady state is valid for component A:

$$[\text{incoming A by diffusion through the gas film}] + [\text{generated A}] = 0. \tag{8.73}$$

This means that the flux through the interface equals the reaction in the interface, expressed in terms of mathematics accordingly (mass balance):

$$N_A A + r_A A = 0, \tag{8.74}$$

where A is the size of the interface. For a spherical particle, interface A is

$$A = 4\pi r^2 \tag{8.75}$$

and the reaction rate r_A is expressed with the stoichiometric relation (Equation 8.11). The mass balance can now be written as

$$N_A + \nu_A R = 0, \tag{8.76}$$

where R is the reaction rate.

The reaction rate R is defined as a function of the surface concentrations in the system, $R = R(c^s)$. For an arbitrary component reacting in the gas phase, Equation 8.76 is generalized to

$$N_i + \nu_i R\left(c^s\right) = 0. \tag{8.77}$$

For general reaction kinetics, the unknown surface concentrations must be solved using a balance equation of a nature similar to Equation 8.77; the flux N_i is always dependent on the surface concentration c_i:

$$N_i = k_{Gi}\left(c_i^b - c_i^s\right). \tag{8.78}$$

For a solid component B, Equation 8.18 can be used as such. A requirement for solving Equation 8.18 is that the reaction rates are expressed through bulk-phase concentrations, c^b. The unknown surface concentrations, c_i^s, can be solved analytically in the balance equation in certain special cases, that is, first-order reactions.

8.2.3.1 First-Order Reactions

For a first-order reaction, the rate equation

$$R = kc_A^s \tag{8.79}$$

and the flux N_A as in Equation 8.72 are inserted into the mass balance Equation 8.76, and the result is

$$k_{GA}\left(c_A^b - c_A^s\right) + \nu_A k c_A^s = 0. \tag{8.80}$$

The surface concentration c_A^s is solved as

$$c_A^s = \frac{c_A^b}{1 - (\nu_A k/k_{GA})}. \tag{8.81}$$

Substituting this expression into the rate equation yields the time dependence of the particle radius for a first-order reaction:

$$\frac{dr}{dt} = \frac{M}{x_B \rho_p} \frac{\nu_B k c_A^b}{1 - (\nu_A k/k_{GA})}. \tag{8.82}$$

For a shrinking particle, the dependence of the gas film coefficient and particle size must be considered. According to the film theory, the gas film coefficient is related to the gas film thickness:

$$k_{GA} = \frac{D_{GA}}{\delta_G}, \tag{8.83}$$

where D_{GA} is component A's diffusion coefficient in the gas phase and δ_G is the gas film thickness. During the course of the reaction, the size of the particle decreases and the gas film becomes thinner, which means that the numerical value of the gas film coefficient k_{GA} increases. The following correlation equation has been proposed by Ranz and Marshall [3]:

$$\frac{k_{GA} d_p}{D_{GA}} = 2 + 0.6 Sc^{1/3} Re^{1/2}, \tag{8.84}$$

where d_p is the particle diameter, and *Schmidt* (*Sc*) and *Reynolds* (*Re*) numbers are defined by well-known expressions:

$$Sc = \frac{\mu_G}{\rho_G D_{GA}}, \tag{8.85}$$

$$Re = \frac{d_p w_G \rho_G}{\mu_G}. \tag{8.86}$$

In these well-known formulas, μ_G and ρ_G are the gas viscosity and the density, respectively, whereas w_G denotes the flow velocity. For low gas flow velocities (Stokes regime), the relation in Equation 8.76 is simplified to (note that the diameter, $d = 2r$, and the velocity, w_G, are small)

$$k_{GA} = \frac{D_{GA}}{r}. \tag{8.87}$$

Inserting Equation 8.87 into Equation 8.82 yields

$$\frac{dr}{dt} = \frac{M \nu_B k c_A^b}{x_B \rho_B \left(1 - (\nu_A k r / D_{GA})\right)}. \tag{8.88}$$

By inserting the dimensionless *Thiele modulus* ϕ'' into Equation 8.88,

$$\phi'' = -\frac{\nu_A k R}{D_{GA}} \tag{8.89}$$

a new form is obtained:

$$\frac{dr}{dt} = \frac{M \nu_B k c_A^b}{x_B \rho_B \left(1 + \phi''(r/R)\right)}. \tag{8.90}$$

If the rate constant is time-independent, the differential equation, Equation 8.90, can be easily integrated:

$$\int_R^r \left(1 + \phi'' \frac{r}{R}\right) \mathrm{d}r = \frac{M \nu_B k c_{Ab}}{x_B \rho_B} \int_0^t c_A^b \, \mathrm{d}t. \tag{8.91}$$

Let us define a parameter a that, once again, denotes the right-hand side of Equation 8.91:

$$a = -\frac{M \nu_B k}{x_B \rho_B} \int_0^t c_A^b \, \mathrm{d}t. \tag{8.92}$$

Consequently, integrating the left-hand side of Equation 8.91 and applying the integration limits yield

$$r - R + \frac{\phi'' R}{2} \left(\left(\frac{r}{R}\right)^2 - 1 \right) = -a. \tag{8.93}$$

At the total reaction time ($t = t_0, r = 0$), parameter a has the value

$$a_0 = -\frac{M \nu_B k}{x_B \rho_B} \int_0^{t_0} c_A^b \, \mathrm{d}t. \tag{8.94}$$

At the end of the reaction ($r = 0$), Equation 8.93 attains the new form

$$-R - \frac{\phi'' R}{2} = -a_0. \tag{8.95}$$

Let us now divide Equation 8.93 by Equation 8.95:

$$\frac{a}{a_0} = \frac{2\left(1 - (r/R)\right) + \phi''\left(1 - (r/R)^2\right)}{2 + \phi''}, \tag{8.96}$$

where, in a manner similar to the treatment in Section 8.2.2 (Product Layer Model), a/a_0 is given by

$$\frac{a}{a_0} = \frac{\int_0^t c_A^b \, \mathrm{d}t}{\int_0^{t_0} c_A^b \, \mathrm{d}t}. \tag{8.97}$$

Equation 8.96 has two interesting limiting cases: the surface reaction alone determines the reaction rate, or diffusion through the gas film is the rate-determining step.

If the *surface reaction determines the reaction rate* ($\phi'' \approx 0$), then Equation 8.96 is simplified to

$$\frac{a}{a_0} = 1 - \frac{r}{R}. \tag{8.98}$$

On the other hand, if *film diffusion is the rate-determining step* ($\phi'' = \infty$), then Equation 8.96 is simplified to

$$\frac{a}{a_0} = 1 - \left(\frac{r}{R}\right)^2. \tag{8.99}$$

8.2.3.2 Arbitrary Reaction Kinetics: Diffusion Resistance in the Gas Film as the Rate-Determining Step

For a shrinking particle, a general expression a/a_0 can be derived for the case in which diffusion through the gas film is the rate-determining step. The concentration on the particle surface, c_A^s, is in this case much lower than the concentration in the bulk phase, that is, $c_A^s \ll c_A^b$. This is applied to the flux N_A in Equation 8.78, and the reaction rate, R, is expressed through the flux N_A as in Equation 8.77. The expression thus obtained is inserted into the equation for the time derivative of the particle radius, Equation 8.18. The integration is easy, and the following simple expression is obtained:

$$\frac{a}{a_0} = 1 - \left(\frac{r}{R}\right)^2. \tag{8.100}$$

This ratio, a/a_0, is again the relationship between the integrated time dependencies of the bulk-phase concentrations c_A^b.

8.3 MASS BALANCES FOR REACTORS CONTAINING A SOLID REACTIVE PHASE

In this section, we consider mass balances for three common reactors that can be used in processing a solid reactive phase: a BR, a semibatch reactor, and a packed bed reactor. BRs are commonly used in reactions where the reactive solid reacts with a liquid, that is, leaching reactions. The semibatch reactor considered here is assumed to have a high gas throughput, and the gas content in the reactor can therefore be assumed as constant. These kinds of reactors are often used in the study of the kinetics of gas–solid reactions. Packed beds, where the gas or the liquid flows through stagnant solid catalyst particles, are used, for instance, in combustion processes and ion-exchange reactions. At the beginning of the reaction, the solid particles are assumed to be of the same size, although cases with particle size distributions could be considered. It is further assumed that BRs and semibatch reactors are completely backmixed, and the gas phase in packed beds is characterized by plug flow conditions. Radial and axial dispersion effects are assumed to be negligible.

8.3.1 BATCH REACTOR

For a BR with a constant volume, balance Equation 8.9 for a single particle can be generalized, being valid throughout all of the reactor contents. For n_p equally sized particles in the reactor, we obtain

$$\frac{d(n_p n_B)}{dt} = n_p A r_B, \tag{8.101}$$

where n_B denotes the molar amount of component B in a particle. The previous equation can now be rewritten as

$$\frac{dr}{dt} = \frac{M}{x_B \rho_B} \nu_R R(c^s). \tag{8.102}$$

As can be seen, Equation 8.102 is similar to Equation 8.18. The total molar amount of component B, n'_B, in the reactor at the time t is given by

$$n'_B = n_p x_B \frac{\rho_p (4/3)\pi r^3}{M}. \tag{8.103}$$

For a gas-phase component i reacting with a solid-phase component B, a mass balance can be written as

$$[\text{outflux } i \text{ from the particle}] + [\text{accumulated } i \text{ in the gas phase}] = 0. \tag{8.104}$$

As a mathematical equation, this can be expressed in the following way:

$$N_i n_p A + \frac{dn_i}{dt} = 0, \tag{8.105}$$

where n_i is the molar amount of i in the gas phase. The molar amount n_i can be expressed as the concentration of i in the gas bulk, c_i^b, and the gas-phase volume, V_G:

$$n_i = c_i^b V_G. \tag{8.106}$$

The volume of the gas phase (V_G) can be written as a function of the gas holdup (ε_G) and the reactor volume (V_R):

$$V_G = \varepsilon_G V_R. \tag{8.107}$$

Inserting Equations 8.106 and 8.107 into the derivative, Equation 8.105, yields

$$\frac{dn_i}{dt} = \frac{d\left(c_i^b \varepsilon_G V_R\right)}{dt}. \tag{8.108}$$

The quantity $n_p A$ gives the size of the interfacial area. The ratio between the interfacial area and the reactor volume is denoted as

$$a_p = \frac{n_p A}{V_R}. \tag{8.109}$$

After inserting these expressions into the mass balance, Equation 8.105, and assuming a constant reactor volume, the mass balance can be reformulated as follows:

$$\frac{d\left(\varepsilon_G c_i^b\right)}{dt} - N_i a_p. \tag{8.110}$$

Further development of the mass balance depends on whether the particle is shrinking or whether it has a porous product layer.

8.3.1.1 Particles with a Porous Product Layer

For particles with a porous product layer, the interfacial area, $n_p A$, is constant during the reaction:

$$a_p = \frac{n_p A_0}{V_R} = a_{0p}, \tag{8.111}$$

where A_0 is the interfacial area at the beginning of the reaction; $A_0 = \frac{1}{3}\pi R^3$ for a spherical particle. The gas holdup also remains constant during the reaction, $\varepsilon_G = \varepsilon_{0G}$.

The expressions for the ratio between the interfacial area and reactor volume (a_p) and the gas holdup (ε_G) are inserted into the balance Equation 8.110, and we obtain

$$\frac{dc_i^b}{dt} = -N_i \frac{a_{0p}}{\varepsilon_{0G}}. \tag{8.112}$$

The flux N_i and the surface concentration c^s are given in Equations 8.50 and 8.51, respectively.

For a general system containing N components in the gas phase, the coupled system of $N + 1$ differential equations, Equations 8.110 and 8.18, is solved. The flux N_i and the surface concentration c_i^s are given in Equations 8.50 and 8.51, respectively. The coupled differential equations must be solved numerically using the tools and methods introduced, for instance, in Appendix 2. For first-order reactions, however, a simplified procedure is possible.

For a first-order reaction, with the reaction kinetics

$$R = k c_A^s, \tag{8.113}$$

the expression for the surface concentration c_A^s (Equation 8.51) finally transforms to Equation 8.56. Inserting Equation 8.56 into the first-order reaction kinetics formula and taking into account Equation 8.51 gives the flux

$$N_A = \frac{-\nu_A k c_A^b}{1 + \phi'(r/R)\,[1 - (r/R)\,(1 - (1/Bi_{AM}))]}. \tag{8.114}$$

Inserting the expression for the flux N_A into the balance equation, Equation 8.112, yields

$$\frac{dc_A^b}{dt} = \frac{\nu_A k a_{0p}}{\varepsilon_{0G}} \frac{c_A^b}{1 + \phi'(r/R)\,[1 - (r/R)\,(1 - (1/Bi_{AM}))]}. \tag{8.115}$$

If this expression is divided by the time derivative of the particle radius (dr/dt), Equation 8.58, we obtain

$$\frac{dc_A^b}{dr} = \frac{x_B \rho_B \nu_A a_{0p}}{\nu_B \varepsilon_{0G}}. \tag{8.116}$$

After integrating, we obtain the concentration in the bulk phase:

$$c_A^b = c_{0A}^b - \frac{x_B \rho_p \nu_A a_{0p} R}{M \nu_B \varepsilon_{0G}} \left(1 - \frac{r}{R}\right). \tag{8.117}$$

The expression for the bulk-phase concentration, c_A^b, is inserted into the radius time derivative, Equation 8.58, and we obtain

$$\frac{dr}{dt} = \frac{M\nu_B k}{x_B \rho_p} \frac{\left[c_{0A}^b - (x_B \rho_p \nu_A a_{0p} R / M\nu_B \varepsilon_{0G})\,(1 - (r/R))\right]}{[1 + \phi'(r/R)\,[1 - (r/R)\,(1 - (1/Bi_{AM}))]]}. \tag{8.118}$$

Integration of this expression gives the reaction time that is required by a certain particle radius:

$$t = \frac{x_B \rho_p}{M\nu k} \int_R^r \frac{\left[1 + \phi'(r/R)\,(1 - (r/R)\,(1 - (1/Bi_{AM})))\right]}{c_{0A}^b - (x_B \rho_p \nu_A a_{0p} R / M\nu_A \varepsilon_{0G})\,(1 - (r/R))}. \tag{8.119}$$

8.3.1.2 Shrinking Particles

In shrinking particles, the interfacial area changes during the reaction due to particle shrinkage. The interfacial area-to-reactor volume is given by

$$a_p = \frac{n_p A}{V_R}, \tag{8.120}$$

where the interfacial area is $A = 4\pi r^2$ for spherical particles. At the beginning of the reaction, the interfacial area is $A_0 = 4\pi R^2$ and the ratio of the interfacial area-to-reactor volume can be written as

$$a_{0p} = \frac{n_p A_0}{V_R} = n_p \frac{4\pi R^2}{V_R}. \tag{8.121}$$

At time t, the interfacial area-to-reactor volume relation is

$$a_p = \frac{n_p A_0}{V_R} \frac{A}{A_0} = a_{0p} \left(\frac{r}{R}\right)^2. \tag{8.122}$$

The gas holdup ε_G also changes due to the reaction. This change is not self-evident: if a product layer is peeled off the surface of the solid particle, a certain part of the solid material remains in the reactor. However, if only gas-phase products are being formed, then the value of the gas holdup ε_0 approaches unity (1) as the reaction proceeds. Here we will assume that it approaches unity ($\varepsilon_G = l$). The gas holdup ε_G is defined by

$$\varepsilon_G = \frac{V_G}{V_R} = \frac{V_R - V_s}{V_R}, \tag{8.123}$$

where V_s is the volume of particles in the reactor. The volume of spherical particles is given by

$$V_s = n_p \frac{4}{3}\pi r^3 = n_p \frac{4}{3}\pi R^3 \left(\frac{r}{R}\right)^3. \tag{8.124}$$

At time $t = 0$, the particle volume is $V_{s0} = n_p(4/3)\pi R^3$ and the gas holdup ε_G is

$$\varepsilon_G = 1 - \frac{V_s}{V_R} = 1 - \frac{V_{s0}}{V_R}\left(\frac{r}{R}\right)^3. \tag{8.125}$$

On the other hand, the holdup at the beginning of the reaction is instead described accordingly:

$$\varepsilon_{0G} = \frac{V_R - V_{s0}}{V_R} = 1 - \frac{V_{s0}}{V_R} \tag{8.126}$$

or

$$\frac{V_{s0}}{V_R} = 1 - \varepsilon_{0G}. \tag{8.127}$$

After inserting this expression into Equation 8.125, we obtain a new formula for the holdup:

$$\varepsilon_G = 1 - (1 - \varepsilon_{0G})\left(\frac{r}{R}\right)^3. \tag{8.128}$$

Inserting Equations 8.122 and 8.128 into the mass balance Equation 8.110 yields

$$\frac{d\left[\left(1 - (1 - \varepsilon_{0G})\,(r/R)^3\right)\right] c_i^b}{dt} = -N_i a_{0p}\left(\frac{r}{R}\right)^2. \tag{8.129}$$

Now, let us return to the flux N_i, which is given by Equations 8.77 and 8.78:

$$N_i = k_{Gi}\left(c_i - c_i^s\right) = -\nu_i R\left(c^s\right). \tag{8.130}$$

For an arbitrary kinetic model, the surface concentrations c_i^s are solved by Equation 8.130 and the flux thus obtained, N_i, is inserted into the differential Equation 8.129. This equation is then solved numerically as an initial value problem (Appendix 2). A simplified solution procedure is possible for a first-order reaction.

The kinetics for a first-order reaction is

$$R = kc_A^s. \tag{8.131}$$

Combining Equations 8.131 and 8.130 gives the surface concentration c_A^s as in Equation 8.81.

Substituting Equation 8.81 into Equation 8.131 and inserting the expression thus obtained for the reaction rate, in Equation 8.130, yield the flux

$$N_A = \frac{-\nu_A k c_A^b}{1 - (\nu_A k/k_{GA})}. \tag{8.132}$$

The mass balance Equation 8.129 can now be written as

$$\frac{\mathrm{d}\left\{\left[1-(1-\varepsilon_{\mathrm{G}})\,(r/R)^3\right]c_{\mathrm{A}}^{\mathrm{b}}\right\}}{\mathrm{d}t}=\frac{\nu_{\mathrm{A}}kc_{\mathrm{A}}^{\mathrm{b}}a_{0\mathrm{p}}}{1-(\nu_{\mathrm{A}}k/k_{\mathrm{GA}})}\left(\frac{r}{R}\right)^2. \tag{8.133}$$

Division by the radius time derivative, Equation 8.82, yields

$$\frac{\mathrm{d}\left\{\left[1-(1-\varepsilon_{0\mathrm{G}})\,(r/R)^3\right]c_{\mathrm{A}}^{\mathrm{b}}\right\}}{\mathrm{d}r}=\frac{\nu_{\mathrm{A}}x_{\mathrm{B}}\rho_{\mathrm{p}}a_{0\mathrm{p}}}{\nu_{\mathrm{B}}M}\left(\frac{r}{R}\right)^2 \tag{8.134}$$

and integration yields the following result:

$$\left[1-(1-\varepsilon_{0\mathrm{G}})\left(\frac{r}{R}\right)^3\right]c_{\mathrm{A}}^{\mathrm{b}}-\left[1-(1-\varepsilon_{0\mathrm{G}})\right]c_{0\mathrm{A}}^{\mathrm{b}}=\frac{\nu_{\mathrm{A}}x_{\mathrm{B}}\rho_{\mathrm{p}}a_{0\mathrm{p}}}{3\nu_{\mathrm{B}}M}(r^3-R^3), \tag{8.135}$$

from which we are able to extract the following expression for $\varepsilon_{\mathrm{G}}c_{\mathrm{A}}^{\mathrm{b}}$:

$$\varepsilon_{\mathrm{G}}c_{\mathrm{A}}^{\mathrm{b}}=\varepsilon_{0\mathrm{G}}c_{0\mathrm{A}}^{\mathrm{b}}-\frac{\nu_{\mathrm{A}}x_{\mathrm{B}}\rho_{\mathrm{p}}a_{0\mathrm{p}}R}{3\nu_{\mathrm{B}}M}\left[1-\left(\frac{r}{R}\right)^3\right]. \tag{8.136}$$

Inserting the concentration $c_{\mathrm{A}}^{\mathrm{b}}$ obtained from Equation 8.136 into the differential equation describing the change in the particle radius, Equation 8.90, yields

$$\frac{\mathrm{d}r}{\mathrm{d}t}=\frac{\nu_{\mathrm{B}}Mk}{x_{\mathrm{B}}\rho_{\mathrm{p}}}\frac{\left[(\varepsilon_{0\mathrm{G}}/\varepsilon_{\mathrm{G}})c_{0\mathrm{A}}^{\mathrm{b}}-(\nu_{\mathrm{A}}x_{\mathrm{B}}\rho_{\mathrm{p}}a_{0\mathrm{p}}R/3\nu_{\mathrm{B}}M)\left(1-(r/R)^3\right)\right]}{1+\phi''(r/R)}. \tag{8.137}$$

The reaction time required to reach the particle radius, r (shrinking particle), is determined by the integral

$$t=\frac{x_{\mathrm{B}}\rho_{\mathrm{p}}}{M\nu_{\mathrm{B}}k}\int_R^r\frac{\left(1+\phi''(r/R)\right)\varepsilon_{\mathrm{G}}\,\mathrm{d}r}{\varepsilon_{0\mathrm{G}}c_{0\mathrm{A}}^{\mathrm{b}}-(\nu_{\mathrm{A}}x_{\mathrm{B}}\rho_{\mathrm{p}}a_{0\mathrm{p}}R\left(1-(r/R)^3\right)/3\nu_{\mathrm{B}}M)}, \tag{8.138}$$

where the gas holdup ε_{G} is given by

$$\varepsilon_{\mathrm{G}}=1-(1-\varepsilon_{0\mathrm{G}})\left(\frac{r}{R}\right)^3. \tag{8.139}$$

The result is valid for a *shrinking particle*. Integration of Equation 8.138 is performed numerically.

8.3.2 SEMIBATCH REACTOR

Let us consider a special case of a semibatch reactor: a reactor in which the gas flows in large excess passing the solid particles. In this case, the composition of the gas phase can be

assumed to be constant in all parts of the reactor. This kind of semibatch reactor is often used in thermogravimetric analysis studies of, for instance, gas–solid reaction kinetics.

To this kind of a semibatch reactor, balance Equation 8.18 can be applied for the solid-phase component B:

$$\frac{\mathrm{d}r}{\mathrm{d}t} = \frac{M}{x_\mathrm{B}\rho_\mathrm{B}}\nu_\mathrm{B}R\left(c_i^\mathrm{s}\right). \tag{8.140}$$

For first-order reaction kinetics, Equation 8.54, the balance Equation 8.140 assumes different forms depending on whether the particle has a product layer and whether it shrinks.

8.3.2.1 Particle with a Porous Product Layer

For a particle with a porous layer, Equation 8.66 was derived for a first-order reaction. The ratio a/a_0 once again, in Equation 8.66, is given by Equation 8.67. If the gas concentration $\left(c_\mathrm{A}^\mathrm{b}\right)$ is constant, the ratio a/a_0 is equal to the time ratio t/t_0 in Equation 8.67 ($a/a_0 = t/t_0$).

The reaction time t can now be written as

$$\frac{t}{t_0} = \frac{6(1-(r/R)) + 3\phi'\left(1-(r/R)^2\right) - 2\phi'\left(1-(r/R)^3\right)(1-(1/Bi_\mathrm{AM}))}{6+\phi'(1+(2/Bi_\mathrm{AM}))}. \tag{8.141}$$

Depending on whether diffusion through the product layer or diffusion through the gas film is the rate-determining step, different limiting cases for Equation 8.141 are obtained. These limiting cases were already mentioned in Section 8.2.2.

The dependence, that is, particle radius as a function of reaction time, for the different cases, is illustrated in Figure 8.5 [1].

8.3.2.2 Shrinking Particle

Earlier, Equation 8.96 was derived for a first-order reaction, assuming the ratio a/a_0. For a constant gas concentration $\left(c_\mathrm{A}^\mathrm{b}\right)$, the ratio $a/a_0 = t/t_0$ and the reaction time are obtained as

$$\frac{t}{t_0} = \frac{2\,(1-(r/R)) + \phi''\left(1-(r/R)^2\right)}{2+\phi''}. \tag{8.142}$$

Depending on the rate-determining step, either diffusion through the gas film or chemical reaction as the rate-determining step, Equation 8.142 is transformed to various different forms. Some limiting cases were considered in Section 8.2.3.

8.3.3 PACKED BED

Let us now consider a stagnant packed bed with a continuous gas flow. The reactor operates, in this case, in a semibatch mode: solid particles form the continuous phase, whereas gas is the discontinuous phase. The mass balances must be derived for the transient state for the

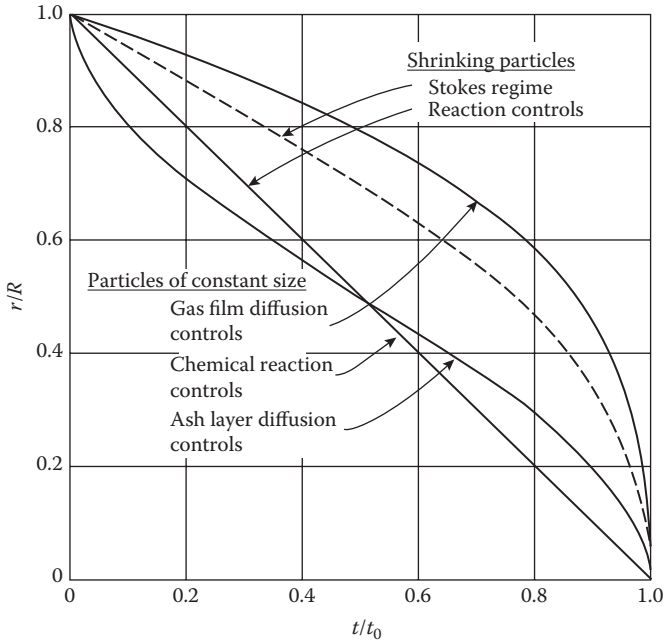

FIGURE 8.5 Particle radius (r) versus the reaction time (t) for a particle containing a product layer. Case: shrinking particle. (Data from Levenspiel, O., *Chemical Reaction Engineering*, 3rd Edition,Wiley, New York, 1999.)

volume element ΔV_R. If we assume that there are Δn_p solid particles in the volume element ΔV_R, the mass balance is

$$\frac{d(\Delta n_p n_B)}{dt} = \Delta n_p A r_p, \tag{8.143}$$

where n_B is the molar amount of component B in the particle. With the same considerations as in Section 8.2.1, the mass balance can be written as

$$\frac{dr}{dt} = \frac{M}{x_B \rho_p} \nu_B R(c^s). \tag{8.144}$$

The analogy to Equation 8.18 is obvious.

For a gas component i reacting with the solid component B, the mass balance is given by

$$\begin{aligned}[\text{inflow of } i] = [\text{outflow of } i] + [\text{flux of } i \text{ into the particle}] \\ + [\text{accumulated } i \text{ in the gas phase}].\end{aligned} \tag{8.145}$$

The balance can be written in a mathematical form accordingly:

$$\dot{n}_{i,in} = \dot{n}_{i,out} + N_i \Delta A + \frac{dn_i}{dt}. \tag{8.146}$$

Let us now combine it with the definition

$$\Delta A = a_v \Delta V_R \tag{8.147}$$

and with the difference $\dot{n}_{i,out} - \dot{n}_{i,in} = \Delta \dot{n}_i$. The molar amount of component i in the volume element n_i is expressed in terms of concentration as:

$$n_i = c_i \Delta V_G = c_i \varepsilon_G \Delta V_R. \tag{8.148}$$

Inserting the definitions for ΔA and n_i, followed by division by the volume element ΔV_R, yields

$$\frac{d(\varepsilon_G c_i)}{dt} + N_i a_v + \frac{\Delta \dot{n}_i}{\Delta V_R} = 0. \tag{8.149}$$

Allowing the value of the volume element to approach zero, $\Delta V_R \to 0$, the balance can be written in the following form:

$$\frac{d(\varepsilon_G c_i)}{dt} = -N_i a_v - \frac{d\dot{n}_i}{dV_R}. \tag{8.150}$$

Equations 8.149 and 8.150 describe a *semibatch* packed bed. Changes in the gas phase are much more rapid than those in the liquid phase. Therefore, we can assume that the gas phase is in *a pseudo-steady-state* and that the time derivative in Equation 8.150 can sometimes be ignored:

$$\frac{d\dot{n}_i}{dV_R} = -N_i a_v. \tag{8.151}$$

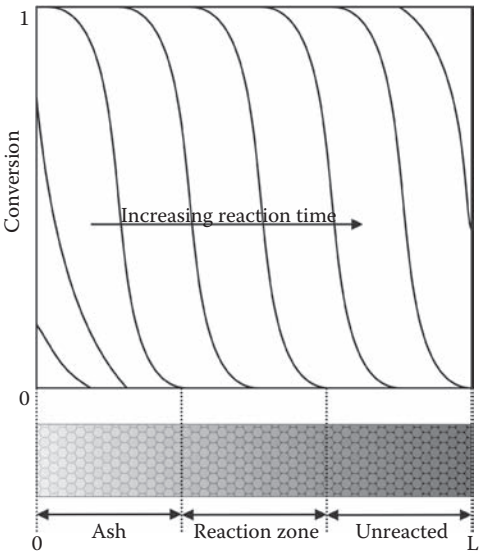

FIGURE 8.6 Conversion of a solid reactant in a packed bed at different reaction times.

A suitable expression for the flux N_i must, of course, be used.

Examples of the development of concentration profiles in packed beds are shown in Figure 8.6 [4]. This figure is valid for particles with a porous product layer. The development of a reaction zone moving from the inlet toward the outlet is a typical behavior of packed beds. At the reactor inlet, the particles have reacted completely, whereas the particles close to the outlet are totally unreacted.

REFERENCES

1. Levenspiel, O., *Chemical Reaction Engineering*, 3rd Edition, Wiley, New York, 1999.
2. Sohn, H.Y. and Szekely, J., A structural model for gas–solid reactions with a moving boundary-III. A generalized dimensionless representation of the irreversible reaction between a porous solid and a reactant gas, *Chem. Eng. Sci.*, 27, 763–778, 1972.
3. Ranz, W.E. and Marshall, W.R., Evaporation from droplets, *Chem. Eng. Prog.*, 48, 141–173, 1952.
4. Trambouze, P., van Landegehem, H., and Wauquier, J.P., *Chemical Reactors—Design/Engineering/* Editions Technip, Paris, 1988.

CHAPTER 9

Toward New Reactor and Reaction Engineering

9.1 HOW TO APPROACH THE MODELING OF NOVEL REACTOR CONCEPTS?

The reactors considered in the previous chapters form the core of chemical reaction engineering, that is, classical, well-established structures, for which a number of practical industrial applications exist. For existing reactor configurations, even the mathematical modeling, simulation, and optimization are in a mature stage. Plug flow, laminar flow, axial dispersion, and complete backmixing models are the dominant ones for conventional reactor technology. Considerable deviations from these flow models are treated by detailed flow modeling, computational fluid dynamics (CFD). Particularly, the modeling of fluidized beds requires a very advanced approach, combining kinetics, mass transfer, and detailed fluid description.

Conventional reactor technologies such as fixed beds and slurry reactors suffer from serious drawbacks. Mass transfer resistance is the crucial factor in the scaleup of processes. Laboratory experiments are often carried out with catalyst particles with diameters clearly less than 1 mm, whereas industrial reactors typically operate with larger catalyst particles ranging from 1 mm to 1 cm. The scale dimensions are illustrated in Figure 9.1. Intrinsic kinetics is thus inevitably coupled to the modeling of mass transfer, as has been illustrated in previous chapters. Internal mass transfer limitations can be suppressed by decreasing the particle size, but the particle sizes in industrial processes cannot be diminished limitlessly, because this would lead to a tremendous increase in the pressure drop. To overcome this problem, new innovations and structured reactors have been developed, such as catalytic packing element reactors, monoliths, and fiber structures. The aim of these innovations has

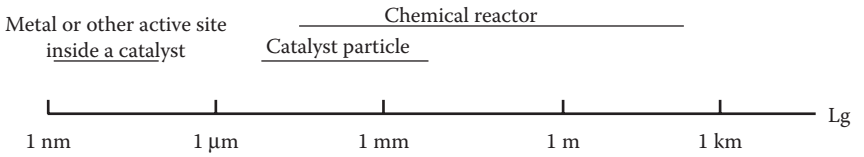

FIGURE 9.1 Scales in the modeling of chemical processes involving solid catalysts.

been to decouple the catalyst layer thickness and pressure drop effects. At the laboratory scale, it is possible to minimize the external mass transfer resistance using high stirring rates, but in industrial reactors, this is not always feasible. The stirring effect per reactor volume at the laboratory scale is typically less prominent than that in industrial operations. Consequently, external and internal mass and heat transfer often play a significant role in large-scale reactors. Fixed bed reactors typically suffer from heavy internal mass transfer due to large catalyst particles, and slurry reactors suffer from external mass transfer resistance due to insufficient stirring. These problems can, at least partially, be resolved by utilizing structured reactors that take advantage of thin catalyst layers.

Conventional industrial processes operate continuously and at steady state. Steady-state operation, however, is sometimes less economical, particularly in cases where considerable energy effects are encountered. For example, classical sulfur dioxide oxidation processes involve a large reactor–heat exchanger system to force conversion of the reactant to an acceptable level. By non-steady-state operation, the reactor volume can be considerably diminished. Unconventional operation modes are much more sensitive than conventional steady-state modeling. Very advanced dynamic modeling concepts are thus needed.

Unconventional, often sophisticated reactor technologies, such as the use of various structural catalysts (monoliths, coated static mixer elements, woven catalytic fiber cloths, Sulzer Katapaks®, etc.) or various loop configurations, can essentially be treated and modeled with classical concepts. The reactor models presented in the previous chapters can even be applied in the case of novel reactor concepts: We just divide the system into logical units that can be described with existing theories. Nowadays, advanced tools such as CFD are available, which enable the more precise prediction and description of the reactor system performance. The use of novel tools is necessary in some cases. Improved catalyst synthesis based on high throughput (parallel) catalyst screening and multifunctional reactor design is the current trend. As catalysts achieve higher intrinsic activities and selectivities and processes are pushed to a higher conversion, integration of new catalyst synthesis and reactor concepts can also improve existing technologies to a significant extent.

Basic concepts can easily be adopted: a reactor operates in a batch, a semibatch, or a continuous mode; the catalyst is either in suspension or immobilized (fixed or structured beds, monoliths); the flow of gas and liquid is counter or concurrent, following plug flow, stirred tank (backmixing or no backmixing), or fluidized bed behavior; and mass transfer limitations (at the phase boundaries or within a phase) can prevail (Chapters 5 through 8). The biggest challenge might arise from recognizing a potentially unique unit operation (equipment-specific feature) that might emerge in a system and that the combination of

classical modeling principles cannot handle adequately: in these cases, a nontraditional approach might lead to a better description of the reality. For instance, in the case of monoliths, the flow distribution anomalies are best dealt with by CFD. However, when analyzing the system as a whole, the established principles can always be applied to describing the vast majority of cases.

A product-oriented approach is the slogan of the twenty-first century. Reaction engineering of the future is to focus more on fine and speciality chemicals, bioengineering applications, and treatment of natural products, such as pulp and paper making, health-promoting compounds, and pharmaceuticals. In parallel, the reaction engineering of bulk chemicals will be refined, for instance, by introducing improved kinetics and chemometric concepts as well as detailed fluid dynamics. Typically, hydrogenation and oxidation reactions of complex organic molecules tend to give rise to complex reaction networks involving multiple consecutive, consecutive-competitive, and mixed reactions. Nontraditional reactor concepts are more likely to be used for two reasons. First, it is easier for more expensive concepts that are typically applied on a somewhat smaller scale to surpass the investment threshold in fine chemicals processes than in bulk processes. Secondly, the complexity of many reaction systems (multiple side reactions producing undesired waste compounds) requires more innovative reactor technologies that suppress side reactions and favor the formation of desired compounds.

The goal of the novel reactor technology is a more efficient, more selective, and less energy-consuming process. The introduction of new reactor technologies should lead to a reduction in the physical size of the existing processes. This methodology, called process intensification or, more specifically, reaction intensification, comprises new reactor structures, unconventional operation modes, utilization of unconventional forms of energy (such as ultrasound and microwave), and novel reaction media [e.g., supercritical fluids (SCFs) and ionic liquids (ILs)]. In this chapter, we will describe some of the new avenues of reactor technology and reaction engineering. Our treatment is essentially qualitative and holistic. The concepts of kinetics, mass, and heat transfer as well as fluid dynamics introduced earlier are also applicable to the new reaction engineering concepts. We will leave it to the readers to develop models of their own in the forthcoming research and development efforts; the cases treated below should be regarded as approaches to novel technologies, not final solutions.

9.2 REACTOR STRUCTURES AND OPERATION MODES

A multitude of reactor structures have been developed for special applications. This is why we are not aiming at an exhaustive listing and analysis of each and every kind of reactor here. Instead, the reader is given a short introduction to some of the most prominent new reactor technologies.

9.2.1 REACTORS WITH CATALYST PACKINGS

Column reactors with static packing elements provide an attractive alternative for conventional packed bed reactors, since they essentially combine the benefits of classical fixed beds and slurry reactors: static mixing elements give rise to local turbulence, catalyst separation

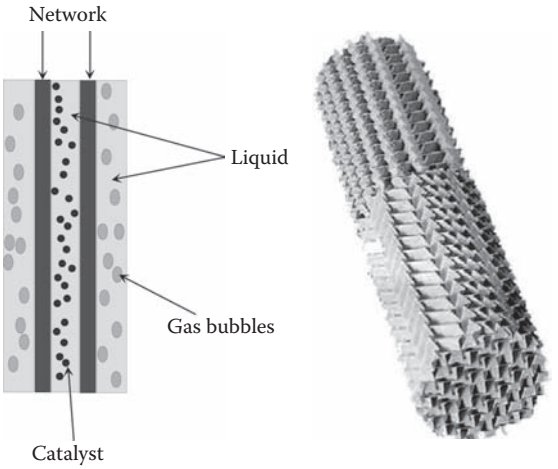

FIGURE 9.2 A packing element in a column reactor.

(filtration) is avoided, and small catalyst particles can be utilized. An illustration is provided in Figure 9.2. The modeling of column reactors is based on verified hypotheses on prevailing hydrodynamic and mass transfer conditions. In essence, a dynamic model accounting for the accumulation of substance in gas and liquid phases as well as in the pores of the catalyst can be compiled [1]. Previous experience has convincingly shown that dynamic and pseudodynamic models are preferred not only to predict transient operations, but also to obtain improved robustness in the numerical solution, particularly in the case of a countercurrent operation. The gas and liquid flow patterns were described using the axial dispersion concept (Section 4.5), coupled to the plug flow model. CFD calculations were applied to study the distribution of local liquid and gas velocities inside and outside the catalyst network [2,3]. The velocity profiles in Katapak elements calculated by CFD are illustrated in Figure 9.3. Mass transfer and convection take place through the network via molecular diffusion and

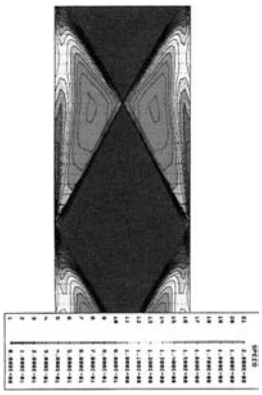

FIGURE 9.3 Velocity profiles in Katapak elements (CFD calculations, water at 20°C).

turbulence. In fact, mass transfer in the catalyst pores was described by a classical reaction–diffusion model, whereas the flow and mass transfer between the fluid phases inside and outside the packing network were treated as a system with an effective transport coefficient. In the special case studied in the above-mentioned publications [2,3] (oxidation of ferric sulfate to ferrous sulfate by molecular oxygen), both catalytic and noncatalytic reactions proceed simultaneously.

The modeling of column reactors is based on verified hypotheses concerning the hydrodynamics and mass transfer conditions. The following fundamental assumptions can be applied to the modeling of column reactors:

- The model is completely dynamic, accounting for the accumulation of mass in the bulk phases of gas and liquid as well as in the pores of the catalyst particles. Our previous experience [3] has demonstrated that dynamic (or pseudodynamic) models should be preferred not only because of the prediction of transient operation periods, but also to ensure an improved robustness in the numerical solution of the model equations, particularly for countercurrent operations.
- The liquid phase is distributed in the pores of the catalyst as well as inside and outside the packing network. Gas bubbles exist exclusively outside the packing network, since they are not able to penetrate through the network, the size of which is only 0.5 mm.
- The gas and liquid flow patterns are described by a reaction–diffusion model, whereas an approach based on the effective transport coefficient is applied to the flow and the mass transfer between the liquid phases existing inside and outside the catalyst packing network.
- Both catalytic and noncatalytic reactions proceed simultaneously inside the wetted catalyst pores.
- Isothermal cases are modeled; energy balances are thus omitted.

A schematic illustration of the modeling principles is illustrated in Figure 9.4.

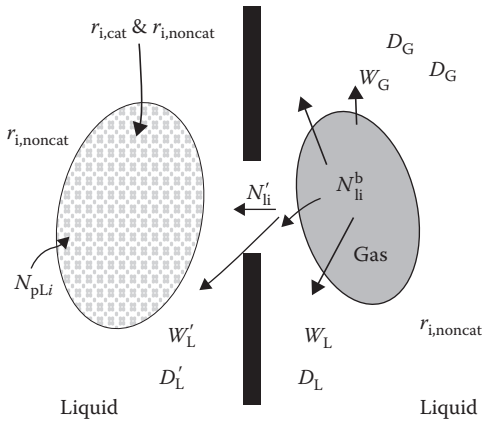

FIGURE 9.4 Schematic illustration of the modeling principles.

9.2.1.1 Mass Balances for the Gas and Liquid Bulk Phases

Based on the hypotheses presented above, the mass balances can be written as follows.

The liquid phase outside the packing network is described by

$$\frac{\mathrm{d}c_{\mathrm{L}i}}{\mathrm{d}t} = \frac{1}{\varepsilon_{\mathrm{L}}}\left(-w_{\mathrm{L}}\frac{\mathrm{d}c_{\mathrm{L}i}}{\mathrm{d}l} + \varepsilon_{\mathrm{L}}D_{\mathrm{L}}\frac{\mathrm{d}^2c_{\mathrm{L}i}}{\mathrm{d}l^2} + N^{\mathrm{b}}_{\mathrm{L}i}a_{\mathrm{v}} - N'_{\mathrm{L}i}a'_{\mathrm{v}} + \varepsilon_{\mathrm{L}}r_{\mathrm{noncat},i}\right), \tag{9.1}$$

where $N^{\mathrm{b}}_{\mathrm{L}i}a_{\mathrm{v}}$ denotes the diffusion flux from the gas bubbles to the liquid bulk and $N'_{\mathrm{L}i}a'_{\mathrm{v}}$ denotes the transport from the liquid bulk into the network, principally consisting of two contributions: molecular diffusion and turbulent exchange between the material inside and outside the network.

For the gas phase outside the packing network:

$$\frac{\mathrm{d}c_{\mathrm{G}i}}{\mathrm{d}t} = \frac{1}{\varepsilon_{\mathrm{G}}}\left[\pm\left(\frac{\mathrm{d}c_{\mathrm{G}i}}{\mathrm{d}l}w_{\mathrm{G}} + \alpha_1\frac{\mathrm{d}w_{\mathrm{G}}}{\mathrm{d}l}c_{\mathrm{G}i}\right) - \alpha_2 c_{\mathrm{G}i}\frac{\mathrm{d}\varepsilon_{\mathrm{G}}}{\mathrm{d}t} + \varepsilon_{\mathrm{G}}D_{\mathrm{G}}\frac{\mathrm{d}^2c_{\mathrm{G}i}}{\mathrm{d}l^2} - N^{\mathrm{b}}_{\mathrm{L}i}a_{\mathrm{v}}\right], \tag{9.2}$$

where $\alpha_1 = 0$ or 1 and $\alpha_2 = 0$ or 1; $\alpha_1 = \alpha_2 = 1$ for cases when it is necessary to account for changes in the volumetric flow rate and holdup of the gas, for instance, in cases in which the gas phase is consumed due to the reaction. Typically, the dispersion coefficient in the gas phase (D_{G}) is rather low, and the system approaches a plug flow. In Equation 9.2, the $-$ and $+$ signs denote the concurrent and countercurrent operation, respectively.

Inside the packing network, only liquid is present, and the balance becomes

$$\frac{\mathrm{d}c'_{\mathrm{L}i}}{\mathrm{d}t} = \frac{1}{\varepsilon'_{\mathrm{L}}}\left[-w'_{\mathrm{L}}\frac{\mathrm{d}c'_{\mathrm{L}i}}{\mathrm{d}l} + \varepsilon'_{\mathrm{L}}D'_{\mathrm{L}}\frac{\mathrm{d}^2c'_{\mathrm{L}i}}{\mathrm{d}l^2} - N_{\mathrm{pL}}a_{\mathrm{p}} + N'_{\mathrm{L}i}a'_{\mathrm{v}} + \varepsilon' r_{\mathrm{noncat},i}\right]. \tag{9.3}$$

The model consists of a set of parabolic PDEs 9.1 through 9.3. For the reactor inlet and outlet, the classical boundary conditions of Danckwerts are applied. The boundary conditions for the inlet are (Chapter 4)

$$\frac{\mathrm{d}c_{\mathrm{L}i}}{\mathrm{d}l} = \frac{w_{\mathrm{L}}}{\varepsilon_{\mathrm{L}}D_{\mathrm{L}}}\left(c_{\mathrm{L}i} - c_{\mathrm{L}0i}\right); \quad \frac{\mathrm{d}c'_{\mathrm{L}i}}{\mathrm{d}l} = \frac{w'_{\mathrm{L}}}{\varepsilon'_{\mathrm{L}}D'_{\mathrm{L}}}\left(c'_{\mathrm{L}i} - c'_{\mathrm{L}0i}\right), \tag{9.4}$$

$$\frac{\mathrm{d}c_{\mathrm{G}i}}{\mathrm{d}l} = \frac{w_{\mathrm{G}}}{\varepsilon_{\mathrm{G}}D_{\mathrm{G}}}\left(c_{\mathrm{G}i} - c_{\mathrm{G}0i}\right), \tag{9.5}$$

and for the outlet we have

$$\frac{\mathrm{d}c_{\mathrm{L}i}}{\mathrm{d}l} = 0; \quad \frac{\mathrm{d}c'_{\mathrm{L}i}}{\mathrm{d}l} = 0; \quad \frac{\mathrm{d}c_{\mathrm{G}i}}{\mathrm{d}l} = 0. \tag{9.6}$$

The initial conditions valid at $t = 0$ are evident: $c_{\mathrm{L}i}$, $c'_{\mathrm{L}i}$, and $c_{\mathrm{G}i}$ are assigned known profiles throughout the column, that is, constant values inside the column.

9.2.1.2 Interfacial Transport

The fluxes at the gas–liquid interfaces (N_{Li}^{b}) are obtained by equating the fluxes in the gas and liquid films. Moreover, a thermodynamic equilibrium is assumed to prevail at the interface. According to Fick's law, the flux is obtained from a simple two-film expression (Chapters 6 and 7):

$$N_{Li}^{b} a_v = \frac{\left(c_{Gi}^{b}/K_i\right) - c_{Li}^{b}}{(1/K_i a_v) + (1/k_{Gi} a_v K_i)}. \tag{9.7}$$

The exchange of substance between the liquid bulk and the network (N'_{Li}) is described by the phenomenological equation

$$N'_{Li} a'_v = k_{net} a_v \left(c'_{Li} - c_{Li}\right). \tag{9.8}$$

It should be noted that the transfer coefficient (k_{net}) is not a pure mass transfer coefficient, but it is also dependent on the exchange flow rate through the network. Principles similar to those of Kunii and Levenspiel for fluidized beds are thus applied (Chapter 5).

9.2.1.3 Mass Balances for the Catalyst Particles

For the description of molecular and Knudsen diffusion inside the catalyst particles, the concept of the effective diffusion coefficient (D_{ei}) combined with Fick's law is applied. Different catalyst geometries are accounted for by the shape factor ($a = 1$ for slabs, $a = 2$ for infinite cylinders, and $a = 3$ for spheres; see Chapter 5). Catalytic and noncatalytic reactions are assumed to proceed simultaneously in completely wetted catalyst pores.

Consequently, for the concentration profiles inside the catalyst particles, the component mass balance equation is written using dimensionless coordinates:

$$\frac{\varepsilon_p R_p^2}{D_{ei}} \frac{dc_i}{dt} = \frac{d^2 c_i}{dx^2} + \frac{(a-1)}{x} \frac{dc_i}{dx} + \frac{R_p^2}{D_{ei}} \left(\rho_p r_{i,cat} + \varepsilon_p r_{i,noncat}\right). \tag{9.9}$$

The boundary conditions are listed below:

$$\frac{dc_i}{dx} = 0 \quad \text{at } x = 0; \qquad \frac{dc_i}{dx} = Bi\,(c_{0i} - c_i) \quad \text{at } x = 1, \tag{9.10}$$

where the Biot number for mass transfer is

$$Bi = \frac{k_{Lsi} R_p}{D_{ei}}. \tag{9.11}$$

At the beginning of the reaction, the concentration profiles inside the catalyst particles were known, that is, they were set equal to the bulk-phase concentrations.

The flux into the particles (N_p) is, in principle, obtained from the concentration gradients at the outer surface of the catalyst particle, but numerically a more robust way is to utilize the whole concentration profile, that is, the integrated generation rates:

$$N_{pi}(x=1) = \rho_p R_p \int_0^1 r_{i,\text{cat}} x^{a-1}\,dx + \varepsilon_p R_p \int_0^1 r_{i,\text{noncat}} x^{a-1}\,dx. \tag{9.12}$$

The approach presented above in Equation 9.12 suppresses the effect of numerical errors originating from the solution of the differential equation, Equation 9.9. The effectiveness factors are obtained by dividing the flux in Equation 9.12 with the rate calculated with bulk-phase concentrations.

For cases in which diffusion resistance inside the catalyst particles can be neglected, the generation rates (r_i) are constant in the particle, the integration of Equation 9.12 becomes trivial, and we obtain

$$N_{pi}(x=1) = \frac{R_p}{a}\left(\rho_p r_{i,\text{cat}} + \varepsilon_p r_{i,\text{noncat}}\right). \tag{9.13}$$

9.2.1.4 Numerical Solution of the Column Reactor Model

Mathematically, the system consists of parabolic PDEs, which were solved numerically by discretization of the spatial derivatives with finite differences and by solving the ODEs thus created with respect to time (Appendix 2). Typically, 3–5-point difference formulae were used in the spatial discretization. The first derivatives of the concentrations originating from a plug flow (Equations 9.1 through 9.3) were approximated with BD formulae, whereas the first and second derivatives originating from axial dispersion in the bulk phases and diffusion inside the catalyst particles were approximated by central difference formulae. Some simple backward (Equation 9.14) and central difference (Equation 9.15) formulae are shown here as examples:

$$\left(\frac{dy}{dx}\right)_{x=x_0} = \frac{1}{60\,h}\left(147y_0 - 360y_{-1} + 450y_{-2} - 400y_{-3} + 225y_{-4} - 72y_{-5} + 10y_{-6}\right), \tag{9.14}$$

$$\left(\frac{d^2y}{dx^2}\right)_{x=x_0} = \frac{1}{180}\left(2y_{-3} - 27y_{-2} + 270y_{-1} - 490y_0 + 270y_{+1} - 27y_{+2} + 2y_{+3}\right). \tag{9.15}$$

The system of ODEs thus created is sparse and stiff. This is why the ODE solution methodology was based on the program package of Hindmarsh (Appendix 2), which utilizes the BD method of Henrici, often called Gear's method. The results of the modeling effort are shown in Figures 9.5 and 9.6. The strong diffusion limitation inside the catalyst pellets is illustrated in Figure 9.6. A model neglecting the internal mass transfer resistance inside the catalyst pellet would be completely wrong.

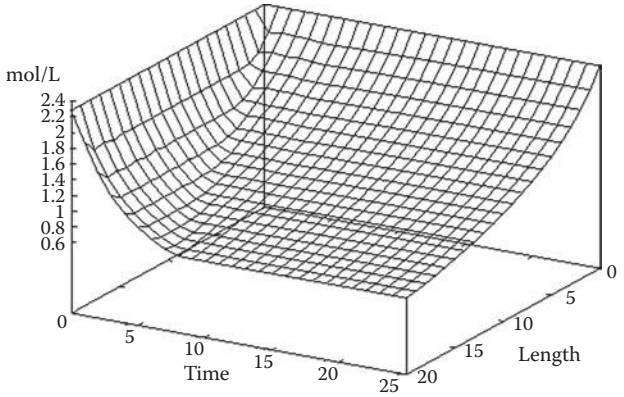

FIGURE 9.5 Contour plot of concentration (Fe^{2+}) in the column reactor (4.7 bar oxygen, 120°C).

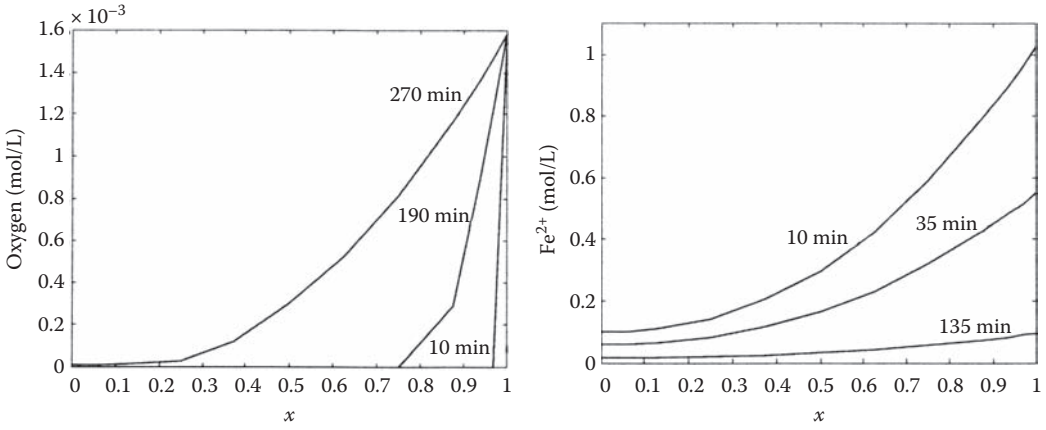

FIGURE 9.6 Concentration of oxygen (left) and $FeSO_4$ (right) inside a catalyst particle at different reaction times (60°C, 6 bar).

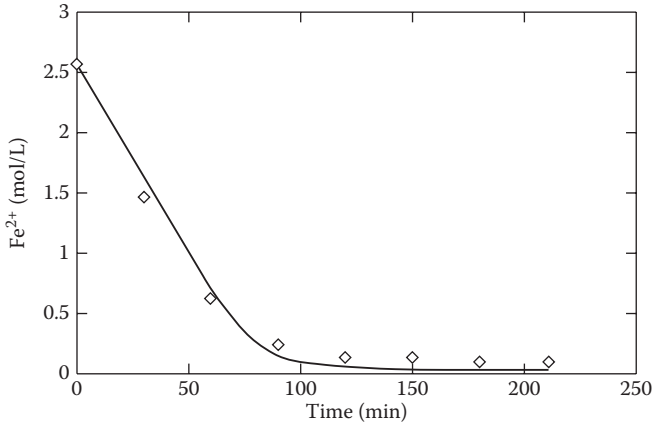

FIGURE 9.7 Model verification experiment (120°C, 4.7 bar oxygen).

Some results from model verification experiments are shown in Figure 9.7. The liquid flow rates were so high that ferrous sulfate conversion was low during one cycle through the catalyst bed. This is why the liquid phase was recirculated several times through the column in order to obtain measurable conversions. The kinetic, thermodynamic, and diffusion parameters were implemented in the simulation model, and the value of the gas–liquid mass transfer parameter was adjusted for the best possible fit to the experimental data. The results are illustrated in Figure 9.7, which shows a fairly good agreement between the model and the experimental data.

9.2.1.5 Concluding Summary

A dynamic mathematical model of the three-phase reactor system with catalyst particles in static elements was derived, which consists of the following ingredients: simultaneous reaction and diffusion in porous catalyst particles; plug flow and axial dispersion in the bulk gas and liquid phases; effective mass transport and turbulence at the boundary domain of the metal network; and a mass transfer model for the gas–liquid interface.

The model parameters were estimated from pulse experiments and CFD calculations. The liquid velocities at different locations of the reactor system were studied off-line with the aid of CFDs, which were used to obtain realistic values for superficial velocities inside the catalyst packing network.

The governing parabolic PDEs describing the model were discretized with respect to the spatial coordinates of the catalyst particles and the column length coordinate. The resulting ODEs were solved numerically with the sparse version of the stiff ODE solver, LSODES (Appendix 2).

The model solution procedure turned out to be robust and reliable, as illustrated by the reactor simulations (Figure 9.7). The model was verified with a realistic test system, oxidation of ferrous sulfate to ferric sulfate (Figure 9.6). The sample chemical system is relevant in the production of ferric sulfate, an efficient coagulation agent used in water purification. The model was able to describe the progress of the reaction in a Katapak column reactor, where the gas phase was continuous and the liquid phase was recycled. A good agreement was obtained between the experimental data and the model simulations. This modeling concept is a general one: it can be applied to any chemical system in a column reactor containing structural packing elements.

9.2.2 MONOLITH REACTORS

Traditionally, monolith reactors have demonstrated their performance in gas-phase reactions, particularly in the treatment of automotive exhaust gases. Today, virtually all vehicles are equipped with catalytic converters. Here we will consider three-phase applications. These have been studied by a few authors and research groups such as Moulijn and coworkers [4,5] and Irandoust and Andersson [6]. Certain industrial processes such as hydrogenation of anthraquinone in the production of hydrogen peroxide are also examples of the monolith reactor technology being established on an industrial scale. Monolith

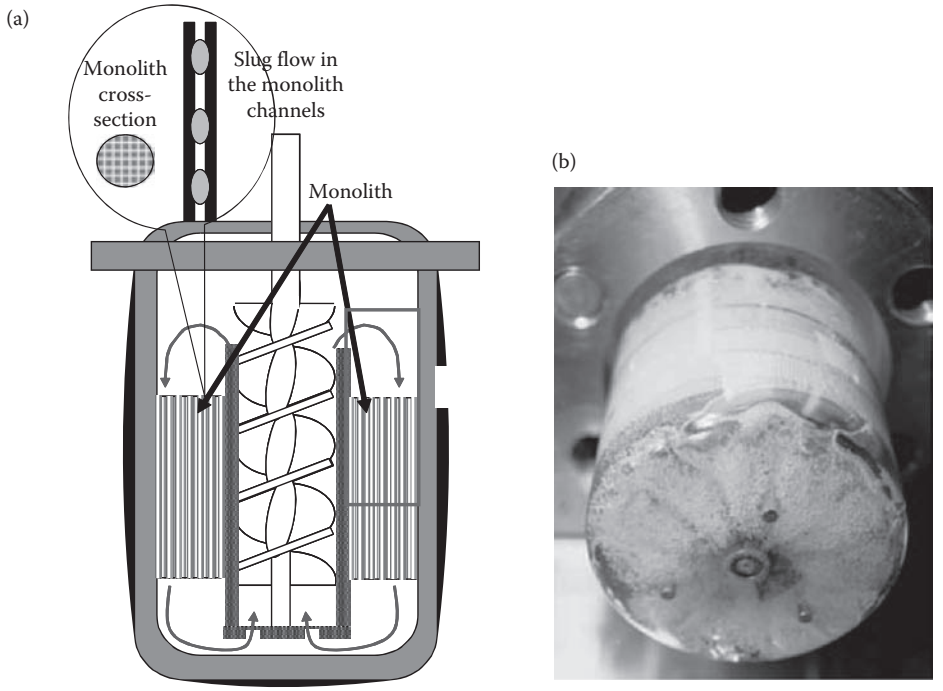

FIGURE 9.8 Laboratory-scale monolith test reactor (a) schematically and (b) in reality.

reactors combine the benefits of slurry reactors (thin catalyst layer) and fixed beds (low pressure drop).

Kinetics can be screened in a screw impeller-stirred reactor (SISR) [7] (Figure 9.8). The reactor system comprises a screw impeller that pumps the liquid upwards, and the high exit velocity of the liquid results in an effective foam formation in the top section of the reactor. A slug flow (Chapter 6) is thus established in the monolith channels. Consequently, the liquid and gas are pumped from the lower section to the upper section of the reactor, over and over again. In fact, the concept resembles that of a loop reactor. Cylindrical monoliths are placed in the stator of an SISR (Figure 9.8), and a foam of gas and liquid is forced through the monolith channels by a screw.

We will next look at a three-phase hydrogenation reaction in the production of fine chemicals. The monolith catalyst was prepared by a commercial cordierite skeleton. On the walls of the parallel channels, a solid catalyst phase was synthesized. The basic treatment of the reactor system is very straightforward, since the system can be characterized as a "frozen" slurry reactor, that is, a traditional batch or a semibatch approach can be utilized.

Traditional modeling concepts can be complemented by new elements: if we consider the RTD in the channels, CFD becomes useful. The information from the CFD model can be transferred to a simplified simulation model, in which the monolith and the mixing system are described by parallel tubular reactors coupled to a mixing space.

RTD is a classical tool in predicting the comportment of a chemical reactor: provided that the reaction kinetics and mass transfer characteristics of the system are known, reactor

performance can be calculated by combining kinetic and mass transfer models with an appropriate RTD model. RTDs can be determined from pulse or step response experiments (Chapter 4). This technique is elegant in principle, but it requires access to a real reactor system. In large-scale production, experimental RTD studies are not always possible or allowed.

The current progress of CFD enables computational "experiments" in a reactor apparatus to reveal the RTD. Typically, CFD is used for nonreactive fluid systems, but nowadays reactive systems can also be computed as discussed in Ref. [8]. The difficulties of CFD, however, increase considerably as multiphase systems with chemical reactions are examined. For this reason, a logical approach is to utilize CFD to catch the essential features of the flow pattern and to use this information in classical reactor models based on RTDs.

9.2.2.1 Flow Distribution from CFD Calculations

In monolith reactors, the distribution of fluid into the channels is typically at least somewhat uneven [9]; this is why it is very important to predict the flow distribution and include it in the quantitative modeling. Experimental techniques can also be used to study the flow distribution in monolith channels; this method is introduced in Figure 9.9 [10]. CFD calculations make it possible to obtain the flow characteristics of the experimental system. In this case, the calculations were performed using the software CFX.4.4 [7]. The flow profiles in the gas and liquid phases were described by the turbulent k–ε method (320,000 calculation elements), and to evaluate the distribution of gas bubbles, the multiple size group method was applied. The results from the CFD calculations gave the flow velocities for gas

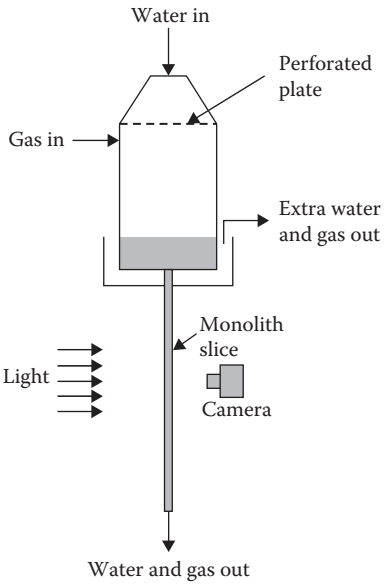

FIGURE 9.9 Experimental setup to study the gas and liquid flow distributions in monolith channels.

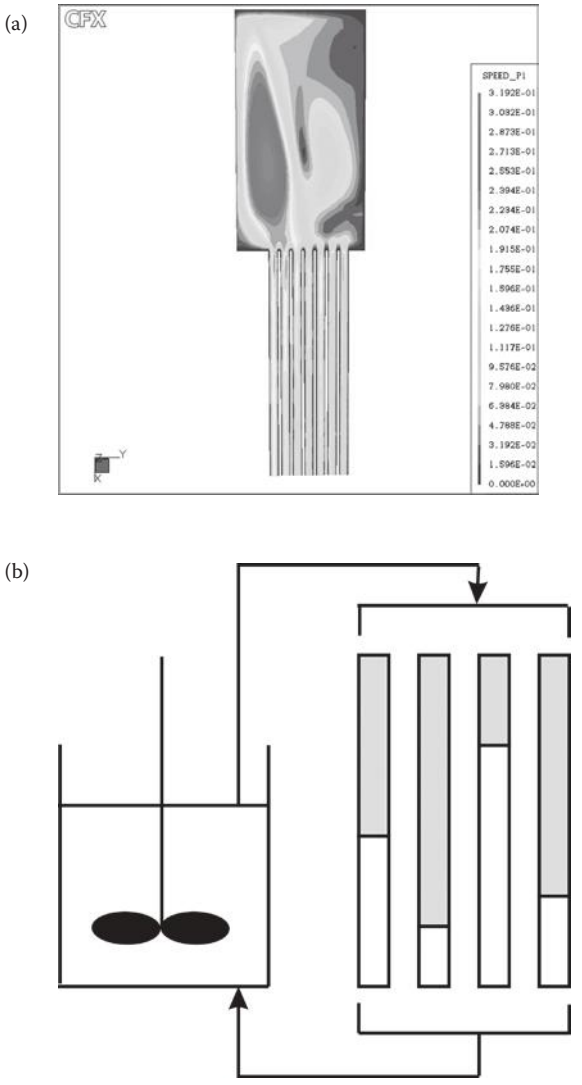

FIGURE 9.10 (a) Flow distribution calculated in the monolith channels by CFD and (b) a simplified flow sheet of the monolith system described as parallel tube reactors and stirred mixing volume.

and liquid, the bubble sizes, and the gas and liquid holdups in the channels (Figure 9.10). This information can be utilized in the conventional reactor model. The predicted slug flow (Taylor flow) conditions in the monolith channels were also confirmed by a visual investigation of the flow by replacing the autoclave with a glass vessel of an equal size (Figure 9.8). Schematically, the reactor can be regarded as a system of parallel tubes with varying residence times. The screw acts as a mixer, which implies that the outlet flows from the channels are merged together and the inlet flows to the monolith channels have a uniform chemical composition. The principal flow sheet is displayed in Figure 9.10. The simplified mass balance equations are derived on the basis of this flow sheet.

9.2.2.2 Simplified Model for Reactive Flow

The surroundings of the monolith can be regarded as a perfectly backmixed system, in which no reactions take place [7]. The monolith channels can be described using the plug flow concept. The gas–liquid and the liquid–solid mass transfer resistances are easily included in the model. Since the catalyst layer is very thin (few micrometers) and the reactions considered in the present case were slow, the internal mass transfer resistance in the catalyst layer was neglected. The gas-phase pressure in the reactor was maintained constant by the controlled addition of hydrogen. Temperature fluctuations during the experiments were negligible; the energy balances were thus not needed. Conversions of the reactants were minimal during one cycle through the monolith, which implies that a constant gas holdup was assumed for each channel. The reactions were carried out in inert solvents, and the liquid density did not change during the reaction. Based on this background information, the dynamic mass balance for the liquid phase in each channel can be written as follows:

$$\dot{n}_{\mathrm{L},ij,\mathrm{in}} + N_{\mathrm{L},ij}\Delta A_{\mathrm{L}} = N_{\mathrm{L},ij} + \dot{n}_{\mathrm{L},ij,\mathrm{out}} + \frac{\mathrm{d}n_{\mathrm{L},ij}}{\mathrm{d}t}, \tag{9.16}$$

where i and j denote the component and the channel, respectively. Due to the assumption of constant density, the volumetric flow rate does not change, and the model can be expressed by concentrations. The basic volume element is allowed to shrink, and the hyperbolic PDE is obtained:

$$\frac{\mathrm{d}c_{\mathrm{L},ij}}{\mathrm{d}t} = N_{\mathrm{L},ij}a_{\mathrm{L}} - N_{\mathrm{S},ij}a_{\mathrm{S}} - \frac{1}{\tau_{\mathrm{L},j}\varepsilon_{\mathrm{L},j}}\frac{\mathrm{d}c_{\mathrm{L},ij}}{\mathrm{d}z}. \tag{9.17}$$

This complete model is valid for all of the components but, actually, the gas–liquid mass transfer ($N_{\mathrm{L},ij}$) term is nonzero for hydrogen only. The PDE model can be further simplified by taking into account the fact that conversion is minimal during one cycle through the channel, and the concentration profile in the channel can be assumed to be almost linear, that is, the differential reactor concept can be applied. The entire model can now be expressed by the average (c^*) and the outlet concentration (c_0):

$$\frac{\mathrm{d}c^*_{\mathrm{L},ij}}{\mathrm{d}t} = N^*_{\mathrm{L},ij}a_{\mathrm{L}} - N^*_{\mathrm{L},ij}a_{\mathrm{S}} - \frac{2}{\tau_{\mathrm{L},j}\varepsilon_{\mathrm{L},ij}}\left(c^*_{\mathrm{L},ij} - c_{0\mathrm{L},ij}\right). \tag{9.18}$$

The exact formulations of the fluxes (N^*) depend on the particular model being used for mass transfer; principally, the whole scope is feasible, from Fick's law to the complete set of Stefan–Maxwell equations. Since the only component of importance for the gas–liquid mass transfer is hydrogen, which has limited solubility in the liquid phase, the simple two-film model along with *Fick's law* was used, yielding the flux expression

$$N^*_{\mathrm{L},ij} = k'_{\mathrm{L},ij}\left(\frac{c^*_{\mathrm{G},ij}}{K_i} - c^*_{\mathrm{L},ij}\right). \tag{9.19}$$

For the liquid–solid interface, a local quasi-steady-state mass balance takes the form

$$N^*_{\mathrm{L},ij} a_\mathrm{S} + r^*_{ij} \rho_\mathrm{B} = 0. \tag{9.20}$$

In case the liquid–solid mass transfer is rapid, the bulk and surface concentrations coincide, and the rate expression is directly inserted into the balance equation, which becomes

$$\frac{\mathrm{d}c^*_{\mathrm{L},ij}}{\mathrm{d}t} = r^*_{ij} \rho_\mathrm{B} - \frac{2}{\tau_{\mathrm{L},j} \varepsilon_{\mathrm{L},j}} \left(c^*_{\mathrm{L},ij} - c_{0\mathrm{L},ij} \right). \tag{9.21}$$

The surroundings of the monolith are described by the concept of complete backmixing, which leads to the following overall mass balance for the components in the surrounding liquid phase:

$$\frac{\mathrm{d}c_{0\mathrm{L},ij}}{\mathrm{d}t} = \frac{1}{\tau_\mathrm{L}} \left(\sum \left(2c^*_{\mathrm{L},ij} - c_{0\mathrm{L},ij} \right) \alpha_{\mathrm{L},j} - c_{0\mathrm{L},j} \right). \tag{9.22}$$

The treatment of the gas phase is analogous to that of the liquid phase. The flux describing the gas–liquid mass transfer is given by Equation 9.19. Consequently, the dynamic mass balance for the monolith channels can be written as

$$\frac{\mathrm{d}c^*_{\mathrm{G},ij}}{\mathrm{d}t} = -N^*_{\mathrm{L},ij} a_\mathrm{L} - \frac{2}{\tau_{\mathrm{G},j} \varepsilon_{\mathrm{G},j}} \left(c_{\mathrm{G},ij} - c_{0\mathrm{G},i} \right). \tag{9.23}$$

For the monolith surroundings, the concept of complete backmixing leads to the formula

$$\frac{\mathrm{d}c_{0\mathrm{G},i}}{\mathrm{d}t} = \frac{1}{\tau_\mathrm{G}} \left(\sum \left(2c^*_{\mathrm{G},ij} - c_{0\mathrm{G},ij} \right) \alpha_{\mathrm{G},j} - c_{0\mathrm{G},j} \right). \tag{9.24}$$

The model for the schematic system (Figure 9.10) consists of the simple ODEs, Equations 9.21 through 9.24, which form an initial value problem (IVP). In case pure hydrogen is used, its pressure is kept constant and the liquid-phase components are nonvolatile, the gas-phase balance Equations 9.23 and 9.24 are discarded, and the gas-phase concentration is obtained, for example, from the ideal gas law. The initial conditions, that is, the concentrations at time $t = 0$, are equal everywhere in the system, and the IVP can be solved numerically by any stiff ODE solver (Appendices 2 and 3).

9.2.2.3 Application: Catalytic Three-Phase Hydrogenation of Citral in the Monolith Reactor

Hydrogenation of citral was selected as an example, because it nicely illustrates a case with complex stoichiometry and kinetics, which is characteristic for fine chemicals. The stoichiometric scheme is shown in Figure 9.11. The reaction system is relevant for the manufacture of fragrances, since some of the intermediates, citronellal and citronellol, have a pleasant smell, while the final product 3,7-dimethyloctanol is useless. This is why the

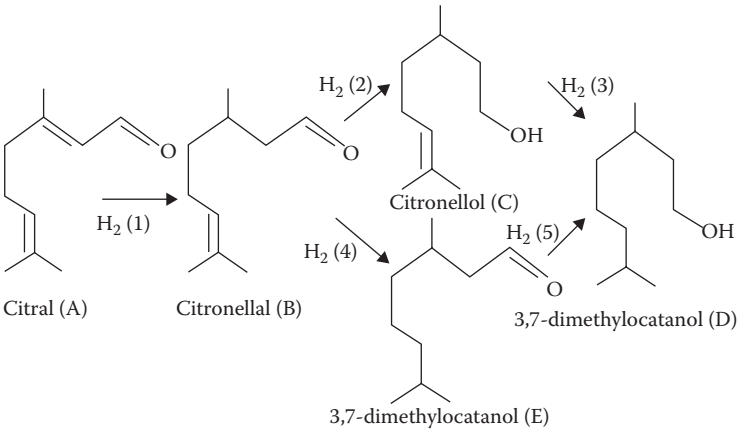

FIGURE 9.11 Stoichiometric scheme for citral hydrogenation.

optimization of product yield is of crucial importance. Isothermal and isobaric experiments were carried out under hydrogen pressure in a monolith reactor system at various pressures and temperatures (293–373 K, Figure 9.11).

The product distribution depends considerably on the reaction conditions: at low temperatures and hydrogen pressures, the system operates under kinetic control, and the desired intermediate products were obtained in high yields. As the temperature and hydrogen pressure were increased, the final product was favored. The individual mass transfer coefficients were estimated using the molecular diffusion coefficient of hydrogen in the liquid phase along with the hydrodynamic film thickness [11]. Different modeling concepts, that is, a quasi-homogeneous batch model versus the parallel tube model, in combination with flow data for the channels obtained from CFD calculations, were compared in Figure 9.12 [7]. Since the film thickness depends on the local velocity, the mass transfer coefficient was different in different channels. The rate equations describing the reaction scheme (Figure 9.11) can be found in Ref. [7]. The kinetic parameters were determined by nonlinear regression (Appendix 10).

The weighted sum of squares between measured and estimated concentrations (Appendix 10) was minimized by a hybrid Simplex–Levenberg–Marquardt algorithm. The model equations were solved *in situ* in the parameter estimation by the BD method (Appendix 2). The estimated parameters were the kinetic and adsorption equilibrium constants of the system. The simulation results revealed that the model was able to describe the behavior of the system. The parameter values were reasonable and comparable with the values obtained from citral hydrogenation in a slurry reactor [12].

9.2.3 FIBER REACTOR

Another new class of structured reactors consists of different kinds of fiber or matt structures, coated with catalytically active materials. Typically, the fiber structures can be made from different polymeric materials, for example, polyethylene. These fibers can be free-standing (such as Smoptech Smopex®, [13]) or knitted structures [14,15] with catalytically

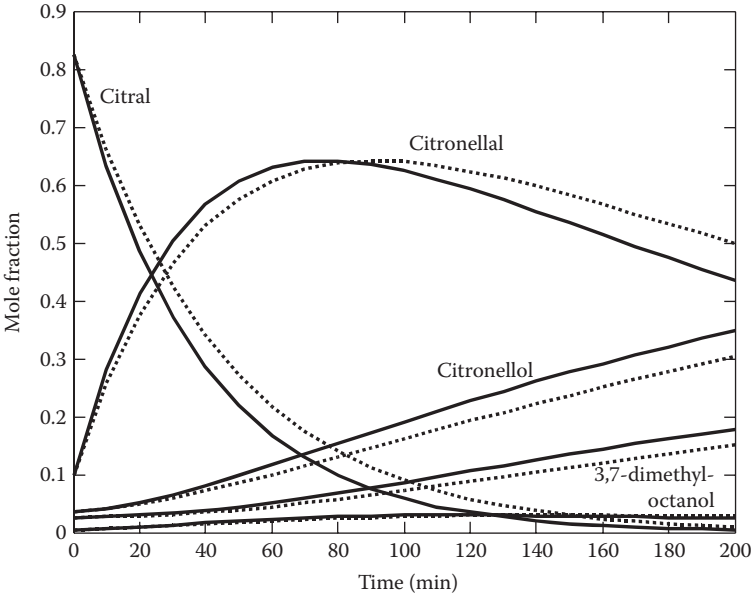

FIGURE 9.12 Comparison of two modeling approaches in the hydrogenation of citral on a Ni catalyst. Simulation with a BR model (—) and CSTR connected to parallel tubes with a plug flow model (·····).

active materials attached to the structure. These structures can be utilized as such in slurry reactors, freely floating or attached to special, tailor-made agitator devices. A very natural solution is, however, to use them, especially in the case of knitted carpet structures, in fixed bed reactors. The structures of knitted fiber catalysts, of silica and polymer-active carbon types, are introduced in Figures 9.13 and 9.14.

The application was studied as an example, namely, the continuous enantioselective hydrogenation of 1-phenyl-1,2-propanedione with Pt on a silica fiber modified with chiral (–)-cinchonidine (natural alkaloid) [14]. The main goal is to produce one of the optical isomers, namely (R)-1-hydroxy-1-phenylpropanone, in high yields. This isomer is an important intermediate in the synthesis of pharmaceuticals. The complete reaction scheme is introduced in Figure 9.15.

For this system, the existence of mass transfer limitations was investigated by changing the amount of the catalyst and, at the same time, keeping the space time constant but varying the liquid flow rate. Interesting new results were obtained by transient experiments, in which the modifier flow was stopped and started, resulting in variations in the enantioselectivity (Figure 9.16) and regioselectivity. The behavior of the system was described by a dynamic axial dispersion model. The value of the dispersion coefficient was determined with pulse experiments, using an inert tracer (Figure 9.17). An example of the model's fit to experimental data is provided by Figure 9.17, which shows that the model description is adequate.

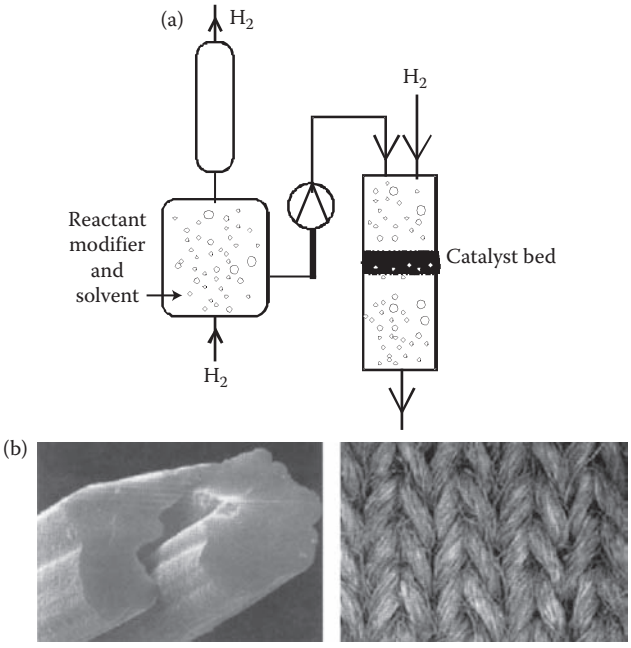

FIGURE 9.13 (a) Three-phase continuous hydrogenation of an organic compound over a metal supported on silica fibers. (b) A scanning electron microscopy (SEM) image of a knitted silica fiber catalyst.

9.2.4 MEMBRANE REACTOR

Equilibrium-limited processes are a huge challenge for reaction engineering and reactor technology. For instance, if dehydrogenation of a reactant (A) molecule on a solid catalyst is to be carried out, the products (P and hydrogen) retard the reaction rate as soon as

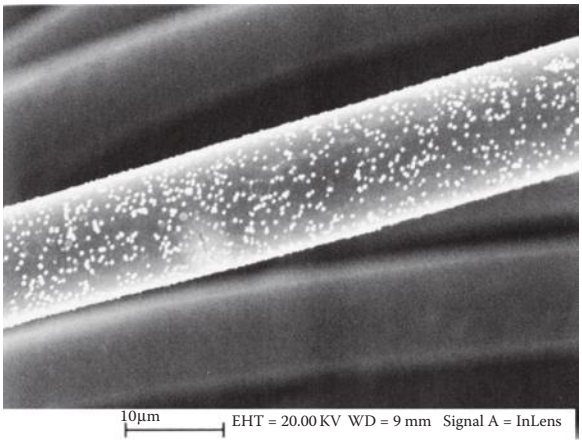

FIGURE 9.14 An SEM image of Pt on Kynol®-activated carbon fiber catalyst.

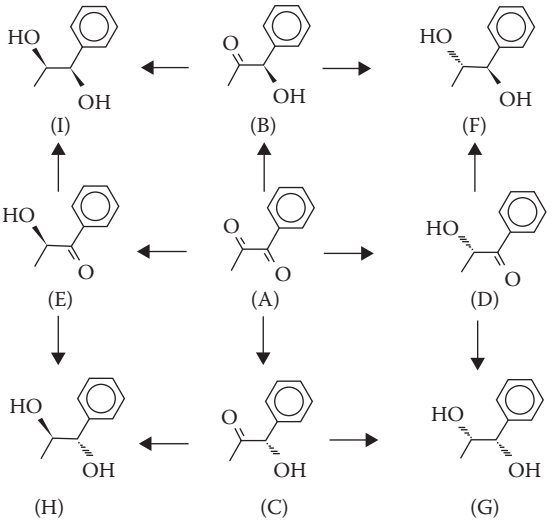

FIGURE 9.15 Reaction scheme of 1-phenyl-1,2-propanedione hydrogenation on supported Pt. Catalyst modifier: cinchonidine.

they appear:

$$A + \text{cat} \rightleftarrows P + H_2.$$

One way of forcing the reaction toward high conversion is to combine the catalyst and membrane technologies. The reaction is carried out in a porous membrane tube covered with the catalyst material. The principal concept is shown in Figure 9.18. The reaction proceeds on metal spots deposited on the membrane material. Simultaneously, the smallest product molecules (in this case H_2) diffuse out of the system through the membrane. In this way, the equilibrium limitation is removed, and the process proceeds almost as an irreversible reaction in the ideal case. The additional benefit is that the components of the product gas are directly separated, and the construction of a specific separation unit is avoided. For the reactor construction, see Figure 9.19. From the reaction engineering

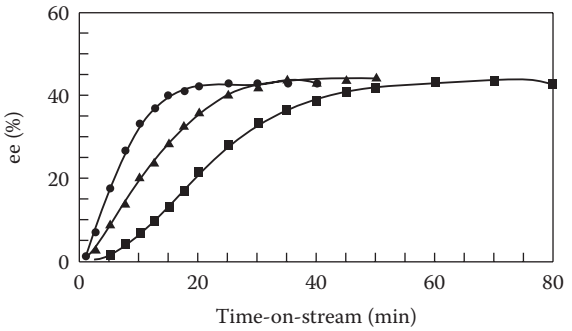

FIGURE 9.16 Enantiomeric excess ($ee = (c_B - c_c)/(c_B + c_c)$) as a function of space time (● 22 s, ◀ 30 s, ■ 44 s) in a fiber reactor. For the reaction scheme, see Figure 9.15.

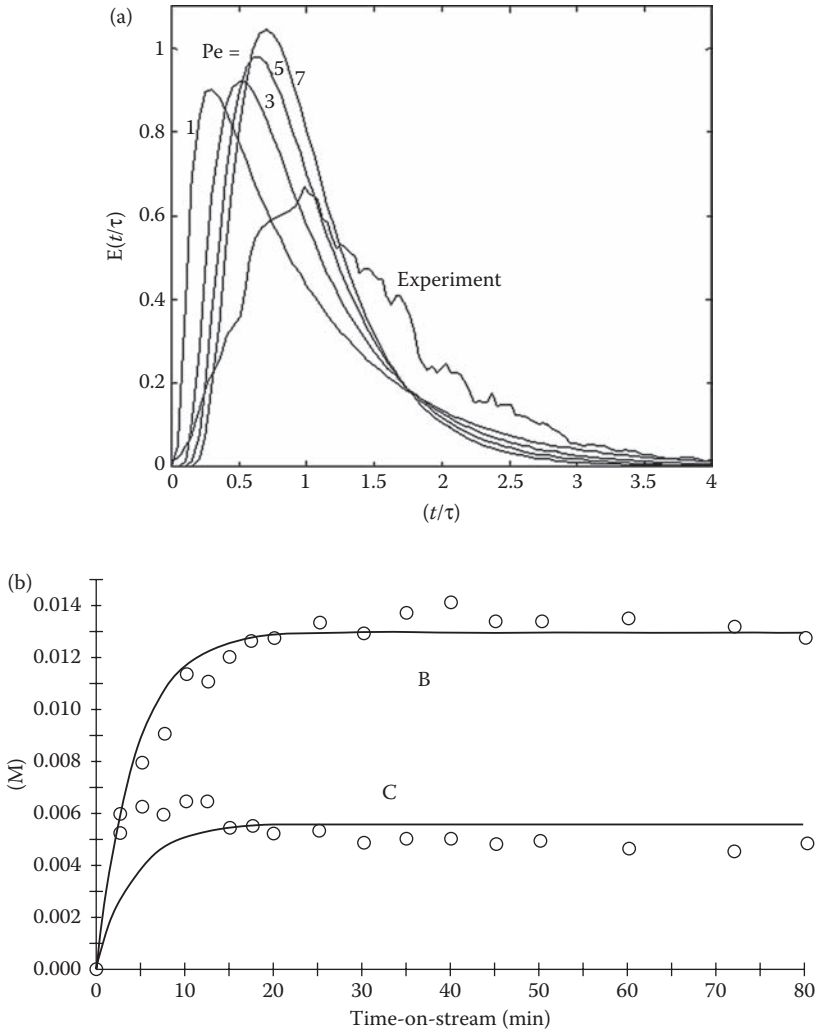

FIGURE 9.17 (a) Tracer experiments in a three-phase tubular reactor with knitted silica catalyst layers. (b) A fit of the kinetic model based on transient data (Figure 9.15).

viewpoint, it is not a problem to model the simultaneous reaction and separation in the porous membrane layer. The real challenge lies in the development of selective and durable membrane materials.

9.2.5 MICROREACTOR

In recent years, research activities have paid increasing attention to reactions on a very small scale. The development of manufacturing technology has also enabled the production of miniature components for chemical reactor technology. Microstructured or microchannel reactors are called microreactors. They can also be defined as miniaturized reaction systems. The channel dimensions in microreactors are typically $\approx 50\,\mu m$ to 2 mm. Microreactor manufacturers provide microstructured mixers, heat exchangers,

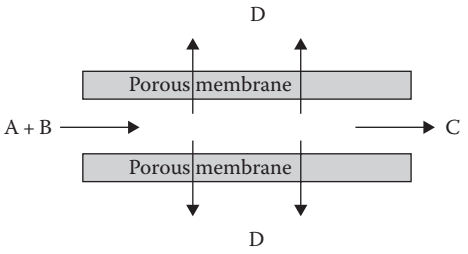

FIGURE 9.18 General function principle of a catalytic membrane reactor, reversible reaction $A + B \rightleftarrows C + D$.

and reaction modules for gas- and liquid-phase reactions. Generally, these components consist of microstructured plates including flow channels for fluids. Even microstructured separation units and gas–liquid reactor devices are available. The reactor modules for liquid-phase and gas–liquid-phase reactions usually consist of combined reaction channel heat exchanger units. For a few examples of microstructured reactor systems, see Figures 9.20 and 9.21.

Microreactor technology (MRT) satisfies three basic requirements for a chemical reaction: it can easily provide for an optimal reaction time (contact time), introduction or removal of heat into the reaction zone, and sufficient mass transfer. The reduced dimensions of MRT systems make them applicable to reactions that require good transport properties. An important feature is their high surface area-to-volume ratio. This is particularly important for reactions that require efficient heat transfer, that is, highly exothermic or endothermic reactions. In a traditional stirred tank reactor, the reaction rate can be compromised because of the limited heat transfer capacity and, in the case of hazardous reactions such as nitrations, a run-away might be induced by inefficient heat transfer. In the case of

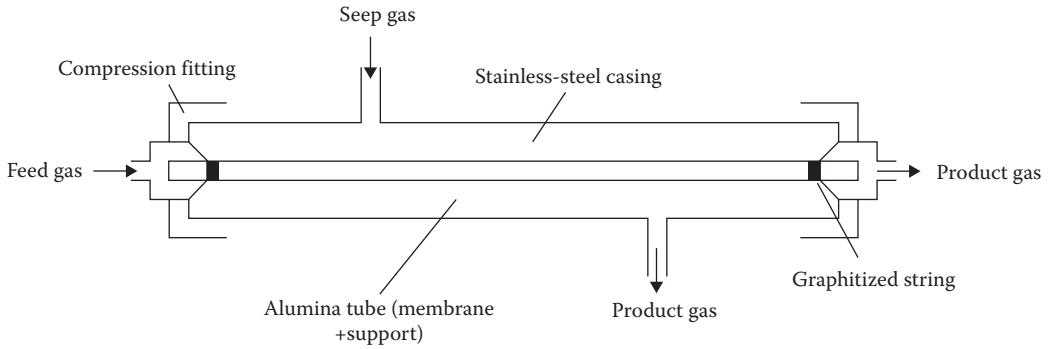

FIGURE 9.19 Membrane reactor in practice. The application: dehydrogenation of ethane, $CH_3CH_3 \rightleftarrows CH_2 = CH_2 + H_2$. The ceramic tube consists of a multilayered composite: Pt crystallites. (Data from Moulijn, J.A., Makkee, M., and van Diepen, A., *Chemical Process Technology*, Wiley, 2001.)

FIGURE 9.20 Microstructured reactor setup for gas-phase studies (parts manufactured by Institut für Mikrotechnik Mainz Gmbh).

microreactors, the overall reaction rate can be controlled by intrinsic kinetics. Moreover, precise temperature control is facilitated. Isothermal reaction conditions and short contact times give rise to improved yields and selectivities in comparison with conventional reaction technology. Small dimensions facilitate short diffusion distances for the chemical species, also providing efficient mixing in the case of laminar flow conditions. Uniform concentration distributions countereffect the by-product formation. The small volumes and small reagent amounts, together with efficient heat transfer and easy process control properties, improve plant safety.

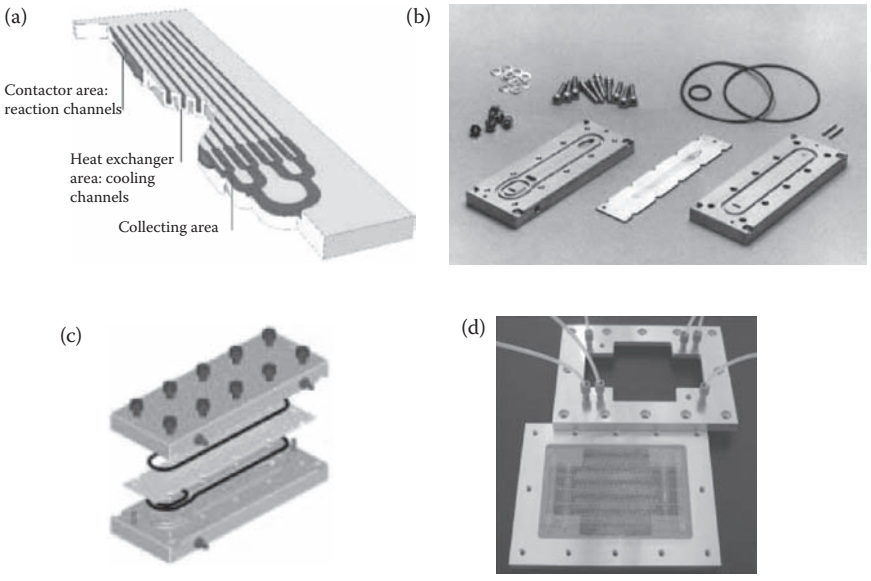

FIGURE 9.21 Specialized reactor components for liquid-phase reactions: (a) reaction plate, (b) individual reactor parts, (c) assembly of the microreactor, by Institut für Mikrotechnik Mainz Gmbh (IMM), and (d) microreactor by Mikroglas Chemtech.

In laboratory-scale kinetic studies, microreactors show especially promising features. Typical tasks, such as the determination of reaction kinetics and catalyst screening in combination with the small amounts of reactants needed, enhance the work. A large number of experiments can be carried out on a shorter time scale. The small dimensions of the flow channels enable kinetic measurements in the absence of mass and heat transfer limitations, mixing is efficient, and, consequently, the disturbances introduced into kinetic data are eliminated. The thickness of the liquid layer in micromixers is in the range of a few tens of micrometers, resulting in mixing times measured in milliseconds, in some cases even nanoseconds. This kind of mixing times cannot be achieved in any conventional equipment. Since the flow channel diameters can be in the range of 50–500 μm, the heat transfer area-to-volume ratios achieved are 10,000–50,000 m^2/m^3. In conventional laboratory- and industrial-scale equipment, we can maximally attain values ranging from 100 to 1000 m^2/m^3. Moreover, the heat transfer coefficient in microreactors can achieve values up to 25,000 W/m^2 K, which is a much higher value than that achieved in traditional equipment. In multiphase applications, the characteristic surface ratios between the phases can reach values up to 5000–30,000 m^2/m^3, whereas in traditional bubble columns, values around 100 m^2/m^3 are attainable (in best laboratory-scale experiments with traditional equipment some 2000 m^2/m^3) [17,18].

When using MRT, the step from the laboratory to the industrial scale, that is, scaleup, is easy: in the best case, the industrial unit is constructed by multiplication of parallel small units, similar to those used in laboratory experiments. This procedure is sometimes called number-up. On the other hand, MRT offers the possibility of decentralized production, so that multiple relatively small on-site units are used instead of one, large production facility in line with conventional strategy. According to the Institut für Mikrotechnik Mainz Gmbh, the upper capacity limit for MRT is around 1000 t/a. It has been calculated that 20% of the chemicals produced within the European Union (EU) have a production volume smaller than 10 t/a. Most of these processes are carried out in stirred tank reactors to produce fine chemicals. This is why, especially in the production of high value-added chemicals, the higher cost of MRT can be overcome by the benefits of this exciting new technology.

9.3 TRANSIENT OPERATION MODES AND DYNAMIC MODELING

The nonstationary (transient) operation of chemical reactors is traditionally applied in kinetic research in order to reveal reaction mechanisms. Pulses and step changes can be introduced in continuous reactors, and concentration changes at the reactor outlet are monitored by on-line or off-line analysis. The method is applicable to both gas- and liquid-phase systems. Isotope exchange can be commenced wherein H_2/D_2 (hydrogen/deuterium) experiments can reveal the role of hydrogen in a catalytic process. Some examples of catalytic isomerizations are displayed in Figure 9.22. A reaction network for hydrocarbon isomerization is shown in Figure 9.22.

Mathematical modeling can be applied to transient data. The crucial issue is to include the accumulation term (dn_i/dt) in all mass balances and to take into account the changes

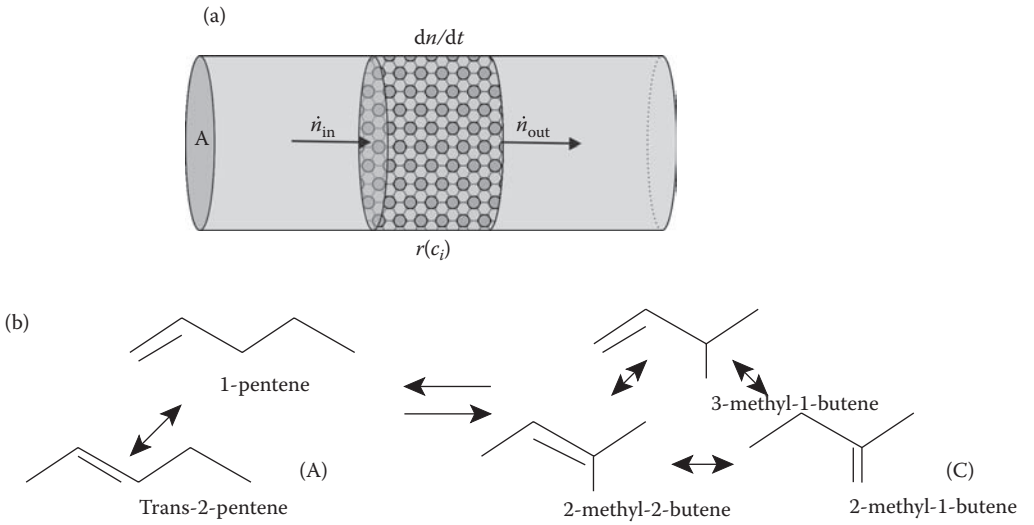

FIGURE 9.22 (a) Reactor volume element and (b) the chemical system for skeletal isomerization.

in surface coverages of adsorbed species. In addition, a model for catalyst deactivation is included.

Let us look at a reactor volume element as illustrated in Figure 9.22. The mass balance of a component in the volume element is

$$\dot{n}_{\mathrm{L,in}} + r_i \Delta V \rho_{\mathrm{B}} = \dot{n}_{i,\mathrm{out}} + \frac{\mathrm{d}n_i}{\mathrm{d}t}, \tag{9.25}$$

where $\dot{n}_i$ is the molar flow, ΔV is the volume element, ρ_{B} is the catalyst bulk density, and r_i is the reaction rate. We will introduce the notations $\dot{n}_{i,\mathrm{out}} - \dot{n}_{i,\mathrm{in}} = \delta \dot{n}_i$ and, recalling that $\dot{n}_i = c_i \Delta V_{\mathrm{L}} = c_i \varepsilon_{\mathrm{L}} \Delta V$, a rearrangement yields

$$\frac{\mathrm{d}c_i}{\mathrm{d}t} \varepsilon \Delta V = \Delta V r_i \rho_{\mathrm{B}} - \Delta \dot{n}_i, \tag{9.26}$$

where c_i is the component concentration and ε is the liquid holdup. By assuming a constant flow, we rewrite $\Delta V = \mathrm{A}\Delta \mathrm{l}$, $\Delta \dot{n} = w \Delta c_i \mathrm{A l}$ and divide by $\varepsilon \Delta V$. We introduce the dimensionless quantities $z = 1/\mathrm{L}$ and $\Delta z \to 0$, which finally yield the dynamic model for a fixed bed reactor

$$\frac{\mathrm{d}c_i}{\mathrm{d}t} = \frac{1}{\varepsilon} \left(-\frac{w}{L} \frac{\mathrm{d}c_i}{\mathrm{d}z} + r_i \rho_{\mathrm{B}} \right). \tag{9.27}$$

For the adsorbed surface components, the mass balance is written as

$$\frac{\mathrm{d}c_j^*}{\mathrm{d}t} \Delta A' = r_j \Delta m_{\mathrm{cat}}, \tag{9.28}$$

where $\Delta A'$ denotes the accessible catalyst surface area in the volume element. We denote $\Delta m_{\text{cat}}/(\Delta A' c_0^*) = \alpha$, which yields

$$\frac{\mathrm{d}\Theta_j}{\mathrm{d}t} = \alpha r_j, \tag{9.29}$$

where the surface coverage of the component (j) is $\Theta_j = c_j^*/c_0^*$ and α^{-1} represents the sorption capacity of the catalyst.

The component generation rates are obtained from the stoichiometry

$$r_i = \sum \nu_{ik} r_k \tag{9.30}$$

for gas-phase components and

$$r_j = \sum \nu_{jk} r_k, \tag{9.31}$$

for surface species, where r_k denotes the rate of surface step k. The initial conditions arise from the actual experiment reality. Typically, the concentration profile in the reactor is known at the beginning of the experiment:

$$c_i = c_i(z) \quad \text{at } t = 0. \tag{9.32}$$

The initial condition for the system is that the inlet concentrations are known during the experiment:

$$c_{0i} = c_{0i}(t) \quad \text{at } t \geq 0. \tag{9.33}$$

As Figure 9.23 shows, it is possible to describe the transient behavior quantitatively.

9.3.1 PERIODIC SWITCHING OF FEED COMPOSITION

Over the years, researchers have investigated the possibility of applying periodic operation to chemical reactors for production purposes. For instance, it has been shown that alternating the concentrations of two reactants might be beneficial. Two components (A and B) react on the catalyst surface. One of them (A) has a high adsorption affinity, while the other (B) adsorbs only weakly. By alternating the A and B concentrations in the inlet flow, it is possible to increase the surface coverage of B (θ_B). Thus the surface reaction rate expressed by surface coverages (θ_A, θ_B) and concentrations (c) is maximized:

$$R = k\theta_A\theta_B = \frac{k' c_A c_B}{(1 + K_A c_A + K_B c_B)^2}. \tag{9.34}$$

A typical example of surface coverage optimization is the reaction between CO and O_2. A periodic change in the inlet composition has a particularly important application, namely the catalytic automotive exhaust cleaning. The feed to the catalytic monolith changes periodically, both in composition and in temperature. In this way, the highest possible reaction rate according to Equation 9.34 is achieved.

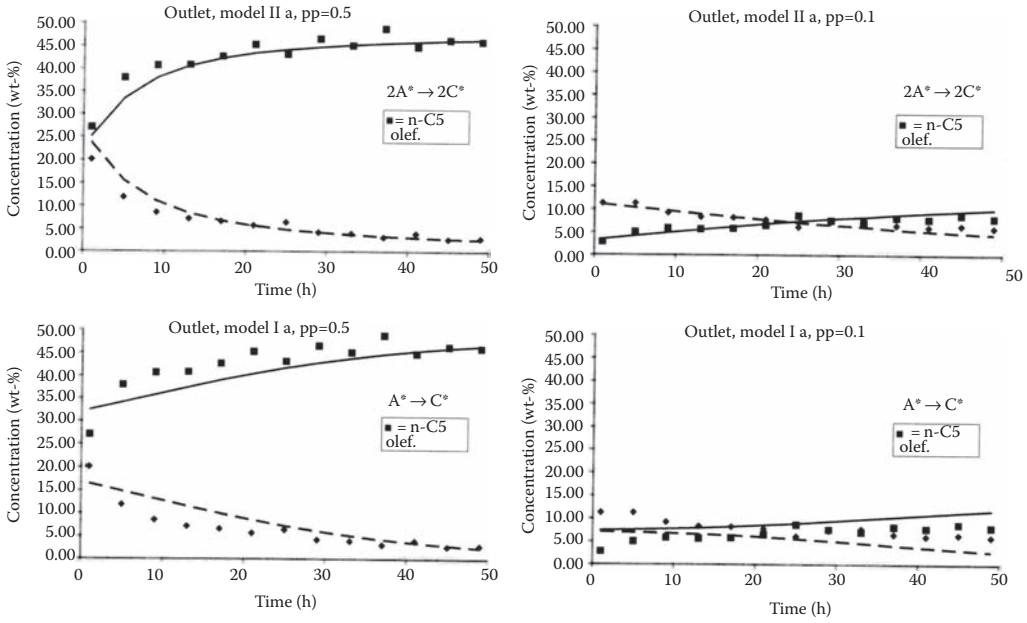

FIGURE 9.23 Transient experiments in the gas phase. Case study: pentene isomerization on a ferrierite catalyst (Figure 9.22).

9.3.2 REVERSE FLOW REACTORS

The most prominent practical success of transient operation has been attained in cases in which the temperature profile inside the reactor is optimized. This approach is based on making use of the solid catalyst material for heat storage. In some catalytic processes, the temperature profile that develops spontaneously in the reactor is unfavorable. Typical examples are highly exothermic reactions in adiabatic fixed beds, where the temperature has a tendency to increase considerably as a function of the bed length. For reversible reactions, however, the optimal temperature profile would be the opposite. A high temperature is advantageous at the inlet to guarantee a high forward reaction rate, but a decreasing temperature profile in the bed is desirable to minimize the rate of the backward reaction. As an example, the reversible and exothermic catalytic reaction

$$\mathrm{A} \rightleftarrows \mathrm{P}$$

is considered. The rate is given by the expression

$$R = k\left(\frac{c_\mathrm{A} - c_\mathrm{P}}{K}\right), \tag{9.35}$$

where the rate constant is given by the Arrhenius law

$$k = \mathrm{A}k^{-E_\mathrm{a}/RT} \tag{9.36}$$

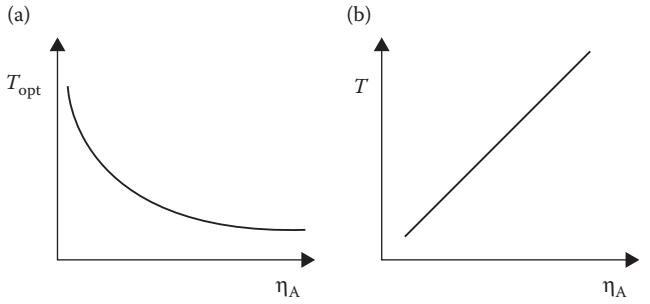

FIGURE 9.24 Optimal (a) and real (b) temperature profiles for an exothermic, reversible reaction (b: an adiabatic bed).

and the temperature dependence of the equilibrium constant is given by the van't Hoff law

$$K = K_0 \, \mathrm{e}^{-\Delta H_r/RT}, \tag{9.37}$$

where R denotes the general gas constant. As $-\Delta \mathrm{H_r}$ is positive for exothermic reactions, K decreases with increasing temperatures. The term c_P/K in the rate expression thus increases with increasing temperature and conversion and has a deteriorating effect on the overall reaction rate. By introducing the conversion of A

$$c_\mathrm{A} = (1 - \eta_\mathrm{A}) c_{0\mathrm{A}} \quad \text{and} \quad c_\mathrm{P} = \eta_\mathrm{A} c_{0\mathrm{A}}, \quad c_{0\mathrm{P}} = 0 \tag{9.38}$$

into the rate equation along with the Arrhenius and van't Hoff expressions, it is possible to show that the optimal temperature for a fixed value of conversion is obtained from the condition $\partial R/\partial T = 0$. The result is

$$T_\mathrm{opt} = \frac{E_\mathrm{a}^- - E_\mathrm{a}^+}{R \ln[\mathrm{A}^- E_\mathrm{a}^- \eta_\mathrm{A}/\mathrm{A}^+ E_\mathrm{a}^+ (1 - \eta_\mathrm{A})]}. \tag{9.39}$$

The profile is illustrated in Figure 9.24. In conventional fixed bed technology, this problem is resolved by coupling adiabatic fixed beds and heat exchangers in series, as illustrated in Figure 9.25.

With this arrangement, a zigzag around the optimal temperature curve (Figure 9.26) is obtained.

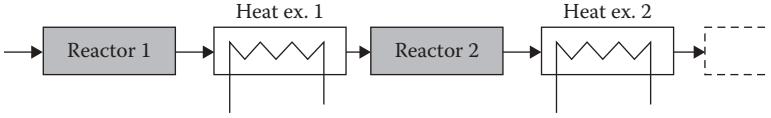

FIGURE 9.25 Conventional technology for reversible exothermic processes.

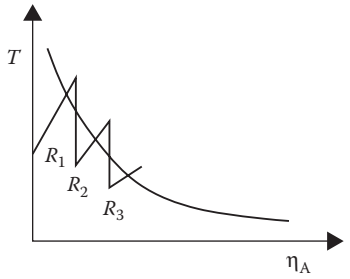

FIGURE 9.26 The zigzag temperature profile obtained with conventional technology.

The concept is, for instance, used in conventional sulfuric acid plants to carry out the catalytic oxidation of SO_2 to SO_3 on V_2O_5 catalysts. Non-steady-state operations can, however, provide an elegant solution to the problem. Let us imagine the following experiment: We start a reversible, exothermic reaction by blowing the reaction gas through a cold catalyst bed. The bed is heated up, and we obtain an increasing temperature profile. Then, the flow direction is switched and consequently a good, decreasing temperature profile is obtained [19]. The heat released by the reaction of course destroys this profile, but then the flow direction is switched again. A temperature wave is built up that travels inside the bed as illustrated in Figure 9.27.

The technical arrangement in which the reverse flow can be materialized is called a reverse flow reactor and is displayed schematically in Figure 9.28.

As valves *A* are open and valves *B* are closed, we obtain the flow direction 1. With the opposite arrangement (*A* closed, *B* open), the flow direction 2 is obtained. Optimization of the flow switching is the crucial factor for success. A fully dynamic reactor model including the solid catalyst phase is needed to simulate the system behavior and to discover the optimized operating conditions.

The application of reverse flow reactors is not limited to reversible, exothermic reactions only, but extends to all systems for which it is beneficial or necessary to heat up the feed.

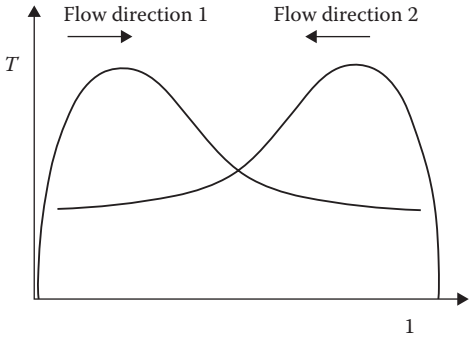

FIGURE 9.27 Temperature waves inside a reverse flow reactor.

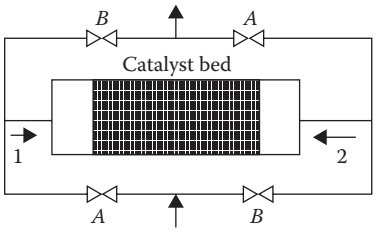

FIGURE 9.28 Schematic of a reverse flow reactor.

The combustion of volatile organic compounds (VOCs) is a typical example; commercial units are in operation. An example of the reverse flow technology in combustion is shown in Figure 9.29 [20].

9.4 NOVEL FORMS OF ENERGY AND REACTION MEDIA

New, exciting means of delivering energy and new reaction media to the reaction environment have emerged in recent years. The general aim is to obtain smaller, cleaner, and more energy-efficient processes. This approach is called process intensification, or more specifically reaction intensification. Examples of the first category are acoustic irradiation (ultrasound) and microwave dielectric heating, whereas the use of SCFs (e.g., carbon dioxide) and ("room temperature") ILs belongs to the latter one. SCFs are mixtures of compounds with properties between typical gases and typical liquids. ILs, on the other hand, are salt melts typically composed of bulky, organic cations and inorganic anions. For more detailed information on the utilization of new forms of energy in connection with chemical reactions, the reader is referred to a review article [21].

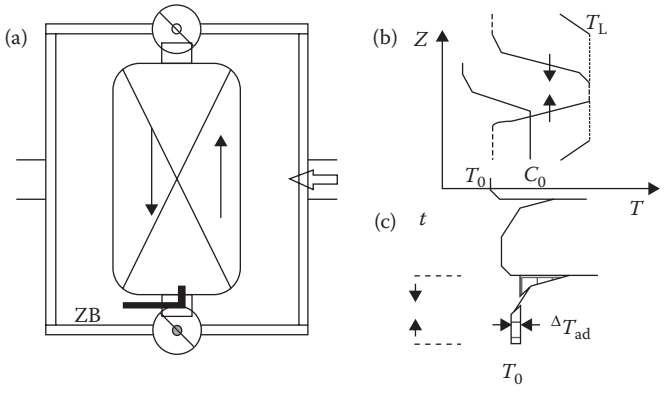

FIGURE 9.29 Reactor with a periodic flow reversal (autothermal fixed bed reactor for catalytic combustion of VOCs). (a) Reactor configuration, (b) temperature profiles at the time of flow reversal, and (c) exit temperature versus time.

9.4.1 ULTRASOUND

Ultrasound is sound pitched above the frequency bond of human hearing. It is a part of sonic spectrum ranging from 20 kHz to 10 MHz (wavelengths from 10 to 10^{-3} cm). The application of ultrasound in association with chemical reactions is called sonochemistry. The range from 20 kHz to around 1 MHz is used in sonochemistry, since acoustic cavitation in liquids can be efficiently generated within this frequency range. However, common laboratory and industrial equipment typically utilize a range between 20 and 40 kHz.

Chemical application of ultrasound has become an exciting field of research rather recently, although the interest in ultrasound and the cavitational effect dates back to over 100 years. The first report on cavitation was published in 1895 by Thornycroft and Barnaby, as they noticed that the propeller of their submarine, the H.M.S. Daring, was pitted and eroded. The first commercial application appeared in 1917, as the French physician Paul Langevin invented and developed an "echo-sounder." The original "echo-sounder" later on became an underwater sonar for submarine detection during World War II. In the same year, Lord Rayleigh published the first mathematical model for cavitational collapse, predicting enormous local temperatures and pressures. In 1927, Richards and Loomis published the first paper on the chemical effects of ultrasound. In 1980, Neppiras used the term "sonochemistry" for the first time in a review of acoustic cavitation. The First International Meeting on Sonochemistry took place at Warwick University in 1986, which accelerated the renaissance of sonochemistry research.

The origin of sonochemical effects in liquids is acoustic cavitation. Ultrasound is transmitted through a medium via pressure waves by inducing vibrational motions of molecules, which alternately compress and stretch the molecular structure of the medium due to a time-varying pressure. Molecules start to oscillate around their mean position, and provided that the strength of the acoustic field is sufficiently intense, cavities are created in liquids. This will happen if the negative pressure exceeds the local tensile strength of the liquid.

The beneficial impact of acoustic irradiation on chemical synthesis (heterogeneous or homogeneous) can be utilized in connection with free radical formation under ultrasound, as it promotes additional reaction pathways. In the case of organic systems, the enhancing effect of ultrasound is not necessarily directly related to thermal effects as in aqueous systems, but is rather a result of single-electron-transfer (SET) process acceleration. The SET step is required as the initial stage in some reactions, for example, cycloadditions involving carbodienes and heterodienes. In systems in which the reaction mechanism does not require a SET step, ultrasound has a minor or no direct effect on the overall reaction rate—although the mass transfer characteristics of a system can significantly alter and thus result in an upgraded performance.

As a cavitation bubble collapses violently in the vicinity of a solid surface, liquid jets are produced, and high-speed jets of liquid are driven into the particle surface (Figure 9.30). These jets and shock waves cause surface coating removal, produce localized high temperatures and pressures, and improve the liquid–solid mass transfer. Moreover, surface pitting may result. With increasing external pressure (P_h), the cavitation threshold and the intensity of bubble collapse are increased. There will no longer be a resultant negative pressure phase of the sound wave (since $P_h - P_A > 0$), and cavitation bubbles cannot be created. However,

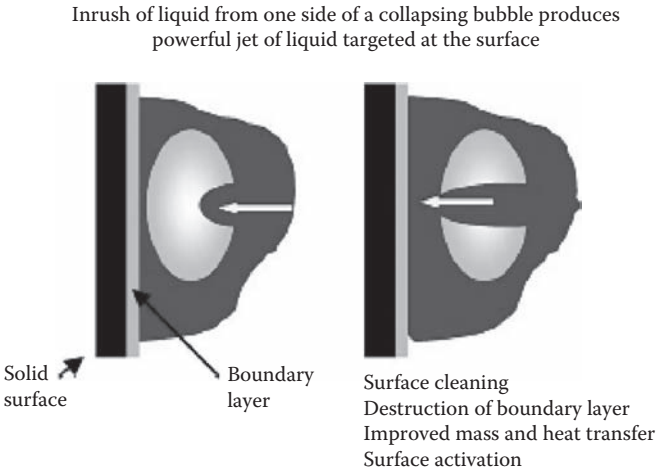

FIGURE 9.30 Cavitation in practice and collapse of a cavitation bubble near a solid surface. (Data from Suslick, K.S., *Sonocatalysis Handbook of Heterogeneous Catalysis*, pp. 1350–1357, VCH Verlagsgesellschaft mbH,Weinheim, Germany, 1997.)

a sufficiently large increase in the intensity (I) of the applied ultrasonic field can produce cavitation, even at higher overpressures, since it will generate larger values of P_A, making $P_h - P_A < 0$. Since P_m (the pressure of a collapsing bubble) is approximately $P_h + P_A$, increasing the value of P_h will lead to a more rapid collapse: $P_A = P_{0A} \sin(2\pi ft)$, where P_A is the applied acoustic pressure, t the time, f the frequency, and P_{0A} the pressure amplitude. For the collapse time (t), the following equation is valid:

$$t = 0.915\, R_m \left(\frac{\rho}{\rho_m}\right)^{1/2} \left(1 + \frac{P_{vg}}{P_m}\right), \tag{9.40}$$

where t is the collapse time, R_m is the radius of the cavity at the start of collapse, ρ is the density of the medium, and P_m is the pressure in the liquid:

$$P_{max} = P \left\{\frac{P_m(K-1)}{P}\right\}^{K/(K-1)}, \tag{9.41}$$

where P_{max} is the maximum pressure developed in the bubble, P_m is the pressure in the liquid at the time of transient collapse, P is the pressure in the bubble at its maximum size, and K is the polytropic index of the gas mixture. The figure illustrates the collapse of a cavitation bubble near a solid surface. Moulton et al. investigated the hydrogenation of soybean oil at a high hydrogen pressure (14 bar) and observed a negligible enhancement of the catalyst activity. At a lower hydrogen pressure (8.5 bar), on the other hand, the ultrasonic effect was more profound. Torok et al. observed a similar trend when studying cinamaldehyde hydrogenation on a Pt/SiO_2 catalyst. At 30 bar of hydrogen pressure, the enhancement of the catalyst activity under ultrasound was almost negligible. As the pressure was decreased to 1 bar, the catalyst activity was significantly enhanced by ultrasound [22].

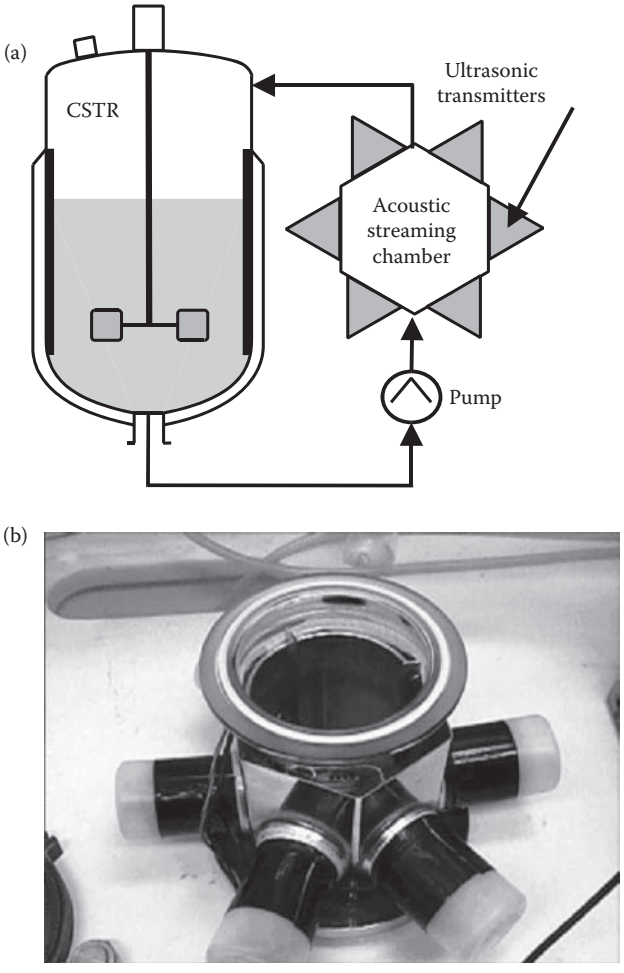

FIGURE 9.31 (a) A sonication loop reactor configuration on an industrial-scale and (b) a laboratory-scale equipment.

To generate an ultrasonic field, two basic philosophies of applying acoustic power to liquid loads are used: acoustic fields generated by probe/horn systems and piezoelectric vibrators or hydrodynamic cavitation. For laboratory experiments, low-intensity systems of 1–2 W/cm^2 (an ultrasonic bath) and high-intensity systems yielding hundreds of W/cm^2 (a horn/vibrator system) are available. An industrial loop reactor configuration for sonication is introduced in Figure 9.31. As regards the application of ultrasound, we will discuss an industrial application, namely the production of sweeteners.

Hydrogenation of xylose to xylitol is an important process in the production of sweeteners, and the sponge nickel catalyst (often called Raney-Ni) deactivates in the slurry reactor. In successive batches, the catalyst activity declines, and it has to be removed after a few batches and replaced by a new one. However, by applying *in situ* ultrasound treatment, the catalyst deactivation was considerably suppressed as illustrated in Figure 9.32. In this way, the catalyst life time can be considerably prolonged [23].

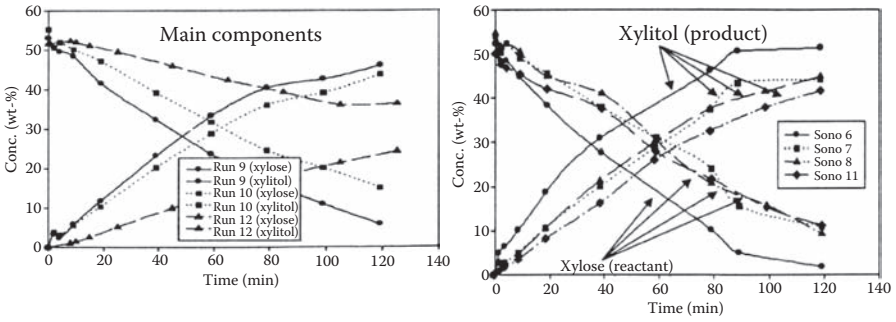

FIGURE 9.32 Suppression of catalyst deactivation using ultrasound: hydrogenation of xylose to xylitol (left: silent conditions, right: ultrasound treatment).

9.4.2 MICROWAVES

Microwaves have recently received attention as an alternative energy source for chemical processes. Microwave irradiation is a form of electromagnetic energy. Microwaves consist of an electric component as well as a magnetic one. The microwave region of the electromagnetic spectrum is situated between infrared radiation and radio frequencies. Microwave irradiation ranges from 30 GHz to 300 MHz, corresponding to wavelengths of 1 cm to 1 m. Microwave heaters use specific, fixed frequencies 2.45 GHz (wavelength 12.2 cm) or 0.9 GHz (wavelength 33.3 cm), in an effort to avoid interferences with RADAR (wavelength from 1 to 25 cm) and telecommunication applications. All domestic microwave ovens operate at the frequency of 2.45 GHz. In comparison with conventional heating, energy transfer does not primarily occur by convention and conduction but by dielectric loss in the case of microwave heating [21,24].

During World War II, Randall and Booth, working at the University of Birmingham, designed a magnetron to generate microwaves in connection with the development of radar. As with many other great inventions, the microwave oven was a by-product of research efforts. In 1946, Percy Spencer realized that a candy bar in his pocket melted during the tests of a vacuum tube called magnetron. Gedye et al. published the first pioneering report on utilizing microwave irradiation in chemical synthesis in 1986. During the last decade, microwave heating has been increasingly applied in carrying out organic synthesis.

Most of the industrial applications of electromagnetic heating are found as a change of state where nonconductive matter is involved (e.g., defrosting, dehydration with the change of state of water) [21]. Another important use of microwave is the sintering and fusion of solids. Microwave heating is also used in the food industry for drying fruit, berries, and corn.

Microwave dielectric heating depends on the ability of an electric field to polarize charges in materials and their inability to follow rapid changes in an electric field space. Total polarization is a sum of several components:

$$\alpha_1 = \alpha_e + \alpha_a + \alpha_d + \alpha_i, \tag{9.42}$$

where α_e is the electronic polarization, α_a is the atomic polarization, α_d is the dipolar polarization, and α_i is the interfacial polarization (the Maxwell–Wagner effect). The time scale of the electronic and atomic polarization/depolarization is much smaller than microwave frequencies, which is why they do not contribute to microwave dielectric heating. Microwave energy can affect molecules in two principal ways: (a) by dipolar polarization and (b) by ionic conduction. A third mechanism, (c) interfacial polarization, can also take place, although it is often of limited importance. The dielectric loss tangent defines the ability of a material to convert electromagnetic energy into heat energy at a certain frequency and temperature:

$$\tan\delta = \frac{\varepsilon''}{\varepsilon'}, \tag{9.43}$$

where ε' is the dielectric constant describing the ability of a molecule to be polarized by the electric field and ε'' is the dielectric loss describing the efficiency at which the energy of the electromagnetic irradiation can be converted into heat. Both parameters, the dielectric loss and dielectric constant, are measurable properties.

Materials interact with microwaves in three ways (Figure 9.33). Metals are good conductors, because they tend to reflect microwave energy and do not warm up particularly well. Transparent materials are good insulators, because they are transparent to microwave energy and do not warm up. Absorbing materials receive microwave energy and are heated. These different material interactions with microwaves enable *selective heating*.

The advantage of microwave irradiation as an energy source for heterogeneously catalyzed systems is that microwaves, in many cases, do not substantially heat up the adsorbed organic layers, but interact directly with the metal sites on the catalyst surface, and hot spots might be created. The temperature of the reactive sites was calculated to reside 9–18 K above the bulk temperature.

The rate of the temperature increase in a batch system due to the dielectric field of microwave radiation in a BR is determined by the following equation:

$$\frac{dT}{dt} = k\frac{\varepsilon'' f E^2_{\text{r.m.s}}}{\rho c_p}, \tag{9.44}$$

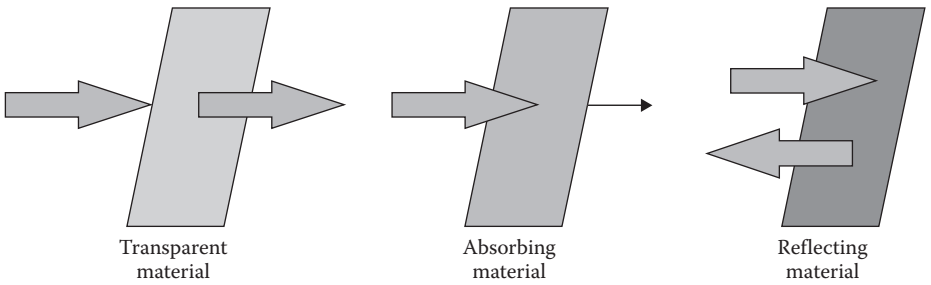

FIGURE 9.33 Interaction of transparent (insulator), absorbing (dielectric), and reflecting (conductor) materials with microwave energy.

where $E^2_{\text{r.m.s}}$ is the r.m.s. field intensity, ρ is the density, c_p is the specific heat capacity, k is a proportionality coefficient constant, ε'' is the dielectric loss, and f is the frequency. Depending on the parameters in Equation 9.44, the temperature increase may become substantial. The main advantage of microwave heating is that it is instantaneous unlike conventional heating.

Microwave equipment can be divided into two categories: (a) multimode and (b) single-mode cavities. If we consider an empty metallic volume, the electric field repartition into that volume is very heterogeneous, if the dimensions of that volume are too large compared with the wavelength. This is the case for multimode applicators (such as the domestic microwave oven). The repartition is well mastered and stable, if the applicator dimensions are close to the single-mode structure. The use of wave guides emitting the fundamental mode at a fixed frequency allows us to master and, above all, control the power transmission, as the aim is to study the influence of a microwave electromagnetic field on the behavior of chemical reactions. This approach enables us to scaleup the results as well as the equipment to an industrial scale. For a single-mode microwave loop reactor configuration on a laboratory scale, see Figure 9.34.

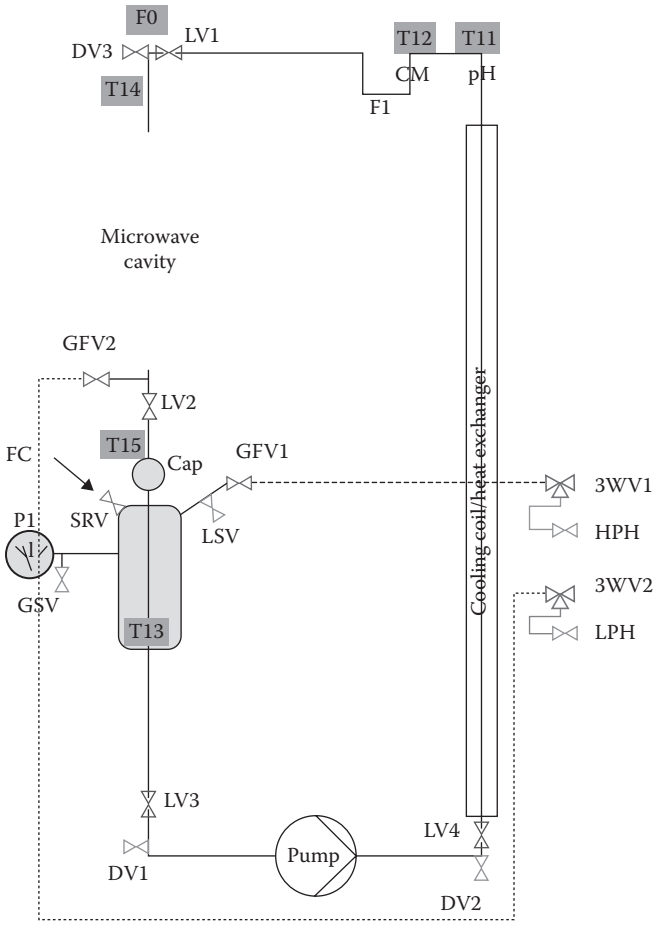

FIGURE 9.34 A single-mode microwave loop reactor.

A very important advantage of microwave irradiation is the possibility of carrying out many chemical syntheses rapidly and with good yields in solutions as well as in the absence of a solvent. This leads to the enhancement of selectivity and gives rise to an inherently greener chemical production.

9.4.3 SUPERCRITICAL FLUIDS

SCFs are gaseous compounds, or mixtures thereof, having properties between typical gases and liquids. These properties can be fine-tuned by varying the pressure. Over one hundred industrial plants using SCFs are in operation around the world in process and production technology [25]. High-pressure *sc*-CO_2 is probably the process best known to the large public, although supercritical conditions are by no means restricted to the use of carbon dioxide. Extraction of valuable cmponents from solid material with supercritical CO_2 is applied in many processes. Other substances, such as water or hydrocarbons including ethene, are commonly applied in their supercritical states. Highly compressed ethylene is known as a good solvent for organic compounds and, consequently, industrial processes exist, for example, for high-pressure polymerization of ethene [26].

9.4.3.1 Case: Hydrogenation of Triglycerides

For some 100 years, hydrogenation of fats and fat derivatives has been an important high-pressure reaction. Tens of millions of tons of biological oils are hydrogenated annually. The goal is to increase the melting point by reducing the number of C=C double bonds in the fatty acid chains of unsaturated triglycerides. These hardened fats are used, for example, in margarine production and in further processed products [27].

Typically, conversion rates in these processes are slow, the reason being the low solubility of hydrogen in liquid oils. High temperatures and rather long residence times in the presence of a catalyst may promote unwanted by-product formation. In the case of triglycerides, *trans*-fatty acids might form, which are physiologically unfavorable. In the 1990s, a few authors investigated the hydrogenation of fats in the presence of SCFs [28–31]. Considerable rate enhancement was observed compared with conventional technology. Reaction rates obtained on the lab scale were hundreds of times higher than in the absence of SCFs. It is very important to understand why a solvent not directly taking part in the chemical reaction itself so dramatically influences the overall rate. The thermodynamic behavior of the mixture is considered as the key for understanding this. In Figure 9.35, the phases present in classical hydrogenation are displayed.

The substrate to be hydrogenated is liquid, and hydrogen forms a separate gas phase. The two compounds must be brought to contact on the surface of the solid catalyst. This is why hydrogen is dissolved into the liquid phase and its maximum solubility is determined by the thermodynamic equilibrium, which is temperature- and pressure-dependent. During the hydrogenation of triglycerides, double bonds of the fatty acid side chains are saturated. If triglycerides are considered as pure substances, the reaction mixture comprises four components. The miscibility of the oils/fats with SCFs does not depend strongly on the degree of saturation. The reactant(s) and product(s) thus possess miscibilities similar to

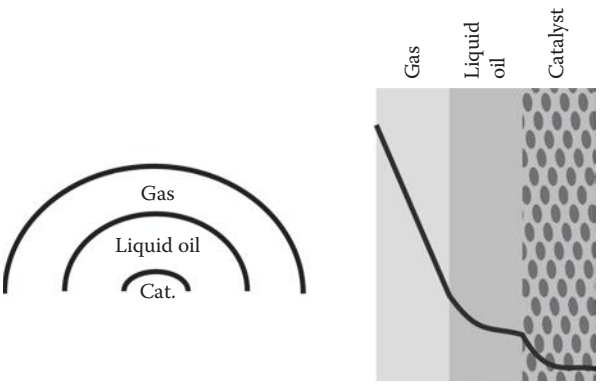

FIGURE 9.35 Hydrogenation of triglycerides by heterogeneous catalysis phases and concentration profiles of hydrogen.

an SCF. Therefore, the quaternary system is reduced to a pseudoternary system containing triglycerides, hydrogen, and an SCF.

For the phase behavior of triglycerides and hydrogen with CO_2, a typical ternary diagram can be constructed. In Figure 9.36, the rectangles on the sides of the triangle represent

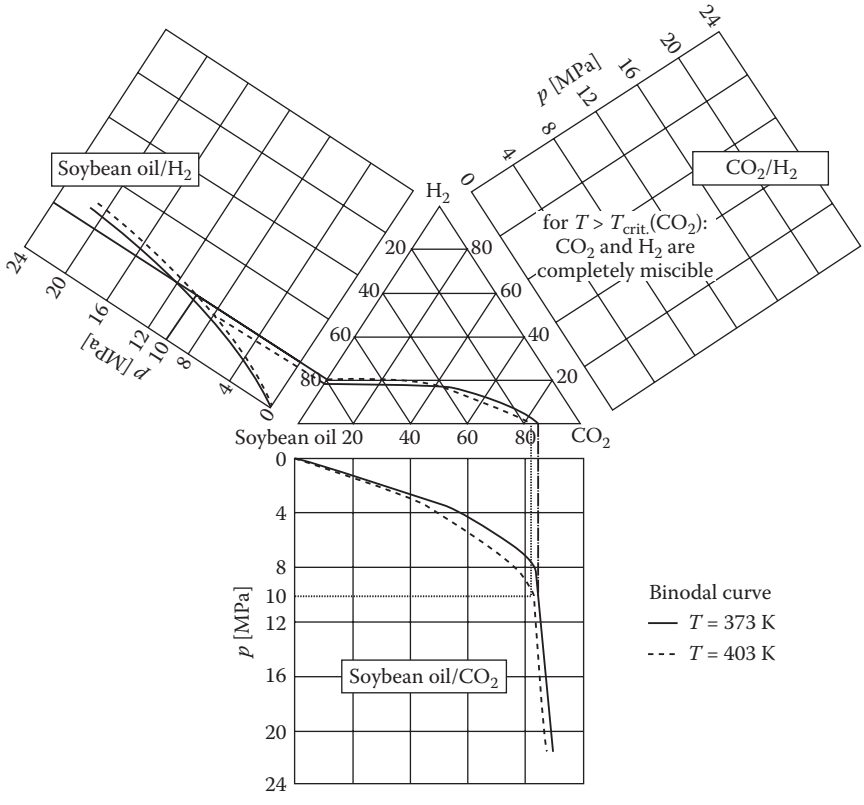

FIGURE 9.36 Phase behavior of soybean oil, hydrogen, and carbon dioxide. (Data from Weidner, E., Brake, C., and Richter, D., in *Supercritical Fluids as Solvents and Reaction Media*, G. Brunner (Ed.), Elsevier B. V., Amsterdam, The Netherlands, 2004.)

the phase equilibria of binary mixtures in pressure–composition plots at two different temperatures. The lower triangle illustrates the phase behavior of soybean oil and carbon dioxide. Carbon dioxide dissolves almost no oil at all, whereas it has a rather good solubility in the oil phase. The solubility of the gas in the oil increases with increasing pressure and/or decreasing temperature. The binary hydrogen–soybean oil system shows a different behavior: with increasing temperature, the solubility of hydrogen in oil increases. The solubility of hydrogen in oil is also much lower than that of carbon dioxide. The binary mixing gaps on the lower and the left-hand side of the triangle are connected with the binodal curve, this being determined experimentally. Due to the different temperature dependencies of the gas solubilities (carbon dioxide and hydrogen) in soybean oil, the binodal isotherms of the ternary system must have an intersection. The shaded area in Figure 9.36 represents a region where a gas-saturated liquid phase coexists with a gas phase, mainly containing hydrogen and carbon dioxide. Due to the low solubility of soybean oil in the gases, the gas-phase composition is almost identical to the right side of the triangle. The area below the curve corresponds to the single-phase region, where the gas mixture is homogeneously miscible with soybean oil [32].

The example presented here illustrates the fact that supercritical technologies may have huge potential for a variety of chemical processes, although the supercritical solvent as such would not be needed. In light of this example, another current "hot topic," biodiesel processing from renewable resources, could presumably also benefit from this technology.

9.4.4 IONIC LIQUIDS

Room-temperature IL (RTILs) are a novel class of materials that can be utilized, for instance, as bulk solvents in biphasic operations, separations, and electrochemistry. The key features of these neoteric solvents are as follows: generally, RTILs have a negligible or at least a very low vapor pressure; in most cases, they are considered nonflammable; RTILs are recyclable and possess unique solvation properties (high concentrations of solute, up to 2:1; some of them can dissolve cellulose and mineral rock); they have a wide liquidus range (from around $-100°C$ to $+400°C$) and selective stabilization properties (immobilization of catalytically active species and nanoparticles); they are tunable in terms of polarity and co-miscibility with molecular solvents; many have high solubility of various industrially important gases such as H_2, O_2, and CO_2; and supercritical CO_2 is often infinitely soluble in ILs, whereas ILs do not dissolve in *sc*-CO_2 (separation aspect).

The first IL was discovered in the early twentieth century, soon to be followed by the chloroaluminates, which were primarily targeted for improved battery technology. The problem with chloroaluminates is that they are both moisture and oxygen sensitive, and they are only stable in an inert atmosphere. Much later, at the beginning of the 1990s, Wilkes et al. discovered the first moisture- and air-stabile ILs. Until today, the scope of possible cation–anion combinations and as a new trend, zwitterionic compounds, has expanded tremendously: for example, various alkyl-imidazolium, alkyl-pyridium, quaternary phosphonium, quaternary ammonium, and thiazolinium cations can be coupled with a multitude of anions such as $[PF_6]^-$, $[BF_4]^-$, $[C1]^-$, $[Br]^-$, and $[A1C1]^-$. Moreover, deep

eutectic melts such as choline chloride coupled to a multitude of other substrates (such as zinc chloride) have emerged as alternative "ionic-liquid-like" solutions.

ILs have shown promise in upgrading existing chemical processes such as the IFP Dimersol to Difasol (oligomerization). Butene dimerization can be carried out through a Difasol liquid–liquid biphasic reaction (IL is the other liquid), resulting in an increased yield, selectivity, and cost savings compared with the original Dimersol monophasic reaction. The process is widely used industrially for the dimerization of alkenes, typically propene and butene, to the more valuable branched hexenes and octenes [33]. Numerous reports have also been published on the utilization of ILs in electrochemical applications, liquid–liquid extractions, hydrogenations, oxidations, catalysis, and even enzymatic processes.

9.4.4.1 Case: Heterogenized ILs as Catalysts

Traditionally, catalytically active transition metal particles are introduced into heterogeneous catalysts by various impregnation and precipitation, and so on, methods—or by direct mixing of the metal precursors during the synthesis of the solid material—followed by (thermal) decomposition, restructuring, and redistribution of the resulting active metal sites during calcination and reduction steps. The catalytic properties of the resulting material are largely determined by the conditions prevailing under these post-treatment operations, such as the final temperature during calcination and reduction, temperature gradients during these processes, reduction method (chemical or molecular hydrogen), oxygen effects, nature of the precursors, and so on. Additionally, the counterdeactivation characteristics of a particular catalyst depend not only on the process conditions applied but also on the details of the synthesis process and the precursors used. This is why the development of a well-performing heterogeneous catalyst involves a tedious process in which a huge amount of experimental work and characterization is required. An alternative strategy for the preparation of heterogeneous catalysts by means of an immobilized IL layer, into which the metallic transition metal species have been dissolved, is illustrated in Figure 9.37.

This approach allows a general strategy for the preparation of supported IL and transition metal complex/nanoparticles [34]. There are a few feasible means of immobilization of ILs, which in turn immobilize the active metal species. In case the IL is insoluble in the bulk solvent, no special covalent anchoring is required to retain the IL on the support structure. However, if this is not the case, covalent anchoring of the cation or the anion is required. This can be facilitated, for example, by introducing a side branch containing a silyl group that is bound to the surface hydroxide moieties of the support, or a vinyl group that enables polymerization of the IL. Naturally, the metal species can also be directly incorporated into the IL cation or anion. In Figure 9.38, hydrogenation of citral is introduced by means of a supported IL catalyst (Pd in IL) containing transition metal moieties. As the figure shows, the catalyst works.

The engineering modeling of IL environments is yet to emerge, and measurements of physico-chemical properties (such as viscosities, densities, gas solubilities, diffusion coefficients, toxicology, etc.) are only available for a very limited number of compounds. Moreover, new correlations need to be developed to account for, for example, the complex equilibrium behavior of ILs and traditional solvents.

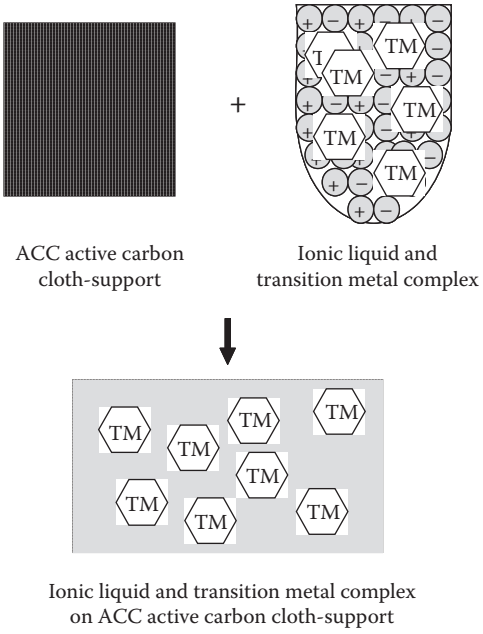

FIGURE 9.37 The concept of IL and transition metal supported on an active carbon cloth (ACC) support.

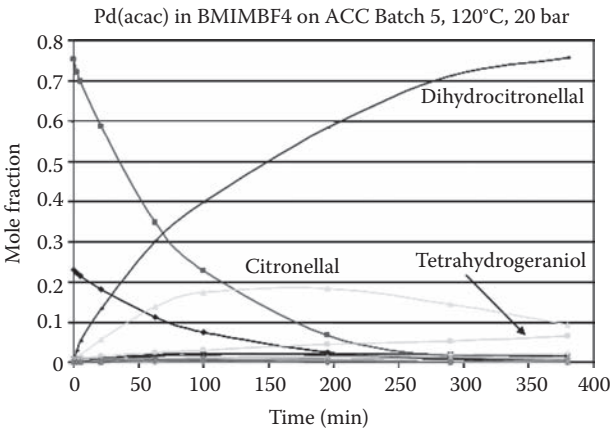

FIGURE 9.38 Mole fractions of components as a function of time upon hydrogenation of citral with a Pd/IL/ACC catalyst at 120°C, 20 bar.

9.5 EXPLORING REACTION ENGINEERING FOR NEW APPLICATIONS

The utilization of classical reaction engineering and reactor technology has established itself long ago as a standard policy in the bulk industries. However, many other fields of chemical industries, such as pharmaceutical, alimentary, or paper and pulping industries, are only slowly beginning to discover the benefits of it. The reasons for this are several, such

as differences in corporate cultures, education of engineers and chemists for these special areas, and, perhaps most importantly, the complexity of many organic systems for which the recent development of computational capacity and chemical analysis has opened a realistic window to enter the world of modeling. Moreover, the lack of ready-made, tailored models accounting for a complex interaction of simultaneous, different phenomena (e.g., the huge number of parallel, consecutive, and mixed reactions, large number of unknown species, complex mass, and heat transfer effects) has slowed down the development. In this section, we will introduce an attempt to penetrate such a complex system, namely delignification of wood chips, in line with classical chemical engineering concepts. In the processing of wood to cellulose and paper, the approach has traditionally been very empirical.

9.5.1 CASE STUDY: DELIGNIFICATION OF WOOD

The alkaline delignification of wood in the pulp industry is an example of a particularly complex system involving hundreds of reactions. This process is the key step in the production of cellulose via chemical pulping. The lignin material in the wood (L) is partially decomposed and dissolved in the cooking liquor, whereas cellulose fibers remain in a solid state. A part of hemicelluloses is also dissolved. The process can be roughly described as (without exact stoichiometry) [35]

$$\mathrm{L(s), HS(s)} + \mathrm{OH^-/HS^-} \rightarrow \mathrm{L(1), HS(1)}.$$

Very little attention has been paid to modeling of these kinds of systems. The reason for this is that the research and development involving paper and pulp processes has the tradition of remaining isolated from the mainstream of chemical engineering research. The chemical complexity and large variations in the raw material composition have led to the notion that modeling these systems is too challenging a task. The pulp and paper industry does not represent a very significant portion of the chemical industry in the countries that are leading in chemical engineering. The key concept is to identify the most important reactions and to merge certain classes of compounds, much in line with the modeling of petrochemical or refining processes, where we are dealing with similar kinds of challenges, that is, varying feed compositions and complex reactions. The apparatus used in the paper and pulp industry is somewhat different from that used in classical chemical industry, but in any case it can be divided into logical units in accordance with the concepts described in the previous chapters.

A model for a porous, reactive particle is considered in Figure 9.39. A two-dimensional time-dependent model is required, describing the wood material in the radial and longitudinal directions. In the particle, simultaneous reaction and diffusion take place, and the porosity changes with time as lignin is dissolved. Furthermore, the porosity variations in time are different in the x and y directions.

The lignin content of the wood material typically decreases as an S-shaped curve in a nonisothermal batch process as shown in Figure 9.40.

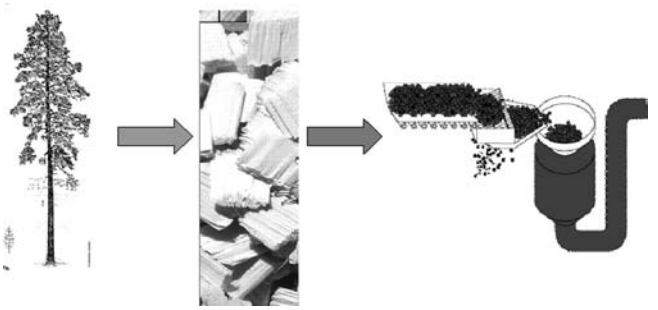

FIGURE 9.39 The fate of a porous, reactive particle (wood chip).

The mass balance for a reacting component in the wood chip can be expressed as follows:

$$\frac{\mathrm{d}\left(\varepsilon_{\mathrm{p}} c_i\right)}{\mathrm{d}t} = D_{\mathrm{e}i}\left(\varepsilon'_x \frac{\mathrm{d}^2 c_i}{\mathrm{d}x^2} + \varepsilon'_y \frac{\mathrm{d}^2 c_i}{\mathrm{d}y^2}\right) + r'_i, \tag{9.45}$$

where $D_{\mathrm{e}i}$ is the diffusion coefficient (Appendices 4 and 6), and ε'_x and ε'_y denote modified porosity-to-tortuosity ratios.

The following boundary conditions need to be taken into account: $c_i = c_{\mathrm{L}i}$ at $x = \mathrm{L}_x$ and $y = \mathrm{L}_y$ and $\mathrm{d}c_i/\mathrm{d}x = \mathrm{d}c_i/\mathrm{d}y = 0$ at $x = y = 0$. In the mass balance of the bulk liquid, the classical concepts can be applied, for example, BR model and the fluxes of dissolved components diffusing into the liquid main bulk; for the liquid bulk, the following mass balance is obtained:

$$\frac{\mathrm{d}c_{\mathrm{L}i}}{\mathrm{d}t} = N_{ix} a_x + N_{iy} a_y. \tag{9.46}$$

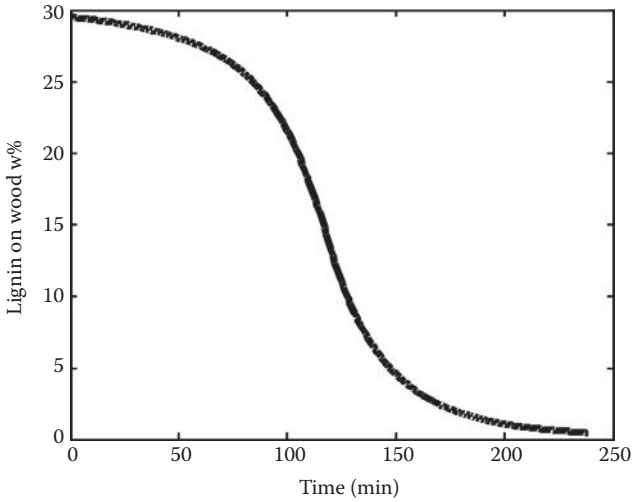

FIGURE 9.40 Lignin on wood (wt%) as a function of the reaction time.

As lignin is dissolved from the wood chip, the porosity (ε_p, ε'_x, ε'_y) increases with time. The overall porosity increase over time is described by the formula

$$\varepsilon_p = \varepsilon_{0,p} + \left(\varepsilon_\infty - \varepsilon_{0,p}\right)\left[1 - \left(1 - \eta_L^{\alpha'}\right)\right], \tag{9.47}$$

where $\varepsilon_{0,p}$ and ε_∞ denote the initial and the final porosities, respectively, η_L is the conversion of lignin, and α' is an empirical, adjustable exponent (Figure 9.41).

In the mathematical description of the model, the parabolic PDEs were converted into ODEs by the method of lines and, consequently, a large number of ODEs were solved. The conversion of PDEs to ODEs is carried out using central difference formulae for the derivatives d^2c_i/dx^2. The kinetic model for the components can be described as follows:

$$r_i = k_i \left(c_{OH}^a c_{HS}^b + k_2\right) w_i, \tag{9.48}$$

where w_i denotes the wt% of lignin, cellulose, carbohydrates, and xylanes, respectively, and c_{OH} and c_{HS} denote the concentrations of the cooking chemicals (NaOH and NaHS). We should keep in mind that the concentrations of the species in the liquid bulk as well as in line with the two coordinate axes (x, y) vary differently in time, partially since the porosity changes evolve differently in the x and y directions. After performing the calculations, the relevant concentration profiles and the porosity can be obtained by means of simulations (Figures 9.42).

The model can be used for process intensification, since it provides information about the effect of temperature, concentrations, and wood chip sizes on the cooking time required. A more comprehensive treatment can be found, for example, in Refs. [35,36]. As can be seen, classical chemical engineering concepts are applicable and can be successfully adapted in cases of very complex natural materials. The main challenge of the model development is the description of the chemical system. However, it is expected that the delignification reactors of future, the digesters, will be designed on the basis of rational chemical engineering principles.

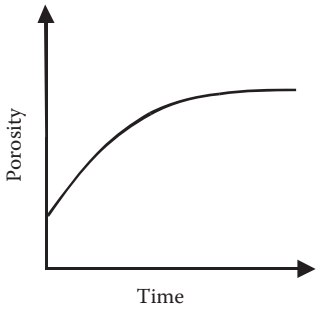

FIGURE 9.41 The porosity evolvement in a wood chip over time.

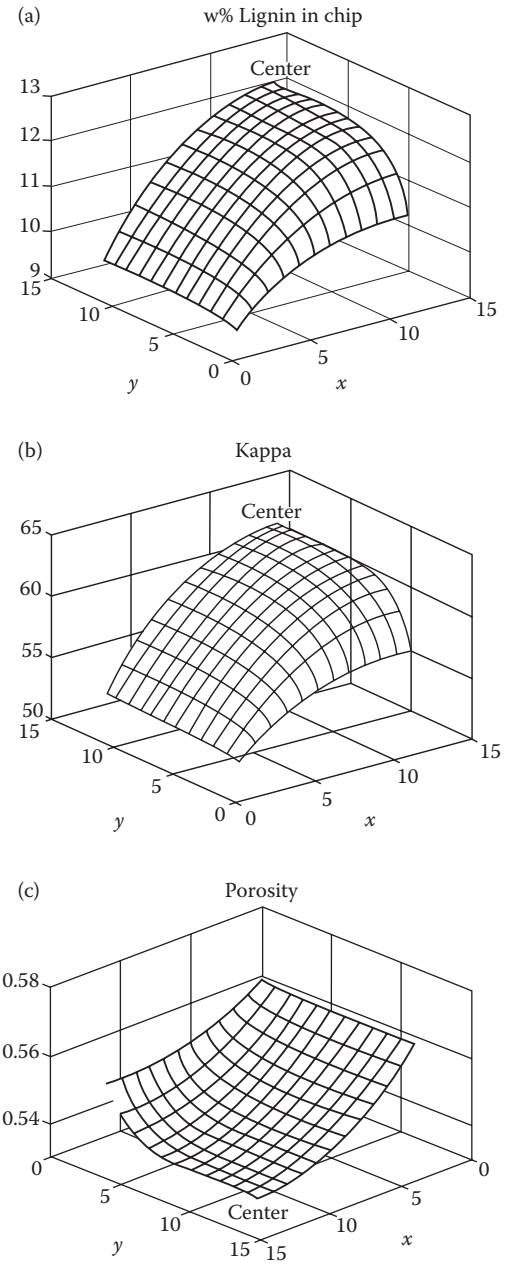

FIGURE 9.42 Simulated concentration profile of (a) lignin (w%), (b) the Kappa number, and (c) porosity inside a wood chip during the cook. The Kappa number is a measure of the lignin content.

9.6 SUMMARY

As was demonstrated in this chapter, we could state that even in the case of nontraditional reactor concepts, classical modeling is the basis of the approach: we only need to divide the system into logical parts to which the established concepts are applicable. The basic

concepts and mathematics required for the modeling of most peculiar reactors have been introduced in this volume. We therefore leave it to the well-educated readers of this book to complete the picture as novel technologies emerge.

As processes move through their various developmental phases, for example, conception, development, commercialization, and evolutionary optimization, additional improvements eventually often require major innovations and breakthroughs. In this volume, several approaches have been indicated to demonstrate that we can squeeze a higher performance out of existing processes by revisiting the fundamentals of reaction engineering and science. To achieve an optimum success, multidisciplinary teams should address the current and future needs of the process industry. Good engineering teams bring together experts from many areas of special expertise as well as knowledgeable reaction engineers. Furthermore, industry–university collaboration is encouraged. This provides highly synergistic effects, since the participants can extend and reinforce their efforts, taking full advantage of the complementary capabilities of engineering sciences of the twenty-first century.

REFERENCES

1. Salmi, T., Wärnå, J., Rönnholm, M., Turunen, I., Luoma, M., Keikko, K., Lewering, W., von Scala, C., and Haario, H., Dynamic modelling of catalytic column reactors with packing elements, in Rönnholm, M., Doctoral thesis, Åbo Akademi, Turku/Åbo, Finland, 2001.
2. Rönnholm, M., Wärnå, J., and Salmi, T., Comparison of three-phase reactor performances with and without packing elements, *Catal. Today*, 79–80, 285–291, 2003.
3. Wärnå, J. and Salmi, T., Dynamic modelling of catalytic three phase reactors, *Comput. Chem. Eng.*, 20, 39–47, 1996.
4. Kapteijn, F., Nijhuis, T.A., Heiszwolf, J.J., and Moulijn, J.A., New non-traditional multiphase catalytic reactors based on monolithic structures, *Catal. Today*, 66, 133–144, 2001.
5. Nijhuis, T.A., Kreutzer, M.T., Romijn, A.C.J., Kapteijn, F., and Moulijn, J.A., Monolithic catalysts as more efficient three-phase reactors, *Catal. Today*, 66, 157–165, 2001.
6. Irandoust, S. and Andersson, B., Monolithic catalysts for nonautomobile applications, *Catal. Rev. Sci. Eng.*, 30, 341–392, 1988.
7. Salmi, T., Wärnå, J., Mikkola, J.-P., Aumo, J., Rönnholm, M., and Kuusisto, J., Residence time distributions from CFD in monolith reactors—combination of avant-garde and classical modelling, *Comput. Aided Chem. Eng.*, 14, 905–910, 2003.
8. Baldyga, J. and Bourne, J.R., *Turbulent Mixing and Chemical Reactions*, Wiley, New York, 1999.
9. CFX 4.4, User's guide, CFX International, UK, 2000.
10. Haakana, T., Kolehmainen, E., Turunen, I., Mikkola, J.-P., and Salmi, T., The development of monolith reactors: General strategies with a case study, *Chem. Eng. Sci.*, 59, 5629–5635, 2004.
11. Irandoust, S. and Andersson, B., Liquid film in Taylor flow through a capillary, *Ind. Eng. Chem. Res.*, 28, 1685–1688, 1989.
12. Aumo, J., Wärnå, J., Salmi, T., and Murzin, D., Interaction of kinetics and internal diffusion in complex catalytic three-phase reactions: Activity and selectivity in citral hydrogenation, *Chem. Eng. Sci.*, 61, 814–822, 2006.
13. Lilja, J., Murzin, D., Salmi, T., Aumo, J., Mäki-Arvela, P., and Sundell, M., Esterification of different acids over heterogeneous and homogeneous catalysts and correlation with the Taft equation, *J. Mol. Catal.*, 182–183, 555–563, 2002.

14. Toukoniitty, E., Wärnå, J., Salmi, T., Mäki-Arvela, P., and Murzin, D.Yu., Application of transient methods in three-phase catalysis: Hydrogenation of a dione in a catalytic plate column, *Catal. Today*, 79–80, 383, 2003.
15. Mikkola, J.-P., Aumo, J., Murzin, D., and Salmi, T., Structured, but not overstructured: Woven active carbon fibre matt catalyst, *Catal. Today*, 105, 323–330, 2005.
16. Moulijn, J.A., Makkee, M., and van Diepen, A., *Chemical Process Technology*, Wiley, 2001.
17. The Process Technology of Tomorrow-catalogue, Institut für Microtechnik Mainz GmbH, 2007.
18. Hessel, V., Hardt, S., and Lowe, H., *Chemical Micro Processing Engineering*, Wiley-VCH, 2004.
19. Matros, Yu.Sh. and Burimovich, G.A., Reverse-flow operation in fixed bed catalytic reactors, *Catal. Rev. Sci. Eng.*, 38, 1–68, 1996.
20. Niecken, U., Kolios, G., and Eigenberger, G., Limiting cases and approximate solutions for fixed-bed reactors with periodic flow reversal, *AIChE J.*, 41, 1915–1925, 1995.
21. Toukoniitty, B., Mikkola, J.-P., Murzin, D.Yu., and Salmi, T., Utilization of electromagnetic and acoustic irradiation in enhancing heterogeneous catalytic reactions, a review, *Appl. Catal. A: General*, 279, 1–22, 2005.
22. Suslick, K.S., *Sonocatalysis Handbook of Heterogeneous Catalysis*, pp. 1350–1357, VCH Verlagsgesellschaft mbH, Weinheim, Germany, 1997.
23. Mikkola, J.-P. and Salmi, T., In-situ ultrasonic catalyst rejuvenation in three-phase hydrogenation of xylose, *Chem. Eng. Sci.*, 54, 1583–1588, 1999.
24. Moyes, R.B. and Bond, G., Microwave heating in catalysis, in *Handbook of Heterogeneous Catalysis*, VCH Verlagsgesellschft, Weinheim, Germany, 1997.
25. Brunner, G. (Ed.), *Supercritical Fluids as Solvents and Reaction Media*, Elsevier B.V., Amsterdam, The Netherlands, 2004.
26. Luft, G., in A. Bertucco and G. Vetter (Eds), *High Pressure Process Technology*, Elsevier, Amsterdam.
27. Bockisch, M., *Fats and Oils Handbook*, AOCS Press, 1998.
28. Pickel, K.H. and Steiner, R., Supercritical fluid solvents for reactions, *Proc. of the 3rd Int. Symp. on Supercritical Fluids*, Strasbourg, 1994.
29. Tacke, T., Wieland, S., and Panster, P., Hardening of fats and oils in supercritical CO_2, *Proc. of the 3rd Int. Symp. on High Pressure Chemical Engineering*, Zürich, 1996.
30. Härröd, M. and Møller, P., Hydrogenation of fats and oils at supercritical conditions, in P. Rudolf von Rohr and C. Trepp (Eds), *High Pressure Chemical Engineering*, Elsevier Science, Amsterdam, 1996.
31. Degussa A.G., WO 95/22591, *Hydrogenation of Unsaturated Fats, Fatty Acids or Fatty Acid Esters*, 1995.
32. Weidner, E., Brake, C., and Richter, D., in G. Brunner (Ed.), *Supercritical Fluids as Solvents and Reaction Media*, Elsevier B. V., Amsterdam, The Netherlands, 2004.
33. Chauvin, Y., Olivier, H., Wyrwalski, C.N., Simon, L.C., de Souza, R., and Dupont, J., Oligomerization of n-butenes catalyzed by nickel complexes dissolved in organochloroaluminate ionic liquids, *J. Catal.*, 165, 275–278, 1997.
34. Mikkola, J.-P., Virtanen, P., Karhu, H., Murzin, D.Yu., and Salmi, T., Supported ionic liquid catalysts for fine chemicals: Citral hydrogenation, *Green. Chem.*, 8, 197–205, 2006.
35. Salmi, T., Wärnå, J., Mikkola, J.-P., and Rönnholm, M., Modelling and simulation of porous, reactive particles in liquids: Delignification of wood, *Comput. Aided Chem. Eng.*, 20B, 325–330, 2005.
36. Sandelin, F., Salmi, T., and Murzin, D., An integrated dynamic model for reaction kinetics and catalyst deactivation in fixed bed reactors: Skeletal isomerization of 1-pentene over ferrierite, *Chem. Eng. Sci.*, 61, 1157–1166, 2006.

CHAPTER 10

Chemical Reaction Engineering: Historical Remarks and Future Challenges

10.1 CHEMICAL REACTION ENGINEERING AS A PART OF CHEMICAL ENGINEERING

The well-known researcher and teacher in chemical reaction engineering, professor Jacques Villermaux from Nancy, defines chemical reaction engineering in the following manner:

> Génie de la réaction chimique est un branche du génie des precédés qui traite des méthodes de mise en oevre rationelle des transformations de la matière et des appareils dans lesques sont conduites les réactions: les réacteurs.

A free translation can be given as follows: Chemical reaction engineering is the field of process engineering, which, in a rational way, treats the transformation of the components as well as the apparatus where the transformations take place, namely chemical reactors. The French word *génie* refers to not only engineering but also genius and spirit. The history of chemical reaction engineering covers all these aspects and meanings. We will try and provide a brief insight into the roots of chemical reaction engineering and its development as a vital part of chemical engineering.

10.2 EARLY ACHIEVEMENTS OF CHEMICAL ENGINEERING

From a historical viewpoint, chemical reaction engineering is one of the youngest branches of chemical engineering. The development of chemical engineering started with the industrial revolution during the second half of the nineteenth century. The first applications of chemical engineering were in relation to distillation processes: mainly the distillation of oil products in America and that of alcohol in Europe. Caustic soda, sulfuric acid, and bleaching chemicals were the key products during the pioneering era of industrial revolution. One of the great inventors of the application of systematic scientific methods to the design of chemical processes was Eugen Solvay from Belgium, who scaled up the production process for the manufacture of soda (sodium carbonate) from sodium chloride, ammonia, and carbon dioxide. This happened 50 years before the well-known Haber–Bosch process for industrial production of ammonia from atmospheric nitrogen was developed. In the synthesis of organic chemicals, the success of the application of chemical engineering principles was much more modest, since these chemicals were manufactured according to traditional recipes in small amounts in inexpensive, batchwise operated vessels.

The pioneering age of chemical engineering was characterized by the innovations of self-made men, who made marvelous contributions to the empirical development of chemical processes on a large scale. Organized education in chemical technology started in the golden city of Prague, at the prestigious Charles University. The education was focused on brewery technology, which represented one of the core competences of the Czech part of the Austro-Hungarian double monarchy.

The United States was the pioneering country of chemical engineering. A curriculum in chemical engineering was started at the Massachusetts Institute of Technology (MIT) in 1880. The old Europe followed the trend, starting from Denmark, Great Britain, and Imperial Russia.

In 1895, the Danish Technical University in Copenhagen started to send its undergraduates to the chemical industry to produce their master's theses, related to the design of chemical processes in practice. In 1909, a chair devoted to processes and apparatuses in chemical technology was established at the Institute of Chemical Technology in Saint Petersburg. The Imperial College in London initiated a curriculum in chemical engineering in 1911. In Germany, the viewpoint was slightly different: Chemistry (*Chemie*) and technology (*Verfahrenstechnik*) were regarded as rather separate disciplines, and their integration was not considered an issue. As a historical paradox, it can be noticed that many of the pioneers in chemical engineering at MIT, such as Norton, Thorp, Noyes, Walker, and Lewis, had obtained their academic education in physical or organic chemistry at a prestigious German university such as Göttingen, Heidelberg, Leipzig, or Breslau. The German researcher Eugen Hausbrand wrote in the 1890s a book about various separation apparatuses. Hausbrand is one of the fathers of the concept of "unit operations," which is still one of the cornerstones for understanding chemical processes on an industrial scale.

The education of chemical engineers advanced dramatically in the 1920s. In 1920–1925, new chairs in chemical engineering were established at 14 American universities. Politecnico di Milano formed a chair in chemical engineering in 1927 and, in 1928, the Technical

University of Karlsruhe established an institute of chemical engineering, the first one on German soil. In the 1920s, chemical engineering education was established in Scandinavia.

As the description indicates, chemical engineering focused heavily on separation processes such as distillation, absorption, and crystallization. The core of a chemical process is, however, the chemical reaction itself, which implies transformation of raw materials to products. Chemical engineering essentially includes mathematical modeling, simulation, and optimization of processes. As chemical reactions are always involved in chemical reaction engineering, the mathematical treatment is usually rather complicated. This might be the reason why chemical reaction engineering emerged much later than many other branches of chemical engineering.

10.3 THE ROOTS OF CHEMICAL REACTION ENGINEERING

It might be impossible to pinpoint a precise time of birth for chemical reaction engineering, but some milestones are worth noting. The central issue in chemical reaction engineering is to determine the residence time, which is needed to obtain the desired product with specified quality requirements. This idea has existed in the human mind since time immemorial, starting from food preparation over an open flame. An excellent example of an early developed chemical reactor is the empirical construction of a blast furnace for the treatment of iron ores: a semibatch reactor with an optimized shape. The equipment was developed empirically throughout centuries, whereas today advanced mathematical modeling is applied to predict the behavior of iron production units.

A characteristic feature of industrially applied chemical processes is the prominent role of reaction kinetics. The vast majority of industrially applied chemical reactors are slow, and chemical equilibria do not prevail in the system. This is why the classical branch of physical chemistry, namely chemical kinetics, plays a central role in chemical reaction engineering. Kinetics provides us with a method to predict the residence times needed for product formation.

The first quantitative experimental data on chemical kinetics were recorded by the well-known French chemist, Louis Jacques Thénard, who, in 1818, studied the decomposition rate of hydrogen peroxide, a component he himself had discovered. Nowadays, the importance of hydrogen peroxide is growing, because it is an environmentally friendly bleaching agent. As regards quantitative kinetic modeling—and even reactor modeling—an early work could be said to be one of the important milestones of chemical reaction engineering. The British chemist Augustin Harcourt carried out kinetic experiments in a BR and registered the appearance and disappearance of chemical compounds as a function of the reaction time. Because Harcourt was a pure chemist, he did not have extensive knowledge of integral calculus. He thus turned to a mathematician, William Esson, who solved the coupled differential equations for the consecutive reaction system $A \rightarrow R \rightarrow S$. This was de facto the solution of the mass balances of components in a complex reaction system. The work was published in 1865–1867. Nowadays, this model system is the standard material in every basic course in chemical reaction engineering.

Two pioneers of chemical kinetics who made great contributions should not be forgotten, namely, the Dutch and Swedish Nobel Prize winners Jacobus Henricus van't Hoff and Svante Arrhenius. In his monograph *Études dynamique chimique*, van't Hoff described the temperature dependences of rate and equilibrium constants with exponential functions ($\exp(-E/(RT))$), which have a sound physical background and are sufficiently accurate for most industrial applications. Svante Arrhenius demonstrated the usefulness of this expression in many practical cases. The Arrhenius equation is still the most common expression used for the temperature dependence of rate constants.

The majority of industrially applied chemical processes involve the use of solid, heterogeneous catalysts, which make the processes feasible by enhancing the rates of chemical reactions. This is why the quantitative development of catalytic kinetics has been of crucial importance for successful chemical reaction engineering. The Nobel Prize winners Irving Langmuir from New York and Cyril Hinshelwood from Oxford made breakthroughs in the development of theories for catalytic processes on ideal, uniform solid surfaces. The theory of adsorption, desorption, and surface reaction on ideal surfaces was extended to nonideal (nonuniform) surfaces by Mikhail Temkin, who worked at the Karpov Institute of Physical Chemistry, Moscow. These concepts of catalytic kinetics are nowadays used everywhere, and always, when kinetics is needed to predict the behavior of a catalytic reactor. In the field of polymerization kinetics, the Nobel Prize winner Paul Flory carried out pioneering work on stagewise polymerization kinetics.

10.4 UNDERSTANDING CONTINUOUS REACTORS AND TRANSPORT PHENOMENA

An important breakthrough in the development of chemical reaction engineering was the quantitative treatment of continuous reactors. For many experts, real engineering implies a continuous operation. This is where the flow pattern of the reactor along with heat and mass transfer effects enters the arena. The pioneering effort on continuous reactors was made by the German scientist Gerhard Damköhler. After obtaining his doctoral degree at the University of Munich and spending some years in the industry, at the age of 26 he was invited to the Institute of Physical Chemistry in Göttingen. The chief of the institute, professor Arnold Eucken, proposed that the young doctor should study reaction rates in continuous flow reactors. This research resulted in a series of papers devoted to the topic *Einflüsse der Strömung, Diffusion und das Wärmeüberganges auf die Leistung von Reaktionsöfen*, that is, the influence of flow, diffusion, and heat transfer on the performance of reaction furnaces. Damköhler applied mass, energy, and momentum balances to the description of chemical reactors and discovered four dimensionless numbers, nowadays known as the Damköhler numbers.

At the end of the 1930s, some research work was published on the coupling between chemical reaction rates and mass transfer. The Russian physicist D.A. Frank-Kamenetskii developed a theory for coupled chemical reactions and mass transfer on nonporous solid surfaces in connection with combustion processes. This work remained ignored for a long

time in the Western world, until it was translated into English in 1955 under the title *Diffusion and Heat Exchange in Chemical Kinetics*. G. Damköhler in Germany, E.W. Thiele in United States, and B. Zeldovich in Russia developed the theory of simultaneous reaction and diffusion in porous catalyst particles toward the end of the 1930s. A new dimensionless number was introduced by Thiele to relate the intrinsic rate of a chemical reaction to the diffusion rate inside catalyst pores. This dimensionless number is nowadays called the Thiele modulus.

10.5 POSTWAR TIME: NEW THEORIES EMERGE

The period after World War II marked a great breakthrough in the development of theories in chemical engineering. In a classical paper appearing in the *Chemical Engineering Science* in 1953, a war veteran, professor Peter Danckwerts from Cambridge, developed the language of treatment for a nonideal flow, the functions that are nowadays known as $E(t)$ and $F(t)$ functions, used to characterize residence times in chemical reactors. The theories of a nonideal flow, including the principles of segregation and maximum mixedness (micromixing and macromixing), were developed further by Bourne, Zwietering, and many others.

The problem of adequately describing the gas–liquid contact is still a difficult one. The early two-film theory for gas–liquid interfaces is still the dominant one in reaction engineering practice, but researchers have for long recognized its artificial nature and aimed at physically more meaningful descriptions. Here the penetration theory of Higbie and particularly the surface renewal theory of P.V. Danckwerts are important milestones. Again, professor Danckwerts made a classical contribution to chemical reaction engineering by writing the book *Gas–Liquid Reactions*, which made his idea of mosaic-like structures at fluid–fluid interfaces understandable for a wide audience of chemical engineers.

A new era brought about the discovery of new reactors. The fluidized beds technology was developed in the 1940s, originally to make catalytic cracking more efficient and economical. A fluidized bed is a challenging topic from both the operational and the modeling viewpoints. Conventional mathematical models for fluidized beds based on the use of residence time functions or dispersion coefficients are not adequate, because a fluidized bed consists of segregated regions, in which the catalyst bulk density varies. A sound understanding of this dilemma was provided by D. Kunii and O. Levenspiel, who developed a hydrodynamic model for fluidized beds, and distinguished between "'bubble," "cloud," "wake," and "emulsion" phases. These phases are visible in real beds. A reliable description of the fluidized bed is based on local reaction rates combined to mass transfer between the different regions—today, this approach is called the Kunii–Levenspiel model, and numerous extensions of it have been developed.

The very mathematical orientation of chemical reaction engineering led to avant-garde research on American soil. Professor Neil Amundson from Minnesota published a pioneering work on the stability of chemical reactors, and professor Rutherford Aris from the same university published a monumental treatise on reaction and diffusion in porous catalysts. In parallel, the optimization aspects of chemical reactors were developed further by many

researchers, such as Levenspiel, Aris, and many members of the Dutch school in chemical reaction engineering (Westerterp, Beenackers, and van Swaaij).

The exciting issue of steady-state multiplicity has attracted the attention of many researchers. First the focus was on exothermic reactions in continuous stirred tanks, and later on catalyst pellets and dispersed flow reactors as well as on multiplicity originating from complex isothermal kinetics. Nonisothermal catalyst pellets can exhibit steady-state multiplicity for exothermic reactions, as was demonstrated by P.B. Weitz and J.S. Hicks in a classical paper in the Chemical Engineering Science in 1962. The topic of multiplicity and oscillations has been put forward by many researchers such as D. Luss, V. Balakotaiah, V. Hlavacek, M. Marek, M. Kubicek, and R. Schmitz. Bifurcation theory has proved to be very useful in the search for parametric domains where multiple steady states might appear. Moreover, steady-state multiplicity has been confirmed experimentally, one of the classical papers being that of A. Vejtassa and R.A. Schmitz in the *AIChE Journal* in 1970, where the multiple steady states of a CSTR with an exothermic reaction were elegantly illustrated.

The description of fluid–solid reactions is particularly challenging, since the structure of solid material changes during the reaction. We can have topochemical reactions on essentially nonporous materials, reactions coupled to diffusion throughout a porous particle, or diffusion through a porous product layer to a reaction plane or a reaction zone. Yagi and Kunii made a breakthrough (1955, 1961) by providing a quantitative description of product layer behavior. Later, Szekely and Evans developed a new model for solid particles to achieve a more realistic description of solid materials: the particle consists of nonporous grains, which are coupled together as a porous structure—the grain model. The development of new microscopic techniques might provide an inspiration for new model development in the future.

10.6 NUMERICAL MATHEMATICS AND COMPUTING DEVELOP

A field that has considerably contributed toward the development of chemical reaction engineering, particularly in the 1970s and 1980s, is numerical mathematics, along with the development of computing capacity. Most problems in chemical reaction engineering are highly nonlinear, and they include several coupled algebraic or differential equations. The nonlinearity has two basic reasons: nonlinear kinetics and highly nonlinear temperature dependence of rate and equilibrium constants. This is why the coupling between mass and energy balances is very nonlinear. In addition, the problems concerning complex reaction networks are often of a stiff nature, since rapid and slow reactions coexist. Many researchers have contributed toward the successful numerical solution of stiff differential equations, such as Henrici, Gear, Hindmarsh, Buzzi Ferraris, Rosenbrock, Michelsen, Kaps, and Wanner (Appendix 2). It is interesting to note that these researchers represent both mathematical and chemical engineering communities. BD and semi-implicit Runge–Kutta methods have turned out to be the best ones for IVPs in chemical reaction engineering. The well-known computer code for stiff IVPs developed by Alan Hindmarsh at Lawrence Livermore Laboratory has become a standard tool for engineers. Very stiff problems are best treated by

semi-implicit Runge–Kutta methods, for example, the method of Kaps and Wanner. The BD treatment has been extended to differential-algebraic systems by Linda Petzold.

Several central models in chemical reaction engineering, such as reaction–diffusion in porous media and in fluid layers, are boundary value problems. In the distant past, the numerical solution of boundary value problems was cumbersome and uncertain, since the approach was mostly based on a trial-and-error approach (shooting method). A breakthrough was made in the late 1960s and early 1970s by Warren Stewart in Wisconsin and John Villadsen and Michael Michelsen in Copenhagen, who developed a polynomial approximation method, orthogonal collocation, to such a mature stage that it works in practice for chemical engineering problems. The first development of collocation was based on global approximation, that is, the use of one single polynomial for the entire domain, but later on, the collocation approach was extended to cope with very steep concentration and temperature profiles by introducing a piecewise approximation (collocation on fine elements). The books by Villadsen and Michelsen as well as those by Bruce Finlayson became standard texts for researchers and engineers throughout the chemical engineering community. The collocation method has been combined with the BD method for the solution of PDEs appearing in many engineering problems—the adaptive grid concept has been successfully applied to reactor models—a typical example is the work by Alirio Rodrigues and his coworkers.

Today, the above-mentioned numerical methods are inbuilt in standard, public-domain software or incorporated into high-level programming languages (e.g., MATLAB® and Mathematica)—undergraduates can perform advanced simulations without knowing anything about the underlying numerical algorithms! However, many challenges still remain. Parameter estimation from experimental data is a demanding task and a risky business. The most common algorithms used today, for instance, the simplex and Levenberg–Marquardt algorithms for optimum search, are of a local nature, and a trial-and-error approach is frequently used to avoid the termination of the calculations in a suboptimum. Genetic algorithms may in the future show whether this dilemma can be surmounted.

10.7 TEACHING THE NEXT GENERATION

Writing excellent textbooks has always been a good tradition among the researchers in chemical reaction engineering. We still remember the thin, clear, and concise book from the Cambridge School of Chemical Engineering: *Chemical Reactor Theory* by Denbigh and Turner. It convinced many generations that chemical reaction engineering is a real science. If we asked people working in chemical reaction engineering to mention just one textbook, the majority would cite *Chemical Reaction Engineering* by Octave Levenspiel, Oregon State University. The title was perfect and so was the pedagogic approach. As the book appeared in 1962, it directly led to a revolution in chemical reaction engineering education. Logical, bright, and rich with graphical illustrations and clarifying pictures, it made chemical reaction engineering attractive for a wide audience, even for students not very keen on mathematics. It is admirable that after more than 30 years, professor Levenspiel came out with a third, updated edition of the book.

One other textbook deserves a special mention. The book by G. Froment and K. Bischoff, *Chemical Reactor Analysis and Design*, aims not to be easy but elegant, introducing the reader directly to the advanced theories of reaction engineering and to the frontiers of research by including complex reaction networks, advanced models for catalytic systems, multicomponent diffusion, and the surface renewal theory for gas–liquid contact. The book is excellent for students who wish to become scientists in chemical reaction engineering.

It has been delightful to see that textbook writing has not been limited to the English language only. Advanced textbooks and pedagogical texts have been written by J. Villermaux in French, by H. Hofmann, A. Renken, and M. Baerns in German, and by people in Italy, Spain, Portugal, Russia, and Scandinavia. Besides the current *lingua franca* in science, we need terminology in the students' mother tongue to develop their deep understanding of the subject and to give them communication skills with their closest surroundings. New forms of pedagogics, such as virtuality, are entering the universities. However, learning by reading and problem-solving still remain at the core.

10.8 EXPANSION OF CHEMICAL REACTION ENGINEERING: TOWARD NEW PARADIGMS

The last decades of the twentieth century have brought about a tremendous expansion and diversification of chemical reaction engineering, from the treatment of very complex reaction networks to transient operation of chemical reactors and oscillating systems. In parallel to this, the systems engineering approach has emerged for the optimization of chemical processes, as well as integration of reaction and separation, reactive distillation being an example of a huge commercial success. CFD has entered the world of chemical reaction engineering. Simultaneously, we have gone back to the basics again. It is not enough to improve on the description of conventional reactors, but we wish to discover new reactor structures such as monoliths, catalyst packings, and fiber reactors; to introduce nonconventional forms of energy such as microwave and ultrasound; and to introduce new reaction media such as ILs and supercritical media. Some of the milestones are listed in Table 10.1.

Since the reaction engineering community is large, Table 10.1 can never be exhaustive; we apologize to those who are not mentioned—Table 10.1 should only be used as an orientation in the subject. By running a computer search of the persons mentioned in Table 10.1, it will be easy to come across new names through the references.

In recent decades, the application of chemical reaction engineering has made a real breakthrough; elegant academic exercises have been turned into industrial practice. Chemical reaction engineering is no longer only applied to the production of bulk chemicals but also to fine and speciality chemicals. New application areas have emerged, such as bioreactors, processes in the electronics industry, conversion of molecules from nature, and production of pulp and paper.

Topics of chemical reaction engineering are discussed by a multitude of scientific congresses and colloquia devoted to chemical engineering and catalysis. The flagship of these events in reaction engineering is the International Symposium in Chemical Reaction Engineering (ISCRE), which started in the late 1950s as a European—North American effort.

TABLE 10.1 Fields of Chemical Reaction Engineering with Well-Known Research Teams

Transient (dynamic) models for catalytic reactors	M. Kobayashi, J. Koubek, C.O. Bennett, M. Baerns, J. Hanika, H. Hofmann, G. Eigenberger, R. Lange, A. Renken, G. Marin, A. Seidel-Morgenstern, and P. Silveston
Three-phase reactor technology	B. McCoy, G. Baldi, J. Hanika, R. Lange, and R. Chaudhari
Combination of reaction and diffusion in catalyst pellets to real reactor models	G. Froment, H. Delmas, C. Julcour, S. Toppinen, and P. Schneider
New approach to modeling of porous solids	L.K. Doraiswamy, K. Jensen, M. Marek, and F. Stepanek
Novel gas–liquid technologies	M.M. Sharma, N. Midoux, J.-C. Charpentier, G. Wild, and G. Astarita
High-temperature reactor technology	L.D. Schmidt
CFD in chemical reactors	J. Baldyga, J.R. Bourne, G. Eigenberger, M. Dudukovic, R. Krishna, and many others
Nonlinear dynamics	M. Marek, M. Kubicek, and A. Varma
Reactive distillation	Many companies and research groups such as U. Hoffman, K. Sundmacher, and R. Krishna
Bioreaction engineering	J. Villadsen, Nielsen, J. Bailey, and D. Ollis
Polymer reaction engineering	P. Flory, B. Nauman, D.H. Solomon, M. Tirreu, A. Kumar, R.K. Gupta, and A. Renken
Simulating moving beds and chromatographic reactors	A. Rodrigues, M. Morbidelli, and A. Seidel-Morgenstern
Monolith technology	B. Andersson, S. Irandoust, J. Moulijn, F. Kapteijn, M. Kreutzer, and A. Stankiewitz
Catalyst packings	A.G. Sulzer
Fiber reactors	M. Sheintuch, A. Renken, L. Kiwi-Minsker, and A. Kalantar
Membrane reactors	van Swaaij and A. Seidel-Morgenstern
Reverse flow reactors	G. Boreskov, Yu Matros, and G. Eigenberger
Microreactors	Mikrotechnik (Mainz) along with several companies and K. Jensen

Today, it is a global forum alternating among America, Asia, and Europe. Chemical reaction engineering has a strong position in national and international chemical engineering organizations. We should not forget that the first three presidents of the European Federation of Chemical Reaction Engineering come from the field of reaction engineering: H. Hofmann (Erlangen–Nürnberg), K. Westerterp (Twente–Enschede), and J.-C. Charpentier (Nancy and Lyon).

New paradigms of chemical reaction engineering will appear; the processes of the future should be more intensive, more selective, and more product-oriented, because of global competition and environmental aspects. A broad-minded view is needed to meet the

challenges of the future; as one of the presidents of European Federation of Chemical Engineering, professor Charpentier, has stated the link between molecular-level phenomena, processes, and products, *processus–procedés–produits* is crucial. Chemists, material scientists, physicians, mathematicians, and chemical engineers have to work together to meet the future challenges. Chemical reaction engineering is a hard science promoting the green values of a globalizing society.

FURTHER READING

Aris, R., *Introduction to the Analysis of Chemical Reactors*, Prentice-Hall, Englewood Cliffs, NJ, 1965.

Aris, R., *Elementary Chemical Reactor Analysis*, Prentice-Hall, Englewood Cliffs, NJ, 1969.

Baerns, M., Hofmann, H., and Renken, A., *Chemische Reaktionstechnik*, Georg Thieme Verlag, Stuttgart, 1992.

Baldyga, J. and Bourne, J.R., *Turbulent Mixing and Chemical Reactions*, Wiley, New York, 1999.

Butt, J.B., *Reaction Kinetics and Reactor Design*, 2nd Edition, Marcel Dekker, New York, 2000.

Carberry, J.J., *Chemical and Catalytic Reaction Engineering*, McGraw-Hill, New York, 1976.

Denbigh, K.G. and Turner J.C.R., *Chemical Reactor Theory*, 2nd Edition, Cambridge University Press, Cambridge, 1971.

Emig, G. and Klemm, E., *Technische Chemie—Einfuhrung in die Chemische Reaktionstechnik*, Fünfte Auflage, Springer, Heidelberg, 2005.

Fogler, H.S., *Elements of Chemical Reaction Engineering*, 3rd Edition, Prentice-Hall, Englewood Cliffs, NJ, 1999.

Froment, G.B. and Bischoff, K.B., *Chemical Reactor Analysis and Design*, 2nd Edition, Wiley, New York, 1990.

Hayes, R.-E., *Introduction to Chemical Reactor Analysis*, Gordon and Breach Science Publishers, Amsterdam, 2001.

Hill, C.G., Jr., *An Introduction to Chemical Engineering Kinetics and Reactor Design*, Wiley, New York, 1977.

Levenspiel, O., *Chemical Reaction Engineering*, 3rd Edition, Wiley, New York, 1999.

Metcalfe, I.S., *Chemical Reaction Engineering: A First Course*, Oxford University Press, New York, 1997.

Missen, R.W., Mims, C.A., and Saville, B.A., *Chemical Reaction Engineering and Kinetics*, Wiley, Toronto, 1999.

Nauman, E.B., *Chemical Reactor Design*, Wiley, Toronto, 1987.

Nauman, E.B., *Chemical Reactor Design, Optimization and Scaleup*, McGraw-Hill, New York, 2001.

Rase, H.F., *Chemical Reactor Design for Process Plants I-II*, Wiley, New York, 1997.

Rose, L.M., *Chemical Reactor Design in Practice*, Elsevier, Amsterdam, 1981.

Schmidt, L.D., *The Engineering of Chemical Reactions*, Oxford University Press, New York, 1998.

Smith, J.M., *Chemical Engineering Kinetics*, 3rd Edition, McGraw-Hill, New York, 1981.

Trambouze, P. and Euzen, J.-P., *Les Réacteurs Chimiques, de la Conception à la Mice en Oeuvre*, Editions Technip, Paris, 2002.

Trambouze, P., van Landeghem, H., and Wauquier, J.P., *Chemical Reactors—Design/Engineering Operation*, Editions Technip, Paris, 1988.

Walas, S.M., *Chemical Reaction Engineering Handbook of Solved Problems*, Gordon and Breach Science Publishers, Amsterdam, 1995.

Westerterp, K.R., van Swaaij, W.P.M., and Beenackers, A.A.C.M., *Chemical Reactor Design and Operation*, Wiley, New York, 1984.

Villermaux, J., *Génie de la Réaction Chimique—Conception et Fonctionement des Réacteurs*, Lavoiser, Paris, 1985.

CHAPTER 11

Exercises*

CONTENTS

SECTION I. KINETICS, EQUILIBRIA, AND HOMOGENEOUS REACTORS

1. Tertiary amyl-ether (TAME) is a gasoline additive. The degradation products of TAME are 2-methyl-1-butene (M1B), 2-methyl-2-butene (M2B), and methanol (M). The MIB is further isomerized to M2B during the reaction. The reaction scheme can thus be written as follows:

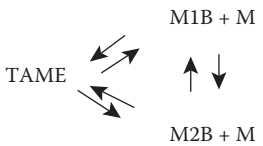

Here, the reactions can be regarded as elementary and reversible, taking place on the surface of a catalytic ion-exchange resin.

*Some of the exercises are based on the literature data. A list of literature references is provided at the end of this chapter.

a. Define the stoichiometric matrix for the system.
b. How many stoichiometrically independent reactions does the above scheme contain?
c. Give generation rates for the components TAME, M1B, M2B, and M. (Use the previously defined symbols for the compounds.)
d. Select suitable key components and define the mass balances for all components in a tube reactor based on the concentrations of these key components. In this case, the reactions can be considered as homogeneous liquid-phase reactions.

2. In a catalytic exhaust gas converter (monolith catalyst), the following reactions take place on a Pt catalyst:

$$2CO + O_2 \rightleftarrows 2CO_2, \tag{1}$$

$$2C_3H_6 + 9O_2 \rightleftarrows 6CO_2 + 6H_2O. \tag{2}$$

Propene (C_3H_6) and carbon monoxide (CO) were used as model compounds to study the activity of a freshly prepared Pt catalyst. The experiments were carried out in a test reactor operating at atmospheric conditions in the absence of diffusion effects. The conversions of CO and propene (HC), η_{CO} and η_{HC}, were measured at the reactor outlet. Initial concentrations at the reactor inlet were known ($x_{0,CO}, x_{0,HC}, x_{0,O_2}, \ldots, x_{0,H_2O}$).

a. Give the stoichiometric matrix for the system.
b. How is the composition of the product gas, at the reactor outlet, calculated from the conversions η_{CO} and η_{HC} and the initial concentrations? Give the result in mole fractions.

3. Originally, 0.054 mol/dm^3 of methanol reacted with 0.106 mol/dm^3 triphenylmethyl chloride in a solution of dry benzene:

$$CH_3OH + (C_6H_5)_3CCl \rightarrow (C_6H_5)_3COCH_3 + HCl.$$

The reaction follows the second-order kinetics as regard to CH_3OH and the first-order kinetics as regard to $(C_6H_5)_3CCl$. Determine the rate constant from the data given in the table below:

t (min)	426	1150	1660	3120
$c_{CH_3OH\ (mol/dm^3)}$	0.0351	0.0222	0.0186	0.0124

4. Acetylation of benzoyl chloride is carried out in an aqueous medium at 102°C:

$$\underset{(A)}{C_6H_5CH_2Cl} + \underset{(B)}{NaAc} \rightarrow \underset{(C)}{C_6H_5CH_2Ac} + \underset{(D)}{NaCl}.$$

a. The following data were obtained from an experiment carried out in a BR with equimolar initial concentrations of A and B ($c_{0A} = 0.757\,\text{kmol/m}^3$):

t (ks)	10.8	24.48	46.08	54.72	69.48	88.56	109.4	126.7	133.7
c_A/c_{0A}	0.945	0.912	0.846	0.809	0.779	0.730	0.678	0.638	0.619

Determine the reaction order and rate constant for this reaction.

b. Calculate the production capacity of C that can be obtained in a PFR with the volume 500 dm^3, if the reactor is fed with a volumetric flow rate of 0.3 dm^3/ min, containing 10 kmol/m^3 of A and 12 kmol/m^3 of B.

c. What production capacity of C could be obtained in a reactor cascade consisting of three identical CSTRs in series, with a total volume of 500 dm^3? The volumetric flow rate and initial concentrations are the same as in case b.

5. The reaction between ethylene chlorohydrine and sodium hydrogen carbonate can be used in the synthesis of ethylene glycol:

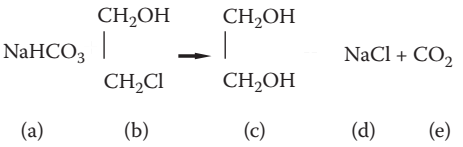

a. The kinetics of this reaction was studied at 82°C in a BR with a volume of 200 mL. The laboratory experiment was conducted with equimolar amounts of ethylene chlorohydrine and sodium carbonate. The experiment's results are listed in the table below. Determine the reaction order and the rate constant k.

A pilot reactor is used to determine the economic feasibility of ethylene glycol production from two available process streams containing 1.79 mol/dm^3 sodium bicarbonate and 3.73 mol/dm^3 ethylene chlorohydrine in water.

b. What is the required volume of a PFR necessary for the production of 20 kg/h of ethylene glycol with a conversion of 95% of the equimolar mixture that has been developed by suitable proportional mixing of the two process streams?

c. What is the required volume of a CSTR operating under similar conditions as the PFR in case b?

d. How much could the total reactor volume be diminished, if the CSTR in case c was replaced by three equally sized CSTRs in series, comprising the same total volume as in case c?

Laboratory experiment

t (h)	c_A (mol/dm^3)
0	2.0
0.05	1.316
0.1	0.980
0.2	0.649
0.3	0.485
0.4	0.388
0.5	0.323
1.0	0.175
2.0	0.092
5.0	0.038

6. Determine the reaction order and rate constant for the gas-phase degradation of ditertiary butyl peroxide:

$$\underset{(A)}{(CH_3)COOC(CH_3)_3} \rightarrow \underset{(B)}{C_2H_6} + \underset{(C)}{2CH_3\ COCH_3}.$$

The reaction proceeded on a laboratory scale in an isothermal BR, where the total pressure (P) was logged. The experimental data are denoted in the table below. Pure ditertiary butyl peroxide was used as a reactant.

Calculate the ratio $V_k/\dot{V}_0$ for a tube reactor to ensure that exactly the same conversion of A is obtained as with the BR in 20 min.

t (min)	P (kPa)
0.0	1.00
2.5	1.40
5.0	1.67
10.0	2.11
15.0	2.39
20.0	2.59

7. Dinitrogen oxide degrades at elevated temperatures to nitrogen and oxygen following the reaction

$$N_2O \rightarrow N_2 + \tfrac{1}{2}O_2.$$

The reaction was studied at 967 K by registering the total pressure (assuming pure N_2O at 200 torr):

t (s)	0	86	234	440	1080	1900
P (torr)	200	212	227	241	263	275

a. What is the required size of a tube reactor to ensure that 90% of dinitrogen oxide would react at 967 K and 2 bar, assuming a volumetric flow rate of 1000 L/h which contains 20 vol% N_2O and the rest being an inert gas?
b. During maintenance work on a tube reactor, it is necessary to use a tank reactor ($2.00\,m^3$) instead. How much is the production capacity affected, provided that a similar degradation efficiency is desired and the gas composition remains unchanged?

8. Diarsine trioxide that emerges as a by-product in the oxidation of arsine-containing sulfide ores is the most important raw material in the manufacture of various arsinic compounds.

Ammonium metavanadite dissolved in a strong acid reacts with diarsine trioxide during the formation of diarsine pentoxide following the overall reaction:

$$\underset{(A)}{As_2O_3(aq)} + \underset{(B)}{4V(V)(aq)} + 2H_2O \rightarrow \underset{(R)}{As_2O_5(aq)} + \underset{(S)}{4V(IV)(aq)} + 4H^-.$$

To determine the reaction kinetics, an experiment was conducted at 318 K in a BR. The initial concentration was $c_{0A} = 1.056\,10^{-2}$ mol/dm^3. The concentration of B was recorded during the reaction, and the following results were obtained:

t (min)	$10^{-2}c_B$ (mol/dm^3)
0	2.00
14.9	1.68
49.5	1.17
68.2	0.98
98.3	0.75
123.1	0.61

a. Determine the reaction order and rate constant.
b. Calculate the production capacity that is obtainable in an isothermal tank reactor with a volume of 100 dm^3 and a volumetric flow rate of 0.5 m^3/h. The reactor was fed with a stoichiometric mixture of A and B, $c_{0A} = 0.025$ mol/dm^3.
c. Give the production capacity of a tube reactor operated under similar conditions as in case b.

9. Thermal decomposition of dimethyl ether was studied at 504°C in a BR operating at a constant volume:

$$(CH_3)_2O \rightarrow CH_4 + H_2 + CO.$$

Determine the rate expression and the rate constant for the reaction using the table below. The experiment was initiated with pure dimethyl ether.

Data:

t (s)	P (torr)
0	312
390	408
777	488
1195	562
3155	779
∞	931

Here t denotes the time and P denotes the total pressure in the reactor.

The reaction was carried out at 504°C in a tube reactor with an inner diameter of 2.5 cm and a length of 5 m. The pressure at the inlet was 1 atm and the inflow contained 50 mol% dimethyl ether. The volumetric flow rate was 100 mL/min at the reactor inlet. Calculate and illustrate graphically the conversion as a function of the reactor length. What is the residence time of the gas in the tube reactor?

10. Acetaldehyde can be produced from ethanol in the following reaction:

$$\underset{\text{(A)}}{CH_3CH_2OH} + \tfrac{1}{2}O_2 \rightarrow \underset{\text{(R)}}{CH_3CHO} + H_2O. \tag{1}$$

Unfortunately, acetaldehyde is oxidized further to carbon dioxide:

$$\underset{\text{(R)}}{CH_3CHO} + \tfrac{5}{2}O_2 \rightarrow \underset{\text{(S)}}{2CO_2} + 2H_2O. \tag{2}$$

The oxygen excess is large, and this is why reactions (1) and (2) can be considered to follow the first-order kinetics in terms of ethanol and acetaldehyde, respectively. Since the ethanol concentration in the process is low (0.1% A at the reactor inlet), the volumetric flow rate can be assumed to be constant.

To study the reaction kinetics, an experiment was carried out in a tube reactor with four different volumetric flow rates at 518 K. The ethanol and acetaldehyde concentrations were determined by chemical analysis. On the basis of the analytical data, the yield of acetaldehyde (c_R/c_{0A}) and the conversion of ethanol were calculated.

a. Estimate k_2/k_1 based on the data listed in the table below.

Experiment in a Tube Reactor

Experiment Number	η_A	c_R/c_{0A}
1	0.175	0.152
2	0.351	0.255
3	0.614	0.300
4	0.956	0.074

b. Calculate and sketch c_R/c_{0A} as a function of η_A at 518 K. Furthermore, add the experimental points in the graph.

c. At which degree of ethanol conversion should the reactor operate to achieve the maximal yield of acetaldehyde (c_R/c_{0A})?

11. Nobel Prize winner Paul Flory studied the kinetics of several poly esterification reactions in a BR, on a laboratory scale. The experimental data of esterification of adipic acid with lauryl alcohol are given in the table below. Initial concentrations of the reactants were 1.0 mol/L. The reaction kinetics can be described with the rate expression

$$r = k\, c_{COOH}^{n}\, c_{OH},$$

where c_{COOH} and c_{OH} denote the concentrations of adipic acid and lauryl alcohol, respectively, and k is the rate constant. The exponent, n, is a number varying between 1 and 2 according to a semi-empirical relation:

$$n = 2^X$$

if $q = 1$ and

$$n = (1 - (1 - 2^{1-q})X)^{1/(1-q)}$$

if $q \neq 1$; X is the conversion of adipic acid and q an empirical exponent.

a) Derive the balance equations that are required for the simulation of the concentrations in a batch reactor.
b) Determine the rate constant on the basis of the data listed in Table 1:

t (min)	X_A
0	0
6	0.1379
12	0.2470
23	0.3675
37	0.4975
59	0.6080
88	0.6865
129	0.7513
170	0.7894
203	0.8161
235	0.8349
270	0.8500
321	0.8672
397	0.8837
488	0.8974
596	0.9084
690	0.9163
900	0.9273
1008	0.9303
1147	0.9354
1370	0.9405
1606	0.9447

X_A = the conversion of adipic acid.

12. The reaction kinetics of the homogeneous liquid-phase reaction

$$2S_2O_3^{2-} + 4H_2O_2 \rightarrow S_3O_6^{2-} + SO_4^{2-} + 4H_2O \qquad (1)$$

was studied in an adiabatic stirred tank reactor (CSTR) under transient conditions, measuring the temperature rise caused by the exothermic reaction (1) as a function of time. The inlet concentrations of thiosulfate and hydrogen peroxide were determined by chemical analysis before the experiment, but no chemical analyses were performed in the course of the experiment. Reaction (1) follows second-order kinetics in thiosulfate and hydrogen peroxide. The density of the reaction mixture as well as the heat capacity remained more or less constant during the reaction.

a. How can the mass and energy balances be coupled in order to have the reaction temperature as the only independent variable in the system?
b. Explain how the parameters incorporated into the rate constant can be determined on the basis of the temperature–time curve, using regression analysis as a tool. Which principal difficulties are incorporated into this methodology?
c. Determine the kinetic parameters by regression analysis.

Data: $R = 8.3143\,\text{J/K mol}$, $c_P = 4.186 \cdot 10^3\,\text{J/kg K}$, $\rho = 1000\,\text{kg/m}^3$,
$\Delta H = -1004.3 \cdot 10^3\,\text{J/mol}$, $T_0 = 25.2°\text{C}$, $c_{0A} = 316.8\,\text{mol/m}^3$,
$\text{A} = S_2O_3^{2-}$, $c_{0B} = 2 \cdot c_{0A}$, $\text{B} = H_2O_2$, $V_R = 110 \times 10^{-6}\,\text{m}^3$,
$V = 130 \times 10^{-6}\,\text{m}^3/\text{s}$.

The temperature profile in the reactor:

t (min)	0	0.5	1.0	1.5	2.0	2.5	3.0	4.0	4.5
T (°C)	25.4	27.9	32.9	39.6	46.1	50.4	53.1	55.5	56.0
t (min)	5.0	5.5	6.0	6.5	7.0	7.5			
T (°C)	56.2	56.5	56.3	56.5	56.5	56.4			

13. The reaction between ammonia and formaldehyde can be used for the production of hexamine:

$$4NH_3 + 6HCHO \rightarrow (CH_2)_6N_4 + 6H_2O.$$
(A) (B) (C) (D)

The reaction kinetics is given by the expression

$$r = kc_Ac_B^2,$$

where $k = 0.01611\,\mathrm{dm^3/mol^2\ s}$ at 309 K. The reactor was fed at a volumetric flow rate of $1.50\,^3/\mathrm{s}$, containing $4.00\,\mathrm{mol/dm^3}$ of ammonia and $6.00\,\mathrm{mol/dm^3}$ of formaldehyde. The temperature was set at 309 K. Determine c_A, c_B, and c_C as well as η_A in a stirred tank reactor in a PFR with a volume of $490\,\mathrm{cm^3}$.

14. Acetic acid anhydride needs to be hydrolyzed in a continuously operating cascade reactor consisting of four identical stirred tank reactors. The first reactor operates at 10°C, the second one at 15°C, the third at 25°C, and the fourth at 40°C. The hydrolysis reaction can be assumed to follow first-order kinetics in diluted aqueous solutions, and the rate constant has the following values at the given temperatures:

T (°C)	k ($\mathrm{mm^{-1}}$)
10	0.0567
15	0.0806
25	0.1580
40	0.3800

a. How large should the stirred tank reactors be to achieve a conversion of 0.95 at the outlet of the cascade, assuming a volumetric flow rate of 90 L/min?
b. How many reactors in series of the size calculated in A are required in case all of the reactors operate at 15°C?

15. It is desirable to figure out the dependence on the conversion of different reactor sizes and types in adiabatic operations, for example, for the strongly exothermic reaction:

$$2S_2O_3^{2-} + 4H_2O_2 \rightarrow S_3O_6^{2-} + SO_4^{2-} + 4H_2O.$$

This second-order reaction has the following rate constant

$$k_{S_2O_3} = e^{31.35} \cdot e^{-E_a RT}(1/\mathrm{mol/min})$$

and the activation energy

$$E_a = 76.59\,\mathrm{kJ/mol}.$$

a. Derive an expression for the generation velocity, $r_{S_2O_3}$, provided that $c_{0,S_2O_3} = 0.5c_{0,H_2O_2}$.
b. Calculate the ratio, $\rho c_p/(-\Delta H_{S_2O_3})$, which is presumed to remain constant and independent of the temperature. Further, an aqueous solution with the initial concentration of 0.33 S_2O_3/L and 0.668 mol H_2O_2/L under adiabatic conditions in a BR attained the conversion of 1.0 at 64°C, as the initial temperature was 20°C.
c. At what temperature (in an adiabatic BR) is the conversion of 0.5 obtained for the reaction in question, taking into account the data given and calculated in b? What is the value of velocity, $r_{S_2O_3}$, at this temperature?

16. For the reversible liquid-phase reaction,

$$\underset{(A)}{CH_3COOH} + \underset{(B)}{C_2H_5OH} \underset{k_-}{\overset{k_+}{\rightleftarrows}} \underset{(R)}{CH_3COOC_2H_5} + \underset{(S)}{H_2O}$$

the rate expression $r_A = k_+ c_A c_B - k_- c_R c_S$ is valid. As 4500 L/h of the solution with the initial composition

$$\begin{aligned} \text{Data: } c_{0A} &= 3.9\ \text{mol/L} \\ c_{0B} &= 10.2\ \text{mol/L} \\ c_{0R} &= 0\ \text{mol/L} \\ c_{0S} &= 17.6\ \text{mol/L} \end{aligned}$$

at 100°C and under vigorous agitation flows through a tank reactor of 16,000 L, a conversion level of 0.35 is obtained for acetic acid. Experiments on a smaller scale have demonstrated that with more moderate flow rates, the conversion level of 0.54 is asymptotically approached. Calculate the numerical values of k_+ and k_- at 100°C. Which value obtains the equilibrium constant? The density of the solution can be assumed to be independent of the conversion level.

17. Butadiene and acrolein react in a BR with a constant temperature and volume.

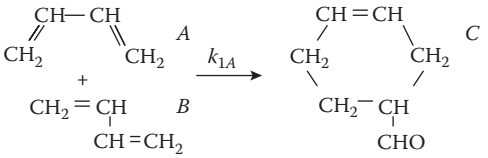

However, a side reaction takes place simultaneously:

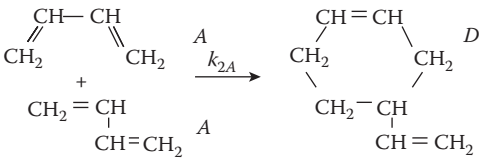

Reactions (1) and (2) can be assumed to be elementary.

a. Derive an expression that yields c_A as a function of c_B in a BR.
b. How large a fraction of butadiene has reacted at the reaction time t (see the table below)?

c. Give the total yields of C and D at time t.

$$\text{Data: } c_{0A} = c_{0B} = 0.01 \text{ mol/dm}^3$$
$$k_{1A} = 5.86 \text{ dm}^3/\text{mol min}$$
$$k_{2A} = 1.44 \text{ dm}^3/\text{mol min}$$

The rate constants are given at 330°C.

The reaction times (t, min) are 20, 40, and 60 min.

18. Pyrolysis of acetoxy propionate yields acetic acid and methyl acrylate following the reaction scheme

$$CH_3COOCH(CH_3)COOCH_3 \rightarrow CH_3COOH + CH_2 = CHCOOCH_3.$$

Below 565°C, the pyrolysis reaction is of first order and has the rate constant

$$k = 7.8 \cdot 10^9 \cdot e^{-19{,}220(T/K)} (s^{-1}).$$

a. A pilot reactor operating isothermally at 500°C is used. How long a reactor is required to achieve a conversion of 90%? The reactor consists of a tube with an inner cross-sectional area of 36 cm^2. The total pressure is 5 atm and the incoming flow of acetoxy propionate is 226.8 kg/h.

b. Calculate the residence time for the gas mixture in the pilot unit. Compare the residence time with $V/\dot{V}_0$.

Remember that

$$\bar{t} = \int_0^V \frac{dV}{\dot{V}}.$$

c. How long should the reactor take, if it operates batchwise as an autoclave, to reach the same conversion and production capacity as specified in case a, provided that the conditions otherwise are similar to those defined in case a?

19. At temperatures exceeding 200°C, 5-methyl-2-oxazolidinone (A) reacts with N-(2-hydroxypropyl)-imdazolidinon (B) and carbon dioxide (C):

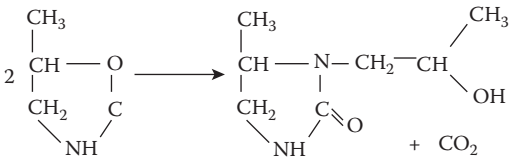

The generation velocity of B can be described by the expression

$$r_B = k_1 c_A^2 + k_2 c_A c_B.$$

A conversion of η_A (see the table below) should be obtained. Calculate the required residence time when the reaction is carried out in

a. A CSTR
b. A PFR without recirculation
c. A PFR with recirculation
d. In an optimal cascade consisting of suitable reactor units
e. What kind of reactor would you recommend for the final design?

$$\text{Data}: k_1 = 1.02\,\text{m}^3/(\text{kmol Ms}),$$
$$k_2 = 75\,\text{m}^3/(\text{kmol Ms}),$$
$$c_{0A} = 30\,\text{mol/dm}^3$$

Use the conversion of η_A: 0.80, 0.90, 0.95, and 0.99.

20. Saponification of diethyl adipate takes place in two steps:

$$\text{A} + \text{B} \rightarrow \text{R} + \text{E}, \quad (1)$$
$$\text{R} + \text{B} \rightarrow \text{S} + \text{E}, \quad (2)$$

where $\text{A} = (CH_2)_4(COOC_2H_5)_2$, $\text{B} = \text{NaOH}$, $\text{R} = (CH_2)_4(COONa)(COOC_2H_5)$, $\text{S} = (CH_2)_4(COONa)_2$, and $\text{E} = C_2H_5OH$.

The rate constants have the following values: $k_1 = 0.3346\,\text{dm}^3/\text{mol s}$ and $k_2 = 0.1989\,\text{dm}^3/\text{mol s}$. An isothermal reactor should be designed in such a way that the maximum concentration of R is obtained at the outlet. The reactor is fed with two separate inflows as in the data listed below. Subscripts 1 and 2 denote the flows 1 and 2, respectively.

a. Calculate the maximum concentrations of R that can be obtained in CSTRs and PFRs.
b. How large a volumetric flow rate is required in a CSTR to attain the maximal concentration of R?
c. How can we determine the residence time of a PFR that yields the maximal concentration of R?

$\dot{V}$ (dm³/min)	$\dot{V}_2$ (dm³/min)	$c_{0A,1}$ (mol/dm³)	$c_{0B,2}$ (mol/dm³)
0.5	0.5	0.10	0.20
0.5	0.5	0.10	0.16

$c_{0A,2} = 0, c_{0B,1} = 0, c_{0R} = c_{0S} = 0.$

21. Saponification of diethyl adipate is a mixed reaction, which, under alkaline conditions, follows the reaction scheme

$$\mathrm{A} + \mathrm{B} \rightarrow \mathrm{R} + \mathrm{E}, \tag{1}$$

$$\mathrm{R} + \mathrm{B} \rightarrow \mathrm{S} + \mathrm{E}, \tag{2}$$

where $\mathrm{A} = (\mathrm{CH_2})_4(\mathrm{COOC_2H_5})_2$, $\mathrm{B} = \mathrm{NaOH}$, $\mathrm{R} = (\mathrm{CH_2})_4(\mathrm{COONa})(\mathrm{COOC_2H_5})$, $\mathrm{S} = (\mathrm{CH_2})_4(\mathrm{COONa})_2$, and $\mathrm{E} = \mathrm{C_2H_5OH}$.

By investigating the reaction kinetics, the rate constants k_1 and k_2 for reactions (1) and (2) were determined:

$$k_1 = 4.87 \times 10^6 \ \exp(-5080\,\mathrm{K/T})\ \mathrm{dm^3/mol/s},$$

$$k_2 = 3.49 \times 10^3 \ \exp(-3010\,\mathrm{K/T})\ \mathrm{dm^3/mol/s}.$$

A tube reactor is fed with a solution containing $2\,\mathrm{mol/dm^3}$ diethyl adipate (A) and $3\,\mathrm{mol/dm^3}$ sodium hydroxide (B). The reactor is assumed to operate adiabatically. Determine the residence time (space time) by numerical simulations, which gives the maximum yield of the intermediate product, R.

Data: Reaction enthalpies, $\Delta H_{\mathrm{r}1} = -45.2\,\mathrm{kJ/mol}$, $\Delta H_{\mathrm{r}2} = -68.0\,\mathrm{kJ/mol}$,

Heat capacity of the mixture, $c_\rho = 4.20\,\mathrm{kJ/K/dm^3}$,

Concentrations and temperatures at the reactor inlet, $c_{0\mathrm{A}} = 2.0\,\mathrm{mol/dm^3}$,

$c_{0\mathrm{B}} = 3.0\,\mathrm{mol/dm^3}$, the remaining concentrations, $c_{0i} = 0\,\mathrm{mol/dm^3}$,

$T_0 = 300\,\mathrm{K}$.

22. Many industrially interesting organic syntheses follow the reaction scheme

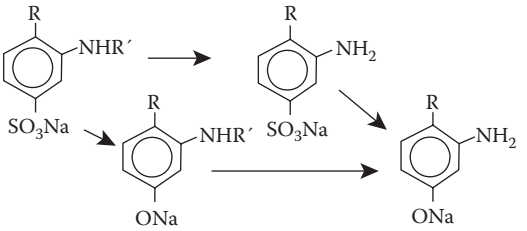

As an example, the production of substituted alkylamine phenols takes place as follows:

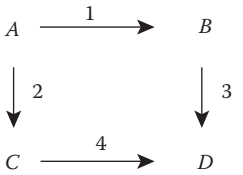

For the model system, some first-order rate constants, k_1, k_2, k_3, and k_4, have been determined. The numerical values are listed in the table below.

Rate Constants	
k_1 (h^{-1})	0.010
k_2 (h^{-1})	0.020
k_3 (h^{-1})	0.018
k_4 (h^{-1})	0.012

a. Derive the expressions of c_A, c_B, and c_C as a function of the reaction time in a BR.
b. Determine the optimal residence time leading to the maximum concentrations of B and C in a PFR. Which values are thus obtained for the concentrations of B and C, if the initial concentration is $c_{0A} = 1.00$ mol/dm^3?
c. What will be the numerical value of the optimal mean residence time that yields the maximum concentrations of B and C in a CSTR? Also, calculate the maximum concentrations of B and C.

23. Oxidation of SO_2 to SO_3 is carried out in a contact process at atmospheric pressure, using oxygen in air as one of the reactants. The catalyst is V_2O_5 and the temperature at the outlet is around 420°C. For the reaction

$$2SO_2 + O_2 \rightleftarrows 2SO_3,$$

the thermodynamic equilibrium constant, K_p, is given by the equation

$$\lg\left(\frac{K_p}{\text{atm}^{-1}}\right) = \frac{9910}{(T/K)} - 9.36.$$

a. Investigate which equilibrium conversion could be achieved if the oxidation takes place at 550°C and 30 MPa. Assume a stoichiometric mixture of sulfur dioxide and pure oxygen gas.
b. Which equilibrium conversion can be attained by assuming the same initial composition of the reaction mixture and temperature, but a total pressure of 100 kPa?

24. The methanol synthesis reaction

$$CO(g) + 2H_2(g) \rightleftarrows CH_3OH(g)$$

is carried out at 350°C and 213 atm. By means of a new type of catalyst, some companies have managed to carry out the synthesis at 230°.

Start with a stoichiometric mixture of CO and H_2 and calculate the total pressure required to reach the same equilibrium composition at 230°C as at 350°C and 213 atm. Give the equilibrium mole fractions for all the components.

The equilibrium constant is given by

$$\lg(K_p/\mathrm{atm}^{-2}) = 5304/(T/K) - 12.89.$$

25. Many industrially important reactions follow the scheme

$$\mathrm{A} + \mathrm{B} \underset{k_2}{\overset{k_1}{\longrightarrow}} \mathrm{R}$$

$$\mathrm{R} + \mathrm{B} \rightarrow \mathrm{S}$$

$$\mathrm{S} + \mathrm{B} \xrightarrow{k_3} \mathrm{T}$$

as illustrated below.

Industrially Important Complex Reactions

Reactants		**Products**		
A	**B**	**R**	**S**	**T**
Water, ammonia	Ethylene oxide[a]	Ethylene glycol	Diethylene glycol	Triethylene glycol
	Ethylene oxide[a]	Monoethanolamine	Diethanolamine	Triethanolamine
Methyl, ethyl, or butyl alcohol	Ethylene oxide[a]	Monoglycol ether	Diglycol ether	Triglycol ether
Benzene	Chlorine	Monochlorobenzene	Dichlorobenzene	Trichlorobenzene
Methane	Chlorine	Methyl chloride	Dichloromethane	Trichloromethane

[a] The same sets of reactions are also carried out using propylene oxide.

a. Derive equations that make it possible to calculate the product distribution (c_R, c_S, c_T) as a function of the concentration of reactant A ($c_{0R} = c_{0S}$, $c_{0T} = 0$) in a CSTR. Assume that the reactions can be regarded as elementary.
b. Apply the derived equations on the production of glycols by calculating and sketching $c_R/(c_R + c_S + c_T)$, $c_S/(c_R + c_S + c_T)$, and $c_T/(c_R + c_S + c_T)$ as a function of reacted A. The reaction is carried out at 25°C and the rate constants have the following values:

$$k_1 = 7.37 \times 10^{-7}\ \mathrm{dm}^3/\mathrm{mol\ min}, \qquad k_2/k_1 = k_3/k_1 = 2.0.$$

c. The commercial demand for glycols follows the approximate relation, R:S:T=90:8:2 (in wt%). At which conversion level of water should a CSTR operate to reach the desired product distribution at 25°C?
d. Calculate the residence time in a CSTR that produces glycols according to the distribution mentioned in case c; a 95% conversion level of ethene oxide is required, and the inflow contains 55 mol/dm^3 water. Can 25°C be considered as a realistic operation temperature for an industrial process?

26. Ketene is an important intermediate for the organic-chemical industry. It can be produced by cracking of acetone:

$$\underset{(A)}{CH_3COCH_3} \rightarrow \underset{(B)}{CH_2CO} + \underset{(C)}{CH_4} \tag{1}$$

The reaction (11) is of first order in acetone. The rate constant is given by the expression

$$\ln k = \left(34.34 - 34222/(T/K)\right)s^{-1} \tag{2}$$

20% of the acetone (pure) in the inflow should be converted into ketene in a reactor system that consists of 25 mm tubes in parallel.

a. How large a total volume is required, if the isothermal reactor system is fed with 8000 kg/h acetone at 1025 K and 162 kPa?
b. What kind of reactor configuration would you recommend (the length and the number of tubes)?

27. Formic acid decomposes according to irreversible reactions (11) and (2):

$$HCOOH \rightarrow H_2O + CO, \tag{1}$$

$$HCOOH \rightarrow H_2 + CO_2. \tag{2}$$

The activation energy for the reaction (11) is 52.0 kJ/mol and $k_1 = 2.79 \times 10^{-3}$ min^{-1} at 236°C. At 396°C, the product flow from the reactor contained equal volume fractions of H_2O, CO, H_2, and CO_2.

a. What is the value of the activation energy for reaction (2) if $k_2 = 1.52 \times 10^{-4}$ min^{-1} at 237°C?
b. A plug flow regime can be assumed in a laboratory-scale reactor with a volume of 0.500 dm^3, operating at 396°C and 1.00 bar. Which level of conversion can be obtained, if the reactor is fed with an inflow of 0.03 mol/h of pure formic acid?

28. Butadiene is dimerized at 638°C, following a reversible and an elementary gas-phase reaction path:

$$2A \rightleftarrows B.$$

The forward and backward rate constants k_+ and k_- have the values 87 dm^3/mol s and 0.915 s^{-1}, respectively.

The reaction ought to be carried out at 638°C and 1 bar in a PFR with an inner diameter of 10 cm. Butadiene and steam (an inert dilutant) are fed into the reactor in a molar ratio of 3:1.

a. Give the maximally attainable conversion level of butadiene, if the reactor is fed with a flow of 9.0 kmol/h butadiene and water.
b. How long should the reactor tube be if 45% of the butadiene should be dimerized?

29. For the homogeneous gas-phase reaction,

$$C_2H_4 + Br_2 \rightleftarrows C_2H_4Br_2$$

the rate constants, $k_1 = 156$ L/mol and $k_2 = 0.218\ \text{min}^{-1}$, are valid at 427°C. The plan is to carry out the reaction continuously in a PFR operating at 427°C and 1.5 bar. The ideal gas law is assumed to be valid for the feed gas mixture, at the given temperature and pressure, containing 40 vol% C_2H_4 and 60 vol% Br_2.

a. Calculate the maximally attainable conversion of C_2H_4.
b. Introduce an expression that makes the reactor design possible. Explain the nomenclature of the expression carefully.
c. How large a reactor volume is required to reach 60% of the maximum conversion of C_2H_4, in case the value of the incoming volumetric flow rate is 600 m^3/h (measured at 427°C and 1.5 bar)?

30. A mixture of oxygen gas and ozone (10 vol% ozone in oxygen) is fed into a PFR operating at 100°C and 1 atm. What is the required tube length to reduce 50%? The gas velocity at the inlet is 1.52 cm/s at 100°C. The ozone decomposition reaction

$$2O_3 \rightarrow 3O_2$$

is irreversible and is of second order. The numerical value of k is 0.086 L/mol s at 100°C and 1 atm.

31. Oxidation of nitric oxide

$$2NO + O_2 \rightarrow 2NO_2$$

is an important step in the production of nitric acid from ammonium. The reaction is carried out in an isothermal tube. The incoming gas has the composition 8.8% O_2, 8.2% NO, and the balance N_2. The generation rate of NO is given by

$$r_{NO} = -k_{NO}c_{NO}^2 c_{O_2}.$$

Mr. X (MSc), a recently employed process engineer, claims that an additional inflow of air into the reactor would decrease the required reactor volume or increase the production capacity of the existing one. The shorter residence time would be compensated by the increased reaction rate, claims Mr. X. The Chief Engineer of the plant, Mr. Y (Dr. Sc.), is skeptic. At the very end, he bitterly agrees to investigate the matter.

a. How large a reactor is required, if no add-on air flow is used?
b. Figure out whether a reduction in the reactor volume can be obtained by the add-on air flow. To what percentage can the volume reduction maximally amount? Comment on this.

$$\text{Data:} \quad T = 303\,\text{K}, \qquad P = 1\,\text{atm},$$
$$k_{\text{NO}} = 8.0 \times 10^3\,\text{m}^6/\text{kmol}^2\,\text{s}, \qquad \dot{V}_0 = 30\,\text{dm}^3/\text{min}.$$

Composition of air: 79% N_2, 21% O_2.
Conversion level of NO: 0.80, 0.90, and 0.95.

32. A CSTR is to be used for the polymerization of styrene (A). The reactor is fed with a monomer flow at 300 K. The mean residence time is 2 h. The reaction can be assumed to be approximately of first order. The rate constant is expressed by

$$k = 10^{10} \exp(-10{,}000\,K/T)\text{h}^{-1}.$$

Laboratory-scale experiments were carried out in an adiabatic BR. The monomer reacted completely and a temperature rise of 400°C was registered.

a. Calculate the steady state in adiabatic operation. Can the reactor be operated adiabatically if the highest allowed temperature is 450 K because of safety precautions?
b. Polymerization will be carried out at 413 K to reach the desired distribution of molecular weight. What conversion level of the monomer can thus be achieved? At what temperature should the cooling jacket of the reactor be, if the heat transfer parameter, $\alpha = UA/\rho\dot{V}c_P$, assumes the following values: $\alpha = 50$, 20, or 10?
c. Which is the limiting value of α to enable a stable operation at 413 K? Calculate the limiting temperature of the cooling jacket. Define the conditions for multiple steady states.

33. A reactor is planned for the production of chemical compound B. The reaction needs to be carried out in an isothermally and continuously operating liquid-phase reactor. The situation is complicated by the fact that B can undergo consecutive decomposition to C, and reactant A is able to react bimolecularly to D:

$$\begin{array}{l} \text{A} \xrightarrow{k_1} \text{B} \xrightarrow{k_2} \text{C} \\ + \\ \text{A} \\ \downarrow k_3 \\ \text{D} \end{array}$$

$k_1 = 0.20\ \text{min}^{-1}, k_2 = 0.10\ \text{min}^{-1}, k_3 = 0.20\,\text{dm}^3/\text{mol}/\,\text{min}.$

The reactions are assumed to be elementary.

Mr. P (MSc) suggests that a CSTR should be selected, since backmixing in parallel reactions always favors the reaction of the lowest order, that is, A → B. Mr. Q (MSc), however, claims that when dealing with reactions of the type A → B → C, one should always select a PFR, because a PFR favors the formation of the intermediate product, B. Mr. Q backs up his argument with the tables below, which illustrate c_B/c_{0A} as a function of the conversion level of A. The tables (calculated by Mr. Q) are, however, valid for PFRs only. To resolve the conflict, the boss Mr. H (PhD) delegated to Miss S (a student) the task of finding out the possibilities for utilizing a CSTR. Let us assume that you are Miss S!

a. Compare c_B/c_{0A} for different η_A and a CSTR and a PFR. Can a higher concentration of B be obtained in a CSTR? Can the conclusion be generalized?
b. What residence time is required in a CSTR and PFR, respectively, if both operate at a conversion level of A that maximizes the concentration of B?

The table of Mr. Q for PFRs is as follows:

c_{0A} (mol/dm^3)	0.25	2.5	5.0
η_A	c_B/c_{0A}	c_B/c_{0A}	c_B/c_{0A}
0.0	0.000	0.000	0.000
0.1	0.067	0.0173	0.0095
0.2	0.133	0.0361	0.01995
0.3	0.197	0.0565	0.03152
0.4	0.259	0.0788	0.0445
0.5	0.317	0.1033	0.0592
0.6	0.367	0.1301	0.0760
0.7	0.405	0.1589	0.0955
0.8	0.419	0.1875	0.1179
0.9	0.382	0.2046	0.1395
0.92	0.361	0.203	0.1421
0.95	0.313	0.190	0.1397
1.0	0.000	0.0000	0.0000

34. Saponification of the ethyl ester of formic acid is carried out in a column reactor equipped with a static mixer:

$$CH_3COOCH_2CH_3 + NaOH \rightarrow Na^+CH_3COO^- + CH_3CH_2OH.$$
$$(A + B \rightarrow C + D)$$

The reaction takes place isothermally in an aqueous solution at 25°C, and it can be considered as being approximately of second order. The reaction kinetics is thus given by

$$r = kc_Ac_B.$$

The rate constant, k, has the value 6.5 $dm^3/mol/min$ at 25°C. An experiment was carried out in the column reactor with the inlet concentrations $c_{0A} = c_{0B} = 0.04\,mol/dm^3$ and the average residence time of $\tau = 5.84$ min. The conversion level of A at the reactor outlet was 0.483. On the basis of this experiment, we wish to set up a tanks-in-series model for the column and describe the column with equally large CSTRs coupled in series. The density of the reaction mixture can be considered as constant during the reaction.

a. Describe (in detail, utilizing balance equations and numerical methods) how this problem can be solved.
b. Write a computer program to calculate the number of CSTRs on the basis of the outlet concentration of A that was determined experimentally.

35. Maleic acid hexylmonoester (C) is formed as maleic acid (A) and hexanol (B) react following the reaction below:

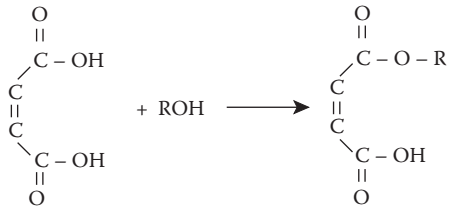

No solvent is present, and pure reactants are thus mixed together in a reaction vessel. The reaction mixture is heated until all A has melted at 53°C. After this, the concentrations of A and B are as follows: $c_{0A} = 4.55\,mol/dm^3$ and $c_{0B} = 5.34\,mol/dm^3$. The reaction is of second order, and the rate constant is given by

$$k = 1.37 \times 10^{12}\ \exp(-12{,}628\,K\mathrm{T})\,dm^3/mol\,s.$$

The reaction enthalpy, $\Delta H_r = -33.5\,kJ/mol$, and the heat capacity of the mixture, $\rho c_P = 1980\,J/dm^3\,K$, are known. The temperature limit of 100°C must not be exceeded, because the reaction is in principle reversible, and diesterification can take place. A stirred BR with a volume of $5.0\,m^3$ is available. Heat conductivity between the reactor and the surroundings can be approximated to $U = 250\,W/m^2\,K$.

Suggest a suitable BR design (inlet and outlet temperatures, heat exchange, etc.) that gives a high conversion level of maleic acid (min. 95%). How long a reaction time is required? What will be the production capacity? Could the BR be operated adiabatically?

The time required for refilling and recharging the reactor contents can be neglected.

36. Maleic acid hexylmonoester (C) is formed as maleic acid (A) and hexanol (B) react following the reaction below:

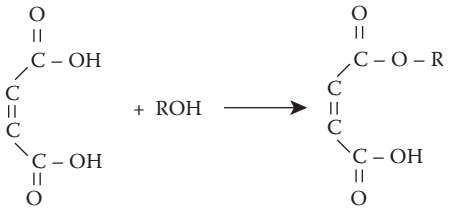

The reaction should be carried out adiabatically in a semibatch reactor, feeding hexanol into the liquid maleic acid. The reactor volume is 500 dm^3, and no solvent is used. Maleic acid melts at 53°C. A maximum temperature of 100°C may not be exceeded due to the formation of by-products. The reaction is of second order, and the rate constant is expressed as

$$k = 1.37 \times 10^{12} \exp(-12{,}628\,\mathrm{KT})\mathrm{dm}^3/\mathrm{mol\,s}.$$

The reaction enthalpy, $\Delta H_r = -33.5$ kJ/mol, and the heat capacity of the mixture, $\rho c_P = 1980\,\mathrm{J/dm}^3\,\mathrm{K}$, are known. The volumetric flow rate of hexanol should follow the equation

$$\dot{V} = a_0 + a_1 t,$$

where a_0 and a_1 are adjustable parameters. The parameters can obtain values in such a range that the maximum temperature of 100°C is not exceeded. The total molar amounts of both reactants are 2.5 kmol. The density of hexanol is 820 kg/m^3 and the molar mass is 102 kg/mol.

a. Introduce the molar and energy balances.
b. Write a computer program for the simulation of the molar amounts and temperatures in the semibatch reactor. The program should be used to determine the volumetric flow rate parameters (a_0 and a_1) in such a way that the reaction time is minimized. However, no global optimization of the procedure is required.

37. A batch of 180 kg of pure ethyl alcohol (density = 0.789 kg/dm^3) was stored in a container. Pumping of an aqueous solution of acetic acid (42.6 wt% acetic acid; density 0.958 kg/dm^3) into the container was initiated. A continuous, constant inflow of 1.8 kg/min was maintained for 120 min. The reaction temperature was 100°C. The reaction

$$CH_3COOH + C_2H_5OH \rightleftarrows CH_3COOC_2H_5 + H_2O$$

has rate constants that obtain the following values at 100°C:

$$k_+ = 4.76 \times 10^{-4}\,\mathrm{dm}^3/\mathrm{mol\,min},$$
$$k_- = 1.63 \times 10^{-4}\,\mathrm{dm}^3/\mathrm{mol\,min}.$$

The density of the reaction mixture can be assumed to be approximately constant in the course of the reaction.

a. Which reactor type was utilized to carry out the reaction?
b. Give the molar balances of the components.
c. Simulate the concentrations and the conversion level of acetic acid as functions of the reaction time.

38. Several industrially important reactions follow a consecutive–parallel reaction scheme of the following type:

$$\begin{array}{ccccc} A & \xrightarrow{1} & R & \xrightarrow{2} & S \\ & \searrow^{3} & & & \\ & & S & & \end{array}$$

The rate constants k_1, k_2, and k_3 for the isothermal liquid-phase reaction are given in the table below. A continuous reactor is fed with a solution containing only 1.0 mol/dm^3 of A.

Determine the required residence time for a PFR and a CSTR to maximize the concentration of R. What will be the maximum concentration of R in a PFR and CSTR, respectively?

Rate Constants
$k_1 = 0.05\ \text{min}^{-1}$
$k_2 = 0.03\ \text{min}^{-1}$
$k_3 = 0.02\ \text{min}^{-1}$

39. Determine the reaction order and the rate constant for the catalytic decomposition of di-*tert*-butylperoxide:

$$(CH_3)_3\,COOC\,(CH_3)_3 \rightarrow C_2H_6 + 2CH_3CCH_3.$$

The reaction was carried out in a laboratory autoclave by registering the total pressure as a function of reaction time. The experiment was started with pure di-*tert*-butylperoxide.

The experimental data are listed below:

***t* (min)**	***P* (torr)**
0	7.5
2.5	10.5
5	12.5
10	15.8
15	17.9
20	19.4

What will the final pressure in the autoclave be?

How long a space time is required for a continuous tube reactor to achieve the same conversion as was obtained in the autoclave at 20 min?

40. The reactions

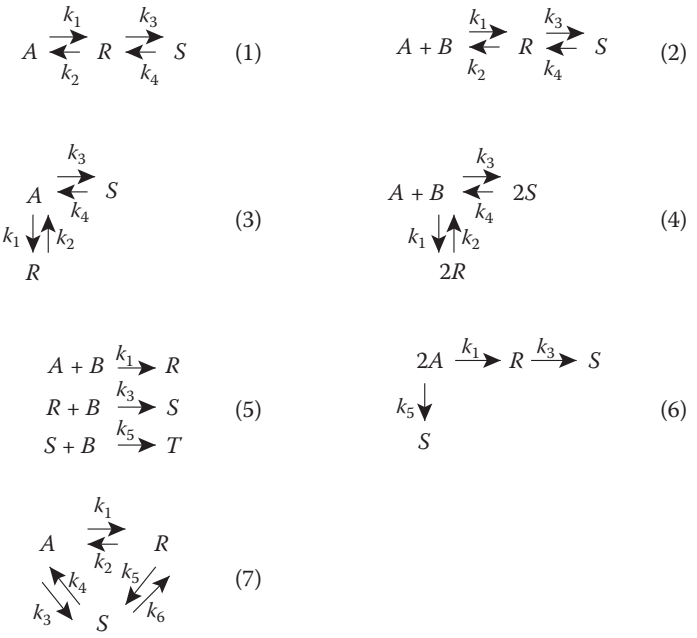

are carried out in a PFR and CSTR. The reaction steps are elementary, and the density of the reaction mixture can be assumed to be constant.

a. Give the rate expressions, $r_A, r_B, \ldots, r_T$, for reactions (11) through (7).
b. Design computer subroutines for a suitable simulation software to calculate numerically the reactant and product concentrations as functions of the mean residence time for reactions (11) through (7).
c. Illustrate graphically the concentrations of A, R, S, and T as functions of the mean residence time.
d. Compile the results into a report. The report should contain
   - Derivation of the mass balances
   - Program listings
   - Program execution listings with results
   - Graphical illustration of the concentrations as functions of the (average) residence time.

Case	k_1	k_2	k_3	k_4	k_5	k_6
1	0.1	0	0.1	0	0	0
	0.1	0	0.02	0		
	0.02	0	0.1	0		
	0.1	0.05	0.1	0.05		
	0.1	0.1	0.01	0.01		
2	Same as case (11) above, but try $c_{0A} = c_{0B} = 1$ mol/dm^3 and $c_{0A} = 1.0$ mol/dm^3 and $c_{0B} = 2.0$ mol/dm^3					
3	Same as case (11) above					
4	Same as case (11) above, but try $c_{0B} = c_{0A}$, $c_{0B} = 2$ and $c_{0B} = 0.5c_{0A}$					
5	0.1	0	0.1	0	0.1	
Try the cases	0.1		0.02		0.02	
$c_{0B} = c_{0A}$	0.1		0.1		0.02	
$c_{0B} = 2c_{0A}$	0.02		0.1		0.02	
$c_{0B} = 3c_{0A}$	0.02		0.02		0.1	
	0.02		0.1		0.1	
6	As case 5					
7	0.1	0.05	0.1	0.05	0.1	0.05
	0.1	0.01	0.1	0.01	0.1	0.01
	0.1	0.1	0.01	0.01	0.1	0.1

41. A tube reactor is characterized using a step change experiment taking advantage of an inert tracer compound. The concentration evolvement of the tracer is given in the table below.

a. Which flow model is the best fit with the experimental data?
b. Determine the mean residence time on the basis of the data listed below.
c. Derive functions $F(t)$, $E(t)$, and $\lambda(t)$.

Results of the Experiment

t (min)	c (mol/L)
0	0
5	0.611
7.0	0.979
8.0	1.219
9.0	1.383

continued

continued

t (min)	c (mol/L)
10.0	1.500
12.0	1.653
20.0	1.875
30.0	1.944
60.0	1.986
∞	2.000

42. A well-known researcher in the field of chemical reaction engineering, Mr. Axel Eklundh, studied liquid-phase decomposition reactions and obtained certain products in the gas phase. His reactor system is displayed in figure below. Some of the reaction products migrate into the gas phase, which was analyzed quantitatively by a quadruple mass spectrometer.

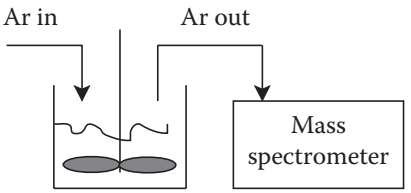

The reactor system

The question remains, however, which flow model should be applied to the description of the gas phase. To solve this dilemma, pulse experiments with argon as an inert tracer were conducted. For the resulting response curve, see figure below.

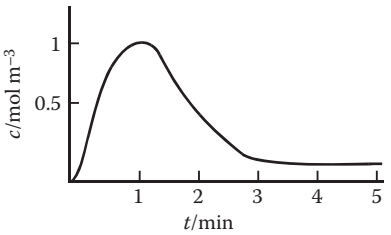

Experimental data obtained from a pulse experiment.

Can the backmixing model be applied to these data? Determine the average residence time of the gas phase.

43. A reactor system consists of two equally sized tanks-in-series reactors with recycle, as illustrated in the below figure. The recycle ratio has a value R. A pulse of an inert tracer is

introduced at the inlet of the first reactor.

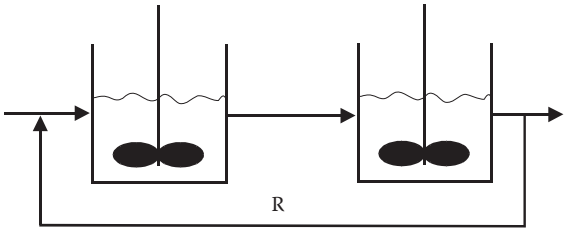

The reactor system with recirculation.

a. Derive the theoretical expression for the concentration of the inert tracer at the outlets of the reactor vessels.
b. At what time (in dimensionless time units) has the pulse response reached 50%, 90%, and 99% of its maximal value?

Use the recycle ratios (R): 0.1, 1.0, and 10.

44. A tracer (A) that reacts following the elementary reaction

$$A \rightarrow P$$

was introduced into a tank reactor in two separate experiments: in the first one, a step change was introduced, and in the second one, a pulse was introduced. The average residence time in the reactor was t. The reactor vessel was carefully flushed with an inert solvent between the experiments. When introducing the step change, the concentration of A at the inlet was instantaneously raised from 0 to c_{0A} and maintained at this level. Before starting this experiment, the reactor was filled with an inert solvent. In the pulse experiment, a certain amount of the tracer (A) was introduced into the reactor, so that the concentration of A obtained the value c_{0A}. The inflow into the reactor remained free of the tracer.

a. Derive a mathematical expression for the concentration of A in the reactor as a function of time for the step change.
b. Derive a mathematical expression for the concentration of A in the reactor as a function of time for the pulse experiment.
c. Calculate and plot the normalized concentration c_A/c_{0A} for cases a and b. The rate constant and the average residence time obtain the following values: $k = 0.015\ \text{min}^{-1}$ and $t = 20$ min.
d. Give the conversion of A at steady state in the step-change experiment.

45. Your task is to analyze the results of the experiment carried out at the marvelous piece of urban art, "The Flow of Time," by the famous Finnish sculptor and academician Kain Tapper (see figure above), located at the Old City Hall Square, Turku. The experiment involved the addition of a pulse of NaCl as the tracer into the flowing water. The experimental results are presented in the figure below and the measured data are given in the table below.

The Experimental Data

Time (s)	**Conductivity**
0	0.152
20	0.151
45	0.152
85	0.151
100	0.151
118	0.151
135	0.152
150	0.151
165	0.151
180	0.15
205	0.48
216	6.63
230	13.76
245	9.08
259	4.89
268	2.66
278	1.66
288	1.03
300	0.75
313	0.51
323	0.41
337	0.33
348	0.29
356	0.25
370	0.22
391	0.2
415	0.19
430	0.18

The sculpturer Kain Tapper

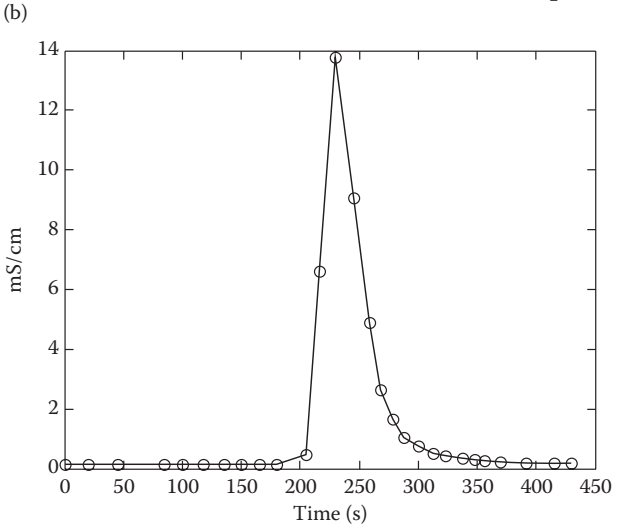

Experimental data obtained from tracer experiments.

a. Determine the functions $E(t)$ and $F(t)$.
b. Which flow model can describe the experimental data (complete backmixing, tanks in series, plug flow, or laminar flow)?
c. Determine the parameter(s) of the model that best describes the reality on the basis of the experimental data available.

46. A reversible first-order reaction

$$A \rightarrow P$$

is to be carried out in a cascade reactor consisting of two equally sized backmixed reactors (CSTR).

a. Which value is obtained for the conversion of component A?
b. Calculate the production capacity of component B.

Data: $k = 0.015\,\text{min}^{-1}$

$K = 3.0$

Volume of first reactor: 10 L

Volume of second reactor: 8 L

Volumetric flow rate: 0.5 L/min

Initial concentration of component A at the inlet of the first reactor: 2.0 mol/L.

47. Loop reactors, that is, reactors with recycle, are used industrially, for example, for catalytic hydrogenation. A schematic sketch of the reactor equipment is introduced below:

To map the prevailing flow conditions, a tracer experiment was carried out by introducing a pulse of an inert tracer in the loop and continuously monitoring the concentration of the tracer by an analysis instrument located in the loop.

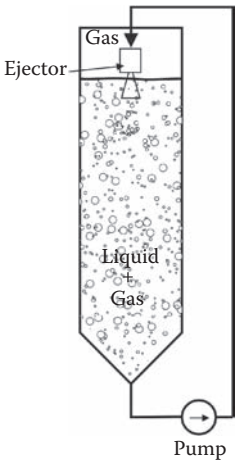

a. Assume that the reactor itself can be described as two equally large CSTRs coupled in series, and the loop characterized using the plug flow model. Derive the mass balance for tracer concentrations in the loop and the reactor.
b. Describe qualitatively how the concentration of the tracer component varies in the loop as a function of time.

48. A first-order irreversible reaction A → B is described by a tanks-in-series model. The total volume (and total residence time) of the system is fixed, but the number of tanks can be changed. Which limit approaches $c_{A,out}/c_{0A}$ as the number of tanks approaches infinity? Prove this mathematically.

49. A second-order, irreversible, and elementary reaction

$$A + B \rightarrow C + D$$

was carried out with equimolar reactant amounts in a reactor system consisting of two CSTRs in parallel.

a. Calculate and plot the step changes of concentrations of A and C.
b. Calculate the conversion of A at steady state.
c. Determine the point in time when the steady state has been attained. As a criterion for steady state can be used for the conversion of A reaching 99% of the steady-state value.

Data	
Rate constant	$k = 0.015\,\text{L/mol min}$
Concentration of A at the inlet	3.5 mol/L
Total reactor volume	20 L
Volume ratio of the reactors in parallel	1:2
Total volumetric flow rate	0.5 L/min

50. A second-order irreversible reaction

$$A + B \rightarrow C$$

was carried out in a tank reactor, which was completely backmixed. The reaction was started by filling the reactor vessel with an inert solvent and instantaneously switching on the flow containing both components A and B.

a. Calculate and plot the step responses of A and C at the reactor outlet.
b. How long does it take before the steady state has been attained? As a practical criterion for having reached the steady state, the concentration of A for obtaining a value that is 99% of the steady-state value can be used.

Data: Reactor volume: 10 L

Volumetric flow rate: 0.2 L/min

Reactant concentrations at the inlet: 2.0 mol/L (equimolar)

Rate constant: 0.015 L/mol min

51. The hydrolysis of an ester (A) with sodium hydroxide (B) can be described with second-order kinetics

$$A + B \rightarrow C + D,$$

where C and D denote the reaction products. The reaction should be carried out in a tube reactor, in which the flow is laminar. Relevant data are listed in the table below.

a. Derive the design equation for a laminar reactor with radial diffusion.
b. Which form does the design equation assume in case the radial diffusion can be considered negligible?
c. Calculate the degree of conversion for component A according to the model in case b.

Data	
Rate constant	0.025 L/mol min
Average residence time	10 min
Concentration of A at the inlet	5.0 mol/L
Concentration of B at the inlet	4.0 mol/L
Molecular diffusion coefficient of A	5×10^{-8} m^2/s
Dynamic viscosity	1.1 cP
Density	1.05 kg/L
Reactor length	3 m
Reactor diameter	5 cm

52. A tube reactor is used to carry out a first-order reaction, in which reactant A decomposes to B and C. Which value is obtained for the degree of conversion of A in case the prevailing flow conditions are

a. Turbulent?
b. Laminar?
c. Explain philosophically the underlying reason for the difference of the results obtained for cases a and b.

Data: $k = 0.10\ \text{min}^{-1}$

$V = 0.5$ L

Volumetric flow rate: 0.025 L/min

53. A first-order, irreversible, and elementary liquid-phase reaction

$$A \rightarrow P$$

was carried out in a column reactor, where a certain degree of backmixing prevails. An experiment with an inert tracer indicated that the reactor column can schematically be described by two tanks in series with recycle as in the figure below:

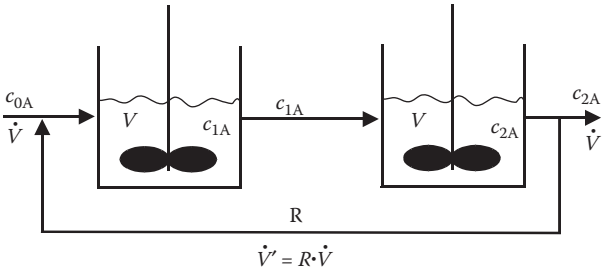

The quantity R in the figure denotes the recycle ratio. At the beginning of the process, the whole system is filled with an inert solvent. The reaction was started by switching on a pump that supplies a liquid with the concentration level of c_{0A} into the reactor.

a. Determine the dynamic mass balance of component A in both tank units. The reactor volume and the volumetric flow rate are assumed to be constant.
b. Solve the balances in time plane and denote the point in time at which the step response of A has reached 90% of its steady-state value.
c. Determine the conversion of A and the yield of P at steady state.

Data: Rate constant: 0.05 L/min

Average residence time in a tank: 20 min

Recycle ratio: 3.0

54. Several enzymatic processes in which a reactant (a substrate) S is transformed to product P can be described by Michaelis–Menten kinetics

$$r = \frac{k\,K c_E\, c_S}{(1 + K c_S)}.$$

What value can the substrate (S) obtain in case the reactor is described by the segregated tanks-in-series model with $j = 2$, and the tanks in series as an entity is completely segregated?

Data: $k = 0.01\ \text{min}^{-1}$

$c_{\text{E}} = 1.0\ \text{mol/L}$ (enzyme concentration, constant)

$K = 2.0\ \text{L/mol}$

$c_{0\text{S}} = 3.0\ \text{mol/L}$

$\bar{t} = 10\ \text{min}$

55. A third-order reaction

$$3\text{A} \rightarrow \text{B}$$

is utilized in order to synthesize the trimer B. The reaction medium is highly viscous and therefore segregation prevails in the liquid phase.

a. Determine the conversion of A and the yield of B according to the segregated tanks-in-series model ($j = 3$). The tanks in series as an entity is assumed to be segregated.
b. For the sake of comparison, calculate the degree of conversion that the "conventional" tanks-in-series model and the plug flow model might predict.
c. Determine the relaxation time as well as the time required for the formation of a micromixture.

Data: $k = 0.01\ \text{(L/mol)/ min}$

$c_{0\text{A}} = 15\ \text{mol/L}$

Average residence time: 5 min

Molecular diffusion coefficient of A: $2 \times 10^{-10}\ \text{m}^2/\text{s}$

Length of the microturbulent eddies: $100\ \mu\text{m}$

56. A second-order irreversible reaction

$$\text{A} + \text{B} \rightarrow \text{C} + \text{D}$$

was carried out in a reactor that can be described by the axial dispersion model. The reactor was supplied with equimolar amounts of reactants A and B. Calculate the conversion (in %) of A in case the average residence time is 30 min.

Data : $c_{0\text{A}} = 5.0\ \text{mol/L}$

$k = 0.012\ \text{L/(mol min)}$

$Pe = 6.7$

57. A zero-order chemical reaction

$$\text{A} \rightarrow \text{P}$$

following the kinetics $r = k$ (k denotes the reaction rate constant) is carried out in a tube reactor in which axial dispersion prevails.

a. Derive a theoretical expression for the concentration profile of A in the reactor. At the inlet as well as the outlet, the classical boundary condition of P.V. Danckwerts is assumed to be valid (Chapter 4). Calculate the conversion of A according to the axial dispersion model and the plug flow model.

Data: $A = 0.01\,\text{mol/(L min)}$

$c_{0A} = 2.0\,\text{mol/L}$

Average residence time: 20 min

$Pe = 20$

58. A second-order, irreversible, and bimolecular liquid-phase reaction

$$\text{A} + \text{B} \rightarrow \text{C}$$

is carried out in a tube reactor. The tube diameter is 5.0 cm and the length is 120 cm. The average residence time is 36 s. At the reactor inlet, the concentrations of both A and B are 10.0 mol/L. The reaction rate constant obtains the value $k = 1.2\,\text{L/(mol min)}$. The physical properties of the reaction medium are listed in the table below.

a. Is the flow laminar or turbulent?
b. Estimate the value of the Peclet number.
c. Calculate the conversion of A according to the axial dispersion model as well as the segregated and maximum-mixed axial dispersion models.

Physical Properties	
Dynamic viscosity	$\mu = 1.5\,\text{cP}$
Density	$\rho = 1.25\,\text{kg/L}$
Molecular diffusion coefficients	$D_A = D_B = 0.8 \times 10^{-8}\,\text{m}^2/\text{s}$

59. The hydrolysis of an ester (A) with sodium hydroxide (B) can be described by means of second-order kinetics

$$\text{A} + \text{B} \rightarrow \text{C} + \text{D},$$

where C and D are the reaction products. The reaction should be carried out in a tube reactor, to which both the axial dispersion and the tanks-in-series models can, in principle, be applied. Relevant data are listed in the table below.

a. Give the molecular reaction formula in case that propionic acid methyl ester is hydrolyzed by sodium hydroxide.
b. Calculate the axial dispersion coefficient and the Peclet number.
c. Calculate the degree of conversion of A according to the following models:

- Axial dispersion model
- Tanks-in-series model
- Segregated axial dispersion model
- Segregated tanks-in-series model (the tanks in series as a whole segregated)

Data
Rate constant: 0.025 L/(mol min)
Average residence time: 10 min
Concentration of A at the inlet: 5.0 mol/L
Concentration of B at the inlet: 5.0 mol/L
Molecular diffusion coefficient of A: 5×10^{-8} m^2/s
Dynamic viscosity: 1.1 cP
Density: 1.05 kg/L
Reactor length: 3 m
Reactor diameter: 5 cm

60. A third-order elementary reaction

$$2\mathrm{A} + \mathrm{B} \rightleftarrows \mathrm{C} + \mathrm{D}$$

is carried out in a tube reactor. A computer simulates the concentrations of components at the reactor outlet by using

a. The axial dispersion model
b. The segregated tanks-in-series model
c. The segregated axial dispersion model
d. The maximum-mixedness axial dispersion model
e. Give the degree of conversion of A in all of the above cases.

Data:

Inlet concentrations: $c_{0\mathrm{A}} = 5.0\,\mathrm{mol/L}, c_{0\mathrm{B}} = 3.0\,\mathrm{mol/L}$

Reaction rate constant: $k = 0.012(\mathrm{L/mol})^2/\mathrm{min}$

Equilibrium constant: $K_{\mathrm{eq}} = 5.0\,\mathrm{L/mol}$

Average residence time: $\tau = 10$ min

Peclet number: $Pe = 20$

61. Ceramic and metallic monoliths are extensively used for exhaust cleaning. In the channels of monoliths, laminar flow conditions often prevail. A typical reaction in exhaust cleaning is the catalytic oxidation of carbon monoxide:

$$\mathrm{CO} + \tfrac{1}{2}\mathrm{O_2} \rightarrow \mathrm{CO_2}.$$

A rate expression is written as

$$r = \frac{k c_{\mathrm{CO}} c_{\mathrm{O_2}}^{\alpha}}{\left(1 + K_{\mathrm{CO}} c_{\mathrm{CO}} + K_{\mathrm{O_2}} c_{\mathrm{O_2}}^{\alpha}\right)^2}.$$

a. Derive a mathematical model for the monolith channel. Use the following assumptions: laminar flow without radial diffusion, isothermal conditions, and change in the volumetric flow rate due to the chemical reaction.
b. Simulate numerically the monolith performance (search for suitable kinetic data in contemporary literature).

SECTION II. CATALYTIC REACTORS

1. Catalytic dehydrogenation of ethylbenzene to styrene takes place following the reaction scheme below:

$$\text{Ethyl benzene} \rightleftarrows \text{Styrene} + \text{H}_2 \tag{1}$$

The reaction velocity is given by the expression

$$R = k(p_\text{E} - p_\text{S}p_\text{H}/K), \tag{2}$$

in which the rate constant k and the equilibrium constant K are given by Equations (3) and (4), respectively:

$$k = 0.0345\ \exp(-10{,}980\,K/T)\text{mol}/(\text{s Pa}), \tag{3}$$

$$K = 4.656 \times 10^{11} \times \exp(-14{,}651\,K/T)\text{Pa}. \tag{4}$$

The reaction will be carried out in an adiabatic packed bed. The reaction is endothermic, and cofeeding of hot water vapor into the bed is therefore applied. The conversion level $\eta_\text{E} = 0.45$ is required. Determine the necessary bed length and the temperature of the outlet gas.

Data		
Total pressure	$P_0 = 121\,\text{kPa}$	
Reactor inlet temperature	$T = 898\,\text{K}$	
Catalyst bulk density	$\rho_\text{B} = 1440\,\text{kg/m}^3$	
Reaction enthalpy	$\Delta\text{H}_r = 139\,\text{kJ/mol}$	
Specific heat capacity for the mixture	$c_\text{p} = 2.18\,\text{kJ/(kgK)}$	
Molar flows at the reactor inlet	$\dot{n}_{0,\text{E}} = 1.80\,\text{mol/s}$,	$\dot{n}_{0,\text{H}_2\text{O}} = 34\,\text{mol/s}$

2. Methyl-tertiary-butylether (MTBE) is used as an additive in engine gasoline. In the presence of a catalyst, an ion-exchange resin, MTBE, decomposes to isobutene and methanol following the scheme below:

$$(\text{CH}_3)_3\text{C} - \text{O} - \text{CH}_3 \rightarrow \text{CH}_2 = \overset{\displaystyle\text{CH}_3}{\overset{|}{\text{C}}} - \text{CH}_3 + \text{CH}_3\text{OH}.$$

The reaction is of first order and follows the reaction kinetics as in the equation

$$r = k\, c_{\mathrm{MTBE}}.$$

Your task is to calculate the temperature profile and conversion of MTBE in a nonadiabatic tube reactor. How large a volume is required to obtain the conversions η as in the table below? The real reactor system will comprise a number of parallel tubes with a length of 5 m and an inner diameter of 0.025 m. How many tubes are required to achieve the desired production capacity?

What would be the outlet temperature, if the reactor were operated adiabatically? Is it possible to run the reactor adiabatically, taking into account the boundary condition set by the outlet temperature?

Rate constant	$K = A\mathrm{e}^{-E_\mathrm{a}/RT}$
	$A = 22{,}800\ \mathrm{mol/kg/s/(mol/m^3)}$
	$E_a = 79{,}620\ \mathrm{J/mol}$
Reaction enthalpy	$\Delta H_r = 73{,}900\ \mathrm{J/mol}$ (endothermic reaction)
Heat capacity	$c_\mathrm{p} = 2100\ \mathrm{J/kg/K}$
Catalyst bulk density	$\rho_\mathrm{B} = 700\ \mathrm{kg/m^3}$
Temperature at the reactor inlet	$T_0 = 503$–$523\ \mathrm{K}$ (see below)
Pressure at the reactor inlet	$P = 506,500\ \mathrm{Pa}$
Reaction mixture composition (inlet)	$x_{0,\mathrm{MTBE}} = 0.9$
	$x_{0,\mathrm{N}} = 0.1$
Inflow of MTBE at the inlet	$\dot{n}_{0,\mathrm{MTBE}} = 140{,}000\ \mathrm{mol/h}$
Heat transfer parameter	$U = 15\ \mathrm{J/m^2/s/K}$
Temperature of the heating oil	$T_C = 513$–$533\ \mathrm{K}$ (see below)

η	T_0/(K)	T_C/(K)
0.85	503	513
	503	523
	503	533
0.85	513	523
	513	533
	523	533
0.95	523	533

3. Decomposition of (MTBE A) into isobutene (B) and methanol (C) follows the reaction scheme below:

$$(\mathrm{CH_3})_3\mathrm{C} - \mathrm{O} - \mathrm{CH_3} \rightarrow \mathrm{CH_2} = \overset{\overset{\mathrm{CH_3}}{|}}{\mathrm{C}} - \mathrm{CH_3} + \mathrm{CH_3OH}. \qquad (1)$$

The reaction takes place on the surface of a solid catalyst and it can be considered as elementary. Since the reaction is endothermic, it is carried out in parallel tubes heated with oil (a multitubular reactor). The tubes are packed with catalyst particles.

a. Give the reaction kinetics for reaction (1).
b. Determine the mass and energy balances for a single reactor tube, if the radial concentration and temperature gradients are negligible as well as the mass and heat transfer of the catalyst particles.
c. To consider the reactor design, a computer program for the simulation of concentration and temperature profiles inside the tubes is needed. Compile a suitable code to calculate the concentration and temperature profiles in the reactor tubes and simulate the molar flows and temperatures as a function of the reactor volume.

Data	
Rate constant	$K = A\mathrm{e}^{-E_\mathrm{a}/RT}$
	$A = 22{,}800\ \mathrm{mol/kg/s/(mol/m^3)}$
	$E_\mathrm{a} = 79{,}620\ \mathrm{J/mol}$
Reaction enthalpy at 298 K	$\Delta H_\mathrm{r} = 75{,}000\ \mathrm{J/mol}$
Molar heat capacities	$c_{\mathrm{pm}i} = a_{0i} + a_{1i}\,(T/K) + a_{2i}\,(T/K)^2 + a_{3i}\,(T/K)^3\ \mathrm{J/kg/K}$ (see below)
Catalyst bulk density	$\rho_\mathrm{B} = 700\ \mathrm{kg/m^3}$
Temperature at the reactor inlet	$T_0 = 503\ \mathrm{K}$
Pressure at the reactor inlet	$P = 506.5\ \mathrm{kPa}$
Gas composition (inlet)	$x_{0,\mathrm{A}} = 0.9, x_{0,\mathrm{N_2}} = 0.1$
Total molar inflow at the inlet	$\dot{n}_0 = 43.21\ \mathrm{mol/s}$
Overall heat transfer parameter	$\mathrm{U} = 15.0\ \mathrm{W/m^2/s/K}$
Temperature of the heating oil	$T_C = 523\ \mathrm{K}$

M/kg/mol	a_{0i}	a_{1i}	a_{2i}	a_{3i}	
0.08815	0.2534E+1	0.5136	−0.2596E−3	0.4303E−7	MTBE
0.05611	0.1605E+2	0.2804	−0.1091E−3	0.9098E−8	ISOBUTENE
0.03204	0.2115E+2	0.7092E−1	0.2587E−4	−0.2852E−7	METHANOL
0.02801	0.3115E+2	−0.1357E−1	0.2680E−4	−0.1168E−7	N_2

4. A catalytic reaction of isobutene to *tert*-butanol takes place on an ion-exchange resin following the reaction

$$\underset{\text{(A)}}{\mathrm{CH_3-\overset{\overset{\mathrm{CH_2}}{\|}}{C}-CH_3}} + \underset{\text{(B)}}{\mathrm{H_2O}} \rightarrow \underset{\text{(C)}}{\mathrm{(CH_3)_3COH}}.$$

Water is available in a large excess, which implies that the reaction can be assumed to follow the first-order kinetics. A packed bed is fed with a liquid mixture containing 2 mol/L isobutene. A 50% conversion level of isobutene is required.

a. Calculate the space time of the liquid (= V/V) and the catalyst mass in the reactor. What will the effectiveness factor be?
b. How large will the error be (in %), if the internal mass transfer resistance is ignored?

Data: $k = 0.0016\,\mathrm{m^3/(kg\,s)}$
$\rho_B = 500\,\mathrm{kg/m^3}$
$D_{ei} = 2.0\,10^{-9}\,\mathrm{m^2/s}$
$R = 0.0213\,10^{-2}\,\mathrm{m}$ (the radius of a spherical catalyst particle)
$\rho_P = 1000\,\mathrm{kg/m^3}$

5. Hydrogenation of nitrobenzene to aniline takes place in a nonadiabatic fixed bed reactor following the scheme below:

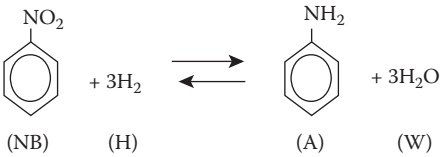

Calculate and graphically illustrate the conversion level of nitrobenzene and temperature in the reactor as a function of the reactor length.

Reaction enthalpy	$\Delta H_r = -660\,\mathrm{kJ/mol}$
Reaction kinetics	$R = k \cdot p_B^{0.5} \cdot p_H^{0.5}$ $k_{\rho_B} = 21.9368 \cdot e^{(-8240/T/K)}\,\mathrm{mol/(m^3\,s\,Pa)}$
Molar flow of nitrobenzene at the inlet	$\dot{n}_{0,NB} = 4.0\,\mathrm{mol/s}$
Specific heat capacity	$c_P = 1540\,\mathrm{J/kg\,K}$
Composition of the feed mixture	$x_{0,NB} = 0.1$ $x_{0,H} = 0.5$ $x_{0,N_2} = 0.4$
Reactor diameter	$d_T = 0.025\,\mathrm{m}$
Heat transfer parameter	$U = 150\,\mathrm{W/m^2\,sK}$
Temperature of the cooling media	$T_C = T_0$
Temperature of the inflow	$T_0 = 575$, 600, or 625 K
Catalyst bulk density	$\rho_B = 200\,\mathrm{kg/m^3}$

6. Acetaldehyde is industrially manufactured via oxidation of ethanol on a suitable metallic catalyst (e.g., Ag). Filho and Dominiques (*Chem. Eng. Sci.*, **47**, 2571–2576) studied the

oxidation of ethanol on a commercial Fe–Mo catalyst and concluded that the kinetics of the oxidation process

$$CH_3CH_2OH + \tfrac{1}{2}O_2 \;\rightleftarrows\; CH_3CHO + H_2O$$

is given by the expression

$$R = \frac{2k_1k_2p_{O_2}p_{EtOH}}{D},$$

where

$$D = k_1p_{EtOH} + 2k_2p_{O_2} + k_3k_4p_Ap_{H_2O} + k_3k_1p_{EtOH}p_A + 1.$$

EtOH and A denote ethanol and acetaldehyde, respectively. The temperature dependence of constants $k_1 - k_4$, is given by the expression $k_i = a_i \exp(b_i/(RT))$, where a_i and b_i are given in the table below:

		a_i	b_i
k_1	$Nm^3/(s\ kg_{cat}\ Pa)$	2.7988560	−7260.7632
k_2	$Nm^3/(s\ kg_{cat}\ Pa)$	174.483331	−96,787.2852
k_3	Pa^{-1}	6.01961E−10	42,233.2832
k_4	$Nm^3/(s\ kg_{cat}\ Pa)$	295,435.68	−104,486.9283

The reaction is carried out in an isothermal packed bed at atmospheric pressure. Select a suitable reactor model and calculate how long a space time τ is required to achieve a 98% conversion of ethanol to acetaldehyde.

Data: Total pressure, $P_0 = 101.3\,kPa$

Temperature, $T = 210°C$

Catalyst bulk density, $\rho_B = 500\,kg/m^3$

Gas composition at the reactor inlet: $x_{EtOH} = 0.05,\ x_{O_2} = 0.20,\ x_{N_2} = 0.75$

7. The industrial production of sulfuric acid is based on the absorption of sulfur trioxide in water following the reaction

$$SO_3 + H_2O \rightleftarrows H_2SO_4. \tag{1}$$

Sulfur trioxide is formed in the catalytic oxidation of sulfur dioxide over a vanadium pentoxide (V_2O_5) catalyst:

$$SO_2 + \tfrac{1}{2}O_2 \rightleftarrows SO_3. \tag{2}$$

Reaction (2) is exothermic and reversible. It takes place in cascades of adiabatic packed beds at atmospheric pressure. The catalyst is rather inactive at low temperatures, and the

minimum temperature for the reactors thus is 703 K. Determine the space time, $\tau = V/\dot{V}_0$, for an adiabatic packed bed taking into account the fact that the degree of conversion of SO_2 should be at least 0.7. What will the temperature at the reactor outlet be?

Reaction kinetics	$R = k_1 p_{SO_2}^{1/2} p_{O_2} - k_2 p_{SO_2}^{1/2} p_{O_2}^{1/2} p_{SO_3}$
	$k_1 = 5.412\ \exp(-129{,}791\ \text{J/mol}/RT)\ \text{mol/s kg Pa}^3$
	$k_2 = 7.490 \times 10^7\ \exp(-224{,}412\ \text{J}/RT)\ \text{mol/s kg Pa}$
Catalyst bulk density	$\rho_B = 600\ \text{kg/m}^3$
Thermodynamics	$\Delta H_r = (-102.99 \times 10^3 + 8.33(\text{T/K}))\ \text{J/mol}$
	$c_P = 1046.7\ \text{J/kg K}$
Composition of the incoming gas mixture	$T_0 = 703\ \text{K}$
	$P_0 = 101.3 \times 10^3\ \text{Pa}$
	$x_{0,SO_2} = 0.085, x_{0,O_2} = 0.090, x_{0,N_2} = 0.825$

8. Carbon monoxide can be catalytically converted into methane in a high-pressure reactor. The reaction kinetics is given by the expression

$$R = \frac{k_1 p_{CO_2} p_{H_2}^4}{D^5},$$

where

$$D = 1 + K_1 p_{H_2} + K_2 p_{CO_2}.$$

The constants obtain the following values at 314°C and 30 atm:

$$k = 7.0\ \text{kmol/kgh atm}^5,\ K_1 = 1.73\ \text{atm}^{-1},\ K_2 = 0.30\ \text{atm}^{-1}.$$

The reactor is fed with an inflow of 100 kmol/h of CO_2 and a stoichiometric feed of H_2. A conversion level of 20% for CO_2 is desired. Calculate the catalyst mass required in the catalytic bed so that the required conversion is obtained. Assume that the bed can be described with a pseudohomogeneous, one-dimensional model.

9. The water–gas shift reaction is carried out in an isothermal packed bed:

$$CO + H_2O \rightleftarrows CO_2 + H_2.$$

The bed is filled with iron–chromium oxide catalyst particles. The catalyst particles are cylindrical and have a diameter and a height of 3.2 mm. The temperature in the reactor is 683 K and the total pressure is 1 atm. The reaction rate (R') can be described by the equation

$$R' = k\, c_{CO}(1 - B),$$

where $B = c_{CO_2} c_{H_2}/(K\, c_{CO}\, c_{H_2O})$ K denotes the equilibrium constant of the reaction, and k is the first-order rate constant. The effectiveness factor $\eta_{e,CO}$ is given by the expression

$$\eta_{e,CO} = \left(\frac{3}{\varphi}\right)\left(\frac{1}{\tanh\varphi} - \frac{1}{\varphi}\right),$$

where $\varphi^2 = R^2(k\rho_p/D_{e,CO})$. The effective diffusion coefficient $D_{e,CO}$ is given by

$$D_{e,CO} = \left(\frac{\varepsilon_p}{\tau_p}\right)\left(\frac{1}{D_{m,CO}} + \frac{1}{D_{K,CO}}\right)^{-1},$$

where $D_{m,CO}$ and $D_{K,CO}$ denote the molecular and Knudsen diffusion coefficients, respectively. The diffusion coefficients and the rate constant k were determined by Keiski et al. (1992). A few values are given in the table below:

T (K)	D_m (cm^2/s)	D_K (cm^2/s)	k (cm$_3$/g/s)
723	1.40	0.107	14.4
703	1.33	0.105	9.36
683	1.27	0.104	5.81
663	1.20	0.102	3.5

What value should the space time ($\tau = V_R/\dot{V}_0$) obtain so that the equilibrium conversion of CO could be approximately reached? Use as the criterion $\eta_{CO} = 0.999\ \eta^*_{CO}$, where η^*_{CO} denotes the equilibrium conversion level.

Composition of the incoming gas:

$$x_{0,CO} = 0.07, x_{0,CO_2} = 0.03, x_{0,H_2} = 0.20, x_{0,N_2} = 0.20, x_{0,H_2O} = 0.50.$$

Catalyst bulk density	$\rho_B = 0.95$ g/cm^3
Catalyst porosity and tortuosity	$\varepsilon_P/\tau_P = 0.25$
Density of the catalyst particle	$\rho_P = 1.55$ g/cm^3
Equilibrium constant of the reaction	$K = e^{(4577.8\ K/T - 4.33)}$

10. Oxidation of sulfur dioxide, $SO_2 + 1/2O_2 \rightleftarrows SO_3$, is industrially carried out in fixed beds filled with V_2O_5 catalyst particles. Kinetic studies have indicated that the reaction rate can be described by an expression of the following kind:

$$-r_{SO_2} = \frac{k_1 p_{SO_2} p_{O_2} - k_2 p_{SO_3} p_{O_2}^{1/2}}{p_{SO_2}^{1/2}}.$$

The reaction is carried out in two nonisothermal reactors coupled in series.

a. Calculate and illustrate graphically the temperature and conversion level of SO_2 as functions of the reactor length in the first reactor. The conversion level (ηSO_2) after the first reactor should remain at 0.75–0.80 (see the table). The temperature at the inlet to the second reactor must not exceed 673 K. How large a temperature difference needs to be realized with a heat exchanger?
b. Calculate the value of the equilibrium constant of the reaction as well as the equilibrium conversion for η_{SO_2} at the outlet of the first reactor.

Data

The rate constants	$k_1 = 5.412/\exp(-129{,}791\ \text{J}/RT\ \text{mol})/\text{mol/s/kg/Pa}^{3/2}$
	$k_2 = 7.49010^7 \exp(-224{,}412\ \text{J/RTmol})/\text{mol/s/kg/Pa}$
Reaction enthalpy	$\Delta H_r = (-102.99 + 8.33 \cdot 10^{-3}(\text{T/K})) \cdot 10^3$ J/mol
Specific heat capacity	$c_p = 1046.7$ J/kgK
Catalyst bulk density	$\rho_B = 600$ kg/m^3
Temperature of the incoming gas	$T_0 = 643 - 663$ K (see the table below)
Composition of the incoming gas	$x_{SO_2} = 0.08, x_{O_2} = 0.13, x_{N_2} = 0.79$
Conversion level at the outlet	$\eta_{SO_2} = 0.99$
Total pressure	$P = 1.01325 \cdot 10^5$/Pa
Production capacity	50 ton/H_2SO_4/d
Diameter of the reactors	$d = 1.8$ m
Temperature of the surroundings	$T_C = 294$ K
Heat transfer coefficient	$U = 6.81$ J/m^{2}sK

Table

η_{SO_2}	T_0/K
0.80	643
0.80	663
0.75	643
0.75	663

11. In the industrial production of phthalic anhydride, the oxidation of either naphthalene or *o*-xylene can be utilized. The reaction mechanism in the oxidation of *o*-xylene over V_2O_5 catalyst particles can be described in a simplified manner by a parallel–consecutive reaction, which leads to the following rate expressions:

$$r_1 = k_1 p_A p_{O_2} \rho_B, \tag{1}$$

$$r_2 = k_2 p_B p_{O_2} \rho_B, \tag{2}$$

$$r_3 = k_3 p_A p_{O_2} \rho_B. \tag{3}$$

The reaction scheme is

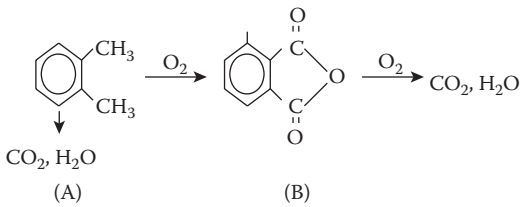

Oxidation is carried out in the presence of a large excess of air in fixed bed reactors comprising several tubes surrounded by a salt solution [$NaNO_2/KNO_3$ (11)]. The salt solution acts as the cooling medium. Because of the prevailing explosion hazard, the *o*-xylene content in the inlet flow must be kept below 1 vol%. The temperature may not exceed 660 K, as the catalyst will be deactivated in elevated temperatures.

a. Calculate and illustrate graphically the temperature and phthalic anhydride concentrations as a function of the reactor length in a pilot plant reactor containing a single tube and operating in the given conditions (see the table).
b. What will be the maximum temperature in the reactor? Which way should the conditions be changed, if the limiting temperature value of 660 K is exceeded?
c. Which conversion level of A and which yield of B can be reached in the reactor?
d. How would an increase in the temperature of the inflow affect the yield of B?

Data	
Activation energies	$E_{a1} = 1.133 \times 10^5$ J/mol
	$E_{a2} = 1.301 \times 10^5$ J/mol
	$E_{a3} = 1.200 \times 10^5$ J/mol
Frequency factors	$A_1 = 1.145 \times 10^8$ atm^{-2} mol/kg/s
	$A_2 = 3.185 \times 10^8$ atm^{-2} mol/kg/s
	$A_3 = 4.577 \times 10^7$ atm^{-2} mol/kg/s
Reaction enthalpies	$\Delta H_{m1} = -1.2845 \times 10^6$ J/mol
	$\Delta H_{m2} = -3.276 \times 10^6$ J/mol
Specific heat capacity	$c_P = 1.046 \times 10^3$ J/kg/K
Catalyst bulk density	$\rho_B = 1300$ kg/m^3
Total pressure	P = 1.0 atm
Inlet conditions	$x_{0A} = 0.0093, x_{0O_2} = 0.208, x_{0N_2} = 0.783$
Molar mass of the inflow	$M = 29.48 \times 10^{-3}$ kg/mol
Reactor diameter and length	$d = 0.025$ m, $z = 3.00$ m
Heat transfer parameter	$U = 96.116$ J/m^2/s/K
Temperature of the cooling agent	$T_{cool} = T_0$
Temperature of the inflow	T_0/K: 625, 630, 633, 635

12. A reversible and elementary gas-phase reaction

$$A \rightarrow 2P$$

is to be carried out in an adiabatic packed bed. The catalyst particles are spherical and the diffusion limitation regime prevails inside the particles. The temperature gradients inside the particles are, however, negligible. Additionally, the mass and heat exchange resistances in the gas film around the particles are discarded. The radial concentration and temperature gradients in the reactor tube are assumed to be negligible; so a one-dimensional model can be applied. For more data, see the table below.

a. Develop an expression to calculate the conversion level of A (η_A) as a function of space time (τ) in the reactor.
b. Calculate the value of space time that is required to convert 95% of A.

Catalyst	$k = 1.0 \times 10^{-2}$ m^3/(kg s) at 700 K,
	$E_a = 80{,}000$ J/mol, $k_A e^{-E_a/RT}$
	$\rho_P = 1300$ kg/m^3 (particle density)
	$R = 1.5 \times 10^{-3}$ m (particle radius)
	$D_{eA} = 0.1(T/298\,\text{K})^{1.75} \times 10^{-4}$ m^2/s
	$\rho_B = 1500$ kg/m^3 (catalyst bulk density)

continued

continued

Reaction enthalpy and heat capacity	$\Delta H_r = -150\times10^3$ J/mol
	$c_p = 1.25 \times 10^3$ J/(kg K)
Composition and conditions of the incoming gas mixture	$X_{0A} = 0.5$
	$P_0 = 5.0$ atm
	$T_0 = 473$ K (the temperature of the inflow)
	$\rho_0 = 3.5$ kg/m^3

13. A first-order, irreversible catalytic gas-phase reaction

$$A \rightarrow P$$

should be carried out in an isothermal fluidized bed. The conversion level $\eta_A = 0.95$ is required. Calculate the bed height based on the Kunii–Levenspiel model.

$$\begin{aligned}
\text{Data: } \rho_{Bb} &= 7.5\,\text{kg/m}^3 \\
\rho_{Bb} &= V_c/V_b = 290\,\text{kg/m}^3 \\
\rho_{Be} &= V_e/V_b = 1020\,\text{kg/m}^3 \\
K_{bc} &= 1.4\,\text{s}^{-1} \\
K_{ce} &= 0.9\,\text{s}^{-1} \\
k &= 1.5\,\text{m}^3/(\text{kg h}) \\
w &= 1800\,\text{m/h} \\
w_{mf} &= 20.5\,\text{m/h} \\
d_b &= 0.1\,\text{m}
\end{aligned}$$

14. A continuous and completely backmixed slurry reactor is used for the polymerization of ethene. The catalyst is suspended in cyclohexane, which is fed into the reactor by an inflow of 10^5 cm^3/ min. The liquid volume of the reactor is 10^4 cm^3. Pure ethene gas is supplied into the reactor by the inflow of 10^5 cm^3/ min, at $T = 373$ K and P = 10 bar. The gas bubbles have a diameter of 3 mm, and the gas–liquid volume ratio in the reactor is $V_G/V_L = 0.09$. The catalyst amount (mass of catalyst/liquid volume) is 0.10 g/cm^3 and the particle density is $\rho_P = 1.0$ g/cm^3.

The mass transfer coefficients of ethene obtain the following values: $k_L = 0.07$ cm/s (gas–liquid) and $k_{LS} = 0.03$ cm/s (liquid–solid).

The reaction can be assumed to be approximately of first order in ethene. The reaction rate is given by the expression

$$r_{ethene} = -k a_p c_{LS,ethene},$$

where $k = 0.01$ cm/s. The gas–liquid equilibrium constant for ethene in cyclohexane is $K = 5.0$. How many moles of ethene per hour react in this system?

15. Catalytic hydrogenation of alkylbenzene to cyclic compounds proceeds in the liquid phase on the surface of a suspended (Ni/Al_2O_3) catalyst according to the stoichiometry

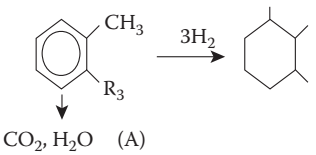

The reaction rate is defined as

$$R = \frac{kK_A K_H c_A c_H}{\left(3K_A c_A + (K_H c_H)^{1/\gamma} + 1\right)^{\gamma+1}},$$

where $\gamma = 2$.

Numerical values for the kinetic parameters are listed in the table below.

Kinetic Parameters and Catalyst Properties

$k(T_0)$ mol/kgs	2.1	Efficient radius (mm)	0.25
K_A (dm^3/mol)	0.25	Porosity	0.4
K_H (dm^3/mol)	37.0	Tortuosity	4
T_0 (K)	373.2	Density (kg/m^3)	1300

The solubility of hydrogen in toluene and methylcyclohexane is $x^*_{H_2} = 0.014$ at $P_{H_2} = 20$ bar and $T = 373$ K.

The hydrogenation of toluene takes place in a BR at 373 K and at a hydrogen pressure of 20 bar. Suspended Ni/Al_2O_3 is used as the catalyst. The reaction starts with pure toluene in the reactor. The reactor volume is 1.1 dm^3 and the liquid volume in the reactor is 1.0 dm^3. The initial concentration of toluene is 9.5 mol/dm^3, and toluene and methylcyclohexane are assumed to stay in the liquid phase at the prevailing conditions.

a. How much catalyst is needed to obtain a 99% conversion of toluene in the reactor, provided that the stirring of the reactor is very vigorous?
b. What is the required reaction time, if the stirring is less vigorous and the gas–liquid mass transfer coefficient for hydrogen is $k_{L,H_2}a = 0.1\ s^{-1}$? The mass transfer resistance at the catalyst particle surface can be ignored.

16. An organic component (A) is hydrogenated catalytically in a fixed bed reactor

$$A + H_2 \xrightarrow{\text{cat}} AH_2.$$

The reaction kinetics is of first order with respect to hydrogen and almost of zero order with respect to A. The reactor itself can be described by the plug flow model, but both internal and external (at the gas–liquid interphase) mass transfers limit the hydrogenation rate. The gas phase consists of pure hydrogen, which flows in a large excess. The density of the liquid phase is assumed to be constant. Give the balance equations of the components.

a. In gas and liquid phases.
b. Solve the balance equations of the liquid phase for hydrogen and AH_2. Give the result in the form of dimensionless quantities and discuss the impacts of various parameters.
c. Sketch the concentration profiles as a function of the liquid residence time (τ_L). Use relevant values for the parameters.

17. Derive an expression for the effectiveness factor for a first-order three-phase catalytic system, for which

a. Gas–liquid mass transfer resistance is a limiting factor and other mass transfer resistances are negligible.
b. Liquid–solid mass transfer resistance limits the overall rate. Other mass transfer resistances are ignored.
c. Internal mass transfer resistance in the porous catalyst particle (spherical) is determining the rate.
d. All possible mass transfer resistances control the process.

18. A catalytic gas–liquid reaction is carried out in a slurry reactor with small catalyst particles, for which the internal mass transfer resistance is negligible. Mixing in the reactor is inefficient, and thus some external mass transfer resistance remains at the outer surfaces of the catalyst particles. The overall stoichiometry is given by

$$2\mathrm{A(l)} + \mathrm{B(g)} \rightarrow \mathrm{C(l)}$$

and the reaction kinetics is given by

$$R = kc_{\mathrm{A}}^2 c_{\mathrm{B}}.$$

The gas–liquid mass transfer rate is high, and the concentration of B in the liquid phase is thus close to the saturation concentration.

a. Derive an expression for the effectiveness factor of A.
b. Simulate the concentration of A in a semibatch reactor, where the pressure of B is kept constant.

19. A catalytic oxidation process is going to be carried out in a fluidized bed with spherical catalyst particles. Calculate all the parameters of oxygen needed for the Kunii–Levenspiel model, starting from the physical data given below:

Data	
Gas composition	20 vol% O_2, 80 vol% N_2
Temperature	200°C
Pressure	1 bar
Catalyst particle diameter	10 μm
Density of particle	1.2 kg/dm^3
V_{sb}/V_b	0.005
α	0.3
Bubble diameter	10 cm

20. Derive steady-state and nonsteady-state mass and energy balances for a catalyst monolith channel in which several chemical reactions take place simultaneously. External and internal mass transfer limitations are assumed to prevail. The flow in the channel is laminar, but radial diffusion might play a role. Axial heat conduction in the solid material must be accounted for. For the sake of simplicity, use cylindrical geometry. Which numerical methods do you recommend for the solution of the model?

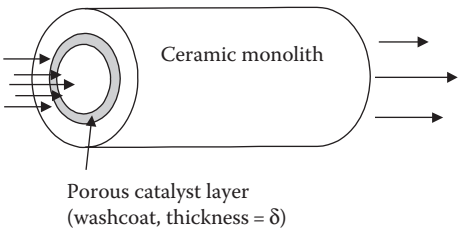

SECTION III. GAS–LIQUID REACTORS

1. Chlorination of benzene takes place in a liquid phase following the stoichiometry below:

$$C_6H_6 + Cl_2 \rightarrow C_6H_5Cl + HCl, \quad (1)$$

$$C_6H_5Cl + Cl_2 \rightarrow C_6H_4Cl_2 + HCl, \quad (2)$$

$$C_6H_4Cl_2 + Cl_2 \rightarrow C_6H_3Cl_3 + HCl, \quad (3)$$

where $C_6H_6 = A$, $C_6H_5Cl = R$, $C_6H_4Cl_2 = S$, and $C_6H_3Cl_3 = T$. The reaction is carried out in an isothermal BR at 55°C. A continuous flow of chlorine gas is fed into the reactor, so that the concentration of chlorine in the liquid phase is maintained at a constant (saturated) level during the chlorination. The volume of the reaction mixture is assumed to remain unaltered. At 55°C, the ratio between the rate constants is as follows: $k_1/k_2 = 8$ and $k_1/k_3 = 240$.

a. Formulate the rate expressions and mass balances for all components.
b. Calculate and illustrate graphically c_R/c_{0A} and c_S/c_{0A} as a function of reacted benzene.
c. Which is the maximum concentration of monochlorobenzene in relation to the initial benzene concentration, and at which conversion level of benzene is this concentration obtained?
d. How large a fraction of benzene is in the unreacted form as the maximum concentration of monochlorobenzene is reached?
e. How large a fraction of benzene has been transformed to dichlorobenzene at the maximum concentration of monochlorobenzene?
f. Calculate the maximum concentration of dichlorobenzene in relation to the initial benzene concentration and give the conversion level of benzene for which this concentration is obtained.

2. *o*-Methyl-benzoic acid can be produced by the oxidation of *o*-xylene in a gas–liquid reactor. The reaction should be carried out batchwise in an autoclave, at an initial pressure of 20 bar and at 160°C. The reaction is of pseudo-first-order following the kinetics

$$R = kc_{O_2},$$

where $k = 2.4 \times 10^3$ (r is given in mol/dm^3, h and c in mol/dm^3). For additional data, see the table below. The reaction scheme is written as

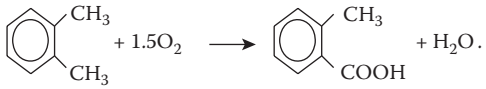

(B) (A)

The gas phase contains pure oxygen at the beginning of the reaction. Assume that the reaction belongs to the group of "rapid reactions" ($c^b_{LO_2} = 0$) and calculate the required reaction time for the pressure to drop to 2 bar in the gas phase.

$D_{LO_2} = 5.2 \times 10^{-6}$ m^2/h	$He_{O_2} = 126.6$ dm^3 bar/mol	$e_G = 0.5$
$a_v = 20$ m^{-1}	$k_{LO_2} = 1.5$ m/h	k_{GO_2} = large

3. Pure toluene should be chlorinated to monochlorotoluene in the presence of a homogeneous catalyst, $SnCl_4$, at atmospheric pressure and 20°C following the reaction

$$\text{Toluene} + Cl_2 \rightarrow \text{Monochlorotoluene} + HCl. \quad (1)$$

The reaction kinetics can be described as

$$R = kc_{LA}c_{LB}c_{cat}, \quad (2)$$

where c_{LA}, c_{LB}, and c_{cat} denote chlorine, toluene, and catalyst concentrations, respectively. The catalyst concentration remains constant during the reaction. Since the product gas, HCl, is desorbed approximately at the same velocity as Cl_2 is absorbed, the volumetric gas flow can be assumed to be constant. The reaction should be carried out in a bubble column, operating according to the concurrent operations principle.

a. Which expression(s) is feasible for the calculation of the absorption flux of chlorine?
b. Calculate the enhancement factor, E_A, at the reactor inlet.

Data

$T = 293K$	$k = 1.34 \times 10^{-7}\,m^6mol^2/s$	$D_{LA} = 3.5 \times 10^{-9}\,m^2/s$	$K_A = 0.0185$
$k_{LA} = 4.0 \times 10^{-6}\,m/s$	$k_{GA} = 1.29 \times 10^{-4}\,m/s$	$a_v = 500\,m^2/m^3$	$\varepsilon_L = 0.6$
$p_{0A} = 101.3 \times 10^3\,Pa$	$c_{0LB} = 9360\,mol/m^3$	$c_{cat} = 0.5\,mol/m^3$	Cl_2 excess at the reactor inlet = 2

4. *p*-Cresol is chlorinated to monochloro-*p*-cresol following the reaction

$$A + B \rightarrow C + D,$$

where A, B, C, and D denote chlorine, *p*-cresol, monochloro-*p*-cresol, and hydrogen chloride, respectively. The reaction takes place at 1 atm total pressure and 0°C. The molar fraction of chlorine in the gas phase is 0.5. Carbon tetrachloride (CCl_4) is used as the solvent. The reaction can be considered as an elementary and irreversible one. Relevant data are listed in the table below.

What value is obtained for the enhancement factor? Give your comments on this. In which category does this reaction belong?

Data

$T = 273\,K$	$K_A = 0.02$	$K = 5.626\,dm^{-3}\,(mol\,s)$	$k_{GA} = large$
$\delta_L = 1.5 \times 10^{-5}\,m$	$c^b_{LB} = 10\,mol/dm^3$		

The diffusion coefficients can be estimated from the Wilke–Chang equation

$$D_i = \frac{7.4\,10^{-12}(\Phi M)^{1/2}T}{(\eta\, V_i^{0.6})}\ m^2/s,$$

where M is the molar mass (g/mol) of the solvent, Φ is the association factor of the solvent, η is the solvent viscosity (cP), T is the temperature (K), and V_i denotes the molar volume of the solute at its boiling point. For chlorine and *p*-cresol, $V_A = 49.2\,cm^3$ mol and

$V_B = 125.6\,cm^3$ mol. The association factor (Φ) is 1 for CCl_4. The viscosity of the solvent (in cP) can be calculated from the equation below:

$$\ln(\eta/cP) = A + B/T + CT + DT^2.$$

The temperature is in K and the parameters A . . . D are given as follows:

CCl_4, carbon tetrachloride: −20°C to 283°C			
$A = -1.303E+01$	$B = 2.290E+03$	$C = 2.339E-02$	$D = -2.011E-05$

5. In the chlorination of carboxylic acids, it is important to know the diffusion coefficient of chlorine gas in the liquid phase. It is thus possible to determine how the reaction is affected by the diffusion of chlorine in the liquid film. Here, we will estimate the diffusion coefficient of chlorine in acetic acid. The association factor of acetic acid can be assumed to be equal to two.

a. Which equations can be used in the calculation of D_{Cl_2}?
b. Calculate the diffusion coefficient of chlorine in acetic acid at 70°C.

6. Monochloroacetic acid is, for instance, used in the synthesis of cellulose derivatives (such as CMC). Monochloroacetic acid is produced by the chlorination of acetic acid in the presence of a homogeneous catalyst dissolved in the liquid phase, such as acetyl chloride:

$$\underset{(A)}{CH_3COOH} + \underset{(B)}{Cl_2} \xrightarrow{\text{Cat.}} \underset{\text{Cat.} = \text{catalyst (C)}}{ClCH_2COOH + HCl}$$

If the solution is kept saturated with Cl_2, an experimentally determined rate expression is valid:

$$r = (k_1 + k_2 c_B^{1/2}) c_C.$$

A stirred tank reactor is supplied with a mixture of acetic acid and acetyl chloride (60 kg/h, see the table below).

a. Which conversion of acetic acid is obtained as the reactor is operated continuously at 85°C?
b. Is the performance of the reactor improving/impairing in the case of batchwise operation? How much? Assume that the time consumed on charging and discharging the reactor is negligible in comparison to the reaction time.
c. Would it be possible to obtain a higher conversion level in a PFR supplied with recycle? Why?

Data	
Reactor volume	$V = 200\ \mathrm{dm}^3$ (= liquid volume)
Density of the liquid mixture	$\rho \approx 1\ \mathrm{kg/dm}^3$
Rate constants at 85°C	$k_1 = 0.0133\ \mathrm{min}^{-1}$
	$k_2 c_0^{1/2} = 0.0512\ \mathrm{min}^{-1}$
Catalyst amount (mole fraction acetyl chloride)	$x_c = 0.05$ or 0.07

$c_0 = c_A + c_B + c_C$ = constant, c_0 = total concentration of the liquid.

7. α-Monochloropropanoic acid (MCA) can be synthesized through the catalytic chlorination of propanoic acid:

$$CH_3CH_2\overset{\text{Cat.}}{COOH} + Cl_2 \rightarrow CH_3CHClCOOH + HCl. \tag{1}$$

As the homogeneous catalyst, propionyl chloride or chlorosulfonic acid (among others) can be used, α,α-dichloro propanoic acid (DCA) is formed as a by-product:

$$CH_3CH_2COO\overset{\text{Cat.}}{H} + 2Cl_2 \rightarrow CH_3Cl_2COOH + 2HCl. \tag{2}$$

The reaction kinetics for the chlorination of propanoic acid was studied by Mäki-Arvela et al. (1995) (*Chem. Eng. Sci.* **50**, 2275–2288). Chlorosulfonic acid ($ClSO_3H$) was used as the catalyst. For a sample illustration (concentration versus time) of the reaction progress, see figure above. The reaction mechanism is introduced in the figure below.

The process (11) is autocatalytic at low and intermediate conversion levels of propionic acid. At constant chlorine and catalyst concentrations, the generation velocity of MCA can be expressed by

$$r_{MCA} = f c_0 (p_1 y_{MCA}^{1/2} + p_1') - c_0 p_1'' y_{MCA}, \quad f = 1 - e^{-b(1-y_{MCA})}, \tag{3}$$

where c_0 denotes the total concentration of the liquid and y_{MCA} denotes the mole fraction of MCA. The parameters p_1, p_1', p_1'', and b have been determined on the basis of the experimental data (Figure 1). The parameter values are listed in the table below.

Kinetic Parameters			
$p_1/\mathrm{min}^{-1} = 0.0103$	$p_1'/\mathrm{min}^{-1} = 0.3 \cdot 10^{-8}$	$p_1''/\mathrm{min}^{-1} = 0.00013$	$b = 3.4$

a. At which mole fraction of MCA, y_{MCA}, does the generation velocity of MCA attain its maximum?
b. The mole fraction $y_{MCA} = 0.95$ is desired. Calculate the reaction time (or residence time) needed to reach this mole fraction. Compare the following reactors: a BR, CSTR, PFR, and a PFR equipped with a recirculation loop.

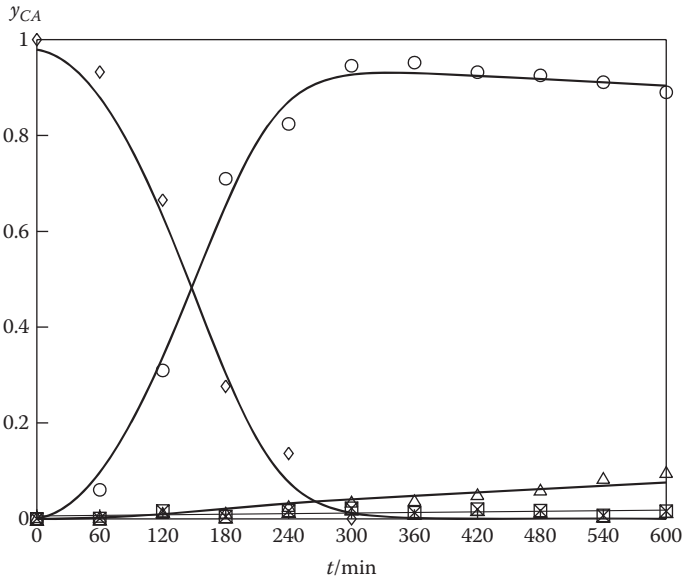

FIGURE 1 Chlorination of propanoic acid at 110°C. Catalyst amount: $y_{ClSO_3H} = 0.082$. Symbols: (◊) propionic acid, (O) α-monochloropropanoic acid, (▲) α,α-dichloropropanoic acid, and (□) α, β-dichloropropanoic acid.

8. Chlorination of butanoic acid to α-monochloro- and α,α-dichlorobutanoic acid was studied on the laboratory scale in a semibatch reactor:

$$CH_3CH_2CH_2COOH + Cl_2 \rightarrow CH_3CH_2CHClCOOH + HCl, \quad (1)$$

$$CH_3CH_2CH_2COOH + 2Cl_2 \rightarrow CH_3CH_2CCl_2COOH + 2HCl. \quad (2)$$

Chlorine and oxygen were bubbled continuously through the liquid phase in the reactor. An inorganic acid catalyst (chlorosulfonic acid) was continuously supplied into the reaction mixture, maintaining the relative amount of acid catalyst in the liquid phase constant during the experiment. The experiment results (Figures 1 and 2) suggest that α-monochloro- and α,α-dichlorobutanoic acids are formed through parallel reaction routes. It also seems that the generation rates are enhanced as the reaction time increases (autocatalytic reactions).

A researcher suggests that an acid-catalyzed enolization of the original carboxylic acid or the acid chloride (formed from the carboxylic acid and the inorganic acid catalyst) might be the rate-determining reaction step. The double bond of the enolic species is, consequently, chlorinated parallel to the monochloro- and dichlorocarboxylic acids. According to the reaction mechanism, the researcher suggests that the following rate equations could be used to describe the kinetics of the chlorination mechanisms (11) and (2):

$$r_{MC} = 1/(1+\alpha)(k_1' y_{MC}^{1/2} + k_1'' y_{DC}^{1/2} + k_2 y_C^{1/2} + k' y_{cat}^{1/2}) y_{cat}^{1/2} (n_0/V_L), \quad (3)$$

$$r_{DC} = \alpha/(1+\alpha)(k_1' y_{MC}^{1/2} + k_1'' y_{DC}^{1/2} + k_2 y_C^{1/2} + k' y_{cat}^{1/2}) y_{cat}^{1/2} (n_0/V_L), \quad (4)$$

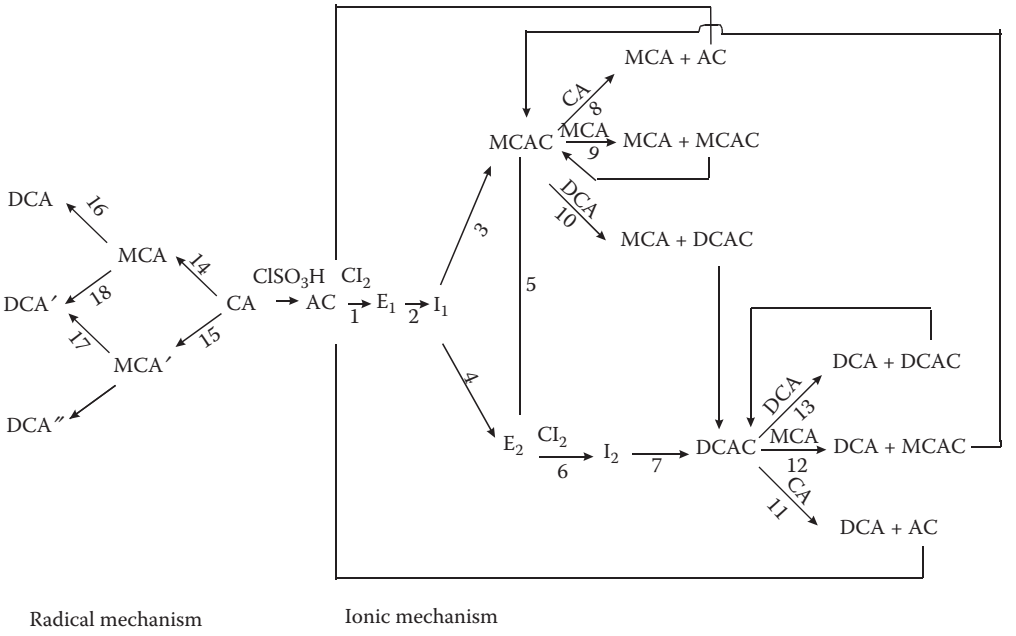

FIGURE 2 Reaction scheme for the chlorination of propanoic acid.

where r_{MC} and r_{DC} give the generation rates for monochloro- and dichlorocarboxylic acids, respectively. The symbols y_C, y_{MC}, y_{DC}, and y_{cat} denote the mole fractions of the original carboxylic acid, monochlorocarboxylic acid, dichlorocarboxylic acid, and the inorganic acid catalyst, respectively. The kinetic parameters are α, k_1', k_1'', k_2, and k'. The parameter α is given by

$$\alpha = \frac{k_{DC}}{k_{MC}}, \tag{5}$$

where k_{DC} and k_{MC} denote the rate constants for mono- and dichlorination of the intermediate enol. The chlorine concentration $[Cl_2]$ in the liquid phase can be presumed constant during the experiments. The mole fractions y_C, y_{MC}, and y_{DC} are related by Equation (6) as follows:

$$y_C + y_{MC} + y_{DC} = 1. \tag{6}$$

The catalyst amount (y_{cat}) in the system is so low that its contribution to balance (6) can be ignored.

a. Set up the mass balances for the carboxylic acids in the liquid phase.
b. List the fundamental kinetic parameters that can be determined from the experimental data (Figures 1 and 2, Table 1).
c. Determine the values of kinetic parameters using suitable regression software.

TABLE 1 Experimental Data

T (°C)	t (min)	y_{MCA}	y_{DCA}
90	0	0	0
	200	0	0
	400	0.0119	0.0002
	600	0.0246	0.0006
	800	0.0567	0.0041
	1000	0.1113	0.0046
	1200	0.1556	0.0072
110	0	0	0
	200	0.013	0.0003
	400	0.0386	0.0013
	600	0.0929	0.0053
	800	0.178	0.0092
	1000	0.2769	0.0147
	1200	0.3876	0.0374
120	0	0	0
	200	0.0153	0.0009
	400	0.0543	0.00322
	600	0.1934	0.0115
	800	0.3099	0.0184
	1000	0.4594	0.0273
	1200	0.5901	0.035
130	0	0	0
	200	0.0493	0.0026
	400	0.1199	0.0058
	600	0.2648	0.0151
	800	0.4235	0.0232
	1000	0.5875	0.0347
	1200	0.7442	0.0442

d. Compare the experimental results with those obtained from the model. Is it possible to state that kinetic equations (3) and (4) describe the experimental data satisfactorily?

9. Dodecanoic acid can, in the presence of a homogeneous catalyst, be chlorinated to α-monochlorodecanoic acid according to the stoichiometry

$$RCH_2COOH + Cl_2 \rightarrow RCHClCOOH + HCl,$$

where $R = C_{10}H_{21}$. The reaction can be considered as a zero-order reaction at the end. The gas phase is primarily pure chlorine, and the diffusion resistance in the gas film is thus negligible. Estimate the enhancement factor E_{Cl_2}. Assume here that the concentration of chlorine in the liquid phase is close to zero. Where does the reaction primarily take place—in the liquid film or in the bulk of the liquid?

Data	
Temperature	$T = 130°C$
Pressure	$P = 101.3\,kPa$
Zero-order rate constant	$k = 0.0838\,mol/dm^3\,min$
Chlorine solubility	$He'_{Cl_2} = 212.4\,bar$
Diffusion coefficient of chlorine in liquid	$D_{Cl_2} = 0.284 \times 10^{-8}\,m^2/s$
Liquid film thickness	$\delta_L = 10^{-4}\,m$
Total concentration of the liquid	$c_L = 4.63\,mol/dm^3$

10. Component A in the gas phase reacts irreversibly and instantaneously with component B in the liquid phase according to the stoichiometry below:

$$A(g) + B(l) \rightarrow C(l).$$

The reaction is carried out in an isothermal BR with a constant volume (an autoclave). Equimolar amounts of A and B are consumed. How long a reaction time is required to obtain a 90% conversion of A?

Data	
Total pressure at the beginning	$P_0 = 1\,atm$
Initial mole fraction of A in the gas phase	$x_{0A} = 0.5$
Temperature	$T = 320\,K$
Reactor volume	$V_R = 0.1\,dm^3$
Volume fraction gas in the reactor	$\varepsilon_G = 0.5$
Volume fraction liquid in the reactor	$\varepsilon_L = 0.5$
Equilibrium constants	$K_A = 0.5, K_B = 0.0$
Ratio between the diffusion coefficients, in the liquid phase	$D_{LB}/D_{LA} = 2.0$
Mass transfer parameters	$k_{LA}a_v = 1.0 \times 10^{-2}\,s^{-1}$
	$k_{GA}a_v = 5.0 \times 10^{-2}\,s^{-1}$

11. Let us consider an irreversible and infinitely rapid gas–liquid reaction

$$A(g) + B(l) \rightarrow C(l).$$

The reaction should be carried out at atmospheric pressure in a column reactor. Give the absorption flow of A and the enhancement factor at the reactor inlet. The liquid contains 5.0 mol/dm^3 of B, and the partial pressure of A in the gas phase is 0.075 atm.

Data:

$$T = 293\,\mathrm{K}$$
$$D_{\mathrm{LA}} = 5.5 \times 10^{-9}\,\mathrm{m^2/s}$$
$$\mathrm{D_{LB}} = 8.3 \times 10^{-9}\,\mathrm{m^2/s}$$
$$K_{\mathrm{A}} = 0.0185$$
$$k_{\mathrm{LB}} = 6.0 \times 10^{-6}\,\mathrm{m/s}$$
$$k_{\mathrm{GA}} = 1.5 \times 10^{-4}\,\mathrm{m/s}$$
$$a_{\mathrm{v}} = 500\,\mathrm{m^2/m^3}$$

12. Absorption of dihydrogen sulfide (H_2S) in amine solutions is, for instance, applied in the desulfurization stages of oil refining processes. H_2S and monoethanol amine (MEA) react in an aqueous solution following the formula below:

$$\mathrm{H_2S + HOCH_2CH_2NH_2 \rightarrow HS^- + HOCH_2CH_2NH_3^+}.$$

The reaction is irreversible and instantaneous.

From an air flow containing 5 vol% H_2S, the aim is to absorb at least 95% of H_2S. A column filled with 1″ ceramic Raschig rings operating at 25°C and a total pressure of 20 bar is used. The absorbing medium is an aqueous solution containing 0.5 mol/dm^3 of MEA; 90% of MEA should react in the column. The volumetric flow rate of gas at 25°C and 20 bar is 5000 m^3/h. The diameter of the absorption column is assumed to be 1.2 m. Determine the column height.

Data:

$$D_{\mathrm{G,H_2S}} = 0.0090\,\mathrm{cm^2/s}$$
$$k'_{\mathrm{G,H_2S}} a_{\mathrm{v}} = 1.2 \times 10^{-5}\,\mathrm{mol/(cm^3\,bar\,s)}$$
$$D_{\mathrm{L,H_2S}} = 2.06 \times 10^{-5}\,\mathrm{cm^2/s}$$
$$k_{\mathrm{L,H_2S}} a_{\mathrm{v}} = 1.4 \times 10^{-2}\,\mathrm{s^{-1}}$$
$$D_{\mathrm{L,H_2S}}/D_{\mathrm{L,MEA}} = 1.62$$
$$He_{\mathrm{H_2S}} = 9.8\,\mathrm{dm^3\,bar/mol}$$

SECTION IV. REACTORS WITH A REACTIVE SOLID PHASE

1. Combustion of graphite takes place as follows:

$$\mathrm{C(s) + O_2(g) \rightarrow CO_2(g)}. \qquad (1)$$

Graphite particles of various sizes were burnt at 900°C in an air flow containing 10 vol% oxygen. The following data were recorded during the combustion:

R (mm)	0.1	1.0	R = initial radius
t_0/(min)	1.6	22.7	t_0 = the total combustion time

Is it correct to assume that the chemical reaction is the rate-determining step in the combustion process? What might be plausible reasons to disagree?

Data:

$$k_{O_2,s} = 20.0\,\text{cm/s at } T = 900°\text{C} \quad \text{and} \quad P = 101.3\,\text{kPa}, \quad \rho_C = 2.26\,\text{g/cm}^3.$$

2. Sulfur dioxide can be adsorbed from flue gases on sodium aluminate, $Na_2O \cdot xAl_2O_3$. The dominating reaction in the system is

$$SO_2(g) + Na_2O_3(s) \rightarrow Na_2SO_3(s).$$

In the testing of an adsorbent (spherical sodium aluminate particles), the following data were recorded (see the table below). The particle volume can be assumed to remain unaffected by the conversion level.

Sorbent weight = 227 mg, saturation weight gain = 111 mg

Time (min)	**Weight Gain**
0	0
0.5	3.3
1	6.8
1.5	9.8
2	12.8
2.5	15
3	17.3
4	21.5
5	25.4
6	28.6
7	32.6
8	35.3
10	42

continued

continued

Time (min)	Weight Gain
12	46.8
14	52.0
16	56.0
18	60.1
20	63.9
22	67.6
24	70.6
26	73.0
29	76.6
32	80.0
35	83.0
38	85.5

Is it possible that the chemical reaction or the product layer diffusion at any point in time might be the rate-determining step in the process? Justify your answer.

3. Carboxyalkylation of cellulose (for instance, the production of CMC) takes place in a BR at a constant temperature under atmospheric pressure. The Na cellulose particles suspended in the solvent (a branched alcohol) react with dissolved α-halogenated carboxylic acid anions leading to the formation of carboxyalkyl cellulose. In each and every glucose unit in a cellulose molecule, there are three (3) hydroxyl groups, HO-2, HO-3, and HO-6, with different reactivities at carbon atoms 2, 3, and 6. In the scheme below, the substitution of HO-6 in Na cellulose with monochloro acetate is illustrated:

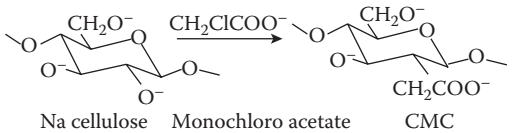

The most important factor for product quality is the degree of substitution (DS) that is defined as

$$\mathrm{DS} = \frac{c_{\mathrm{P2}} + c_{\mathrm{P3}} + c_{\mathrm{P6}}}{c_0},$$

where c_{P2}, c_{P3}, and c_{P6} denote the concentrations of the substituted HO groups in carbon atoms 2, 3, and 6, respectively, and c_0 denotes the initial concentration of cellulose at time $t = 0$. The amount of carboxylic acid at $t = 0$ is assumed to be $c_{\mathrm{HA},0}$.

The reaction between the hydroxyl group in the cellulose molecule and the carboxylic acid molecule is assumed to be elementary and takes place as in the case of a homogeneous liquid-phase reaction. The rate constants for the reaction between the hydroxyl groups

HO-2, HO-3, and HO-6 obtain values k_2, k_3, and k_6, respectively. The constants are given in the table below.

Kinetic Data

$T/°C$	k_0	a_0
30	0.004	3.62
40	0.005	0.763
50	0.0263	1.433
60	0.0135	1.002

A company called MS Ltd. desires to obtain a better control over the carboxylation process in future, which takes place in an isothermal BR. In this context, Mr. Y—the pragmatist—turns to the university and requests that a technology student develop a mathematical model for the process and design of a computer program for the simulation of the DS as a function of time in the carboxymethylation of cellulose in a BR. Miss S, a technology student, accepts the challenge. Imagine that you are Miss S!

a. Describe the reaction kinetics for the formation of P2, P3, and P6.
b. Formulate the molar balances for P2, P3, and P6 as well as for the carboxylic acid HA, in a BR.
c. Design a simulation software for the calculation of c_{P2}, c_{P3}, c_{P6}, c_{HA}, and DS as a function of time. Simulate these concentrations as a function of time.

The DS is obtained from the sum of the substituted groups:

$$DS = \sum_i C_i.$$

The decline of the reactivities of the hydroxyl groups is probably attributed to a decrease in the chemical reactivity and to diffusional limitations. The decrease in reactivity during the substitution is described by a simple phenomenological approach. The rate constants for the substitution of sites HO-2, HO-3, and HO-6 (k_i') can be written as

$$k_i' = \alpha k', \quad i = 2, 3, 6, \ldots$$

where α_i is a proportionality coefficient. The parameter k' is supposed to decline as the substitution proceeds.

We obtain the following exponential relationship between k' and DS

$$k' = k_0 e^{-a_0 DS}.$$

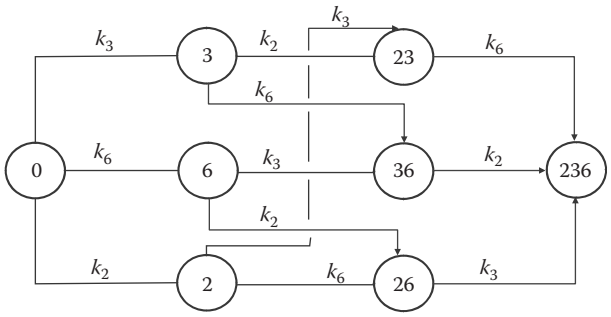

4. A gas–solid reaction

$$\mathrm{A(g)} + \mathrm{B(s)} \rightarrow \mathrm{C(s)}$$

was studied experimentally. This was accomplished by measuring the total reaction time (t_0) for a number of particles with varying radii (R). The gas was supplied in a large excess. Thus c_A was, in practice, constant during the reaction. On the basis of the below-mentioned data, determine which step—the surface reaction or diffusion through the product layer—is the rate-determining step.

R (mm)	t_0 (min)
0.063	5.0
0.125	10.0
0.250	20.0

5. A liquid-phase component (A) reacts with a solid component (B) in a BR to form a dissolved component (P):

$$\mathrm{A(l)} + \mathrm{B(s)} \rightarrow \mathrm{P(l)}.$$

The reaction kinetics is of first order with respect to A. The solid particles are spherical and equal sized. The shrinking particle model can be applied on the particles consisting exclusively of B.

Simulate the dimensionless concentration of A ($y = c_A/c_{0A}$) and dimensionless radius of B ($z = r/R$) as a function of the reaction time in an isothermal BR. The necessary data are given below.

Molar mass of B (M_B) = 60 g/mol
Initial amount of B to liquid volume (n_{0B}/V_L) = 2 mol/L
Density of particles (ρ_P) = 1500 kg/m^3
Initial particle radius (R) = 0.5 mm
Rate constant (k) = 4.17×10^{-5} m/min

REFERENCES*

Section I. Kinetics, Equilibria, and Homogeneous Reactors

1. Rihko, L., *Lic. Technol.*, Thesis, Helsinki University Technology, Espoo, 1994.
3. Fogler, H.S., *Elements of Chemical Reaction Engineering*, Prentice-Hall, Englewood, NJ, 1986.
4. Hill, C.G., *An Introduction to Chemical Engineering Kinetics and Reactor Design*, Wiley, New York, 1976.
5. Levespiel, O., *Chemical Reaction Engineering*, 2nd Edition, Wiley, New York, 1972.
8. Campbell, I.M., *An Example Course in Reaction Kinetics*, International Textbook Company, New York, 1980.
11. Flory, P., Kinetics of polyesterification: A study of the effects of molecular weight and viscosity on reaction rate, *J. Am. Chem. Soc.*, 61, 3334–3340, 1939.
17. Hill, C.G., *An Introduction to Chemical Engineering Kinetics and Reactor Design*, Wiley, New York, 1976.
18. Hill, C.G., *An Introduction to Chemical Engineering Kinetics and Reactor Design*, Wiley, New York, 1976.
19. Hill, C.G., *An Introduction to Chemical Engineering Kinetics and Reactor Design*, Wiley, New York, 1976.
20. Newberger, M.R. and Kadler, R.H., Kinetics of the saponification of diethyl adipate, *AIChE J.*, 19, 1272–1275, 1973.
21. Newberger, M.R. and Kadler, R.H., *AIChE J.*, 19, 1972, 1973.
22. Lehtonen J., Salmi, T., Vuori, A., Haario H., and Nousiainen P., Modelling of the kinetics of alkali fusion, *Ind. Eng. Chem. Res.*, 34, 3678–3687, 1995.
25. Russell, T.W.F. and Denn, M.M., *Introduction to Chemical Engineering Analysis*, Wiley, New York, 1972.
26. Nielsen, P., Ph.D. thesis, Danmarks tekniske højskole, Lyngby, 1985.
32. Nauman, E.B., *Chemical Reactor Design*, Wiley, New York, 1987.
33. Carberry, J.J., *Chemical and Catalysis Reaction Engineering*, McGraw-Hill, New York, 1976.
40. Salmi, T., A computer exercise in chemical reaction engineering and applied kinetics, *J. Chem. Educ.*, 64, 876–878, 1987.

Section II. Catalytic Reactors

1. Smith, J.M., *Chemical Engineering Kinetics*, 3rd Edition, McGraw-Hill, Singapore, 1981.
4. Smith, J.M., *Chemical Engineering Kinetics*, 3rd Edition, McGraw-Hill, Singapore, 1981.
6. Filho, R.M. and Dominigues, A., A multitubular reactor for obtention of acetaldehyde by oxidation of ethyl alcohol, *Chem. Eng. Sci.*, 47, 2571–2576, 1992.

*The numbers refer to the respective problem number.

7. Hill, C.G., *An Introduction to Chemical Engineering Kinetics and Reactor Design*, Wiley, New York, 1976.
8. Smith, J.M., *Chemical Engineering Kinetics*, 3rd Edition, McGraw-Hill, Singapore, 1981.
9. Keiski, R.L., Salmi, T., and Pohjola, V.J., Development and verification of a detailed simulation model for fixed bed reactors, *Chem. Eng. J.*, 48, 17–29, 1992.
10. Hill, C.G., *An Introduction to Chemical Engineering Kinetics and Reactor Design*, Wiley, New York, 1976.
11. Rase, H.F., *Chemical Engineering Kinetics*, 3rd Edition, McGraw-Hill, Singapore, 1981.
12. Smith, J.M., *Chemical Engineering Kinetics*, 3rd Edition, McGraw-Hill, Singapore, 1981.
15. Toppinen, S., Rantakylä, T.-K., Salmi, T., and Aittamaa, J., Kinetics of the liquid phase hydrogenation of benzene and some monosubstituted alkylbenzenes over a Ni catalyst, *Ind. Eng. Chem. Res.*, 35, 1824–1833, 1996.

Section III. Gas–Liquid Reactors

1. Russell, T.W.F. and Denn, M.M., *Introduction to Chemical Engineering Analysis*, Wiley, New York, 1972.
2. Froment, G.F. and Bischoff, K.B., *Chemical Reactor Analysis and Design*, 2nd Edition, Wiley, New York, 1972.
4. Darde, T., Midoux, N., and Charpentier, J.-S., Réactions gaz-liquide complexes: Contribution à la recherche d'un outil de modèlisation et de prédiction de la sélectivité, *Entropie*, 19, 92–109, 1983.
6. Martikainen, P., Salmi, T., Paatero, E., Hummelstedt, L., Klein, P., Damen, H., and Lindroos, T., Kinetics of the homogeneous catalytic chlorination of acetic acid, *J. Chem. Technol. Biotechnol.*, 40, 259–274, 1987.
7. Mäki-Arvela, P., Salmi, T., Paatero, E., and Sjöholm, E., Selective synthesis of monochloropropanoic acid, *Ind. Eng. Chem. Res.*, 34, 1976–1993, 1995.
8. Salmi, T., Paatero, E., and Fagerstolt, K., Kinetic model for synthesis of chlorocarboxylic acids, *Chem. Eng. Sci.*, 48, 735–751, 1993.
9. Salmi, T., Paatero, E., and Fagerstolt, K., *Chem. Eng. Sci.*, 48, 735–751, 1993.

Section IV. Reactors Containing a Reactive Solid Phase

3. Salmi, T., Valtakari, D., Paatero, E., Holmbom, B., and Sjöholm, R., Kinetic study of the carboxymethylation of cellulose, *Ind. Eng. Chem. Res.*, 33, 1454–1459, 1994.
4. Smith, J.M., *Chemical Engineering Kinetics*, 3rd Edition, McGraw-Hill, Singapore, 1981.

Solutions of Selected Exercises

SECTION I/2

The reactions are

$$2CO + O_2 \rightleftarrows 2CO_2,$$
$$2C_3H_6 + 9O_2 \rightleftarrows 6CO_2 + 6H_2O.$$

Let us introduce the notation

$$\underline{a}^{\mathrm{T}} = [\mathrm{CO}\,\mathrm{O_2}\,\mathrm{CO_2}\,\mathrm{C_3H_6}\,\mathrm{H_2O}] = [\mathrm{C}\,\mathrm{O}\,\mathrm{D}\,\mathrm{P}\,\mathrm{W}]\,.$$

The key component vector is

$$\underline{a}_k^{\mathrm{T}} = [\mathrm{CO}\,\mathrm{C_3H_6}] = [\mathrm{C}\,\mathrm{P}]\,.$$

The stoichiometric matrix is written as

$$\underline{\nu} = \begin{bmatrix} -2 & 0 \\ -1 & -9 \\ +2 & +6 \\ 0 & -2 \\ 0 & 6 \end{bmatrix}.$$

Equation 3.86, Section 3.5.2, gives the relationship

$$\underline{x} = \frac{\underline{x}_0 + \underline{\nu}\left(-\underline{\nu}_k^{-1}\right)\eta'_k}{1 + \underline{i}^{\mathrm{T}}\underline{\nu}\left(-\underline{\nu}_k^{-1}\right)\eta'_k},$$

where $\eta'_k = x_{0k}\,\eta_k$, in which η_k denotes the relative conversion. The stoichiometric matrix of the key components is

$$\underline{\nu}_k = \begin{bmatrix} -2 & 0 \\ 0 & -2 \end{bmatrix}.$$

Inversion of $\underline{\nu}_k$ gives $\underline{\nu}_k^{-1}$, which becomes

$$\underline{\nu}_k^{-1} = \begin{bmatrix} -\frac{1}{2} & 0 \\ 0 & -\frac{1}{2} \end{bmatrix}.$$

The product $\underline{\nu}(-\underline{\nu}_k^{-1})\eta'_k$ is calculated:

$$\begin{bmatrix} -2 & 0 \\ -1 & -9 \\ 2 & 6 \\ 0 & -2 \\ 0 & 6 \end{bmatrix} \begin{bmatrix} \frac{1}{2} & 0 \\ 0 & \frac{1}{2} \end{bmatrix} \begin{bmatrix} \eta'_{\mathrm{c}} \\ \eta'_{\mathrm{p}} \end{bmatrix} = \begin{bmatrix} -2 & 0 \\ -1 & -9 \\ 2 & 6 \\ 0 & -2 \\ 0 & 6 \end{bmatrix} \begin{bmatrix} \frac{1}{2}\eta'_{\mathrm{c}} \\ \frac{1}{2}\eta'_{\mathrm{p}} \end{bmatrix} = \begin{bmatrix} -\eta'_{\mathrm{c}} \\ -\frac{1}{2}\eta'_{\mathrm{c}} - \frac{9}{2}\eta'_{\mathrm{p}} \\ \eta'_{\mathrm{c}} + 3\eta'_{\mathrm{p}} \\ -\eta'_{\mathrm{p}} \\ 3\eta'_{\mathrm{p}} \end{bmatrix}.$$

The term $\alpha = \underline{i}^{\mathrm{T}}(\underline{\nu}_k^{-1})\underline{\eta}'_k$ implies the sum of all relative conversions:

$$\alpha = -\eta'_{\mathrm{c}} - \frac{1}{2}\eta'_{\mathrm{c}} - \frac{9}{2}\eta'_{\mathrm{p}} + \eta'_{\mathrm{c}} + 3\eta'_{\mathrm{p}} - \eta'_{\mathrm{p}} + 3\eta'_{\mathrm{p}},$$

$$\alpha = \frac{1}{2}\eta'_{\mathrm{c}} - \frac{1}{2}\eta'_{\mathrm{p}},$$

$$\begin{bmatrix} x_{\mathrm{C}} \\ x_{\mathrm{O}} \\ x_{\mathrm{D}} \\ x_{\mathrm{P}} \\ x_{\mathrm{W}} \end{bmatrix} = \left(1 - \frac{1}{2}\eta'_{\mathrm{c}} + \frac{1}{2}\eta'_{\mathrm{p}}\right)^{-1} \left(\begin{bmatrix} x_{0\mathrm{C}} \\ x_{0\mathrm{O}} \\ x_{0\mathrm{D}} \\ x_{0\mathrm{P}} \\ x_{0\mathrm{W}} \end{bmatrix} + \begin{bmatrix} -\eta'_{\mathrm{c}} \\ -\frac{1}{2}\eta'_{\mathrm{c}} - \frac{9}{2}\eta'_{\mathrm{p}} \\ \eta'_{\mathrm{c}} + 3\eta'_{\mathrm{p}} \\ -\eta'_{\mathrm{p}} \\ 3\eta_{\mathrm{p}}{}' \end{bmatrix} \right).$$

The above equation can more conveniently be written as follows:

$$x_{\mathrm{C}} = (1 + \alpha)^{-1}\left(x_{0\mathrm{C}} - \eta'_{\mathrm{C}}\right),$$

$$x_{\mathrm{O}} = (1 + \alpha)^{-1}\left(x_{0\mathrm{O}} - \frac{1}{2}\eta'_{\mathrm{C}} - \frac{9}{2}\eta'_{\mathrm{p}}\right),$$

$$x_{\mathrm{D}} = (1+\alpha)^{-1}\left(x_{0\mathrm{D}} - \eta'_{\mathrm{C}} + 3\eta'_{\mathrm{p}}\right),$$
$$x_{\mathrm{P}} = (1+\alpha)^{-1}\left(x_{0\mathrm{P}} - \eta'_{\mathrm{p}}\right),$$
$$x_{\mathrm{W}} = (1+\alpha)^{-1}\left(x_{0\mathrm{W}} + 3\eta'_{\mathrm{p}}\right).$$

Now all mole fractions can be calculated from the relative conversions of P and C.

SECTION I/4

a. The reaction scheme is

$$\mathrm{A} + \mathrm{B} \longrightarrow \mathrm{C} + \mathrm{D}.$$

Since the reaction is bimolecular and irreversible, the second-order kinetics is assumed:

$$r = kc_{\mathrm{A}}c_{\mathrm{B}}, \quad r_{\mathrm{A}} = \nu_{\mathrm{A}}r, \quad \text{and} \quad r_{\mathrm{B}} = \nu_{\mathrm{B}}r.$$

Stoichiometry gives a relation between component concentrations. For the constant volume system, we obtain

$$\zeta' = \frac{(c_{\mathrm{A}} - c_{0\mathrm{A}})}{\nu_{\mathrm{A}}} = \frac{(c_{\mathrm{B}} - c_{0\mathrm{B}})}{\nu_{\mathrm{B}}}.$$

Since $c_{0\mathrm{A}} = c_{0\mathrm{B}} = 0.757\ \mathrm{mol/L}$ and $\nu_{\mathrm{B}} = \nu_{\mathrm{A}} = -1$, we obtain $c_{\mathrm{B}} = c_{\mathrm{A}}$. Thus, r becomes

$$r = kc_{\mathrm{A}}^2.$$

The mass balance is

$$\frac{\mathrm{d}c_{\mathrm{A}}}{\mathrm{d}t} = r_{\mathrm{A}} = -kc_{\mathrm{A}}^2,$$

which on integration becomes

$$-\int_{c_{0\mathrm{A}}}^{c_{\mathrm{A}}} \frac{\mathrm{d}c_{\mathrm{A}}}{c_{\mathrm{A}}^2} = k\int_0^t \mathrm{d}t$$

yielding

$$1/c_{\mathrm{A}} - 1/c_{0\mathrm{A}} = kt \Longrightarrow c_{0\mathrm{A}}/c_{\mathrm{A}} - 1 = kc_{0\mathrm{A}}t.$$

The equation has the form

$$y = k'x, \quad \text{where } y = c_{0\mathrm{A}}/c_{\mathrm{A}} - 1, \quad x = t, \quad \text{and} \quad k' = kc_{0\mathrm{A}}.$$

The transformed data are presented in the table below:

t(ks)	$c_{0A}/c_A - 1 = y$
0	0
10.8	0.0582
24.48	0.09649
46.08	0.1820
54.72	0.2361
69.48	0.2837
88.56	0.36986
109.4	0.47493
126.7	0.5674
133.7	0.6155

The linear plot is shown below. The slope is $kc_{0A} = 0.00429\ \text{ks}^{-1}$ (ks = kilosecond = 10^3 s) yielding k ($c_{0A} = 0.757$ mol/L). We obtain $k = 0.00566$ L/(mol/ks).

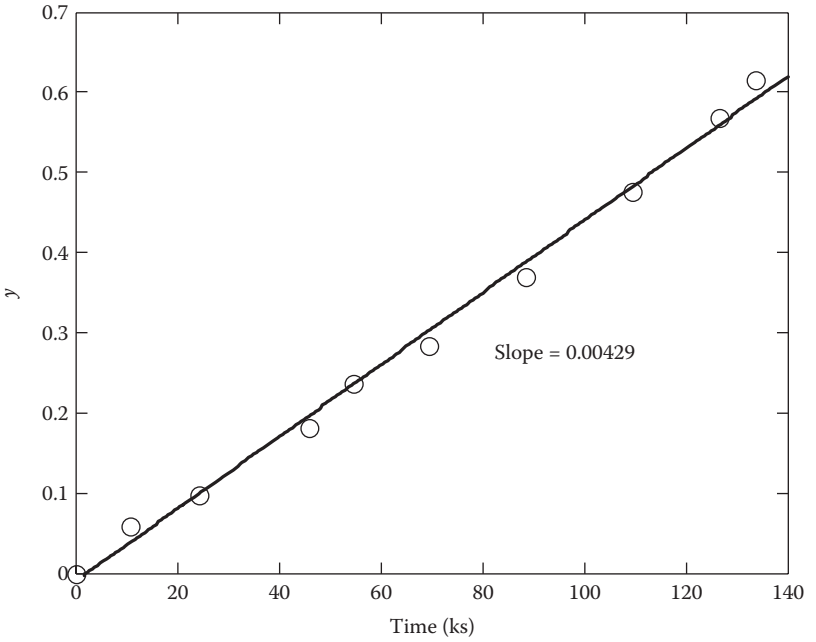

b. The inlet flow is nonequimolar, which is why we use the form

$$\frac{dc_A}{d\tau} = r_A = -kc_Ac_B$$

and the relation between c_A and c_B is obtained from

$$\zeta = \frac{c_A - c_{0A}}{\nu_A} = \frac{c_B - c_{0B}}{\nu_B}, \quad \nu_A = \nu_B = -1,$$

in which $c_B = c_{0B} - c_{0A} + c_A = a + c_A$, where $a = c_{0B} - c_{0A}$. Thus we obtain

$$\frac{dc_A}{d\tau} = -kc_A\,(a + c_A)\,,$$

which is solved by the separation of variables

$$\int_{c_{0A}}^{c_A} \frac{dc_A}{c_A\,(a + c_A)} = -k \int_0^{\tau} d\tau.$$

The term $1/(c_A(a + c_A))$ is developed into partial fractions

$$\frac{1}{c_A\,(a + c_A)} = \frac{A}{c_A} + \frac{B}{a + c_A},$$

that is, $A(a + c_A) + Bc_A = 1$, which in turn yields $Aa + (A + B)x = 1 \Rightarrow Aa = 1$ and $A + B = 0$. Finally, we obtain $A = 1/a$ and $B = -1/a$. The integral is now easily solved:

$$\int \frac{A\,dc_A}{c_A} + \int \frac{B\,dc_A}{a + c_A} = A \ln c_A + B \ln\,(a + c_A)\,.$$

The limits are inserted and we obtain

$$\frac{1}{a} \ln\left(\frac{c_A}{c_{0A}}\right) - \frac{1}{a}\left(\frac{a + c_A}{a + c_{0A}}\right) = -k\tau,$$

which is rewritten as

$$\ln\left(\frac{c_A\,(a + c_{0A})}{c_{0A}\,(a + c_A)}\right) = -ka\tau.$$

Recalling that $a = c_{0B} - c_{0A}$, the equation is transformed to

$$\ln\left(\frac{c_{0A}\,(c_{0B} - c_{0A} + c_A)}{c_{0B}c_A}\right) = k(c_{0B} - c_{0A})\tau,$$

from which c_A is solved:

$$\frac{c_{0A}\,(c_{0B} - c_{0A} + c_A)}{c_{0B}c_A} = e^{k(c_{0B} - c_{0A})\tau},$$

and we obtain

$$c_A = \frac{c_{0B} - c_{0A}}{(c_{0B}/c_{0A})\,e^{k(c_{0B} - c_{0A})\tau} - 1}.$$

The numerical values are

$$c_{0B} - c_{0A} = 12\,\text{mol/L} - 10\,\text{mol/L} = 2\,\text{mol/L},$$
$$\frac{c_{0B}}{c_{0A}} = \frac{12}{10} = \frac{6}{5} = 1.2,$$
$$\tau = \frac{V}{\dot{V}} = 500\frac{1}{0.3}\,\text{L/min} = 1666.667\,\text{min} = 27.778\,\text{h},$$
$$k(c_{0B} - c_{0A})\tau = 0.02038\,(\text{L/(mol/h)})\,2\,\text{mol/L}\,27.778\,\text{h} = 1.13222,$$
$$c_A = 2\,\text{mol/L}/(1.2e^{1.13222} - 1) = 0.73447\,\text{mol/L}.$$

Since no C was present in the feed, $c_C = c_{0A} - c_A = 9.2655\,\text{mol/L}$. Consequently, the production capacity of C is

$$\dot{n}_C = c_C\dot{V} = 9.2655\,\text{mol/L} \cdot 0.3\,\text{L/min} = 2.7796\,\text{mol/min} = 166.78\,\text{mol/h}.$$

c. For a CSTR, the following balance equation is valid:

$$\frac{c_A - c_{0A}}{\bar{\tau}} = r_A = -kc_Ac_B, \quad \text{where} \quad \bar{\tau} = \frac{V}{3\dot{V}}.$$

Again, we have for $c_B = c_{0B} - c_{0A} + c_A = a + c_A$. The balance equation becomes

$$c_A - c_{0A} = -k\bar{\tau}c_A\,(a + c_A), \quad \text{that is,} \quad k\bar{\tau}c_A^2 + (1 + k\bar{\tau}a)\,c_A - c_{0A} = 0,$$

which has the solution

$$c_A = \frac{-(1 + k\bar{\tau}a) \pm \sqrt{(1 + k\bar{\tau}a)^2 + 4k\bar{\tau}c_{0A}}}{2k\bar{\tau}}.$$

This equation is valid for the first reactor, that is, $c_A = c_{1A}$.

To obtain c_{2A}, c_{1A} is solved and inserted instead of c_{0A}, and c_{2A} is solved. An analogous treatment is applied to the third reactor, giving c_{3A}. The production capacity of C is once again, obtained from

$$c_C = c_{0A} - c_{3A} \quad \text{and} \quad \dot{n}_C - c_C\dot{V}.$$

SECTION I/10

The reaction can be written as

$$A \xrightarrow[1]{O_2} R \xrightarrow[2]{O_2} S.$$

For a tube reactor (PFR) with a constant volumetric flow rate, we have the mass balances $\mathrm{d}c_i/\mathrm{d}\tau = r_i$, where $\tau = V/\dot{V}$. In the current case, $r_\mathrm{A} = -r_1, r_\mathrm{R} = +r_1 - r_2$, and the reaction rates are given by $r_1 = k_1 c_\mathrm{A}$ and $r_2 = k_2 c_\mathrm{R}$. The balances of A and R become

$$\frac{\mathrm{d}c_\mathrm{A}}{\mathrm{d}\tau} = -k_1 c_\mathrm{A},$$
$$\frac{\mathrm{d}c_\mathrm{R}}{\mathrm{d}\tau} = +k_1 c_\mathrm{A} - k_2 c_\mathrm{R}.$$

Division of the balances yields

$$\mathrm{d}c_\mathrm{R}/\mathrm{d}c_\mathrm{A} = -1 + (k_2/k_1)(c_\mathrm{R}/c_\mathrm{A}).$$

The substitution $c_\mathrm{R}/c_\mathrm{A} = z$ is introduced, yielding

$$\frac{\mathrm{d}c_\mathrm{R}}{\mathrm{d}c_\mathrm{A}} = \frac{\mathrm{d}\,(c_\mathrm{A} z)}{\mathrm{d}c_\mathrm{A}} = \frac{\mathrm{d}z}{\mathrm{d}c_\mathrm{A}} c_\mathrm{A} + z.$$

The differential equation becomes

$$\frac{\mathrm{d}z}{\mathrm{d}c_\mathrm{A}} c_\mathrm{A} + z = -1 + \frac{k_2}{k_1} z, \quad \text{that is,} \quad \frac{\mathrm{d}z}{\mathrm{d}c_\mathrm{A}} c_\mathrm{A} = \left(\frac{k_2}{k_1} - 1\right) z - 1 = \alpha z - 1.$$

The variables are easily separated, $c_\mathrm{A}/\mathrm{d}c_\mathrm{A} = (\alpha z - 1)/\mathrm{d}z$. The integration is carried out ($z = 0$ at the beginning as $c_\mathrm{A} = c_{0\mathrm{A}}$)

$$\int_{c_{0\mathrm{A}}}^{c_\mathrm{A}} \frac{\mathrm{d}c_\mathrm{A}}{c_\mathrm{A}} = \int_0^z \frac{\mathrm{d}z}{\alpha z - 1} \Leftrightarrow \ln \frac{c_\mathrm{A}}{c_{0\mathrm{A}}} = \frac{1}{\alpha} \ln \left(\frac{\alpha z - 1}{-1}\right),$$

which is solved as follows:

$$\frac{c_\mathrm{A}}{c_{0\mathrm{A}}} = (1 - \alpha z)^{1/\alpha}, \quad \text{where} \quad z = \frac{c_\mathrm{R}}{c_\mathrm{A}}.$$

We obtain from the above

$$1 - \alpha \frac{c_\mathrm{R}}{c_\mathrm{A}} = \left(\frac{c_\mathrm{A}}{c_{0\mathrm{A}}}\right)^\alpha \Leftrightarrow \alpha \frac{c_\mathrm{R}}{c_\mathrm{A}} = 1 - \left(\frac{c_\mathrm{A}}{c_{0\mathrm{A}}}\right)^\alpha.$$

Finally, we obtain

$$\frac{c_\mathrm{R}}{c_{0\mathrm{A}}} = \alpha \left(\frac{c_\mathrm{A}}{c_{0\mathrm{A}}}\right)\left(1 - \left(\frac{c_\mathrm{A}}{c_{0\mathrm{A}}}\right)^\alpha\right), \quad \text{where} \quad \alpha = \frac{k_2}{k_1} - 1 \quad \text{and} \quad \frac{c_\mathrm{A}}{c_{0\mathrm{A}}} = 1 - \eta_\mathrm{A}.$$

The mathematical model to be used for the data displayed in the table thus becomes

$$\frac{c_\mathrm{R}}{c_{0A}} = \alpha(1 - \eta_A)(1 - (1 - \eta_A)^\alpha),$$

from which $\alpha = (k_2/k_1) - 1$ is obtained. The problem is nonlinear with respect to α, and, therefore, nonlinear regression analysis is principally the best method. Further, α can be obtained by a trial-and-error search of the best fit to the data. A shortcut is to utilize the maximum of function f, where $(1 - \eta_A) = c_A/c_{0A}$:

$$f = \frac{c_A}{c_{0A}}\left(1 - \left(\frac{c_A}{c_{0A}}\right)^{\alpha}\right).$$

We denote $c_A/c_{0A} = x$ and obtain

$$f(x) = x - x^{\alpha+1}.$$

Differentiation yields $f'(x) = 1 - (\alpha + 1)x^{\alpha}$. At the maximum, $f'(x) = 0$. Consequently, $(\alpha + 1)x^{\alpha} = 1$, and x becomes

$$x = \frac{1}{(\alpha + 1)^{1/\alpha}} = \left(\frac{c_A}{c_{0A}}\right)_{\max}.$$

The figure below indicates that the maximum is at around $\eta_A = 0.55$, that is, $(c_A/c_{0A})_{\max} = 0.45$. The value, $\alpha = 0.6$, approximately satisfies the above equation. Consequently, $k_2/k_1 = 1 + \alpha = 1.6$. We conclude that $k_2/k_1 \approx 1.6$, and the maximum yield of R (c_R/c_{0A}) is obtained with the conversion level of A having the value 0.55.

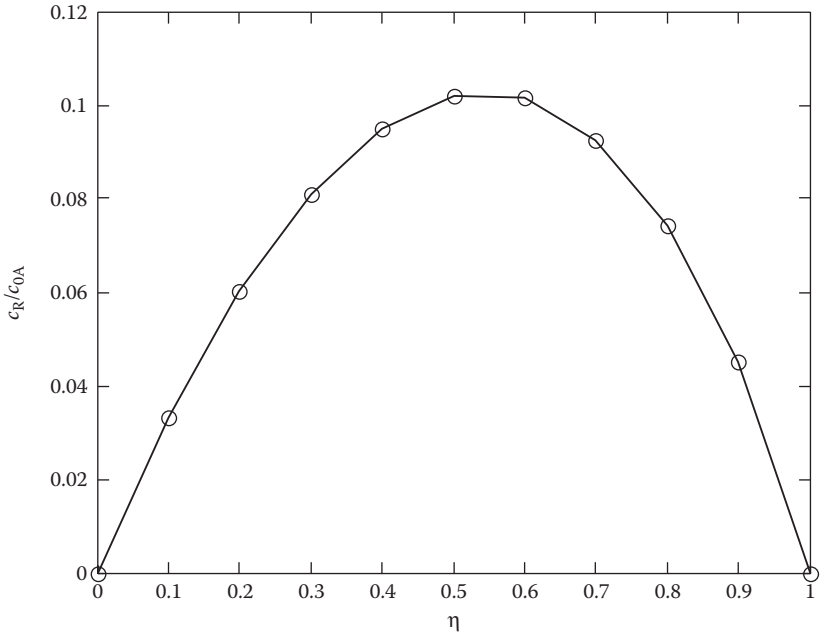

SECTION I/12

The reaction is given by

$$2SO_2O_3^{2-} + 4H_2O_2 \longrightarrow \text{products},$$

that is, $2A + 4B \rightarrow$ products.

The transient mass balance of A in a CSTR is given by

$$c_{0A}\dot{V} + r_A V = c_A\dot{V} + \frac{dn_A}{dt}.$$

Since the volume is constant, we can write $dn_A/dt = V(dc_A/dt)$.

Further, the generation rate of A is $r_A = \nu_A r$. The mean residence time is introduced, $\tau = V/\dot{V}$.

We obtain $c_{0A} + \nu_A r\tau = c_A + \tau(dc_A/dt)$, which is rewritten as

$$\frac{dc_A}{dt} = \frac{c_{0A} - c_A}{\tau} + \nu_A r. \qquad [A]$$

The transient energy balance obtains the form ($U = 0$, for an adiabatic reactor)

$$r\,(-\Delta H_r)\,V\,dt = \dot{m}c_p\,(T - T_0)\;dt + c_p m\,dT.$$

Here we assumed that $c_p \approx$ constant and $c_p \approx c_v$ for the system. The time derivative of the temperature thus becomes

$$\frac{dT}{dt} = \frac{1}{c_p m}\left[r(-\Delta H_r)V - \dot{m}c_p(T - T_0)\right].$$

The liquid mass is $m = \rho_0 V_0 \approx \rho_0 V$ and the mass flow is $\dot{m} = \rho_0\dot{V}_0$. The balance is rewritten as

$$\frac{dT}{dt} = \frac{1}{c_p\rho_0}\left(r(-\Delta H_r) - \frac{\rho_0 c_p}{\tau}(T - T_0)\right),$$

that is,

$$\frac{dT}{dt} = \frac{T_0 - T}{\tau} + \beta r, \quad \text{where } \beta = \frac{-\Delta H_r}{c_p\rho_0}. \qquad [B]$$

Equations [A] and [B] have similar structures, and the reaction rate can thus be eliminated:

$$-\beta\frac{dc_A}{dt} = -\beta\left(\frac{c_{0A} - c_A}{\tau}\right) - \beta\nu_A r,$$

$$\nu_A\frac{dT}{dt} = \nu_A\left(\frac{T_0 - T}{\tau}\right) + \beta\nu_A r.$$

Addition of the above equations yields

$$-\beta\frac{\mathrm{d}c_\mathrm{A}}{\mathrm{d}t}+\nu_\mathrm{A}\frac{\mathrm{d}T}{\mathrm{d}t}=+\frac{\beta}{\tau}c_\mathrm{A}-\frac{\beta}{\tau}c_{0\mathrm{A}}-\frac{\nu_\mathrm{A}}{\tau}T+\frac{\nu_\mathrm{A}}{\tau}T_0.$$

We define new variables $y=\beta c_\mathrm{A}-\nu_\mathrm{A}T$ and $y_0=\beta c_{0\mathrm{A}}-\nu_\mathrm{A}T_0$. The equation becomes

$$-\frac{\mathrm{d}y}{\mathrm{d}t}=\frac{y}{\tau}-\frac{y_0}{\tau},$$

which is easily solved by separation of variables

$$\int_{y(0)}^{y}\frac{\mathrm{d}y}{y_0-y}=\int_0^t\frac{\mathrm{d}t}{\tau}=\frac{t}{\tau}.$$

The solution becomes

$$-\int_{y(0)}^{y}\ln\left(y_0-y\right)=\frac{t}{\tau}\Rightarrow\ln\left(\frac{y_0-y}{y_0-y(0)}\right)=-\frac{t}{\tau}$$

yielding y accordingly:

$$y=y_0-\left(y_0-y\left(0\right)\right)\mathrm{e}^{-t/\tau}.$$

After this, c_A is obtained from

$$c_\mathrm{A}=\beta^{-1}\left(y+\nu_\mathrm{A}T\right).$$

The variable y at $t=0$ is $y(0), y(0)=\beta 0-\nu_\mathrm{A}T(0)=-\nu_\mathrm{A}T(0)$, where $T(0)$ is the initial temperature ($c_\mathrm{A}(0)=0$).

We return to the energy balance $\mathrm{d}T/\mathrm{d}t=(T_0-T)/\tau+\beta r$ and insert the rate equation, which is $r=kc_\mathrm{A}c_\mathrm{B}$.

The stoichiometry yields the relation

$$\zeta=\frac{c_\mathrm{A}-c_{0\mathrm{A}}}{\nu_\mathrm{A}}=\frac{c_\mathrm{B}-c_{0\mathrm{B}}}{\nu_\mathrm{B}},\quad c_\mathrm{B}=c_{0\mathrm{B}}+\frac{\nu_\mathrm{B}}{\nu_\mathrm{A}}(c_\mathrm{A}-c_{0\mathrm{A}}).$$

The rate equation receives the form (remember that $k=\mathrm{e}^{-E_\mathrm{a}/RT}$)

$$r=A^{-E_\mathrm{a}/RT}c_\mathrm{A}\left(c_{0\mathrm{B}}+\frac{\nu_\mathrm{B}}{\nu_\mathrm{A}}\left(c_\mathrm{A}-c_{0\mathrm{A}}\right)\right).$$

The algorithm is thus summarized as follows:

1. $y=y_0-(y_0-y(0))\mathrm{e}^{-t/\tau}$, where $y(0)=-\nu_\mathrm{A}T(0)$ and $y_0=\beta c_{0\mathrm{A}}-\nu_\mathrm{A}T_0$;
2. $c_\mathrm{A}=\beta^{-1}(y+\nu_\mathrm{A}T)$, where $\beta=-\Delta H_\mathrm{r}/c_\mathrm{p}\rho_0$;

3. $r = Ae^{E_a/RT} c_A \left(c_{0B} + \frac{\nu_B}{\nu_A}(c_A - c_{0A}) \right)$;
4. $\frac{dT}{dt} = \frac{T_0 - T}{\tau} + \beta r$.

The differential equation in step 4 is solved numerically using various values of A and E_a, until the best fit to the experimental data is obtained. In practice, the calculations are carried out by nonlinear regression analysis. The best fit to the data was obtained for the following values:

$$A = 2.74 \times 10^{18}\,\mathrm{m^3/mol\,min} \quad \text{and} \quad E_a = 127\,\mathrm{kJ/mol}$$

The fit is displayed in the figure below.

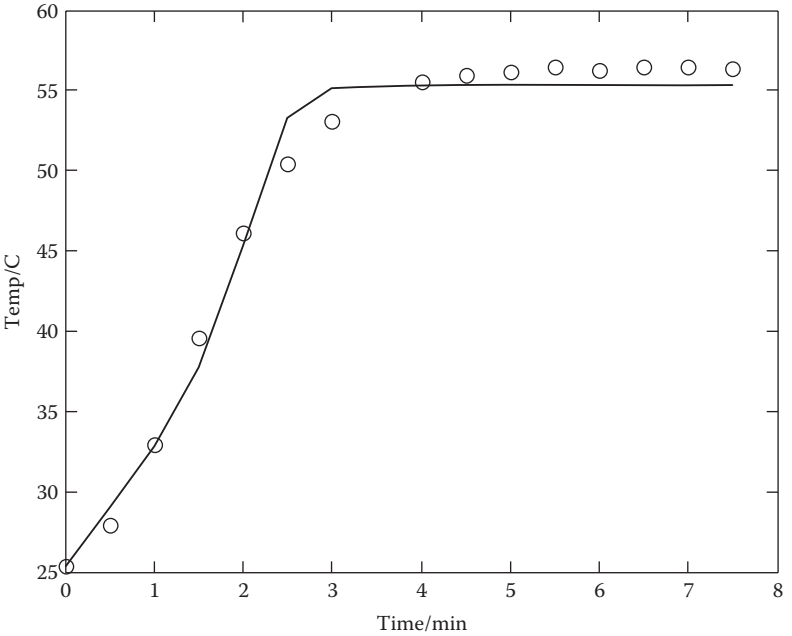

Fit of the model to the experimental data.

SECTION I/18

The reaction is given by

$$A \rightarrow B + C.$$

The design equation for the tube reactor is $d\dot{n}_A/dV = r_A$, where $r_A = kc_A = k(\dot{n}_A/\dot{V})$.

We insert the definition of conversion $\eta_A = (\dot{n}_{0A} - \dot{n}_A)/\dot{n}_{0A}$, which yields $\dot{n}_A = (1 - \eta_A)\dot{n}_{0A}$.

The derivative thus becomes $d\dot{n}_A/dV = -\dot{n}_{0A}(d\eta_A/dV)$.

The balance becomes

$$\frac{\mathrm{d}\eta_\mathrm{A}}{\mathrm{d}V} = \frac{k\dot{n}_\mathrm{A}}{\dot{n}_{0\mathrm{A}}\dot{V}} = \frac{k(1-\eta_\mathrm{A})}{\dot{V}}.$$

The updating formula for the volumetric flow rate is $\dot{V} = \dot{V}_0(1 + x_{0\mathrm{A}}\delta_\mathrm{A}\eta_\mathrm{A})$, and we obtain

$$\frac{\mathrm{d}\eta_\mathrm{A}}{\mathrm{d}V} = \frac{k(1-\eta_\mathrm{A})}{\dot{V}_0(1 + x_{0\mathrm{A}}\delta_\mathrm{A}\eta_\mathrm{A})}.$$

A new variable, the space time, is introduced: $\tau = V/\dot{V}_0$, giving $\mathrm{d}V = \dot{V}_0\mathrm{d}t$. A simple equation

$$\frac{\mathrm{d}\eta_\mathrm{A}}{\mathrm{d}\tau} = \frac{k(1-\eta_\mathrm{A})}{1 + x_{0\mathrm{A}}\delta_\mathrm{A}\eta_\mathrm{A}}$$

is obtained.

The notation $x_{0\mathrm{A}}\delta_\mathrm{A} = \alpha$ is introduced and the variables are separated:

$$\int_0^{\eta_\mathrm{A}} \left(\frac{1+\alpha\eta}{1-\eta_\mathrm{A}}\right)\mathrm{d}\eta_\mathrm{A} = k\int_0^{\tau}\mathrm{d}\tau \Rightarrow \int_0^{\eta_\mathrm{A}} \left(\frac{1+\alpha}{1-\eta_\mathrm{A}} - \alpha\right)\mathrm{d}\eta_\mathrm{A} = k\tau,$$

$$-(1+\alpha)\Big/_0^{\eta_\mathrm{A}} \ln(1-\eta_\mathrm{A}) - \alpha\Big/_0^{\eta_\mathrm{A}} \eta_\mathrm{A} = k\tau,$$

$$(1+\alpha)\ln(1-\eta_\mathrm{A})^{-1} - \alpha\eta_\mathrm{A} = k\tau,$$

which yields the required space time:

$$\tau = k^{-1}\left[(1+\alpha)\ln(1-\eta_\mathrm{A})^{-1} - \alpha\eta_\mathrm{A}\right],$$

for which the rate constant (k) and the conversion (η_A) are given, whereas α is calculated. The inflow consists of A(= acetoxy propionate), thus $X_{0\mathrm{A}} = 1$.The factor δ_A gets the value

$$\delta_\mathrm{A} = \sum \frac{\nu_i}{(-\nu_\mathrm{A})} = \frac{-1+1+1}{-(-1)} = 1,$$

$$1 + x_{0\mathrm{A}}\delta_\mathrm{A} = 2.$$

At 500°C (=773 K), the rate constant becomes $k = 7.8 \times 10^9 \mathrm{e}^{-\left(\frac{19{,}220}{773}\right)}\,\mathrm{s}^{-1} = 0.124\,\mathrm{s}^{-1}$. The required conversion is $\eta_\mathrm{A} = 0.9$. We obtain

$$\tau = (0.124)^{-1}\ \mathrm{s}\left[2\ln(1-0.9)^{-1} - 0.9\right] = 29.88\ \mathrm{s}.$$

The space time is defined as $\tau = V/\dot{V}_0$. The inlet volumetric flow rate is calculated as follows. The ideal gas law tells us that $P_0\dot{V}_0 = \dot{n}_0 RT_0$, where the molar flow ($\dot{n}_0$) consists of pure A.

Consequently,

$$\dot{n}_0 = \frac{\dot{m}_{0\mathrm{A}}}{M_\mathrm{A}} = \frac{226.8\,\mathrm{kg\,mol}}{3600\,\mathrm{s} \times 146 \times 10^{-3}\,\mathrm{kg}} = 0.4315\,\mathrm{mol/s}.$$

The volumetric flow becomes

$$\dot{V}_0 = \frac{0.4315 \times 8.3143 \times 773}{5 \times 101.3 \times 10^3}\,\mathrm{m^3/s} = 5.4754 \times 10^{-3}\,\mathrm{m^3/s}\,(= 5.4754\,\mathrm{L/s}).$$

The reactor volume is $V = \dot{V}_0\tau = 5.4754 \times 10^{-3}\,\mathrm{m^3/s} \times 29.88\,\mathrm{s} = 0.1636\,\mathrm{m^3}$.

The reactor consists of the tube, that is, $V = \pi d^2/4\,L$, from where we obtain $L = 4V/\pi d^2$ and the required reactor length is obtained:

$$L = \frac{4 \times 0.1636\,\mathrm{m^3}}{\pi\left(36 \times 10^{-2}\right)^2\,\mathrm{m^2}} = 1.61\,\mathrm{m}.$$

b. The mean residence time is defined as

$$\bar{t} = \int_0^V \frac{\mathrm{d}V}{\dot{V}}.$$

This equation is solved using the conversion of A. The design equation is

$$\frac{\mathrm{d}\eta_\mathrm{A}}{\mathrm{d}V} = \frac{k(1-\eta_\mathrm{A})}{\dot{V}_0(1+\alpha\eta_\mathrm{A})}, \quad \text{that is,} \quad \frac{\mathrm{d}V}{\mathrm{d}\eta_\mathrm{A}} = \frac{\dot{V}_0(1+\alpha\eta_\mathrm{A})}{k(1-\eta_\mathrm{A})},$$

and we have $\dot{V} = \dot{V}_0(1+\alpha\eta_\mathrm{A})$. Consequently, $\mathrm{d}V/\dot{V}$ becomes $\dfrac{\mathrm{d}V}{\dot{V}} = \dfrac{(1+\alpha\eta_\mathrm{A})\mathrm{d}\eta_\mathrm{A}}{k(1-\eta_\mathrm{A})(1+\alpha\eta_\mathrm{A})}$ $= \dfrac{\mathrm{d}\eta_\mathrm{A}}{k(1-\eta_\mathrm{A})}$ and the very simple integral is obtained:

$$\bar{t} = \int_0^{\eta_\mathrm{A}} \frac{\mathrm{d}\eta_\mathrm{A}}{k(1-\eta_\mathrm{A})}.$$

The integral becomes $\bar{t} = k^{-1}\,\ln(1-\eta_\mathrm{A})^{-1}$ and we obtain the numerical value

$$\bar{t} = (0.124)^{-1}\,\mathrm{s}\,\ln\,(1-0.9)^{-1} = 18.6\,\mathrm{s}.$$

Observe that $\bar{t} < \tau\,(= V/\dot{V}_0)$ because $\dot{V}$ increases continuously inside the reactor tube.

c. For a batchwise operating autoclave, we have $\mathrm{d}c_\mathrm{A}/\mathrm{d}t = r_\mathrm{A} = -kc_\mathrm{A}$, which has the solution $c_\mathrm{A}/c_{0\mathrm{A}} = e^{-kt}$.

For a constant volume BR, $\eta_\mathrm{A} = (c_{0\mathrm{A}} - c_\mathrm{A})/c_{0A} = 1 - (c_\mathrm{A}/c_{0\mathrm{A}})$, and we insert η_A:

$$1 - \eta_\mathrm{A} = \mathrm{e}^{-kt},$$

giving $t = k^{-1}\,\ln(1-\eta_\mathrm{A})^{-1}$. This expression is calculated in case b and it gave $t = 18.6\,\mathrm{s}$.

The production capacity for a BR is given by $P_{BR} = \eta_A n_{0A}/(t + t_0)$, where t_0 is the time for refilling and cleaning. Provided that $t_0 \ll t$ we can neglect it.

For the continuous tube reactor, the production capacity is $P_{PFR} = \eta_A \dot{n}_{0A}$. In this case, $P_{PFR} = P_{BR}$ and we get formally $\eta_A n_{0A}/t = \eta_A \dot{n}_{0A}$, that is, $n_{0A} = \dot{n}_{0A} t$, where the initial amount is

$$n_{0A} = c_{0A} V_{BR} = x_{0A} c_0 V_{BR}.$$

The total concentration (c_0) is obtained from the ideal gas law, $P_0 = c_0 R T_0$. In the present case $x_{0A} = 1$ (pure reactant), and finally we obtain

$$c_0 V_{BR} = \dot{n}_{0A} t, \quad \text{that is, } V_{BR} = \frac{\dot{n}_{0A} t R T_0}{P_0}.$$

The BR volume becomes

$$V_{BR} = \frac{0.4315\,\text{mol} \times 18.569\,\text{s} \times 8.3143\,\text{J} \times 773\,\text{K m}^2}{\text{s mol K}\, 5 \times 101.3 \times 10^3\,\text{N}} = 0.10167\,\text{m}^3,$$

which gives the length $L = 1.0$ m.

A remark: de facto the volume ratio could be obtained in a straightforward manner from the space time and batch time ratio ($\tau = V_{BR}/\dot{V}_0$)

$$\frac{t_{BR}}{\tau} = \frac{V_{BR}}{V_{PFR}} = \frac{L_{BR}}{L_{PFR}}, \quad \text{that is, } L_{BR} = \frac{t_{BR}}{\tau} L_{PFR} = \frac{18.569\,\text{s}}{29.88\,\text{s}} \times 1.61\,\text{m} = 1.0\,\text{m}.$$

SECTION I/22

The reaction scheme is

$$\begin{array}{ccc} \text{A} & \xrightarrow{1} & \text{B} \\ \downarrow 2 & & \downarrow 3 \\ \text{C} & \xrightarrow{4} & \text{D} \end{array}$$

For a BR, a general component balance is written as

$$\frac{\mathrm{d}c_i}{\mathrm{d}t} = r_i.$$

The generation rates are obtained from $r_i = \sum \nu_{ij} R_J$:

$$r_A = -r_1 - r_2,$$
$$r_B = r_1 - r_4,$$
$$r_C = r_2 - r_3,$$
$$r_D = r_3 + r_4.$$

A first-order irreversible kinetics is assumed for each reaction

$$r_1 = k_1 c_\mathrm{A},$$
$$r_2 = k_2 c_\mathrm{A},$$
$$r_3 = k_3 c_\mathrm{C},$$
$$r_4 = k_4 c_\mathrm{B}.$$

The component balance equations become

$$\frac{\mathrm{d}c_\mathrm{A}}{\mathrm{d}t} = -(k_1 + k_2)c_\mathrm{A},$$
$$\frac{\mathrm{d}c_\mathrm{B}}{\mathrm{d}t} = k_1 c_\mathrm{A} - k_4 c_\mathrm{B},$$
$$\frac{\mathrm{d}c_\mathrm{C}}{\mathrm{d}t} = k_2 c_\mathrm{A} - k_3 c_\mathrm{C},$$
$$\frac{\mathrm{d}c_\mathrm{D}}{\mathrm{d}t} = k_3 c_\mathrm{C} + k_4 c_\mathrm{B}.$$

The first differential equation is easily solved by separation of variables

$$\int_{c_{0\mathrm{A}}}^{c_\mathrm{A}} \frac{\mathrm{d}c_\mathrm{A}}{c_\mathrm{A}} = -(k_1 + k_2)\int_0^t \mathrm{d}t \Rightarrow \ln\left(\frac{c_\mathrm{A}}{c_{0\mathrm{A}}}\right) = -(k_1 + k_2)t,$$

giving the reactant concentration $c_\mathrm{A} = c_{0\mathrm{A}}\mathrm{e}^{-(k_1+k_2)t}$. This is inserted into the second balance equation, which after a rearrangement obtains the form

$$\frac{\mathrm{d}c_\mathrm{B}}{\mathrm{d}t} + k_4 c_\mathrm{B} = k_1 c_{0\mathrm{A}}\mathrm{e}^{-(k_1+k_2)t}.$$

We denote $c_\mathrm{B} = y$ and $t = x$. The differential equation is of the type

$$y' + f(x)y = g(x), \quad \text{where } f(x) = k_4 \quad \text{and} \quad g(x) = k_1 c_{0\mathrm{A}}\mathrm{e}^{-(k_1+k_2)x}.$$

The general solution of a first-order differential equation is

$$y = \mathrm{e}^{-\int f\,\mathrm{d}x}\left(C + \int g(x)\mathrm{e}^{\int f\,\mathrm{d}x}\right),$$

where C is the integration constant.

The integrals become

$$\int f(x)\,\mathrm{d}x = \int k_4\,\mathrm{d}x = k_4 x,$$

$$\int g(x)\mathrm{e}^{\int f\,\mathrm{d}x}\,\mathrm{d}x = \int k_1 c_{0\mathrm{A}}\mathrm{e}^{-(k_1+k_2)x}\mathrm{e}^{k_4 x}\,\mathrm{d}x = k_1 c_{0\mathrm{A}}\int \mathrm{e}^{-(k_1+k_2-k_4)x}\,\mathrm{d}x$$

$$= \frac{k_1 c_{0\mathrm{A}}\mathrm{e}^{-(k_1+k_2-k_4)x}}{-(k_1+k_2-k_4)}.$$

Thus we have

$$y = C\mathrm{e}^{-k_4 x} + \frac{\mathrm{e}^{-k_4 x}\times k_1 c_{0\mathrm{A}}\mathrm{e}^{-(k_1+k_2-k_4)x}}{-(k_1+k_2-k_4)} \Rightarrow y = C\mathrm{e}^{-k_4 x} - \frac{k_1 c_{0\mathrm{A}}\mathrm{e}^{-(k_1+k_2)x}}{k_1+k_2-k_4}.$$

From the initial condition, $t(=x)=0, y(=c_{\mathrm{B}})=0$, the integration constant (C) can be determined:

$$0 = C\mathrm{e}^0 - \frac{k_1 c_{0\mathrm{A}}\mathrm{e}^0}{k_1+k_2-k_4}, \quad \text{which yields } C = \frac{k_1 c_{0\mathrm{A}}}{k_1+k_2-k_4}.$$

The solution for the concentration of B becomes $(y = c_{\mathrm{B}})$

$$c_{\mathrm{B}} = \left(\frac{k_1 c_{0\mathrm{A}}}{k_1+k_2-k_4}\right)\left(\mathrm{e}^{-k_4 t} - \mathrm{e}^{-(k_1+k_2)t}\right).$$

For component C, a separate derivation is not needed, since the balances of B and C are analogous, as shown in the table below.

The Balance of B	The Balance of C
k_1	k_2
k_2	k_1
k_4	k_3

Thus we directly obtain

$$c_{\mathrm{C}} = \left(\frac{k_2 c_{0\mathrm{A}}}{k_1+k_2-k_3}\right)\left(\mathrm{e}^{-k_3 t} - \mathrm{e}^{-(k_1+k_2)t}\right).$$

The maximum concentrations of c_{B} and c_C are obtained from the condition

$$f(t) = \mathrm{e}^{-\alpha t} - \mathrm{e}^{-\beta t}$$

(e.g., for c_{B}, $\alpha = k_4$ and $\beta = k_1 + k_2$).

The maximum is obtained at $f'(t) = 0$:

$f'(t) = -\alpha^{-\alpha t} + \beta e^{-\beta t} = 0$, that is, $\alpha^{-\alpha t} = \beta e^{-\beta t}$, which yields $\ln \alpha - \alpha t = \ln \beta - \beta t$.

We finally obtain $t_{\max}$,

$$t_{\max} = \frac{\ln(\alpha/\beta)}{\alpha - \beta}.$$

For B, we obtain $\alpha = k_4$ and $\beta = k_1 + k_2$, $\alpha = 0.012\,\mathrm{h}^{-1}$ and $\beta = 0.03\,\mathrm{h}^{-1}$:

$$t_{\max,\mathrm{B}} = \frac{\ln(0.012/0.03)}{0.012 - 0.03}\ \mathrm{min} = 50.905\ \mathrm{min}.$$

Analogously, the time of maximum C is

$$t_{\max,\mathrm{C}} = \frac{\ln(0.018/0.03)}{0.018 - 0.03}\ \mathrm{min} = 42.569\ \mathrm{min}.$$

The maximum concentrations of B and C are obtained by inserting the $t_{\max}$ values into the corresponding expressions for B and C.

The problem can be solved numerically using, for example, MATLAB®. The mass balances for each component are typed into an *m* file as shown below:

```
function ex_1_22

[x,y]=ode23(@alkylamine,[0 100],[1 0 0 0])
plot(x,y)
return

function dcdt=alkylamine(t,c)
% rate constant 1/h
k1=0.01;
k2=0.02;
k3=0.018;
k4=0.012;

cA=c(1);
cB=c(2);
cC=c(3);
cD=c(4);

% first order kinetics
r1=k1*cA;
r2=k2*cA;
```

```
r3=k3*cC;
r4=k4*cB;

%mass balances
dcdt(1,1)=-r1-r2;
dcdt(2,1)= r1-r4;
dcdt(3,1)= r2-r3;
dcdt(4,1)= r3+r4;
return
```

The numerical solution obtained is

Time (min)	c_A (mol/dm^3)	c_B (mol/dm^3)	c_C (mol/ dm^3)	c_D (mol/dm^3)
0	1.0000	0	0	0
0.0040	0.9999	0.0000	0.0001	0.0000
0.0240	0.9993	0.0002	0.0005	0.0000
0.1240	0.9963	0.0012	0.0025	0.0000
0.6240	0.9815	0.0062	0.0123	0.0001
1.6644	0.9513	0.0161	0.0320	0.0006
2.7182	0.9217	0.0257	0.0509	0.0017
3.9920	0.8871	0.0367	0.0726	0.0036
5.6527	0.8440	0.0502	0.0987	0.0070
7.7722	0.7920	0.0661	0.1290	0.0129
10.4342	0.7312	0.0839	0.1626	0.0223
13.7396	0.6622	0.1032	0.1978	0.0367
17.8143	0.5860	0.1231	0.2328	0.0581
22.8226	0.5042	0.1423	0.2648	0.0886
28.9900	0.4190	0.1595	0.2907	0.1308
36.6485	0.3330	0.1729	0.3067	0.1874
45.8897	0.2523	0.1802	0.3091	0.2584
55.8897	0.1868	0.1803	0.2980	0.3349
65.8897	0.1383	0.1751	0.2784	0.4081
75.8897	0.1024	0.1666	0.2544	0.4766
85.8897	0.0759	0.1561	0.2286	0.5395
95.8897	0.0562	0.1446	0.2029	0.5963
100.0000	0.0497	0.1397	0.1927	0.6180

The simulation result is displayed graphically in the figure below. The concentration maxima are very flat, which is beneficial for process operation: the reactor performance is not very sensitive to small fluctuations of the residence time.

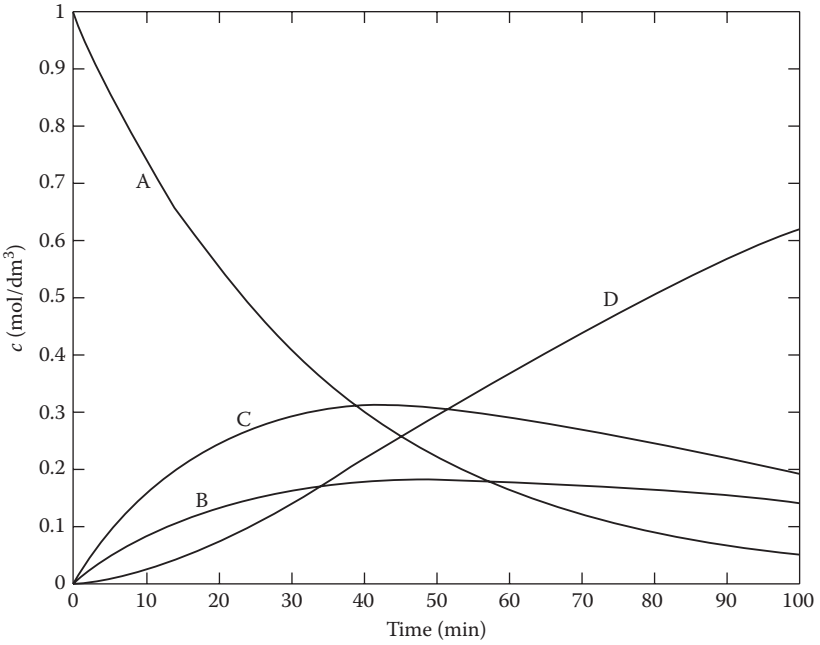

SECTION I/23

a. Case a

The oxidation of sulfur dioxide to sulfur trioxide follows the stoichiometry

$$2SO_2 + O_2 \leftrightarrows 2SO_3, \quad \text{that is, } 2A + B \leftrightarrows 2C.$$

The equilibrium constant is defined as $K_p = p_C^2/p_A^2 p_B$, provided that the ideal gas law can be applied—if this is not the case, fugacity coefficients would be included in the above expression.

For an ideal gas, the mole fraction and partial pressure are related by $p_i = x_i P$, where P is the total pressure. Thus, we obtain

$$K_p = \frac{x_C^2}{x_A^2 x_B} P^{-1}.$$

The initial mixture is stoichiometric, that is, $x_{0A} = 2x_{0B}$ (and $n_{0A} = 2n_{0B}$) and we obtain

$$\zeta = \frac{n_A - n_{0A}}{\nu_A} = \frac{n_B - n_{0B}}{\nu_B}, \quad \text{that is, } \frac{2n_{0B} - n_A}{2} = \frac{n_{0B} - n_B}{1} \Rightarrow n_B = \frac{n_A}{2},$$

which implies that $n_A = 2n_B$ throughout the reaction and, of course, also that $x_A = 2x_B$. In addition, for the mole fractions the general rule is valid

$$x_A + x_B + x_C = 1.$$

We obtain $2x_B + x_B + x_C = 1$, yielding $x_C = 1 - 3x_B$.

The equilibrium expression becomes

$$K_p P = \frac{(1 - 3x_B)^2}{4x_B^3}.$$

Below, we denote $4K_p P = K$ and $x_B = x$. A third-degree equation is obtained:

$$Kx^3 - (1 - 3x)^2 = 0,$$

from which the mole fraction (x) is solved. The value of K_p is calculated from

$$\log\left(\frac{K_p}{\text{atm}^{-1}}\right) = \frac{9910}{550 + 273} - 9.36 = 2.68131,$$

$$K_p P = 142{,}175.2715 = 0.142175 \times 10^6.$$

Equation $Kx^3 - (1 - 3x)^2 = 0$ is solved iteratively, for example, by the Newton–Raphson method:

$$f(x) = Kx^3 - (1 - 3x)^2,$$

$$f(x) = 3Kx^2 - 2(1 - 3x)(-3), \quad \text{that is,} \quad f'(x) = 3Kx^2 + 6(1 - 3x).$$

The algorithm is

$$x_{(k+1)} = x_{(k)} - \frac{f_{(k)}(x)}{f'_{(k)}(x)},$$

where k is the iteration index.

After a few iterations, the solution becomes

$$x = x_B = 0.0184,$$

$$x_A = 2x = 0.0368,$$

$$x_C = 0.9448.$$

The conversion of A is calculated from the definition

$$\eta_A = \frac{n_{0A} - n_A}{n_{0A}} = 1 - \frac{n_A}{n_{0A}} = 1 - \frac{x_A n}{x_{0A} n_0}.$$

The ratio between the total amounts is calculated from

$$\frac{n}{n_0} = 1 + x_{0A}\delta_A\eta_A, \quad \text{where} \quad \delta_A = \frac{\sum \nu_i}{-\nu_A}.$$

We denote $x_{0A}\delta_A$ by α and obtain $n/n_0 = 1 + \alpha\eta_A$, which is inserted into the definition of η_A:

$$\eta_A = 1 - \frac{x_A}{x_{0A}}(1 + \alpha\eta_A).$$

The equation has the solution

$$\eta_A = \frac{x_{0A}/x_A - 1}{\alpha + x_{0A}/x_A}.$$

The numerical values are

$$x_{0A} = \frac{2}{3} \quad \left(x_B = \frac{1}{3}\right),$$

$$x_A = 0.0368,$$

$$\frac{x_{0A}}{x_A} = 18.11594,$$

$$\alpha = x_{0A}\delta_A = \frac{2}{3}\frac{(-2 - 1 + 2)}{-(-2)} = -\frac{1}{3}.$$

Thus we obtain

$$\eta_A = \frac{18.11594 - 1}{-(1/3) + 18.11594} = 0.963.$$

The equilibrium conversion is high since the pressure is high. To compare the result, a comparative calculation is recommended, in which the nonideality of the gas mixture is taken into account.

b. Case b is solved exactly in the same manner as case a, but the value of the total pressure (P) is 100 kPa.

SECTION I/28

The dimerization reaction is given by

$$2A \leftrightarrows B.$$

The reaction rate is defined by

$$r = k_+ c_A^2 - k_- c_B.$$

With the aid of the molar flows, we obtain

$$r = \frac{k_+ \dot{n}_A^2}{\dot{V}^2} - k_- \frac{\dot{n}_B}{\dot{V}}.$$

The extent of reaction yields the relation between the molar amounts

$$\xi = \frac{\dot{n}_A - \dot{n}_{0A}}{\nu_A} = \frac{\dot{n}_B - \dot{n}_{0B}}{\nu_B}.$$

The feed contains no B, thus $\dot{n}_{0B} = 0$, and we obtain

$$\dot{n}_B = \frac{\nu_B}{\nu_A}(\dot{n}_A - \dot{n}_{0A}) = \frac{\nu_B}{-\nu_A}\dot{n}_{0A}\eta_A.$$

Furthermore, we obtain $\dot{n}_A = (1 - \eta_A)\dot{n}_{0A}$.

The update of the volumetric flow rate is $\dot{V} = \dot{V}_0(1 + x_{0A}\delta_A\eta_A)$, where $\delta_A = \sum \nu_i/\nu_A$.

The final form of the rate equation is

$$r = \frac{k_+(1 - \eta_A)^2\dot{n}_{0A}^2}{\dot{V}_0^2(1 + x_{0A}\delta_A\eta_A)^2} - \frac{k_-(\nu_B/-\nu_A)\eta_A\dot{n}_{0A}}{\dot{V}_0(1 + x_{0A}\delta_A\eta_A)}.$$

To simplify the notation, we introduce $\dot{n}_{0A}/\dot{V}_0 = c_{0A}$ and $x_{0A}\delta_A = \alpha$. Thus we obtain

$$r = \frac{k_+ c_{0A}^2(1 - \eta_A)^2}{(1 + \alpha\eta_A)^2} - \frac{k_-(\nu_B/-\nu_A)c_{0A}\eta_A}{1 + \alpha\eta_A}.$$

The mass balance of A is written as

$$\frac{\mathrm{d}\dot{n}_A}{\mathrm{d}V} = r_A = \nu_A r,$$

where $\dot{n}_A = (1 - \eta_A)\dot{n}_{0A}$ and $\mathrm{d}V = \dot{V}_0\mathrm{d}\tau$ ($\tau = V/\dot{V}_0$, the space time).

We obtain

$$-\frac{\mathrm{d}\eta_A}{\mathrm{d}\tau}\frac{\dot{n}_{0A}}{\dot{V}_0} = \nu_A r, \quad \text{that is,} \quad \frac{\mathrm{d}\eta_A}{\mathrm{d}\tau} = -\nu_A c_{0A}^{-1} r.$$

The rate expression is inserted giving the expression

$$\frac{\mathrm{d}\eta_A}{\mathrm{d}\tau} = -\nu_A\left[\frac{k_+ c_{0A}(1 - \eta_A)^2}{(1 + \alpha\eta_A)^2} - \frac{k_-(\nu_B/-\nu_A)\eta_A}{1 + \alpha\eta_A}\right]. \qquad [A]$$

This differential equation can be conveniently solved by numerical simulation from $\tau = 0$ toward higher τ values. The asymptotic value of η_A represents the equilibrium conversion.

The classical approach is possible, but cumbersome. We denote $-\nu_A k_+ c_0 A = \beta$ and $k_- \nu_B = \gamma$. The balance equation becomes

$$\frac{d\eta_A}{d\tau} = \frac{\beta(1-\eta_A)^2}{(1+\alpha\eta_A)^2} - \frac{\gamma\eta_A}{1+\alpha\eta_A},$$
$$\frac{d\eta_A}{d\tau} = \frac{\beta(1-\eta_A)^2 - \gamma\eta_A(1+\alpha\eta_A)}{(1+\alpha\eta_A)^2},$$

The separation of variables gives

$$\int_0^{\eta_A} \frac{(1+\alpha\eta_A)^2 d\eta_A}{\beta(1-\alpha\eta_A)^2 - \gamma\eta_A(1+\alpha\eta_A)} = \int_0^r d\tau = \tau. \qquad [B]$$

The integral on the left-hand side can be solved analytically or numerically.

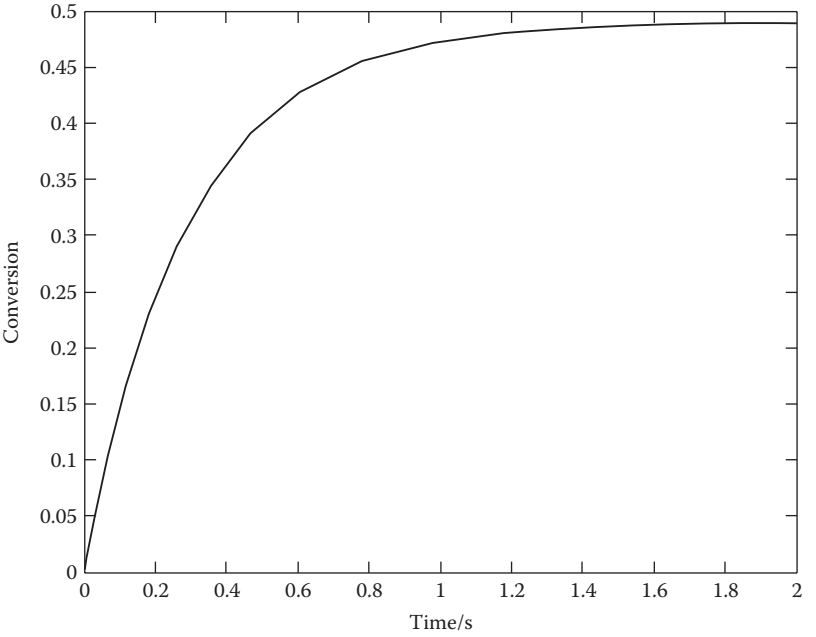

Numerical solution of Equation [A].

The results of the numerical solution of Equation [A] are displayed in the figure above, which shows that the equilibrium conversion is $\eta_A^* = 0.49$ and that the conversion $\eta_A = 0.45$ is obtained for $\tau = 0.7$ s.

The numerical values needed for the simulation are explained below.

The inlet concentration of A:$c_{0A} = x_{0A} \times c_0$, where $c_0 = P_0/RT_0$.

$$x_{0A} = 0.75 (x_{0,\text{water}} = 0.25; \text{ the molar ratio was } 3:1),$$
$$c_{0A} = 0.75 \cdot \frac{100 \times 10^3 \text{ Pa}}{8.3143 \text{ J/(K mol)}(638+273) \text{ K}} = 9.90187 \text{ mol/m}^3.$$

The inlet volumetric flow rate is calculated as follows:

$$P_0\dot{V}_0 = \dot{n}_0 RT_0,$$

$$\dot{V}_0 = \frac{\dot{n}_0 RT_0}{P_0} = \frac{9.0 \times 10^3 \text{ mol} \times 8.3143 \text{ J}(638 + 273) \text{ K}}{3600 \text{ s K mol} \times 100 \times 10^3 \text{ Pa}} = 0.189358 \text{ m}^3/\text{s}.$$

The reactor volume thus becomes $V = \dot{V}_0\tau$.

Time (s)	**η**
0	0
0.0000	0.0001
0.0003	0.0005
0.0014	0.0025
0.0072	0.0123
0.0302	0.0492
0.0678	0.1034
0.1187	0.1658
0.1828	0.2297
0.2610	0.2906
0.3554	0.3450
0.4691	0.3909
0.6074	0.4276
0.7793	**0.4548**
0.9793	0.4720
1.1793	0.4807
1.3793	0.4852
1.5793	0.4875
1.7793	0.4887
1.9793	0.4893
2.0000	0.4893

SECTION I/32

Styrene polymerization is carried out in a CSTR:

$$\text{A} \rightarrow \text{Polymer}.$$

The reaction rate is given by $r = kc_\text{A}$. The mass balance of A is

$$\frac{c_\text{A} - c_{0\text{A}}}{\tau} = r_\text{A}, \quad \text{where } r_\text{A} = \nu_\text{A} r.$$

The energy balance is given by

$$\frac{T - T_0}{\tau} = \frac{1}{c_p \rho_0} \left(r\,(-\Delta H_r) - \frac{UA}{V}\,(T - T_C) \right).$$

For adiabatic operation, we have $U = 0$.
Division of the mass and energy balances yields

$$\frac{c_A - c_{0A}}{T - T_0} = \frac{\nu_A r c_p \rho_0}{r(-\Delta H_r)}, \quad \text{that is,}$$
$$\frac{T - T_0}{c_{0A} - c_A} = \frac{-\Delta H_r}{-\nu_A c_p \rho_0}, c_{0A} - c_A = c_{0A}\eta_A,$$
$$T - T_0 = \frac{(-\Delta H_r) c_{0A} \eta_A}{-\nu_A c_p \rho_0},$$

which de facto gives the adiabatic temperature change $\Delta T_{ad} = T - T_0$.
From the experimental data, ΔT_{ad} is obtained and the parameter β becomes

$$\beta = \frac{(-\Delta H_r)\, c_{0A}}{-\nu_A c_p \rho_0} = \frac{T - T_0}{\eta_A} = \frac{400\,\text{K}}{1} = 400\,\text{K}.$$

We thus have in general $T = T_0 + \beta\eta_A$.
The reactor performance is calculated from the mass balance

$$\frac{c_A - c_{0A}}{\tau} = r_A = \nu_A r = -k c_A.$$

We insert $\eta_A = (c_{0A} - c_A)/c_{0A}$ and obtain

$$\frac{c_{0A}\eta_A}{\tau} = k(1 - \eta_A)c_{0A}, \quad \text{that is, } \eta_A = k\tau(1 - \eta_A).$$

The temperature dependence of the rate constant k is inserted:

$$k = A e^{-(E_a/RT)}, \text{ where } T = T_0 + \beta\eta_A.$$

Finally, we have

$$\eta_A - A\tau e^{-(E_a/R(T_0+\beta\eta_A))}(1 - \eta_A) = 0,$$

which is solved iteratively by using the following numerical values:

$$A\tau = 10^{10}\,\text{h}^{-1} \times 2\,\text{h} = 2 \times 10^{10},$$
$$E_a/R = 10{,}000\,\text{K},$$

$$T_0 = 573\,\text{K},$$
$$\beta = 400\,\text{K}.$$

The iterative solution gives $\eta_A = 0.999$ and consequently $T = T_0 + \beta\eta_A = 973\,\text{K}$.

The temperature exceeds the allowable maximum (450 K). Hence a cooling device is required.

b. If the polymerization is carried out at $T = 413\,\text{K}$, the conversion can be calculated from the balance equation $(c_A - c_{0A})/\tau = r_A$, which in this case becomes

$$\frac{c_{0A}\eta_A}{\tau} = k(1-\eta_A)c_{0A}, \quad \text{that is, } \eta_A = k\tau(1-\eta_A)$$

yielding

$$(1+k\tau)\eta_A = k\tau \Rightarrow \eta_A = \frac{k\tau}{1+k\tau}.$$

The rate constant attains the value

$$k = 10^{10}\text{e}^{-10{,}000/413}\,\text{h}^{-1} = 0.305\,\text{h}^{-1},$$
$$k\tau = 0.305 \times 2 = 0.6101$$

and we obtain

$$\eta_A = \frac{0.6101}{1+0.6101} = 0.3789.$$

The cooling jacket temperature is obtained from the energy balance

$$r(-\Delta H_r) - \frac{UA}{V}(T - T_C) = \frac{c_p\rho_0(T-T_0)}{\tau}, \quad \text{that is, } V = \dot{V}_0\tau,$$
$$\frac{UA}{\dot{V}_0\tau}(T - T_C) = r\,(-\Delta H_r) - \frac{c_p\rho_0}{\tau}(T - T_0).$$

The balance is manipulated further to get the parameter, $\alpha = UA/\rho_0 c_p \dot{V}_0$, involved:

$$\frac{UA}{\rho_0 c_p \dot{V}_0}\left(\frac{T - T_C}{\tau}\right) = \frac{kc_{0A}\,(-\Delta H_r)\,(1-\eta_A)}{\rho_0 c_p} - \frac{T - T_0}{\tau},$$
$$\frac{UA}{\rho_0 c_p \dot{V}_0} = \alpha, \quad \text{and} \quad \frac{-\Delta H_r c_{0A}}{\rho_0 c_p} = \beta; \text{ in this case } (-\nu_A = 1).$$

Thus we have

$$\frac{\alpha(T - T_C)}{\tau} = k\beta(1 - \eta_A) - \frac{(T - T_0)}{\tau}, \text{ which yields } T - T_C:$$

$$T - T_C = \frac{k\tau\beta\,(1 - \eta_A)}{\alpha} - \frac{(T - T_0)}{\alpha}.$$

The numerical values are inserted:

$$T - T_C = \frac{0.6101 \cdot 400 \cdot (1 - 0.3789)\,\mathrm{K}}{50} - \frac{(413 - 300)}{50} = 0.77146\,\mathrm{K},$$

$$T_C = T - 0.77146\,\mathrm{K} = 412\,\mathrm{K}.$$

For a lower value of a, namely $\alpha = 10$, we obtain $T - T_C = 3.8573\,\mathrm{K}$, which gives the coolant temperature $T_C = 409.14\,\mathrm{K}$.

SECTION I/39

The reaction

$$\mathrm{A} \rightarrow \mathrm{B} + 2\mathrm{C}$$

proceeds in a pressurized vessel with a constant volume. The balance of A is

$$\frac{\mathrm{d}c_A}{\mathrm{d}t} = r_A.$$

We assume first-order kinetics, $r_A = -kc_A$, yielding

$$\frac{\mathrm{d}c_A}{\mathrm{d}t} = -kc_A,$$

which has the solution

$$\frac{c_A}{c_{0A}} = \mathrm{e}^{-kt}. \qquad [A]$$

The concentration of A is related to the total pressure via the relation

$$\frac{P}{P_0} = 1 + x_{0A}\delta_A\eta_A,$$

where $\delta_A = \sum \nu_i/(-\nu_A)$, and η_A is the conversion, defined here as (V = constant)

$$\eta_A = \frac{c_{0A} - c_A}{c_{0A}} = 1 - \frac{c_A}{c_{0A}}.$$

The mole fraction $x_{0A} = 1$ in this case since a pure reactant was used.

$$\delta_A = \frac{-1+1+2}{-(-1)} = 2.$$

We obtain for $\frac{P}{P_0} = 1 + 2\eta_A = 1 + 2 - 2\frac{c_A}{c_{0A}}$,

$$\frac{P}{P_0} = 3 - 2\frac{c_A}{c_{0A}},$$

which yields $\frac{c_A}{c_{0A}} = \frac{(3 - P/P_0)}{2}$, which is inserted into the exponential expression [A]

$$\frac{3 - P/P_0}{2} = e^{-kt}.$$

After taking the logarithm, we have

$$-\ln\left(\frac{3 - P/P_0}{2}\right) = kt,$$

which has the form $y = kx$, where $y = -\ln((3 - P/P_0)/2)$ and $x = t$.

The transformed data are listed in the table below:

$t/\text{min} = x$	$-\ln\left(\frac{3-P/P_0}{2}\right) = y$
0	0
2.5	0.2231
5	0.40797
10	0.8097
15	1.1874
20	1.5847

A plot of y versus x is linear and gives the slope $\approx 0.08\ \text{min}^{-1}$. The slope is equal to the rate constant k.

For the tube reactor, isothermal plug flow conditions are assumed. The mass balance of A is

$$\frac{d\dot{n}}{dV} = r_A = -kc_A = -k\frac{\dot{n}}{\dot{V}}.$$

The balance is written with the conversion of A; $\dot{n}_A = (1 - \eta_A)\dot{n}_{0A} \Rightarrow \frac{d\dot{n}}{dV} = -\dot{n}_{0A}\frac{d\eta_A}{dV}$.

For the volumetric flow rate we have $\dot{V} = \dot{V}_0(1 + x_{0A}\delta_A\eta_A)$, $\quad \delta_A = \frac{\sum \nu_i}{-\nu_A}$.

The balance becomes

$$\frac{\mathrm{d}\eta_\mathrm{A}}{\mathrm{d}V}\dot{n}_{0\mathrm{A}} = \frac{k(1-\eta_\mathrm{A})\dot{n}_{0\mathrm{A}}}{\dot{V}_0(1+x_{0\mathrm{A}}\delta_\mathrm{A}\eta_\mathrm{A})}.$$

The relation $V/\dot{V}_0$ is denoted by τ,

$$\mathrm{d}V = \dot{V}_0\mathrm{d}\tau,$$

and the balance is simplified to

$$\frac{\mathrm{d}\eta_\mathrm{A}}{\mathrm{d}\tau} = \frac{k(1-\eta_\mathrm{A})}{1+x_{0\mathrm{A}}\delta_\mathrm{A}\eta_\mathrm{A}}.$$

We denote $x_{0\mathrm{A}}\delta_\mathrm{A} = \alpha$ and separate the variables

$$\int_0^{\eta_\mathrm{A}} \frac{1+\alpha\eta_\mathrm{A}}{1-\eta_\mathrm{A}}\,\mathrm{d}\eta_\mathrm{A} = k\int_0^{\tau}\mathrm{d}\tau = k\tau.$$

The integration of the left-hand side is carried out as follows:

$$\frac{1+\alpha\eta_\mathrm{A}}{1-\eta_\mathrm{A}} = \frac{1}{1-\eta_\mathrm{A}} + \frac{\alpha\,(\eta_\mathrm{A}-1+1)}{1-\eta_\mathrm{A}} = \frac{1}{1-\eta_\mathrm{A}} - \alpha + \frac{\alpha}{1-\eta_\mathrm{A}} = \frac{\alpha+1}{1-\eta_\mathrm{A}} - \alpha.$$

The integral becomes

$$\begin{aligned}\int_0^{\eta_\mathrm{A}} \frac{(\alpha+1)}{1-\eta_\mathrm{A}}\,\mathrm{d}\eta_\mathrm{A} - \alpha\int_0^{\eta_\mathrm{A}}\mathrm{d}\eta_\mathrm{A} &= (\alpha+1)\Big/_0^{\eta_\mathrm{A}} - \ln(1-\eta_\mathrm{A}) - \alpha\Big/_0^{\eta_\mathrm{A}}\eta_\mathrm{A} \\ &= (\alpha+1)\ln(1-\eta_\mathrm{A})^{-1} - \alpha\eta_\mathrm{A} = k\tau,\end{aligned}$$

from which $\tau = V_\mathrm{k}/\dot{V}_0$ is solved:

$$\tau = k^{-1}[(1+x_{0\mathrm{A}}\delta_\mathrm{A})\ln(1-\eta_\mathrm{A})^{-1} - (1+x_{0\mathrm{A}}\delta_\mathrm{A})\eta_\mathrm{A}].$$

The conversion (η_A) would be equal to that obtained from the BR after 20 min reaction:

$$\begin{aligned}&\frac{c_\mathrm{A}}{c_{0\mathrm{A}}} = \mathrm{e}^{-kt}, \quad \eta_\mathrm{A} = 1 - \frac{c_\mathrm{A}}{c_{0\mathrm{A}}}, \\ &\eta_\mathrm{A} = 1 - \mathrm{e}^{-0.08\times 20} = 0.7981, \\ &1 + x_{0\mathrm{A}}\delta_\mathrm{A} = 1 + 2 = 3, \\ &1 - \eta_\mathrm{A} = 0.2019, \\ &\tau = 0.08^{-1}\ \mathrm{min}[3\ \ln\,(0.2019)^{-1} - 3\times 0.7981] = 30.07\ \mathrm{min}.\end{aligned}$$

$V_k/\dot{V}_0 = 30$ min is required to achieve the conversion in the tube reactor. The space time is longer than that in an autoclave, because the volumetric rate increases the reactor. Neglecting

the change in the volumetric flow rate, $\dot{V}(\delta = 0)$ would give the very erroneous result $\tau_{error} = V_k/\dot{V}_0 = 20$ min.

SECTION I/42

Except for the small time delay at the beginning, the data resemble pulse experiments from a CSTR. This is why the model of complete backmixing is tried. The function $E(t)$ is defined for a CSTR:

$$E(t) = \frac{e^{-t/\bar{t}}}{\bar{t}}.$$

The actual data are proportional to $E(t)$; the signal is $S = \alpha E(t)$, where α is a calibration constant. Thus we obtain

$$S = \frac{\alpha e^{-t/\bar{t}}}{\bar{t}},$$

which yields

$$\ln(S) = \ln\left(\frac{\alpha}{\bar{t}}\right) - \frac{t}{\bar{t}},$$

that is,

$$-\ln(S) = \frac{t}{\bar{t}} - \ln\left(\frac{\alpha}{\bar{t}}\right).$$

By plotting $-\ln(S)$ versus t, a straight line is obtained, if the data follow the backmixing model. The inverse of the slope gives the mean residence time (the slope $= 1/\bar{t}$). The value of ln (S) is directly available from the figure. From the figure, the following table is compiled:

t (s)	S (mm)	$\ln(S) = \ln[\alpha E(t)]$
600	35	3.555
1200	26	3.258
1800	17.4	2.856
2400	12.2	2.5014
3000	8.5	2.14
3600	6.2	1.8245
4200	4.5	1.504

The plot $-\ln(S)$ versus t is provided by the figure below. As shown in the figure, it provides a fairly good straight line. The slope is $1/\bar{t} = 0.005933\,s^{-1}$, which gives $\bar{t} = 1685\,s = 28.1$ min.

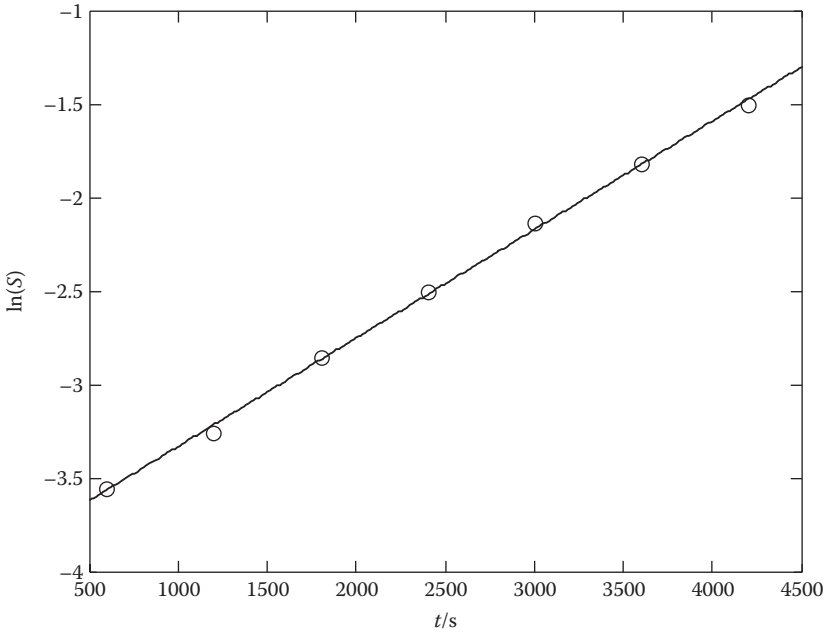

SECTION I/43

The notations displayed in the figure below are introduced for the reaction system.

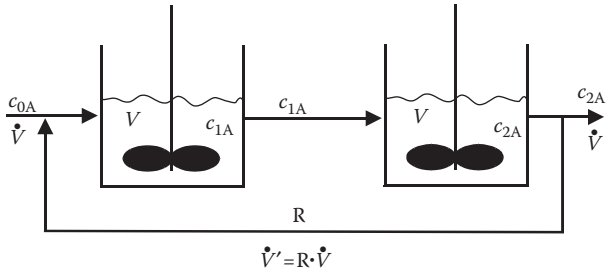

The balance for the first reactor is (an inert tracer is introduced, thus $r_A = 0$)

$$c_{0A}\dot{V} + c_{2A}R\dot{V} = c_{1A}(1+R)\dot{V} + V\frac{dc_{1A}}{dt}.$$

Analogously, for the second reactor, we have

$$c_{1A}\dot{V}(1+R)\dot{V} = c_{2A}(1+R)\dot{V} + V\frac{dc_{2A}}{dt}.$$

Since the inert was added pulsewise, not stepwise, the concentration $c_{0A} = 0$. In addition, we denote $V/\dot{V} = \tau$. The balance equations become

$$\frac{dc_{1A}}{dt} = \frac{c_{2A}R}{\tau} - \frac{c_{1A}(1+R)}{\tau},$$
$$\frac{dc_{2A}}{dt} = \frac{c_{1A}(1+R)}{\tau} - \frac{c_{2A}(1+R)}{\tau}.$$

By introducing a dimensionless time $\theta = t/\tau$, we obtain

$$\frac{dc_{1A}}{d\theta} = -(1+R)c_{1A} + Rc_{2A},$$
$$\frac{dc_{2A}}{d\theta} = (1+R)(c_{1A} - c_{2A}).$$

The Laplace transformation is applied:

$$L\left(\frac{dc_{1A}}{d\theta}\right) = sC_1 - c_{1A}(0),$$
$$L\left(\frac{dc_{2A}}{d\theta}\right) = sC_2 - c_{2A}(0),$$

where C_1 and C_2 are the Laplace transforms of c_{1A} and c_{2A}, respectively. Furthermore, $c_{2A}(0) = 0$ and we denote $c_{1A}(0) = C_0$. The transforms become

$$sC_1 - C_0 = -(1+R)C_1 + RC_2,$$
$$sC_2 = (1+R)(C_1 - C_2),$$

and C_1 and C_2 are solved:

$$\frac{C_2}{C_1} = \frac{(1+R)}{s+1+R},$$
$$\frac{C_1}{C_0} = \frac{s+1+R}{(s+1)^2 + R(2s+1)},$$

yielding C_2/C_0:

$$\frac{C_2}{C_0} = \frac{1+R}{(s+1)^2 + R(2s+1)},$$

which is rewritten as

$$\frac{C_2}{C_0} = \frac{1+R}{s^2 + 2s(R+1) + R + 1}.$$

We introduce $R + 1 = \alpha$ and obtain

$$\frac{C_2}{C_0} = \frac{1 + R}{\left(s + \alpha + \sqrt{\alpha(\alpha - 1)}\right)\left(s + \alpha - \sqrt{\alpha(\alpha - 1)}\right)}.$$

An inverse Laplace transformation yields

$$\frac{C_2(\theta)}{C_0} = \frac{\alpha}{2\surd}\left(\mathrm{e}^{(-\alpha+\surd)\theta} - \mathrm{e}^{(-\alpha-\surd)\theta}\right), \qquad [\mathrm{A}]$$

where $\alpha = R + 1$ and $\surd = \sqrt{\alpha(\alpha - 1)} = \sqrt{R(R + 1)}$.

The pulse has a maximum, which is obtained by the differentiation of the function $C_2(\theta)/C_0$. In this case, it is sufficient to consider the function

$$f(\theta) = e^{(-\alpha+\surd)\theta} - e^{(-\alpha-\surd)\theta}.$$

Differentiation of $f(\theta)$ with θ and setting $f'(\theta) = 0$ finally yield

$$\theta_{\max} = \frac{\ln((R + 1 + \sqrt{R(R + 1)})/(R + 1 - \sqrt{R(R + 1)}))}{2\sqrt{R(R + 1)}}.$$

For instance, for $R = 1$ we obtain

$$\theta_{\max} = \frac{\ln\left(\left(2 + \sqrt{2}\right)\Big/\left(2 - \sqrt{2}\right)\right)}{2\sqrt{2}} = 0.623,$$

which can be substituted in Equation [A] to yield the maximum value of $C_2(\theta)/C_0$.

For $R = 1$ we obtain $\alpha = 2$ and $\sqrt{R(R + 1)} = \sqrt{2}$. Equation [A] becomes

$$\frac{C_2(\theta)}{C_0} = \frac{1}{\sqrt{2}}\left(\mathrm{e}^{\left(-2+\sqrt{2}\right)\theta} - \mathrm{e}^{\left(-2-\sqrt{2}\right)\theta}\right).$$

A simulated plot $C_2(\theta)/C_0$ versus θ is shown below.

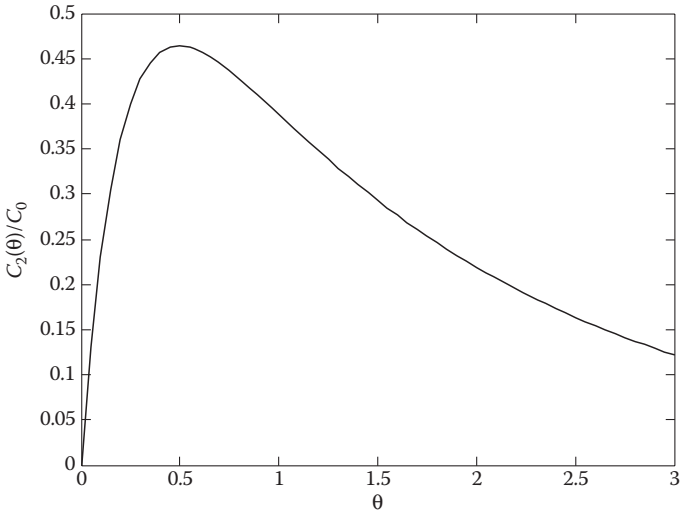

SECTION I/49

The reaction is A + B → C. For a CSTR, a dynamic balance equation can be written as (V = constant)

$$c_{0A}\dot{V} + r_A V = c_A\dot{V} + V\frac{dc_A}{dt}.$$

We denote $V/\dot{V} = \tau$, which after rearrangement gives

$$\frac{dc_A}{dt}\tau = c_{0A} - c_A + r_A\tau.$$

By introducing a dimensionless term $\theta = t/\tau$, we yield

$$\frac{dc_A}{d\theta} = c_{0A} - c_A + r_A\tau.$$

The reaction rate is obtained from

$$R = kc_Ac_B.$$

Since equimolar amounts were used, $c_A = c_B$. Thus $r_A = \nu_A R = -kc_Ac_B = -kc_A^2$ in this case. The rate expression is inserted into the balance equation, which becomes

$$\frac{dc_A}{d\theta} = c_{0A} - c_A + k\tau c_A^2.$$

The differential equation is solved by separation of variables and integration:

$$\int_{c_A(0)=0}^{c_A} \frac{dc_A}{k\tau c_A^2 + c_A - c_{0A}} = -\int_0^{\theta} d\theta = -\theta.$$

The integral on the left-hand side is of the type

$$\int \frac{dx}{ax^2 + bx + c}, \quad \text{where } x = c_A,\ a = k\tau,\ b = 1, \text{ and } c = -c_{0A},$$

which is a standard case having the solution

$$\frac{1}{\sqrt{b^2 - 4ac}} \Big/_{x=0}^{x=c_A} \ln\left[\frac{\sqrt{b^2 - 4ac} - b - 2ax}{\sqrt{b^2 - 4ac} + b + 2ax}\right] = -\theta.$$

The physical quantities are inserted:

$$\ln\left[\frac{(\sqrt{1 + 4kc_{0A}\tau} - 1 - 2k\tau c_A)(\sqrt{1 + 4kc_{0A}\tau} + 1)}{(\sqrt{1 + 4kc_{0A}\tau} - 1 + 2k\tau c_A)(\sqrt{1 + 4kc_{0A}\tau} - 1)}\right] = -\sqrt{1 + 4kc_{0A}\tau}\,\theta.$$

We denote $\surd + 1 = \alpha$ and $\surd - 1 = \beta$ and obtain

$$\ln\left[\frac{\alpha(\beta - 2k\tau c_A)}{\beta(\alpha + 2k\tau c_A)}\right] = -\surd\theta, \quad \text{that is,} \quad \frac{\alpha(\beta - 2k\tau c_A)}{\beta(\alpha + 2k\tau c_A)} = e^{-\surd\theta}.$$

From the above equation, c_A is solved after some straightforward algebraic manipulations:

$$c_A = \frac{\beta\left(1 - e^{-\surd\theta}\right)}{2k\tau\left(1 + (\beta/\alpha)e^{-\surd\theta}\right)}, \quad \text{where} \quad \surd = \sqrt{1 + 4kc_{0A}\tau} \quad \text{and,}$$

$$\alpha = \surd{+1} \quad \text{and} \quad \beta = \surd{-1}.$$

In the Damköhler space, $Da = kc_{0A}\tau$, the result can be presented in an elegant way:

$$\frac{c_A}{c_{0A}} = \frac{(\surd - 1)\left(1 - e^{-\surd\theta}\right)}{Da\left[1 + \left((\surd - 1)/(\surd + 1)\right)e^{-\surd\theta}\right]}, \quad \text{where} \quad \surd = \sqrt{1 + Da}.$$

It should be noted that the solution is compressed to

$$\frac{c_A}{c_{0A}} = \frac{\surd - 1}{Da}$$

at steady state, that is, to a solution that can be obtained directly from the steady-state model $c_{0A} - c_A + r_A\tau = 0$, $r_A = -kc_A^2$.

SECTION I/51

The reaction is A → B + C. The first-order Damköhler number is $Da = k\bar{t}$, where $\bar{t} = V/\dot{V}$, and we obtain

$$k\bar{t} = 0.1\,\text{min}^{-1} \times 0.5\,\text{dm}^3/0.025\,\text{dm}^3/\text{min} = 2.$$

For turbulent conditions, the plug flow model is used, yielding

$$\frac{c_\text{A}}{c_{0\text{A}}} = \text{e}^{-k\bar{t}} = \text{e}^{-2} = 0.135,$$

$$\eta_\text{A} = 1 - \frac{c_\text{A}}{c_{0\text{A}}} = 0.865.$$

For laminar conditions, the laminar flow model should be applied. The simplest one, laminar flow without radial diffusion, gives for first-order reactions

$$\frac{c_\text{A}}{c_{0\text{A}}} = 4\int_0^1 \text{e}^{(-k\bar{t}/2(1-x^2))}(1-x^2)x\,\text{d}x.$$

The result is readily calculated. See Figure 4.38 Section 4.6, which gives for $k\bar{t} = 2$, $c_\text{A}/c_{0\text{A}} = 0.206$, for the laminar flow model. The conversion becomes $\eta_\text{A} = 1 - c_\text{A}/c_{0\text{A}} = 0.794$. The laminar flow model gives a lower conversion than the plug flow model.

SECTION I/53

The stoichiometry is

$$\text{S} \rightarrow \text{P}$$

and the kinetics is determined by

$$r = \frac{kKc_\text{E}c_\text{S}}{1 + Kc_\text{S}}.$$

The product kKc_E is constant and denoted by $\alpha = kKc_E$ below. Thus, for the substrate, we obtain

$$r_\text{S} = -\frac{\alpha c_\text{S}}{1 + Kc_\text{S}}.$$

The segregation model gives the average concentration $\bar{c}_\text{S}$:

$$\bar{c}_\text{S} = \int_0^\infty c_{\text{S,B}}(t)E(t)\,\text{d}t, \qquad \text{[A]}$$

where $c_{\text{S,B}}$ is obtained from the BR model

$$\frac{\text{d}c_{\text{S,B}}}{\text{d}t} = r_\text{S}.$$

For simplicity, we denote $c_{S,B} = c_S$. The BR model becomes

$$\frac{dc_S}{dt} = -\frac{\alpha c_S}{1 + Kc_S}.$$

Separation of the variables gives

$$-\int_{c_{0S}}^{c_S} \frac{1 + Kc_S}{c_S}\, dc_S = \alpha \int_0^t dt,$$

which is equivalent to

$$-\int_{c_{0S}}^{c_S} \frac{dc_S}{c_S} - \int_{c_{0S}}^{c_S} K\, dc_S = dt,$$

that is,

$$-\ln\left(\frac{c_S}{c_{0S}}\right) + K\,(c_{0S} - c_S) = \alpha t,$$

$$Kc_{0S}\left(1 - \frac{c_S}{c_{0S}}\right) - \ln\left(\frac{c_S}{c_{0S}}\right) = \alpha t, \qquad [B]$$

from which $c_S/c_{0S}(= c_{S,B}/c_{0S})$ can be solved iteratively for each reaction time (t). The $E(\theta)$ function for the tanks-in-series model $(j = 2)$ is

$$E(\theta) = \frac{j^j}{(j-1)!}\theta^{j-1}e^{-j\theta} = 4\theta e^{-2\theta}.$$

Also, we have the relation (Table 4.1)

$$E(t) = \frac{E(\theta)}{\bar{t}},$$

$$E(t) = \frac{4t}{\bar{t}^2}e^{-2(t/\bar{t})},$$

which is inserted into Equation [A]

$$\bar{c}_S = \frac{4}{\bar{t}^2}\int_0^\infty c_S(t)te^{-2(t/\bar{t})}\, dt$$

and transformed to a dimensionless form

$$\frac{\bar{c}_S}{c_{0S}} = \frac{4}{\bar{t}^2}\int_0^\infty \left(\frac{c_S(t)}{c_{0S}}\right)te^{-2(t/\bar{t})}\, dt. \qquad [C]$$

We introduce the dimensionless quantities $y = c_S(t)/c_{0S}$ and $\bar{y} = \bar{c}/c_{0S}$. The final equations become ($\beta = Kc_{0S}$)

$$\beta(1 - y) - \ln(y) - \alpha t = 0, \qquad [D]$$

$$\bar{y} = \frac{4}{\bar{t}^2} \int_0^\infty yt e^{-2(t/\bar{t})}\, dt. \qquad [E]$$

The parameter values are

$$\alpha = kKc_E = 0.01\,\text{min}^{-1} 2.0\,\text{dm}^3/\text{mol} \cdot 1.0\,\text{mol/dm}^3 = 0.02\,\text{min}^{-1},$$

$$\beta = Kc_{0S} = 2\,\text{dm}^3/\text{mol} \cdot 3.0\,\text{mol/dm}^3 = 6,$$

$$4/\bar{t}^2 = 4/100\,\text{min}^2 = 0.04\,\text{min}^{-2}.$$

The value of $y(= c_{S,B}/c_{0S})$ versus t is displayed in the figure below (Equation [D]).

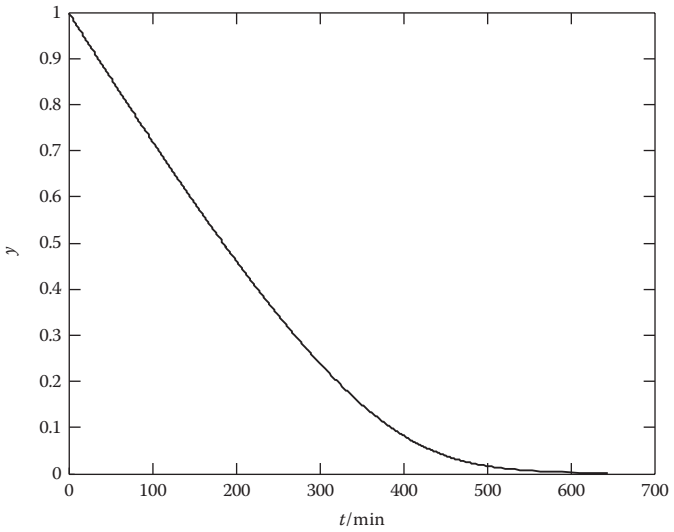

Numerical integration of Equation [E] yields $\bar{y}(= \bar{c}_S/c_{0S}) = 0.9519$.

SECTION I/57

The second-order reaction is

$$A + B \rightarrow C.$$

The flow type is obtained by calculating the Reynolds number, $Re = wd/\nu$. The average velocity (w) is

$$w = \frac{L}{\bar{t}} = \frac{120\,\text{cm}}{36\,\text{s}} = 0.0333\,\text{m/s}.$$

The kinematic viscosity is $\nu = \mu/\rho$:

$$\nu = \frac{1.5\,\text{cP}}{1.25\,\text{kg/dm}^3} = \frac{1.5 \times 10^{-2} \times 0.1\,\text{Nsm}^{-2} \times 10^{-3}\,\text{m}^3}{1.25\,\text{kg}} = 1.2 \times 10^{-6}\,\text{m}^2/\text{s}.$$

The Reynolds number becomes ($d = 5 \cdot 10^{-2}$ m)

$$Re = \frac{0.0333\,\text{m/s} \times 5 \times 10^{-2}\,\text{m}}{1.2 \times 10^{-6}\,\text{m}^2/\text{s}} = 1389.16.$$

The conclusion is that $Re < 2000$ indicating a laminar flow.
The axial dispersion coefficient is thus calculated from

$$D = D_\text{m} + \frac{w^2 d^2}{192\,D_\text{m}},$$

where $D_\text{m} = 0.8 \times 10^{-8}\,\text{m}^2/\text{s}$ for both A and B. We obtain

$$D = \left(0.8 \times 10^{-8} + \frac{0.0333^2 (5 \times 10^{-2})^2}{192 \times 0.8 \times 10^{-8}}\right) \text{m}^2/\text{s} = 1.808\,\text{m}^2/\text{s}.$$

The axial Peclet number becomes

$$Pe = \frac{wL}{D}, \quad Pe = \frac{0.0333\,\text{m/s} \times 1.2\,\text{m}}{1.808\,\text{m}^2/\text{s}} = 0.022,$$

which is very low.
The dimensionless Damköhler number is

$$R = k\bar{t} c_{0\text{A}} \left(\frac{\nu_\text{B}}{\nu_\text{A}}\right),$$

$$R = \frac{1.2\,\text{dm}^3}{\text{mol min}} \frac{36}{60} \text{min}\, 10 \frac{\text{mol}}{\text{dm}^3} \left(\frac{-1}{-1}\right) = 7.2.$$

Parameter $M = \nu_\text{A} c_{0\text{B}}/\nu_\text{B} c_{0\text{A}} = 1$ in this case.
The reactor performance can now conveniently be calculated from Figure 4.34 (Section 4.5.2). We obtain ($y = c_\text{A}/c_{0\text{A}}$)

$$y_\text{D} = 0.3,$$

$$y_\text{SD} - y_\text{D} = -0.064,$$

$$y_\text{MD} - y_\text{D} = +0 \text{ (very close to 0 but positive)}.$$

Thus we have

$$y_D = c_{AD}/c_{0A} = 0.3 \text{ (axial dispersion model)},$$
$$y_{SD} = c_{ASD}/c_{0A} = 0.236 \text{ (segregated axial dispersion model)},$$
$$y_{MD} = c_{AMD}/c_{0A} \geq 0.3 \text{ (maximum mixed axial dispersion model)}.$$

In general, for reaction orders $\geq 1, y_{SD} < y_D < y_{MD}$ and consequently, $\eta_{MD} < \eta_D < \eta_{SD}$ ($\eta = 1 - y$).

The segregated model predicts the highest conversion for reaction orders ≥ 1.

SECTION II/1

Catalytic dehydrogenation of ethylbenzene

$$E \rightarrow S + H,$$

where E = ethylbenzene, S = styrene, and H = hydrogen (H_2).

The reaction rate is given by

$$r = k\left(\frac{p_E - p_S p_H}{K}\right).$$

The generation rate of ethylbenzene is

$$r_E = \nu_E r = -r,$$

and the mass balance for the key component (E) in the fixed bed is written as

$$\frac{d\dot{n}_E}{dV} = r_E \rho_B.$$

The ideal gas law is applied ($P_0 = 121$ kPa, which is a low value) and the partial pressures in the rate equation can thus be replaced by concentrations. The relation $p_i = c_i RT$ is valid and we obtain

$$r = k\left(c_E RT - \frac{c_S c_H (RT)^2}{K}\right).$$

In addition, the concentrations are replaced by molar flows and volumetric flow rates

$$c_i = \frac{\dot{n}_i}{\dot{V}}.$$

The update of the flow rate is $\dot{V} = \dot{V}_0(1 + x_{0E}\delta_E\eta_E)(T/T_0)$.

Thus the rate equation becomes

$$r = k\left(\frac{\dot{n}_\mathrm{E}}{\dot{V}}RT - \frac{\dot{n}_\mathrm{S}\dot{n}_\mathrm{H}}{\dot{V}^2}(RT)^2/K\right).$$

The calculations are carried out with the conversion of E (η_E)

$$\dot{n}_\mathrm{E} = (1 - \eta_\mathrm{E})\,\dot{n}_{0\mathrm{E}}.$$

For the reaction products, we have

$$\xi = \frac{\dot{n}_\mathrm{S} - \dot{n}_{0\mathrm{S}}}{\nu_\mathrm{S}} = \frac{\dot{n}_\mathrm{H} - \dot{n}_{0\mathrm{H}}}{\nu_\mathrm{H}} = \frac{\dot{n}_\mathrm{E} - \dot{n}_{0\mathrm{E}}}{\nu_\mathrm{E}}.$$

The inlet flows of S and H_2 are zero ($\dot{n}_{0\mathrm{S}} = \dot{n}_{0\mathrm{H}} = 0$). We obtain $\dot{n}_\mathrm{S} = \dot{n}_\mathrm{H} = \dot{n}_{0\mathrm{E}} - \dot{n}_\mathrm{E}$ in this case. The difference $\dot{n}_{0\mathrm{E}} - \dot{n}_\mathrm{E}$ is equal to $\dot{n}_{0\mathrm{E}}\eta_\mathrm{E}$. Finally, we obtain $\dot{n}_\mathrm{S} = \dot{n}_{0\mathrm{E}}\eta_\mathrm{E}$ and $\dot{n}_\mathrm{H} = \dot{n}_{0\mathrm{E}}\eta_\mathrm{E}$.

The rate equation becomes

$$r = k\left(\frac{\dot{n}_{0\mathrm{E}}(1 - \eta_\mathrm{E})RT}{\dot{V}_0(1 + x_{0\mathrm{A}}\delta_\mathrm{E}\eta_\mathrm{E})(T/T_0)} - \frac{\dot{n}_{0\mathrm{E}}^2\eta_\mathrm{E}^2(RT)^2}{\dot{V}_0^2(1 + x_{0\mathrm{A}}\delta_\mathrm{E}\eta_\mathrm{E})^2(T/T_0)^2K}\right),$$

where

$$\delta_\mathrm{E} = \sum \frac{\nu_i}{-\nu_\mathrm{E}}.$$

To make the equation more aesthetic, some relations are included. The factor $\dot{n}_{0\mathrm{E}}/\dot{V}_0 = c_{0\mathrm{E}} = x_{0\mathrm{E}}c_0$. The total concentration at the inlet is denoted by c_0.

$$c_0 = \frac{P_0}{RT_0}.$$

The rate equation is thus simplified to

$$r = k\left(\frac{x_{0\mathrm{E}}P_0(1 - \eta_\mathrm{E})}{(1 + x_{0\mathrm{A}}\delta_\mathrm{E}\eta_\mathrm{E})} - \frac{x_{0\mathrm{E}}^2P_0^2\eta_\mathrm{E}^2}{(1 + x_{0\mathrm{A}}\delta_\mathrm{E}\eta_\mathrm{E})^2K}\right).$$

The molar flow in the mass balance is replaced by the conversion $\dot{n}_\mathrm{E} = (1 - \eta_\mathrm{E})\dot{n}_{0\mathrm{E}}$, which implies

$$\frac{\mathrm{d}\dot{n}_\mathrm{E}}{\mathrm{d}V} = -\frac{\mathrm{d}\eta_\mathrm{E}}{\mathrm{d}V}\dot{n}_{0\mathrm{E}}.$$

Furthermore, $V/\dot{V}_0 = \tau$ and $\dot{n}_{0\mathrm{E}} = c_{0\mathrm{E}}\dot{V}_{0\mathrm{G}}$, which yields

$$\frac{\mathrm{d}\dot{n}_\mathrm{E}}{\mathrm{d}V} = -\frac{\mathrm{d}\eta_\mathrm{E}}{\mathrm{d}\tau}c_{0\mathrm{E}} = -\frac{\mathrm{d}\eta_\mathrm{E}}{\mathrm{d}\tau}\frac{x_{0\mathrm{E}}P_0}{RT_0}.$$

We now have

$$\frac{\mathrm{d}\eta_\mathrm{E}}{\mathrm{d}\tau}\frac{x_{0\mathrm{E}}P_0}{RT_0} = k\left(\frac{x_{0\mathrm{E}}P_0(1-\eta_\mathrm{E})}{1+x_{0\mathrm{E}}\delta_\mathrm{E}\eta_\mathrm{E}} - \frac{x_{0\mathrm{E}}^2P_0^2\eta_\mathrm{E}^2}{(1+x_{0\mathrm{E}}\delta_\mathrm{E}\eta_\mathrm{E})^2K}\right)\rho_\mathrm{B},$$

yielding the design equation

$$\frac{\mathrm{d}\eta_\mathrm{E}}{\mathrm{d}\tau} = RT_0k\rho_\mathrm{B}\left(\frac{(1-\eta_\mathrm{E})}{1+x_{0\mathrm{E}}\delta_\mathrm{E}\eta_\mathrm{E}} - \frac{x_{0\mathrm{E}}P_0\eta_\mathrm{E}^2}{(1+x_{0\mathrm{E}}\delta_\mathrm{E}\eta_\mathrm{E})^2K}\right). \qquad [\mathrm{A}]$$

However, the temperature changes inside the reactor, and therefore the energy balance is also needed. The energy balance for an adiabatic packed bed ($U = 0$) is written as

$$\frac{\mathrm{d}T}{\mathrm{d}V} = \frac{1}{\dot{m}c_\mathrm{p}}\rho_\mathrm{B}r(-\Delta H_\mathrm{r}),$$

which is combined with the mass balance

$$\frac{\mathrm{d}\dot{n}_\mathrm{E}}{\mathrm{d}V} = \rho_\mathrm{B}r_\mathrm{E} = \nu_\mathrm{E}\rho_\mathrm{B}r.$$

A division of the above equations yields

$$\frac{\mathrm{d}T}{\mathrm{d}\dot{n}_\mathrm{E}} = \frac{-\Delta H_\mathrm{r}}{\dot{m}c_\mathrm{p}\nu_\mathrm{E}},$$

that is, easily integrated (ΔH_r and c_p are assumed to be constant here):

$$\int_{T_0}^{T}\mathrm{d}T = -\frac{\Delta H_\mathrm{r}}{\dot{m}c_\mathrm{p}\nu_\mathrm{E}}\int_{\dot{n}_{0\mathrm{E}}}^{\dot{n}_\mathrm{E}}\mathrm{d}\dot{n}_\mathrm{E},$$

$$T - T_0 = \frac{-\Delta H_\mathrm{r}}{-\nu_\mathrm{E}\dot{m}c_\mathrm{p}}(\dot{n}_{0\mathrm{E}} - \dot{n}_\mathrm{E}),$$

where $\dot{n}_{0\mathrm{E}} - \dot{n}_\mathrm{E} = \dot{n}_\mathrm{E}\eta_\mathrm{E} = x_{0\mathrm{E}}\dot{n}_0\eta_\mathrm{E}$.

The mass flow is $\dot{m} = \dot{n}_0M_0$ (where M_0 is the molar mass of the feed). We obtain

$$T - T_0 = \frac{-\Delta H_\mathrm{r}x_{0\mathrm{E}}\dot{n}_0\eta_\mathrm{E}}{-\nu_\mathrm{E}\dot{n}_0M_0c_\mathrm{p}},$$

from which the temperature is updated:

$$T = T_0 + \frac{-\Delta H_\mathrm{r}x_{0\mathrm{E}}\eta_\mathrm{E}}{-\nu_\mathrm{E}M_0c_\mathrm{p}}. \qquad [\mathrm{B}]$$

The model of the system consists of Equations [A] and [B] (remember that k and K are dependent on temperature).

The numerical values are calculated below:

$R = 8.3143\,\mathrm{J/K\,mol}$,
$T_0 = 898\,\mathrm{K}$,
$\rho_\mathrm{B} = 1440\,\mathrm{kg/m^3}$,
$x_{0\mathrm{E}} = 1.8\,\mathrm{mol/s}/(1.8\,\mathrm{mol/s} + 34\,\mathrm{mol/s}) = 0.05028$,

$$\delta_\mathrm{E} = \frac{-1+1+1}{-(-1)} = 1 \Rightarrow x_{0\mathrm{E}}\delta_\mathrm{E} = 0.05028.$$

The quantity $\beta = (-\Delta H_\mathrm{r} x_{0\mathrm{E}})/(-\nu_\mathrm{E} M_0 c_\mathrm{p})$ is calculated.
The molar mass of the feed is

$$M_0 = x_{0\mathrm{E}} M_\mathrm{E} + x_{0\mathrm{W}} M_\mathrm{W},$$

$$x_{0\mathrm{W}} = 1 - x_{0\mathrm{E}} = 1 - 0.05028 = 0.95,$$

$$M_\mathrm{E} = 106 \times 10^{-3}\,\mathrm{kg/mol},$$

$$M_\mathrm{W} = 18 \times 10^{-3}\,\mathrm{kg/mol},$$

$$M_0 = (0.05 \times 106 + 0.95 \times 18) \times 10^{-3}\,\mathrm{kg/mol} = 22.4 \times 10^{-3}\,\mathrm{kg/mol},$$

$$\beta = \frac{-139 \times 10^3\,\mathrm{J/mol} \times 0.05028}{-(-1) \times 22.4 \times 10^{-3}\,\mathrm{kg/mol} \times 2.18 \times 10^3\,\mathrm{J/(kgK)}} = -142.324\,\mathrm{K}.$$

The rate and the equilibrium constants are

$$k = 0.0345 \cdot \mathrm{e}^{(-10{,}980K/T)}\,\mathrm{mol/(sPa)}, \quad K = 4.656 \cdot 10^{11} \cdot \mathrm{e}^{(-14{,}651\,K/T)}\,\mathrm{Pa}.$$

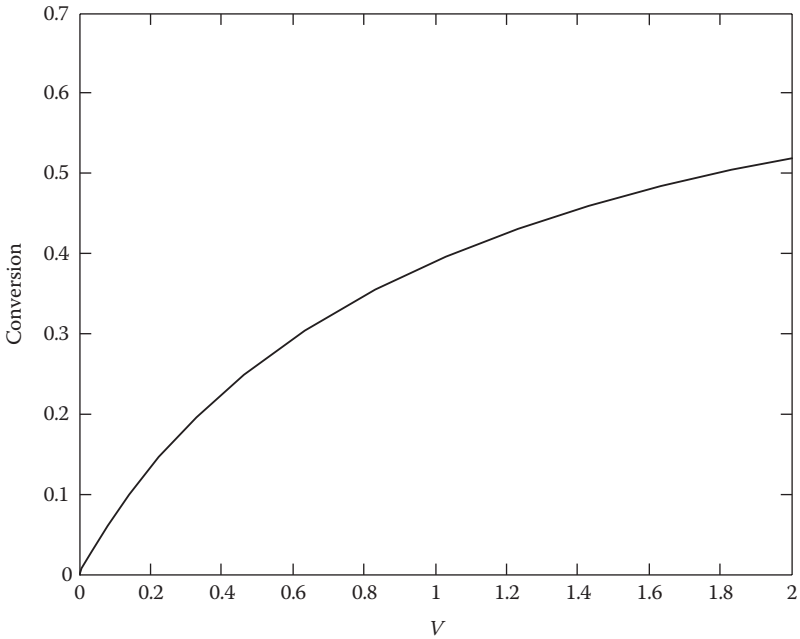

Conversion of ethylbenzene as a function of the reactor volume ($\mathrm{m^3}$).

The reactor volume at the conversion $\eta_E = 0.45$ can be read in the figure above, and it is $1.4\,m^3$.

The reactor volume can also be calculated by solving the mass balances for all of the components and the energy balance. The MATLAB® code for this solution is listed below:

```
function ex_2_1
% solve mass and energy balances
[x,y]=ode23(@exe,[0 2],[1.8 0 0 898])
eta=(y(1,1)-y(:,1))/y(1,1) % calculate conversion
plot(x,eta)
xlabel('Volume');
ylabel('Conversion')
title('ex 2.1');
return

function ds=exe(v,s)
ne=s(1);
ns=s(2);
nh=s(3);
T=s(4);
nh2o=34;
ntot=ne+ns+nh+nh2o;
Rgas=8.3143;
p0=121e3;
ptot=p0;
% partial pressures
pe=ne/ntot*ptot;
ps=ns/ntot*ptot;
ph=nh/ntot*ptot;

x0e=0.05028;
M=22.4e-3;
m=M*ntot;
cp=2.18e3;
dH=139e3;
rhoB=1440;
% reaction kinetics
k=0.0345*exp(-10980/T);
Keq = 4.656e11*exp(-14651/T);
rate=k*(pe-ps*ph/Keq);
% mass balances
ds(1,1)=-rate*rhoB;
ds(2,1)=rate*rhoB;
```

```
ds(3,1)=rate*rhoB;
% energy balance
ds(4,1)=1/m/cp*rhoB*rate*(-dH);
return
```

SECTION II/4

The liquid-phase reaction scheme is given by

$$\mathrm{A} + \mathrm{B} \rightarrow \mathrm{C},$$

where A = isobutene, B = water, and C = *tert*-butanol.

The reaction is assumed to be of first order:

$$r = kc_{\mathrm{A}}.$$

Internal mass transfer resistance influences the global rate; the mass balance of A thus obtains the form

$$\frac{\mathrm{d}\dot{n}_{\mathrm{A}}}{\mathrm{d}V} = \rho_{\mathrm{B}}\eta_{\mathrm{eA}}r_{\mathrm{A}},$$

where $r_{\mathrm{A}} = \nu_{\mathrm{A}}r$ and r is expressed with the bulk-phase concentrations. The molar flow is constant; we thus obtain $\dot{n} = c_{\mathrm{A}}\dot{V}$ and the derivative becomes

$$\frac{\mathrm{d}\dot{n}_{\mathrm{A}}}{\mathrm{d}V} = \frac{\mathrm{d}c_{\mathrm{A}}}{\mathrm{d}V}\dot{V} = \frac{\mathrm{d}c_{\mathrm{A}}}{\mathrm{d}\tau}$$

since $V/\dot{V} = \tau$, the space time of the liquid.

The balance attains the form ($\nu_{\mathrm{A}} = -1$)

$$\frac{\mathrm{d}c_{\mathrm{A}}}{\mathrm{d}\tau} = -\rho_{\mathrm{B}}\eta_{\mathrm{eA}}kc_{\mathrm{A}}.$$

For first-order reactions, the effectiveness factor is independent of the concentration, and the model equation can be solved in a straightforward manner:

$$\int_{c_{0\mathrm{A}}}^{c_{\mathrm{A}}} \frac{\mathrm{d}c_{\mathrm{A}}}{c_{\mathrm{A}}} = -k\rho_{\mathrm{B}}\eta_{\mathrm{eA}}\int_0^{\tau}\mathrm{d}\tau$$

yielding

$$\ln\left(\frac{c_{\mathrm{A}}}{c_{0\mathrm{A}}}\right) = -k\rho_{\mathrm{B}}\eta_{\mathrm{eA}}\tau,$$

from which the space time is obtained:

$$\tau = (\eta_{\mathrm{eA}}k\rho_{\mathrm{B}})^{-1}\ln\left(\frac{c_{0\mathrm{A}}}{c_{\mathrm{A}}}\right).$$

The effectiveness factor for first-order kinetics in spherical particles is obtained from the Thiele modulus. An absence of external mass transfer is assumed, since no information about the Biot number is available (here we assume that $Bi_m \to \infty$, Equation 5.85 in Section 5.2.2)

$$\eta_{eA} = \frac{3}{\phi}\left(\frac{1}{\tanh\ \phi} - \frac{1}{\phi}\right),$$

where the Thiele modulus (ϕ) is defined by

$$\phi = \sqrt{\frac{-\nu_A \rho_p k}{D_{eA}} R}$$

(Equation 5.59 in Section 5.2.2).

The value of ϕ is calculated as follows:

$$\phi = \sqrt{\frac{1.1000\,\text{kg/m}^3 \times 0.0016\,\text{m}^3/(\text{kgs})}{2.0 \times 10^{-9}\,\text{m}^2/\text{s}}} 0.0213 \times 10^{-2}\,\text{m} = 6.02455.$$

The effectiveness factor becomes

$$\eta_{eA} = \frac{3}{6.02455}\left(\frac{1}{\tanh\ 6.02455} - \frac{1}{6.02455}\right) = 0.4153.$$

The factor $\eta_e k \rho_B$ becomes

$$(\eta_e k \rho_B)^{-1} = (0.4153 \times 0.0016\,\text{m}^3/(\text{kgs}) \times 500\,\text{kg/m}^3)^{-1} = 3.0099\,\text{s}.$$

The conversion level required is $\eta_A = 0.5$.

We have $\eta_A = 1 - c_A/c_{0A}$, which yields $c_A/c_{0A} = 1 - \eta_A = 0.5$ and $(c_A/c_{0A})^{-1} = 0.5^{-1} = 2$.

The space time is thus finally obtained from

$$\tau = (\eta_e k \rho_B)^{-1} \ln (c_A/c_{0A})^{-1},$$
$$\tau = 3.0099\,\text{s}\ \ln(2) = 2.09\,\text{s}.$$

If the mass transfer resistance were simply neglected, $\eta_c = 1$, we would obtain

$$\tau = (k \rho_B)^{-1} \ln (c_A/c_{0A})^{-1},$$
$$\tau = 1.25\,\text{s}\ \ln(2) = 0.87\,\text{s}.$$

The example demonstrates that the intraparticle mass transfer resistance plays a crucial role and it cannot be discarded, since this would lead to a large error in the reactor sizing.

SECTION II/9

The equilibrium conversion of the water–gas shift reaction

$$\underset{\text{(A)}}{\text{CO}} + \underset{\text{(B)}}{\text{H}_2} \rightleftarrows \underset{\text{(C)}}{\text{CO}_2} + \underset{\text{(D)}}{\text{H}_2}$$

is calculated first. Since the total pressure is low ($P = 1$ atm), the ideal gas law can be applied. The equilibrium expression is

$$K_\text{p} = \frac{p_\text{C} p_\text{D}}{p_\text{A} p_\text{B}}.$$

The ideal gas law yields $p_i = x_i P$, where $i = \text{A, B, C, D}$, which is inserted into K_P yielding

$$K_\text{P} = \frac{x_\text{C} x_\text{D}}{x_\text{A} x_\text{B}}.$$

Equation 3.67 in Section 3.5.2 gives a relation between the molar fractions and conversion of the key component (A),

$$x_1 = \frac{x_{0i} + \nu_i x_{0\text{A}}(\eta_\text{A}/-\nu_\text{A})}{1 + \sum \nu_i x_{0\text{A}}(\eta_\text{A}/-\nu_\text{A})}.$$

The term $\sum \nu_i x_{0\text{A}} \eta_\text{A}/(-\nu_\text{A})$ is $(-1 - 1 + 1 + 1)x_{0\text{A}}\eta_\text{A}/1 = 0$ (no change in the total amount of substance). Thus we have

$$\begin{aligned} x_\text{A} &= x_{0\text{A}}\,(1 - \eta_\text{A}), \\ x_\text{B} &= x_{0\text{B}} - x_{0\text{A}}\eta_\text{A}, \\ x_\text{C} &= x_{0\text{C}} - x_{0\text{A}}\eta_\text{A}, \\ x_\text{D} &= x_{0\text{D}} - x_{0\text{A}}\eta_\text{A}, \end{aligned}$$

which are inserted into the equilibrium expression

$$K_\text{P} = \frac{(x_{0\text{C}} + x_{0\text{A}}\eta_\text{A})\,(x_{0\text{D}} + x_{0\text{A}}\eta_\text{A})}{x_{0\text{A}}\,(1 - \eta_\text{A})\,(x_{0\text{B}} - x_{0\text{A}}\eta_\text{A})} \qquad \text{[A]}$$

and developed into a second-degree equation ($K_\text{P} = K$, $\eta_\text{A} = \eta$ below)

$$x_{0\text{A}}^2(1 - K)\eta^2 + \left(x_{0\text{A}}x_{0\text{C}} + x_{0\text{A}}x_{0\text{D}} + Kx_{0\text{A}}x_{0\text{B}} + Kx_{0\text{A}}^2\right)\eta + x_{0\text{C}}x_{0\text{D}} - Kx_{0\text{A}}x_{0\text{B}} = 0. \qquad \text{[B]}$$

The numerical value of $K(= K_\text{P})$ is

$$K = \text{e}^{4577.8K/T - 4.33}, \text{ where } T = 683\,\text{K}, K = 10.724.$$

We introduce the notations

$$a = x_{0A}^2 (1 - K), \quad b = x_{0A}x_{0C} + x_{0A}x_{0B} + Kx_{0A}x_{0B} + Kx_{0A}^2,$$
$$c = x_{0C}x_{0D} - Kx_{0A}x_{0B}.$$

Equation [B] becomes

$$a\eta^2 + b\eta + c = 0, \qquad [C]$$

where $a = -0.0476$, $b = 0.44399$, and $c = -0.36934$. The solution of Equation [C] is

$$\eta = \frac{-b \pm \sqrt{b^2 - 4ac}}{2a}.$$

We get the equilibrium conversion $\eta = \eta_A^* = 0.9234$.
For the packed bed reactor, it is required that $\eta = 0.999 \times \eta_A^* = 0.9225$.
The design equation for the packed bed is (one-dimensional model)

$$\frac{d\dot{n}_A}{dV} = \eta_{eA} r_A \rho_B, \qquad [D]$$

where r_A refers to intrinsic kinetics and η_{eA} is the effectiveness factor.
The molar flow is related to the conversion

$$\eta_A = \frac{\dot{n}_{0A} - \dot{n}_A}{\dot{n}_{0A}},$$

which yields

$$\dot{n}_A = (1 - \eta_A)\dot{n}_{0A}.$$

Differentiation yields

$$\frac{d\dot{n}_A}{dV} = -\dot{n}_{0A}\frac{d\eta_A}{dV}.$$

The inlet molar flow is $\dot{n}_{0A} = c_{0A}\dot{V}_0$. Thus the derivative becomes $d\dot{n}_A/dV = -c_{0A}(d\eta_A/d\tau)$, where $\tau = V/\dot{V}_0$. The mass balance [D] is thus rewritten as

$$\frac{d\eta_A}{d\tau} = -\frac{\eta_{eA} r_A \rho_B}{c_{0A}}. \qquad [E]$$

The inlet concentration is obtained from the ideal gas law: $c_{0A} = x_{0A}c_0$, where $c_0 = P_0/RT_0$.
The intrinsic kinetics is written as

$$r_A = \nu_A R' = -R' \quad R' = kc_A(1 - B) \quad B = \frac{c_C c_D}{K_P c_A c_B} = \frac{x_C x_D}{K x_A x_B}, \quad (K = K_P).$$

The rate equation becomes

$$r_A = -kx_A c\left(1 - \frac{x_C x_D}{K x_A x_B}\right),$$

where the total concentration c is

$$c = \frac{P}{RT} = \frac{P_0}{RT_0}. \qquad (P \text{ and } T \text{ are constant})$$

The expressions for x_A, x_B, x_c, and x_D are inserted:

$$r_A = -\frac{kP}{RT} x_{0A}(1 - \eta_A)\left(1 - \frac{(x_{0C} + x_{0A}\eta_A)\,(x_{0D} + x_{0A}\eta_A)}{K x_{0A}(1 - \eta_A)\,(x_{0B} - x_{0A}\eta_A)}\right).$$

For simplicity, the effectiveness factor for irreversible first-order reactions in spherical particles is used (the reader should note that this is an approximation, which should be applied with care).

$$\eta_{eA} = \frac{3}{\phi}\left(\frac{1}{\tanh(\phi)} - \frac{1}{\phi}\right), \qquad [F]$$

where the Thiele modulus is

$$\phi = \sqrt{\frac{k\rho_P}{D_{eA}}} \cdot R.$$

The balance equation of A finally becomes

$$\frac{d\eta_A}{d\tau} = \frac{3}{\phi}\left(\frac{1}{\tanh(\phi)} - \frac{1}{\phi}\right) k\,(1 - \eta_A)\,(1 - B)\rho_B, \qquad [G]$$

$$B = \frac{(x_{0C} + x_{0A}\eta_A)\,(x_{0D} + x_{0A}\eta_A)}{K x_{0A}\,(1 - \eta_A)\,(x_{0B} - x_{0A}\eta_A)}.$$

The parameters of Equation [G] are calculated *a priori*, $k\rho_B = 5.81\,\text{cm}^3/\text{g s} \times 0.95\,\text{g/cm}^3 = 5.5195\,\text{s}^{-1}$.

The effective diffusion coefficient is

$$D_{eA} = \frac{\varepsilon_p}{\tau_p}\left(\frac{1}{D_{mA}} + \frac{1}{D_{KA}}\right)^{-1},$$

$$D_{eA} = 0.25 \cdot \left(1.27^{-1} + 0.104^{-1}\right)^{-1}\,\text{cm}^2/\text{s} = 0.0240\,\text{cm}^2/\text{s}.$$

In the Thiele modulus, the characteristic dimension of the catalyst particle is needed (R), that is, $R = a_p/2 = h/2 = 3.2\,\text{mm}/2 = 1.6\,\text{mm}$. The Thiele modulus becomes

$$\phi = \sqrt{\frac{5.81\,\text{cm}^3 1.55\,\text{g s}}{\text{g s cm}^3\ 0.0240\,\text{cm}^2}} \times 0.16\,\text{cm} = 3.099.$$

The effectiveness factor is obtained from Equation [F], $\eta_{eA} = 0.6596$, which implies that the diffusion resistance is considerable.

The factor $\eta_{eA} k \rho_B = \dfrac{3}{\phi}\left[\dfrac{1}{\tanh(\phi)} - \dfrac{1}{\phi}\right] k\rho_B$ is denoted by α, which becomes

$$\alpha = 0.6596 \times 5.5195\,\mathrm{s}^{-1} = 3.6408\,\mathrm{s}^{-1}.$$

Finally, the differential equation can be solved numerically:

$$\frac{d\eta_A}{d\tau} = \alpha(1 - \eta_A)(1 - B), \quad B = \frac{(x_{0C} + x_{0A}\eta_A)\,(x_{0D} + x_{0A}\eta_A)}{K x_{0A}\,(1 - \eta_A)\,(x_{0B} - x_{0A}\eta_A)}, \qquad [H]$$

where $\alpha = 3.6408\,\mathrm{s}^{-1}$, $x_{0A} = 0.07$, $x_{0B} = 0.50$, $x_{0C} = 0.03$, $x_{0D} = 0.2$, and $K = 10.742$.

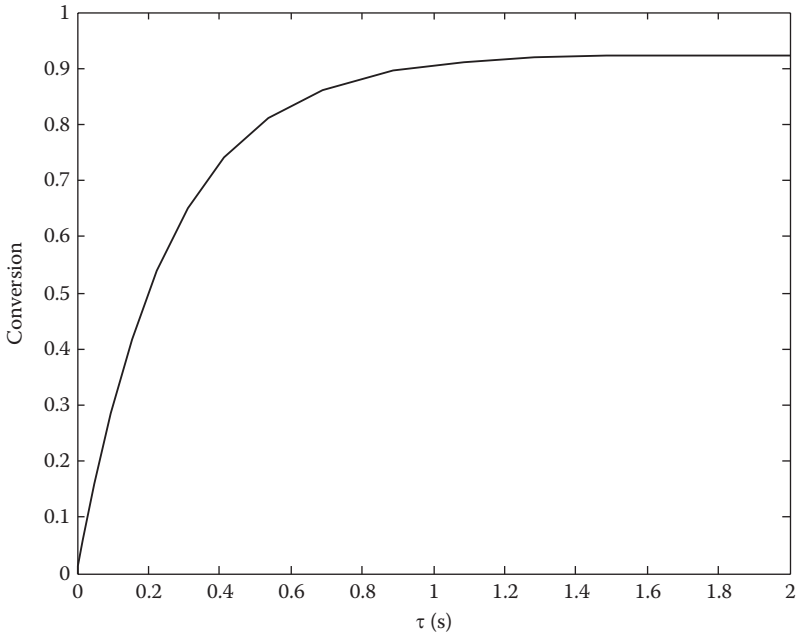

For the result of the numerical solution, see the figure. The space time needed for $\eta_A = 0.9225$ is $\tau = 1.7$ s.

τ (s)	η_A
0	0
0.0000	0.0001
0.0001	0.0005
0.0007	0.0025
0.0035	0.0124
0.0174	0.0605

continued

continued

τ (s)	η_A
0.0491	0.1604
0.0947	0.2847
0.1532	0.4153
0.2247	0.5397
0.3103	0.6496
0.4125	0.7406
0.5355	0.8113
0.6873	0.8625
0.8850	0.8964
1.0850	0.9115
1.2850	0.9182
1.4850	0.9211
1.6850	**0.9224**
1.8850	0.9229
2.0000	0.9231

SECTION II/13

The first-order reaction

$$A \rightarrow P$$

is carried out in an isothermal fluidized bed, to which the Kunii–Levenspiel model is applied. The bed length can principally be calculated from

$$\frac{d\dot{n}_{bi}}{dV_G} = r_{bi}\rho_{Bb} - K_{bci}\,(c_{bi} - c_{ei}).$$

The volumetric flow rate is constant, and $d\dot{n}_{bi}/dV_b$ can be replaced by $dc_{bi}/d\tau_b$, where

$$\tau_b = \frac{V_b}{\dot{V}_b}.$$

However, the concentrations in the cloud and wake phases, c_{ci}, have to be calculated. We have

$$K_{bci}\,(c_{bi} - c_{ci}) + r_{ci}\rho_{Bc}\frac{V_c}{V_b} = K_{cei}(c_{ci} - c_{ei}),$$

where the concentration in the emulsion phase, c_{ei}, appears again. For the emulsion phase, the balance equation is

$$K_{cei}\,(c_{ci} - c_{ei}) + r_{ei}\rho_{Be}\frac{V_e}{V_b} = 0.$$

Since the reaction kinetics is linear of first order, an analytical solution is possible. We introduce the reaction kinetics in the phases as follows:

$$r_{bi} = -kc_{bi},$$
$$r_{ci} = -kc_{ci},$$
$$r_{ei} = -kc_{ei}.$$

Because just one component ($i = \mathrm{A}$) is considered, the component index is omitted below.

For the emulsion phase, we have

$$K_{ce}(c_c - c_e) - kc_e\alpha_e = 0, \quad \alpha_e = \frac{\rho_{Be}V_e}{V_b}.$$

This yields

$$K_{ce}c_c = K_{ce} + k\alpha_e c_e$$

and

$$c_e = \frac{K_{ce}c_c}{K_{ce} + k\alpha_e} = \frac{c_c}{1 + k\alpha_e/K_{ce}}.$$

For the cloud and wake phases, an analogous treatment is applied:

$$K_{bc}(c_b - c_c) - kc_c\alpha_c = K_{ce}(c_c - c_e), \quad \text{where } \alpha_c = \frac{\rho_{Bc}V_c}{V_b}.$$

From this expression, c_e can be obtained after some straightforward algebraic operations. We insert the expression for c_e:

$$K_{bc}c_b - k_{bc}c_c - k\alpha_c c_c = K_{ce}c_c - \frac{K_{ce}c_c}{1 + k\alpha_e/K_{ce}}.$$

From the above equation, the concentration c_c is obtained:

$$c_c = \frac{K_{bc}c_b}{K_{bc} + K_{ce}[1 - (1/(1 + k\alpha_e/K_{ce}))] + k\alpha_c},$$

which can be simplified to

$$c_c = \frac{c_b}{1 + [(K_{ce}k\alpha_e/K_{ce})/K_{bc}(1 + k\alpha_e/K_{ce})] + (k\alpha_c/K_{be})}.$$

Finally, we have

$$c_c = \frac{c_b}{1 + (k\alpha_c/K_{bc}) + [(k\alpha_e)/(K_{bc}(1 + k\alpha_e/K_{ce}))]}.$$

The denominator is a constant, and it can be expressed as $1 + \beta$; we obtain

$$c_c = \frac{c_b}{1+\beta}.$$

We return to the initial design equation

$$\frac{dc_b}{d\tau_b} = -kc_b\rho_{Bb} - K_{bc}(c_b - c_c), \quad \text{that is,} \quad \frac{dc_b}{d\tau_b} = -\left(k\rho_{Bb} + K_{bc} - K_{bc}(1+\beta)^{-1}\right)c_b.$$

The expression is easily integrated:

$$\int_{c_{0b}}^{c_b} \frac{dc_b}{c_b} = -\left(k\rho_{Bb} + K_{bc} - K_{bc}(1+\beta)^{-1}\right)\int_0^{\tau_b} d\tau_b$$

yielding

$$\ln\frac{c_b}{c_{0b}} = -\left(k\rho_{Bb} + K_{bc} - K_{bc}(1+\beta)^{-1}\right)\tau_b.$$

This yields the space time of the bubbles, and the conversion of A (η_A) is introduced as

$$\frac{c_b}{c_{0b}} = 1 - \eta_A,$$

$$\tau_b = \frac{\ln(1-\eta_A)^{-1}}{k\rho_{Bb} + K_{bc} - K_{bc}(1+\beta)^{-1}},$$

where $\beta = (k\alpha_c/K_{bc}) + (k\alpha_e/K_{bc}(1 + k\alpha_e/K_{ce}))$, $\alpha_c = \rho_{Bc}V_c/V_b$, and $\alpha_e = \rho_{Be}V_e/V_b$.

The numerical values are calculated below:

$$\alpha_c = 290\,\text{kg/m}^3,$$

$$\alpha_e = 1020\,\text{kg/m}^3,$$

$$\beta = \frac{1.5\,\text{m}^3 \times 290\,\text{kg/m}^3}{\text{kg h}\,1.4\,\text{s}^{-1}} + \frac{1.5\,\text{m}^3 \times 1020\,\text{kg/m}^3}{\text{kg h}\,1.4\,\text{s}^{-1}(1 + (1.5\,\text{m}^3 \times 1020\,\text{kg})/(\text{kg h m}^3/0.95))},$$

$$\beta = 0.0863095 + \frac{0.30357}{1 + 0.47222} = 0.2925.$$

The denominator becomes

$$k\rho_{Bb} + K_{bc} - K_{bc}(1+\beta)^{-1} = \frac{1.5\,\text{m}^3}{\text{kg}\;3600\,\text{s}} + 1.4\,\text{s}^{-1} - 1.4\,\text{s}^{-1}(1 + 0.2925)\,\text{s}^{-1}$$

$$= 0.31995\,\text{s}^{-1}.$$

Finally, we obtain ($\eta_A = 0.95$)

$$\tau_b = \frac{\ln(1-0.95)^{-1}}{0.31995\,s^{-1}} = 9.363\,s.$$

The bed height is calculated from the relation

$$L = \tau_b w_b,$$

where w_b is obtained from the correlation given in the book:

$$w_b = w - w_{mf} + 0.711\sqrt{g d_b},$$

$$w_b = \frac{1800\,m}{3600\,s} - \frac{20.5\,m}{3600\,s} + 0.711\sqrt{9.816 \cdot 0.1}\,m/s = 1.1987\,m/s.$$

The bed length becomes

$$L = 9.363\,s \times 1.1987\,m/s \text{ giving } L = 11.22\,m.$$

SECTION II/15

The catalytic hydrogenation of alkylbenzenes is given by the reaction formula

$$A + 3H_2 \rightarrow B,$$

where A is the alkylbenzene and B is the alkylcyclohexane.

The reaction is carried out in a BR, to which hydrogen is continuously added in such a way that the pressure is maintained constant.

In the absence of mass transfer resistances, the mass balance of A is written as

$$\frac{dc_A}{dt} = \rho_B r_A,$$

where $r_A = \nu_A r$.

In the present case, the reaction rate is given by

$$r = \frac{kK_A K_H c_A c_H}{\left(3K_A c_A + (K_H c_H)^{1/\gamma} + 1\right)^{\gamma+1}},$$

where $\gamma = 2$.

Furthermore, the constants in the nominator can be merged, $k' = kK_A K_H c_H$, because the liquid phase is saturated with respect to hydrogen, that is, c_H is constant ($= c_H^*$). Analogously,

the sum $(K_H c_H)^{1/\gamma} + 1 = \alpha$ is a constant, because c_H is a constant. We denote $3K_A$ by β. The rate expression becomes

$$r = \frac{k' c_A}{(\alpha + \beta c_A)^3}.$$

The mass balance of A is rewritten as ($\nu_A = -1$)

$$\frac{dc_A}{dt} = -\frac{k' \rho_B c_A}{(\alpha + \beta c_A)^3}.$$

The separation of variables yields

$$\int_{c_{0A}}^{c_A} \frac{(\alpha + \beta c_A)^3}{c_A} dc_A = -k' \rho_B \int_0^t dt = -k' \rho_B t.$$

The left-hand side is developed further:

$$\begin{aligned}
\int &= \int_{c_{0A}}^{c_A} \left(\frac{\alpha^3 + 3\alpha^2\beta c_A + 3\alpha\beta^2 c_A^2 + \beta^3 c_A^3}{c_A} \right) dc_A \\
&= \alpha^3 \int_{c_{0A}}^{c_A} \frac{dc_A}{c_A} + 3\alpha^2\beta \int_{c_{0A}}^{c_A} dc_A + 3\alpha\beta^2 \int_{c_{0A}}^{c_A} c_A dc_A + \beta^3 \int_{c_{0A}}^{c_A} c_A^2 \, dc_A \\
&= \alpha^3 \ln\left(\frac{c_A}{c_{0A}} \right) + 3\alpha^2\beta \, (c_A - c_{0A}) + \frac{3}{2}\alpha\beta^2 \left(c_A^2 - c_{0A}^2 \right) + \frac{\beta^3}{3} \left(c_A^3 - c_{0A}^3 \right).
\end{aligned}$$

The bulk density of the catalyst is defined as

$$\rho_B = \frac{m_{cat}}{V_L}.$$

The conversion level is $\eta_A = 1 - c_A/c_{0A} = 0.99$, that is, $c_A/c_{0A} = 0.01$. The integrated result is transformed to

$$\begin{aligned}
&\alpha^3 \ln(1 - \eta_A)^{-1} + \alpha^2\beta c_{0A}\eta_A + \frac{3}{2}\alpha\beta^2 c_{0A}^2 \left(1 - (1 - \eta_A)^2 \right) + \frac{\beta^3}{3} c_{0A}^3 \left(1 - (1 - \eta_A)^3 \right) \\
&\quad = \frac{k' m_{cat} t}{V_L},
\end{aligned}$$

from which m_{cat} can be solved.

b. In case that external mass transfer resistance influences the reactor performance, the following expression is valid (Section 6.2.4):

$$\frac{dn_{LA}}{dt} = \left(N_{LA}^b a_v - N_{LA}^s a_p \right) V_R.$$

Since the mass transfer resistance at the particles is negligible, N_{LA}^{s} is given by

$$N_{LA}^{s} = -\frac{\varepsilon_L \rho_B}{a_p} r_A,$$

and we obtain

$$\frac{dn_{LA}}{dt} = \left(N_{LA}^{b} a_v + \varepsilon_L \rho_B r_A\right) V_R.$$

The liquid volume remains constant, we thus have $n_{LA} = c_{LA} V_L$ and $dn_{LA}/dt = V_L dc_{LA}/dt$, and the balance equation becomes ($\varepsilon_L V_R = V_L$)

$$V_L \frac{dc_{LA}}{dt} = N_{LA}^{b} a_v V_R + V_L \rho_B r_A,$$

that is,

$$\frac{dc_{LA}}{dt} = \frac{N_{LA}^{b} a_v}{\varepsilon_L} + \rho_B r_A.$$

The interfacial (gas–liquid) flux is given by

$$N_{LA}^{b} = \frac{c_{GA}^{b} - K_A c_{LA}^{b}}{(K_A/k_{LA}) + (1/k_{GA})}.$$

For the aromatic compound (A), the volatility is neglected ($K_A \approx 0$ and $c_{GA}^{b} = 0$). Thus we only have ($r_A = \nu_A r$)

$$\frac{dc_{LA}}{dt} = \rho_B \nu_A r.$$

For hydrogen, all of the terms in the mass balance are important, yielding

$$\frac{dc_{LB}}{dt} = \frac{N_{LB}^{b} a_v}{\varepsilon_L} + \rho_B \nu_B r,$$

where

$$N_{LB}^{b} = k_{LB}\left(\frac{c_{GB}^{b}}{K_B} - c_{LB}^{b}\right).$$

The concentration in the gas bulk (c_{GB}^{b}) is obtained from the ideal gas law

$$p_H V_G = n_H RT, \quad \frac{n_H}{V_G} = c_{GB}^{b} \Rightarrow c_{GB}^{b} = \frac{p_H}{RT}.$$

We denote c_{LB}^{b} by $c_{LB} = c_B$ and analogously c_{LA} by c_A.

The final form of the mathematical model is

$$\frac{\mathrm{d}c_\mathrm{A}}{\mathrm{d}t} = \rho_\mathrm{B}\nu_\mathrm{A}r,$$

$$\frac{\mathrm{d}c_\mathrm{B}}{\mathrm{d}t} = \frac{k_\mathrm{LB}a_\mathrm{v}}{\varepsilon_\mathrm{L}}\left(\frac{p_\mathrm{H}}{RTK_\mathrm{B}} - c_\mathrm{B}\right) + \rho_\mathrm{B}\nu_\mathrm{B}r,$$

where

$$r = \frac{kK_\mathrm{A}K_\mathrm{H}c_\mathrm{A}p_\mathrm{H}/(RT)}{\left(3K_\mathrm{A}c_\mathrm{A} + \left(K_\mathrm{H}p_\mathrm{H}/(RT)\right)^{1/2} + 1\right)^3}.$$

The coupled differential equations are solved numerically by the BD method implemented in the software LSODE. The main program and the model subroutine written in Fortran 90 for the toluene hydrogenation process are listed below:

```
!  Example 2 15
!  Compile this file with a Fortran compiler and
!  link it with the lsode solver
!  The Lsode solver can be downloaded from www.netlib.org
    Program Batch_reactor
    implicit none
    integer,parameter :: ncom=3  ! number of components, equations
    real(8) c(ncom),rwork(22+9*ncom+ncom**2)
        real(8) atol(ncom),rtol(ncom)
    integer iwork(20+ncom),lrw,liw
    integer mf,istate,itask,iopt,itol
        real(8) t,tout,tstep
    external batch,jex


    lrw=22+9*ncom+ncom**2  ! work vectors for lsode
    liw=20+ncom
    atol   = 1.0d-9 ! absolute tolerance
    rtol   = 1.0d-9 ! relative tolerance
    mf     = 22     ! method flag for lsode
    istate = 1      ! state of calculations
    itask  = 1      ! task to be perfomed
    iopt   = 0      ! optional input (no)
    itol   = 4      ! type of error control
    tstep  = 200    ! time step (s)
                    ! initial concentrations (mol/dm3)
    c(1)   = 9.5d0  ! Toluene
    c(2)   = 0.0d0  ! Hydrogen
    c(3)   = 0.0d0  ! Methylcyclohexane
    t      = 0.0d0  ! start at time = 0 seconds
    tout   =t+tstep ! solution at time=tout

!  open data file and write initial conditions to screen and file
    open(21,file='toluene.dat')
```

```
    write(*,'(f8.0,1x,4(f6.3,1x))') t,c(1:3),(1.0d0-c(1)/9.5)*100
    write(21,'(f8.0,1x,4(f6.3,1x))') t,c(1:3),(1.0d0-c(1)/9.5)*100

    do while ((1.0d0-c(1)/9.5).lt.0.9999) ! calculate until conversion=99%
      ! call solver
      call dlsode(batch,ncom,c,t,tout,itol,rtol,atol,itask,istate, &
                  iopt,rwork,lrw,iwork,liw,jex,mf)
!    write results to screen and file
      write(*,'(f8.0,1x,4(f6.3,1x))') tout,c(1:3),(1.0d0-c(1)/9.5)*100
      write(21,'(f8.0,1x,4(f6.3,1x))') tout,c(1:3),(1.0d0-c(1)/9.5)*100
            tout=tout+tstep  ! increase time for next calculation
        end do
        end program

!  Batch reactor model
    subroutine batch(ncom,t,c,dcdt)
    implicit none
    integer :: ncom
    real(8) :: t,c(ncom),dcdt(ncom)
    real(8) :: KA=0.25, KH=37.0, kla=0.1, k=2.1
    real(8) :: Rgas=8.3143d0, Temp=373.0d0, Pres=20.0d0
    real(8) :: xstar=0.014
    real(8) :: cA,cH,ctot
    real(8) :: mcat=0.040,VL=1.0,VR=1.1
    real(8) :: Rate,Keq,Flux,rhoB,epsL


    ctot=sum(c(1:ncom)) ! total concentration
    cA=c(1)             ! Toluene
    cH=c(2)             ! Hydrogen
    rhoB=mcat/VL ! catalyst bulk density
    epsL=VL/VR   ! liquid holdup

!  gas-liquid equilibrium constant
    Keq=Pres*101.3d3/Rgas/Temp/ctot/xstar*1.0d-3

!  Flux of hydrogen from gas to liquid phase
    Flux=kla/epsL*(Pres*101.3d0/Rgas/Temp/Keq-cH)

!  Reaction rate
    Rate=k*KA*KH*cA*cH/(3.0d0*KA*cA+sqrt(KH*cH)+1.0d0)**3

!  Mass balances
    dcdt(1)=-rhoB*Rate
    dcdt(2)=-3.0d0*rhoB*Rate+Flux
    dcdt(3)= rhoB*Rate

    return
    end

    subroutine jex ! dummy routine
    return
    end
```

The simulation results are displayed in the figure above, which shows that a reaction time of 135 min (8100 s) is needed to achieve a 99% conversion. As shown in the figure, the process is heavily influenced by mass transfer resistance. The dissolved hydrogen concentration only starts to approach the saturation concentration after practically all of toluene has reacted.

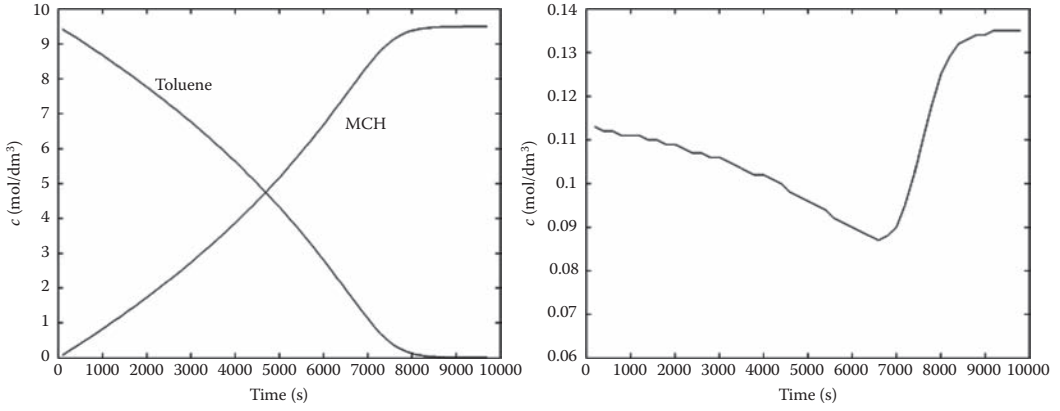

Concentration of toluene and methylcyclohexane in the reactor as a function of time (left) and concentration of hydrogen in the liquid phase during the reaction (right).

SECTION II/16

The three-phase reaction

$$A + H_2 \rightarrow AH_2$$

follows first-order kinetics $r = kc_{H_2}$; we will below denote $c_{H_2} = c_H$.

The mass balances of hydrogen in the liquid and gas phases are given by the following expression (Section 6.2.2):

$$\frac{d\dot{n}_{LH}}{dV_R} = N^b_{LH} a_v - N^s_{LH} a_p,$$

$$\frac{d\dot{n}_{GH}}{dV_R} = -N^b_{LH} a_v,$$

where

$$N^b_{LH} = \frac{c^b_{GH} - K_H c^b_{LH}}{K_H/k_{LH} + 1/k_{GH}}$$

and

$$N^s_{LH} = -\frac{\rho_B \varepsilon_L}{a_p} \eta_{eH} r_H,$$

where

$$r_H = V_H r.$$

The above expression N^s_{LH} is used (with η_e) because internal diffusion affects the rate.

Pure hydrogen is used in excess, thus $c^b_{GH} \approx$ constant and a_v can also be regarded as constant.

We denote

$$(K_H/k_{LH} + 1/k_{GH})^{-1} = K.$$

The liquid-phase balance equation becomes ($V = V_R$)

$$\frac{d\dot{n}_{LH}}{dV} = K\left(c^b_{GH} - K_H c^b_{LH}\right)a_v + \rho_B \varepsilon_L \eta_{eH}\left(-k c^b_{LH}\right).$$

The volumetric flow rate of the liquid is constant, that is, $d\dot{n}_{LH}/dV = \dot{V}_L(dc^b_{LH}/dV)$.

The notation is simplified: $c^b_{LH} = c_H$ and $c^b_{GH} = c$.

We have

$$\dot{V}_L \frac{dc_H}{dV} = Ka_v(c - K_H c_H) - \rho_B \varepsilon_L k \eta_{eH} c_H,$$

$V/\dot{V}_L = \tau_L$ is inserted, yielding

$$\frac{dc_H}{d\tau_L} = Ka_v c - (Ka_v K_H + \rho_B \varepsilon_L k \eta_{eH}) c_H.$$

The following notation is introduced: $Ka_v c = \beta$ and $Ka_v K_H + \rho_B \varepsilon_L k \eta_{eH} = \alpha$ yielding

$$\frac{dc_H}{d\tau_L} = \beta - \alpha c_H.$$

The separation of variables yields

$$\int_{c_{0H}}^{c_H} \frac{dc_H}{\beta - \alpha c_H} = \int_0^{\tau_L} d\tau_L = \tau_L.$$

The integral becomes

$$-\frac{1}{\alpha} \Big/_{c_{0H}}^{c_H} \ln(\beta - \alpha c_H) = -\frac{1}{\alpha} \ln\left(\frac{\beta - \alpha c_H}{\beta - \alpha c_{0H}}\right) = \tau_L \Rightarrow \frac{\beta - \alpha c_H}{\beta - \alpha c_{0H}} = e^{-\alpha \tau_L},$$

from which the liquid-phase concentration of H_2 is solved:

$$c_H = \frac{\beta - (\beta - \alpha c_{0H})\, e^{-\alpha \tau_L}}{\alpha}. \qquad [A]$$

The formation rate of AH_2 is

$$\eta_{eH} r_{AH_2} = \nu_{AH_2} \eta_{eH} r = +r\eta_{eH} = k\eta_{eH} c_H.$$

Because AH_2 is essentially nonvolatile, its balance equation can be written as

$$\frac{d\dot{n}_{LAH_2}}{dV} = -N^s_{LAH_2} a_p \quad \text{where } N^s_{LAH_2} = -\frac{\rho_B \varepsilon_L \eta_{eH_2} r_{AH_2}}{a_p}$$

and $d\dot{n}_{LAH_2}/dV = d\left(c_{AH_2}\dot{V}_L\right)/dV = dc_{AH_2}/d\tau_L$ in this case ($\dot{V}_L$ = constant).

We have

$$\frac{dc_{AH_2}}{d\tau_L} = \rho_B \varepsilon_L \eta_{eAH_2} r_{AH_2},$$

when $\eta_{eAH_2} r_{AH_2}/\nu_{AH_2} = \eta_{eH} r_H/\nu_H = \eta_e r$, from which we obtain

$$\eta_{eAH_2} r_{AH_2} = \frac{\nu_{AH_2}}{\nu_H}\eta_{eH}\nu_H r = \nu_{AH_2}\eta_{eH} r = k\eta_{eH} c_H, \text{ since } \nu_{AH_2} = +1 \text{ and } \nu_H = -1.$$

The balance equation becomes

$$\frac{dc_{AH_2}}{d\tau_L} = \rho_B \varepsilon_L \eta_{eH} k c_H,$$

in which c_H is inserted from Equation [A]

$$\frac{dc_{AH_2}}{d\tau_L} = \frac{\rho_B \varepsilon_L \eta_{eH} k}{\alpha}\left(\beta - (\beta - \alpha c_{0H})e^{-\alpha\tau_L}\right).$$

We denote $\rho_B \varepsilon_L \eta_{eH} k/\alpha = \omega$ and separate the variables. The result is

$$\int_0^{c_{AH_2}} dc_{AH_2} = \omega \int_0^{\tau_L} \left(\beta - (\beta - \alpha c_{0H})\, e^{-\alpha\tau_L}\right) d\tau_L$$

$$\Rightarrow c_{AH_2} = \omega\left(\beta\tau_L + \left(\frac{\beta - \alpha c_{0H}}{\alpha}\right)(e^{-\alpha\tau_L} - 1)\right).$$

The concentrations of H_2 and AH_2 in the liquid phase can now be computed from Equations [A] and [B] as a function of the liquid-phase space time (τ_L).

SECTION II/17

a. Equation 6.1 is used:

$$N^b_{Li} = \frac{c^b_{Gi} - K_i c^b_{Li}}{(K_i/k_{Li}) + (1/k_{Gi})}. \tag{6.1}$$

It gives the flux into a liquid phase. In this case, it equals the reaction rate

$$N^b_{Li} A = -r_i m_{cat}.$$

We divide this by the reactor volume (V_R) and remember that $a = A/V_R$ and $\rho_B = m_{cat}/V_L = m_{cat}/(\varepsilon_L V_R)$. Thus we obtain

$$N_{Li}^b a = -r_i \varepsilon_L \rho_B.$$

In this case, $r_i = \nu_i k c_i$; here $c_i = c_{Li}^b$ and we have

$$K_i' \left(c_{Gi}^b - K_i c_{Li}^b\right) a = -\varepsilon_L \rho_B \nu_i k c_{Li}^b, \quad \text{where} \quad K_i' = \left(\frac{K_i}{k_{Li}} - \frac{1}{k_{Gi}}\right)^{-1}, \text{ we obtain}$$

$$c_{Gi}^b - K_i c_{Li}^b = -\frac{\varepsilon_L \rho_B \nu_i k}{K_i' a} c_{Li}^b = \alpha c_{Li}^b,$$

in which c_{Gi}^b is solved:

$$c_{Li}^b = \frac{c_{Gi}^b}{\alpha + K_i}. \qquad [A]$$

In case of no gas–liquid mass transfer resistance, the concentrations are related by the equilibrium

$$c_{Li}^* = \frac{c_{Gi}^*}{K_i}.$$

Intrinsic kinetics becomes (r_i')

$$r_i' = \nu_i k c_{Li}^* = \frac{\nu_i k_i c_{Gi}^*}{K_i} = \frac{\nu_i k_i c_{Gi}^b}{K_i}. \qquad [B]$$

Equation [A] is transformed to ($\alpha/K_i = \beta$)

$$c_{Li}^b = \frac{c_{Gi}^b}{K_i (1 + \beta)}.$$

The rate becomes

$$r_i = \nu_i k c_{Li}^b = \frac{\nu_i k c_{Gi}^b}{K_i (1 + \beta)}. \qquad [C]$$

The effectiveness factor is defined as

$$\eta_e = \frac{N_i}{N_i'} = \frac{r_i}{r_i'},$$

which becomes (see Equations [B] and [C])

$$\eta_e = \frac{1}{1 + \beta}, \qquad [D]$$

where

$$\beta = \frac{\varepsilon_L \rho_B (-\nu_i) k}{a} \left(\frac{1}{k_{Li}} + \frac{1}{k_{Gi} K} \right).$$

For pure gas $k_{Gi} \to \infty$ and we obtain

$$\beta = \frac{\varepsilon_L \rho_B (-\nu_i) k}{k_{Li} a}.$$

b. In the case of liquid–solid mass transfer resistance, Equation 6.11 is valid:

$$k_{LSi} \left(c_{Li}^b - c_{Li}^s \right) a_p = \varepsilon_L \rho_B r_i.$$

In the present example, first-order kinetics is applied, and we have $r_i = \nu_i k c_{Li}^s$ which is inserted:

$$k_{LSi} a_p \left(c_{Li}^b - c_{Li}^s \right) = \varepsilon_L \rho_B (-\nu_i) k c_{Li}^s,$$

from which the concentration at the particle surface is solved:

$$c_{Li}^b - c_{Li}^s = \frac{\varepsilon_L \rho_B (-\nu_i) k}{k_{LSi} a_p} c_{Li}^s = \gamma c_{Li}^s,$$

$$c_{Li}^s = \frac{c_{Li}^b}{1 + \gamma}.$$

The flux becomes

$$N_{LSi} = -\frac{\varepsilon_L \rho_B r_i}{a_p} = \frac{\varepsilon_L \rho_B}{a_p} \frac{(\nu_i) k c_{Li}^b}{1 + \gamma}.$$

If the mass transfer resistance is negligible, the flux is

$$N'_{LSi} = \frac{\varepsilon_L \rho_B}{a_p} \nu_i k c_{Li}^b.$$

The effectiveness factor becomes

$$\eta_e = \frac{N_{LSi}}{N'_{LSi}} = \frac{1}{1 + \gamma}, \qquad [E]$$

where

$$\gamma = \frac{\varepsilon_L \rho_B (-\nu_i) k}{k_{LSi} a_p}.$$

c. For pure internal mass transfer resistance for a completely wetted spherical particle, Equation 5.79 is valid:

$$\eta_e = \frac{3}{\phi} \left(\frac{1}{\tanh \phi} - \frac{1}{\phi} \right), \qquad [F]$$

where

$$\phi = \sqrt{\frac{-\nu_i \rho_p k}{D_{ei}}}.$$

d. If all the resistances are present simultaneously, the overall effectiveness factor $(\eta_{e,overall})$ is obtained from Equations [D], [E], and [F]:

$$\eta_{e,overall} = [D][E][F],$$

$$\eta_{e,overall} = \frac{3}{(1+\beta)(1+\gamma)\phi}\left(\frac{1}{\tanh\ \phi} + \frac{1}{\phi}\right),$$

where the dimensionless moduli are

$$\beta = \frac{\varepsilon_L \rho_B (-\nu_i) k}{k_{Li} a},$$

$$\gamma = \frac{\varepsilon_L \rho_B (-\nu_i) k}{k_{LSi} a_p},$$

$$\phi = \sqrt{\frac{-\nu_i \rho_p k}{D_{ei}}}.$$

Note that in the above formulae, the rate is calculated from

$$r_i = \eta_{e,overall} \frac{\nu_i k c_{Gi}^b}{K_i}.$$

The effectiveness factor is independent of the reactant concentration.

SECTION II/18

For the liquid–solid mass transfer, the following equation (Equation 6.11) is valid:

$$k_{LSi}\left(c_{Li}^b - c_{Li}^s\right) a_p = -\varepsilon_L \rho_B r_i.$$

In the present case, $i = A$ and $r_i = -2k\left(c_{LA}^s\right)^2 c_{LB}^b$.

We denote $k' = 2kc_{LB}^b$ and obtain $k_{LSA} a_p \left(c_{LA}^b - c_{LA}^s\right) = k' \varepsilon_L \rho_B \left(c_{LA}^s\right)^2$, which can be brought into a dimensionless form

$$1 - \left(\frac{c_{LA}^s}{c_{LA}^b}\right) = \frac{\varepsilon_L \rho_B k' c_{LA}^b}{k_{LSA} a_p} \left(\frac{c_{LA}^s}{c_{LA}^b}\right)^2,$$

that is, $1 - y = \alpha y^2$, where

$$\alpha = \frac{\varepsilon_L \rho_B k' c_{LA}^b}{k_{LSA} a_p}$$

$\alpha y^2 + y - 1 = 0$ (a dimensionless modulus), $y = c_{LA}^s / c_{LA}^b$.

The solution becomes

$$y = \frac{-1 \pm \sqrt{1^2 - 4\alpha\,(-1)}}{2\alpha}.$$

For our case the root

$$y = \frac{\sqrt{1 + 4\alpha} - 1}{2\alpha} \qquad [A]$$

is physically relevant.

The effectiveness factor is in this case defined as

$$\eta_e = \frac{k' \varepsilon_L \rho_B {c_{La}^s}^2}{k' \varepsilon_L \rho_B {c_{La}^b}^2} = y^2,$$

that is,

$$\eta_e = \frac{\left(\sqrt{1 + 4\alpha} - 1\right)^2}{4\alpha^2}. \qquad [B]$$

The value of η_e is plotted against the modulus α.

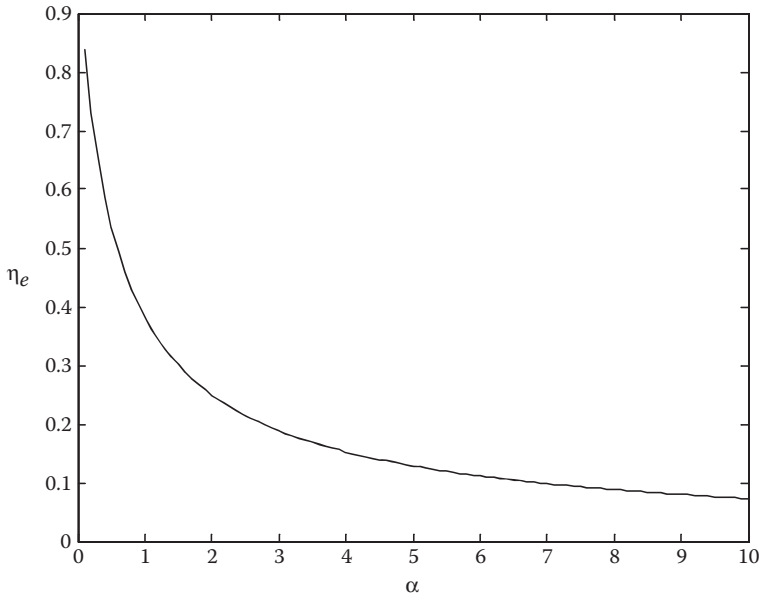

b. For the liquid-phase components, mass balance (Equation 6.39) is used,

$$\frac{dn_{Li}}{dt} = \left(N_{Li}^b a_v - N_{Li}^s a_p\right) V_R.$$

Since A is nonvolatile, $N_{\mathrm{LA}}^{\mathrm{b}} = 0$. Furthermore, $n_{\mathrm{L}i} = c_{\mathrm{L}i}^{\mathrm{b}} V_{\mathrm{L}}$ and V_{L} is constant. We obtain

$$V_{\mathrm{L}} \frac{\mathrm{d}c_{\mathrm{LA}}^{\mathrm{b}}}{\mathrm{d}t} = -N_{\mathrm{LSA}} a_{\mathrm{p}} V_{\mathrm{R}}, \quad \text{where} \quad N_{\mathrm{LSA}} = k_{\mathrm{LSA}} \left(c_{\mathrm{LA}}^{\mathrm{b}} - c_{\mathrm{LA}}^{\mathrm{s}} \right),$$

that is,

$$N_{\mathrm{LSA}} = \frac{k' c_{\mathrm{L}} \rho_{\mathrm{B}} {c_{\mathrm{LA}}^{\mathrm{s}}}^2}{a_{\mathrm{p}}} \quad \text{and} \quad V_{\mathrm{L}}/V_{\mathrm{R}} = \varepsilon_{\mathrm{L}}.$$

These quantities are inserted into the balance equation, and we obtain

$$\frac{\mathrm{d}c_{\mathrm{LA}}^{\mathrm{B}}}{\mathrm{d}t} = -k' \rho_{\mathrm{B}} {c_{\mathrm{LA}}^{\mathrm{s}}}^2 = k' \rho_{\mathrm{B}} {c_{\mathrm{LA}}^{\mathrm{b}}}^2 y^2,$$

that is,

$$\frac{\mathrm{d}c_{\mathrm{LA}}^{\mathrm{b}}}{\mathrm{d}t} = -k' \rho_{\mathrm{B}} {c_{\mathrm{LA}}^{\mathrm{b}}}^2 \left(\frac{\sqrt{1 + 4\alpha} - 1}{2\alpha} \right)^2,$$

where

$$\alpha = \frac{\varepsilon_{\mathrm{L}} \rho_{\mathrm{B}} k'}{k_{\mathrm{LAS}} a_p} c_{\mathrm{LA}}^{\mathrm{b}}.$$

A dimensionless concentration $x = c_{\mathrm{LA}}^{\mathrm{b}} / c_{0\mathrm{LA}}^{\mathrm{b}}$ is introduced and we obtain $\left(c_{0\mathrm{LA}}^{\mathrm{b}} = c_{0\mathrm{A}} \right)$

$$\frac{\mathrm{d}x}{\mathrm{d}t} = -k' \rho_{\mathrm{B}} c_{0\mathrm{A}} x^2 \left(\frac{\sqrt{1 + 4\beta x} - 1}{2\beta x} \right)^2, \qquad [\mathrm{C}]$$

where

$$\beta = \frac{\varepsilon_{\mathrm{L}} \rho_{\mathrm{B}} k' c_{0\mathrm{A}}}{k_{\mathrm{LAS}} a_{\mathrm{p}}}, \quad \text{at} \quad t = 0,\ x = 1.$$

Equation [C] can be presented in Damköhler space by introducing a Damköhler number (Da) as follows: $Da = k' \rho_{\mathrm{B}} \ c_{0\mathrm{A}}$. We obtain

$$\frac{\mathrm{d}x}{\mathrm{d}Da} = -x^2 \left(\frac{\sqrt{1 + 4\beta x} - 1}{2\beta x} \right)^2,$$

at $Da = 0, x = 1$.

In general, the solution of Equation [D] is obtained numerically. Two limiting cases are of interest. For a negligible mass transfer resistance, $\beta = 0$, $\eta_e = 1$, and the parenthesis

expression in Equation [D] approaches 1. We have

$$\frac{\mathrm{d}x}{\mathrm{d}Da} = -x^2,$$

that is,

$$x = (1 + Da)^{-1}.$$

In case of a heavy mass transfer resistance, the effectiveness factor (Equation [B]) approaches (a is large) the expression

$$\eta_e = \frac{\left(\sqrt{4\alpha}\right)^2}{4\alpha^2} = \frac{1}{\alpha}.$$

The parenthesis in Equation [D] approaches for large β ($\beta \to \infty$)

$$\left(\frac{\sqrt{1 + 4\beta x} - 1}{2\beta x}\right)^2 \to \left(\frac{\sqrt{4\beta x}}{2\beta x}\right)^2 = \frac{1}{\beta x}.$$

The mass balance [D] in this case becomes

$$\frac{\mathrm{d}x}{\mathrm{d}Da} = -\frac{1}{\beta}x,$$

which has the solution

$$x = \mathrm{e}^{-Da/\beta},$$

that is, the system approaches first-order behavior as the mass transfer resistance increases.

What is Da/β? From the definitions of Da and β, we obtain

$$\frac{Da}{\beta} = \frac{k'\rho_B c_{0A} k_{LSA} a_p}{\varepsilon_L \rho_B k' c_{0A}} = \frac{k_{LSA} a_p}{\varepsilon_L},$$

which means that the system is described by

$$x = \mathrm{e}^{-k_{LSA} a_p/\varepsilon_L},$$

that is, exclusively by the mass transfer resistance parameter. A full numerical solution of Equation [D] for various values of β is provided in the figure below.

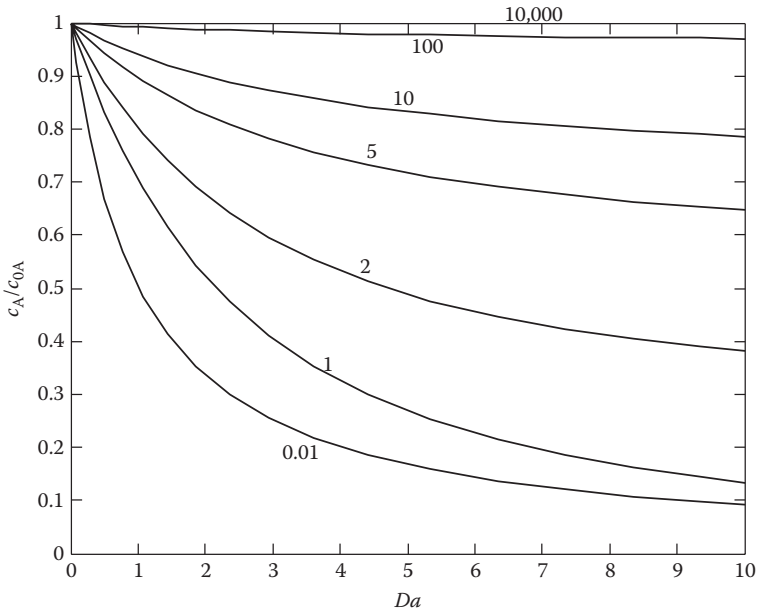

SECTION III/2

The reaction scheme is written as follows.

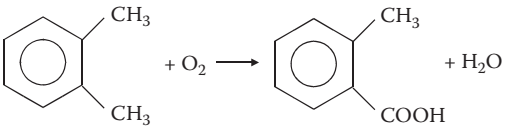

The reaction rate is given by

$$R = kc_{O_2}.$$

For the liquid and gas phases, we have the balances for a BR (Section 7.2.3)

$$\frac{dn_{Li}}{dt} = \left(N_{Li}^{b} a_v + \varepsilon_L r_i\right) V_R,$$

$$\frac{dn_{Gi}}{dt} = -N_{Gi}^{b} a_v V_R.$$

The reaction is assumed to be rapid. The expression for the flux of a first-order reaction is (Equation 7.112 in Section 7.2.4)

$$N_{Li}^{s} = N_{Gi}^{b} = \frac{c_{Gi}^{b} - \left(K_i / \cosh\sqrt{M}\right) c_{Li}^{b}}{\left(\tanh\sqrt{M}/\sqrt{M}\right)(K_i/k_{Li}) + (1/k_{Gi})}.$$

Because the reaction is rapid, $c^{\mathrm{b}}_{\mathrm{L}i} = c^{\mathrm{b}}_{\mathrm{LO_2}} \approx 0$, and the flux expression is simplified to

$$N^{\mathrm{b}}_{\mathrm{GO_2}} = \frac{c^{\mathrm{b}}_{\mathrm{GO_2}}}{\left(\tanh\sqrt{M}/\sqrt{M}\right)\left(K_{\mathrm{O_2}}/k_{\mathrm{LO_2}}\right) + \left(1/k_{\mathrm{G_2}}\right)} = \frac{c^{\mathrm{b}}_{\mathrm{GO_2}}}{\beta^{-1}},$$

where

$$\sqrt{M} = \left(\frac{-\nu_{\mathrm{O_2}} k D_{\mathrm{LO_2}}}{k^2_{\mathrm{LO_2}}}\right)^{1/2},$$

that is, the Hatta number.

The gas-phase mass balance is

$$\frac{\mathrm{d}n_{\mathrm{GO_2}}}{\mathrm{d}t} = \frac{\mathrm{d}c^{\mathrm{b}}_{\mathrm{GO_2}}}{\mathrm{d}t} V_{\mathrm{G}} = -N^{\mathrm{b}}_{\mathrm{GO_2}} a_{\mathrm{v}} V_{\mathrm{R}}$$

yielding ($V_{\mathrm{G}} = \varepsilon_{\mathrm{G}} V_{\mathrm{R}}$)

$$\frac{\mathrm{d}c^{\mathrm{b}}_{\mathrm{GO_2}}}{\mathrm{d}t} = -\frac{N^{\mathrm{b}}_{\mathrm{GO_2}} a_{\mathrm{v}}}{\varepsilon_{\mathrm{G}}} = -\frac{\beta a_{\mathrm{v}}}{\varepsilon_{\mathrm{G}}} c^{\mathrm{b}}_{\mathrm{GO_2}}.$$

The separation of variables yields

$$\int_{c_{0\mathrm{GO_2}}}^{c_{\mathrm{GO_2}}} \frac{\mathrm{d}c^{\mathrm{b}}_{\mathrm{GO_2}}}{c^{\mathrm{b}}_{\mathrm{GO_2}}} = -\frac{\beta a_{\mathrm{v}}}{\varepsilon_{\mathrm{G}}} \int_0^t \mathrm{d}t,$$

that is,

$$\ln\left(\frac{c^{\mathrm{b}}_{\mathrm{GO_2}}}{c^{\mathrm{b}}_{0\mathrm{GO_2}}}\right) = -\frac{\beta a_{\mathrm{v}}}{\varepsilon_{\mathrm{G}}} t,$$

which yields the required reaction time

$$t = \frac{\varepsilon_{\mathrm{G}}}{\beta a_{\mathrm{v}}} \ln\left(\frac{c^{\mathrm{b}}_{\mathrm{GO_2}}}{c^{\mathrm{b}}_{0\mathrm{GO_2}}}\right)^{-1}.$$

The concentrations are obtained from the pressures as follows:

$$P_{0\mathrm{O_2}} = c^{\mathrm{b}}_{0\mathrm{GO_2}} R T_0 \quad \text{and} \quad P_{\mathrm{O_2}} = c^{\mathrm{b}}_{\mathrm{GO_2}} R T,$$

that is,

$$\left(\frac{c^{\mathrm{b}}_{\mathrm{GO_2}}}{c^{\mathrm{b}}_{0\mathrm{GO_2}}}\right) = \left(\frac{P_{\mathrm{O_2}}}{P_{0\mathrm{O_2}}}\right) = \left(\frac{2\,\mathrm{bar}}{20\,\mathrm{bar}}\right)^{-1} = 10.$$

Finally, we have

$$t = \frac{\varepsilon_G}{\beta a_v} \ln(10).$$

The parameter values are calculated below

$$K_{O_2} = \frac{c^*_{GO_2}}{c^*_{LO_2}}, \quad \text{but} \quad He_{O_2} = \frac{P^*_{O_2}}{c^*_{LO_2}} = \frac{c^*_{GO_2}}{c^*_{LO_2}} RT = K_{O_2} RT.$$

Thus

$$K_{O_2} = \frac{He_{O_2}}{RT} = \frac{126\,\text{dm}^3\text{Kmol}\,100 \times 10^3\,\text{Pa}}{\text{mol}\,8.3143\,\text{J}(273+160)\text{K}} = 3.49991.$$

Since k_{GO_2} is large, β becomes

$$\beta = \left(\frac{\tanh\sqrt{M}}{\sqrt{M}} \frac{K_{O_2}}{k_{LO_2}} \right)^{-1}.$$

The Hatta number $\sqrt{M}$ is calculated:

$$\sqrt{M} = \left(\frac{3/2 \times 2.4 \times 10^3\,\text{h}^{-1} \times 5.2 \times 10^{-6}\,\text{m}^2/\text{h}}{1.5^2\,\text{m}^2/\text{h}^2} \right)^{1/2} = 0.0912.$$

Thus we have

$$\beta = \frac{\sqrt{M}}{\tanh\sqrt{M}} \frac{k_{LO_2}}{K_{O_2}} = \frac{0.0912}{\tanh(0.0912)} \frac{1.5\,\text{m/h}}{3.49991} = 0.4297\,\text{m/h}.$$

The factor $\beta a_v/\varepsilon_G$ becomes

$$\frac{\beta a_v}{\varepsilon_G} = \frac{0.4297\,\text{m/h} \times 20\,\text{m}^{-1}}{0.5} = 17.1882\,\text{h}^{-1},$$

$$t = \frac{\varepsilon_G}{\beta a_v} \ln(10) = 0.13396\,\text{h} = 8.03\ \text{min}.$$

The required reaction time is 8 min.

SECTION III/4

Chlorination of *p*-cresol can be expressed in a simplified way as

$$A + B \rightarrow C + D,$$

where A is chlorine and B is *p*-cresol. Various expressions can be used to estimate E_A, for example, from the van Krevelen–Hoftijzer approximation or the expressions collected in Table 7.4.

We start by calculating E_i

$$E_i = 1 + \frac{\nu_A D_{LB} c^b_{LB}}{\nu_B D_{LA} c^s_{LA}}.$$

The diffusion coefficients are obtained from the Wilke–Chang equation

$$D_{LA} = \frac{7.4 \cdot 10^{-12} \sqrt{\phi M_{solvent}}\, T}{\eta \nu_A^{0.6}}$$

and similarly for B we can obtain D_{LB}. The ratio becomes

$$\frac{D_{LB}}{D_{LA}} = \left(\frac{\nu_A}{\nu_B}\right)^{0.6} = \left(\frac{49.2}{125.6}\right)^{0.6} = 0.56988.$$

The concentration of c^s_{LA} is obtained from solubility data: $K_A = c^s_{GA}/c^s_{LA}$,

$$c^s_{LA} = \frac{c^s_{GA}}{K_A} = \frac{P_A}{RTK_A} = \frac{x_A P}{RTK_A}.$$

We obtain

$$c^s_{LA} = \frac{0.5 \cdot 101.3 \times 10^3 \text{ Pa}}{8.3143 \text{ J/mol K} \times 273 \text{ K} \times 0.02} = 1.1157 \text{ k mol/m}^3.$$

Now the factor E_i is obtained:

$$E_i = 1 + 0.56988 \frac{10}{1.1157} = 6.1077.$$

To progress further, the Hatta number ($\sqrt{M}$) is needed:

$$M = -\frac{\nu_A k c^b_{LB}}{D_{LA}} \delta_L^2,$$

that is,

$$\sqrt{M} = \sqrt{\frac{-\nu_A k c^b_{LB}}{D_{LA}}}\, \delta_L.$$

The diffusion coefficient of A is included in D_{LA}, First the viscosity is calculated from the empirical equation

$$\ln\left(\frac{\mu}{\text{cP}}\right) = -1.303 \times 10^{1} + \frac{2.290 \times 10^{3}}{297} + 2.339 \times 10^{-2} \times 273 - 2.011 \times 10^{-5} \times 273^{2}$$
$$= 0.24497$$
$$\mu = 1.27758 \text{ cP}.$$

The molar mass of the solvent (CCl_4) is

$$M_{CCl_4} = (12 + 4 \times 35.45) \text{ g/mol} = 153.8 \text{ g/mol}.$$

The diffusion coefficient becomes

$$D_{LA} = \frac{7.4 \times 10^{-12}\sqrt{1 \times 153.8} \times 273}{1.27758 \times 49.2^{0.6}} \text{m}^2/\text{s} = 1.894 \times 10^{-9} \text{ m}^2/\text{s}.$$

The Hatta number obtains the value

$$\sqrt{M} = \sqrt{\frac{-(-1) \times 5.626 \times 10^{-3} \text{ m}^3/\text{mols} \times 10 \text{ mol/L}}{1.894 \times 10^{-9} \text{ m}^2/\text{s}}} \times 1.5 \times 10^{-5} \text{ m} = 0.08176.$$

The famous formula of van Krevelen and Hoftijzer yields

$$E_A = \frac{\sqrt{M(E_i - E_A/E_i - 1)}}{\tanh\sqrt{M(E_i - E_A/E_i - 1)}},$$

where $\sqrt{M} = 2.038$ and $E_i = 6.1077$. An iterative solution of the above equation yields $E_A = 1.0022$. The Hatta value is low, E_i has rather a low value, and in addition c_{LB} is high. We can conclude that a pseudo-first-order reaction is probable.

SECTION III/6

This reaction is very slow and it has extraordinary autocatalytic kinetics (independent of chlorine concentration). The system can thus be treated as a homogeneous liquid-phase system, for which the mass transfer effects are negligible.

a. We have the balance equation for a CSTR $(c_B - c_{0B})/\tau_L = r_B$, where B is the monochloroacetic acid and $\tau_L = V/\dot{V}_L$, $c_{0B} = 0$ (no B in the feed), and $r_B = r$.

From the above equations, we obtain

$$c_B = \tau_L c_C\left(k_1 + k_2 c_B^{1/2}\right).$$

The mole fraction and the total concentration ($c_i = x_i c_0$) are introduced:

$$x_B c_0 = \tau_L x_C c_0 \left(k_1 + k_2 c_0^{1/2} x_B^{1/2} \right),$$

which is simplified to

$$x_B - k_1 \tau_L x_C = k_2 c_0^{1/2} \tau_L x_C x_B^{1/2}.$$

We denote $k_2 c_0^{1/2} \tau_L x_C = \alpha$ and $k_1 \tau_L x_C = \beta$, that is, $x_B - \beta = \alpha x_B^{1/2}$, which yields a second-degree equation:

$$(x_B - \beta)^2 = \alpha x_B \text{ equivalent to}$$
$$x_B^2 - 2\beta x_B - \alpha x_B + \beta^2 = 0,$$

giving the mole fraction of B:

$$x_B = \frac{2\beta + \alpha \pm \sqrt{\alpha^2 + 4\alpha\beta}}{2}.$$

Numerically, we obtain

$$\alpha = k_2 c_0^{1/2} \tau_L x_C,$$
$$\tau_L = \frac{V}{\dot{V}_L} = \frac{V\rho}{\dot{m}} = \frac{200\,\text{L} \times 1\,\text{kg/L} \times 60\ \text{min}}{60\,\text{kg}} = 200\ \text{min},$$
$$\alpha = 0.0512 \times 200 \times 0.05 = 0.515,$$
$$\beta = k_1 \tau_L x_C = 0.0133\,\text{min}^{-1} \times 200\ \text{min}\ \times 0.05 = 0.133,$$
$$2\beta + \alpha = 0.781,$$
$$x_B = \frac{0.781 \pm \sqrt{0.781^2 - 0.070756}}{2},$$
$$x_B = \frac{0.781 \pm 0.7343}{2} = 0.75765.$$

[The second root (–) does not satisfy the original equation.]

In this case, the conversion of A is defined by

$$\eta_A = \frac{c_{0A} - c_A}{c_{0A}} = \frac{x_{0A} - x_A}{x_{0A}} = 1 - \frac{x_A}{x_{0A}}$$

and we have $c_0 = c_A + c_B + c_C$, that is, $x_A + x_B + x_C = 1$ and $x_{0A} + x_{0B} + x_{0C} = 1$.

Furthermore, $x_C = x_{0C}$ (constant), which yields $x_A + x_B = x_{0A} + x_{0B}$ and $x_{0B} = 0$.

Thus $x_A = x_{0A} - x_B = 0.95 - 0.75765 = 0.1924$.

$$\eta_A = 1 - \frac{0.1924}{0.95} = 0.797.$$

The conversion is $\eta_A \approx 0.80$.

b. For batchwise operation, we have the balance equation

$$\frac{dc_B}{dt} = r_B.$$

The rate expression is inserted and we obtain

$$\frac{dc_B}{dt} = \left(k_1 + k_2 c_B^{1/2}\right) c_C.$$

The mole fraction x_B is defined as $x_B = c_B/c_0$:

$$\frac{dx_B}{dt} c_0 = \left(k_1 + k_2 c_0^{1/2} x_B^{1/2}\right) c_0 x_C,$$

yielding

$$\frac{dx_B}{dt} = \left(k_1 + k_2 c_0^{1/2} x_B^{1/2}\right) x_C.$$

We denote $k_1 x_C = \beta$ and $k_2 c_0^{1/2} x_C = \alpha$.
The separation of variables yields

$$\int_0^{x_B} \frac{dx_B}{\alpha x_B^{1/2} + \beta} = \int_0^t dt = t.$$

The substitution $x_B^{1/2} = y$ is introduced.
We obtain $x_B = y^2$ and $dx_B = 2y\,dy$.
The integral becomes

$$\int_0^y \frac{2y\,dy}{\alpha y + \beta} = \frac{2}{\alpha}\int_0^y \frac{(\alpha y + \beta - \beta)}{\alpha y + \beta} dy = \frac{2}{\alpha}\int_0^y \left(1 - \frac{\beta}{\alpha y + \beta}\right) dy$$
$$= \frac{2}{\alpha}\Big/_0^y \left(y - \frac{\beta}{\alpha}\ln(\alpha y + \beta)\right) = \frac{2}{\alpha}\left(y - \frac{\beta}{\alpha}\ln(\alpha y + \beta) + \frac{\beta}{\alpha}\ln(\beta)\right).$$

Rearrangement and backsubstitution yields

$$\frac{2}{\alpha}\left(x_B^{1/2} + \frac{\beta}{\alpha}\ln\left(\frac{\beta}{\alpha x_B^{1/2} + \beta}\right)\right) = t.$$

The numerical values are listed below:

$$\alpha = k_2 c_0^{1/2} x_C = 0.0512 \times 0.05\,\text{min}^{-1} = 0.00256\,\text{min}^{-1},$$
$$\beta = k_1 x_C = 0.0133\,\text{min}^{-1} \times 0.05 = 0.000665\,\text{min}^{-1}.$$

The equation is rewritten as

$$2x_B^{1/2} + \frac{2\beta}{\alpha}\ln\left(\frac{1}{(\alpha/\beta)x_B^{1/2}+1}\right) - \alpha t = 0 \quad \text{and} \quad x_B^{1/2} = y.$$

The final form is

$$2y - 2\frac{\beta}{\alpha}\ln\left(\frac{\alpha}{\beta}y + 1\right) - \alpha t = 0, \qquad [A]$$
$$\alpha/\beta = 3.8496 \quad t = \tau_L = 200\ \text{min}.$$

Equation [A] is solved numerically giving $y = 0.55$. Finally, we obtain $x_B = y^2$, $x_B = 0.3025$. This is less than what was obtained for the CSTR ($x_{B,CSTR} = 0.76$), which is a direct consequence of the autocatalytic kinetics.

SECTION III/11

The reaction is written as A(G) + B(L) → products.

For an adsorption column, the following design equation is valid (Section 7.2.6):

$$V_R = \frac{(1 - x_{0A})\,\dot{n}_{0G}}{a_v}\int_{x_A}^{x_{0A}} \frac{dx_A}{N_{LA}^s\,(1 - x_A)^2}.$$

For infinitely fast reactions, the flux is given by

$$N_{LA}^s = \frac{c_{GA}^b + (\nu_A D_{LB}/\nu_B D_{LA}) K_A c_{LB}^b}{(K_A/k_{LA}) + (1/k_{GA})},$$

where

$$c_{GA}^b = x_A c_0 = x_A \frac{P}{RT}.$$

The flux expression is inserted into the design equation (Section 7.2.6)

$$V_R = (1 - x_{0A})\,\dot{n}_{0G}\left(\frac{K_A}{k_{LA}a_v} + \frac{1}{k_{GA}a_v}\right)\int_{x_A}^{x_{0A}} \frac{d_{x_A}}{\left(x_A P/RT + \omega\, c_{LB}^b\right)(1 - x_A)^2},$$

where $\omega = (\nu_A D_{LB}/\nu_B D_{LA}) K_A$ and

$$c^b_{LB} = c^b_{1LB} + \frac{\nu_B}{\nu_A}\left(\frac{x_{0A} - x_A}{1 - x_A}\right)\frac{\dot{V}_{0G}}{\dot{V}_{0L}}\frac{P}{RT},$$

$$c^b_{1LB} = c^b_{0LB} - \frac{\nu_B}{\nu_A}\left(\frac{x_{0A} - x_{1A}}{1 - x_{1A}}\right)\frac{\dot{V}_{0G}}{V_{0L}}\frac{P}{RT}.$$

The boundaries are calculated below. According to the requirements, 95% of A should react and $x_{0A} = 0.05$.

We have

$$\eta_A = \frac{\dot{n}_{0A} - \dot{n}_A}{\dot{n}_{0A}} = 1 - \frac{\dot{n}_A}{\dot{n}_{0A}} = 0.95,$$

that is,

$$\frac{\dot{n}_A}{\dot{n}_{0A}} = 0.05.$$

The total flow at the inlet and the outlet is $\dot{n}_0 = \dot{n}_{inert} + \dot{n}_A$, where the subscript "inert" refers to the inert gas and

$$\dot{n} = \dot{n}_{inert} + \dot{n}_A.$$

The first equation gives $\dot{n}_{inert} = \dot{n}_0 - \dot{n}_0 x_{0A} = \dot{n}_0 (1 - x_{0A})$. Analogously, the second equation gives $\dot{n}_{inert} = \dot{n} (1 - x_A)$ leading to

$$1 = \frac{\dot{n} (1 - x_A)}{\dot{n}_0 (1 - x_{0A})},$$

that is,

$$\frac{\dot{n}}{\dot{n}_0} = \frac{1 - x_{0A}}{1 - x_A}.$$

The conversion value yields

$$\eta_A = 1 - \frac{x_A}{x_{0A}}\frac{\dot{n}}{\dot{n}_0} = 1 - \frac{x_A (1 - x_{0A})}{x_{0A} (1 - x_A)},$$

from which x_A is elegantly solved:

$$x_A = \frac{(1 - \eta_A) x_{0A}}{1 - x_{0A} + (1 - \eta_A) x_{0A}}.$$

We obtain the solution $x_A = 0.00265$ from the above equation.

The expression for c^b_{1LB} gives the ratio between the volumetric flow rates $\dot{V}_{0G}/\dot{V}_{0L}$, as will be expressed below.

The conversion of B is fixed to

$$\eta_B = \frac{c_{0B} - c_{1B}}{c_{0B}} = 0.9, \quad \text{which gives} \quad \frac{c_{1LB}}{c_{0LB}} = 0.1.$$

The expression for c_{1LB} yields

$$\frac{c_{1LB}}{c_{0LB}} + \frac{\nu_B}{\nu_A}\left(\frac{x_{0A} - x_{1A}}{1 - x_{1A}}\right)\frac{P\dot{V}_{0G}}{c_{0LB}RT\dot{V}_{0L}} = 1 \quad \text{leading to}$$

$$\frac{\dot{V}_{0G}}{\dot{V}_{0L}} = A\left(1 - \frac{c_{1LB}}{c_{0LB}}\right),$$

that is,

$$\frac{\dot{V}_{0G}}{\dot{V}_{0L}} = \frac{\nu_A\,(1 - x_{1A})\,c_{0LB}RT}{\nu_B\,(x_{0A} - x_{1A})\,P}\left(1 - \frac{c_{1LB}}{c_{0LB}}\right).$$

We obtain

$$\frac{\nu_A\,(1 - x_{1A})\,c_{0LB}RT}{\nu_B\,(x_{0A} - x_{1A})\,P} = \frac{(-1)(1 - 0.00265) \times 500\,\text{mol/m}^3 \times 8.3143\,\text{J/(K mol)} \times 298\,\text{K}}{(-1)(0.05 - 0.00265) \times 20 \times 100 \times 10^3\,\text{Pa}}$$

$$= 13.046967.$$

$$\frac{\dot{V}_{0G}}{\dot{V}_{0L}} = 13.046967(1 - 0.1) = 11.74227,$$

$$\dot{V}_{0L} = \frac{\dot{V}_{0G}}{11.74227} = \frac{5000\,\text{m}^3}{3600\,\text{s} \times 11.74227} = 0.11828\,\text{m}^3/\text{s}.$$

The factor P/RT is

$$\frac{P}{RT} = \frac{20 \times 100 \times 10^3\,\text{Pa}}{8.3143\,\text{J/K mol} \times 298\,\text{K}} = 807.2128\,\text{mol/m}^3,$$

$$\frac{P}{RT}\frac{\dot{V}_{0G}}{\dot{V}_{0L}} = 9478.51\,\text{mol/m}^3.$$

We obtain

$$c_{LB}^{b} = 50\,\text{mol/m}^3 + 9478.51\,\text{mol/m}^3\left(\frac{x_{0A} - x_A}{1 - x_A}\right).$$

The parameter ω will be calculated; He_A is converted to K_A accordingly:

$$\text{He}_A = \frac{p_A}{c_{LA}} = \frac{c_{GA}RT}{c_{LA}} = K_A RT,$$

$$K_A = \frac{\text{He}_A}{RT} = \frac{9.8 \times 10^{-3}\,\text{m}^3 \times 100 \times 10^3\,\text{Pa K mol}}{\text{mol}\,8.3143\,\text{J} \times 298\,\text{K}} = 0.39553,$$

$$\omega = \frac{\nu_A D_{LB}}{\nu_B D_{LA}}K_A = \frac{(-1) \times 1.62^{-1} \times 0.39553}{(-1)} = 0.244157.$$

The mass transfer parameter is

$$\frac{K_A}{k_{LA}a_v} + \frac{1}{k_{GA}a_v}.$$

The gas-phase mass transfer parameter is not given in standard units, but in pressure units, that is,

$$k'_{GA}\Delta c = k'_{GA}\Delta P = k'_{GA}\Delta cRT,$$

which yields

$$k_{GA}a_v = k'_{GA}a_vRT = \frac{1.2 \times 10^{-5}\,\text{mol} \times 8.3143\,\text{J} \times 298\,\text{K}}{\text{K mol}\,10^{-6}\,\text{m}^3 \times 100 \times 10^3\,\text{Pa s}} = 0.297319\,\text{s}^{-1},$$

$$\frac{1}{k_{GA}a_v} = 3.36339\,\text{s}.$$

The factor $K_A/k_{LA}a_v$ becomes

$$\frac{K_A}{k_{LA}a_v} = \frac{0.39553}{1.4 \cdot 10^{-2}}\,\text{s} = 28.252\,\text{s}.$$

Both gas- and liquid-side mass transfer resistances are significant, since $1/(k_{GA}a_v)$ and $K_A/(k_{GA}a_v)$ are of comparable size. The proportionality factor becomes

$$F = (1 - x_{0A})\,\dot{n}_{0G}\left(\frac{K_A}{k_{LA}a_v} + \frac{1}{k_{GA}a_v}\right),$$

where

$$\dot{n}_{0G} = \frac{\dot{V}_{0G}}{RT} = \frac{20 \times 100 \times 10^3\,\text{Pa} \times 5000\,\text{m}^3 \times \text{K mol}}{8.3143\,\text{J} \times 298\,\text{K} \times 3600\,\text{s}} = 1121.129\,\text{mol/s},$$

and

$$1 - x_{0A} = 0.95.$$

Finally, we obtain

$$F = 0.95 \cdot 1121.129\,\text{mol/s}(28252 + 3.36339)\,\text{s} = 33672.68\,\text{mol}.$$

The design algorithm can now be simplified as follows:

$$V_R = F\int_{x_A}^{x_{0A}} \frac{dx_A}{\left(x_AP/RT + \omega c^b_{LB}\right)(1 - x_A)^2},$$

where

$$c_{\mathrm{LB}}^{\mathrm{b}} = \left(50 + 9478.51\left(\frac{x_{0\mathrm{A}} - x_{\mathrm{A}}}{1 - x_{\mathrm{A}}}\right)\right) \mathrm{mol/m^3},$$

where

$$x_{0\mathrm{A}} = 0.05,$$
$$\omega = 0.244157,$$
$$P/RT = 807.21\ \mathrm{mol/m^3},$$
$$F = 33,672.68\ \mathrm{mol}.$$

Numerical integration is carried out from $x_{\mathrm{A}} = 0.00264$ to $x_{0\mathrm{A}} = 0.05$.
The reactor volume becomes $V_{\mathrm{R}} = 20.12\ \mathrm{m^3}$.
The column is cylindrical, that is, $V_{\mathrm{R}} = (\pi \mathrm{d}^2/4)\mathrm{L}$, $d = 1.2$ m,

which gives $L = 4V_{\mathrm{R}}/\pi \mathrm{d}^2$. The column height becomes $L = 17.8$ m.

SECTION III/12

Absorption of H_2S (A) in monoethyleneamine (MEA, B):

$$\underset{(\mathrm{A})}{\mathrm{H_2S}} + \mathrm{HOCH_2}\underset{(\mathrm{B})}{\mathrm{CH_2NH_2}} \rightarrow \mathrm{HS^-} + \mathrm{HOCH_2CH_2NH_3^+}.$$

The column volume can be calculated from Equation 7.177

$$V_{\mathrm{R}} = \frac{(1 - x_{0\mathrm{A}})\,\dot{n}_{0\mathrm{G}} P}{a_{\mathrm{v}}} \int_{P_{\mathrm{A}}}^{P_{0\mathrm{A}}} \frac{\mathrm{d}p_{\mathrm{A}}}{N_{\mathrm{LA}}^{\mathrm{s}} \left(P - p_{\mathrm{A}}\right)^2}, \qquad [\mathrm{A}]$$

and the height of the column is $h = V_{\mathrm{R}}/A$.

For an infinitely fast reaction, the flux $N_{\mathrm{LA}}^{\mathrm{s}}$ is obtained from Equation 7.152

$$N_{\mathrm{LA}}^{\mathrm{s}} = \frac{c_{\mathrm{GA}}^{\mathrm{b}} + (\nu_{\mathrm{A}}/\nu_{\mathrm{B}})(D_{\mathrm{LB}}/D_{\mathrm{LA}})K_{\mathrm{A}} c_{\mathrm{LB}}^{\mathrm{b}}}{(K_{\mathrm{A}}/k_{\mathrm{LA}}) + (1/k_{\mathrm{GA}})}.$$

The concentration $c_{\mathrm{LB}}^{\mathrm{b}}$ is defined in Equation 7.185:

$$c_{\mathrm{LB}}^{\mathrm{b}} = c_{1\mathrm{LB}}^{\mathrm{b}} + \frac{\nu_{\mathrm{B}}}{\nu_{\mathrm{A}}}\left(\frac{x_{0\mathrm{A}} - x_{\mathrm{A}}}{1 - x_{\mathrm{A}}}\right)\frac{\dot{V}_{0\mathrm{G}}}{\dot{V}_{0\mathrm{L}}}\frac{P}{RT}. \qquad [\mathrm{B}]$$

The liquid volumetric flow rate can be obtained from Equation [B] as

$$\dot{V}_{0\mathrm{L}} = \dot{V}_{0\mathrm{G}}\frac{\nu_{\mathrm{B}}}{\nu_{\mathrm{A}}}\left(\frac{x_{0\mathrm{A}} - x_{\mathrm{A}}}{1 - x_{\mathrm{A}}}\right)\frac{1}{c_{\mathrm{LB}}^{\mathrm{b}} - c_{1\mathrm{LB}}^{\mathrm{b}}}\frac{P}{RT}.$$

Liquid-phase outlet concentration of component B is obtained from the conversion

$$\eta_B = \frac{c^b_{LB} - c^b_{1LB}}{c^b_{LB}}, \quad c^b_{1LB} = (1 - \eta_B) c^b_{LB}.$$

The flux can be rewritten as

$$N^s_{LA} a_v = \frac{c^b_{GA} + (\nu_A D_{LB}/\nu_B D_{LA}) K_A c^b_{LB}}{(K_A/k_{LA} a_v) + (1/k_{GA} a_v)}.$$

The concentration of gas component A is obtained from the ideal gas law

$$c^b_{GA} = \frac{p_A}{RT} = \frac{x_A P}{RT}.$$

The concentrations are inserted into the flux term and we obtain

$$N^s_{LA} a_v = \frac{x_A + (\nu_A D_{LB}/\nu_B D_{LA}) K_A \left((RT/P) c^b_{1LB} (\nu_B/\nu_A) \left[(x_{0A} - x_A)/(1 - x_A) \right] \left(\dot{V}_{0G}/\dot{V}_{0L} \right) \right) (P/RT)}{(K_A/k_{LA} a_v) + (1/k_{GA} a_v)}.$$

Transformation from pressure to molar fraction yields

$$p_A = x_A P, \quad \mathrm{d}p_A = P \mathrm{d}x_A, \quad \left(P - p_A \right)^2 = P^2 (1 - x_A)^2 .$$

Now Equation [A] can be written in the form

$$V_R = (1 - x_{0A}) \dot{n}_{0G} \int_{x_{0A}}^{x_{1A}} \frac{\mathrm{d}x_A}{N^s_{LA} a_v (1 - x_A)^2}, \qquad [C]$$

where the gas molar flow rate is obtained from

$$\dot{n}_{0G} = \frac{P \dot{V}_{0G}}{RT}.$$

The outlet mole fraction of component A is $x_{1A} = \dot{n}_{1A}/\dot{n}_{1G}$,

$$\eta_A = \frac{\dot{n}_{0A} - \dot{n}_{1A}}{\dot{n}_{0A}} = 1 - \frac{\dot{n}_{1A}}{\dot{n}_{0A}} = 1 - \frac{x_{1A} \dot{n}_{1G}}{x_{0A} \dot{n}_{0G}}$$

$$\dot{n}_{1G} = \dot{n}_{1A} + \dot{n}_{inert},$$

where

$$\dot{n}_{\text{inert}} = (1 - x_{0A})\,\dot{n}_{0G}, \quad \dot{n}_{1G} = x_{1A}\dot{n}_{1G},$$
$$\dot{n}_{1G} = x_{1A}\dot{n}_{1G} + (1 - x_{0A})\,\dot{n}_{0G}, \qquad (1 - x_{1A})\,\dot{n}_{1G} = (1 - x_{0A})\,\dot{n}_{0G},$$
$$\frac{\dot{n}_{1G}}{\dot{n}_{0G}} = \frac{1 - x_{0A}}{1 - x_{1A}},$$
$$\eta_A = 1 - \frac{x_{1A}\,(1 - x_{0A})}{x_{0A}\,(1 - x_{1A})},$$

from which x_{1A} is solved:

$$x_{1A} = \frac{(1 - \eta_A)\,x_{0A}}{1 - \eta_A x_{0A}}.$$

Equation [C] is integrated numerically using MATLAB®, the program code is listed below.

```
function ex_3_12
x0a=0.05; % initial mole fraction
eta=0.95; % conversion
x1a=(1-eta)*x0a/(1-eta*x0a); % final mole fraction
VR=-quad(@volume,x0a,x1a) % integrate, get volume m3 d=1.2;
% column diameter m h=4*VR/3.1415/d/d % column height m
  return

function int=volume(xa)
% H2S + MEA->HS- + ....
% (A) + (B) ->
R=8.3143;  % J/molK
T=298.15;  % K
nya=-1;
nyb=-1;
V0G=5000/3600; % m3/s
P=20*101325;   % Pa
DLA=2.06e-5;  %cm2/s
DLB=DLA/1.62; %cm2/s
He=9.8;    % dm3bar/mol
klav=1.4e-2; % 1/s
kgav=1.2e-5; % mol/cm3 bar s
kgav=kgav*R*T/1e-6/101.3e3; % 1/s
eta=0.95;
etab=0.9;
x0a=0.05;
```

```
x1a=(1-eta)*x0a/(1-eta*x0a);

c0b=0.5e3;        % mol/m3
c1b=(1-etab)*c0b; % mol/m3

KA=He/1000*100.0e3/R/T;
KK=(KA/klav+1/kgav)^-1;
V0L=V0G*P/R/T*nyb/nya*(x0a-x1a)/(1-x1a)/(c0b-c1b);% m3/s
Nlav=KK*(xa+nya*DLB/nyb/DLA*KA*(R*T/P*c1b+nyb/nya*(x0a-xa)/
(1-xa)*V0G/V0L))*P/R/T;
int=(1-x0a)*P*V0G./R./T./Nlav./(1-xa).^2;

return
```

Results

$$\mathrm{VR} = 20.3281$$

$$\mathrm{h} = 17.9745$$

Column height is 18 m.

SECTION IV/2

The weight gain (w) is directly related to the conversion of the solid component (B), that is,

$$\eta_B = \frac{w}{w_\infty} \; (w_\infty = 111\,\mathrm{mg}).$$

For spherical particles, the dimensionless radius is related to the conversion by

$$\frac{r}{R} = (1 - \eta_B)^{1/3}.$$

By using these formulae, a new table is compiled as shown below:

t/ min	η_B	r/R
0.0	0	1.0000
0.50	0.0297	0.9900
1.00	0.0613	0.9791
1.50	0.0883	0.9697
2.00	0.1153	0.9600
2.50	0.1351	0.9528
3.00	0.1559	0.9451

continued

continued

t/ min	η_B	r/R
4.00	0.1937	0.9308
5.00	0.2288	0.9170
6.00	0.2577	0.9055
7.00	0.2937	0.8906
8.00	0.3180	0.8802
10.00	0.3784	0.8534
12.00	0.4216	0.8332
14.00	0.4685	0.8100
16.00	0.5045	0.7913
18.00	0.5414	0.7711
20.00	0.5757	0.7514
22.00	0.6090	0.7312
24.00	0.6360	0.7140
26.00	0.6577	0.6996
29.00	0.6901	0.6767
32.00	0.7207	0.6537
35.00	0.7477	0.6318
38.00	0.7703	0.6125

The general equation (Equation 8.66) (Section 8.2.2) in case that Bi_{Am} is large (film diffusion negligible) becomes

$$\frac{t}{t_0} = \frac{6\,(1 - r/R) + 3\phi'\left(1 - (r/R)^2\right) - 2\phi'\left(1 - (r/R)^3\right)}{6 + \phi'}, \qquad [A]$$

where $\phi' = -(\nu_A k R/D_{eA})$.

For chemical reaction control, ϕ' is small (negligible), and we obtain

$$\frac{t}{t_0} = 1 - \frac{r}{R}. \qquad [B]$$

For pure product layer diffusion control, ϕ' is large and

$$\frac{t}{t_0} = \frac{3\phi'\left(1 - (r/R)^2\right) - 2\phi'\left(1 - (r/R)^3\right)}{\phi'},$$

and consequently

$$\frac{t}{t_0} = 1 - 3\left(\frac{r}{R}\right)^2 + 2\left(\frac{r}{R}\right)^3. \qquad [C]$$

To check the data, the right-hand sides of Equations [B] and [C] are plotted against the reaction time (t). The figure reveals that neither [B] nor [C] is valid for the entire region,

since the curves are not linear but bended. For model [C], a limited area for linearity can be found.

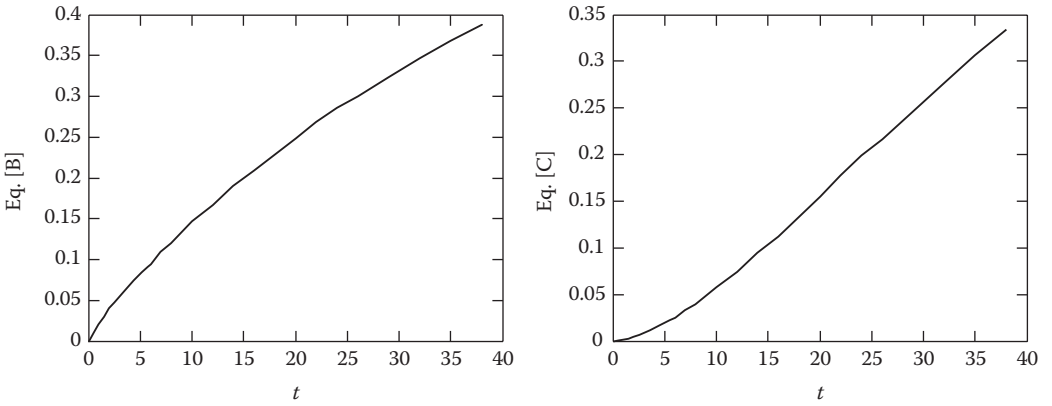

Test of simple models [B] (left) and [C] (right)

A general approach is to determine the Thiele modulus from the general model Equation [A] by nonlinear regression. The value of ϕ' was determined as 76.5.

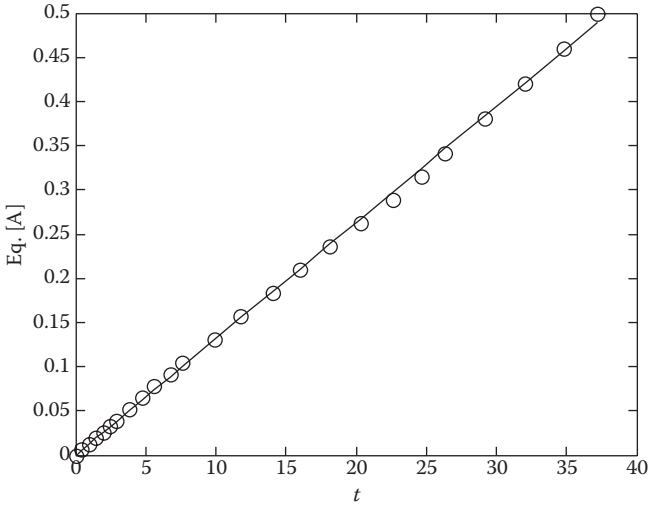

Fit of the general model [A]

The fit of the model to the data is displayed in the figure above. The conclusion is that both the chemical reaction and product layer diffusion contribute to the overall rate.

SECTION IV/4

The total reaction time is obtained from Equation 8.65 (Section 8.2.2).

$$R + \phi'\frac{R}{2} - \phi'\frac{R}{3}\left(1 - \frac{1}{Bi_{\mathrm{Am}}}\right) = a_0, \qquad [\mathrm{A}]$$

where

$$a_0 = \int_0^t c_A^b \, dt$$

and

$$\phi' = -\frac{\nu_A k R}{D_{eA}}.$$

The film diffusion resistance outside the particle is assumed to be negligible; thus $Bi_{Am} \to \infty$. In addition, c_A^b = constant, which yields

$$a_0 = c_A^b \int_0^{t_0} dt = c_A^b t_0.$$

Equation [A] becomes

$$R\left(1 + \frac{\phi'}{6}\right) = c_A^b t_0.$$

Two special cases are considered here.

If the surface reaction is rate-controlling, $\phi'/6 \ll 1$ and

$$R = c_A^b t_0. \qquad [B]$$

If the product layer diffusion is rate-controlling, $\phi'/6 \gg 1$ and we obtain $\frac{R\phi'}{6} = c_A^b t_0$, that is,

$$-\frac{\nu_A k R^2}{D_{eA}} = c_A^b t_0,$$

which becomes

$$R^2 = \frac{D_{eA} c_A^b}{-\nu_A k} = t_0. \qquad [C]$$

Models [B] and [C] are tested by plotting R versus t_0 and R^2 versus t_0.

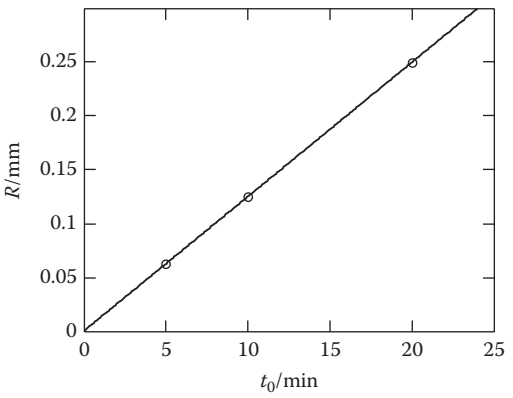

Model [B] is valid

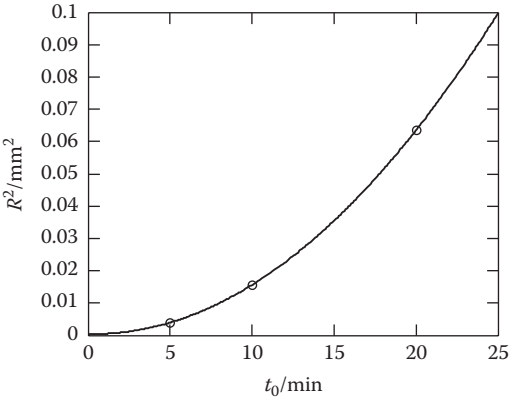

Model [C] is not valid

A straight line provided by model [B] indicates that this model is valid (see the figures below), that is, the surface reaction controls the overall rate.

t_0 (min)	[B] R (mm)	[C] R^2(mm^2)
5	0.063	0.00397
10	0.125	0.015625
20	0.250	0.0635

SECTION IV/5

The rate equation is

$$R' = kc_A.$$

The balance equations for A and B in the BR are written as

$$\frac{dn_A}{dt} = \nu_A R' A, \qquad [A]$$

$$\frac{dn_B}{dt} = \nu_B R' A. \qquad [B]$$

For the liquid phase, we assume a constant volume, that is, $n_A = c_A V_L$ and $dn_A/dt = V_L\,(dc_A/dt)$.

The ratio A/V_L is denoted by $a_p = A/V_L$. At the beginning of the process, we have $a_{0p} = A/V_{0L}$. The balance of [A] becomes

$$\frac{dc_A}{dt} = \nu_A a_p k c_A.$$

The ratio a_p/a_{0p} is

$$\frac{a_p}{a_{0p}} = \frac{A}{A_0} = \frac{n_p 4\pi r^2}{n_p 4\pi R^2} = \left(\frac{r}{R}\right)^2.$$

We thus obtain for c_A:

$$\frac{dc_A}{dt} = \nu_A k a_{0p} \left(\frac{r}{R}\right)^2 c_A,$$

that is,

$$\frac{d\left(c_A/c_{0A}\right)}{dt} = \nu_A k a_{0p} \left(\frac{r}{R}\right)^2 \left(\frac{c_A}{c_{0A}}\right). \qquad [C]$$

Equation [B] is rewritten as (Equation 8.18 in Section 8.2.1)

$$\frac{dr}{dt} = \frac{M}{x_B \rho_p} \nu_B R',$$

which becomes

$$\frac{\mathrm{d}r}{\mathrm{d}t} = \frac{M\nu_\mathrm{B}}{x_\mathrm{B}\rho_\mathrm{p}} k c_\mathrm{A}.$$

By using dimensionless quantities r/R and $c_\mathrm{A}/c_{0\mathrm{A}}$, we obtain

$$\frac{\mathrm{d}\,(r/R)}{\mathrm{d}t} = \frac{\nu_\mathrm{B} M c_{0\mathrm{A}}}{x_\mathrm{B}\rho_\mathrm{p} R a_{0\mathrm{p}}} k a_{0\mathrm{p}} \left(\frac{c_\mathrm{A}}{c_{0\mathrm{A}}}\right). \qquad [\mathrm{D}]$$

The quantity $ka_{0\mathrm{p}}$ is a pseudo-first-order rate parameter denoted by $k = ka_{0\mathrm{p}}$.

Furthermore, $\beta = Mc_{0\mathrm{A}}/x_\mathrm{B}\rho_\mathrm{p} R a_{0\mathrm{p}}$ is a dimensionless parameter. This is why the model can be presented in a very compressed form ($\nu_\mathrm{A} = \nu_\mathrm{B} = -1$):

$$\frac{\mathrm{d}y}{\mathrm{d}t} = -k' y z^2, \quad y = \frac{c_\mathrm{A}}{c_{0\mathrm{A}}}, \quad z = \frac{r}{R}, \qquad [\mathrm{E}]$$

$$\frac{\mathrm{d}z}{\mathrm{d}t} = -\beta k' y. \qquad [\mathrm{F}]$$

Between y and z, a simple relationship is obtained by dividing [E] by [F]:

$$\frac{\mathrm{d}y}{\mathrm{d}z} = \beta^{-1} z^2,$$

which is easily integrated:

$$\int_1^y \mathrm{d}y = \beta^{-1} \int_1^z z^2 \,\mathrm{d}y,$$

yielding

$$y = 1 - \frac{\beta^{-1}}{3}\left(1 - z^3\right).$$

The numerical values of the parameter a_{0p} are calculated. By definition, we have

$$a_{0\mathrm{p}} = \frac{n_\mathrm{p} 4\pi R^2}{V_\mathrm{L}},$$

where n_p is the number of particles. On the other hand, the initial volume of particles is

$$V_{0\mathrm{p}} = n_\mathrm{p} \frac{4}{3} \pi R^3.$$

The initial mass of particles is

$$m_{0\mathrm{p}} = \rho_\mathrm{p} V_{0\mathrm{p}} = M_\mathrm{B} n_{0\mathrm{B}}.$$

Thus V_{0p} is

$$V_{0\mathrm{p}} = \frac{M_{\mathrm{B}} n_{0\mathrm{B}}}{\rho_{\mathrm{p}}}$$

and we obtain n_{p} from

$$n_{\mathrm{p}} = \frac{3V_{0\mathrm{p}}}{4\pi R^3},$$

that is,

$$n_{\mathrm{p}} = \frac{3M_{\mathrm{B}} n_{0\mathrm{B}}}{4\pi R^3 \rho_{\mathrm{p}}}.$$

We now obtain $a_{0\mathrm{p}}$ as follows:

$$a_{0\mathrm{p}} = \frac{3M_{\mathrm{B}} n_{0\mathrm{B}}}{R\rho_{\mathrm{p}} V_{\mathrm{L}}},$$

$$a_{0\mathrm{p}} = \frac{3 \times 60 \times 10^{-3}\,\mathrm{kg/mol} \times 2\,\mathrm{mol}}{0.5 \times 10^{-3}\,\mathrm{m}\,1500\,\mathrm{kg/m^3} \times 10^{-3}\,\mathrm{m^3}} = 480\,\mathrm{m^{-1}}.$$

The pseudo-first-order parameter becomes

$$k' = ka_{0\mathrm{p}} = 4.17 \times 10^{-5} \times 480\,\mathrm{min^{-1}} = 0.02\,\mathrm{min^{-1}}.$$

The parameter β is calculated:

$$\beta = \frac{Mc_{0\mathrm{A}}}{x_{\mathrm{B}}\rho_{\mathrm{p}} R a_{0\mathrm{p}}} = \frac{M_{\mathrm{B}} n_{0\mathrm{A}}}{V_{\mathrm{L}}\rho_{\mathrm{p}} R a_{0\mathrm{p}}} \quad (x_{\mathrm{B}} = 1),$$

$$\beta = \frac{60 \times 10^{-3}\,\mathrm{kg/mol} \times 2\,\mathrm{mol}}{10^{-3}\,\mathrm{m^3} \times 1500\,\mathrm{kg/m^3} \times 0.5 \times 10^{-3}\,\mathrm{m} \times 480\,\mathrm{m^{-1}}} = 0.333.$$

To sum up, we have

$$\frac{\mathrm{d}y}{\mathrm{d}t} = -k' y z^2,$$

$$\frac{\mathrm{d}z}{\mathrm{d}t} = -\beta k' y,$$

where $y = 1$ and $z = 1$ at $t = 0$, $k' = 0.02\,\mathrm{mm^{-1}}$, and $\beta = 0.333$.

The differential equations are simulated numerically. For the simulation results, see the figure below.

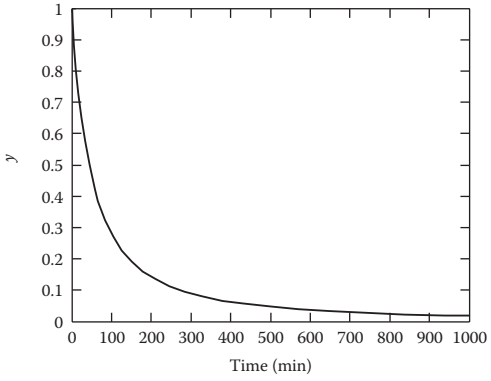

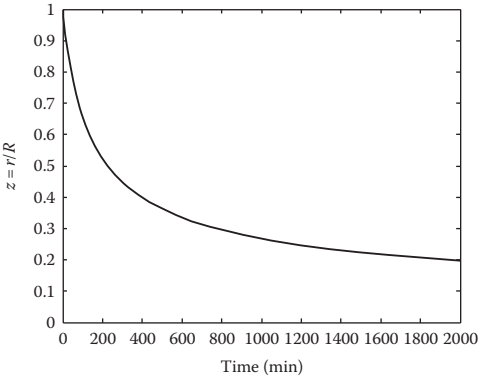

Solutions of Algebraic Equation Systems

Algebraic equation systems

$$f(x, y) = 0 \tag{A1.1}$$

can be solved by the Newton–Raphson method. In the equation system, y denotes the unknown variable and x is a continuity parameter.

The Newton–Raphson algorithm for the solution of the equation is

$$y_k = y_{k-1} - \mathbf{J}^{-1}\boldsymbol{f}_{k-1}, \tag{A1.2}$$

where k denotes the iteration index, $\boldsymbol{f}_k$ is the function vector at iteration cycle k, and $\mathbf{J}^{-1}$is the inverse of the Jacobian matrix. The Jacobian matrix contains the partial derivatives:

$$\mathbf{J} = \begin{bmatrix} \mathrm{d}f_1/\mathrm{d}y_1 & \mathrm{d}f_1/\mathrm{d}y_2 & \mathrm{d}f_1/\mathrm{d}y_3 & \cdots & \mathrm{d}f_1/\mathrm{d}y_N \\ \cdot & & & & \\ \cdot & & & & \\ \cdot & & & & \\ \mathrm{d}f_N/\mathrm{d}y_1 & \mathrm{d}f_N/\mathrm{d}y_2 & \mathrm{d}f_N/\mathrm{d}y_3 & \cdots & \mathrm{d}f_N/\mathrm{d}y_N \end{bmatrix}. \tag{A1.3}$$

The matrix inversion $\mathbf{J}^{-1}$ is performed by the Gauss elimination method applied to linear equations. The derivatives $\mathrm{d}f_i/\mathrm{d}y_j$ are calculated from analytical expressions or numerical approximations. The approximation of the derivatives $\mathrm{d}f_i/\mathrm{d}y_j$ with forward differences is

$$\frac{\mathrm{d}f_i}{\mathrm{d}y_j} \approx \frac{\Delta f_i}{\Delta y_j} = \frac{f_i(y_{j+}\Delta y_j) - f_i(y_j)}{\Delta y_j}. \tag{A1.4}$$

The selection of the difference Δy_j is critical: the smaller the Δy_j, the better the derivative approximation. However, if Δy_j is smaller than the accuracy of the computer, the denominator in Equation A1.4 becomes 0. A criterion for the choice of Δy_j is

$$\Delta y_j = \max\left(\varepsilon_c, \varepsilon_R \left|y_j\right|\right), \tag{A1.5}$$

where ε_R is the relative difference given by the user and ε_c is the round-off error of the computer.

The choice of the initial estimate of $\mathbf{y}_{(0)}$ is critical, as the equation system is solved with the Newton–Raphson method. In many cases, a solution of a problem is expected as a function of the parameter x. The parameter x can be chosen as a continuity parameter: the solution for the equation system, obtained for a certain parameter value x, $\mathbf{y}_{(\infty)}$, can be used as an initial estimate for the next parameter value, $x + \Delta x$:

$$\mathbf{y}_{(0)}(x + \Delta x) = \mathbf{y}_{\infty}(x). \tag{A1.6}$$

The convergence of algorithm (Equation A1.2) is quadratic in most cases.

A termination criterion for the iteration of Equation (A1.2) is usually

$$\left|\frac{y_{i(k)} - y_{i(k-1)}}{y_{i(k)}}\right| < \varepsilon, \quad i = 1, \ldots, N, \tag{A1.7}$$

where ε is the user-defined relative error tolerance.

For a system with a single equation, the algorithm (Equation A1.2) is reduced to

$$y_{(k)} = y_{(k-1)} - \frac{f_{(k-1)}}{f'_{(k-1)}}. \tag{A1.8}$$

The principles described here are implemented in the subroutine NLEODE [1]. In Ref. [1], an application example is described in detail.

REFERENCE

1. Appendix 3 in this book (subroutine NLEODE).

Solutions of ODEs

A first-order differential equation

$$\frac{\mathrm{d}\mathbf{y}}{\mathrm{d}x} = \mathbf{f}(\mathbf{y}, x) \tag{A2.1}$$

with the initial conditions

$$\mathbf{y} = \mathbf{y}_0 \quad \text{at } x = x_0 \tag{A2.2}$$

can be solved by semi-implicit Runge–Kutta methods or by linear multistep methods, which are briefly reviewed below.

A2.1 SEMI-IMPLICIT RUNGE–KUTTA METHOD

The Runge–Kutta methods have a general form

$$\mathbf{y}_n = \mathbf{y}_{n-1} + \sum_{i=1}^{q} b_i \mathbf{k}_i, \tag{A2.3}$$

where $\mathbf{y}_n$ and $\mathbf{y}_{n-1}$ are the solutions of the differential equation at x and $x - \Delta x$. The coefficients $\mathbf{k}_i$ are obtained from

$$\mathbf{k}_i = h\mathbf{f}\left(x_n, \mathbf{y}_n + \sum_{l=1}^{i} a_{il}\mathbf{k}_l\right), \tag{A2.4}$$

where $h = \Delta x$.

If the coefficients $a_{il} = 0$, when $l = 0$, the method is called explicit; if $a \neq 0$, when $l = i$, the method is implicit.

For stiff differential equations, an explicit method cannot be used to obtain a stable solution. To solve stiff systems, an unrealistically short step size h is required. On the other hand, the use of an implicit method requires an iterative solution of a nonlinear algebraic equation system, that is, a solution of $\mathbf{k}_i$ from Equation A2.4. By a Taylor series development of $\mathbf{y}_n + \sum_{l=1}^{i-1} a_{il}\mathbf{k}_i$ and truncation after the first term, a semi-implicit Runge–Kutta method is obtained. The term $\mathbf{k}_i$ can be calculated from [1]

$$(\mathbf{I} - \mathbf{J}a_{ii}h)\,\mathbf{k}_i = \mathbf{f}\left(\mathbf{y}_n + \sum_{l=1}^{i-1} a_{il}\mathbf{k}_l\right)h, \tag{A2.5}$$

where $\mathbf{I}$ is the identity matrix,

$$\mathbf{I} = \begin{bmatrix} 1 & 0 & . & . & . & 0 \\ . & 1 & & & & . \\ . & & & & & . \\ . & & & & & . \\ 0 & 0 & . & . & . & 1 \end{bmatrix}, \tag{A2.6}$$

and $\mathbf{J}$ is the Jacobian matrix,

$$\mathbf{J} = \begin{bmatrix} \mathrm{d}f_1/\mathrm{d}y_1 & \mathrm{d}f_2/\mathrm{d}y_2 & . & . & . & \mathrm{d}f_1/\mathrm{d}y_N \\ . & & & & & . \\ . & & & & & . \\ . & & & & & . \\ \mathrm{d}f_n/\mathrm{d}y_1 & \mathrm{d}f_n/\mathrm{d}y_2 & . & . & . & \mathrm{d}f_n/\mathrm{d}y_N \end{bmatrix}. \tag{A2.7}$$

When using the semi-implicit Runge–Kutta method, the calculation of the Jacobian matrix can be critical. The Jacobian, $\mathbf{J}$, influences directly the values of the parameters $\mathbf{k}_i$ and, thereby, the whole solution of $\mathbf{y}$. An analytical expression of the Jacobian is always preferable over a numerical approximation. If the differentiation of the function is cumbersome, an approximation can be obtained with forward differences

$$\frac{\mathrm{d}f_i}{\mathrm{d}y_j} = \frac{f_i(y_j + \Delta y_j) - f_i(y_j)}{\Delta y_j}, \tag{A2.8}$$

where the increment Δy_j is obtained from the criterion:

$$\Delta y_j = \max\left(\varepsilon_c, \varepsilon_R |y_j|\right), \tag{A2.9}$$

where ε_R is the relative difference and ε_c is the computer round-off criterion.

The equation implies that a linear equation system always has to be solved when the parameter $\mathbf{k}_i$ is calculated. The matrix $\mathbf{I} - \mathbf{J}a_{ij}h$ is inverted using the Gauss elimination.

TABLE A2.1 Coefficients in a Few Semi-implicit Runge–Kutta Methods

I	b_i	a_{ii}	a_{2i}	a_{3i}[a]
		Rosenbrock [1]		
1	−0.413	1.408	0.174	
2	1.413	0.592		
		Caillaud and Padmanabhan [2]		
1	11/27	0.4358	0.75	−0.2746
2	16/27	0.4358		−0.1056
3	1.00000	0.4358		
		Michelsen [3]		
1	1.03758	0.4358	0.75	−0.63017
2	0.83494	0.4358		−0.24235
3	1.00000	0.4358		

[a] In these methods, hf is replaced by $a_{31}k_1 + a_{32}k_2$ in the calculation of k_3.

TABLE A2.2 Coefficients in the ROW4A Method [4]

$a_{ii} = 0.395$	$c_{21} = -1.943744189$
$a_{21} = 0.438$	$c_{31} = 0.4169575310$
$a_{31} = 0.9389486785$	$c_{32} = 1.3239678207$
$a_{32} = 0.0730795421$	$c_{41} = 1.5195132578$
$b_1 = 0.7290448800$	$c_{42} = 1.3537081503$
$b_2 = 0.0541069773$	$c_{43} = -0.8541514953$
$b_3 = 0.2815993624$	
$b_4 = 0.25$	

After calculating $\mathbf{k}_i$ according to Equation A2.4, $\mathbf{y}_n$ is easily obtained from Equation A2.3. The coefficients a_{il} and b_i for some semi-implicit Runge–Kutta methods are summarized in Table A2.1 [1–3].

The Rosenbrock–Wanner (ROW) method is an extension of the semi-implicit Runge–Kutta method. In the ROW method, Equation A2.5 is replaced by the expression

$$(\mathbf{I} - \mathbf{J}a_{ii}h)\,\mathbf{k}_i = \mathbf{f}\left(\mathbf{y}_n + \sum_{l=1}^{i-1} a_{il}\mathbf{k}_l\right)h + \sum_{l=1}^{i-1} c_{il}\mathbf{k}_l. \tag{A2.10}$$

The coefficients of a fourth-order ROW method are listed in Table A2.2.

A2.2 LINEAR MULTISTEP METHODS

The following general algorithm applies to the solution of ODEs [5–7]

$$\mathbf{y}_n = \sum_{i=1}^{K_1} \alpha_i \mathbf{y}_{n-i} + h\sum_{i=0}^{K_2} \beta_i \mathbf{f}_{n-i}. \tag{A2.11}$$

Depending on the values of K_1 and K_2, either the Adams–Moulton (AM) or BD method is obtained [7]:

$$\alpha_1 = 1 \wedge K_1 = 1 \wedge K_2 = q - 1 \quad \text{(AM)}, \tag{A2.12}$$

$$K_1 = q \wedge K_2 = 0 \quad \text{(BD)}. \tag{A2.13}$$

Applying the conditions (Equations A2.12 and A2.13) to Equation A2.11 yields the AM method,

$$\mathbf{y}_n = \mathbf{y}_{n-1} + h \sum_{i=0}^{q-1} \beta_i \mathbf{f}_{n-i} \quad \text{(AM)}, \tag{A2.14}$$

and the BD method,

$$\mathbf{y}_n = \sum_{i=1}^{q} \alpha_i \mathbf{y}_{n-1} + h\beta_0 \mathbf{f}_n \quad \text{(BD)}. \tag{A2.15}$$

Both methods are implicit, since $\mathbf{f}_n$ is usually a nonlinear function of $\mathbf{y}_n$. Methods A2.14 and A2.15 require the solution of a nonlinear, algebraic equation system of the following kind:

$$\mathbf{g}_n = \mathbf{y}_n - h\beta_0 \mathbf{f}_n - \mathbf{a}_n = 0, \tag{A2.16}$$

where $\mathbf{a}_n$ is defined by

$$\mathbf{a}_n = \mathbf{y}_{n-1} + h \sum_{i=0}^{q-1} \beta_i \mathbf{f}_{n-i} \quad \text{(AM)} \tag{A2.17}$$

or

$$\mathbf{a}_n = \sum_{i=1}^{q} \alpha_i \mathbf{y}_{n-i} \quad \text{(BD)}. \tag{A2.18}$$

After solving $\mathbf{y}_n$, $\mathbf{a}_n$ is known from the earlier solutions; the problem thus comprises an iterative solution of equation system A2.16. This is best facilitated by the Newton–Raphson method

$$\mathbf{y}_{n(k+1)} = \mathbf{y}_{n(k)} - \mathbf{P}_n^{-1} \mathbf{g}_n, \tag{A2.19}$$

where $\mathbf{P}_n$ is the Jacobian matrix of system A2.16. Derivation of Equation A2.16 yields a practical expression for $\mathbf{P}_n$,

$$\mathbf{P}_n = \mathbf{I} - h\beta_0 \mathbf{J}, \tag{A2.20}$$

where the identity matrix, $\mathbf{I}$, and the Jacobian, $\mathbf{J}$, are given by Equations A2.6 and A2.7, respectively. The coefficients α_i and β_i of the AM and BD methods of various orders are given in Tables A2.3 and A2.4.

TABLE A2.3 β-Coefficients in the AM Method

I	0	1	2	3	4	5
β_{1i}	1					
$2\beta_{2i}$	1	1				
$12\beta_{3i}$	5	8	−1			
$24\beta_{4i}$	9	19	−5	1		
$720\beta_{5i}$	251	646	−264	106	−19	
$1440\beta_{6i}$	475	1427	−798	482	−173	27

TABLE A2.4 α-Coefficients in the BD Method

I	0	1	2	3	4	5	6
α_{1i}	1	1					
$3\alpha_{2i}$	2	4	−1				
$11\alpha_{3i}$	6	18	−9	2			
$25\alpha_{4i}$	12	48	−36	16	−3		
$137\alpha_{5i}$	60	300	−300	200	−75	12	
$147\alpha_{6i}$	60	360	−450	400	−225	72	−10

Note: $\alpha_{10} = \beta_{10}, \alpha_{20} = \beta_{20}$, and so on.

For stiff differential equations, the BD method is preferred over the AM method. To solve differential equations by means of linear multistep methods, a number of algorithms have been implemented in programming codes, for example, LSODE [8]. LSODE is also known by the name IVPAG, in the International Mathematical and Statistical Library (IMSL) [9]. For large systems of ODEs, a sparse matrix version of LSODE is available (LSODES). Nowadays, there are many public domain codes and program packages for the solution of stiff ODEs, that is, ODEPACK, VODE, CVODE, ROW4A, and so on.

REFERENCES

1. Rosenbrock, H.H., Some general implicit processes for the numerical solution of differential equations, *Comput. J.*, 5, 329–330, 1963.
2. Caillaud, J.B. and Padmanabhan, L., Improved semi-implicit Runge–Kutta method for stiff systems, *Chem. Eng. J.*, 2, 227–232, 1971.
3. Michelsen, M.L., An efficient general purpose method for the integration of stiff ODE, *AIChE J.*, 22, 594–600, 1976.
4. Kaps, P. and Wanner, G., A study of Rosenbrock-type methods of high order, *Numer. Math.*, 38, 279–298, 1981.
5. Salmi, T., Program NLEODE, in T. Westerlund (Ed.), *Chemical Engineering Program Library*, Åbo Akademi, Turku/Åbo, Finland, 1984.
6. Gear, C.W., *Numerical Initial Value Problems in Ordinary Differential Equations*, Prentice-Hall, Englewood Cliffs, NJ, 1971.
7. Henrici, P., *Discrete Variable Methods in Ordinary Differential Equations*, Wiley, New York, 1962.
8. Hindmarsh, A.C., ODEPACK, a systematized collection of ODE-solvers, in R. Stepleman et al. (Eds), *Scientific Computing*, pp. 55–64, IMACS/North Holland Publishing Company, 1983.
9. IMSL, International Mathematical and Statistical Libraries, Houston, TX, 1987.

Computer Code NLEODE

NLEODE is an interactive Fortran code software for solving nonlinear algebraic equation systems of the following kind:

$$\mathbf{f}(\mathbf{y}, x) = 0 \tag{A3.1}$$

with the initial conditions

$$\frac{\mathrm{d}\mathbf{y}}{\mathrm{d}x} = \mathbf{f}(\mathbf{y}) \quad y = y_0 \quad \text{at } x = x_0. \tag{A3.2}$$

Systems 3.1 and 3.2 contain N number of equations. The algebraic equation system can be solved with the Newton–Raphson method [1] and the ordinary differential equations with the semi-implicit Runge–Kutta method, Michelen's semi-implicit Runge–Kutta method [2], or, alternatively, with the Rosenbrock–Wanner semi-implicit Runge–Kutta method [2].

When using the Newton–Raphson method, the subroutine NONLIN [3] is used. The subroutine NONLIN solves the equation system 3.1 with respect to $\mathbf{y}$. Furthermore, x is considered as a continuity parameter. The solution to equation system 3.1 is thus obtained as a function of the parameter x [3]. When using the semi-implicit Runge–Kutta methods, the subroutines SIRKM [4] and ROW4B [5] are used. These are used to solve equation system 3.2.

In order to be able to utilize the NLEODE program code, the operator must, as a minimum, write the program code for the subroutine FCN, in which the functions for the right-hand side of Equations A3.1 and A3.2 are defined. If the Jacobian matrix of the right-hand side in Equations A3.1 and A3.2 is calculated analytically, an additional subroutine, FCNJ, must be written by the operator. In case the elements in the Jacobian matrix are

calculated numerically, an empty subroutine FCNJ only needs to be compiled and linked to the code.

If the differential equations are of a nonautonomous kind,

$$\frac{d\mathbf{y}}{dx} = \mathbf{f}(\mathbf{y}, x), \tag{A3.3}$$

it is necessary at first to transform them to an autonomous system similar to Equation A3.2. This can be achieved by defining a new variable, $y_{N+1} = x$, which has the derivative $dy/dx = 1$. This equation must then be included as an equation number $N + 1$ to the system according to Equation A3.2.

A3.1 SUBROUTINE FCN

Subroutine **FCN**(N, X, Y, YPRIME)
where

N = number of equations/differential equations;
X = the continuity parameter (algebraic equations) or independent variable (differential equations);
Y(N) = dependent variable;
Y(N) = the initial values, $\mathbf{y}_0$, at $x = x_0$ (differential equations);
YPRIME(N) = function **f** in Equations A3.1 and A3.2; and
YPRIME(N) gives the residuals when solving algebraic equations; it gives the derivatives $d\mathbf{y}/dx$ when solving differential equations.

A3.2 SUBROUTINE FCNJ

Subroutine **FCNJ**(N, X, Y, YPRIME, DDY)
where parameters N, X, Y(N), and YPRIME(N) are similar to those in subroutine FCN. Matrix DDY(N, N) contains the elements of the Jacobian

$$\mathbf{J} = \begin{bmatrix} \partial f_1/\partial y_1 & \partial f_1/\partial y_2 & \dots & \partial f_1/\partial y_N \\ \cdot & \cdot & & \cdot \\ \cdot & \cdot & & \cdot \\ \partial f_N/\partial y_1 & \partial f_N/\partial y_2 & \dots & \partial f_N/\partial y_N \end{bmatrix}$$

In other words, DDY(I, J) $= f_i/y_j$. In case the Jacobian is calculated numerically by NLEODE, an empty subroutine FCNJ should be compiled as follows:

```
SUBROUTINE FCNJ(N,X,Y,YPRIME,DDY)
RETURN
END
```

Example 1

Solve the algebraic equation system

$$
\begin{aligned}
y_{01} - y_1 - r_1 &= 0,\\
y_{02} - y_2 - r_1 - r_2 &= 0,\\
y_{03} - y_3 + r_1 - r_2 &= 0,\\
y_{04} - y_4 + r_2 &= 0,\\
y_{05} - y_5 + r_1 + r_2 &= 0,
\end{aligned}
$$

which describes a consecutive-competitive reaction, $A + B \rightarrow R + E, R + B \rightarrow S + E$, in a CSTR. The reaction kinetics is defined by

$$
\begin{aligned}
r_1 &= k_1 y_1 y_2 x,\\
r_2 &= k_2 y_3 y_2 x.
\end{aligned}
$$

The parameters $y_{01}, y_{02}, \ldots, y_{05}$ as well as k_1 and k_2 obtain constant values. The value of the parameter x (residence time) should be between 0 and 5. The subroutines FCN and FCNJ are listed below.

```
c Consecutive-competitive reaction in a CSTR
subroutine fcn(n,x,y,yprime)
implicit real*8 (a-h,o-z)
real*8 y(n),yprime(n)

real* 8 k(2),rate(2),y0(5)

k(1)=5.0d0
k(2)=2.0d0
y0(1)=1.0d0
y0(2)=1.0d0
y0(3)=0.0d0
y0(4)=0.0d0
y0(5)=0.0d0
rate(1)=k(1)*y(1)*y(2)*x
rate(2)=k(2)*y(3)*y(2)*x
yprime(1)=y0(l)-y(1)-rate(1)
yprime(2)=y0(2)-y(2)-rate(1)-rate(2)
yprime(3)=y0(3)-y(3)+rate(1)-rate(2)
```

```
yprime(4)=y0(4)-y(4)+rate(2)
yprime(5)=y0(5)-y(5)+rate(1)+rate(2)

return
end
```

Example 2

Solve the following differential equations

$$\frac{dy_1}{dx} = -r_1$$
$$\frac{dy_2}{dx} = -r_1 - r_2$$
$$\frac{dy_3}{dx} = r_1 - r_2$$
$$\frac{dy_4}{dx} = r_2$$
$$\frac{dy_5}{dx} = r_1 + r_2$$

with the initial conditions, at $x = 0$

$$y_{01} = 1.0,$$
$$y_{02} = 1.0,$$
$$y_{03} = y_{04} = y_{05} = 0.0.$$

The terms r_1 and r_2 are defined as

$$r_1 = k_1 y_1 y_2,$$
$$r_2 = k_1 y_3 y_2.$$

The equations describe a consecutive-competitive reaction, $A + B \rightarrow R + E, R + B \rightarrow S + E$, in a tube or a BR (Example 1).

Parameters k_1 and k_2 obtain constant values. The value of the independent variable x (residence time) should be between 0 and 5. Subroutines FCN and FCNJ are listed below, as well as the numerical results of program code execution.

```
c Consecutive-competitive reaction in a BR or a tubular reactor
subroutine fcn(n,x,y,yprime)
implicit real* 8 (a-h,o-z)
```

```
real*8 y(n),yprime(n)
real*8 k(2),rate(2)

k(1)=5.0d0
k(2)=2.0d0

rate(1)=k(1)*y(1)*y(2)
rate(2)=k(2)*y(3)*y(2)
yprime(1)=rate(1)
yprime(2)=-rate(1)-rate(2)
yprime(3)=rate(1)-rate(2)
yprime(4)=rate(2)
yprime(5)=rate(1)+rate(2)

return
end
```

REFERENCES

1. Solving algebraic equations, *Appendix 1*.
2. Solving ordinary differential equations, *Appendix 2*.
3. Salmi, T., The program code NONLIN for solution of non-linear equations, Institutionen för teknisk kemi, Åbo Akademi, Turku/Åbo, Finland,1990.
4. Salmi, T., The program code SIRKM, Program no. 202, in Westerlund, T. (Ed.), *Chemical Engineering Program Library*, Åbo Akademi, Turku/Åbo, Finland, 1984.
5. Salmi, T., The program code ROW4B, Program no. 201, in Westerlund, T. (Ed.), *Chemical Engineering Program Library*, Åbo Akademi, Turku/Åbo, Finland, 1984.

Gas-Phase Diffusion Coefficients

The theory for diffusion in gas phase is well developed. The diffusion flux of a component $i(N_i)$ depends on all of the components. According to the Stefan–Maxwell theory, the diffusion flux and concentration gradient are governed by the matrix relation

$$\mathbf{FN} = -\frac{\mathrm{d}\mathbf{c}}{\mathrm{d}r}, \tag{A4.1}$$

where **F** is a coefficient matrix. A rigorous computation of the diffusion fluxes requires a numerical inversion of matrix **F**. Matrix **F** contains the contributions of molecular and Knudsen diffusion coefficients. Because the rigorous method is complicated, it is not discussed here further. It is, however, described in detail in Refs. [1–3].

An approximate calculation of the diffusion flux may be based on the concept of effective diffusion coefficients and Fick's law, which yields a simple relation between the diffusion flux and the concentration gradient:

$$N_i = -D_{ei}\frac{\mathrm{d}c_i}{\mathrm{d}x}. \tag{A4.2}$$

This approximation is valid mainly for components in diluted gases, that is, for low concentrations. The effective diffusion coefficient for a gas-phase component in a porous particle can be calculated from the relation

$$D_{ei} = \left(\frac{\varepsilon_p}{\tau_p}\right)D_i, \tag{A4.3}$$

where D_i is the diffusion coefficient, ε_p is the porosity, and τ_p is the tortuosity. The porosity is always <1, whereas the tortuosity shows values >1. The tortuosity factor describes variations from linear pore structures. Satterfield [4] recommends values for tortuosity in the range $1-\sqrt{3}$ for catalyst particles, but values exceeding $\sqrt{3}$ have been reported; many catalysts have tortuosity values in the range 3–4 [4]. More advanced pore models are treated, for example, in Refs. [5] and [6].

The diffusion coefficient (D_i) can be divided into two parts: one originating from intermolecular collisions (D_{mi}) and the other from collisions between the molecules and pore walls, the so-called Knudsen diffusion (D_{Ki}). The diffusion coefficient (D_i) can be estimated from these two parts from the formula

$$\frac{1}{D_i} = \frac{1}{D_{mi}} + \frac{1}{D_{Ki}}. \tag{A4.4}$$

Equation A4.4 is strictly valid for equimolar diffusion in a binary solution ($N_A = -N_B$).

Wilke and Lee [7] have developed an approximate equation for the molecular diffusion coefficient starting from the Stefan–Maxwell theory:

$$D_{mi} = \frac{c - c_i}{\sum_{k=1,k\neq i}^{N} c_k/D_{ik}}, \tag{A4.5}$$

where c is the total concentration of the gas mixture

$$c = \sum_{i=1}^{N} c_i. \tag{A4.6}$$

By introducing more fractions, Equation A4.5 is simplified to

$$D_{mi} = \frac{1 - x_i}{\sum_{k=1,k\neq i}^{N} x_k/D_{ik}}, \tag{A4.7}$$

where D_{ik} is the binary molecular diffusion coefficient. Theoretically, the binary diffusion coefficients can be calculated from the Chapman–Enskog equation [8], but in practice it is shown that a semiempirical modification of the Chapman–Enskog equation gives a better agreement with experimental data. The semiempirical Fuller–Schettler–Giddings equation is

$$D_{ik} = \frac{(T/K)^{1.75}[((g/mol)/M_i) + ((g/mol)/M_k)]^{1/2} \times 10^{-7}}{(P/atm)(v_i^{1/3} + v_k^{1/3})^2} m^2/s, \tag{A4.8}$$

where T and P denote the temperature and the total pressure, respectively. M is the molar mass and v is the diffusion volume of the molecule. The diffusion volumes of some molecules are listed in Table A4.1. It is also possible to estimate the diffusion volumes from atomic increments. Reid et al. [8] deal with different methods for the estimation

TABLE A4.1 Diffusion Volumes of Simple Molecules

He	2.67	CO	18.0
Ne	5.98	CO_2	26.9
Ar	16.2	N_2O	35.9
Kr	24.5	NH_3	20.7
Xe	32.7	H_2O	13.1
H_2	6.12	SF_6	71.3
D_2	6.84	Cl_2	38.4
N_2	18.5	Br_2	69.0
O_2	16.3	SO_2	41.8
Air	19.7		

Source: Data from Reid, R.C., Prausnitz, J.M., and Poling, B.E., *The Properties of Gases and Liquids*, 4th Edition, McGraw-Hill, New York, 1988.

TABLE A4.2 Atomic and Structural Diffusion Volume Increments

C	15.9	F	14.7
H	2.31	Cl	21.0
O	6.11	Br	21.9
N	4.54	I	29.8
Aromatic ring	−18.3	S	22.9
Heterocyclic ring	−18.3		

Source: Data from Reid, R.C., Prausnitz, J.M., and Poling, B.E., *The Properties of Gases and Liquids*, 4th Edition, McGraw-Hill, New York, 1988.

of increments. The best method was probably developed by Fuller et al. Some atomic increments are listed in Table A4.2 [8].

If experimental values of the molecular binary diffusion coefficients exist at one temperature and pressure, Equation A4.7 can be used to estimate the binary diffusion coefficients at other temperatures and pressures. Equation A4.7 is valid for moderate total pressures, but not for extremely high pressures.

For the estimation of the Knudsen diffusion coefficient, the following equation is recommended [4]:

$$D_{\mathrm{K}i} = \frac{8\varepsilon_{\mathrm{p}}}{3S_{\mathrm{g}}\rho_{\mathrm{p}}}\sqrt{\frac{2RT}{\pi M_i}}, \tag{A4.9}$$

where ρ_{p} is the particle density and S_{g} is the specific surface area of the particle. The specific area is mostly measured by nitrogen adsorption, and the result is interpreted with the Brunauer–Emmett–Teller theory [9].

The effective diffusion coefficient can be estimated with Equations A4.3 through A4.9. The highest uncertainty is involved in the estimation of particle porosity and tortuosity. The porosity can be determined by mercury or nitrogen porosimetry. The best way is to experimentally determine the effective diffusion coefficient at room temperature for a

pair of gases and to use available values for the binary diffusion coefficients. The relation (ε_p/τ_p) can then be calculated from Equation A4.3. Now the diffusion coefficient D_i can be estimated at different temperatures and pressures from Equations A4.4 through A4.8. The experimental procedure to determine diffusion coefficient is described in detail in Ref. [4].

REFERENCES

1. Feng, C.F. and Stewart, W.E., *Ind. Eng. Chem. Fundam.*, 12, 143–147, 1973.
2. Fott, P. and Schneider, P., Multicomponent mass transport with complex reaction in a porous catalyst, in *Recent Advances in the Engineering Analysis of Chemically Reacting Systems* (Ed. L.K. Doraiswamy), Wiley Eastern, New Delhi, 1984.
3. Salmi, T. and Wärnå, J., Modelling of catalytic packed bed reactors: Comparison of different diffusion models, *Comput. Chem. Eng.*, 15, 715–727, 1991.
4. Satterfield, C.N., *Mass Transfer in Heterogeneous Catalysis*, MIT Press, Cambridge, MA, 1970.
5. Smith, J.M., *Chemical Engineering Kinetics,* McGraw-Hill, New York, 1981.
6. Froment, G.F. and Bischoff, K.B., *Chemical Reactor Analysis and Design*, Wiley, New York, 1990.
7. Wilke, C.R. and Lee, C.Y., Estimation of diffusion coefficients for gases and vapours, *Ind. Eng. Chem. Res.*, 47, 1253–1257, 1955.
8. Reid, R.C., Prausnitz, J.M., and Poling, B.E., *The Properties of Gases and Liquids*, 4th Edition, McGraw-Hill, New York, 1988.
9. Carberry, J.J., *Chemical and Catalytic Reaction Engineering*, McGraw-Hill, New York, 1976.

Fluid-Film Coefficients

A5.1 GAS–SOLID COEFFICIENTS

Mass and heat transfer between a gas and a solid particle is usually described using dimensionless numbers. There is an analogy between the mass and the heat transfer, of a kind that is discussed in Ref. [1]. Sample results of research are displayed in Figures A5.1 and A5.2. Wakao [2] measured mass and heat transfer between a gas and a solid particle and also summarized earlier results. It became evident that experimental data for heat and mass transfer can be described by Equations A5.1 and A5.2, respectively:

$$Sh = 2 + 1.1 \cdot Sc^{1/3} Re^{0.6}, \tag{A5.1}$$

$$Nu = 2 + 1.1 \cdot Pr^{1/3} Re^{0.6}, \tag{A5.2}$$

where Sh and Nu denote the Sherwood and Nusselt numbers, respectively. They are defined as

$$Sh = \frac{k_{\mathrm{G}i} d_{\mathrm{p}}}{D_{\mathrm{m}i}}, \tag{A5.3}$$

$$Nu = \frac{h d_{\mathrm{p}}}{\lambda_{\mathrm{G}}}, \tag{A5.4}$$

where $k_{\mathrm{G}i}$ and h denote the mass and heat transfer coefficients, respectively, d_{p} the particle diameter, $D_{\mathrm{m}i}$ the molecular diffusion coefficient in the gas phase, and λ_{G} the heat convection ability of the gas. Sh is sometimes called the Biot number for mass transfer and consequently denoted as Bi_{M}. The dimensionless numbers, Pr, Re, and Sc, are defined in Table A5.1.

Correlations A5.1 and A5.2 are considered to be valid for Reynolds numbers in the range $Re \in [3, 3000]$ [2].

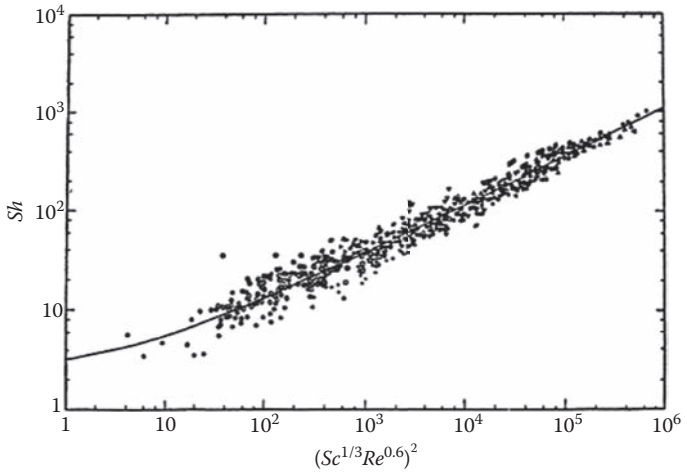

FIGURE A5.1 Behavior of the mass transfer coefficient. [Data from Wakao, N., *Recent Advances in the Engineering Analysis of Chemically Reacting Systems* (Ed. L.K. Doraiswamy),Wiley Eastern, New Delhi, 1984.]

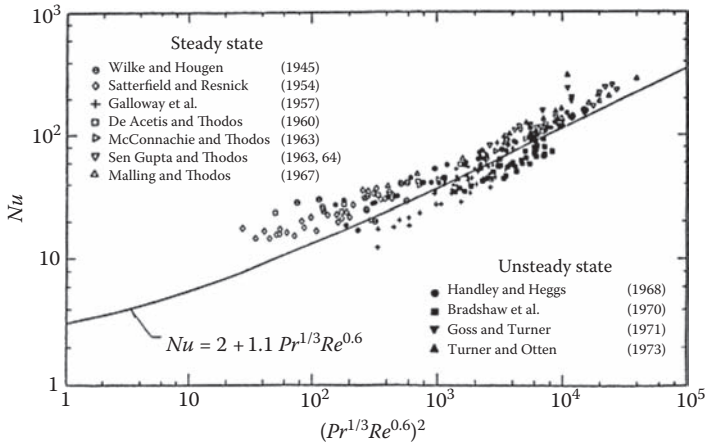

FIGURE A5.2 Behavior of the heat transfer coefficient. [Data from Wakao, N., *Recent Advances in the Engineering Analysis of Chemically Reacting Systems* (Ed. L.K. Doraiswamy),Wiley Eastern, New Delhi, 1984.]

TABLE A5.1 Dimensionless Numbers for Mass and Heat Transfer

Reynolds number	$Re = (\mathrm{G}d_\mathrm{p})/\mu_\mathrm{G}$, where $\mathrm{G} = \dot{m}/\mathrm{A}$ (mass flow/tube cross-section)
Schmidt number	$Sc = \mu_\mathrm{G}/(\rho_\mathrm{G}D_{\mathrm{m}i})$
Prandtl number	$Pr = (c_\mathrm{P}\mu_\mathrm{G})/\lambda_\mathrm{G}$

A5.2 GAS–LIQUID AND LIQUID–SOLID COEFFICIENTS

In general, the relationship

$$Sh = 2 + aSc^{\alpha}Re^{\beta} \tag{A5.5}$$

is applicable to estimate gas–liquid and liquid mass transfer coefficients. A slurry reactor represents a special case in which small solid particles ($d_p \ll 1$ mm) are dispersed in a liquid phase. In the case of a three-phase system, a gas phase is also present. Agitation in slurry reactors is vigorous (often 1000 rpm or even more). For such a case $2 \ll Sc^{\alpha}Re^{\beta}$ and a simplified correlation is proposed

$$Sh = 1.0Sc^{1/3}Re^{1/2}, \tag{A5.6}$$

where the Reynolds number (Re) depends on the specific mixing power (effect dissipated):

$$Re \propto \varepsilon^{1/3}. \tag{A5.7}$$

This leads to the following expressions for the gas–liquid (k_{GLi}) and the liquid–solid (k_{LSi}) mass transfer coefficients:

$$k_{GLi} = \left(\frac{\varepsilon D_{mi}^4 d_B^2 \rho_L}{\mu_L}\right)^{1/6}, \tag{A5.8}$$

$$k_{LSi} = \left(\frac{\varepsilon D_{mi}^4 d_p^2 \rho_L}{\mu_L}\right)^{1/6}, \tag{A5.9}$$

where D_{mi} is the molecular diffusion coefficient in the liquid phase, and d_B and d_p denote the bubble and particle diameters, respectively. The dissipated effect is given as $\varepsilon_{max} = W/m$, where W is the stirring power (in Watt) and m is the mass of suspension. Typically, $\varepsilon < \varepsilon_{max}$. The real effect per suspension mass is best determined experimentally by measuring the dissolution rate of a well-defined solid substance; this yields the mass transfer coefficient (k_{LSi}), from which ε can be calculated. For a detailed description of this procedure, see Ref. [3].

REFERENCES

1. Chilton, C.H. and Colburn, A.P., Mass transfer (absorption) coefficients, *Ind. Eng. Chem.*, 26, 1183, 1934.
2. Wakao, N., Particle-to-fluid heat/mass transfer coefficients in packed bed catalytic reactors, in *Recent Advances in the Engineering Analysis of Chemically Reacting Systems* (Ed. L.K. Doraiswamy), Wiley Eastern, New Delhi, 1984.
3. Hájek, J. and Murzin, D.Yu., Liquid-phase hydrogenation of cinnamaldehyde over Ru-Sn sol–gel catalyst. Part I. Evaluation of mass transfer via combined experimental/theoretical approach, *Ind. Eng. Chem. Res.*, 43, 2030–2038, 2004.

Liquid-Phase Diffusion Coefficients

The theory of molecules diffusing in liquids is not very well developed. A rigorous formulation of multicomponent diffusion, such as the Stefan–Maxwell equation for the gas phase, is not successful in describing diffusion in a liquid phase, because a general theory for calculating binary diffusion coefficients is lacking. However, semiempirical correlations that describe the diffusion of a dissolved component (solute) in a solvent can be used. The concentration of the dissolved component is of course assumed to be low compared with that of the solvent. The diffusion in liquids is very much dependent on whether the molecules are neutral species or ions.

A6.1 NEUTRAL MOLECULES

The treatment of the diffusion of a molecule (A) in a solvent (B) is based on the Stokes–Einstein equation that was developed originally for macromolecules. The diffusion coefficient for a spherical molecule (A) in a solvent (B) can be estimated from [1]

$$D_{AB} = \frac{RT}{6\pi\mu_B R_A}, \tag{A6.1}$$

where μ_B is the viscosity of the solvent and R_A the radius of the molecule (A). It turns out that Equation A6.1 describes the trends in liquid-phase diffusion correctly. The equation has been developed further for more practical use. Estimation of the molecule radius is difficult, especially for nonspherical molecules. Moreover, it is known that polar solvents

TABLE A6.1 Association Factors for Some Common Solvents

Water	2.6
Methanol	1.9
Ethanol	1.5
Nonassociated solvents	1

TABLE A6.2 Molar Volumes (V_A) of Some Molecules

Compound	**Molar Volume (cm^3/mol)**
Methane	37.7
Propane	74.5
Heptane	162
Cyclohexane	117
Ethene	49.4
Benzene	96.5
Fluorobenzene	102
Bromobenzene	120
Chlorobenzene	115
Iodobenzene	130
Methanol	42.5
n-Propanol	81.8
Dimethyl ether	63.8
Ethyl propyl ether	129
Acetone	77.5
Acetic acid	64.1
Isobutyric acid	109
Methyl formate	62.8
Ethyl acetate	106
Diethyl amine	109
Acetonitrile	57.4
Methyl chloride	50.6
Carbon tetrachloride	102
Dichlorodifluoromethane	80.7
Ethyl mercaptan	75.5
Diethyl sulfide	118
Phosgene	69.5
Ammonia	25
Chlorine	45.5
Water	18.7
Hydrochloric acid	30.6
Sulfur dioxide	43.8

associate to dimers and trimers. Considering these factors, Wilke and Chang [2] developed a modified equation

$$D_{AB} = \frac{7.4 \times 10^{-12} \sqrt{\left[\phi M_B/(\text{g/mol})\right]}(T/K)}{(\mu_B/cP)\, V_A^{0.6}} \text{ m}^2/\text{s}, \tag{A6.2}$$

where ϕ is the association factor, and M_B and μ_B denote the molar mass and viscosity of the solvent, respectively. V_A is the molar volume of the solved molecule at the normal boiling point.

The Wilke–Chang equation has been developed further to be valid for mixtures of solvents. For diffusion of component (A) in a mixture (m), Equation A6.2 can be written as

$$D_{Am} = \frac{7.4 \times 10^{-12} \sqrt{\sum_{i=1}^{N} x_k \phi_k M_k} (T/K)}{(\mu_B/cP) V_A^{0.6}} \text{ m}^2/\text{s}, \tag{A6.3}$$

where μ_m is the viscosity of the liquid mixture.

The association factor ϕ is estimated empirically. Table A6.1 lists the values for ϕ for some common solvents. A rule of thumb is that nonpolar organic solvents have the association factor 1, whereas polar solvents have high values.

The molar volume (V_A) is tabulated for some compounds [1]; a few examples are given in Table A6.2. For a general compound, V_A can be estimated from the atomic increments.

TABLE A6.3 Atomic Increments for the Estimation of V_A

	Increment (cm^3/mol) (Le Bas)
Carbon	14.8
Hydrogen	3.7
Oxygen (except as noted below)	7.4
In methyl esters and ethers	9.1
In ethyl esters and ethers	9.9
In higher esters and ethers	11.0
In acids	12.0
Joined to S, P, or N	8.3
Nitrogen	
Doubly bonded	15.6
In primary amines	10.5
In secondary amines	12.0
Bromine	27
Chlorine	24.6
Fluorine	8.7
Iodine	37
Sulfur	25.6
Ring, three-membered	−6.0
Four-membered	−8.5
Five-membered	−11.5
Six-membered	−15.0
Naphthalene	−30.0
Anthracene	−47.5
Double bond between carbon atoms	—
Triple bond between carbon atoms	—

Source: Data from Reid, R.C., Prausnitz, J.M., and Poling, B.E., *The Properties of Gases in Liquids*, 4th Edition, McGraw-Hill, New York, 1988.

TABLE A6.4 Ion Conductivities (λ) at Infinite Dilution in Water at (Ω^{-1}) 25°C

Cation		Anion	
	Monovalent		
Ag^+	61.9	Acetate	40.9
$CH_3NH_3^+$	58.7	Benzoate	32.4
$(CH_3)_2NH_2^+$	51.9	Butyrate	32.6
$(CH_3)_3NH^+$	47.2	Br^-	78.4
Cs^+	77.3	BrO_3^-	55.7
H^+	349.8	Cl^-	76.35
K^+	73.5	ClO_3^-	64.6
Li^+	38.7	ClO_4^-	67.4
Na^+	50.1	Cyanoacetate	41.8
NH_4^+	73.6	F^-	55.4
NMe_4^+	44.9	Formate	54.6
		HCO_3^-	44.5
NEt_4^+	32.7	I^-	76.8
NPr_4^+	23.4	IO_4^-	54.6
NBu_4^+	19.5	N_3^-	69
NAm_4^+	17.5	NO_3^-	71.46
Rb^+	77.8	OH^-	198.6
Tl^+	74.7	Picrate	30.39
		Propionate	35.8
		ReO_4	55
	Bivalent		
Ba^{++}	63.6	CO_3^{--}	69.3
Be^{++}	45	$C_2O_4^{--}$	74.2
Ca^{++}	59.5	SO_4^{--}	80
Co^{++}	55		
Cu^{++}	56.6		
Mg^{++}	53		
Sr^{++}	59.4		
Zn^{++}	52.8		
	Trivalent		
Ce^{3+}	69.8	$Fe(CN)_6^{3-}$	100.9
$CO(NH_3)_6^+$	101.9	P_3O_9	53.6
Dy^{3+}	65.6		
Er^{3+}	65.9		
Eu^{3+}	67.8		
Gd^{3+}	67.3		
HO^{3+}	66.3		
La^{3+}	69.7		
Nd^{3+}	69.4		
Pr^{3+}	69.6		
Sm^{3+}	68.5		
Tm^{3+}	65.4		
Yd^{3+}	65.6		

continued

TABLE A6.4 Ion Conductivities (λ) at Infinite Dilution in Water at (Ω^{-1}) 25°C (continued)

Cation	Anion	
Other		
	$Fe(CN)_6^{4-}$	110
	$P_4O_{12}^{4-}$	94
	$P_2O_2^{4-}$	96
	$P_3O_{10}^{5-}$	109

Reid et al. [1] present values for V_A for the most common atoms. Some atom increments are given in Table A6.3. Alternative equations to Equation A6.2 are presented by Wild and Charpentier [3]. The viscosity of the solvent is an important parameter in Equations A6.2 and A6.3. The viscosity can easily be determined experimentally, and experimental values are always preferred to theoretical correlations. The viscosity is strongly influenced by temperature. The temperature dependence can often be accounted for with simple empirical correlations of the type

$$\mu = AT^B, \tag{A6.4}$$

$$\ln(\mu) = A + \frac{B}{T} + CT + DT^2. \tag{A6.5}$$

The values for A, B, C, and D are given in Ref. [1].

For solvent mixtures, viscosity can in principle be estimated from the clean component viscosities, but the result is uncertain [1].

A6.2 IONS

In electrolyte solutions, both anions and cations diffuse at the same velocity, because the electroneutrality is preserved. Nernst's equation is valid for the diffusion of a completely

TABLE A6.5 Temperature Effects on Ion Conductivities ($l_0 = \lambda_+^0$ or $l_0 = \lambda_-^0$)

$$l^0 = l_{25}^0 + a(t-25) + b(t-25)^2 + c(t-25)^3$$

Ion	A	$b \times 10^2$	$c \times 10^4$
H^+	4.816	−1.031	−0.767
Li^+	0.89	0.441	−0.204
Na^+	1.092	0.472	−0.115
K^+	1.433	0.406	−0.318
Cl^-	1.54	0.465	−0.128
Br^-	1.544	0.447	−0.23
I^-	1.509	0.438	−0.217

dissociated electrolyte at infinite dilution:

$$D_0 = 8.931 \times 10^{-14} \left(\frac{T}{K}\right) \left(\frac{\lambda_+^0 \lambda_-^0}{\lambda_+^0 + \lambda_-^0}\right) \left(\frac{z_+ + z_-}{z_+ z_-}\right), \tag{A6.6}$$

where λ_+^0 and λ_-^0 denote the conductivity of the anion and the cation, respectively, at infinite dilution. The terms z_+ and z_- are the valences of the cation and anion, respectively.

For estimation of the diffusion coefficients in real electrolyte solutions, the following correction term has been proposed for Equation A6.6:

$$D = D_0 \left(1 + \frac{m \, \mathrm{d} \ln (\gamma\pm)}{\mathrm{d}m}\right) \frac{1}{c_{H_2O} V_{H_2O}} \left(\frac{\mu_{H_2O}}{\mu}\right), \tag{A6.7}$$

where m is the molarity of the electrolyte solution (mol electrolyte/kg water), $\gamma\pm$ is the activity coefficient of the electrolyte; c_{H_2O} and V_{H_2O} denote the water concentration and the partial molar volume of water; and μ_{H_2O} and μ are the viscosity of water and the electrolyte solution, respectively. The viscosity is strongly temperature-dependent, and the influence of temperature on conductivity should also be accounted for—if possible. The ion conductivities at 25°C are listed in Table A6.4 [4] and the temperature effect is shown in Table A6.5.

REFERENCES

1. Reid, R.C., Prausnitz, J.M., and Poling, B.E., *The Properties of Gases in Liquids*, 4th Edition, McGraw-Hill, New York, 1988.
2. Wilke, C.R. and Chang, P., Correlation of diffusion coefficients in dilute solutions, *AIChE J.*, 1, 264–270, 1955.
3. Wild, G. and Charpentier, J.-C., *Diffusivité des gaz dans les liquides*, Techniques d' ingénieur, Paris 1987.
4. Perry, R.H. and Chilton, C.H., *Chemical Engineers' Handbook*, 5th Edition, McGraw-Hill, Kogakusha, Tokyo, 1973.

Correlations for Gas–Liquid Systems

An estimation of the mass transfer coefficients (K_G, K_L), the mass transfer area (a_v), and the volume fractions of gas and liquid ($\varepsilon_G, \varepsilon_L$) can be carried out with the correlation equations, which have been developed on the basis of hydrodynamical theories and dimension analysis. The constants incorporated into the equations have subsequently been determined on the basis of experimental data for a number of model systems (such as air–water, oxygen–water, etc.). The dependability of these correlation equations can thus be very different. Usually, the quality of the estimations falls somewhere around 10–30% of the actual values. The correlations presented in the literature should therefore be utilized with great caution, and the validity limitations should be carefully analyzed. However, these correlations are very useful, for example, when performing feasibility studies or planning one's own experimental measurements. A thorough summary of various correlation equations for gas–liquid reactors is presented by Myllykangas [1]. Here we will only treat two common gas–liquid reactors, namely, bubble columns and packed columns, operating in a countercurrent mode.

A7.1 BUBBLE COLUMNS

In a CSTR and a bubble column, the mass transfer resistance is often negligible on the gas-phase side. In other words, the gas film coefficient K_G yields a high value compared with the liquid film coefficient. A simple estimation for K_G can be obtained by assuming that gas bubbles behave like rigid spheres. The gas film coefficient is thus obtained as

$$K_G = \frac{2D\pi^2}{3d_B}, \tag{A7.1}$$

where d_B denotes Sauter's average bubble diameter. The average bubble diameter can be calculated from Equation A7.2, provided that the size distribution of the bubbles is known:

$$d_B = \frac{\sum n_i d_{Bi}^3}{\sum n_i d_{Bi}^2}. \tag{A7.2}$$

A more detailed analysis of the gas film coefficient is presented in Ref. [2]. In this analysis, the experimental results were correlated with Geddes' [3] model (Equation A7.3):

$$k_G = \frac{-d_B}{6t_B} \ln\left[\frac{6}{\pi^2} \exp\left(\frac{Dt_B\pi^2}{(d_B/2)^2}\right)\right]. \tag{A7.3}$$

Hikita et al. [4] proposed the following empirical equation for the calculation of $k_L A$ in bubble columns:

$$k_L a = 14.9\,K\left(\frac{g}{w_G}\right)\left(\frac{w_G\mu_L}{\sigma}\right)^{1.76}\left(\frac{g\mu_L^4}{\rho_L\sigma^3}\right)^{-0.248}\left(\frac{\mu_G}{\mu_L}\right)^{0.243} Sc^{-0.604}, \tag{A7.4}$$

where the value of K depends on the ion strength of the solution (I) as follows:

$$0 < I < 1 \quad K = 10^{0.068I},$$
$$I > 1 \quad K = 1.114 \cdot 10^{0.021I}.$$

Therefore, Equation A7.4 can even be used in the case of electrolyte solutions.

In the case of organic solutions, Özturk et al. [5] recommend the following correlation for $k_L a$:

$$k_L a = 0.62\left(\frac{D}{d_B^2}\right) Sc^{0.5} Bo_B^{0.33} Ga_B^{0.29} Fr_B^{0.68}\left(\frac{\rho_G}{\rho_L}\right)^{0.04}. \tag{A7.5}$$

The bubble diameter was 3 mm during the measurements.

Several correlations are available for the calculation of the mass transfer area per reactor volume (a). In the most simple case, one assumes that all gas bubbles are rigid spheres of a similar volume, and the area is calculated on the basis of bubble size and gas holdup [6]:

$$a = \frac{6\varepsilon_G}{d_B}. \tag{A7.6}$$

Equation A7.6 can only be used after the measurement or estimation of ε_G.

Direct correlations for a_v have been developed by Akita and Yoshida [7].

The correlations are presented below.

$$a = 2600\left(\frac{h_L}{d_R}\right)^{-0.3}\left(\frac{\rho_L\sigma^3}{\mu_L^4 g}\right)^{-0.003}\varepsilon_G. \tag{A7.7}$$

The bubble diameter was assumed to be 3 mm.

The correlation of Akita and Yoshida [7] is written as follows:

$$a = \frac{1}{3d_R} Bo_R^{0.5} Ga_R^{0.1} \varepsilon_G^{1.13}. \tag{A7.8}$$

A requirement for the use of Equation A7.8 is that gas holdup is 0.14 or lower.

For the gas volume fraction, holdup, several correlations are suggested in the literature. The correlation of Akita and Yoshida [7] is valid for columns with a maximal diameter of 60 cm. It can further be utilized in the case of pure liquids and nonelectrolytic solutions:

$$\varepsilon_G = 0.14 Bo_R^{0.113} Ga_R^{0.075} Fr_R^{0.9}. \tag{A7.9}$$

Hikita et al. [4] suggest the following correlation for electrolytic and nonelectrolytic solutions. The measurements were carried out in a column with a diameter of 10 cm:

$$\varepsilon_G = 0.672\, K \left(\frac{w_G \mu_L}{\sigma}\right)^{0.578} \left(\frac{g\mu_L^4}{\rho_L \sigma^3}\right)^{-0.131} \left(\frac{\mu_G}{\mu_L}\right)^{0.107} \left(\frac{\rho_G}{\rho_L}\right)^{0.062}. \tag{A7.10}$$

The value of the parameter K depends on the ion strength (I) as indicated below:

$$\begin{aligned} &I = 0, && K = 1, \\ &0 < I < 1, && K = 10^{0.0414I}, \\ &I > 1, && K = 1.1. \end{aligned}$$

A7.2 PACKED COLUMNS

Sahay and Sharma [8] carried out measurements in a packed column filled with 1″ packing elements. They arrived at the following equation (Equation A7.11) for $k_G a$, in which the coefficients depend on the geometry and the material of packing elements:

$$k_G a = A \cdot 100^{B+C+1} w_G^B w_L^C D^{0.5} RT. \tag{A7.11}$$

A few values for the parameters A, B, and C are tabulated in Table A7.1.

Onda et al. [9] developed the following correlation for k_L in packed columns. The correlation is considered suitable for most packing elements, with the exception of Pall rings. A requirement for using this correlation is that the mass transfer area (a_v) is estimated using some other correlation:

$$k_L = 0.0051 \left(\frac{\rho_L}{\mu_L g}\right)^{-1/3} Re_y^{2/3} Sc^{-1/2} (a_c d_p)^{0.4}. \tag{A7.12}$$

TABLE A7.1 Parameters for Some Packing Elements

Packing Element	Material	A · (10^{-5})	B	C
Raschig ring	Ceramic	35.9	0.64	0.48
	PVC	22.7	0.74	0.41
Intalox saddle	Ceramic	36.5	0.7	0.48
	PP	25.8	0.75	0.45
Pall ring	SS	64.3	0.58	0.38
	PP	33.1	0.64	0.48

Source: Data from Sahay, B.N. and Sharma, M.M., *Chem. Eng. Sci.*, 28, 41, 1973.
PP = polypropylene; PVC = polyvinyl chloride; SS = stainless steel.

For packing elements with a saddle or a ring geometry ($d = 0.95$–7.6 cm), a modification [10] of the traditional Sherwood and Holloway correlation is suggested:

$$k_L a = 530 Sc^{1/2} D \left(\frac{G}{\mu_L}\right)^{0.75}. \tag{A7.13}$$

The most frequently used correlation for the mass transfer area was developed by Onda et al. [9]:

$$\frac{a}{a_c} = 1 - e^{\left(-1.45(\sigma_c/\sigma)^{0.75} Re_Z^{0.1} Fr_p^{-0.05} We_a^{0.2}\right)}, \tag{A7.14}$$

where a_c denotes the so-called "dry area per volume fraction" and σ_c is the critical surface tension.

A few values for these parameters (a_c and σ_c) are tabulated in Tables A7.2 and A7.3.

TABLE A7.2 Packing Element Characteristics

Packing Element	Material	Nominal Size (m)	Estimated *a* (1/m)	Porosity (−)
Raschig ring	Ceramic	0.00635	712	0.62
	Ceramic	0.0127	367	0.64
	Ceramic	0.0254	190	0.74
	Ceramic	0.0508	92	0.74
	Ceramic	0.1016	46	0.8
	Carbon	0.0254	185	0.74
	Steel	0.0254	184	0.86
Pall ring	Ceramic	0.02508	95	0.74
	Steel	0.0254	207	0.94
	PP	0.254	207	0.9
Berl saddle	Ceramic	0.0254	249	0.68
Intalox saddle	Ceramic	0.0254	256	0.77
Tellerett	PE	0.0254	249	0.83

Source: Data from Myllykangas, *J. Rep. Lab. Ind. Chem.*, ÅboAkademi, Åbo, Finland, 1989.

TABLE A7.3 Critical Surface Tension for a Few Materials

Material	Critical Surface Tension (kg/s^2) (10^3)
Carbon	56
Ceramic	61
Glass	73
Paraffin	20
PP	33
PVC	40
Steel	75

Source: Data from Myllykangas, J., *Rep. Lab. Ind. Chem.*, ÅboAkademi, Åbo, Finland, 1989.
PP = polypropylene; PVC = polyvinyl chloride.

The following correlation is suggested [11] for the liquid volume fraction:

$$\varepsilon_L = 2.2\left(\frac{\mu_L w_L}{g\rho_L d_p^2}\right)^{1/3} + Fr_p^{1/2}. \tag{A7.15}$$

The first term in Equation A7.15 is called the *film number*. The equation is valid for ring-shaped packing elements and generally correlates with better than 20% accuracy with the literature data. The following correlation for ring- and saddle-shaped packing elements has been proposed [12]:

$$\varepsilon_L = 4.67\left(\frac{w_L^3 a_c^3 \mu_L}{\rho_L g^2}\right)^{1/4}. \tag{A7.16}$$

A7.3 SYMBOLS

a mass transfer area in water
a_c "dry area" of packing elements divided by their volume
D diffusion coefficient
d_B bubble diameter
d_p particle diameter
d_R reactor diameter
g gravitational acceleration
G mass balanced, linear flow velocity of the liquid: $G = w_L \rho_L$
h_L liquid height level in the reactor
h_R reactor height
I ion strength of the solution
K parameter, Equations A7.4 and A7.10
k_G mass transfer coefficient in the gas phase
k_L mass transfer coefficient in the liquid phase
n_i number of bubbles with a diameter of d_{Bi}
t_B average bubble residence time, $t_B = h_R/w_B$
w linear flow velocity

w_B linear flow velocity of a bubble
ε holdup
μ dynamic viscosity
σ surface tension
σ_d critical surface tension for a packing element
ρ density

A7.4 INDEX

B bubble
G gas
L liquid
P particle
R reactor

A7.5 DIMENSIONLESS NUMBERS

Bo Bond, $Bo_B = gd_B^2\rho_L/\sigma$ $Bo_R = gd_R^2\rho_L/\sigma$
Fr Froude, $Fr_R = w_G/(gd_R)^{1/2}$ $Fr_B = w_G/(gd_B)^{1/2}$ $Fr_P = w_G^2/gd_P$ $Fr_a = G^2a_c/\rho_L^2 g$
Ga Galilei, $Ga_R = gd_R^3\rho_L^2/\mu_L^2$ $Ga_B = gd_B^3\rho_L^2/\mu_L^2$
Re Reynolds, $Re_y = G/(a_w\mu_L)$ $Re_z = G/a_c\mu_L$
Sc Schmidt, $Sc = \mu/\rho D$

REFERENCES

1. Myllykangas, J., Aineensiirtokertoimen, neste—ja kaasuosuuden sekä aineensiirtopintaalan korrelaatiot eräissä heterogeenisissä reaktoreissa, *Rep. Lab. Ind. Chem.*, Åbo Akademi, Åbo, Finland, 1989.
2. Rase, H.F., *Gas–Liquid Reactors, Chemical Reactor Design for Process Plants*, Vol. 1: *Principles and Techniques*, p. 627, Wiley, New York, 1977.
3. Geddes, R.L., Local efficiencies of bubble plate fractionators, *Trans. Am. Inst. Chem. Eng.*, 42, 79, 1946.
4. Hikita, H., Asai, S., Tanigawa, K., Segawa, K., and Kitao, M., The volumetric liquid-phase mass-transfer coefficient in bubble columns, *Chem. Eng. J.*, 22, 61, 1981.
5. Özturk, S.S., Schumpe, A., and Deckwer, W.-D., Organic liquids in a bubble column: Hold-ups and mass-transfer coefficients, *AIChE J.*, 33, 1473, 1987.
6. Miller, D.N., Scale-up of agitated vessels gas–liquid mass-transfer, *AIChE J.*, 20, 445, 1974.
7. Akita, K. and Yoshida, F., Bubble-size, interfacial area and liquid-phase mass-transfer coefficient in bubble columns, *Ind. Eng. Chem. Process Des. Dev.*, 13, 84, 1974.
8. Sahay, B.N. and Sharma, M.M., Effective interfacial area and liquid- and gas-side mass-transfer coefficients in a packed column, *Chem. Eng. Sci.*, 28, 41, 1973.
9. Onda, K., Takeuchi, H., and Okumoto, Y., Mass-transfer coefficients between gas- and liquid-phase in packed columns, *J. Chem. Eng. Jpn*, 1, 56, 1968.
10. Mei Geng Shi and Mersmann A., Effective interfacial area in packed columns, *Ger. Chem. Eng.*, 8, 87, 1985.
11. Perry, J.M., *Chemical Engineer's Handbook*, 5th Edition, McGraw-Hill, New York, 1973.
12. Subramanian, K.N., Sridharan, K., Degaleesan, T.E., and Laddha, G.S., Gas-phase mass-transfer in packed columns, *Ind. Chem. Eng.*, 21, 38, 1979.

Gas Solubilities

For historical reasons, there are several different ways to express gas solubilities in liquids, such as Bunsen's and Ostwald's coefficients. These are not treated here in detail, and the reader is referred to Refs. [1] and [2]. Nowadays, the most common means to express gas solubilities is to turn to the equilibrium molar fractions (x^{s}_{LA} or x) of dissolved gas A and to the temperature and pressure of the gas. From the ratio

$$He'_{A} = \frac{p^{s}_{A}}{x^{s}_{LA}}, \tag{A8.1}$$

from which Henry's constant (He'_{A} or H) can be calculated. Expression A8.1 can be used to predict x^{s}_{LA} at a certain pressure (p^{s}_{A}). The agreement is generally good for low values of x^{s}_{LA} and p^{s}_{A} but compromised at higher pressures. In the case of sparsely soluble gases, Equation A8.1 is a good choice.

Gas solubilities are generally strongly temperature-dependent, so much so that the logarithm of solubility ($\ln x_{g}$) versus inverse temperature ($1/T$) yields a straight line. Intuitively, gas solubility should diminish as a function of the temperature, but experimental measurements have shown that a minimum in gas solubility at a certain temperature is a common behavior (Figure A8.1) [3].

Empirically, the temperature dependence of gas solubility can be described with an equation of the following kind:

$$\ln x = A + \frac{B}{T} + C \ln T + D, \tag{A8.2}$$

where A, B, C, and D are empirical coefficients; coefficients C and D can sometimes be neglected. Fogg and Gerrard [1] have compiled a large amount of literature data in the form of Equation A8.2.

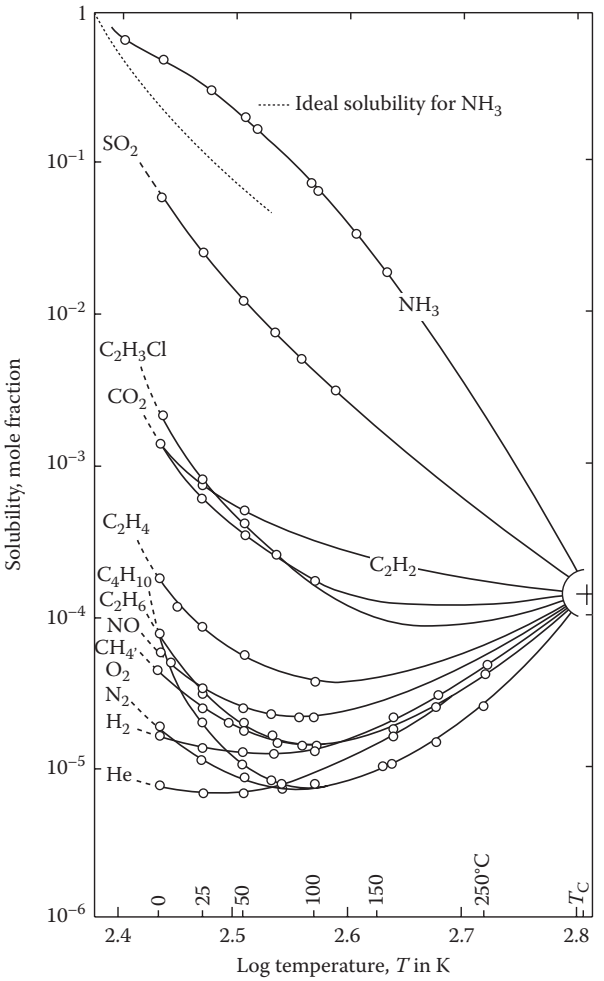

FIGURE A8.1 Solubilities of some common gases in water. (Data from Hayduk, W. and Laudie, H., *AIChE J.*, 19, 1233–1238, 1973.)

Equation A8.2 usually represents a good reproduction of data within the experimental temperature interval, but extrapolation outside the interval is dangerous! A few samples are given in Table A8.1 [1].

The presence of electrolytes in the liquid affects gas solubility. Henry's constant for a pure solvent (H_0) can be corrected with the so-called salting-out factors (h) that are ion-specific parameters. Schumpe [6] has suggested the following equation for electrolyte mixtures:

$$\ln \frac{H}{H_0} = \sum (h_i + h_G)\, c_i, \tag{A8.3}$$

where h_i denotes the salting-out factor for the ion i and h_G the salting-out factor for the gas. Weisenberger and Schumpe [7] expanded Schumpe's original model to be valid for the temperature interval of 273–363 K. The parameter h_G has a linear temperature dependence

TABLE A8.1 Gas Solubilities According to Equation A8.2

Gas	Solvent	*A*	*B*	*C*	*D*	Temperature (*K*)
H_2	H_2O	−123.939	5528.45	16.8893	0	273–345
H_2	Hexane	−5.8952	−424.55	0	0	213–298
	Heptane	−5.6689	−480.99	0	0	238–308
	Octane	−5.6624	−484.38	0	0	248–308
	Benzene	−5.5284	−813.90	0	0	280–336
	Toluene	−6.0373	−603.07	0	0	258–308
	Methanol	−7.3644	−408.38	0	0	213–298
	Ethanol	−7.0155	−439.18	0	0	213–333
O_2	H_2O	−171.2542	8391.24	23.24323	0	273–333
O_2	H_2O	−139.485	6889.6	18.554	0	273–617
O_2	Benzene	−30.1649	874.16	3.53024	0	283–343
O_2	Ethanol	−7.874	126.93	0	0	248–343
CO_2	H_2O	−159.854	8741.68	21.6694	-1.10261×10^{-3}	273–353
	Benzene	−73.824	3804.8	9.8929	0	283–313
	Toluene	−13.391	1512.9	0.6580	0	203–313
Cl_2	Benzene	−9.811	2374	0	0	283–341
	Toluene	−10.030	2457	0	0	288–353
	Ethyl benzene	−8.425	1978	0	0	288–348
	Acetic acid[a] and monochloro acetic acid	−12.98	3072.7	0	0	343–383
	Propionic acid[b] and monochloro propionic acid	−10.474	2356.8	0	0	298–403

Source: Data from Fogg, P.G.T. and Gerrard, W., *Solubility of Gases in Liquids*, Wiley, Chichester, 1991.

[a] Data from Martikainen, P., et al. *J. Chem. Technol. Biotechnol.*, 40, 259–274, 1987.

[b] Data from Mäki-Arvela, P., Kinetics of the chlorination of acetic and propanoic acids, Doctoral Thesis, Åbo Akademi, Turku/Åbo, Finland, 1994.

as follows:

$$h_G = h_{G,0} + h_T(T - 298.15\,\mathrm{K})\,. \tag{A8.4}$$

Numerical values for parameters h_i and h_G are tabulated in Table A8.2 [7].

TABLE A8.2 Salting-Out Factors for Gases and Ions

Cation	h_i (m^3 k mol^{-1})		Anion	h_i (m^3 k mol^{-1})		Gas	$h_{G,0}$ (m^3 k mol^{-1})		$10^3 \times h_r$ (m^3 k mol^{-1})	Temperature[a] (K)
H^+	≡ 0	(57)[b]	OH^-	0.084	(51)[b]	H_2	−0.0218	(75)[a]	−0.299	273–353
Li^+	0.0754	(73)	HS^-	0.085	(1)	He	−0.0353	(20)	0.464	278–353
Na^+	0.1143	(261)	F^-	0.0922	(7)	Ne	−0.008	(57)	−0.913	288–303
K^+	0.0922	(226)	Cl^-	0.032	(421)	Ar	0.0057	(79)	−0.485	273–353
Rb^+	0.084	(21)	Br^-	0.027	(58)	Kr	−0.007	(14)	n.a.[c]	298
Cs^+	0.0759	(36)	I^-	0	(88)	Xe	0.0133	(5)	−0.329	273–318
NR^+	0.0556	(51)	NO_2^-	0.08	(2)	Rn	0.0447	(10)	−0.138	273–301
Mg^{2+}	0.1694	(32)	NO_3^-	0.013	(109)	N_2	−0.001	(38)	−0.605	278–345
Ca^{2+}	0.1762	(17)	ClO_3^-	0.1348	(1)	O_2	≡0	(162)	−0.334	273–353
Sr^{2+}	0.1881	(2)	BrO_3^-	0.1116	(1)	NO	0.006	(1)	n.a.	298
Ba^{2+}	0.2168	(30)	IO_3^-	0.091	(1)	N_2O	−0.009	(78)	−0.479	273–313

continued

TABLE A8.2 Salting-Out Factors for Gases and Ions (continued)

Cation	h_i ($m^3 k mol^{-1}$)		Anion	h_i ($m^3 k mol^{-1}$)		Gas	$h_{G,0}$ ($m^3 k mol^{-1}$)		$10^3 \times h_r$ ($m^3 k mol^{-1}$)	Temperature[a] (K)
Mn^{2+}	0.1463	(14)	ClO_4^-	0.049	(4)	NH_3	−0.0481	(27)	n.a.[c]	298
Fe^{2+}	0.1523	(4)	IO_4^-	0.1464	(1)	CO_2	−0.0172	(50)	−0.338	273–313
Co^{2+}	0.168	(6)	CN^-	0.068	(1)	CH_4	0.0022	(60)	−0.524	273–363
Ni^{2+}	0.1654	(6)	SCN^-	0.063	(1)	C_2H_2	−0.0159	(30)	n.a.[c]	298
Cu^{2+}	0.1537	(8)	$HCrO_4^-$	0.04	(1)	C_2H_4	0.0037	(15)	n.a.[c]	298
Zn^{2+}	0.1537	(10)	HCO_3^-	0.097	(2)	C_2H_6	0.012	(55)	−0.601	273–348
Cd^{2+}	0.1869	(11)	$H_2PO_4^-$	0.091	(8)	C_3H_8	0.024	(17)	−0.702	286–345
Al^{3+}	0.2174	(10)	HSO_3^-	0.055	(1)	n-C_4H_{10}	0.0297	(38)	−0.726	273–345
Cr^{3+}	0.065	(2)	CO_3^{2-}	0.1423	(11)	H_2S	−0.0333	(15)	n.a.[c]	298
Fe^{3+}	0.1161	(6)	HPO_4^{2-}	0.1499	(3)	SO_2	−0.0817	(36)	0.275	283–363
La^{3+}	0.2297	(6)	SO_3^{2-}	0.127	(3)	SF_6	0.01	(10)	n.a.[c]	298
Ce^{3+}	0.2406	(2)	SO_4^{2-}	0.1117	(111)					
Th^{4+}	0.2709	(1)	$S_2O_3^{2-}$	0.1149	(2)					
			PO_4^{3-}	0.2119	(3)					
			$[Fe(CN)_6]^{4-}$	0.3574	(1)					

Source: Data from Weisenberger, S. and Schumpe, A., *AIChE J.*, 42, 298–300, 1996.

[a] Experimental temperature range for the evaluation of the h_r parameter value.

[b] Number of occurrences in the data set (in brackets).

[c] n.a. = not available.

REFERENCES

1. Fogg, P.G.T. and Gerrard, W., *Solubility of Gases in Liquids*, Wiley, Chichester, 1991.
2. Reid, R.C., Prausnitz, J.M., and Poling, B.E., *The Properties of Gases and Liquids*, 4th Edition, McGraw-Hill, New York, 1988.
3. Hayduk, W. and Laudie, H., Solubilities of gases in water and other associated solvents, *AIChE J.*, 19, 1233–1238, 1973.
4. Martikainen, P., Salmi, T., Paatero, E., Hummelstedt, L., Klein, P., Damen, H., and Lindroos, T., Kinetics of the homogeneous catalytic chlorination of acetic acid, *J. Chem. Technol. Biotechnol.*, 40, 259–274, 1987.
5. Mäki-Arvela, P., Kinetics of the chlorination of acetic and propanoic acids, Doctoral Thesis, Åbo Akademi, Turku/Åbo, Finland, 1994.
6. Schumpe, A., The estimation of gas solubilities in salt solutions, *Chem. Eng. Sci.*, 48, 153–158, 1993.
7. Weisenberger, S. and Schumpe, A., Estimation of gas solubilities in salt solutions at temperatures from 273 to 363 K, *AIChE J.*, 42, 298–300, 1996.

Laboratory Reactors

Chemical reactors in the laboratory scale are used to check reactant conversions and product selectivities, chemical equilibria, and reaction kinetics as well as thermal effects. All laboratory reactors can be placed in the well-known categories of homogeneous and heterogeneous reactors. However, laboratory reactors typically possess some characteristic features that are worth discussing in detail: the residence time distribution and temperature are carefully controlled and the flow pattern is maintained as simple as possible. This is due to the primary purpose of laboratory-scale reactors: they are mainly used to screen and determine the kinetics and equilibria of chemical processes, preferably in the absence of heat and mass transfer limitations. Laboratory reactors have a special design to suppress the above-mentioned effects and automated data acquisition is used. The specific phenomena attributed to laboratory reactors will be discussed here. Primary data obtained from laboratory reactors are used to determine the kinetic and thermodynamic parameter values that are important for the process design. For further data processing and estimation of the parameter values, it is important to recognize the mathematical structures of the models. Laboratory reactor structures and modeling aspects are discussed briefly here, whereas parameter estimation from experimental data is described in Appendix 10.

A9.1 FLOW PATTERN IN LABORATORY REACTORS

For kinetic studies in homogeneous tube reactors and catalytic fixed bed reactors, plug flow conditions should prevail to make the interpretation of kinetic data as straightforward as possible. The justification of the plug flow assumption can be checked with available correlations for the Peclet number for homogeneous tube reactors and fixed beds. In terms of fixed beds, three Peclet numbers are used, namely, the Peclet number based on the longitudinal dispersion coefficient (D) and the bed length ($Pe = wL/D$), the Peclet number based

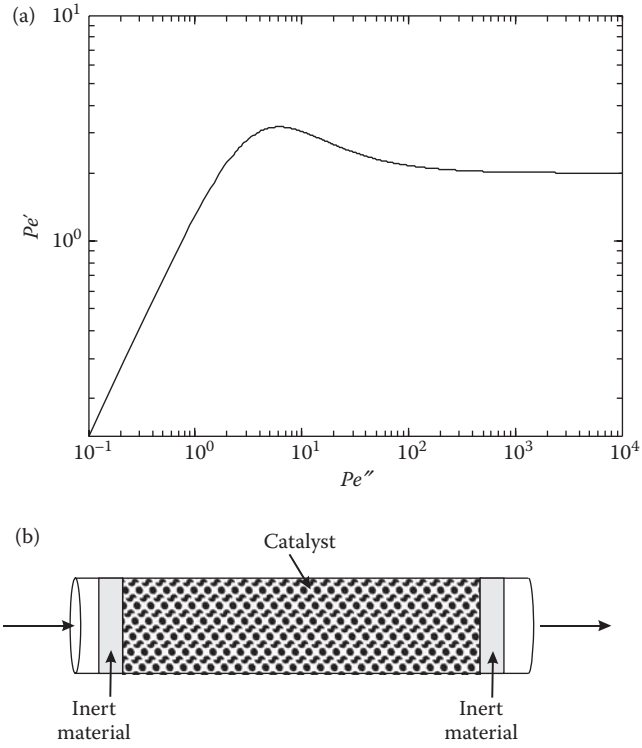

FIGURE A9.1 (a) Flow pattern and different Peclet numbers (Data from Kangas, M., Salmi, T., and Murzin, D., *Ind. Eng. Chem. Res.*, 47, 5413–5426, 2008) and (b) a laboratory-scale fixed bed.

on the longitudinal dispersion coefficient (D) and the particle diameter ($Pe' = wd_P/D$), and the Peclet number based on the molecular diffusion coefficient (D_{mi}) and the particle diameter ($Pe'' = wd_P/D_{mi}$). Edwards and Richardson [1] proposed a correlation equation between Pe' and Pe''. The plot based on the correlation is shown in Figure A9.1 [2]. The approach is straightforward: the molecular diffusion coefficient is measured experimentally or calculated from a model (Appendices 4 and 6), Pe'' is calculated, and Pe' is obtained from Figure A9.1, after which $Pe = (L/d_P)Pe'$. A rough rule of thumb is that Pe should exceed 50 to guarantee the plug flow conditions.

A best way is to determine the residence time distribution experimentally as described in Chapter 4. From the experimentally determined variance (σ) of a pulse experiment, the longitudinal Peclet number is easily obtained by an iterative solution: $\sigma = 2(Pe - 1 + e^{-Pe})/Pe^2$.

A9.2 MASS TRANSFER RESISTANCE

The role of external mass transfer resistance can be checked by the estimation of the Biot number and the mass transfer coefficient as described in Appendix 5. For experimental determination of the role of external mass transfer in fixed beds, a simple test is recommended: the reaction is carried out in the fixed bed with different amounts of catalyst

(m_{cat}) and fluid velocities (inlet volumetric flow rates, $\dot{V}_0$) in such a way that the ratio $R = m_{cat}/\dot{V}_0$ is kept constant. The results should be the same for all of the ratios used, if the external mass transfer limitations are absent. At low flow rates, the reactant conversion will decrease because of increasing external mass transfer resistance. This can be a serious problem in small laboratory-scale reactors with small amounts of catalysts. Low liquid flow rates are used in these reactors to ensure a long enough residence time, which can lead to a pronounced external mass transfer resistance.

To suppress the internal mass transfer resistance in the pores of the solid material, small enough particles should be used. The role of internal mass transfer resistance can be evaluated using the concepts described in Chapter 5, that is, by evaluating the generalized Thiele modulus and the effectiveness factor.

A good experimental approach to check the presence/absence of internal mass transfer resistance is to carry out experiments with various particle sizes. By gradually minimizing the particle size, the conversions, yields, and selectivities should approach a limiting value corresponding to the intrinsic kinetics. Sometimes this approach can, however, lead to a *cul-de-saq*: the pressure drop increases, as the particle size is diminished and the kinetic conditions are not attained. Another type of test reactor should then be considered, for instance, a fluidized bed (for gas-phase reactions) or a slurry reactor (for liquid-phase reactions).

A9.3 HOMOGENEOUS BR

The characteristic feature of a well-stirred homogeneous BR is that neither concentration nor temperature gradients appear inside the reactor vessel. The volume is constant for gas-phase processes carried out in closed reactor vessels (autoclaves) and in practice even often for liquid-phase processes (in many liquid-phase processes, the density change of the reactive mixture is minor) carried out in open vessels. The concentrations in the gas or liquid phases are measured as a function of the reaction time. Various methods for chemical analysis are accessible: continuous methods applied on-line, such as conductometry and photometry, on-line spectroscopic methods as well as discontinuous methods based on sampling and off-line analysis of the samples, such as gas and liquid chromatography. A constant temperature is maintained with a cooling/heating jacket, and the temperature is measured by a thermocouple or an optical fiber. In the case of volatile components, a cooling condenser is placed on top of the reactor. A typical batch-scale laboratory reactor is shown in Figure A9.2, and the results from a kinetic experiment are displayed in Figure A9.3.

The absence of the concentration and temperature gradients in the reactor should be checked by changing the rotation speed of the impeller and plotting the reactant conversion as a function of time for varying impeller speeds.

Provided that the stirring is vigorous enough to guarantee a homogeneous content of the reaction mixture, the mass balance for a component in the BR is written as (Chapter 3)

$$\frac{\mathrm{d}c_i}{\mathrm{d}t} = r_i\,(\mathbf{c}, \mathbf{k}, \mathbf{K}). \tag{A9.1}$$

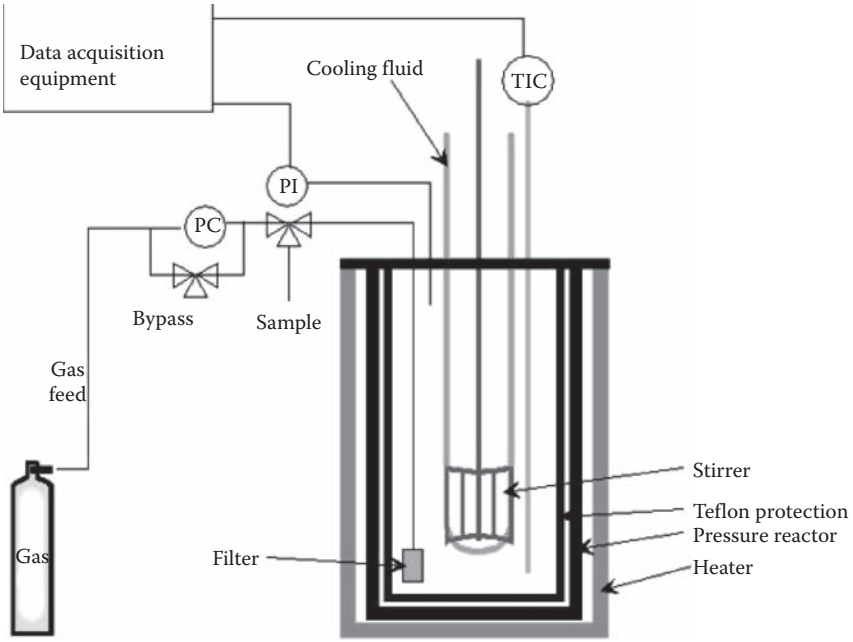

FIGURE A9.2 BR in laboratory scale.

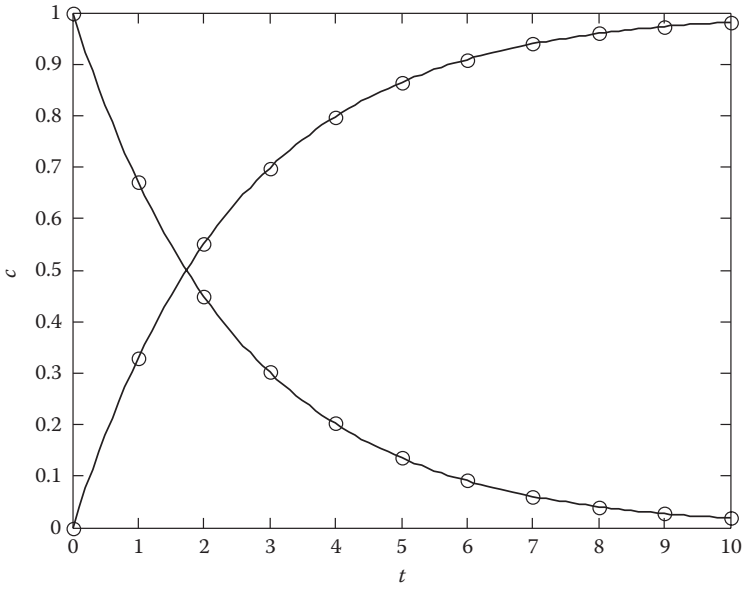

FIGURE A9.3 Results from a BR experiment (A → P).

In effect, Equation A9.1 is a special case of the equations presented for homogeneous tank reactors in Chapter 3.

A9.4 HOMOGENEOUS STIRRED TANK REACTOR

The construction of a laboratory-scale continuous stirred tank reactor (CSTR) resembles of that of a BR, but the reactor is equipped with an inlet and an outlet. Concentration and temperature gradients should be absent because of vigorous stirring. For a homogeneous CSTR, a constant volume and pressure are reasonable assumptions. The concentrations at the reactor outlet are measured as a function of the space time, that is, volumetric flow rate. The steady-state mass balance is written as (Chapter 3)

$$\frac{c_i - c_{0i}}{\tau} = r_i\,(\mathbf{c}, \mathbf{k}, \mathbf{K}), \tag{A9.2}$$

where the space time is defined by

$$\tau = \frac{V}{\dot{V}_0}, \quad \dot{V} = \dot{V}_0. \tag{A9.3}$$

It should be noticed that the volumetric flow rate can have considerable changes for gas-phase reactions because of the change in the number of molecules during the reaction. Measurements of c_i (and c_{0i}, τ) yield r_i directly, that is, the generation rates of the compounds, which represents a great advantage of this reactor as a rapid tool for kinetic experiments. On the other hand, several chemicals are consumed during an experiment. A remedy to this is to reduce the size of the reactor.

An example of the use of a CSTR is given below. The kinetics of the reaction A $\rightarrow$ P is studied in a CSTR. The space time, τ, and possibly the inlet concentration level, c_{0A}, are varied and c_A, r_A-data are obtained. A rate law is assumed, for example, the reaction rate for component A is $r_A = -kc_A$. A plot of the concentration of component A, c_A, versus $-r_A$ gives the rate constant, k, as the slope of the curve, as illustrated in Figure A9.4.

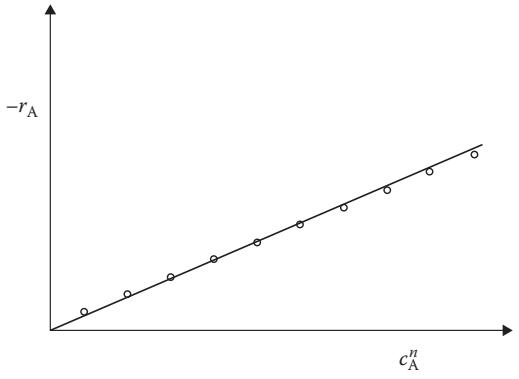

FIGURE A9.4 Evaluation of experimental data obtained from a CSTR.

FIGURE A9.5 Fixed beds in laboratory scale, a system of parallel reactors.

A similar approach can be applied to arbitrary kinetics, provided that the rate can be expressed in the form $-r_A = kf(c)$, where $f(c) = c_A^n, c_A c_B$, and so on.

A9.5 FIXED BED IN THE INTEGRAL MODE

Catalytic fixed beds are frequently used as test reactors for two-phase processes (gas or liquid and a solid catalyst). A laboratory-scale fixed bed reactor is displayed in Figure A9.5. The reactor is placed in an oven or in a thermostat bath. The efficiency of the system can be improved by arranging several fixed beds in parallel. In this way, various temperatures, flow rates, and catalysts can be screened in a single experiment. The gas flows are regulated with mass flow controllers and the liquid feed rates with pumps. Plug flow conditions should prevail, and small enough catalyst particles should be used to suppress the internal diffusion resistance. Provided that these conditions are fulfilled, the mass balance becomes very simple:

$$\frac{\mathrm{d}\dot{n}_i}{\mathrm{d}V} = \rho_\beta r_i. \tag{A9.4}$$

De facto Equation A9.4 is the one-dimensional, pseudohomogeneous model for fixed beds presented in Chapter 5.

The mass of the catalyst in the reactor (m_{cat}) and the catalyst bulk density are related by

$$m_{cat} = \rho_B V_R. \tag{A9.5}$$

The dimensionless coordinate (z) is introduced:

$$V = V_R z, \quad \mathrm{d}V = V_R \mathrm{d}z, \tag{A9.6}$$

which yields

$$\frac{\mathrm{d}\dot{n}_i}{\mathrm{d}z} = m_{cat} r_i, \qquad \text{where } c_i = \frac{\dot{n}_i}{\dot{V}}. \tag{A9.7}$$

Equation A9.7 is solved from $z = 0$ to $z = 1$ to obtain the molar flows at the outlet of the bed, $\dot{n}_i(z = 1)$; these values have typically been measured experimentally. Chemical analysis gives the concentrations (c_i), but they are related to the molar flows as expressed by Equation A9.7. The volumetric flow rate is updated by an appropriate gas law:

$$\dot{V} = \frac{Z\dot{n}RT}{P}, \quad \text{where } \dot{n} = \sum \dot{n}_i. \tag{A9.8}$$

The compressibility factor (Z) is a function of the composition (molar flows, mole fractions), temperature, and pressure. Methods for the calculation of Z from equations of state are discussed in Ref. [3]. For ideal gases, $Z = 1$. The inlet composition is varied in the experiments to obtain varying molar flows.

If the volumetric flow rate and fluid density are constant, the mass balance equation (Equation A9.4) becomes

$$\frac{\mathrm{d}c_i}{\mathrm{d}\tau} = \rho_B r_i, \tag{A9.9}$$

which is formally similar to the balance equation for a homogeneous BR.

For simple cases of kinetics, an analytical solution of the model is possible but, in general, a numerical solution of Equation A9.7 or A9.9 is preferred during the estimation of the kinetic constants. It should be noticed that the analytical solutions obtained for various kinetics in a homogeneous BR (Equation A9.1) can be used for the special case of fixed beds, Equation A9.9, but the reaction time (t) appearing in the solution of the BR model (Equation A9.1) is replaced by the product $\rho_B\tau$ ($\tau = V/\dot{V}_0$) in the fixed bed model. A special case of fixed bed is considered in the next section.

A9.6 DIFFERENTIAL REACTOR

Catalytic differential reactors are frequently mentioned in textbooks as typical test reactors. In fact, a differential reactor used in catalysis is a special case of the fixed bed reactor, nothing else. The conversions are maintained low, which allows us to approximate the molar flow gradients by linear functions:

$$\frac{\mathrm{d}\dot{n}_i}{\mathrm{d}z} = \text{constant} = \frac{\dot{n}_i - \dot{n}_{i0}}{1 - 0} = \dot{n}_i - \dot{n}_{i0}. \tag{A9.10}$$

The approximation is illustrated in Figure A9.6. As shown by the figure, the concentration gradients are practically linear as long as the conversion is low, that is, the rate constant is low and/or the space time is short. In addition, the approximation is better for low reaction orders than for higher ones. For a zero-order reaction (r = constant), the concentration profile is linear, until the reactant is completely consumed. Thus, the differential reactor concept is a perfect description. The higher the reaction order, the more the concentration curves deviate from the linearity, and the risks in using the differential reactor approximation increase. By denoting

$$\dot{n}_i = \dot{n}_i(z = 1) \tag{A9.11}$$

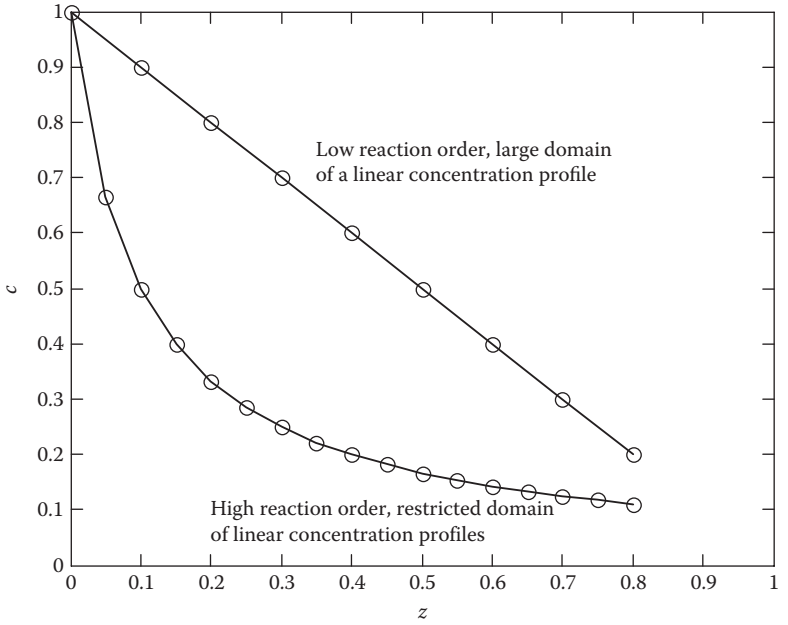

FIGURE A9.6 Concentration profiles in a fixed bed.

and inserting this relation into the balance equation of a catalytic fixed bed, Equation A9.7, we obtain

$$\dot{n}_i - \dot{n}_{0i} = m_{\text{cat}}\bar{r}_i, \tag{A9.12}$$

where r_i indicates the generation rate, which should be calculated as an average of the concentrations or molar flows. The simplest average is

$$\bar{\dot{n}}_i = \frac{1}{2}(\dot{n}_{0i} - \dot{n}_i). \tag{A9.13}$$

The balance can, thus, be rewritten as

$$\bar{\dot{n}}_i - \dot{n}_{0i} = \frac{1}{2}m_{\text{cat}}\bar{r}_i. \tag{A9.14}$$

Using the component concentrations, Equation A9.14 becomes

$$\frac{\bar{c}_i - c_{0i}}{\tau} = \frac{1}{2}\rho_{\text{B}}\bar{r}_i. \tag{A9.15}$$

In principle, r_i is directly obtained by means of a measurement of the molar flow difference, $\dot{n}_i - \dot{n}_{0i}$. Mathematically, the differential reactor model coincides with the model of a gradientless test reactor presented in the next section.

A9.7 GRADIENTLESS REACTOR

Various configurations of gradientless reactors are used to evaluate the heterogeneous catalysts. The catalyst particles are usually placed in a rotating (spinning) or a static basket. For a catalytic gradientless reactor, a constant volume is typically assumed, since pressurized autoclaves are used. Complete backmixing is created by different means, such as by an impeller, a rotating basket inside the reactor, or by recycling. Complete backmixing can be attained by high recycle ratios. Different configurations of the gradientless reactor concept are illustrated in Figure A9.7.

At steady state, the mass balance of an arbitrary component, according to the principles presented in Chapter 5, becomes

$$\frac{\dot{n}_i - \dot{n}_{0i}}{V_R} = \rho_B r_i. \tag{A9.16}$$

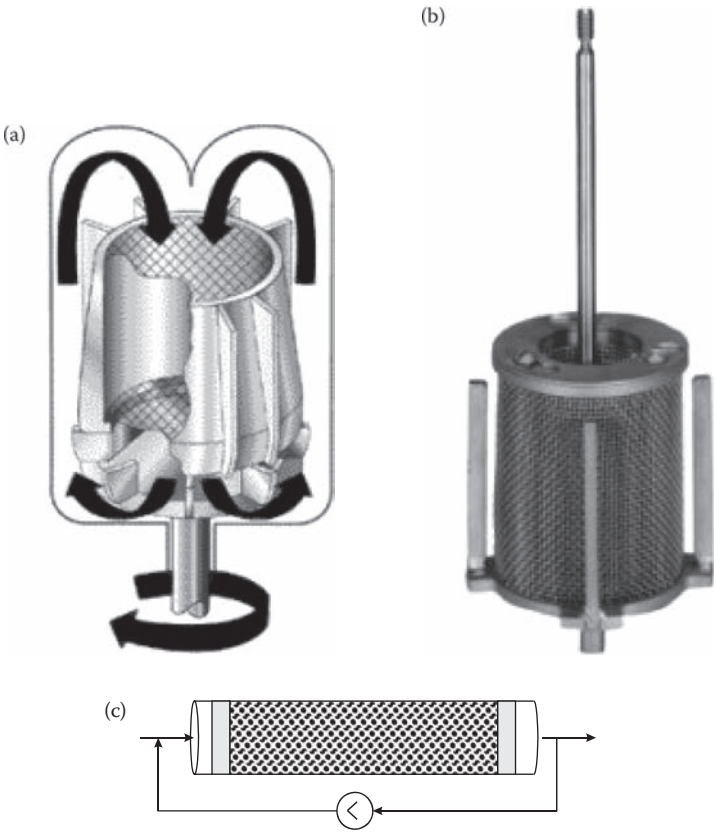

FIGURE A9.7 Configuration alternatives for a gradientless reactor. (a) A stationary catalyst basket (Berty reactor), (b) a rotating catalyst basket (Carberry reactor), and (c) a recycle reactor.

Using the component concentrations, the balance equation (Equation A9.16) can be rewritten as

$$\frac{c_i - c_{0i}}{\tau} = \rho_B r_i. \tag{A9.17}$$

It should be noticed that Equation A9.17 assumes that the volumetric flow rate is constant, whereas Equation A9.16 is a general expression. The great advantage of the gradientless reactor is that the rates are obtained directly by measurement of the molar flows or concentrations at the reactor outlet. Thus the interpretation of the data is completely analogous with the case of a homogeneous CSTR (Figure A9.4).

A9.8 BRs FOR TWO- AND THREE-PHASE PROCESSES

For catalytic three-phase processes, batchwise operating slurry reactors are frequently used in kinetic experiments. The reactor can operate under atmospheric pressure, but a more common approach is to use a pressurized autoclave equipped with a stirrer and catalyst/solvent pretreatment units. The gas-phase pressure is kept constant by regulation. Another option is to use a shaking reactor, which does not require a stirrer, but the stirring is accomplished by vigorous shaking of the equipment. Typical laboratory-scale reactors are shown in Figure A9.8.

The gas–liquid and liquid–solid mass transfer resistances are suppressed by vigorous agitation of the reactor contents, and the mass transfer resistance inside the catalyst particles is minimized by using finely dispersed particles (of micrometer scale). The addition of the gas-phase component is controlled by pressure regulation; thus, the pressure in the gas phase is kept constant, which implies that the mass balance of the gas phase can be excluded from the mathematical treatment. The concentrations of dissolved gases in the liquid phase are equal to the saturation concentrations (Chapter 6). Under these circumstances, the mass

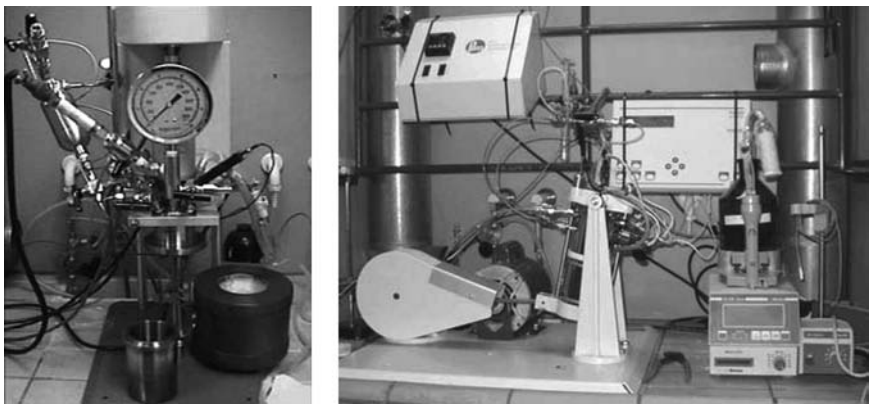

FIGURE A9.8 Test reactors (autoclave and shaking reactor) for the measurement of the kinetics of three-phase processes.

balance of an arbitrary nonvolatile component in the liquid phase becomes

$$\frac{\mathrm{d}c_i}{\mathrm{d}t} = \rho_B r_i, \quad \text{where } \rho_B = \frac{m_{cat}}{V_L}. \tag{A9.18}$$

As shown by Equation A9.18, the formal treatment of the data obtained from the slurry reactor is similar to the procedure for the homogeneous BRs. The only difference arises from using the proportionality factor, that is, the catalyst bulk density, ρ_B.

For noncatalytic and homogeneously catalyzed gas–liquid reaction systems, BRs are frequently used. Provided that the reactor operates at the kinetic regime (mass transfer resistances and reactions in the films are negligible; see Chapter 7), the component mass balance is given by

$$\frac{\mathrm{d}c_i}{\mathrm{d}t} = r_i. \tag{A9.19}$$

Analytical solutions of Equations A9.18 and A9.19 can be obtained for simple cases of isothermal kinetics. The validity of intrinsic kinetics can be checked by plotting the experimentally recorded concentrations (c_i) as a function of the transformed time $t' = \rho_B t$, when experiments are carried out with different amounts of the catalyst, that is, different bulk densities. In a normalized plot (Figure A9.9), all of the curves should coincide, if kinetic

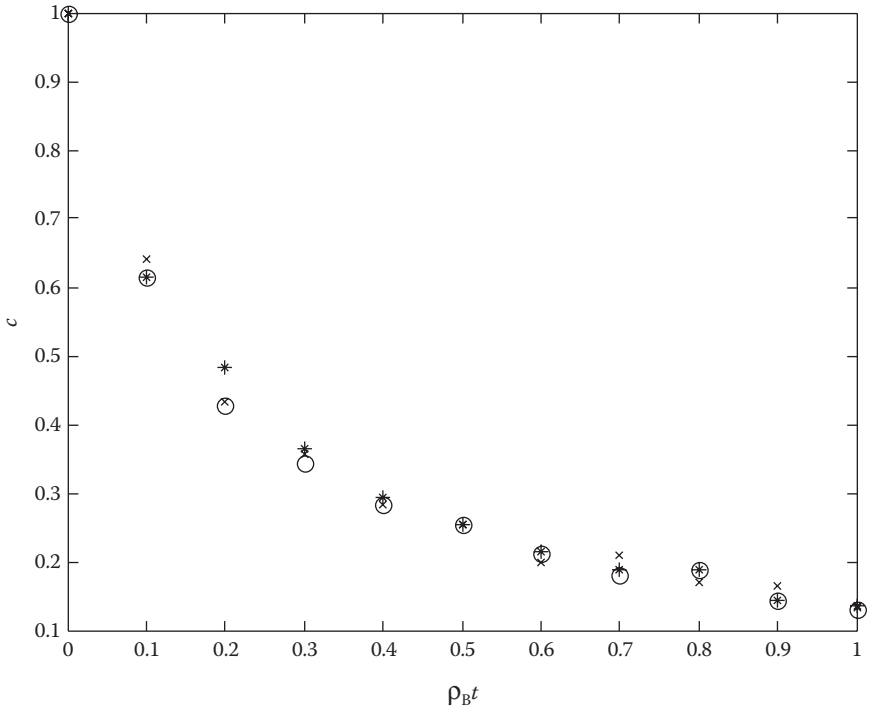

FIGURE A9.9 Verification of the kinetic regime for a three-phase process in a slurry reactor (O, ×, * represent various catalyst amounts).

control prevails. If the mass transfer resistance at the gas–liquid or liquid–solid interphase influences the results, the reactant conversion is slower in the $c_i - t'$ plot (Figure A9.9).

A9.9 CLASSIFICATION OF LABORATORY REACTOR MODELS

The models that were actually used in the estimation of kinetic and thermodynamic parameters are reviewed here. Roughly speaking, two kinds of models are very dominating, namely algebraic models and differential models. Algebraic models consist of nonlinear equation systems (linear equation systems are obtained only for linear kinetics under isothermal conditions), whereas differential models consist of ODEs (provided that ideal flow conditions prevail in the test reactor).

Algebraic models can be represented by the equation

$$\hat{\mathbf{y}} = \mathbf{f}(\mathbf{x}, \mathbf{p}), \tag{A9.20}$$

where $\hat{\mathbf{y}}$ is the dependent variable representing, for instance, the rates measured in CSTRs or differential reactors, and $\mathbf{x}$ is the independent variable, typically the volume, space time, and so on. The kinetic and thermodynamic parameters are included in the vector ($\mathbf{p}$). Equation A9.20 can also represent an analytically integrated balance equation for a component in a BR.

Differential models can generally be described by ODEs, such as

$$\frac{\mathrm{d}\hat{\mathbf{y}}}{\mathrm{d}\theta} = \mathbf{f}(\mathbf{y}, \mathbf{p}), \tag{A9.21}$$

where the symbol θ represents the time, length, volume, and so on, depending on the particular case. The dependent variable ($\hat{\mathbf{y}}$) corresponds to concentrations or molar amounts measured in batch and semibatch reactors, or, concentrations or molar flows at the outlet of a plug flow or, alternatively, a fixed bed. The independent variable (θ) is the reaction time or the reactor length (volume) coordinate. A summary of the test reactor models presented here is given in Table A9.1. Details of the estimation of the kinetic and thermodynamic parameters are discussed in Appendix 10.

TABLE A9.1 Summary of Test Reactor Models

Reactor	Model
Homogeneous batch and semibatch reactor	Differential
Homogeneous tube reactor	Differential
Homogeneous stirred tank reactor	Algebraic
Fixed bed reactor (integral mode)	Differential
Differential reactor	Algebraic
Gradientless reactor	Algebraic
BR for two- and three-phase processes	Differential

REFERENCES

1. Edwards, M.F. and Richardson, J.F., Gas dispersion in packed beds, *Chem. Eng. Sci.*, 23, 109, 1968.
2. Kangas, M., Salmi, T., and Murzin, D., Skeletal isomerization of butene in fixed beds, Part 2, Kinetic and flow modelling, *Ind. Eng. Chem. Res.*, 47, 5413–5426, 2008.
3. Poling, B.E., Prausnitz, J.M., and O'Connell, J.P., *The Properties of Gases and Liquids*, 5th Edition, McGraw-Hill, Boston, 2001.

Estimation of Kinetic Parameters from Experimental Data

The rate constants included in the kinetic expressions, rate equations, can seldom be estimated theoretically based on fundamental theories, such as collision and transition state theories, but an experimental determination of the reaction rates in laboratory-scale reactors is usually unavoidable. Based on experimentally recorded reactant and product concentrations, it is possible to estimate the numerical values of rate constants. Below we will give a brief introduction of the procedures involved in the data acquisition and estimation of kinetic parameters.

A10.1 COLLECTION OF KINETIC DATA

Laboratory experiments can in principle be carried out in all kinds of continuous and discontinuous reactors. In practice, however, the simple, isothermal BR is the most common choice for a test reactor in kinetic experiments. The reactor vessel is filled with a reaction mixture, and the concentrations of the reactants—and preferably even those of the products—are recorded by chemical analysis. The concentrations are measured either on-line by a continuous analysis method or via sampling from the reactor vessel and off-line analysis. Various analytical methods are used nowadays, a brief summary of which is given in Table A10.1.

For kinetic measurements, both continuous and discontinuous analytical methods are applied. Continuous analysis methods such as conductometry or potentiometry are used

TABLE A10.1 Common Analytical Methods Used in Chemical Kinetics

Method	Measurement Principle	Character of the Method
Photometry	Absorption of ultraviolet, visual, or infrared radiation	Continuous or discontinuous
Conductometry	Electrical conductivity of liquid	Continuous or discontinuous
Potentiometry	Voltage	Continuous or discontinuous
Polarography	Electrical current	Discontinuous
Mass spectrometry	Separation of components based on molar masses	Continuous
Gas and liquid chromatography	Separation of components based on their affinities on solid phase	Discontinuous

by placing a sensor directly in the reaction vessel and storing the measurement signal on a computer. Alternatively, a small side-stream can be withdrawn from the reactor to a continuously operating analytical instrument such as a photometer. Discontinuous analysis implies that samples are withdrawn from the reaction vessel, prepared for chemical analysis, and injected into an analytical instrument. Typical applications of this principle are gas and liquid chromatography. The various measurement principles are illustrated in Figure A10.1. Chemical analysis has advanced considerably during the last decades; automatic, continuous analytical methods in particular have developed; and discontinuous methods such as gas and liquid chromatography are equipped with auto-sampling systems. This has considerably improved the precision of kinetic data.

In any case, the primary analytical signal is converted into concentrations, mole fractions, or molar amounts. As an example, Figure A10.2 shows a kinetic curve that has been recorded experimentally for an irreversible second-order reaction $A + B \rightarrow R + S$ in an isothermal BR.

The results from a kinetic experiment carried out in an isothermal BR can be quantitatively interpreted as follows. The mass balance of component A is written as

$$\frac{dn_A}{dt} = r_A V. \tag{A10.1}$$

The volumes of the reaction mixture and the density usually remain approximately constant, and in the present case, the relationship $n_A = c_A V$ yields

$$\frac{dn_A}{dt} = \frac{dc_A}{dt} V. \tag{A10.2}$$

The mass balance Equation A10.1 is thus simplified to

$$\frac{dc_A}{dt} = r_A. \tag{A10.3}$$

Equation A10.3 is the starting point for the treatment of BR data. Further processing of Equation A10.3 depends on the particular rate equation in question.

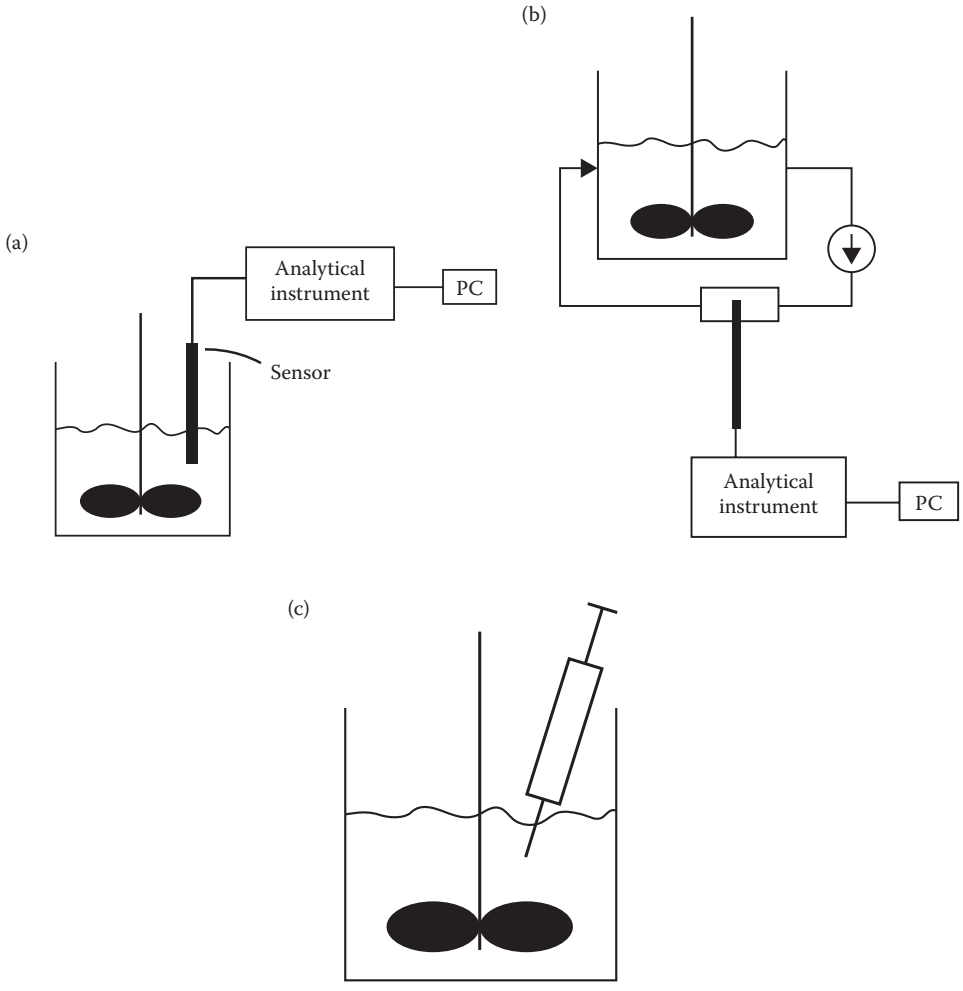

FIGURE A10.1 Principles of chemical analysis applied to kinetic measurements: (a) continuous on-line, *in situ* analysis, (b) continuous on-line analysis of a side-stream, and (c) discontinuous off-line analysis.

For the sake of simplicity, we will consider the irreversible and elementary reaction

$$A \rightarrow P, \tag{A10.4}$$

which follows first-order kinetics

$$r = kc_A, \tag{A10.5}$$

implying that

$$r_A = -kc_A. \tag{A10.6}$$

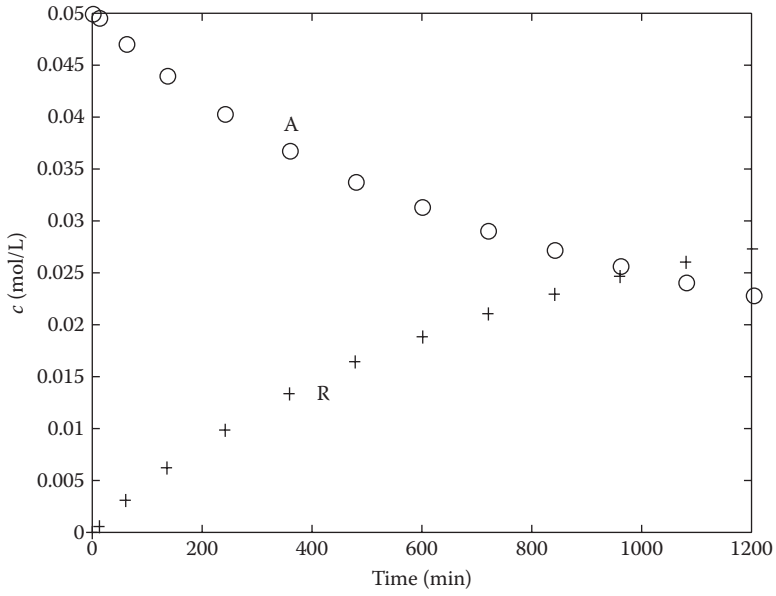

FIGURE A10.2 Concentrations of A and R for a second-order reaction A + B → R + S in an isothermal BR.

The rate expression Equation A10.6 is inserted into the mass balance Equation A10.3, and we obtain

$$\frac{\mathrm{d}c_\mathrm{A}}{\mathrm{d}t} = -kc_\mathrm{A}. \tag{A10.7}$$

For further treatment of Equation A10.7, two possible methods exist, namely, the differential and integral methods, which will be discussed in detail below.

A10.2 INTEGRAL METHOD

The integral method is based on the integration of the mass balance. For instance, Equation A10.7, valid for first-order kinetics, is integrated after a separation of variables

$$-\int_{c_{0\mathrm{A}}}^{c_\mathrm{A}} \frac{\mathrm{d}c_\mathrm{A}}{\mathrm{d}t} = k\int_0^t \mathrm{d}t, \tag{A10.8}$$

yielding the logarithmic relationship

$$-\ln\left(\frac{c_\mathrm{A}}{c_{0\mathrm{A}}}\right) = kt. \tag{A10.9}$$

This expression implies that experimental points $-\ln(c_{\mathrm{A}i}/c_{0\mathrm{A}i})$ versus kt_i (i represents the different samples withdrawn from the reaction mixture) should yield a straight line, if the reaction follows first-order kinetics. A general illustration is provided in Figure A10.3.

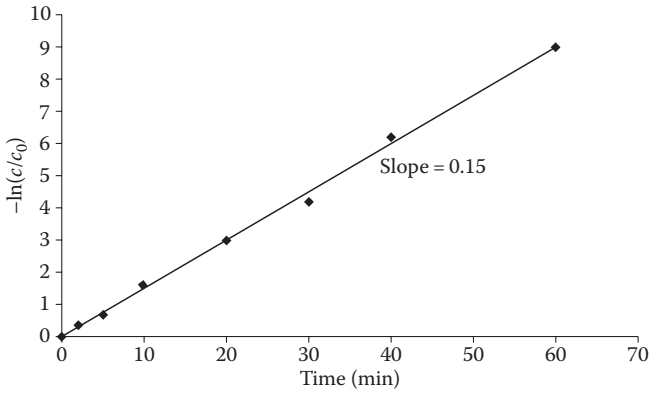

FIGURE A10.3 Determination of the rate constant by the integral method; first-order kinetics $r = kc_A$.

This procedure can be generalized to cover arbitrary kinetics. The expression of r_A depends on the concentrations (c_A, c_B, etc.) only. The reaction stoichiometry gives the concentrations of the other components. In the case of a single reaction, we can use the extent of reaction

$$\xi = \frac{c_A - c_{0A}}{\nu_A} = \frac{c_B - c_{0B}}{\nu_B}, \tag{A10.10}$$

from which all the concentrations are expressed as a function of c_A.

The rate equation can thus be rewritten as

$$r_A = -k_A f(c_A) \; (k_A = |\nu_A| \, k) \, , \tag{A10.11}$$

where $f(c_A)$ depends on the particular form of the kinetics. For instance, second-order kinetics yields $f(c_A) = c_A^2$ or $f(c_A) = c_A c_B$, where $c_B = c_{0B} + (\nu_B/\nu_A)(c_A - c_{0A})$. The mass balance Equation A10.3 is interpreted after the separation of variables

$$\int_{c_{0A}}^{c_A} \frac{\mathrm{d}c_A}{-f(c_A)} = k_A \int_0^t \mathrm{d}t. \tag{A10.12}$$

A general integral function can be denoted by

$$\int \frac{\mathrm{d}c_A}{f(c_A)} = G(c_A). \tag{A10.13}$$

Consequently, Equation A10.12 is rewritten as

$$G(c_{0A}) - G(c_A) = k_A t, \tag{A10.14}$$

which implies that $G(c_{0A}) - G(c_{Ai})$ versus t_i should yield a straight line, if the proposed rate equation is valid. The slope of the plot yields k_A. If the plotted values of the G function

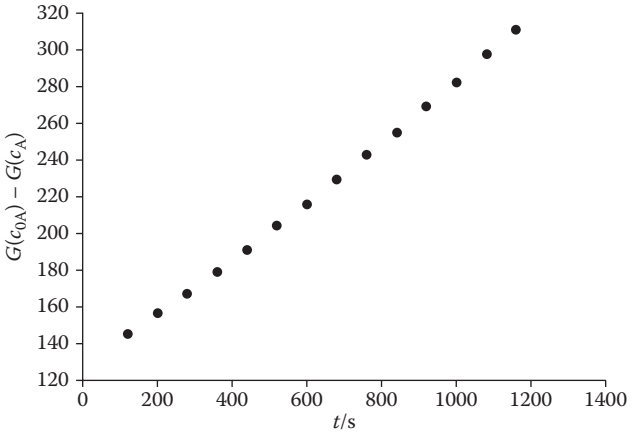

FIGURE A10.4 Estimation of the rate constant according to Equation A10.14 (integral method).

systematically deviate from a straight line, the experimental data evidently do not obey the rate equation proposed, but a new kinetic hypothesis should be adopted and a new test plot should be prepared. For an example plot, see Figure A10.4.

The numerical value of the rate constant can be determined graphically, but the method of least squares is more reliable. This method has been developed by statisticians and is described in detail in many textbooks. Here we will explain the use of the method from a practical viewpoint only.

A set of kinetic data is at our disposal, and the difference $G(c_{0A}) - G(c_{Ai})$ is denoted by y_i. The model Equation A10.14 thus becomes

$$\hat{y}_i = k_A t_i, \tag{A10.15}$$

where the circonflex indicates that the y values are calculated from the kinetic model. The value of the rate constant (c_A) is going to be estimated in such a way that the predicted y values (y_i) deviate as little as possible from the experimental ones (y_i).

An objective function (Q) is formulated by adding together all the quadratic deviations

$$Q = \sum_{i=1}^{n} (\hat{y}_i - y_i)^2, \tag{A10.16}$$

where n denotes the total number of experimental observations. The expression of $\hat{y}_i$ in Equation A10.15 is inserted into Equation A10.16, and we obtain

$$Q = \sum \left(y_i - k_A t_i\right)^2. \tag{A10.17}$$

Our task now is to find such a numerical value of the rate constant (k_A) that the objective function (Q) is minimized. A necessary condition for the minimum is that the first derivative

TABLE A10.2 Expressions for y_i; (Integral Method) for Some Common Kinetics

Reaction	$-r_A$	y
A → Product	kc_A	$\ln(c_{0A}/c_A)$
2A → Product	kc_A^2	$1/c_A - 1/c_{0A}$
A + B → Product	kc_Ac_B	$1/a \ln[(a + c_A)c_{0A}]/[(a + c_{0A})c_A]$, $a = c_{0B} - c_{0A}$
where $c_B = c_A + c_{0B} - c_{0A}$		

is zero

$$\frac{dQ}{dk_A} = 0, \tag{A10.18}$$

where

$$\frac{dQ}{dk_A} = \sum 2\big(y_i - k_A t_i\big)(-t_i) = 0, \tag{A10.19}$$

which is equivalent to

$$\sum y_i t_i - k_A \sum t_i^2 = 0. \tag{A10.20}$$

The rate constant can then be solved explicitly:

$$k_A = \frac{\sum y_i t_i}{\sum t_i^2}. \tag{A10.21}$$

The result implies that the rate constant is obtained from a very simple expression Equation A10.21, which can even be calculated without a computer.

Since the original expression Equation A10.19 is linear with respect to the parameter k_A, this method is called linear regression. Many computer programs exist for the automatic fitting of linear models $y = kx$ and $y = k_0 + k_1x$, and the real expressions for least-square models, such as Equation A10.21, thus remain unknown for the program user.

Now it is time to recall the definition for variable y; it is $y = G(c_{0A}) - G(c_{Ai})$ and thus dependent on the reaction kinetics. The expressions for some common reaction kinetics are presented in Table A10.2 For complex kinetics, the y values can be obtained by numerical integration of Equation A10.12.

Finally, it should be noted that the integral method even enables a very straightforward method of estimation of k_A, namely

$$k_A = \frac{y_i}{t_i}, \tag{A10.22}$$

which can be calculated for each experimental point. The k_A values thus obtained might vary depending on the experimental precision. It is thus reasonable to utilize the entire experimental information and all observations and then take the average:

$$k_A = \frac{\sum (y_i/t_i)}{n}. \tag{A10.23}$$

The major difference between the least-squares expression, Equation A10.21, and the average Equation A10.23 is that the least-squares expression gives the largest weight to high t_i values—since y_i approaches infinity as t_i increases—whereas the average method gives the largest weight to low t_i values. As this discussion reveals, both approaches described have serious disadvantages. Regardless of this, they are useful tools when ascertaining whether a proposed rate equation might be adequate or not. The most objective method for the determination of rate constants, namely nonlinear regression, will be discussed in Section 10.5 in Appendix 10.

A10.3 DIFFERENTIAL METHOD

The use of the differential method is very simple in principle, since it is based on the direct utilization of the generation rate (r_A). For instance, for first-order kinetics, the component mass balance in a BR becomes

$$\frac{dc_A}{dt} = r_A = -k_A c_A, \tag{A10.24}$$

that is, the generation rate is given by dc_A/dt, the concentration derivative, which is evaluated from the kinetic curve as illustrated in Figure A10.5.

The use of the method requires numerical differentiation of the c_A–t curve. For the concentration derivative, the simplest approach is to use the two-point formula

$$\left(\frac{dc_A}{dt}\right)_{t=((t_i+t_{i-1})/2)} = \frac{c_A(t_i) - c_A(t_{i-1})}{t_i - t_{i-1}}. \tag{A10.25}$$

Multipoint differentiation formulae are presented in many handbooks, for example, in that by Abramowitz and Stegun [1].

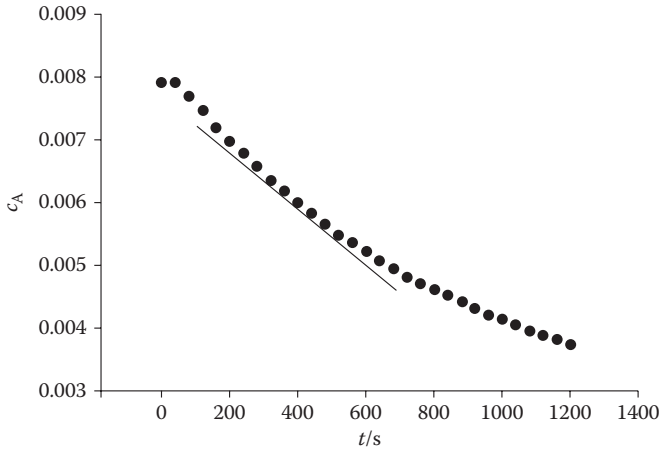

FIGURE A10.5 Determination of the generation rate from an experimentally recorded concentration curve.

In any case, the concentration derivatives are expressed by y_i

$$y_i = -\frac{\mathrm{d}c_{\mathrm{A}i}}{\mathrm{d}t} \tag{A10.26}$$

and the concentration (c_{A}) is denoted by x. The model becomes

$$y_i = k_{\mathrm{A}} x_i, \tag{A10.27}$$

which, for instance, suggests that $y = -\mathrm{d}c_{\mathrm{A}i}/\mathrm{d}t$ versus $c_{\mathrm{A}i}$ should be a straight line, if the experimental data follow first-order kinetics.

The procedure is easily generalized to arbitrary kinetics. The rate expression can be written as

$$r_{\mathrm{A}} = -k_{\mathrm{A}} f(c_{\mathrm{A}}) \tag{A10.28}$$

and the mass balance for a BR becomes

$$-\frac{\mathrm{d}c_{\mathrm{A}}}{\mathrm{d}t} = k_{\mathrm{A}} f(c_{\mathrm{A}})\,. \tag{A10.29}$$

The derivative is denoted by $-\mathrm{d}c_{\mathrm{A}i}/\mathrm{d}t = y_i$ and $f(c_{\mathrm{A}i}) = x_i$, and we obtain

$$y_i = k_{\mathrm{A}} x_i. \tag{A10.30}$$

The expression for x_i depends on the actual case of reaction kinetics, for example, for first-order kinetics $r_{\mathrm{A}} = -kc_{\mathrm{A}}$ and $x_i = c_{\mathrm{A}i}$, and for second-order kinetics $r_{\mathrm{A}} = -kc_{\mathrm{A}}^2$ and $x_i = c_{\mathrm{A}i}^2$, and so on.

The numerical value of the rate constant can now be estimated by linear regression, by the method of least squares. The model is compressed to Equation A10.30, and the objective function thus becomes

$$Q = \sum \left(y_i - k_{\mathrm{A}} x_i\right)^2. \tag{A10.31}$$

The minimization problem is solved as follows:

$$\frac{\mathrm{d}Q}{\mathrm{d}k_{\mathrm{A}}} = \sum 2\left(y_i - k_{\mathrm{A}} x_i\right)(-x_i) = 0. \tag{A10.32}$$

The solution of Equation A10.32 yields the value of k_{A}

$$k_{\mathrm{A}} = \frac{\sum y_i x_i}{\sum x_i^2}, \tag{A10.33}$$

where $y_i = -\mathrm{d}c_{\mathrm{A}i}/\mathrm{d}t$ and x_i depends on the actual reaction kinetics as shown in Table A10.3.

TABLE A10.3 Expressions Valid for x_i for Various Reaction Kinetics (Differential Method)

Reaction	$-r_A$	x_i
A → Product	$k_A c_A$	c_{Ai}
2A → Product	$k_A c_A^2$	c_{Ai}^2
A + B → Product	$k_A c_A c_B$	$c_{Ai}(c_{0B} - c_{0A} + c_{Ai})$
where $c_B = c_A + c_{0B} - c_{0A}$		

A10.4 RECOMMENDATIONS

The differential method is recommended for a preliminary screening of reaction kinetics, particularly for cases in which the expression for r_A is not *a priori* known, and various rate expressions are tried on experimental data until an adequate fit is obtained and systematic deviations between the data and the model have disappeared.

Derivatives $-dc_A/dt$ are evaluated on the basis of the c_A–t curve, and competing hypotheses concerning the reaction kinetics ($r_A = -kc_A$, $r_A = -kc_A^\alpha c_B^\beta$, etc.) are tested. After finding the best expression for r_A, it is highly recommendable to switch to the integral method to carry out a more precise estimation of the rate constant. The integral method is in general more accurate than the differential method, because numerical integration suppresses experimental scattering, while numerical differentiation fortifies it. The performance of the differential method can be improved by using empirical regression formulae, typically polynomials for the determination of the derivatives dc_A/dt on the c_A–t curves. Suitable polynomial regression formulae are presented, for example, by Savitzky and Golay [2]. The use of these formulae leads to the smoothing of the original data, that is, random scattering is diminished. Fortunately, the development of on-line analysis methods and automatic sampling techniques for off-line analysis have considerably reduced experimental scattering and thus made the differential method more attractive.

A10.5 INTRODUCTION TO NONLINEAR REGRESSION

The previously described methods for parameter estimation are based on linear transformations, that is, the model expression is written in such a way that the rate constant (k_A) can be solved from a linear expression. This is convenient from the numerical viewpoint, but the drawback is that the structure of the transformed data becomes biased, as discussed previously (Section 10.2). In effect, the most rational standpoint is to utilize the original experimental data as such, typically the experimentally recorded component concentrations (c_{Ai}), and to compare them with the predicted concentrations (c_{Ai}). The objective function (Q) thus becomes

$$Q = \sum \left(c_{Ai} - \hat{c}_{Ai}\right)^2. \tag{A10.34}$$

This expression is minimized with respect to the rate constant (k_A).

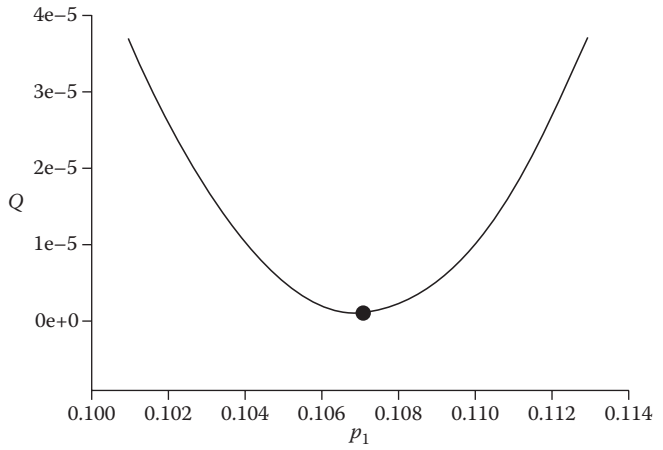

FIGURE A10.6 Determination of the rate constant ($k_A = p_1$) through numerical minimization of the objective function (Q).

For instance, for first-order kinetics ($r_A = -kc_A$), the solution of the BR model, Equation A10.3, becomes

$$\hat{c}_{Ai} = c_{0A}e^{-k_A t_i}. \tag{A10.35}$$

Consequently, the objective function Equation A10.34 assumes the form

$$Q = \sum \left(c_{Ai} - c_{0A}e^{-k_A t_i}\right)^2. \tag{A10.36}$$

The minimum of the objective function is, of course, obtained from the general condition

$$\frac{dQ}{dk_A} = 0, \tag{A10.37}$$

which yields

$$\sum 2\left(c_{Ai} - c_{0A}e^{-k_A t_i}\right) t_i c_{0A}e^{-k_A t_i} = 0. \tag{A10.38}$$

In this case, however, it is not possible to solve the nonlinear Equation A10.38 analytically, but a numerical algorithm, for example, the Newton–Raphson method for the solution of nonlinear equations, should be applied (Appendix 1). A general way to solve the nonlinear regression problem Equation A10.36 is to vary the value of k_A systematically by an optimum search method until the minimum is attained. This method is called nonlinear regression, and it is illustrated in Figure A10.6.

A10.6 GENERAL APPROACH TO NONLINEAR REGRESSION IN CHEMICAL REACTION ENGINEERING

The method of nonlinear regression can be generalized to arbitrary systems with many components and chemical reactions. Furthermore, the method is not limited to BRs, but any reactor model can in principle be used.

The reactor model usually consists either of algebraic equations or ODEs:

$$\frac{dy}{dx} = f(y) \tag{A10.39}$$

and

$$f(y) = \mathbf{0}, \tag{A10.40}$$

where y denotes the concentration, molar amount, or molar flow; x is the reaction time, reactor length, or volume. The parameters to be determined typically are rate (k) or equilibrium (K) constants. The objective function is generally defined as follows:

$$Q = \Sigma\, w_i\left(y_i - \hat{y}_i\right)^2, \tag{A10.41}$$

where w_i is the weight factor of the component (i). In general, tailored weight factors can be used, depending on the experimental data available. Individual weight factors can also be used to exclude data that are wrong for evident reasons (e.g., due to poor sampling or failed chemical analysis). From a statistical viewpoint, different experimental observations should be weighted according to the variances of the data points.

The objective function can be interpreted in a very general way; the values y_i can, for example, comprise the concentrations of various components at various times or spatial locations in the reactor. This is illustrated in Table A10.4.

Various optimum search methods exist for the minimization of objective functions, which can be used for the estimation of kinetic constants [3], for example, the Fibonacci method, the golden section method, the Newton–Raphson method, the Levenberg–Marquardt method, and the simplex method. Recently, even genetic algorithms have been

TABLE A10.4 Model Equations A10.39 and A10.40 for Different Reactor Models

$\frac{d\dot{n}_i}{dV} = r_i\alpha$	Tube reactor, plug flow, general model
$\frac{\dot{n}_i - \dot{n}_{0i}}{V} = r_i\alpha$	Tank reactor, complete backmixing, general model
$\frac{dc_i}{d\tau} = r_i\alpha$	Tube reactor, plug flow, $\dot{V}$ = constant
$\frac{c_i - c_{0i}}{\tau} = r_i\alpha$	Tank reactor, complete backmixing, $\dot{V}$ = constant
$\frac{dc_i}{dt} = r_i\alpha$	BR, V = constant
$\alpha = 1$ for homogeneous reactors	$\tau = V/\dot{V}$
$\alpha = \rho_B (= m_{cat}/V_R)$ for catalytic reactors	t = reaction time

introduced into regression analysis. The details of numerical algorithms are reviewed in many reference books and textbooks, and public domain computer codes are available for regression analysis. Convergence to the real minimum of the objective function is a genuine challenge. It is possible that a local minimum is attained or that the search algorithm diverges. Some rules of thumb are thus of value in the estimation of kinetic parameters:

- Try and use as good initial estimates as possible for the kinetic parameters (an optimization algorithm requires an initial guess of the parameters).
- If possible, transformation of data and application of linear regression are recommendable in obtaining reasonable initial estimates of kinetic parameters.
- If nothing is known a priori, it is usually better to give a low estimate of a kinetic parameter (assuming very slow reactions), and let the optimum search algorithm increase the parameter values. Too high an initial estimate of a rate constant might lead to a rapid consumption of a reactant, whose concentration can even become negative during the computation due to numerical inaccuracies.

The reactor models are in a general case not solved analytically but numerically in the course of parameter estimation. Solvers for nonlinear equations and differential equations (Appendices 1 through 3) are thus frequently used in parameter estimation. The model solution routine [a numerical NLE (nonlinear equation) or ODE solver] works under the parameter estimation routine. The reactor model itself is at the bottom of the system. The structure of a general parameter estimation code is displayed in Figure A10.7. Special codes for kinetics, thermodynamics, and transport phenomena are included, if needed.

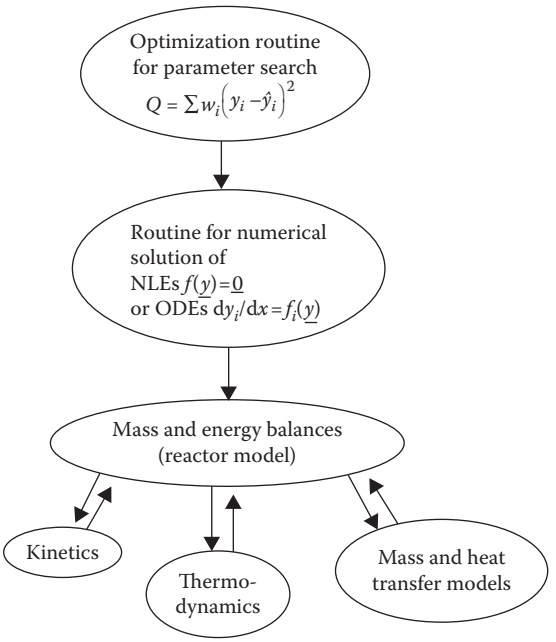

FIGURE A10.7 Parameter estimation in chemical reaction engineering.

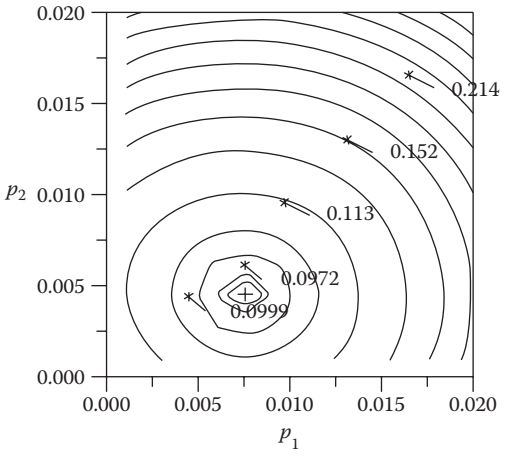

FIGURE A10.8 A "good" contour plot between two parameters (p_1 and p_2).

Parameter estimation is typically followed by a statistical analysis of the parameters, which comprises the variances and confidence intervals of the parameters, correlation coefficients of parameter pairs, contour plots, and a sensitivity analysis. The confidence intervals of the parameters are obtained from standard statistical software; the procedure is not treated in detail here.

Contour plots illustrate the correlation between two parameters. The values of a parameter pair (p_1 and p_2) that give the same value of the objective function (Q) are screened and illustrated graphically. An ideal contour plot is a circle, indicating that the parameters are not mutually correlated as shown in Figure A10.8.

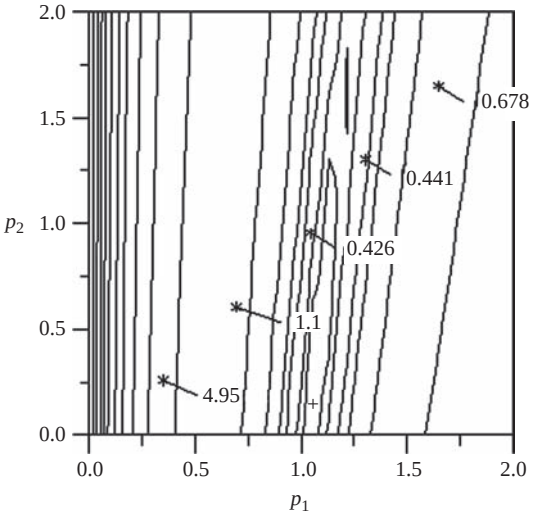

FIGURE A10.9 A "bad" contour plot of two parameters (p_1 and p_2).

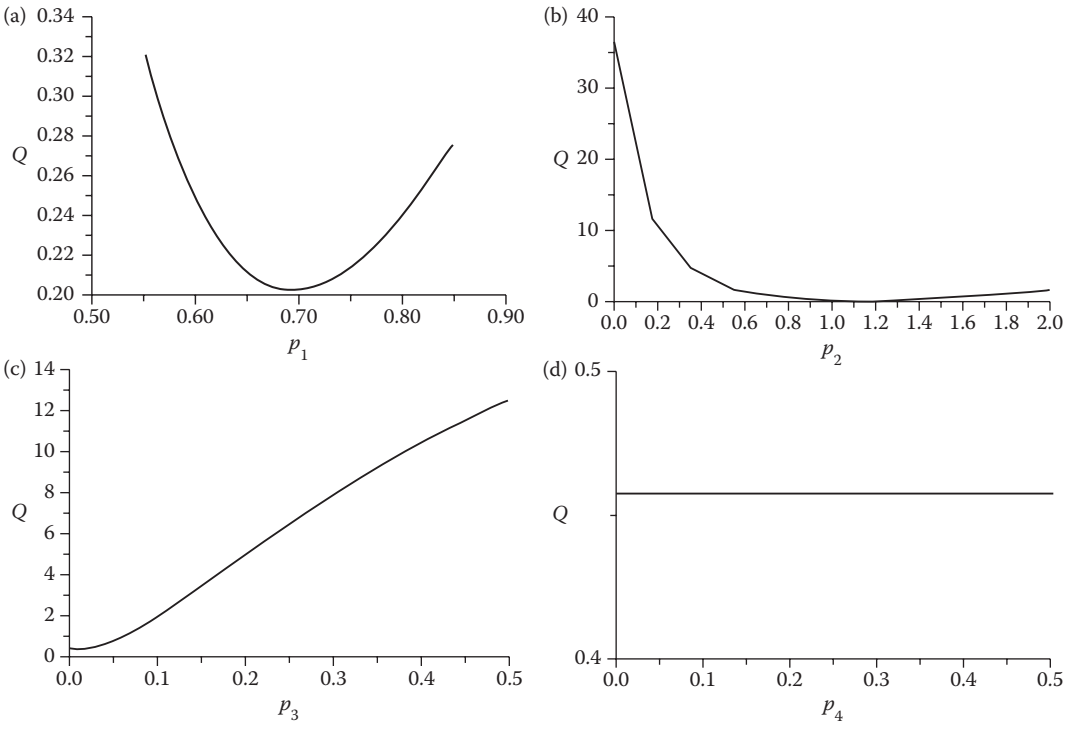

FIGURE A10.10 Sensitivity plots of parameters p_1, p_2, p_3, and p_4 [from left: well-identified (p_1), partially well identified (p_2 and p_3), and not identified (p_4)].

On the other hand, if two parameters are considerably correlated, they can compensate each other, and the absolute values of the parameters remain uncertain. An example of heavily correlated parameters is provided in Figure A10.9.

A very illustrative way to investigate the quality of an estimated parameter is to prepare a sensitivity plot. All parameters except one are fixed on the values, giving the minimum of

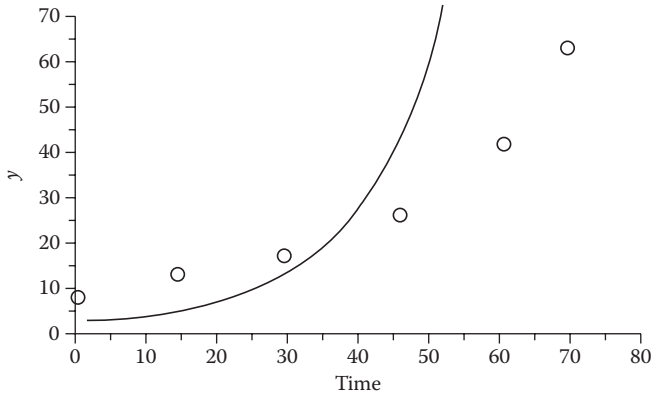

FIGURE A10.11 Parameter estimation results of a "wrong" model with systematic deviations from experimental data.

the objective function (Q), and the value of one parameter is systematically changed and the corresponding value of the objective function is computed. In this way, it is possible to investigate how profound the minimum of Q is. The results can be presented graphically as demonstrated in Figure A10.10. Sensitivity plots indicate the identifiabilities of the parameters better than confidence intervals, since the vicinity of the objective function is necessarily not at all symmetric, but the parameter might be much better identified in one of the directions, as demonstrated in Figure A10.10.

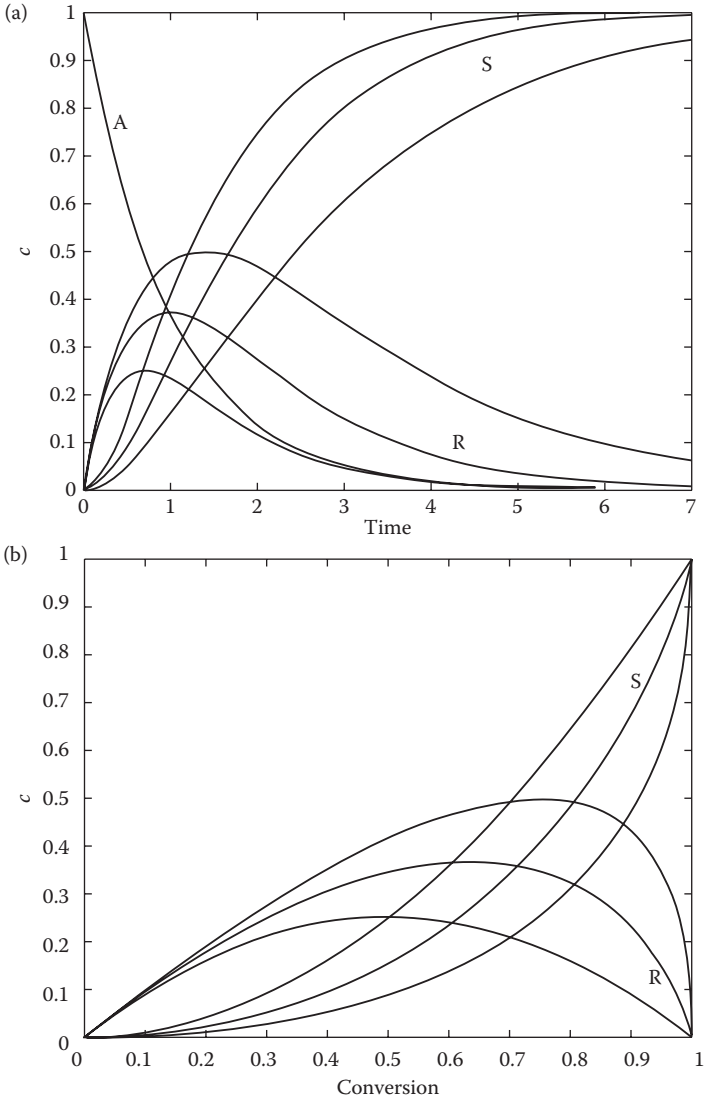

FIGURE A10.12 Kinetic data presented in the time domain (a) and in the stoichiometric domain (b), $A \rightarrow R \rightarrow S$, $dc_A/d\theta = -c_A$, $dc_R/d\theta = c_A - \alpha c_R$, $dc_s/d\theta = \alpha c_R$, $\theta =$ dimensionless time.

The numerical calculation of the sensitivity plots is very simple after the minimum of the objective function has been found; this is why the plots should be used as standard tools in nonlinear regression.

The procedure for the estimation of kinetic parameters comprises several steps as shown by the preceding discussion. The problems caused by scattered experimental data are becoming more and more rare, but the application of parameter estimation explores very complex systems, particularly in the fields of fine and specialty chemicals production. The challenge to find an appropriate model for the system is thus often very demanding. Typically, the first attempts to model a complex system fail, because the proposed model does not provide a chemically adequate description of the system. The parameter estimation procedure

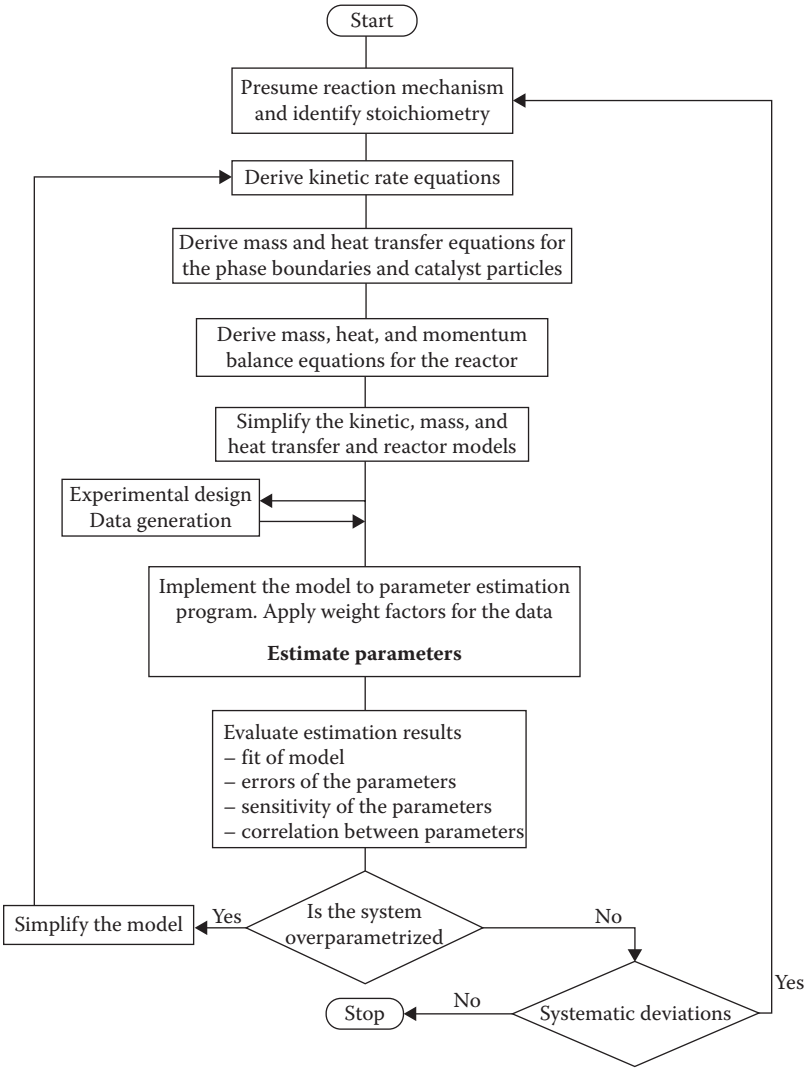

FIGURE A10.13 Parameter estimation in chemical reaction engineering.

works technically, but yields a set of parameters that gives a fit with systematic deviations as illustrated in Figure A10.11.

To detect systematic deviations, graphical plots, for example, experimental versus predicted quantities, are very illustrative tools. It is sometimes difficult to judge whether a deviation is systematic or not, as illustrated for a complex chemical system in Figure A10.12a. Some deviations of the model predictions from experimental data are visible, but their origin remains unclear, as the system is visualized in a concentration–time domain. Transformation of the data to a stoichiometric space might sometimes help. The data displayed in Figure A10.12a are recalculated and plotted in the conversion space as illustrated in Figure A10.12b. Now the systematic deviations become much more clear, and the search for an improved kinetic model can commence.

In general, parameter estimation is an iterative procedure, not only at the algorithmic level but also at the macroscopic level. The first model is checked and evaluated statistically, physically, and graphically; the model is improved and the parameters are reestimated, until a satisfactory fit with physically and statistically meaningful parameters is obtained. For engineering purposes, it is often necessary to simplify the model by leaving out or combining some of the parameters. For a summary of the procedure, see the flow sheet in Figure A10.13 [4]. Application of the procedure is illustrated by solved exercises (Chapters 11 and 12).

REFERENCES

1. Abramowitz, M. and Stegun, I., *Handbook of Mathematical Functions*, Dover Publications, New York, 1972.
2. Savitzky, A. and Golay, M.J.E., Smoothing and differentiation of data by simplified least squares procedure, *Anal. Chem.*, 36, 1627–1639, 1964.
3. Rao, S., *Optimization*, Wiley Eastern, New Delhi, 1979.
4. Tirronen, E. and Salmi, T., Process development in the fine chemical industry, *Chem. Eng. J.*, 91, 103–114, 2003.

The role of the chemical reactor is crucial for the industrial conversion of raw materials into products and numerous factors must be considered when selecting an appropriate and efficient chemical reactor. **Chemical Reaction Engineering and Reactor Technology** defines the qualitative aspects that affect the selection of an industrial chemical reactor and couples various reactor models to case-specific kinetic expressions for chemical processes.

Offering a systematic development of the chemical reaction engineering concept, this volume explores:

- Essential stoichiometric, kinetic, and thermodynamic terms needed in the analysis of chemical reactors
- Homogeneous and heterogeneous reactors
- Residence time distributions and non-ideal flow conditions in industrial reactors
- Solutions of algebraic and ordinary differential equation systems
- Gas- and liquid-phase diffusion coefficients and gas–film coefficients
- Correlations for gas–liquid systems
- Solubilities of gases in liquids
- Guidelines for laboratory reactors and the estimation of kinetic parameters

The authors pay special attention to the exact formulations and derivations of mass energy balances and their numerical solutions. Richly illustrated and containing exercises and solutions covering a number of processes, from oil refining to the development of specialty and fine chemicals, the text provides a clear understanding of chemical reactor analysis and design.

CRC Press
Taylor & Francis Group
an **informa** business
www.crcpress.com

6000 Broken Sound Parkway, NW
Suite 300, Boca Raton, FL 33487
270 Madison Avenue
New York, NY 10016
2 Park Square, Milton Park
Abingdon, Oxon OX14 4RN, UK

92685
ISBN: 978-1-4200-9268-4
90000
9 781420 092684